WCAP-12986
Rev. 2

SG-93-03-005

KEWAUNEE STEAM GENERATOR
TUBE PLUGGING CRITERIA FOR
ODSCC AT TUBE SUPPORT PLATES

MARCH, 1993

Approved by: *T. A. Pitterle for J. N. E.*

J. N. Esposito, Acting Manager
Steam Generator Technology & Engineering

WESTINGHOUSE ELECTRIC COPRPORATION

NUCLEAR SERVICE DIVISION

P. O. BOX 355

PITTSBURGH, PENNSYLVANIA 15230

TABLE OF CONTENTS

KEWAUNEE STEAM GENERATOR TUBE PLUGGING CRITERIA FOR ODSCC AT TUBE SUPPORT PLATES

1.0 INTRODUCTION

This report provides the technical basis for tube plugging criteria for outside diameter stress corrosion cracking (ODSCC) at tube support plate (TSP) intersections in the Kewaunee steam generators (S/Gs). The recommended plugging criteria are based upon bobbin coil inspection voltage amplitude which is correlated with tube burst capability and leakage potential. Repair limits are developed for full implementation of the alternate plugging criteria (APC). Additional margins resulting for interim plugging criteria (IPC) are also developed for varying IPC repair limits less than the APC limit. The recommended criteria are demonstrated to meet the guidelines of Regulatory Guide (R.G.) 1.121.

The tube plugging criteria are based upon the conservative assumptions that the tube to TSP crevices are open (negligible crevice deposits or TSP corrosion) and that the TSPs are displaced under accident conditions. The ODSCC existing within the TSPs is thus assumed to be free span degradation under accident conditions and the principal requirement for tube plugging considerations is to provide margins against tube burst in accordance with R.G. 1.121. The open crevice assumption leads to maximum leak rates compared to packed crevices and also maximizes the potential for TSP displacements under accident conditions. Laboratory testing of incipient denting or dented tube intersections show no leakage or very small leakage such that leakage even under steam line break (SLB) conditions would be negligible.

If the crevices are packed as a consequence of TSP corrosion or if small tube-to-TSP gaps are present, TSP displacements under accident conditions are minimal such that tube burst would be prevented by the presence of the TSPs. TSP displacement analyses under SLB loads were also performed for the open crevice assumption with the further conservative assumption of zero friction at the tube to TSP intersections and at the TSP wedge to wrapper interaction. The wedges are installed in the TSP to wrapper gaps to align the TSPs for tubing of the S/Gs. While the TSP wedges are pressed into the gap during manufacturing, the forces are not known and thus the preload or friction force at the TSP to wrapper interface is not known. It is reasonable to expect that the friction forces at the TSP to wrapper interface would significantly reduce TSP displacements under accident conditions. However, the analytical results based upon the open crevice/zero friction assumptions indicate the potential for TSP displacements under SLB conditions such that prevention of tube rupture cannot be assured for the upper tube support plates of 51 Series S/Gs with the applied analytical assumptions. Even under the conservative assumptions, the analyses show that the bottom two TSPs do not have local yielding of the plates and are expected to provide TSP constraint to prevent tube burst. Conservatively, the requirements for tube burst margins assuming free span degradation have been applied at all TSP elevations to develop the tube plugging criteria for the Kewaunee S/Gs.

The plugging criteria were developed from testing of tube specimens with laboratory-induced ODSCC, extensive examination of pulled tubes from operating S/Gs and field experience for leakage due to indications at TSPs. The recommended criteria represent conservative criteria, based upon Electric Power Research Institute (EPRI) and industry-supported development programs that are continuing to further refine the plugging criteria. The current data base permits use of burst pressures at the lower 95% confidence bound as the basis for the tube plugging limits.

Implementation of the tube plugging criteria is supplemented by 100% bobbin coil inspection requirements at TSP elevations having ODSCC indications, reduced operating leakage requirements, inspection guidelines to provide consistency in the voltage normalization and rotating pancake coil (RPC) inspection requirements for the larger indications left in service to

characterize the principal degradation mechanism as ODSCC. In addition, it is required that potential SLB leakage be calculated for tubes with indications at TSPs left in service to demonstrate that the cumulative leakage is less than allowable limits.

Burst testing has been performed of tubes from plants A-2, D, L and P also having steam generators with 7/8" OD tubing, to support the evaluation. In addition, results of pulled tube examinations from these and other plants have been used to support the tube plugging criteria.

To provide the technical bases for tube plugging due to ODSCC at TSPs, the following activities have been performed as documented in this report:

- Summary of Regulatory Requirements against which the recommended plugging criteria are evaluated - Section 3

- Review of pulled tube examinations from relevant plants - Section 4

- Review of non-destructive examination (NDE) methods to assess the sensitivity associated with application of bobbin coil voltage limits - Section 5

- Review of field experience from pulled tube data and plant leakage occurrences to define the field data base, and supplemented by laboratory tests to develop the plugging criteria - Section 6

- Preparation of laboratory test specimens for non-destructive examination (NDE) and leak testing in a model boiler or doped steam environment for inducing ODSCC cracks, or by cyclic fatigue to produce cracks in the test samples - Section 7

- Description of the burst pressure correlation and development of the voltage-based structural limit for tubing integrity - Section 8

- Correlations of leak test results to relate the NDE parameters to SLB leak rates - Section 9

- Definition of the requirements for analysis of accident conditions, based on accident condition probability assessments - Section 10

- Evaluations to assess TSP displacements under SLB loads, and plant requirements on SLB leakage limits - Section 11

- A description of recent inspection results for Kewaunee, and development of voltage growth rates by cycle and predicted growth rates - Section 12

- Integration of the inspection and burst test results to develop the tube plugging criteria - Section 13

- The eddy current inspection and analysis guidelines that will be used upon implementation of the APC are clearly documented - Appendix A

The overall summary and conclusions for this report are described in Section 2.

2.0 CONCLUSIONS

This report documents the technical support for a Kewaunee alternate plugging criteria (APC) for ODSCC indications at TSPs. Increased tube integrity margins are also identified for interim plugging criteria (IPC) having repair limits less than the APC limit. The database of pulled tube and model boiler specimens used in the evaluation of the APC are described in this report. This database is used to develop correlations relating burst pressure to bobbin voltage and steam line break (SLB) leak rate to bobbin voltage. These correlations are used in the tube integrity assessment to demonstrate Kewaunee APC and IPC margins against Regulatory Guide (RG) 1.121 guidelines for tube plugging limits.

Overall Conclusions

R.G. 1.121 guidelines for tube integrity are conservatively satisfied at end-of-cycle (EOC) conditions for an alternate plugging criteria (APC) implementing the requirements given below. Interim plugging criteria (IPC) having a voltage repair limit less than the APC limit lead to increased R.G. 1.121 margins. The implementation of the alternate plugging criteria (APC) or an interim plugging criteria (IPC, repair limit < APC) for ODSCC at TSPs can be summarized as follows:

Tube Plugging Criterion

APC
Tubes with bobbin coil flaw indications exceeding 2.5 volts will be plugged or repaired.

IPC
Tubes with bobbin flaw indications exceeding the IPC voltage repair limit and ≤2.5 volts will be plugged or repaired if confirmed as flaw indications by RPC inspection. Bobbin flaw indications >2.5 volts attributable to ODSCC will be repaired independent of RPC confirmation.

SLB Leakage Criterion

APC
Predicted end of cycle SLB leak rates from tubes left in service must be less than 9.1 gpm for each S/G, including considerations for NDE uncertainties and ODSCC growth rates.

IPC
Predicted EOC SLB leak rates from tubes left in service must be less than 1.0 gpm for each SG, including considerations for NDE uncertainties and ODSCC growth rates.

Inspection Requirements

APC
A 100% bobbin coil inspection shall be performed for all hot leg TSP intersections and all cold leg intersections down to the lowest cold leg TSP with reported ODSCC indications.

IPC
Same.

Any TSP indication with bobbin coil amplitude exceeding 1.5 volts, if planned to be left in service, shall be inspected by RPC, unless it was it was inspected by RPC during the prior refueling outage. The RPC results shall be evaluated to support ODSCC as the dominant degradation mechanism. Subsequent RPC inspection of 1.5 volt indications shall be performed during alternate refueling outages for reconfirmation as ODSCC.

Any bobbin flaw indication greater than the IPC repair limit shall be inspected if the tube is to be considered for leaving in service. If the IPC repair limit exceeds 1.5 volt, the APC guideline for RPC inspection applies.

Operating Leakage Limits

APC
Plant shutdown will be implemented if normal operating leakage exceeds 150 gpd per SG.

IPC
Same.

Exclusions from Tube Plugging Criterion

APC
Tubes with RPC indications not attributable to ODSCC and tubes with circumferential indications shall be evaluated for tube plugging based on a 50% depth limit.

IPC
Same.

An IPC repair limit less than the APC repair limit of 2.5 volts is expected to result in a maximum EOC voltage comparable to that obtained in the last cycle following implementation of the 50% depth repair limit. Even for a 2.5 volt repair limit, over 99% of the EOC indications would be less than the 4.0 volt Indication found in the last Inspection. For a 2.3 volt IPC, the maximum EOC voltage would be <4.0 volts and the SLB leak rate would be about 0.0017 gpm per 2.3 volt indication. Therefore about 585 indications per SG could be left in service without exceeding a 1.0 gpm SLB leak rate. Further, an IPC repair limit of 2.3 volts would be approximately equivalent to a 50% depth repair limit with maximum EOC voltages of about 4.0 volts and would limit potential SLB leakage to <1.0 gpm for a bounding estimate (585) of the number of indications per SG to be left in service.

Summary of Conclusions

- Tubes pulled from the Kewaunee tubesheet crevice region in 1990 showed OD-initiated cracking caused by secondary side IGSCC. The degradation was primarily axial with some intergranular characteristics. It was concluded that an alkaline environment was associated with this stress corrosion; a similar environment would be expected at the TSP crevices. Although direct examination of pulled tubes from the Kewaunee TSP intersections has not been performed, the existing tube pull data suggest that caustic induced ODSCC to be the degradation mechanism, similar to TSP degradation observed at other plants. The similarity of the TSP region degradation at Kewaunee to that observed at other plants is also supported by RPC results.

- Recommended correlations of bobbin voltage to burst pressure and to SLB leakage, as well as a correlation for the probability of SLB leakage, are developed in this report. These correlations form the basis for determining repair limits and the corresponding margins for burst and leakage as summarized below.

- At EOC, burst pressure capability (expressed as margin ratios relative to $3\Delta P_{N.O.}$ and ΔP_{SLB}) for an APC is expected to have ratios of about 1.01 relative to $3\Delta P_{N.O.}$ at 90% cumulative probability levels and about 1.69 relative to ΔP_{SLB} at 99% cumulative probability levels. For an IPC, the burst margin ratios increase to 1.16 for $3\Delta P_{N.O.}$ and 1.90 for ΔP_{SLB} at a 1.0 volt IPC.

- Potential SLB leakage at EOC conditions with full APC implementation is expected to be well below the allowable limit of 9.1 gpm for the faulted SG as supported by both Monte Carlo and deterministic evaluations including sensitivity analyses. About 3950 indications at 2.5 volts could be left in service without exceeding the 9.1 gpm allowable leak limit developed to the Standard Review Plan guidelines.

- For an IPC repair limit, the allowable SLB leakage limit of 1.0 gpm is not expected to limit the number of indications potentially left in service. About 3125 indications per steam generator at BOC =1.0 volt or about 585 indications per steam generator at BOC = 2.3 volts would be required to exceed the 1.0 gpm leak limit.

- The maximum EOC bobbin voltage indications resulting from BOC indications are projected to be about 2.47 volts for 1.0 volt indications and up to 4.06 volts for 2.5 volt indications, at 99.7% cumulative probability assuming 300 indications at these voltage levels are left in service. Distributing the 300 indications below these BOC voltages would result in lower EOC maximum voltages.

- At the 1992 inspection, following prior tube repair at a 50% depth repair limit, bobbin voltages up to 4.0 volts were found and confirmed with RPC as ODSCC indications. Bobbin indications up to 2.6 volts were found to have depths <50% or were not confirmed by RPC inspection. Implementation of an IPC with a repair limit of 2.3 volts would result in EOC voltages less than 4.0 volts at 99.9% cumulative probability. Thus an IPC = 2.3 volts does not increase the risk for the most limiting indication above that for a 50% repair limit. As noted above, the 2.3 volt repair limit would not result in potential SLB leakage exceeding the 1.0 gpm limit for a bounding (585 indications) number of indications left in service. Therefore an IPC limit of 2.3 volts provides comparable tube integrity margins to the 50% depth limit, and IPC repair limits <2.3 volts are likely to provide increased margins compared to the 50% depth limit.

- The operating leak rate limit of 150 gpd implemented with the APC satisfies R.G. 1.121 guidelines for leak before break. This limit provides for plant shutdown prior to reaching critical crack lengths for SLB conditions at a lower 95% confidence level on leak rates and for $3\Delta P$ conditions at less than nominal leak rates.

- NDE inspection and analysis guidelines of Appendix A will be applied. This includes a probe wear standard to guide probe replacement and a transfer standard calibrated against the reference laboratory standard. These guidelines provide APC implementation consistent with the development and analyses of this report and with prior NRC-approved IPC applications.

3.0 REGULATORY REQUIREMENTS

3.1 General Design Criteria

The eddy current voltage-based plugging criteria, which establishes a basis for repairing tubes experiencing outside diameter stress corrosion cracking (ODSCC) occurring at tube support plate intersections in the Kewaunee steam generators, have been developed to ensure compliance with the applicable General Design Criteria of Appendix A of Part 50 of Title 10 of the Code of Federal Regulations (10CFR50). The GDCs considered are: 2, 4, 14, 15, 31, and 32 and are summarized below.

GDC 2. Design Basis for Protection Against Natural Phenomena, requires that structures, systems and components important to safety be designed to withstand the effects of earthquakes in combinations with the effects of design basis loadings without loss of safety function.

GDC 4. Environmental and Missile Design Bases, requires that structures, systems, and components important to safety are designed to accommodate the effects of and to be compatible with the environmental conditions associated with normal operation, maintenance, testing, and postulated accident condition loadings, including loss-of-coolant accidents.

GDC 14. Reactor Coolant Pressure Boundary, requires the reactor coolant pressure boundary to be designed, fabricated, erected, and tested so as to have an extremely low probability of abnormal leakage, of rapidly propagating to failure, and of gross rupture.

GDC 15. Reactor Coolant System Design, requires the reactor coolant system and associated auxiliary, control, and protection systems to be designed with sufficient margin to assure the design margins of the reactor coolant pressure boundary are not exceeded during any condition of normal operation, including anticipated operating occurrences.

GDC 31. Fracture Prevention of the Reactor Coolant Pressure Boundary, requires that the reactor coolant pressure boundary shall be designed with sufficient margin to ensure that when stressed under operating, maintenance, testing, and postulated accident condition loadings, the boundary behaves in a nonbrittle manner and the probability of a rapidly propagating fracture is minimized.

GDC 32. Inspection of the Reactor Coolant Pressure Boundary, requires that components that are part of the reactor coolant pressure boundary be designed to permit periodic inspection and testing of critical areas to assess their structural and leaktight integrity.

General Design Criteria 2 and 4 are considered in Section 3.3 below where the potential for steam generator tube collapse during the combined effects of loss of coolant (LOCA) plus safe shutdown earthquake (SSE) loadings are addressed for the Kewaunee steam generators.

3.2 Regulatory Guide 1.121

Background

R.G. 1.121, "Bases for Plugging Degraded PWR Steam Generator Tubes" issued for comment in August of 1976, describes a method acceptable to the NRC staff for meeting GDCs 14, 15, 31, and 32 by reducing the probability and consequences of steam generator tube rupture through determining the limiting safe conditions of degradation of steam generator tubing, beyond which tubes with unacceptable cracking, as established by inservice inspection, should be removed

from service by plugging. The recommended plugging criteria for the tube support plate elevation ODSCC occurring in the Kewaunee steam generators may result in tubes with both partial through-wall and through-wall cracks being returned to service. In the limiting case, the presence of a through-wall crack alone is not reason enough to remove a tube from service. The regulatory basis for leaving through-wall cracks in service in the Kewaunee steam generators is provided below.

Steam generator "tube failure" is defined by the NRC within RG 1.83 as the full penetration of the primary pressure boundary with subsequent leakage. Consistent with this definition, upon the implementation of the tube plugging criteria of this report, known leaking tubes will be removed from service from the Kewaunee steam generators. Steam generator tube bundle leak tightness will be re-established by conducting 100% bobbin coil inspection of the S/G tubes. The tube plugging criteria of this report are established such that operational leakage is not anticipated.

The NRC defines steam generator tube rupture within RG 1.121 as any perforation of the tube pressure boundary accompanied by a flow of fluid either from the primary to secondary side of the steam generator or vice versa, depending on the differential pressure condition. As stated within the regulatory guide, the rupture of a number of single tube wall barriers between primary and secondary fluid has safety consequences only if the resulting fluid flow exceeds an acceptable amount and rate.

Consistent with the philosophy of the NRC's definition of tube rupture, during testimony by the NRC staff (on March 24, 1976) to provide information to the Atomic Safety and Licensing Board (ASLB) on the plans for measures to reasonably assure steam generator tube integrity under operating conditions including off-nominal and accident condition loadings at plants of similar design steam generators, the following definition of loss of steam generator tube integrity was provided. Loss of steam generator tube integrity means loss of "leakage integrity". Loss of "leakage integrity" is defined as the degree of degradation by a through-wall crack penetration of a tube wall membrane that can adversely affect the margin of safety leading to "tube failure", burst, or collapse during normal operation and in the event of postulated accidents. Acceptable service in terms of tube integrity limits the allowable primary to secondary leakage rate during normal operating conditions, and assures that the consequences of postulated accidents would be well within the guidelines of 10CFR100. In order to assure steam generator tube integrity is not reduced below a level acceptable for adequate margins of safety, the NRC staff position focused on specific criteria for limiting conditions of operation. These include:

1. Secondary Water Monitoring
2. Primary-to-Secondary tube leakage
3. Steam Generator Tube Surveillance
4. Steam Generator Tube Plugging Criteria

Tubes with through-wall cracks will maintain "leakage integrity" and are acceptable for continued operation if the extent of cracking can be shown to meet the following RG 1.121 criteria:

1. Tubes are demonstrated to maintain a factor of safety of 3 against failure for bursting under normal operating pressure differential.

2. Tubes are demonstrated to maintain adequate margin against tube failure under postulated accident condition loadings (combined with the effects of SSE loadings) and the loadings required to initiate propagation of the largest longitudinal crack resulting in tube rupture. All

hydrodynamic and flow induced forces are to be considered in the analysis to determine acceptable tube wall penetration of cracking.

3. A primary-to-secondary leakage limit under normal operating conditions is set in the plant technical specifications which is less than the leakage rate determined theoretically or experimentally from the largest single permissible longitudinal crack. This action would ensure orderly plant shutdown and allow sufficient time for remedial action(s) if the crack size increases beyond the permissible limit during service.

The voltage-based plugging criteria for indications at tube support plate elevations discussed in this report are shown to meet all of the necessary acceptance criteria.

3.3 Steam Generator Tube Deformation Discussion

In addressing the combined effects of the LOCA and SSE loadings (as required by GDC 2) on the steam generator component, [

]ª.

This issue has been addressed for the Kewaunee steam generators through the application of leak-before-break principles to the primary loop piping. A detailed leak-before-break analysis has been performed for Kewaunee. Based on the results, it is concluded that the leak-before-break methodology (as permitted by GDC 4) is applicable to the Kewaunee reactor coolant system primary loops and, thus, the probability of breaks in the primary loop piping is sufficiently low that they need not be considered in the structural design basis of the plant. Excluding breaks in the RCS primary loops, the LOCA loads from the large branch lines breaks were also assessed and found to be of insufficient magnitude to result in steam generator tube collapse. Using results from recent tests and analysis programs (discussed more fully in section 11.2), no tubes will undergo permanent deformation where the change in diameter exceeds 0.025 inch. Although specific leakage data is not available, it is assumed that deformations of this magnitude will not lead to significant tube leakage. On this basis no tubes need to be excluded from the alternate plugging criteria (APC) for reasons of deformation resulting from combined LOCA + SSE loading.

4.0 PULLED TUBE CRACK MORPHOLOGY

4.1 Introduction

To support the development of the tube plugging criteria for Kewaunee, this section provides summary information on OD-originated corrosion at support plate crevice regions of Alloy 600 tubing pulled from steam generators at various plants. This section provides results of pulled tube examinations at support plate intersections for other plants. The only support plate crevice region data not discussed are primary water stress corrosion cracking and OD circumferential cracking cracking found in Plant G-1 (circumferential cracking at the TSP are excluded from the application of the APC).

Two tubes were pulled from the tubesheet crevice region of the Kewaunee steam generators in March 1990. These tube sections were examined using non-destructive and destructive methods. This evaluation showed OD initiated cracking caused by secondary side intergranular corrosion (IGSCC). The degradation was predominantly axial with some intergranular characteristics. Analyses of OD deposits from the crevice and crack fracture oxide film showed that the presence of an alkaline environment. This provides the environment associated with the stress corrosion. A similar environment would be expected in the tube support plate crevices. Thus it is reasonable to expect that the degradation at the TSP locations is ODSCC in the presence of an alkaline environment. Although direct examination of pulled tubes from the TSP region has not been performed at Kewaunee, the existing tube pull data suggest that caustic induced ODSCC to be the degradation mechanism, similar to TSP degradation observed at other plants. The similarity of TSP region degradation at Kewaunee to those at other plants is also supported by the RPC results described in Section 12.

The type of intergranular corrosion with regard to crack morphology and density (number, length, depth) of cracks can influence the structural integrity of the tube and the eddy current response of the indications. To support the tube repair criteria, the emphasis in the destructive examination is placed upon characterizing the morphology (SCC, IGA involvement), the number of cracks, and characterization of the largest crack networks with regard to length, depth and remaining ligaments between cracks. These crack details support interpretation of structural parameters such as leak rates and burst pressure, crack length and depth, and of eddy current parameters such as measured voltage, with the goal of enhancing structural and eddy current evaluations of tube degradation. In selective cases, such as the 1990 Plant A-2 pulled tubes, the pulled tube evaluations included leak rate measurements in addition to the more standard burst pressure measurements for further support of the integrity and plugging limit evaluations.

4.2 Definitions

Before the support plate region corrosion degradation can be adequately described, some key corrosion morphology terms must to be defined. Intergranular corrosion morphology can vary from IGA to SCC to combinations of the two. IGA (Intergranular Attack) is defined as a three dimensional corrosion degradation which occurs along grain boundaries. The radial dimension has a relatively constant value when viewed from different axial and circumferential coordinates. IGA can occur in isolated patches or as extensive networks which may encompass the entire circumferential dimension within the concentrating crevice. Figure 4-1 provides a sketch of these IGA morphologies. As defined by Westinghouse, the width of the corrosion should be equal to or greater than the depth of the corrosion for the degradation to be classified as IGA. The growth of IGA is relatively stress independent. IGSCC (Intergranular Stress Corrosion Cracking) is defined as a two-dimensional corrosion degradation of grain boundaries that is

strongly stress dependent. IGSCC is typically observed in the axial-radial plane in steam generator tubing, but can occur in the circumferential-radial plane or in combinations of the two planes. The IGSCC can occur as a single two dimensional crack, or it can occur with branches coming off the main plane. Figure 4-2 provides a sketch of these IGSCC morphologies. Both of the IGSCC variations can occur with minor to major components of IGA. The IGA component can occur simply as an IGA base with SCC protruding through the IGA base or the SCC plane may have a semi-three dimensional characteristic. Figure 4-3 provides a sketch of some of the morphologies possible with combinations of IGSCC and IGA. Based on laboratory corrosion tests, it is believed that the latter, SCC protrusions with significant IGA aspects, grow at rates similar to that of SCC, as opposed to the slower rates usually associated with IGA. When IGSCC and IGA are both present, the IGSCC will penetrate throughwall first and provide the leak path.

To provide a semi-quantitative way of characterizing the amount of IGA associated with a given crack, the depth of the crack is divided by the width of the IGA as measured at the mid-depth of the crack, creating a ratio D/W. Three arbitrary D/W categories were created: minor (D/W greater than 20) (all or most PWSCC would be included in this category if it were being considered in this analysis); moderate (D/W between 3 and 20); and significant (D/W less than 3) where for a given crack with a D/W of 1 or less, the morphology is that of patch IGA.

The density of cracking can vary from one single large crack (usually a macrocrack composed of many microcracks which nucleated along a line that has only a very small width and which then grew together by intergranular corrosion) to hundreds of very short microcracks that may have partially linked together to form dozens of larger macrocracks. Note that in cases where a very high density of cracks are present (usually axial cracks) and where these cracks also have significant IGA components, then the outer surface of the tube (crack origin surface) can form regions with effective three dimensional IGA. Axial deformations of the tube may then cause circumferential openings on the outer surface of the tube within the three dimensional network of IGA; these networks are sometimes mistakenly referred to as circumferential cracks. The axial cracks, however, will still be the deeper and the dominant degradation, as compared to IGA.

Recognizing all of the gradations between IGA and IGSCC can be difficult. In addition to observing patch IGA, cellular IGA/SCC has been recently recognized. In cellular IGA/SCC, the cell walls have IGSCC to IGA characteristics while the interiors of the cells have nondegraded metal. The cells are usually equiaxial and are typically 25 to 50 mils in diameter. The cell walls (with intergranular corrosion) are typically 3 to 10 grains (1 to 4 mils) thick. The thickness and shape of the cell walls do not change substantially with radial depth. Visual examinations or limited combinations of axial and transverse metallography will not readily distinguish cellular IGA/SCC from extensive and closely spaced axial IGSCC with circumferential ledges linking axial microcracks, especially if moderate to significant IGA components exist in association with the cracking. Radial metallography is required to definitively recognize cellular IGA/SCC. Cellular IGA/SCC can cover relatively large regions of a support plate crevice (a large fraction of a tube quadrant within the crevice region). Figure 4-4 shows an example of Plant L cellular IGA/SCC.

A given support plate region can have intergranular corrosion that ranges from IGA through individual IGSCC without IGA components.

4.3 Corrosion Degradation of Plant D Steam Generator Tubes

Fifteen (15) tubes have been pulled from the hot leg region of Plant D steam generators. Three (3) tubes were pulled from Plant D-1 SG-4 in 1983. The first support plate region of each tube was destructively examined. In 1984 five tubes were pulled from Plant D-2 SG-1 and two

tubes were pulled from Plant D-2 SG-4. The first support plate region of each of these tubes was destructively examined. In 1985 five tubes were pulled from Plant D-2 SG-2. The first three support plate regions of each tube were pulled, but only eleven of these fifteen locations were destructively examined. In addition, the fourth and fifth support plate regions of two of these tubes were also pulled. Of these additional four support plate locations, three were destructively examined. Of the 24 support plate regions destructively examined from the three tube pulls, a total of 21 had OD origin intergranular corrosion. The following describes the extent and morphology of the degradation found at these hot leg support plate crevice regions as obtained from a review of the final tube examination reports as well as a review of the raw data obtained during the examinations. Examination of the raw data proved to be important since the final reports summarized the support plate crevice region corrosion in a manner that was potentially misleading from an alternative plugging criteria viewpoint. Note that this was especially true regarding the first two tube pull campaigns where much of the examination activities were directed primarily at obtaining local crevice chemistry information. A description of the corrosion degradation at support plate locations was considered complete once intergranular corrosion was found. (More complete descriptions of the corrosion for the two initial tube pull campaigns were provided at the tubesheet locations, the principal focus of these two examinations.) The third tube pull campaign provided more complete support plate corrosion data since the support plate crevice regions were the principal region of interest and since burst testing of some of the degraded support plate crevice regions was also performed.

Plant D-1, 1983 Examination

The first support plate region from the three pulled hot leg tubes (tube R21-C31, R18-C33, and R17-C33) from Plant D-1 SG-4 were destructively examined. The examinations did not completely characterize the extent of cracking within the crevice regions. Conclusions regarding the extent of cracking were primarily based on one transverse metallographic section through each support plate crevice region. From this data the following was concluded. All three support plate crevice locations had some OD initiated intergranular corrosion. The maximum depths of corrosion were 10, 4, and 2% deep, respectively.

Three axial cracks were found on tube R21-C31 at three separate locations around the circumference within the mid-crevice region on the single circumferential metallographic section made and examined from within the crevice region. Their morphology was that of axial IGSCC with moderate IGA aspects (D/W = 5 for the deepest, 10% deep, crack). Some shallow (< 4% deep) intergranular penetrations, possibly IGA, existed nearby. Figure 4-5 shows photomicrographs of these cracks. An axial section through the crevice region revealed small zones with intergranular corrosion, also up to 10% deep. Figure 4-6 shows photomicrographs of two of the deeper areas.

Up to 4% deep intergranular corrosion on tube R18-C33 was found at two locations on a transverse half-ring section cut from within the mid-crevice region. No axial metallography was performed. The shallow intergranular corrosion had a patch IGA morphology that may have been from the early stages of patch IGA development. Alternatively, the degradation could have been local intergranular penetrations at a location where incipient IGSCC was developing. Deeper corrosion degradation would need to have been found to separate these two possibilities. Figure 4-7 shows photomicrographs made of the deepest observed corrosion.

The 2% deep degradation on tube R17-C33 was found at one location on a longitudinal section cut from within the mid-crevice region of the support plate. No corrosion was found on a transverse half-ring section. Again, it is very difficult to discuss the morphology of such shallow corrosion degradation. It appeared that the morphology was that of five very shallow, close together,

intergranular penetrations, possibly that of incipient axial IGSCC. Figure 4-8 shows photomicrographs of the corrosion.

Plant D-2, 1984 Examination

The first support plate regions from seven hot leg tubes (tubes R19-C55 and R21-C58 from Plant D-2 SG-4 and tubes R16-C38, R16-C53, R15-C44, R16-C40, and R16-C42 from Plant D-2 SG-1) were destructively examined. The extent of the degradation was determined from transverse and longitudinal metallographic sections made within the support plate crevice regions. While this type of examination provided crack depth and morphology information, it did not provide information regarding the lengths of individual cracks (microcracks) or the type and extent of crack networks (macrocracks). The following summarizes the support plate degradation observed from this second Plant D tube pull campaign.

No corrosion degradation was detected within the first support plate crevice region of tube R16-C53 and tube R15-C44 from Plant D2 SG-1. Of the remaining 5 tubes, the first support plate crevice regions had OD initiated, intergranular corrosion with depths that ranged from a maximum of 2% to 30% of the tube wall thickness.

The two tubes from Plant D2 SG-4 had the deepest support plate location corrosion, 30% each. Tube R19-C55 was examined within the crevice region using five nearly complete transverse rings and one axial section. Axial IGSCC existed throughout the support plate crevice region. The deeper cracks had D/W ratios that typically ranged from 7 to 14 with one as low as 3. No surface IGA or IGP was present. Figures 4-9 through 4-12 show selected photomicrographs of the corrosion. The first support plate region of tube R21-C58 was examined using nearly complete transverse metallographic rings, as well as, an axial section. Axial IGSCC was found throughout the crevice region, although the corrosion was more concentrated on one half of the circumference within the crevice region. It was estimated that approximately 30 cracks existed at the mid-crevice region. D/W ratios of 5 to 20 were observed for the deeper cracks. Intermittent areas within the crevice regions had shallow intergranular penetrations on the OD surface. Figures 4-13 through 4-16 show photomicrographs of the corrosion.

Three tubes from Plant D2 SG-1 had support plate location degradation. Tube R16-C38 had up to 20% deep intergranular corrosion at one location in the middle of a crevice The morphology was of axial SCC with significant IGA features, D/W ratios of 2 to 4. Approximately 7 cracks were observed intermittently on a transverse half-ring section cut through the mid-crevice region. Figure 4-17 shows two of the deeper ones. Nothing of significance was observed on the single axial section made through the region. Tube R16-C40 had 10% deep intergranular corrosion at one spot within the mid-crevice location. Its morphology was difficult to determine since the corrosion was shallow and the corroded grain boundaries were tight and difficult to see in the photomicrographs. Tube R16-C42 had the most shallow intergranular corrosion, 2% maximum. The intergranular penetrations had IGA aspects.

Plant D-2, 1985 Examination

Fourteen (14) support plate regions of five tubes (R6-C40, R7-C38, R11-C25, R12-C42, and R18-C77) pulled from the hot leg region of Plant D-2 SG-2 were destructively examined. Burst tests had been performed prior to the destructive examination on tube sections from four of the support plate crevice regions (see Table 4.1). Three of the sections were burst tested without simulated support plate collar while the fourth used a collar which caused the burst to occur away from the degraded support plate crevice region. For the three bursts that occurred in the crevice locations, SEM fractography of the burst fracture faces was performed in addition to the more normal metallography. Finally, bend tests (deformation of the tubing to open cracks

for visual purposes) were performed on selected locations to assist in understanding the overall crack distribution.

Thirteen of the fourteen support plate locations examined had intergranular corrosion, primarily as axial SCC, confined to the crevice region. Maximum depths of degradation ranged from a maximum of 13% to 60%. The degradation was located from near the support plate bottom edge to near the top edge with the degradation being in the form of numerous axial microcracks that were frequently close together. No degradation was observed at or beyond the edges of the crevice. In some instances the microcracks had grown together by intergranular corrosion. The first support plate regions of tubes R7-C38 and R18-C77 were found to have the deepest and highest density of SCC (90 or more individual cracks were found at mid-support plate circumferential planes with maximum SCC depths of 60% and 56%, respectively). Correlations were found between the deepest SCC and the number of cracks found. See Figure 4-18. Only a slight decrease in the maximum crack depth was observed with increasing support plate crevice elevation. See Figure 4-19. The SCC aspect ratios (length of the microcrack divided by its depth) from SEM fractography ranged from 1.3 to 15.5 with the larger ratios associated with the more shallow cracks. The aspect ratio was less than 4 and typically 2 to 4 for crack depths of 50% or greater. See Figure 4-20. It was concluded that any individual SCC was short with a maximum length approaching 0.2 inch as the SCC became deeper. Many of the individual cracks (microcracks) were separated by structurally sound, non-corroded metal, that tore by tensile tearing during burst testing. See Figure 4-21. These ligaments between cracks tended to be on the order of 1 mil in width for the support plate locations with the highest densities of SCC. Figure 4-22 shows an SEM montage of the burst fracture face for the highest crack density found (first support plate region of tube R7-C38). The tensile torn ligaments are denoted by the letter "L" in the figure. For low crack density support plate locations, the ligaments were larger, up to 0.12 inch in width.

With respect to crack morphologies, the following is a summary for the support plate locations which were destructively examined. Tube R6-C40 had corrosion at the third support plate location, maximum depth 19%. (The first support plate location had no corrosion and the second was not examined.) The degradation consisted of two adjacent axial cracks that were found in one of two complete transverse rings made at a mid-crevice region and 0.1 inch below. The morphology was of axial IGSCC with a D/W of 20 (Figure 4-23). No surface IGA was observed.

Tube R7-C38 had corrosion at the first, second, and third support plate locations (each of the crevice regions examined). The maximum depths were 60%, 34%, and 26%, respectively. The morphology was of axial IGSCC at all three locations with the first support plate location having the smaller D/W ratios (i.e, with the larger IGA components associated with the cracking). The first support plate region had 90 axial cracks uniformly distributed around the circumference at a mid-crevice location. No cracks were found at the top and bottom support plate crevice locations. Figure 4-24 shows a photomicrograph of one of the smaller D/W ratio cracks. D/W ratios typically varied from 4 to 9 although isolated ratios of greater than 40 were observed. No IGA was observed at the OD surface. The second support plate crevice region had 42 cracks at a mid-crevice region with most of the cracking located on opposite quadrants of the tube. No cracking occurred at the top and bottom crevice edges. D/W ratios were typically near 15 and no IGA was observed at the OD surface. Figure 4-24 also provides a photomicrograph of degradation located at the second crevice region. The third support plate crevice region had 23 axial cracks located at a mid-crevice region with most of the cracking again located on opposite quadrants of the tube. D/W ratios were typically near 24. Figure 4-25 shows a typical crack. The crack is opened wide due to the high burst pressure experienced by this tube section. Intergranular penetrations, approximately 1% deep, were observed at isolated locations on the OD surface.

The results of destructive examination on tubes R11-C25 and R12-C42 were obtained from the tube pull examination report. Tube R11-C25 had corrosion at the third support plate location. (The first and second were pulled but not examined.) The morphology of the 32% deep corrosion was that of axial IGSCC. It is believed that a moderate number of axial cracks were observed around a mid-crevice location, but only 14 were documented by photography and only three of these were included in the final report with attendant photomicrographs. Figure 4-26 presents this data. The D/W ratio of the major crack is approximately 14 and little or no OD surface IGA is observed. Tube R12-C42 had corrosion at the first, third, and fifth support plate locations. The maximum depths of corrosion were 21%, 21%, and 13%, respectively. The first and third support plate locations had an axial IGSCC morphology while the fifth support plate location degradation was difficult to observe in the single photomicrograph reproduction in the final report. It is believed that moderate to minor numbers of axial cracks were present in these three crevice regions based on the text of the final report, but no mention was made of a measurement of the total number of cracks being obtained from the metallographic mounts. Figure 4-27 includes the single photomicrographs of the corrosion documented for the first and third support plate crevice regions. The D/W ratios were 6 and 9, respectively.

Tube R18-C77 had corrosion at the first, second, third, fourth, and fifth support plate locations. The maximum depths of corrosion were 56%, 53%, 35%, 41%, and 47%, respectively. All locations had an axial IGSCC morphology although some locations (particularly the second and fourth support plate crevice regions) had isolated regions with patch IGA, usually at locations where two or three axial cracks were particularly close together. The depth of the patch IGA was less than, but approaching, half the depth of the penetrating axial cracking. A count of the number of cracks observed around a mid-crevice region was made at the first support plate crevice region. Ninety-two (92) cracks were observed and photographs of 43 were taken. The other four TSP regions did not have a total count performed on the original metallographic mounts; however, photomicrographs taken showed 35, 23, 31 and 16 cracks, respectively, at the second, third, fourth and fifth mid-crevice locations. Figures 4-28 through 4-30 show photomicrographs of typical cracks. D/W ratios were obtained from these figures, as well as from the original data records. The ratios for the deeper cracks typically ranged from 6 to 19, 9 to 13, 11 to 17, 9 to 18, and 11 to 24 for the first, second, third, fourth, and fifth support plate crevice regions, respectively. Other than for the locations with IGA patches, only isolated shallow intergranular penetrations were observed on the OD surface away from the cracking.

Summary of Plant D Pulled Tube Data

The tube examination performed in 1983 on Plant D-1 steam generator tubing removed from support plate crevice locations found the beginning of intergranular stress corrosion. Most of the degradation observed was undeveloped and too shallow to form definitive conclusions regarding the corrosion morphology. While recent eddy current inspection data indicates that support plate crevice region corrosion is active, no further destructive examination data has been obtained. It is likely that the Plant D-1 corrosion observed was developing into axial IGSCC. This is based on the examination results obtained from Plant D-2 tube pulls performed in 1984 and 1985. In these examinations, the corrosion was more developed and it was shown that axial IGSCC typically existed at moderate crack densities with crack lengths of approximately 0.05 to 0.10 inch for the deeper cracks. Many of these microcracks had interconnected by corrosion, to varying degrees, prior to the tube pull. During burst testing, networks of these microcracks, further interconnected to form the burst opening. While individual cracks had a normal (moderate) component of IGA associated with the axial cracking, IGA was not observed, other than at some crevice locations on tube R18-C77.

4.4 Corrosion Degradation of S/G Tubes from Plant A (Units 1 and 2)

Because of the special interest regarding the corrosion degradation of support plate regions from Plant A, the following presents a summary of this data. Data available from yet other plants is presented in Sections 4.5 through 4.9.

4.4.1 Plant A Unit 2 1990 Tube Pull Results at TSP Locations

Hot leg tubes R4-C73 and R21-C22 were pulled from Steam Generator B and hot leg tube R38-C46 was pulled from Steam Generator C. The sections pulled included the first support plate region from each tube. Laboratory NDE, leak and burst testing, and destructive examinations were performed. The following summarizes the data obtained at the first support plate region of each tube.

NDE Testing

Laboratory eddy current testing was performed using 0.720 inch diameter bobbin and RPC probes. RPC results showed a main axial indication within the support plate crevice region of tube R4-C73. The length of the signal was 0.44 inch and the depth was estimated as 77 to 82% deep based on an ASME drilled hole standard. In addition to the main signal, a less intense RPC signal was observed parallel to the main axial signal approximately 20 to 30° away. Tube R21-C22 produced a single axial indication within its first support plate crevice region. The 0.5 inch long RPC signal was estimated to be 76 to 81% deep. Tube R38-C46 had a 90% deep RPC signal that was 0.4 inches long. Note that this tube was elongated during the tube pull. As a consequence of the reduced OD dimension, a 0.69 inch diameter RPC probe was used.

Laboratory bobbin probe examination of tubes R4-C73 and R21-C22 was performed using two 0.720 inch diameter bobbin probes. One was a brand new Echoram probe with very stiff spacers (it was difficult to insert the probe into the tube). The other was a slightly used (in terms of length of tubing previously examined) SFRM Zetec probe in which the spacers were less stiff (probe insertion into the tubes was easy). The probes were pulled mechanically through the tubes at speeds similar to those used in the field; however, unlike the field situation, the tubes were examined with the tubes positioned horizontally. In addition, multiple passes were made with each probe with the specimen being rotated between each pass to vary the position of the crack indication. Table 4.2 presents the results. An indication was observed within both support plate crevice locations. Depth estimates were similar for both of the support plate crevice regions and for both of the probes. A range of 86 to 91% deep covered all depth estimates. For tube R4-C73, the Echoram probe voltage variation ranged from 3.6 to 4.3 volts. For tube R21-C22, the Echoram probe voltage variation ranged from 9.6 to 11.6 volts.

While tube R38-C46 was reduced in diameter during the tube pull, the Zetec 0.72 inch diameter bobbin probe could still be used for the lab exam. However, it passed through the deformed tube with difficulty. Consequently, the estimates of depth and voltage are not assumed to be reliable. The field bobbin test produced a 1.4 volt signal with an indicated depth of 68%, and is considered more reliable than the laboratory result of 4.8 volts and 90% depth. Since the tube pull opened crack networks which were readily visible, the larger laboratory voltage is not surprising.

Leak and Burst Testing

Following NDE characterization, the three tube sections from the first support plate region were leak and burst tested. The leak tests were performed in two parts. The specimens were first tested under simulated normal operating conditions. At a test temperature of 616 °F, the primary side of the specimen was connected by insulated pressure tubing to an autoclave

maintained at a pressure of 2250 psi by bottled nitrogen gas. The specimen was located in a second autoclave maintained at 616 °F and a pressure of 750 psi, resulting in a differential pressure of 1500 psi. The 750 psi pressure in the second autoclave was maintained by a back pressure regulator (BPR) connected to the autoclave by pressure tubing. Any water vapor passing through the BPR was then passed through cooling coils immersed in ice water. The amount of condensed water was measured as a function of time. Following the initial leak testing, a simulated steam line break (SLB) leak test was performed using the same system. For the SLB test, the primary pressure was increased to 3050 psi and the secondary side pressure was decreased to 400 psi resulting in a pressure differential of 2650 psi.

Leak test data are presented in Table 4.3. Results from the SLB test are considered reliable. The measured SLB leak rates were [

]^g and no leakage for tube R38-C46. These values are considerably below the maximum leak rate capability of the system, estimated to be approximately 2 l/hr based on a test with the test specimen removed. Results for the normal operating conditions are considered to be less accurate. The observed leak rate for tube R4-C73 was [

]^g for tube R21-C22. No leakage was observed for tube R38-C46. These rates include any overflows from the back pressure regulator (BPR). Leakage through the BPR was encountered, especially with the testing of tube R21-C22. The BPR may have contributed to the entire amount of leakage observed[1] for the normal operating condition test. While this amount of overflow from the BPR is small in comparison to the SLB test leak rates, it is very large in comparison to potential leak rates from the normal operating conditions test. Consequently, the normal operating condition leak rate at the lower end of potential leak rates for these specimens should be considered zero. The upper value presented, at least for tube R21-C22, probably includes significant contributions from the BPR.

Room temperature burst tests were performed on the two specimens following leak testing. The specimens were pressurized with water at a pressurization rate of approximately 1000 psi/sec. Tygon tubing internal bladders were inserted into the specimens to permit testing with their through wall corrosion cracks. No support plate restraints were placed on the specimens. Consequently, the burst pressures measured may be lower than would be observed in the presence of a support plate.

The first support plate region of tube R4-C73 burst at [   ]^g psi, the first support plate region of tube R21-C22 burst at [   ]^g psi, and the first support plate region of tube R38-C46 burst at [   ]^g psi. Table 4.3 presents this data as well as other burst data characterizing the specimens.

---

1. Prior to initiation of the leak tests, the specimen fittings were tested to verify that they were leak tight. The fittings were tested by pressurizing the specimens with 500 to 600 psi air and holding the specimens and their fittings under water. No fitting leaks were observed. The R4-C73 specimen was observed to leak air bubbles at the location of the support plate at a pressure of 500 psi air. The R21-C22 specimen did not leak air bubbles at a pressure of 600 psi. Consequently, it is believed reasonable that the normal operating leak rate for tube R21-C22 should be lower than that for tube R4-C73. This would also be consistent with the SLB leak test results.

Characterization of the Corrosion Cracks

Figure 4-31 shows a sketch of the SEM fractographic observations on the burst fracture face of the first support plate region of tube R4-C73. Within the center of the burst opening, a 0.42 inch long OD origin macrocrack was observed. The macrocrack was located at an orientation[2] of 20° and was entirely confined to within the support plate crevice region. It had only intergranular corrosion features. The macrocrack was composed of four microcracks, all of which had joined together by intergranular corrosion. The crack was through wall for 0.18 inch. A parallel axial macrocrack was observed near 40°. It was 0.46 inch long and up to 69% through wall. In addition, numerous short axial cracks were observed at various locations within the crevice region. The depth of these short cracks ranged from minor penetrations to 34%. Figure 4-31 also provides a sketch estimating the crack distribution within the support plate crevice region as well as a description of the crack morphology of the main macrocrack. Figure 4-32 provides a sketch of the crack distribution and depth within the center of the support plate crevice region as determined by metallography. The main crack morphology was that of SCC with moderate IGA components (D/W = 4). The width of IGA surrounding the SCC is estimated to be approximately 0.012 inch, except at the OD surface where the width was larger.

Other cracks tended to have less IGA components. Figure 4-33 provides micrographs showing both the main crack morphology as well as the crack morphology of one of the lesser cracks. The morphology of the latter crack, which has been opened wide by tube deformation, is more that of IGSCC (D/W = 12).

Figure 4-34 shows a sketch of the SEM fractographic observations on the burst fracture face of the first support plate region of tube R21-C22. Within the center of the burst opening, a 0.50 inch long OD origin macrocrack was observed. The macrocrack was located at an orientation of 330° and was entirely confined to within the support plate crevice region. The corrosion crack had only intergranular features. The macrocrack was composed of four microcracks. Three of the microcracks were joined by intergranular corrosion, while the top most microcrack was still separated from the others by metal. The macrocrack was through wall for approximately 0.15 inch. Figure 4-33 also provides a description of the crack morphology. The crack morphology was that of SCC with significant IGA components. The width of IGA surrounding the SCC is estimated to be approximately 0.030 inch (D/W = 1.7). One additional crack was later observed on the specimen by metallographic examination. Figure 4-35 provides a sketch of the crack distribution and depth observed by metallography. Figure 4-36 provides micrographs of the cracks. As can be observed, the secondary crack morphology had lesser IGA components (D/W = 19 to 37).

Figure 4-37 shows a sketch of the SEM fractographic observations on the burst fracture face of the first support plate region of tube R38-C46. A 0.37 inch long, OD origin, axial macrocrack was observed. The intergranular crack was up to 78% through wall and was contained within the support plate crevice region. The macrocrack was composed of numerous microcracks which had an unusual spatial distribution. They had orientations which ranged from axial to circumferential generating a spider-like crack distribution. It is believed that this network had a cellular IGA/SCC morphology similar to that on Plant L tube R16-C74 at the first support

---

2. In the orientation system used in Westinghouse tube examinations, 0° faces the steam generator divider plate and 90° is clockwise of 0° when looking in the primary flow (up) direction.

plate region. Three other crevice locations had less deep but significant intergranular crack distributions. Their locations are also shown in Figure 4-37. Figure 4-38 shows the crack distribution and depth as determined by transverse metallographic examinations. Figure 4-39 shows photomicrographs of cracks in transverse sections obtained from within the crevice region. The cracks are opened wide by tube deformation. The morphology of the cracks is that of IGSCC with minor to moderate IGA components (D/W = 14 to 28).

4.4.2   Prior Pulled Tube Examinations from Plant A at TSP Locations

Prior to 1990, a total of 10 hot leg support plate intersection locations on steam generator tubing removed from Plant A-2 were examined. In 1985 the first three hot leg support plate regions of tube R34-C44 from Steam Generator A were destructively examined. In 1986 the first support plate region of tube R31-C46 from the hot leg side of Steam Generator C was destructively examined. In 1989 the first three support plate regions of tubes R16-C50 and R16-C53 from the hot leg side of Steam Generator C were destructively examined. Of these 10 support plate locations, 6 were found to have OD origin intergranular corrosion. In addition, a support plate region of a tube removed in 1989 from Plant A-1 was examined. The support plate region of this tube also had OD origin intergranular corrosion. The following describes the extent and morphology of the degradation found.

Plant A-2, 1985 Examination

The first three support plate regions of hot leg tube R34-C44 from Steam Generator A were destructively examined to determine the origin of residual eddy current signals left at the location of the support plates after frequency mixing to eliminate the support plate signal. No corrosion degradation was found by destructive examination at the three support plate locations.

Plant A-2, 1986 Examination

The first support plate region of hot leg tube R31-C46 from Steam Generator C was destructively examined. A 6.16 volt, 81% deep eddy current signal was detected in the field bobbin probe examination using a 400/100 kHz frequency mix. Renormalization to the standard used in this report yielded 7.2 volts. Destructive examination found a 0.52 inch long macrocrack that extended from 0.1 inch above the support plate bottom edge location to 0.2 inch below the top edge location. The crack averaged 80 to 90% through wall with a local area penetrating 100% through wall for a length of 0.02 inch. The macrocrack was composed of a number (at least 4) of axially orientated microcracks which had grown together by corrosion. The intergranular cracking was of OD origin and a number of shallow cracks existed parallel and nearby to the major macrocrack. The morphology of the cracking was predominantly SCC, but moderate IGA components (D/W = 3.2) were also present. Figure 4-40 shows a sketch of SEM fractographic results of the main crack (only the mid to upper portion of the crack was examined). Figure 4-41 shows a sketch of the overall crack distribution and depth as viewed by metallography as well as a transverse micrograph showing the crack morphology. In addition to the main crack (which included a 46% deep axial crack next to the main crack), two smaller axial cracks were observed at other circumferential positions on the half-circumferential section examined.

Plant A-2, 1985 Examination

Two hot leg steam generator tubes from Plant A-2, Steam Generator C were examined to determine the origin of residual eddy current signals at support plate locations. The destructive

examination included the crevice region at support plates 1-3 of tubes R16-C50 and R16-C53.

All six support plate intersections had residual type eddy current signals. The second support plate region of both tubes was chosen for more detailed examination. Following removal of both ID and OD deposits by honing, abrasion, and later by chemical cleaning, the eddy current examination was repeated. No significant change was observed in the eddy current signals indicating that the residuals were not related to surface deposits.

Destructive examination of tube R16-C50 found OD origin intergranular corrosion within the first and second support plate regions. No corrosion degradation was found within the third support plate crevice region. The first support plate region had only an isolated region of minor OD origin, intergranular, axial SCC. The maximum depth of SCC was 0.007 inch. The second support plate region from tube R16-C50 had experienced some negligible (no wall thickness change measurable) OD general corrosion with some intergranular penetrations. While most of the tube OD cracking within the TSP crevice regions had these features, at one location the intergranular corrosion was somewhat deeper though still regarded as minor. At this location, 0.2 inch below the support plate top edge, the penetrations formed two short parallel axial cracks, 0.06 inch long and up to 0.0015 inch deep. Consequently, all three support plate regions of tube R16-C50 had no, or only very minor, IGSCC degradation. Figure 4-42 shows a micrograph of the largest crack found, that within the first support plate crevice region. The morphology is that of IGSCC with only minor to moderate IGA components.

Destructive examination of tube R16-C53 found OD origin intergranular corrosion within all three support plate regions. The first support plate region of tube R16-C53 had numerous OD origin, intergranular, axial stress corrosion cracks, but the depth of cracking was shallow (0.0055 inch maximum depth). At the second support plate of tube R16-C53, axial intergranular stress corrosion cracking was found on the tube OD concentrated near the support plate top edge and to a lesser extent near the support plate bottom edge. There were dozens of very tight stress corrosion cracks located discontinuously around the circumference, but located within all four quadrants of the tube. The maximum depth of penetration was 0.011 inch (22%). The third support plate region also had numerous but relatively shallow OD origin, intergranular, axial SCC. The maximum depth of degradation was 0.0065 inch. Consequently, the only support plate region of tube R16-C53 with corrosion degradation of any potentially noticeable (by eddy current) depth was the second support plate region where the maximum depth was 0.011 inch (22% through wall). The morphology of these cracks ranged from that of IGSCC (Figure 4-43) to that of IGSCC with significant IGA components (Figure 4-44).

In summary, the 1989 pulled tubes were removed primarily to determine the cause of eddy current support plate residual signals. Laboratory eddy current testing showed that the residual eddy current signals were not caused by surface deposits. Destructive examination also showed that the residual signals were not caused by corrosion degradation, even though minor OD origin SCC was present at five of the six support plate locations. For tube R16-C50 the deepest support plate region SCC was 0.007 inch while for tube R16-C53 the deepest crack was 0.011 inch. For the other support plate locations with cracks, the deepest cracks were 0.0015, 0.0055, and 0.0065 inch.

Plant A-1, 1989 Pulled Tube Examination

The first support plate crevice region of hot leg tube R20-C26 from Steam Generator C of Plant A-1 was destructively examined. Dozens of short, OD origin, intergranular, axial stress corrosion cracks existed within the crevice region and just above the crevice region. Most of

these cracks were found within two 30° wide axial bands on opposite sides of the tube. The band located at 255 to 285° extended from the support plate bottom edge to just above the support plate top edge. The deepest crack in this band penetrated 62% through wall and was located approximately 0.2 inch below the top edge. The second band occurred between 75 and 105° with the cracking extending from the bottom edge to approximately 0.275 inch above the support plate top edge. Within the crevice region, the deepest crack in the second band of cracks occurred near the support plate top edge. This crack was 42% through wall. Above the top edge, the depth of cracking decreased rapidly. At 0.13 inch above the top edge, the deepest crack was 10% through wall. With respect to the length of individual cracks, they were typically much less than 0.1 inch long. Where individual cracks had grown together, cracks up to 0.13 inch long were found. Figure 4-45 sketches the crack distribution found within the first support plate crevice region and also provides crack depth data. Figures 4-46 and 4-47 provide photomicrographs of typical cracks as observed in transverse metallographic sections that have been deformed to open cracks. The morphology is that of IGSCC with minor to moderate IGA components (D/W = 17 to 28). Figure 4-48 shows similar transverse micrographs, but ones in which not all cracks were opened during the tube deformation.

Field eddy current inspection (bobbin probe) of the first support plate region revealed (by initial interpretation) no corrosion degradation. Later analysis suggested a very low voltage (0.2 volts) indication signal, partially hidden between larger voltage dent signals. Laboratory bobbin probe inspection produced similar results, with an indication voltage of 0.4 volts within the overall 7 volt dent signal. The phase angle of the indication component, within the overall dent signal, suggested a 61% deep indication. RPC testing revealed many indications confined to within the crevice region.

4.5 Corrosion Degradation of Plant L Steam Generator Tubes

Eight steam generator tubes from Steam Generators C and D of Plant L were examined by ABB Combustion Engineering. Some of the data in this section is considered preliminary in nature. While no major changes are expected in the reported data, some of the quantitative data may be modified based on further information from tests in progress. The source of these data were data obtained from ABB Combustion Engineering, as well as limited laboratory work performed by Westinghouse on six burst crack samples. The following presents a summary of the relevant information.

4.5.1 Corrosion Degradation of Plant L Tube R12-C8, S/G-D

Tube Support Plate 1 (R12-C8)

Extensive OD origin intergranular corrosion was found within the first support plate crevice region of tube R12-C8. This tube was plugged in 1989 and pulled in 1991. From the destructive examination work performed to date, it is difficult to determine if the dominant morphology was that of numerous short axial cracks with moderate amounts of IGA associated with them or if cellular IGA/SCC was the dominant morphology, at least in certain areas. Additional work (radial metallography) would be required to resolve this question. In the mean time, the following summary will describe the degradation as if it were the former morphology, the more usual for support plate region corrosion. At specific locations where cellular IGA/SCC is believed likely, that possibility will be noted.

Within the first support plate crevice region, high densities of axially oriented IGSCC microcracks were observed. Corrosion was not observed outside of the crevice region. The

microcracks had moderate amounts of IGA associated with them. A description of the microcracks would be that of IGA fingers, with the depth of the cracks typically being 6 to 18 times longer than the width of the IGA associated with the crack. The microcracks were less than 0.05 inch long, in axial extent. The density of support plate region cracking was significantly higher than that observed for most other domestic power plants. For a given elevation, crack densities of three to five hundred individual microcracks could be extrapolated to exist around the circumference based on metallographic and SEM fractography data if the maximum local crack density observed extended completely around the circumference. (For tubes examined by Westinghouse at support plate regions, crack densities of 1 to 24 are more typically observed. The highest, support plate region, crack density previously observed in tube examinations by Westinghouse was 20 to 100 at Plant D-2. It has been reported that high crack densities of approximately 300 cracks over the circumference at a given elevation within a support plate region have also been observed in some European steam generators.) Because of the high densities of cracks and the IGA associated with the cracks, local regions sometimes formed effective patches of IGA. (Alternatively, patch IGA may have formed independently of the IGSCC, possibly after the tube was plugged.) The depth of these IGA patches was typically half that of the maximum depth of cracking penetrating through the IGA patch. The largest circumferential length of continuous IGA observed by metallography was 0.05 inch, or approximately 7 degrees, with a maximum depth of 33%. The maximum depth of IGSCC in the same general region was approximately 85%. Figure 4-49 provides supporting metallographic data.

Another aspect of the very high density of axially orientated microcracks, was the formation of larger axial macrocracks. (Before this aspect can be considered, further details regarding the destructive examination need to be mentioned. The first support plate region of the tube was initially separated circumferentially near the center of the crevice region by applying a tensile force axially to the tube. The fracture would have occurred where the volumetric corrosion degradation was deepest. SEM fractography of the separation showed intergranular corrosion greater than 10% deep over 310 degrees of the circumference. Table 4.4 presents complete depth data for the corrosion front. It is believed that the corrosion front was composed of a large number of axially oriented cracks that frequently had interconnecting IGA components.[3] The deepest region of corrosion was 80 to 92% deep, via IGSCC, over approximately 20 degrees of the circumference.) Above this local region with the deepest corrosion, the tubing was deformed to open any axial crack networks. Many were revealed. One of the deeper looking ones was broken apart and SEM fractography was performed. A fairly uniform crack front was observed from the support plate crevice center to the support plate crevice top. The front ranged from 41 to 55% throughwall, with an average depth of 48%. Several ledges were observed in the fractograph where it is believed that individual, axially oriented, microcracks had joined together to form the macrocrack (Figure 4-50). Below the support plate center, only metallography was performed. Transverse metallography revealed the morphology of the axial cracking and IGA. Figure 4-49 already showed the corrosion revealed approximately 0.1 inches below the circumferential fracture face near the location with the deepest cracking. Both IGA patches and IGSCC with moderate IGA components can be observed. Figure 4-51 shows axial metallography from the bottom edge of the crevice to the center of the crevice region, through a region with corrosion. A fairly uniform corrosion front, approximately 50% throughwall, is observed that is similar to that revealed by SEM fractography above the center of the crevice.

---

3. Alternatively, cellular IGA/SCC may have been present in this region. It would have produced similar SEM fractographic and metallographic (both axial and transverse) results.

From this data it is concluded that axial macrocrack networks existed from the bottom edge of the support plate crevice region to the top edge, with the crack fronts having a fairly uniform depth.

Tube Support Plate 2 (R12-C8)

Metallographic data available from the second support plate crevice region of tube R12-C8 indicated the presence of approximately 50 axial penetrations around the circumference. The morphology of the penetrations was that of narrow IGA fingers. The maximum depth of cracking observed was approximately 48% throughwall. In addition to cracking, patch IGA was also present. ABB (CE) conservatively calculated that the maximum depth of the intermittently distributed, patch type IGA was 27% throughwall. Their conservative definition of IGA (corrosion greater than 5 grains wide on a given crack) produced results that were judged not to be directly relevant to a structural integrity analysis. Their definition of patch-type IGA would include corrosion that would behave as axial cracks rather than as IGA patches that would behave as tubing with either a thinned wall or localized pitting. Consequently, the data was reexamined using a definition of IGA judged more relevant to a structural integrity analysis. IGA was identified where corrosion associated with two or more separate cracks intersected or, alternatively, where the corrosion associated with one crack or area (if no cracking was present) had a D/W (depth-to-width ratio) of one or less.

Using this definition, patch IGA was identified at two locations around the circumference at one elevation within the crevice region and at four locations at a second crevice elevation. All patch IGA, that was 10% or more deep, was associated with isolated regions that were very small in circumferential extent. The maximum depths and their corresponding circumferential extents were 11% deep and 1 degree in width for the first elevation and 12% deep and 1 degree in width for the second elevation. The widest IGA patch was 21 degrees (6% of the circumference) with a maximum depth of 6%. For the examined elevations, the largest total circumferential involvement (summation of the widths of the IGA patches) was 22 degrees (6% of the circumference).

From a structural integrity viewpoint, since the IGA patches in the crevice region were isolated from each other and few in number, it is believed that the IGA patches act more like a limited number of pits rather than tubing which has experienced general thinning.

Tube Support Plate 3 (R12-C8)

After burst testing of the third support plate crevice region (burst occurred at 10,500 psi), visual examination revealed numerous, axially oriented, corrosion openings adjacent to the main burst opening. Most of the corrosion appeared to be shallow. SEM fractography performed on the burst opening showed intergranular corrosion existing from the bottom to the top edge of the crevice region. Large ledges were frequently observed between axially orientated microcracks.

Transverse metallography showed approximately 85 axial cracks around the circumference with a morphology of axial IGSCC with moderate IGA aspects. The maximum depth of corrosion was 55%. In addition to cracking, patch IGA was also present. ABB (CE) conservatively calculated that the maximum depth of the intermittently distributed, patch type IGA was 33% throughwall. Again, the data was reexamined using the definition of IGA judged to be more relevant to a structural integrity analysis. Patch IGA was identified at seven locations around the circumference at a mid-support plate crevice region elevation. All patch IGA, that was 10% or more deep, was associated with isolated regions that were very small in circumferential extent. The maximum depths and their corresponding circumferential extents were 21% deep and 0.5

degree in width, 10% deep and 0.3 degree wide, 14% deep and 0.3 degree wide, 14% deep and 0.8 degree wide and 17% and 6 degrees wide. In addition, a number of metallographic grinds were made at the location of the 17% deep and 6 degree wide IGA patch. Patch IGA was found in two of the three grinds at this location. These IGA patches were 10% deep and 2 degrees wide and 8% deep and 1.5 degrees wide. For the mid-crevice region elevation, the total circumferential involvement (summation of the widths of the IGA patches) was 10 degrees (3% of the circumference).

From a structural integrity viewpoint, since the IGA patches in the crevice region were isolated from each other and few in number, it is believed that the IGA patches act more like a limited number of pits rather than tubing which has experienced general thinning.

4.5.2 Corrosion Degradation on Tube R29-C70, S/G-C

Preliminary destructive examination of the first, second, and third support plate regions of tube R29-C70 has produced the following results. All three regions had similar corrosion degradation. Axially oriented IGSCC with only minor to moderate IGA components was present without effective surface IGA (intermittent, minor surface IGA, 1 to 2 grains deep, was occasionally present). The absence of effective surface IGA is in contrast to the results for tube R12-C8. At a mid-support plate elevation, 2-3, 5, and 4 cracks were found distributed around the circumference for the first, second, and third support plate regions, respectively. The presence of such a small number of cracks is typical of support plate cracking at many power plants and is in great contrast to the results for tube R12-C8 from Plant L. The burst strengths for the three regions were 10,400 psi, 9,000 psi, and 10,400 psi, respectively. SEM fractography of the burst faces showed IGSCC macrocracks, confined to the crevice regions, that were 0.29, 0.68, and 0.45 inch long, respectively.[4] These macrocracks were composed of microcracks that were separated by ligaments with dimple rupture features. The numbers of such microcracks were 1, 12, and 6, respectively, for the first, second, and third support plate crevice regions.[5] The maximum spacing between microcrack ledges with tensile overload features was 0.29, 0.26, and 0.14 inches, respectively. The maximum depth of IGSCC observed was 56%, 76%, and 71%, respectively.

4.5.3 Corrosion Degradation on Tube R30-C64, S/G-C

Preliminary destructive examination of the first, second, and third support plate regions of tube R30-C64 has produced the following results. All three regions had similar corrosion degradation. Axially oriented IGSCC with only minor to moderate IGA components was present without effective surface IGA (intermittent, minor surface IGA, 1 to 2 grains deep, was occasionally present). The absence of effective surface IGA is again in contrast to the results for tube R12-C8 and is similar to the results for tube R29-C70. At a mid-support plate elevation, 29, 85 and 30 cracks were found distributed around the circumference at the first, second, and third support plate regions, respectively. The presence of this moderate number of cracks is also typical of support plate cracking at many power plants and is in contrast to the results for

---

4. Note that the macrocrack dimensions were independently measured by both ABB (CE) and Westinghouse. When the results differed, the more conservative value was chosen.

5. Other ligaments or ledges with intergranular features were also present. In the case of the first support plate region, even though only predominantly intergranular ligaments were observed (i.e., one microcrack = one macrocrack), three microcracks were effectively present due to the profile of the scallop-shaped crack front.

tube R12-C8 from Plant L, at least for the first support plate region. The burst strengths for the three regions were 10,500 psi, 8,800 psi, and 10,200 psi, respectively. SEM fractography of the burst faces showed IGSCC macrocracks, confined to the crevice regions, that were 0.74 (0.53),[6] 0.61, and 0.45 inch long, respectively. In the case of the first support plate region, even though predominantly intergranular features were observed on ligaments, i.e., one macrocrack and one microcrack. Three macrocracks were effectively present due to the profile of the scallop-shaped crack front. These macrocracks were composed of microcracks that were separated by ligaments with dimple rupture features. The numbers of such microcracks were 12, 8, and 6, respectively for the first, second, and third support plate crevice regions. [7] The maximum spacing between microcrack ledges with tensile overload features was 0.175, 0.28, and 0.12 inches, respectively. The maximum depth of IGSCC observed was 55%, 65%, and 50%,[8] respectively.

4.5.4 Corrosion Degradation on Tubes R16-C74, R20-C66 and R8-C66 from S/G-D and Tubes R8-C69 and R12-C70 from S/G-C

The first, second and third support plate regions of each of these tubes (except for the second support plate region of tube R12-C70) have been burst tested and SEM fractography has been performed on the axially oriented burst fracture faces. All crevice regions had predominantly axial IGSCC. In addition, nine of the fifteen support plate crevice regions may have had local areas within the crevice region with some cellular IGA/SCC. Table 4.5 (which includes summary corrosion morphology data from many plants) provides further details. The probability of cellular IGA/SCC existing is indicated by the choice of the adjectives definitely, probably, and possibly. The single definite observation is based on radial metallography. The other observations are based on visual observations and standard transverse and longitudinal metallography. Table 4.5 also provides details of the crack densities of these 15 crevice regions from Plant L (all had moderate to low crack densities), as well as details of the extent of IGA associated with the major cracks (most had only minor IGA components) and the extent of OD IGA (only three of the fifteen crevices had IGA, all in the form of a few isolated IGA patches). The lengths and depths of the burst fractures faces and the burst pressures are provided in Table 4.6.

Further, details are presented for the first support plate crevice region on tube R16-C74 where cellular IGA/SCC was confirmed by radial metallography. SEM fractography on the burst opening found numerous axially oriented, OD region, intergranular microcracks, up to 70% deep. Ignoring shallow and isolated cracks near the support plate edges, the main macrocrack was 0.56 inches long and averaged 58% deep. Transverse metallography through the center of the crevice revealed 31 axially oriented intergranular cracks, with minor IGA components. The maximum local depth of cracking was approximately 40%. Negligible uniform IGA (typically 1 to 2 grains deep) was found on most of the OD (and ID) surface. Several small patches of IGA (maximum depth of 19%) were also observed.

---

6. ABB reported that the crack length was greatly increased by the burst test and that a corrected length would be 0.53 inch.

7. Other ligaments or ledges with intergranular features were also present.

8. Note that the macrocrack dimensions were independently measured by both ABB (CE) and Westinghouse. When the results differed, the more conservative value was chosen.

Axial metallography revealed what looked like patch IGA that was up to 52% deep, that was confined to the lower central region of the support plate crevice. (This corrosion was later shown to be cellular IGA/SCC.) In the region near this zone where visual observations revealed a complex mixture of axial and circumferential cracking, in one quadrant of the crevice, radial metallography was performed on a 0.5 x 0.5 inch section of tubing that had been flattened. Cellular IGA/SCC was found on one third of the section. Figures 4-52 and 4-53 show the radial metallography obtained at various radial depths. Later grinding operations performed on this radial section showed that only axial cracks existed at a depth of approximately 70%. At present, it is believed that the cellular IGA/SCC was mostly contained in this region and probably was not the dominant morphology at the burst fracture. This data is highlighted since similar corrosion morphologies may exist at the first support plate region of tube R12-C8.

Summary of Plant L Degradation

All three support plate regions of Plant L plugged tube R12-C8 had multiple axial IGSCC macrocrack networks from the bottom to the top edge of the crevice. The first support plate region had the deepest cracking, 92% through wall. For the second and third support plate regions, the maximum crack depths were 48 and 55%, respectively. In addition, effective IGA patches were observed. In the case of the first support plate crevice location, the IGA patches occurred in regions with the highest crack densities. The depths of the IGA patches were typically half that of the associated axial cracking. For the second and third support plate regions, limited data was directly available regarding the IGA patches, but it was reported by CE that the maximum depths of IGA for these two support plate regions were 27% and 33%, respectively. The twenty-one support plate regions from the other seven pulled Plant L tubes had corrosion more typical of other plants: a small to moderate number of axial IGSCC, minor to moderate IGA components to the cracking, and little or no separate IGA (patch IGA). While the IGSCC on these tubes had IGA components, the appearance was more that of stress corrosion cracking than that of IGA fingers as was observed at the first support plate region of tube R12-C8. Finally, cellular IGA/SCC was locally observed at the first support plate crevice region of tube R16-C74. Cellular IGA/SCC may have also been present, and even played a major roll, in the corrosion degradation at the first support plate region of tube R12-C8. Non-confirmed cellular IGA/SCC was also suspected in local areas of the crevice regions of another eight of the total 24 crevice regions examined.

4.6 Cellular IGA/SCC at Plant E-4

Steam generator tubes at support plate crevice regions in the European Plant E-4 have developed cellular IGA/SCC. The cellular IGA/SCC is localized in the crevice region such that most of the crevice region is free of corrosion. The seventh page of Table 4.5 presents summary corrosion morphology data available from five crevice regions. The crevice regions had moderate crack densities, moderate IGA components associated with individual major cracks, and no significant IGA independent cracking. Burst tests conducted produced the expected axial opening through complex mixtures of axial, circumferential and oblique cracks. For the more affected areas, while the cracking remained multi-directional, there was a predominance of axial cracking. Figures 4-54 and 4-55 provide radial section photomicrographs through two of the more strongly affected areas showing cellular IGA/SCC at Plant E-4.

4.7 Corrosion Degradation in Plant B-1, Support Plate 5

A description of the corrosion found at TSP 5 of Plant B-1 is provided in the following section. This region is singled-out for two reasons. First of all, it has through wall corrosion. Secondly, the tube had a small region believed to have cellular IGA/SCC.

OD origin, axially oriented, intergranular stress corrosion cracks were observed confined entirely within the fifth support plate crevice region on the hot leg side of tube R4-C61 from Steam Generator C of Plant B-1. Six axial macrocracks were observed around the circumference. The largest of these was examined by SEM fractography without any metallography. The macrocrack was 0.4 inch long and through wall for 0.01 inch. However, the crack was nearly (effectively) through wall for 0.1 inch. The macrocrack was composed of seven individual microcracks that had mostly grown together by intergranular corrosion (the separating ledges had intergranular features that ranged from 40 to 90% of the length of the ledges). Since no metallography was performed on the axial cracks, it is not possible to definitively describe the axial crack morphology at this location. At the eighth support plate region of the same tube, metallography showed that the morphology was that of SCC with a crack depth to IGA width ratio (D/W) of 15. Figure 4-56 summarizes the crack distribution and morphology data for the fifth support plate crevice region.

In addition to the OD origin axial macrocracks observed at the fifth support plate region, one location adjacent to the burst crack had five intergranular circumferential cracks. The maximum penetration observed for the circumferential cracking was 46% through wall. The morphology of the circumferential cracking was more that of IGA patches than of SCC. In addition to the 5 main circumferential cracks, the region had numerous smaller cracks aligned in both the axial and circumferential directions providing a crazed appearance. See Figure 4-57. This crazed degradation is now recognized as probably being cellular IGA/SCC. Previously the crazed pattern was thought to represent only shallow IGA type degradation that completely disappeared a short distance below the surface. Figure 4-58 provides micrographs of relevant cracks showing the morphology of axial and circumferential cracks. As stated above, the axial cracks had a morphology of IGSCC with a moderate D/W ratio of 15 while the circumferential cracking had a morphology more like that of IGA, with a D/W ratio of 1.

Field eddy current bobbin probe inspection (in June 1989, just prior to the tube pull) of the fifth support plate crevice region produced a 1.9 volt, 74% deep indication in the 550/100 kHz differential mix.

4.8 Corrosion Degradation of S/G Tubes from Plant P

Two tubes were removed from Plant P in 1991 and were examined for degradation at the tube support plate locations. This work was performed by ABB Combustion Engineering, and a summary of the reported results has been provided below.

4.8.1 Plant P 1991 Tube Pull Results at TSP Locations

Hot leg tubes R11-C48 and R16-C60 were pulled from an unidentified steam generator. In each case, the sections pulled included the first, second, and third tube support plate intersections and the tubesheet expansion transition. Pull forces were 800 lbs. or less during the removal of the tube sections containing the TSP intersections. Laboratory NDE, leak and burst testing, and destructive examinations were performed. The following summarizes the data obtained at each support plate region of the tubes.

NDE Testing

Laboratory eddy current testing was performed using an A740SF/RM bobbin coil probe. Test frequencies were 400 kHz, 200 kHz, 100 kHz, and 10 kHz in differential and absolute modes. The probe speed was 12 in/sec. This probe was calibrated to provide a 4 volt response to a 20% ASME flaw at 400 kHz. The RPC probes were B 720 3 Coil MRPC, calibrated to a 5 volt response to 60% ASME flaws at 400kHz. The RPC probe speed was 0.2 in/sec. Depths were calculated using a 3 point fit curve at 400 kHz. Testing was performed with and without a carbon steel collar utilized to simulate the tube support plate. The effect of the pull forces in potentially opening up cracks was not reported. The relatively low pull forces would indicate that this effect was negligible, but, as reported later in this section, the tube pull was reported to have affected the UT testing. The reported bobbin coil voltages, angular extent, and estimated depths are shown in Table 4.7a, and similar data for RPC are shown in Table 4.7b.

The bobbin coil indicated a very shallow indication (6%) at the second TSP of R16C60 but the MRPC did not suggest the presence of degradation at this location. No comparison of laboratory and field eddy current measurements was included.

Ultrasonic testing was also performed of the samples. UT signals were noisy, as some of the deformation incurred during the tube removal process apparently hampered correct centering of the probe in the tube. Characterization and sizing of defects could not be done accurately. Indications were reported up to 0.2 in. length and 26% deep on R11C48 at the first tube support plate intersection. On R16C60, small crack-like indications 0.1 in. length and 24% and 22% deep were reported at the first and third TSP intersections, respectively.

Radiography did not produce any observable indications.

Visual observation of the tube sections was performed with the unaided eye and with a stereomicroscope with magnifications of up to 40X. Relatively heavy deposits were reported, and metallic copper was observed in the deposits at the TSP locations. At no locations were there any indications visible.

The inside diameter of each tube section was measured using a three point intra-micrometer. As expected from the NDE data, no denting was observed by these measurements.

Leak and Burst Testing

Following NDE characterization, three tube support plate intersections were leak and burst tested. These included :

• R16C60 TSP #1, which laboratory ECT indicated had an 18% throughwall crack.

• R16C60 TSP #2, which laboratory ECT indicated had a 6% throughwall crack.

• R11C48 TSP #1, which laboratory ECT indicated had a 37% throughwall crack.

Burst testing was performed by sealing each end of the tube with mechanical fittings, the upper one of which was connected to 1/8-inch high pressure tubing to permit pressurization of the sample. Some of the fittings leaked initially and were sealed by silver soldering. The pressurizing equipment included:

a.) a hand pump to pump deionized water to pressurize the specimens
b.) a calibrated pressure gage
c.) a pressure transducer connected to a strip chart recorder
d.) 1/8-inch high pressure tubing
e.) a 3000 psi accumulator with valve.

The tests were initially conducted without an internal bladder to determine at what pressure leakage occurred. If a burst was not obtained, the test was interrupted, a bladder was inserted, and the test resumed until a burst, as indicated by a "fish mouth" opening, occurred. A bladder was required in only one case. All failures were axially oriented.

Tube R11C48 TSP #1 was burst test with a thick carbon steel collar to simulate support by the tube support plate. This technique was not employed in the remaining two TSP burst tests, as the presence of the collar provided support to the tube in the area with degradation that bursting occurred in the non-degraded portion of the tube, at 11,500 psig. Tube section R16C60 TSP #1 was prepared for burst testing without using the carbon steel support ring. No fitting leaks were observed, and this section exhibited a final burst pressure of 9,350 psig. Tube section R16C60 TSP#2 was also burst without the use of the carbon steel collar. This section burst at a pressure of 10,200 psig.

Characterization of the Corrosion Cracks

Cracks were examined by a number of techniques including light microscopy, fractography and are reported in this section. Auger emission spectroscopy/X-ray photoelectron spectroscopy of the cracks, base metal characterization, and chemical analysis of tube surface deposits were also performed, but have not been reported here, since they do not directly bear upon crack morphology.

Areas in which indications were observed by NDE or visual examination were examined by cross-sectional metallography to characterize the type and extent of corrosion and to determine crack morphology. The areas containing the crack were cut so that longitudinal and transverse sections could be prepared. The samples were mounted, polished, etched, and examined using conventional metallographic techniques. A dual etching process was performed on longitudinal sections using electrolytic nital and ortho-phosphoric acid. Glyceregia and nital were used as etchants on the transverse sections.

For the burst samples (R16C60 TSP #1 and R16C60 TSP#2), three transverse samples were cut from the upper, mid-plane and lower portion of the "fishmouth" of the burst. For R11C48 TSP #1, three transverse samples were cut from the upper, mid-plane and lower portion of the tube support plate intersection. The sections of tube from the third TSP intersection, R16C60 TSP #3 and R11C48 TSP #3, were examined at the mid-section of the intersection only. No light metallography data were reported for R11C48 TSP #2.

Longitudinal sections were prepared of all six tube support plate intersections with the exception of R11C48 TSP#2.

All mounts were prepared following ASTM procedures. Photomontages of all mid-plane TSP regions as well as top of TSP and bottom of TSP regions for selected tubes were constructed from the burst test transverse sections. Depth of penetration measurements around the circumference of the mid-TSP mounts were taken for each crack directly from the transverse

photomontages for which the magnifications were known. Each crack was identified, and its depth determined with a filar eyepiece. The mean crack depth was calculated and reported. The tube circumference was divided into ten-degree sectors and the maximum penetration within each sector was plotted as a function of angular position.

Tube R16C60 TSP #1

Figure 4-59 is a transverse view of axial cracks near the top of the tube support plate region of the tube. Glyceregia was utilized as an etchant to enhance any potential IGA. After etching the transverse mount, there were only small patches of shallow intergranular attack (IGA) observed in isolated areas along the tube OD. The indications of IGA were between one and four grains deep. Many large OD-initiated indications of intergranular stress corrosion cracking (IGSCC) were present along the entire circumference of the sample. The glyceregia etchant was not used on the remaining transverse sections cut from this tube, since negligible IGA appeared.

From the photomontages for this sample, 160 distinct crack-like indications were reported along the circumference of the sample. The average crack depth was 33% and the maximum depth 53%. The crack depth information for this and all other tube support plate intersections is shown in Table 4.8.

A transverse view of axial cracks at the mid-plane of the tube support plate region is shown in Figure 4-60. This metallographic mount was etched using electrolytic nital. Several cases of IGSCC were observed in the mid-plane region, as can be seen in the 200X photographs. Refer to Table 4.8 for crack depth information.

Figure 4-61 illustrates the maximum penetration (reported as percent throughwall) at ten-degree increments of the circumference for the mid-TSP section as a function of angular position.

A third transverse metallographic mount was prepared from the bottom of the TSP region. This mount was also etched in electrolytic nital, but did not show significant degradation as seen in the upper and mid-plane regions of the TSP. There were no cases of crack-like indications found on this mount. Figure 4-62 includes both high (200X) and low (50X) magnification views of this transverse section.

Tube R16C60 TSP #2

Transverse tube sections were cut from R16C60 TSP #2 at the top, mid-plane and bottom of the tube support plate region of the tube section. In the top of the support plate region, there was a small number of cracks visible at 200X magnification. Figure 4-63 shows photomicrographs at 50X and 200X which show the appearance of the transverse section cut from the top of the TSP region, etched with nital.

Figure 4-64 show the mid-plane transverse TSP section of the tube after a glyceregia etch. Several large indications of IGSCC were found along with small patches of shallow IGA, as seen in the 200X photographs.

Figure 4-65 shows the maximum penetration (reported as percent throughwall) at ten-degree increments of the circumference for the mid-TSP region as a function of angular position. This figure illustrates the burst location.

A third transverse metallographic mount was prepared from the bottom of the TSP region. This mount was also etched with electrolytic nital. There was no evidence of cracking in the transverse sample taken from the bottom of the tube support plate.

Tube R16C60 TSP #3

Minor cracking (less than 20% depth) was observed at in the transverse section at the mid-plane of this intersection. No photomicrographs are presented.

Tube R11C48 TSP #1

After bursting of this specimen with the carbon steel collar in place, the carbon steel support ring was removed from the TSP region. Three transverse mounts were prepared from the tube support plate region of the sample. The top of the support plate region showed only minor degradation due to cracking, as shown in Figure 4-66.

The mid-plane section of this sample showed the greatest extent of IGSCC. Several micrographs of typical examples of cracks found on the OD of this tube are shown in Figure 4-67. Crack depth is again shown in Table 4.8.

The transverse tube section cut from the bottom of the TSP section, like the top of the TSP section, showed minor degradation due to IGSCC. Some examples of cracks are presented in Figure 4-68.

Tube R11C48 TSP #3

Minor cracking (less than 20% depth) was observed at in the transverse section at the mid-plane of this intersection. No photomicrographs are presented.

Fractography

Upon completion of burst testing, a section was removed from two of the TSP intersection burst test specimens (R16C60 TSP #2 and R16C60 TSP #1) for analysis by scanning electron microscope (SEM). Section R11C48 TSP#1 was not examined using SEM since the high burst pressure and location of tube rupture indicated the tube experienced ductile failure. SEM surface examinations were supplemented with energy dispersive spectrometry (EDS) to determine if any contaminants were present on the crack surface. All fractography was performed on one of two axial burst crack faces. SEM/EDS was performed on two TSP region sections which had not been subjected to burst testing.

Selected areas were examined in detail to determine crack morphology, followed by documentation with photomicrographs at 30X or 40X. SEM montages were prepared and compared to the low magnification photographs where the tube support plate location was clearly observable. Identifiable patterns on both the high and low magnification photographs were used to obtain length ratios between the high and low magnification photographs. These ratios were used to compare the crack length to the TSP width and the position of the crack relative to the top of the TSP. With this method, it was also possible to correct the burst crack lengths to the pre-deformation lengths. The method further indicated that the burst cracks for samples R16C60 TSP #2 and R16C60 TSP #1 were contained within the axial extent (thickness) of the tube support plate. No cracking extended beyond the TSP regions in these two samples.

R16C60 TSP #1

A 40X photomontage of the tube section at this intersection was prepared. Table 4.9 illustrates the data from the SEM montages. There were no obvious areas of fatigue, transgranular cracks, etc. There were approximately sixteen ligament-like features present on the fracture surface, oriented in the radial direction. These ligaments represent the material connecting the tips of adjacent and overlapping cracks. Most of the ligaments appeared to have failed in a ductile mode when the sample was burst.

R16C60 TSP #2

A 40X photomontage of this fracture surface was constructed to study the extent of tube degradation at the fracture surface. EDS analysis of this sample showed silicon, which was hypothesized to be contamination from the cutting wheel used to section the tube, and alloy materials. Minor indications of magnesium were also identified on the fracture surface. EDS analysis of the OD deposits identified iron, nickel, chromium, calcium, titanium, lead, aluminum, and potassium. Table 4.10 presents the crack depth and ligament data from the SEM montage.

Summary of Plant P Exam Results

The destructive examination of two tubes from Plant P having various EC indications confirmed the presence of primarily axially-oriented OD-initiated stress corrosion cracks. The cracks were confined to the tube support locations and did not extend beyond the upper and lower boundaries of the tube support plates. The cracks were generally short (<0.2 inch) and were separated by thin ligaments of non-corroded material that provided some structural support. There were no indications of transgranular cracking nor were there any indications of a failure type crack extension during service at any location.

4.9 Summary of Tube Support Plate Region Corrosion Observations

To compare support plate corrosion morphology of the plants described, three ways of data characterization were utilized. All three need to be considered to characterize the corrosion. The first measures cracking density. Since most cracking within support plates is axial in nature, cracking density is usually measured from a transverse metallographic section. If a complete section is available, the cracking density at the given elevation can be directly measured. If only a partial section is available, an estimate by extrapolation can be made. Cracking densities were arbitrarily divided into three density categories: low (1 to 24 cracks); moderate (25 to 100 cracks); and high (greater than 100 cracks). Note that since most axial cracking is composed of short microcracks, usually less than 0.05 inches long, a cracking density of say 25 at a given elevation would correspond to several hundred microcracks within a support plate region. The second way of characterizing the data involved measuring the amount of IGA associated with a given crack. To do this the depth of the crack was divided by the width of the IGA as measured at the mid-depth of the crack, creating a ratio D/W. Again, three arbitrary D/W categories were created: minor (D/W > 20) (all or most PWSCC would be included in this category if it were being considered in this analysis); moderate (D/W 3 to 20); and significant (D/W < 3) where for a given crack with a D/W of 1 or less, the morphology approaches that of patch IGA. The third way of characterizing the data involved considering the extent of IGA present on the the tube, but only the IGA not obviously associated with a single crack was considered. Consequently, IGA independent of cracking is measured and IGA associated with the interaction of more than one crack is measured. The measurement of IGA arbitrarily divided the

circumferential extent of IGA into three categories: negligible (IGA < 5% deep); moderate (IGA 5% to 10% deep); and significant (IGA greater than 10% deep).

Table 4.5 presents a corrosion morphology comparison of support plate region data for plants examined by Westinghouse, and data from laboratory corrosion tests conducted in model boilers. Most plants exhibit only moderate IGA components in association with the axial IGSCC. Significant IGA (greater than 10% through wall) was observed (i.e., excluding isolated IGA patches) only at Plant L (tube R12-C8 only) and Plant M-2. It is believed in the case of Plant L that the formation of IGA in the form of IGA patches is a result of the high cracking densities and IGA aspects associated with the individual cracks. Where the cracks are particularly close together, IGA patches form at the base of the cracks where the width of the IGA is greatest. In the case of Plant M-2, the typical IGA morphology was that of uniform IGA as is shown in the lower two photomicrographs in Figure 4-69. The top photomicrograph in Figure 4-69 also shows uniform IGA but with some axial IGSCC appearing through the uniform IGA.

While not examined by Westinghouse, the following presents data regarding Plant J-1 and Plant N-1. Figure 4-70 shows photomicrographs from the second support plate region of tube R8-C74 of steam generator 2 of European Plant J-1, evidencing extensive intergranular corrosion. Table 4.5 presents qualitative morphological data. The extent of IGA associated with individual cracks has moderate D/W ratios, the extent and depth of IGA is comparable to some domestic units and the origin of the IGA also appears to be that of closely spaced axial IGSCC interacting near the surface to form local IGA patches. It is also interesting that the maximum depth of IGA compared to the depth of IGSCC is similar, typically one-third to one-half of the IGSCC depth. The data from the support plate regions at Plant N-1 was not in a form where firm conclusions regarding corrosion morphology could be made. Table 4.5 presents an attempt to develop conclusions from the available data.

Table 4.1   Burst Test Data from Plant D-2, 1985 Pulled Tubes

Specimen	Burst Pressure (psi)	Burst Δd (%)	Burst Length/Width (inches/inches)	Post-Test Examination
R7C38-4B* 1st S.P.	g	9.0	0.770/0.054	All cracks confined to S.P. region. Intergranular portion of burst crack composed of 12 separate cracks with 11 ligaments; maximum distance between ligaments = 0.17"; typical ligament thickness ~1 mil; total length of macro-crack = 0.74"; maximum depth SCC = 59%; average depth SCC = 40%. Metallography shows ~90 axial SCC's in a given transverse plane, uniformly distributed around the circumference, with many ~50% deep. All SCC confined to S.P. crevice.
R7C38-7A 2nd S.P.		11.4	0.684/0.094	All cracks confined to S.P. region. Intergranular portion of burst crack composed of 13 separate cracks with 12 ligaments; typical ligament thickness ~1 mil; maximum distance between ligaments = 0.15"; total length of macro-crack = 0.65"; maximum depth SCC = 31%; average depth SCC = 23%. Metallography shows ~40 axial SCC's in a given transverse plane, confined to 2 areas, effectively occupying half the circumference, with many cracks ~30% deep. All SCC confined to S.P. crevice.
R7C38-9B 3rd S.P.		23.0	1.071/0.184	Burst crack tips extend ~0.2" beyond S.P. edges; all other cracks confined to S.P. region. Intergranular portion of burst crack is also confined to S.P. region and is composed of 17 separate cracks with 16 ligaments including two very large ligaments (one is 0.12" thick); maximum distance between ligaments = 0.125"; total length at macro-crack = 0.710 inches; max. depth SCC = 16%; average depth SCC = 8%. Metallography shows ~20 axial SCC's in a given plane, confined to 3 areas effectively occupying a third of the circumference, with many cracks ~25% deep. All SCC confined to S.P. crevice.
R11C25-9B 3rd S.P. (S.P. collar used)		25.1	1.624/0.190	Burst was not associated with S.P. location. Tubing uniform expansion has tubing in intimate contact with S.P. collar (16.7 mil gap). Metallography shows SCC in 2/4 of the quadrants with a maximum depth of 30%.

---

* A tensile test of R7C38 showed the 0.878 inch OD, 0.052 inch wall tube had a yield strength of 50.7 KSI and an ultimate tensile strength of 99.3 KSI.

** SCC depth as corrected for wall thinning during the burst test.

Table 4.2

Laboratory Eddy Current Data for Tubes Removed from Plant A-2

Results at Bottom TSP Location for All Tubes

Examination	Tube R4-C73	Tube R21-C22	Tube R38-C46
RPC Exam	Axial indication with faint parallel indication 20 to 30 degrees away; 0.44 inch long, 77-82% deep.	Axial indication; 0.5 inch long, 76-81% deep.	Axial Indication 0.4 Inch long, 90% deep.
Bobbin Exam			
Echoram Probe	Indication 86-88% deep; voltage ranged from 3.6 to 4.3 volts depending on specimen orientation.	Indication 86-87% deep; voltage ranged from 9.6 to 11.6 volts depending on specimen orientation.	Use field data only: 1.4 volts, 68% deep.
Zetec Probe	Indication 86-91% deep; voltage ranged from 2.6 to 5.0 volts depending on specimen orientation.	Indication 86-90% deep; voltage ranged from 7.7 to 14.2 volts depending on specimen orientation.	

Table 4.3

Leak and Burst Data for Tubes Removed from Plant A-2

Results at Bottom TSP Location for All Tubes

Test	Tube R4-C73	Tube R21-C22	Tube R38-C46
Leak Test			
Operating Leak Rate (delta P = 1500 psi)	0 - 0.3 ml/hr	0 - <<7 ml/hr [*]	No Leak
Steam Line Break Rate (delta P = 2650 psi)	174 ml/hr	108 ml/hr	No Leak
Burst Test			
Burst Pressure (psig)	[		] 9
Burst Ductility (% delta D)	5.6	6.8	7.6
Burst Opening Length (inches)	0.459	0.784	0.881
Burst Opening Width (Inches)	0.135 (OD), 0.100 (ID)	0.210 (OD), 0.148 (ID)	0.167

[*] Problems with back pressure regulator increased the measured leak rate.

Table 4.4

Depth of Corrosion Observed on Circumferential Fracture Face from Center of the First Support Plate Crevice Region (Plant L Tube R12-C8)

Circumferential Location (degrees)	Maximum Depth of Penetration (% Through-Wall)
0	62
10	90
20	92
30	78
40	52
50	60
60	52
70	40
80	18
90	60
100	48
110	48
120	56
130	60
140	58
150	60
160	56
170	44
180	56
190	2
200	14
210	10
220	18
230	8
240	14
250	14
260	16
270	14
280	44
290	40
300	44
310	18
320	18
330	0
340	16
350	0

Comparison of Intergranular Corrosion Morphology at Support Plate Regions on S/G Tubing and Laboratory Specimens

Data Source	Cracking Density (as Measured or Estimated for One Plane)*			Extent of IGA Associated with the Major Cracks			Extent of OD IGA (Not Obviously Associated with a Single Crack)		
	Low (1-24 Cracks)	Moderate (25 - 100 Cracks)	High (Greater than 100)	Minor (D/W** >20)	Moderate (D/W 3 to 20)	Significant (D/W <3)	Negligible (<5% Deep)	Moderate (5 to 10% Deep)	Significant (>10% Deep)
Plant D-1									
R21-C31 SP1	3				5			Possible small IGA patches?	
R18-C33 SP1	None?						4% max. for 1% of circ.		
R17-C33 SP1	0 to 5				Inadequate Data		0		
Plant D-2									
R19-C55 SP1	~15				3-14		0		
R21-C58 SP1		~30			5-20		~0		
R16-C38 SP1	~14					2-4	0		
R6-C40 SP3	2				20		0		
R7-C38 SP1		90			4-9		0		
R7-C38 SP2		42			15		0		
R7-C38 SP3	23			24			1% deep intermittently around circumference		
R18-C77 SP1		92			6 to 19		~0	Isolated IGA patches, 10% max. depth	
R18-C77 SP2		>35			9 to 13		~0		Isolated IGA patches, 18% max. depth
R18-C77 SP3	>23				11 to 17		~0		
R18-C77 SP4		>31			9 to 18		~0		Isolated IGA patch, 20% max. depth
R18-C77 SP5	>16				11 to 24		~0		

- - - - - - - - - - - -

* Since most support plate cracking is composed of short axial microcracks, typically 0.02 to 0.05 inch long for a 50% deep crack, a microcracking density of 25 could be associated with more than several hundred individual microcracks within a support plate crevice region.

** D=Depth of SCC as measured from the OD surface exclusive of any surface IGA. W=Width of IGA component to the SCC as measured at the mid-point of the SCC.

Table 4.5 (Continuation)

Comparison of Intergranular Corrosion Morphology at Support Plate Regions on S/G Tubing and Laboratory Specimens

Data Source	Cracking Density (as Measured or Estimated for One Plane)*			Extent of IGA Associated with the Major Cracks			Extent of OD IGA (Not Obviously Associated with a Single Crack)		
	Low (1-24 Cracks)	Moderate (25 - 100 Cracks)	High (Greater than 100)	Minor (D/W** >20)	Moderate (D/W 3 to 20)	Significant (D/W <3)	Negligible (<5% Deep)	Moderate (5 to 10% Deep)	Significant (>10% Deep)
Plant A-2									
R31-C46 SP1	~6				3.2		0		
R4-C73 SP1	~8				4.2		0		
R21-C22 SP1	~2					1.7	0		
R38-C46 SP1	~10			14-28			0		(Possible cellular IGA/SCC in a local area)
Plant B-1									
R4-C61 SP1 (2H)	~4			25			0		
R4-C61 SP2 (5H)	~15 (for axial) ~5 Circ. Cracks				15 (for axial), ~1 (for Circ. Cracks)		2% Deep Intermittently around circumference		
R4-C61-SP5 (12H)	~6 (Circ. Cracks)					1-2	0		(Possible cellular IGA/SCC in a local area)
Plant B-2									
R6-C67 SP1 (2H)	16				18		0		
R6-C67 SP3 (8H)		28			15		4% deep intermittently around circ.		
R6-C67 SP5 (11H)	6				No Data		No Data		

----

* Since most support plate cracking is composed of short axial microcracks, typically 0.02 to 0.05 inch long for a 50% deep crack, a microcracking density of 25 could be associated with more than several hundred individual microcracks within a support plate crevice region.

** D=Depth of SCC as measured from the OD surface exclusive of any surface IGA. W=Width of IGA component to the SCC as measured at the mid-point of the SCC.

Data Source	Cracking Density (as Measured or Estimated for One Plane)*			Extent of IGA Associated with the Major Cracks			Extent of OD IGA (Not Obviously Associated with a Single Crack)		
	Low (1-24 Cracks)	Moderate (25 - 100 Cracks)	High (Greater than 100)	Minor (D/W** >20)	Moderate (D/W 3 to 20)	Significant (D/W <3)	Negligible (<5% Deep)	Moderate (5 to 10% Deep)	Significant (>10% Deep)
Plant L									
R12-C8 SP1			~400 (272-504)		6-18 (Possible cellular IGA/ SCC)				210° at SP Center, less above and below Center (see Table 4.2), max depth 43% by Metallography
R12-C8 SP2		50			Moderate (no quantitative data available)				Intermittently distributed, patch IGA (6% of circ.), max. depth 12%.
R12-C8 SP3		85			Moderate (no quantitative data available)				Intermittently distributed, patch IGA (3% of circ.), max. depth 21%.
R29-C70 SP1	2-3			35			~0		
R29-C70 SP2	5				17		~0		
R29-C70 SP3	4			24 to 50			~0		

....

* Since most support plate cracking is composed of short axial microcracks, typically 0.02 to 0.05 inch long for a 50% deep crack, a microcracking density of 25 could be associated with more than several hundred individual microcracks within a support plate crevice region.

** D=Depth of SCC as measured from the OD surface exclusive of any surface IGA. W=Width of IGA component to the SCC as measured at the mid-point of the SCC.

Table 4.5 (Continuation)

Data Source	Cracking Density (as Measured or Estimated for One Plane)*			Extent of IGA Associated with the Major Cracks			Extent of OD IGA (Not Obviously Associated with a Single Crack)		
	Low (1-24 Cracks)	Moderate (25 - 100 Cracks)	High (Greater than 100)	Minor (D/W** >20)	Moderate (D/W 3 to 20)	Significant (D/W <3)	Negligible (<5% Deep)	Moderate (5 to 10% Deep)	Significant (>10% Deep)
Plant L (Cont.)									
R30-C64 SP1	29				16		~0		Cellular IGA/ SCC possibly present locally
R30-C64 SP2	85				9		~0		
R30-C64 SP3	30			31			~0		
R16-C74 SP1	31			32					A few patches of IGA present, max. depth 19%; Cellular IGA/ SCC definitely present locally
R16-C74 SP2	62			20					A few patches of IGA, 17% max. depth.
R16-C74 SP3	43			21			~0		
R20-C66 SP1	60				4 to 28		~0		Cellular IGA/ SCC probably present locally
R20-C66 SP2	27			21			~0		
R20-C66 SP3	34			36			~0		Cellular IGA/ SCC possibly present locally

- - - - - - - - - - - -

* Since most support plate cracking is composed of short axial microcracks, typically 0.02 to 0.05 inch long for a 50% deep crack, a microcracking density of 25 could be associated with more than several hundred individual microcracks within a support plate crevice region.

* D=Depth of SCC as measured from the OD surface exclusive of any sur███GA. W=Width of IGA component to the SCC as measured at the mid-poi███ the SCC.

Data Source	Cracking Density (as Measured or Estimated for One Plane)*			Extent of IGA Associated with the Major Cracks			Extent of OD IGA (Not Obviously Associated with a Single Crack)		
	Low (1-24 Cracks)	Moderate (25 - 100 Cracks)	High (Greater than 100)	Minor (D/W** >20)	Moderate (D/W 3 to 20)	Significant (D/W <3)	Negligible (<5% Deep)	Moderate (5 to 10% Deep)	Significant (>10% Deep)
Plant L (Cont.)									
R8-C66 SP1		41	.	29			~0		Cellular IGA/ SCC probably present locally
R8-C66 SP2	8				8		~0		Cellular IGA/ SCC probably present locally
R8-C66 SP3	2				16		~0		
R8-C69 SP1		46		60			~0		Cellular IGA/ SCC possibly present locally
R8-C69 SP2		47		32				Intermittent patch IGA present,<10% max. depth	Cellular IGA/ SCC probably present locally
R8-C69 SP3		60		29			~0		Cellular IGA/ SCC probably present locally
R12-C70 SP1		44		22			~0		
R12-C70 SP2	24			32			~0		
R12-C70 SP3		28		33			~0		Cellular IGA/ SCC possibly present locally

- - - - - - - - - - - - - -

* Since most support plate cracking is composed of short axial microcracks, typically 0.02 to 0.05 inch long for a 50% deep crack, a microcracking density of 25 could be associated with more than several hundred individual microcracks within a support plate crevice region.

** D=Depth of SCC as measured from the OD surface exclusive of any surface IGA. W=Width of IGA component to the SCC as measured at the mid-point of the SCC.

Table 4.5 (Continuation)

Data Source	Cracking Density (as Measured or Estimated for One Plane)*			Extent of IGA Associated with the Major Cracks			Extent of OD IGA (Not Obviously Associated with a Single Crack)		
	Low (1-24 Cracks)	Moderate (25 - 100 Cracks)	High (Greater than 100)	Minor (D/W** >20)	Moderate (D/W 3 to 20)	Significant (D/W <3)	Negligible (<5% Deep)	Moderate (5 to 10% Deep)	Significant (>10% Deep)
Plant M-2									
R29-C46CL SP1	0 (~50 if IGA fronts are defined as cracks with L/W ≤ 1)					≤ 1 if crack is defined as being present			≥300° uniform IGA; max. depth 26%
Plant C-2									
R26-C56 SP1 (2H)		36				2-10		2°, max. depth 8%	
Plant P-1									
R16-C60 SP1		82		Minor to moderate, 6 to 25 D/W			0		
R16-C60 SP2		58			11 to 17				A few IGA patches at OD crack locations max. depth 31%; Cellular IGA/SCC probably present locally
R11-C48 SP1		39			10 to 20		~0		
R11-C48 SP3		56			11			IGA and IGA patches, max. depth 9%, less than 20% of circumference	
Plant J-1									
L8-C74 SP1			≤141		14-20				~200°, max. depth ~40%.
L8-C74 SP2			≤176		10-15				~80°, max. depth ~20%.

----

* Since most support plate cracking is composed of short axial microcracks, typically 0.02 to 0.05 inch long for a 50% deep crack, a microcracking density of 25 could be associated with more than several hundred individual microcracks within a support plate crevice region. D=Depth of SCC as measured from the OD surface exclusive of any surf⬤. W=Width of IGA component to the SCC as measured at the mid-point the SCC.

4-34

4 - 35

Data Source	Cracking Density (as Measured or Estimated for One Plane)*			Extent of IGA Associated with the Major Cracks			Extent of OD IGA (Not Obviously Associated with a Single Crack)		
	Low (1-24 Cracks)	Moderate (25 - 100 Cracks)	High (Greater than 100)	Minor (D/W** >20)	Moderate (D/W 3 to 20)	Significant (D/W <3)	Negligible (<5% Deep)	Moderate (5 to 10% Deep)	Significant >10% Deep)
Plant N-1									
L59-C95 SP1			≤340		4 (misleading ratio for these cracks, should be larger value)				45°, max. depth 20%.
L59-C95 SP2	0 (no cracks just IGA)								45°, max. depth 13%.
L120-C12 SP3	3			34 (not accurate since obtained from unetched specimen)			1% deep intermittently around circumference		
Plant E-4									
R19-C35 SP2			~106		9.5		~0		Cellular IGA/ SCC present
R19-C35 SP3		~79			No Data		~0		Cellular IGA/ SCC present
R19-C35 SP4			~103		No Data		~0		Cellular IGA/ SCC present
R42-C49 SP2		~92			3 to 12		~0		Cellular IGA/ SCC present
R8-C47 SP3		~63			4			7% deep IGA, Intermittently around circ.	Cellular IGA/ SCC present
Laboratory Tests									
571-1	1			~50			0		
543-4	5			40			0		
536-1	3			60			0		
543-4	14				14		0		
525-1	5				14		0		
533-3	11			11-40			0		
533-4	13				13		0		

----

* Since most support plate cracking is composed of short axial microcracks, typically 0.02 to 0.05 inch long for a 50% deep crack, a microcracking density of 25 could be associated with more than several hundred individual microcracks within a support plate crevice region.

** D=Depth of SCC as measured from the OD surface exclusive of any surface IGA. W=Width of IGA component to the SCC as measured at the mid-point of the SCC.

Table 4.5 (Continuation)

Data Source	Cracking Density (as Measured or Estimated for One Plane)*			Extent of IGA Associated with the Major Cracks			Extent of OD IGA (Not Obviously Associated with a Single Crack)		
	Low (1-24 Cracks)	Moderate (25 - 100 Cracks)	High (Greater than 100)	Minor (D/W** >20)	Moderate (D/W 3 to 20)	Significant (D/W <3)	Negligible (<5% Deep)	Moderate (5 to 10% Deep)	Significant (>10% Deep)
Laboratory Tests (Cont.)									
532-1	22				16		0		
532-2		25			18		0		Cellular IGA/ SCC possibly present locally
528-2	15				19		0		
535-1	11				12		0		
555-3	7			21			0		
576-2	1			27			0		
576-4	1				13		0		
1015-14B	2			37			0		
1047-13	1			21			0		
1047-15	1				20		0		
509-3	4			41			0		
528-1	8			31			0		
509-2	2			48			0		Cellular IGA/ SCC possibly present locally
510-1	8				10		0		
590-1	3			29			0		
590-2	18				9		0		Cellular IGA/ SCC possibly present locally
591-1	3				14		0		
591-2	12			48			0		
591-4	9			60			0		
596-3	7				10		0		
SL-FH-11	10				11		0		

----

* Since most support plate cracking is composed of short axial microcracks, typically 0.02 to 0.05 inch long for a 50% deep crack, a microcracking density of 25 could be associated with more than several hundred individual microcracks within a support plate crevice region.

** D=Depth of SCC as measured from the OD surface exclusive of any surface IGA. W=Width of IGA component to the SCC as measured at the mid-point of the SCC.

Table 4.6

Summary Data on Tubes Burst from
Third Tube Pull Campaign at Plant L

Tube/TSP	Burst Pressure (psi)	Intergranular Macrocrack Length On Burst Face* (inch)	Maximum Depth (%)	Average Depth (%)
R8-C66 TSP 1				
R8-C66 TSP 2				
R8-C66 TSP 3				
R8-C69 TSP 1				
R8-C69 TSP 2				
R8-C69 TSP 3				
R12-C70 TSP 1				
R12-C70 TSP 3				
R16-C74 TSP 1				
R16-C74 TSP 2				
R16-C74 TSP 3				
R20-C66 TSP 1				
R20-C66 TSP 2				
R20-C66 TSP 3				

g

---

* Direct measurement shows that the pre-burst length does not exceed 0.75 inch.

Table 4.7a

BOBBIN COIL VOLTAGES - LABORATORY RESULTS

Tube	TSP	With Support Ring 400 kHz Diff.	400/100 kHz	Without Support Ring 400 kHz Diff.	400/100 kHz
R11C48	1	3.78 V 70 Deg. 81%	2.50V 102 Deg. 52%	2.48V 129 Deg. 37%	2.16V 97 Deg. 57%
R16C60	1	3.58 V 153 Deg. 16%	2.75V 107 Deg. 48%	4.58V 151 Deg. 18%	2.97V 106 Deg. 49%
R16C60	2	NDD* 153 Deg. 16%	NDD* 107 Deg. 48%	2.12V 164 Deg. 6%	1.29V 146 Deg. 7%

*NDD: No Detectable Degradation

All other tube support plate intersections of the pulled tubes were NDD.

Table 4.7b

RPC VOLTAGES - LABORATORY RESULTS

Tube	TSP	With Support Ring 400 kHz Diff.	400/100 kHz	Without Support Ring 400 kHz Diff.	400/100 kHz
R11C48	1	0.84 V 113 Deg. 28%	1.33V 75 Deg. 31%	0.82V 112 Deg. 31%	1.35V 81 Deg. 0%
R16C60	1	0.92V 145 Deg. 0%	1.08V 94 Deg. 16%	1.28V 149 Deg. 5%	1.28V 113 Deg. 0%

All other tube support plate intersections of the pulled tubes were NDD.

Table 4.8

TUBE SUPPORT PLATE CRACK DATA

Tube	TSP*	Number of Cracks	Maximum Penetration	Average Crack Depth
R16C60	1M	70	33%	20%
R16C60	1T	160	53%	33%
R16C60	2M	53	48%	30%
R11C48	1M	39	54%	40%
R11C48	1B	6	38%	22%

* Designation of T, M and B signifies Top of TSP, Mid-plane of TSP, and Bottom of TSP, respectively.

Table 4.9

SEM MEASUREMENTS FROM R16C60 TSP#1

Crack #	Ligament to Ligament Distance (mils)	Maximum Crack Depth (%)	Ligament Length (mils)
1	25.00	10.0	12.5
2	51.25	22.5	12.5
3	57.50	40.0	15.6
4	20.00	33.5	21.9
5	60.33	46.0	28.1
6	55.00	65.0	34.4
7	41.25	67.5	34.4
8	67.50	62.5	23.4
9	26.25	42.5	25.0
10	31.25	56.3	26.6
11	37.50	50.0	25.0
12	25.00	50.0	25.0
13	67.50	52.5	20.3
14	55.00	30.0	10.9
15	15.00	20.0	12.5
16	65.00	30.0	--

Average Crack Depth = 41%

Burst Crack Length = 0.77 inches

Corrected Crack Length = 0.73 inches

Table 4.10

SEM MEASUREMENTS FROM R16C60 TSP#2

Crack #	Ligament to Ligament Distance (mils)	Maximum Crack Depth (%)	Ligament Length (mils)
1	120.0	32.5	12.5
2	27.5	35.0	15.6
3	36.25	37.5	21.9
4	50.0	50.0	23.4
5	217.5	52.5	21.9
6	137.5	50.0	17.2
7	60.0	47.5	21.9
8	95.0	40.0	18.8
9	57.5	32.5	9.4
10	68.75	20.0	--

Average Crack Depth = 36%

Burst Crack Length = 0.92 inches

Corrected Crack Length = 0.74 inches

tube OD

tube ID

Patch IGA

tube OD

tube ID
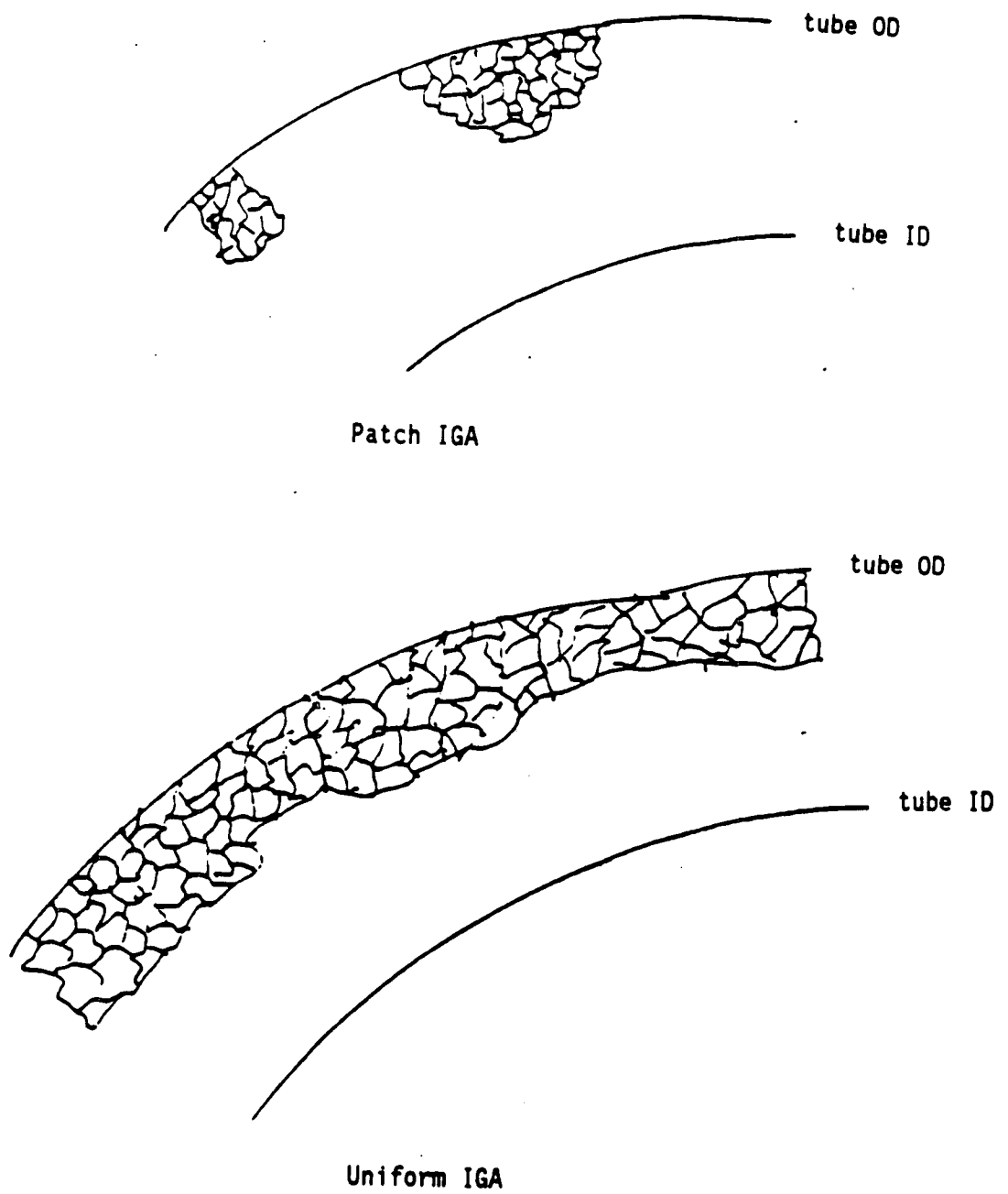
Uniform IGA

Figure 4-1   Patch and uniform IGA morphology as observed in a
transverse tube section. (A similar observation would be
made from a longitudinal section.)

tube OD

tube ID

Branch SCC

Simple SCC

transverse section
schematic

tube OD

tube ID
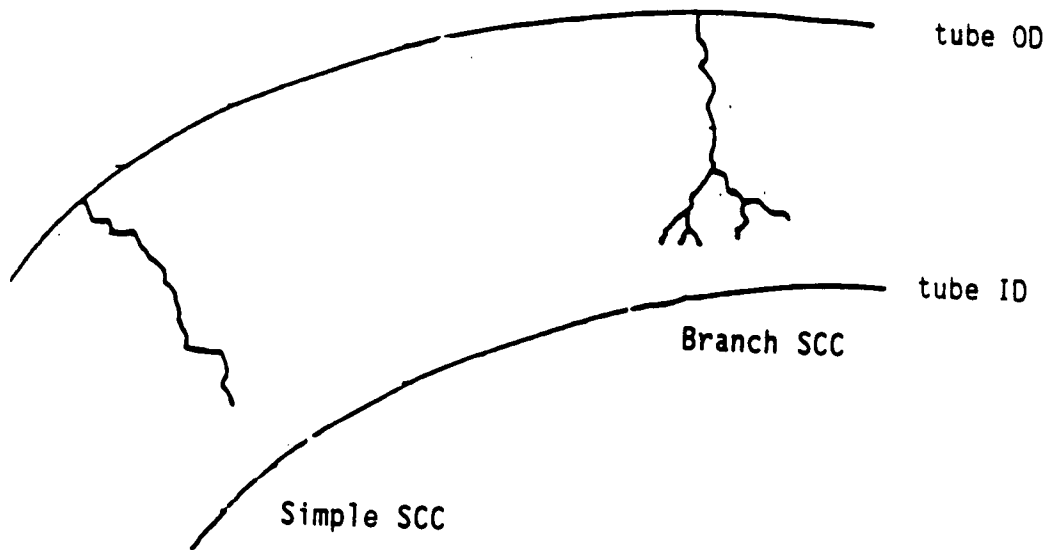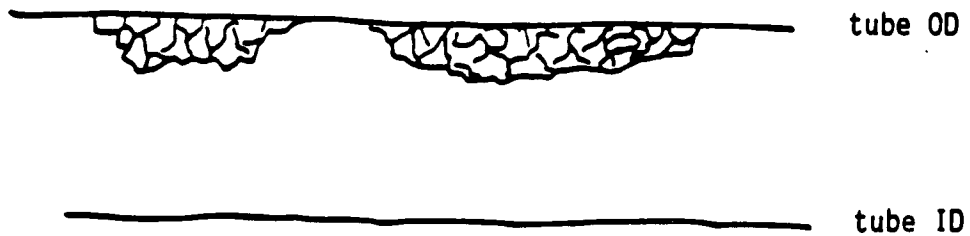
longitudinal section
schematic

Figure 4-2   Schematic of simple IGSCC and branch IGSCC. Note that
              branch and simple IGSCC are not distinguishable from a
              longitudinal metallographic section. From a longitudinal
              section, they also look similar to IGA (See Figure 4.3).

IGA with IGSCC fingers (D/W > 10)

IGA with IGSCC/IGA fingers (D/W = 6)

IGA with IGA fingers (D/W = 1)

tube OD

tube ID

transverse section schematic

tube OD

tube ID

longitudinal section schematic
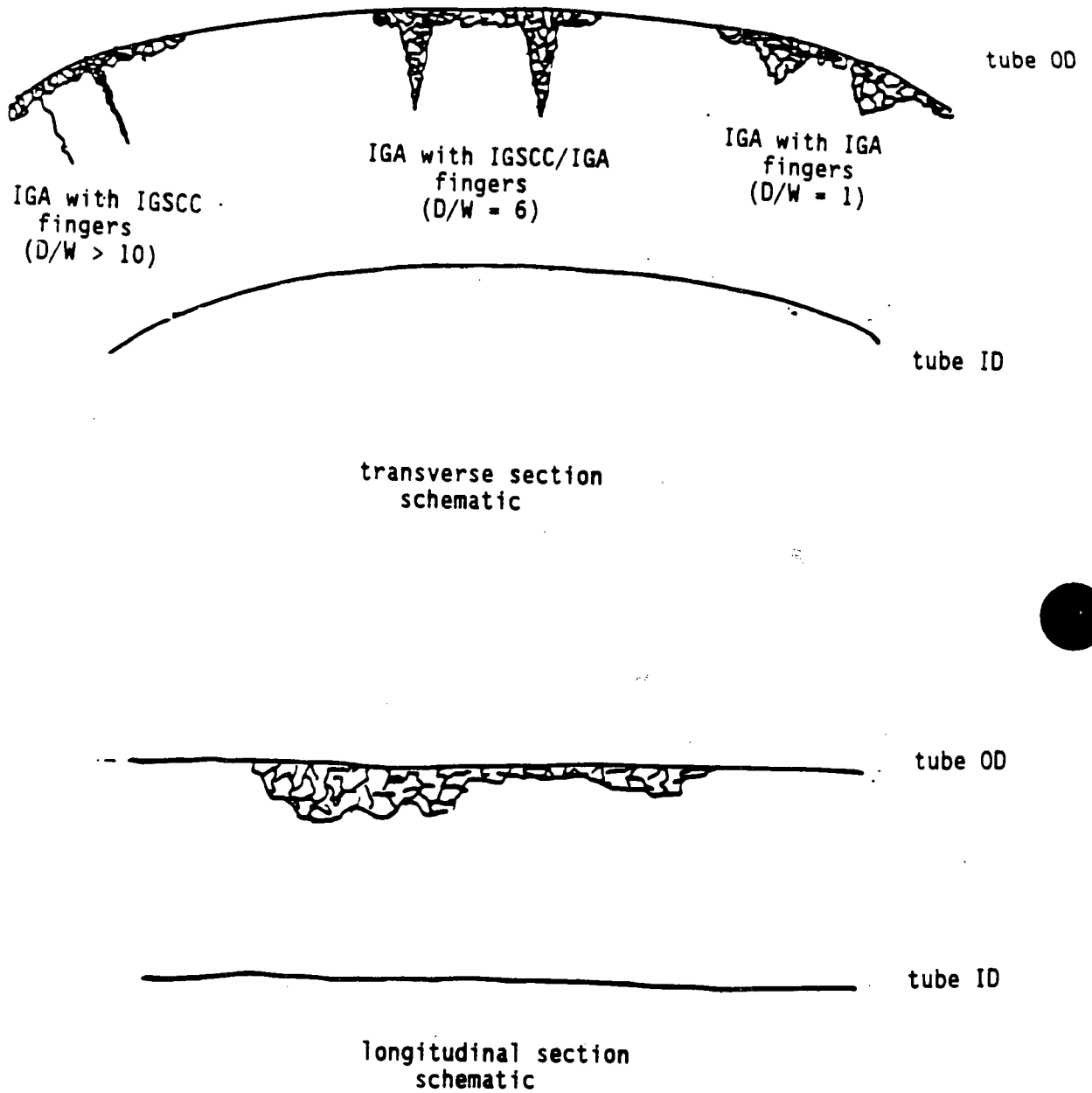
Figure 4-3   Schematic of IGA with IGSCC fingers and IGA with IGA fingers. Note that neither of the above variations can be distinguished from a longitudinal section.

4 - 44

4 Mils Deep   11 Mils Deep   Axial Direction   21 Mils Deep   Mag. 11.5X
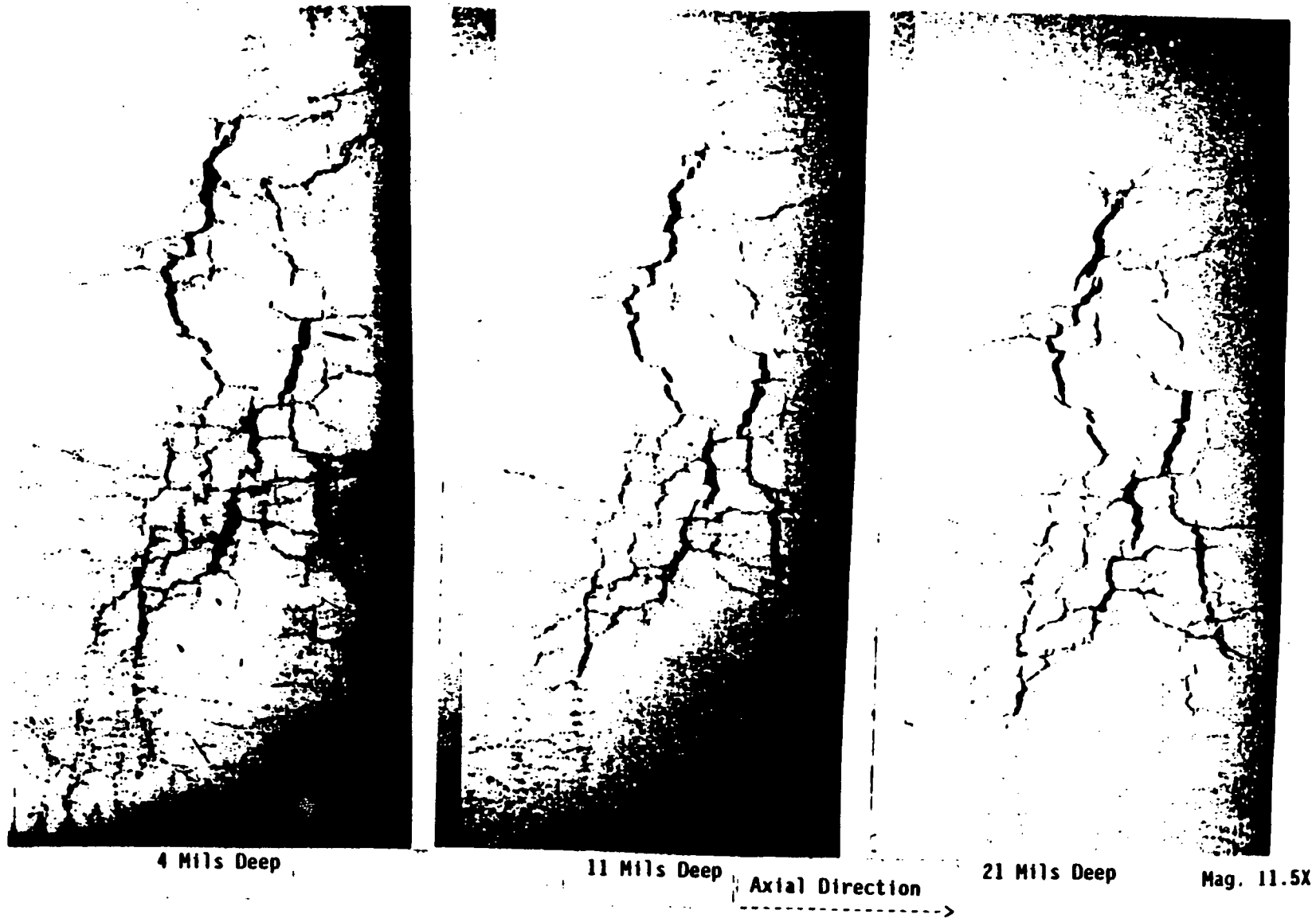
Figure 4-4   Photomicrographs of radial metallography performed on a region with
axial and circumferential degradation on tube R16-C74, support
plate 1. Cellular IGA was found with little change in the cell
shape and cell wall thickness at depths of 4, 11 and 21 mils below
the OD surface. Note that the cut section was flattened,
preferentially opening the circumferential wall of the cells.
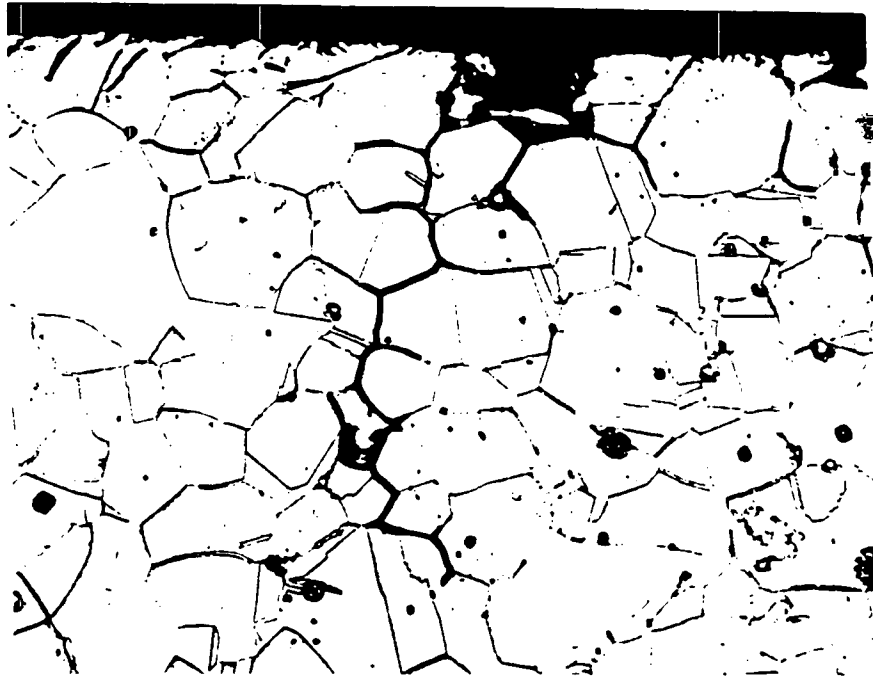
Figure 4-5   Tube R21-C31 from Plant D-1 , first support plate region,
              transverse OD metallography, Mag. 500X.
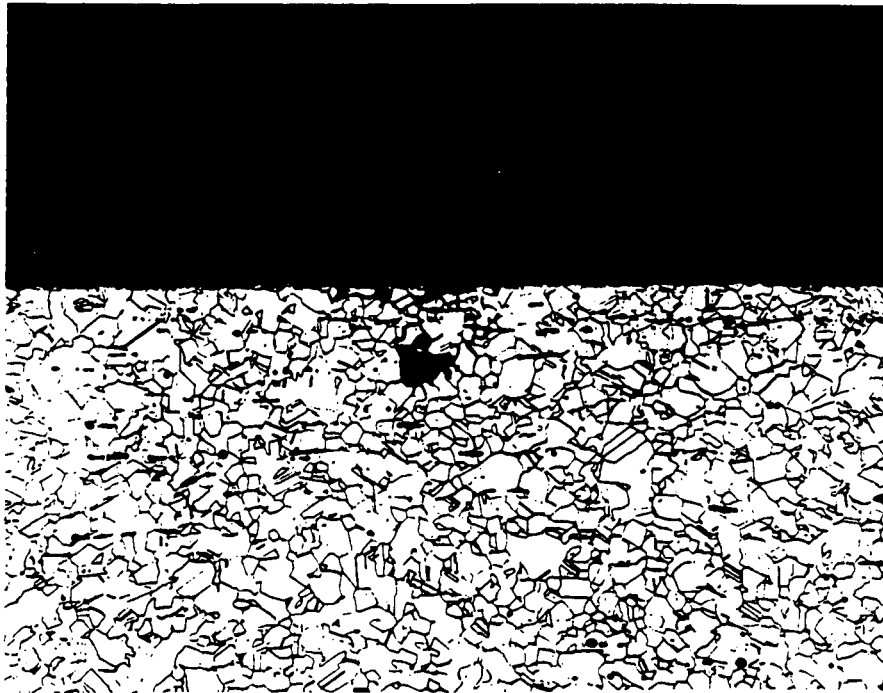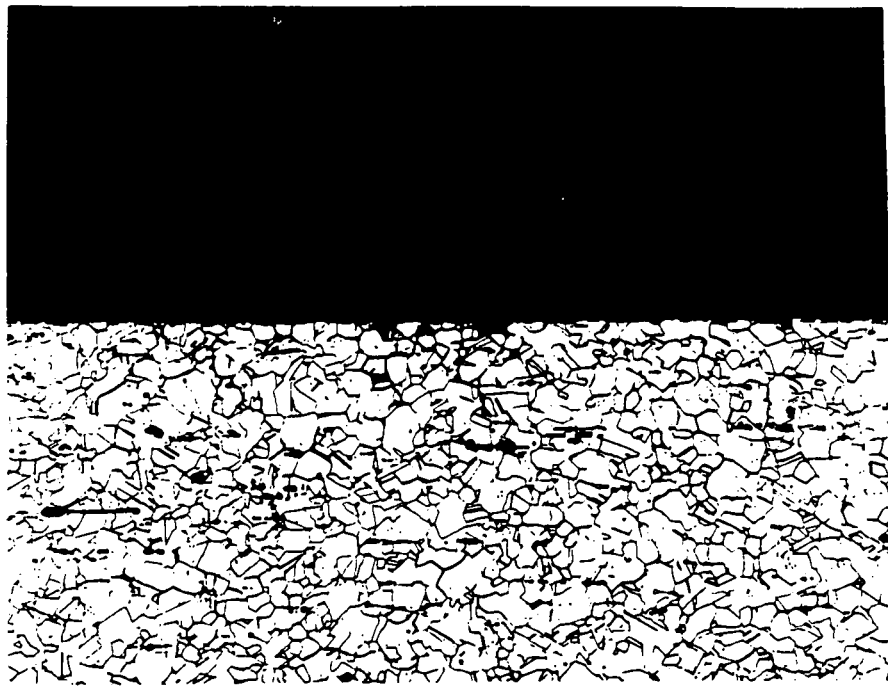
Figure 4-6   Tube R21-C31 from Plant D-1 , first support plate region, longitudinal OD metallography, Mag. 100X.
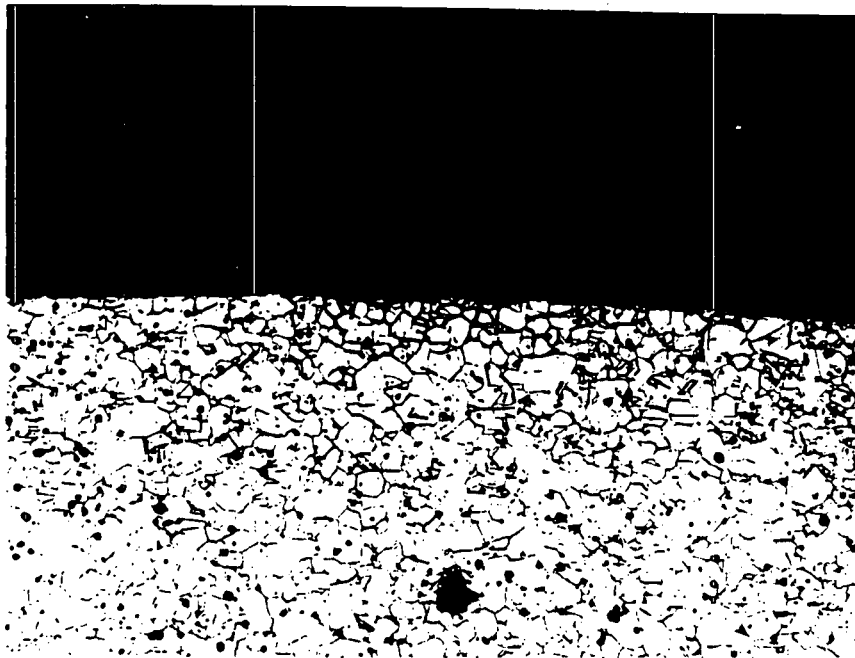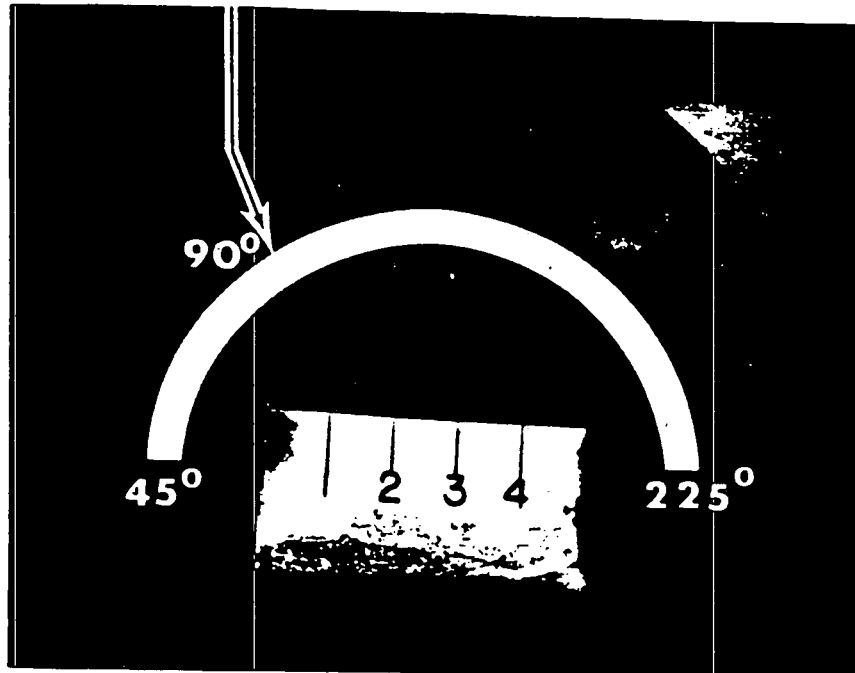
A

Figure 4-7   Tube R18-C33 from Plant D-1, first support plate region,
             longitudinal OD metallography, Mag. 100X (bottom photo).

4 - 48
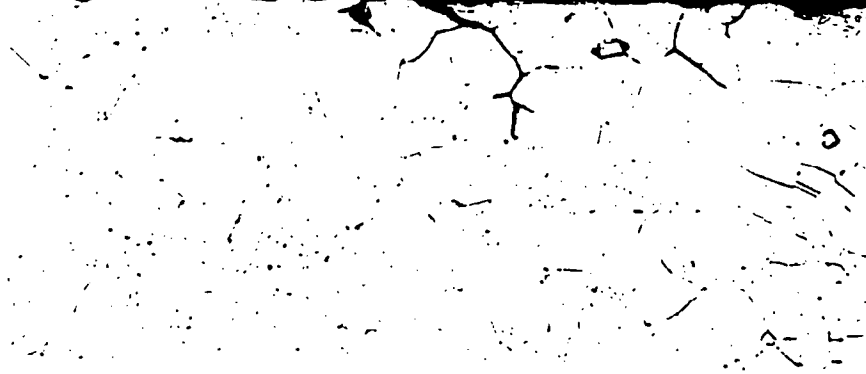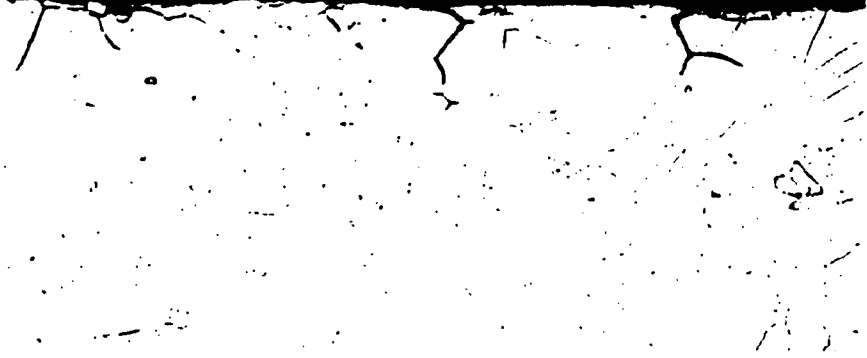
500X

500X

Figure 4-8   Tube R17-C33 from Plant D-1, first support plate region,
              longitudinal OD metallography, Mag. 500X.
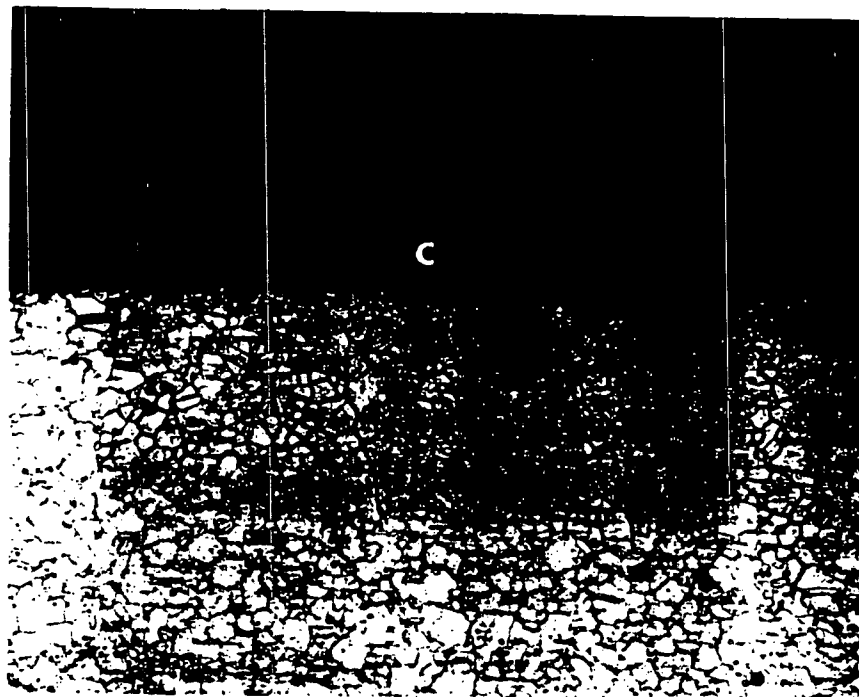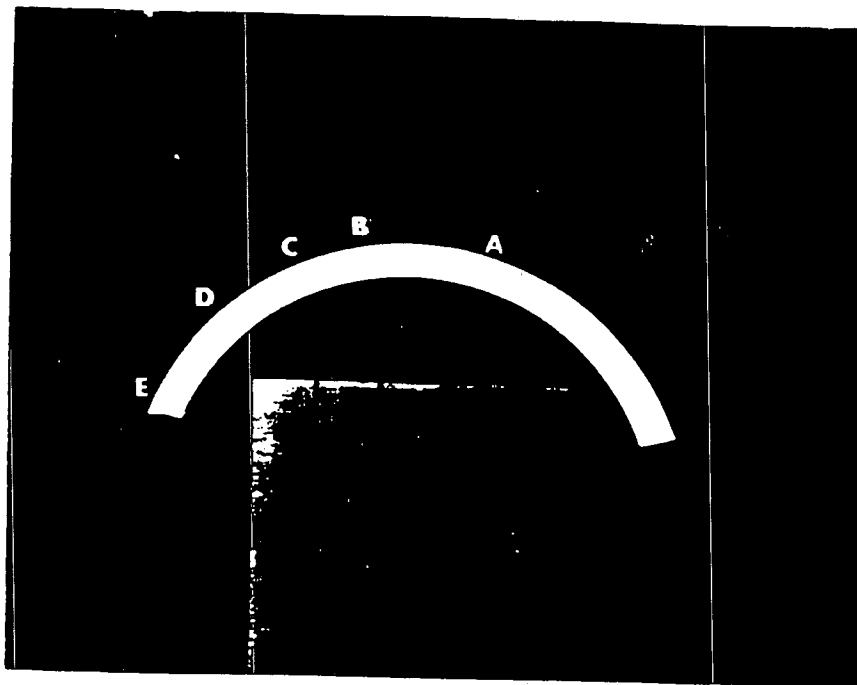
100X

Figure 4-9   Tube R19-C55 from Plant D-2 , first support plate region,
transverse OD metallography, Mag. 100X (bottom photo).
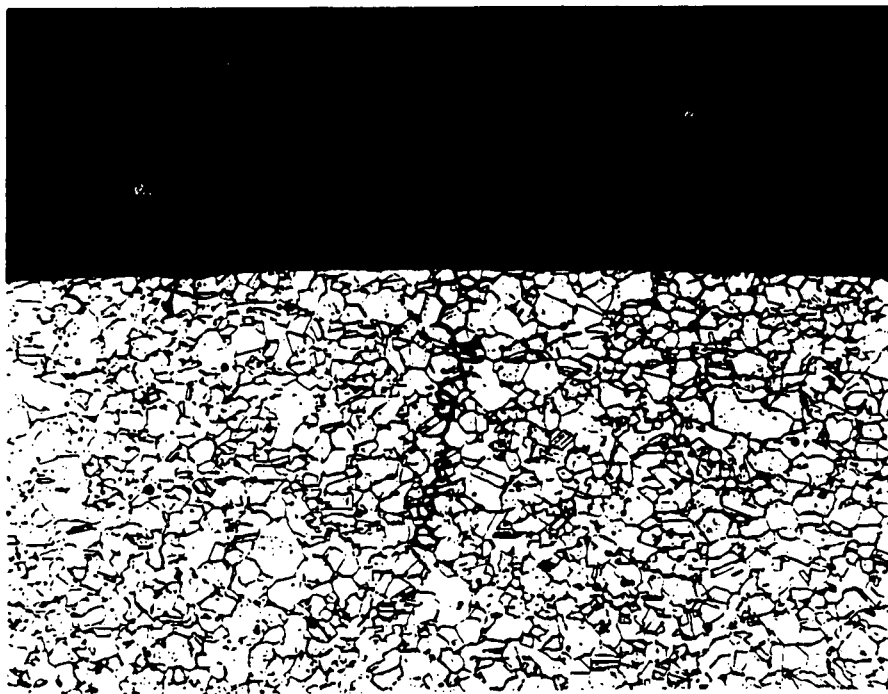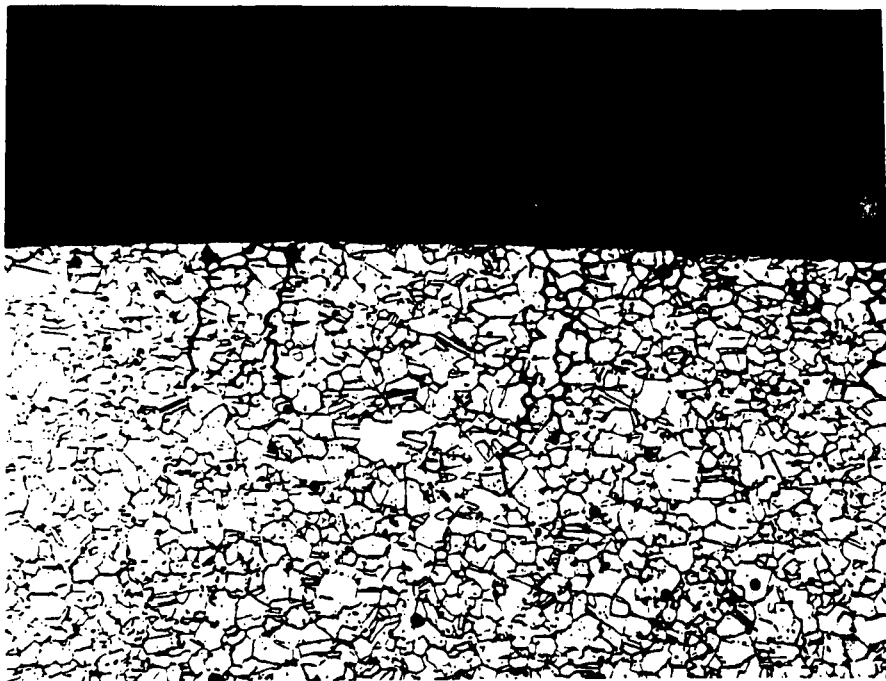
Figure 4-10   Tube R19-C55 from Plant D-2, first support plate region,
transverse OD metallography (from a different section than
the one shown in Figure 4-9), Mag. 100X.
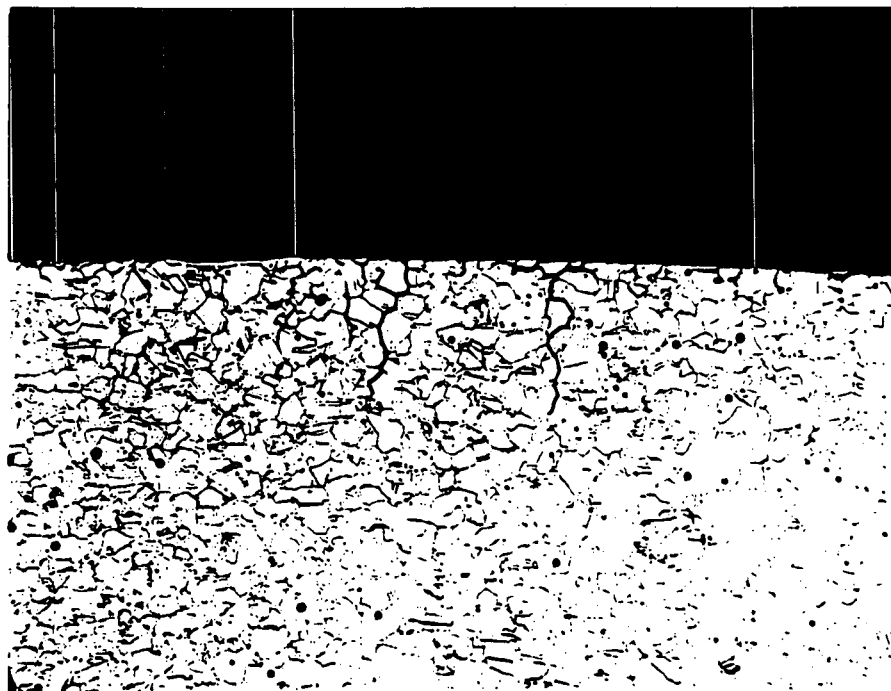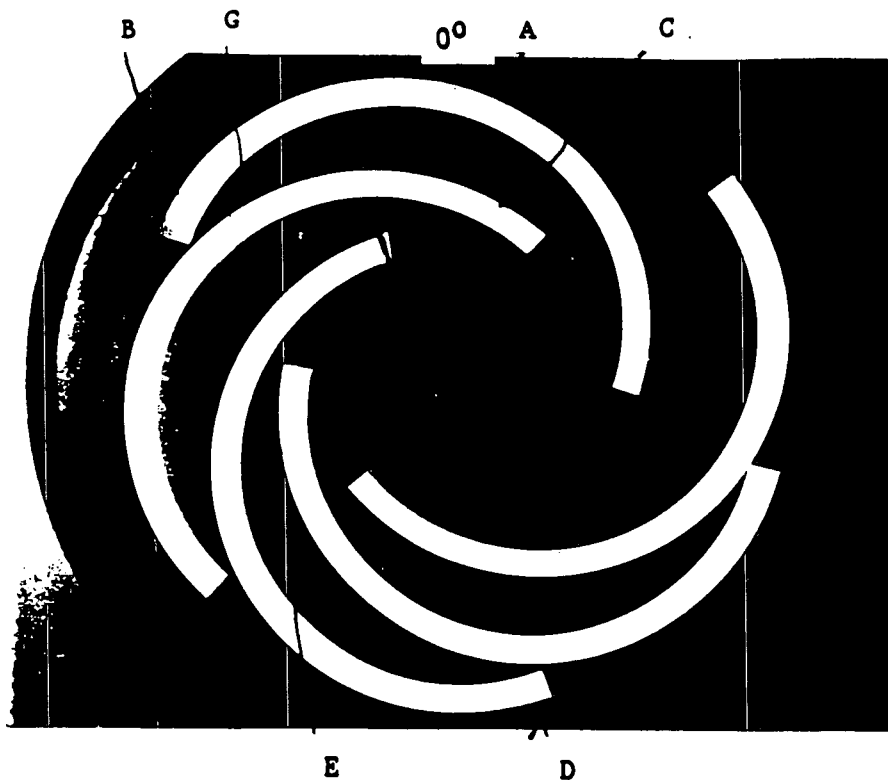
Area C

Figure 4-11   Tube R19-C55 from Plant D-2, first support plate region,
transverse OD metallography (bottom photo is one of many
areas with observed cracking on a series of transverse met.
sections different than those shown in Figures 4-9 and
4-10), Mag. 100X (bottom photo).

4 - 52
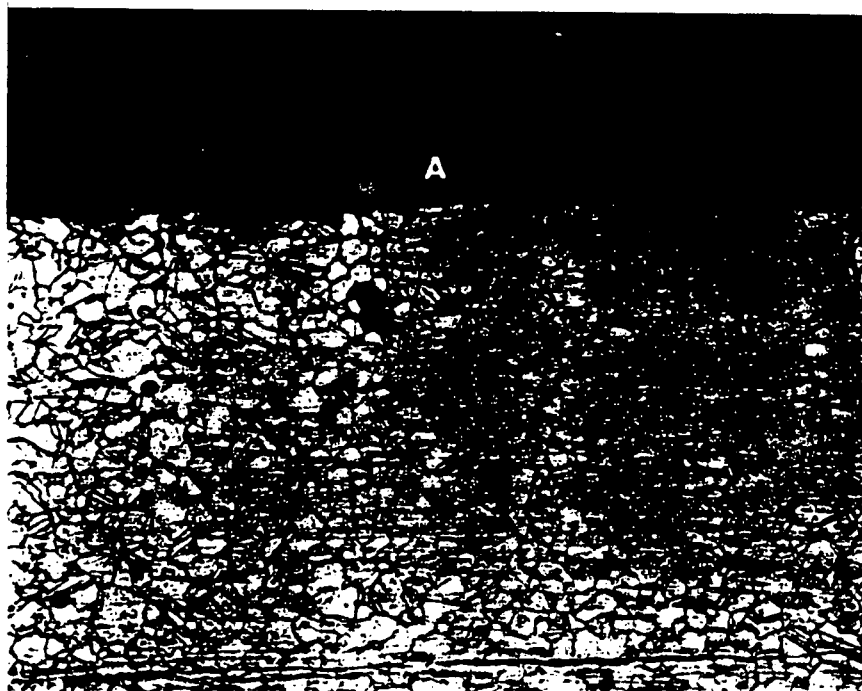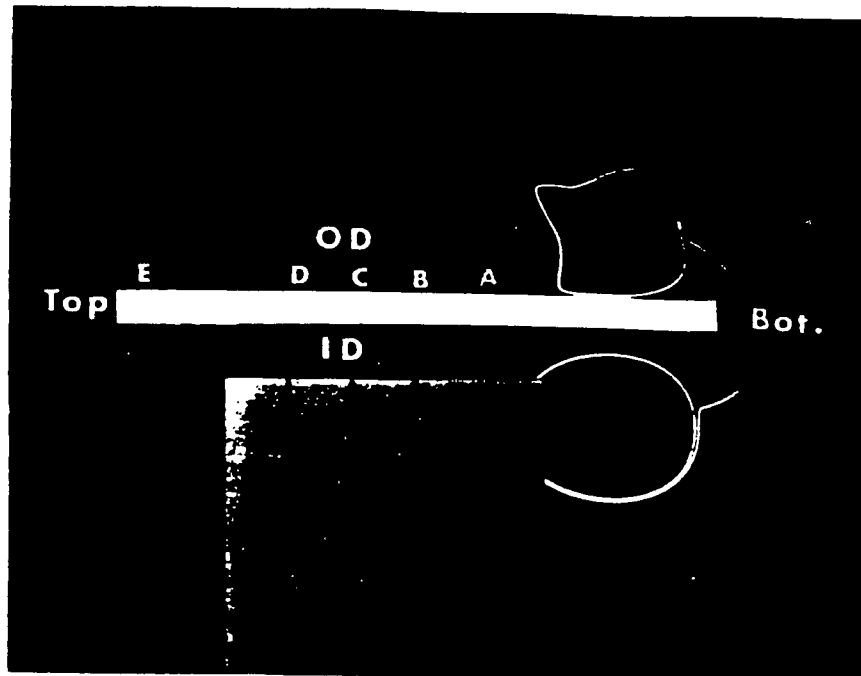
100X

Figure 4-12   Tube R19-C55 from Plant D-2 , first support plate region, longitudinal OD metallography, Mag. 100X (bottom photo).
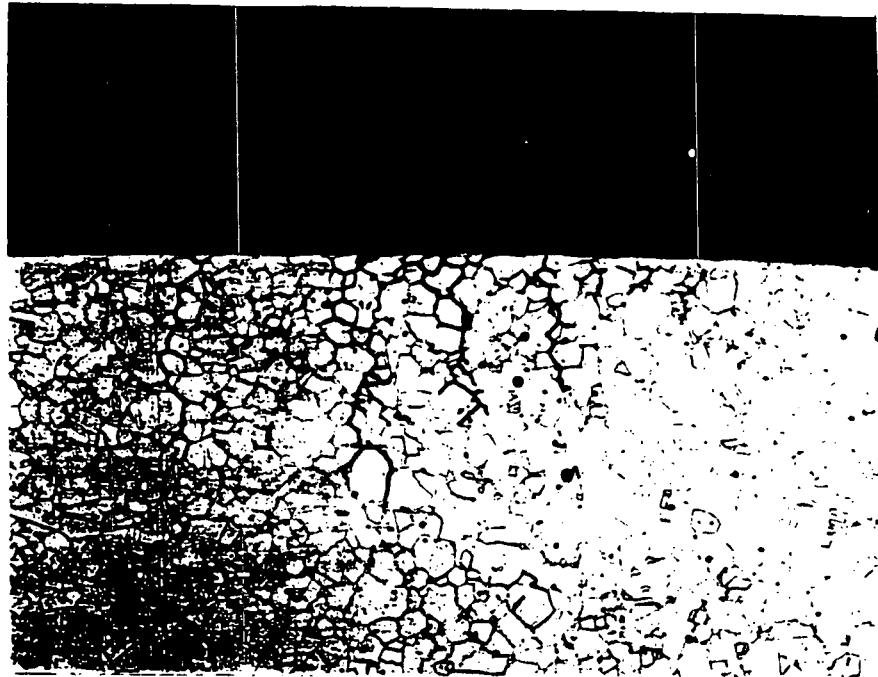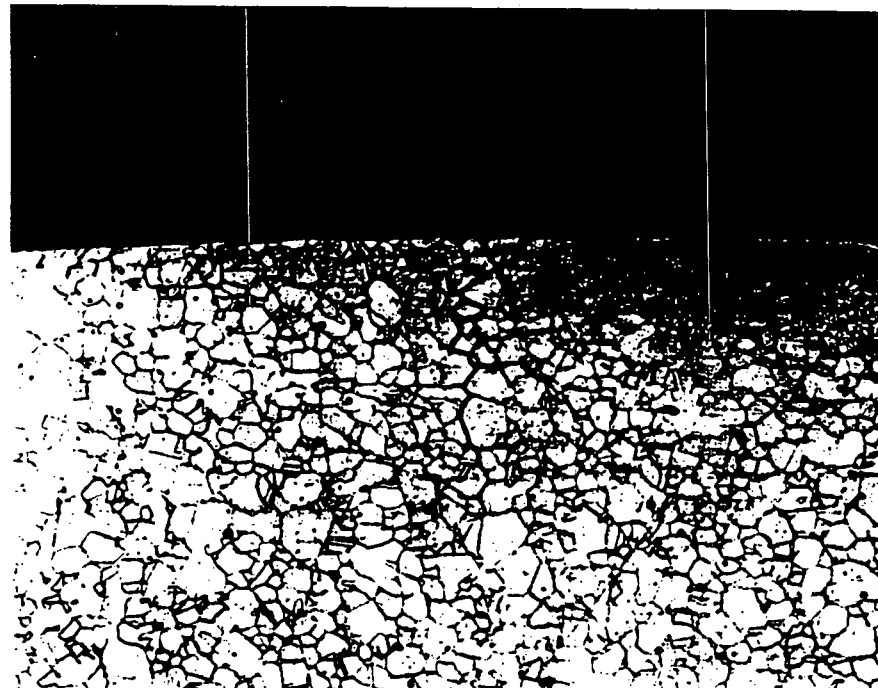
100X

100X

Figure 4-13   Tube R21-C58 from   Plant D-2, first support plate region,
transverse OD metallography, Mag. 100X.

4 - 54
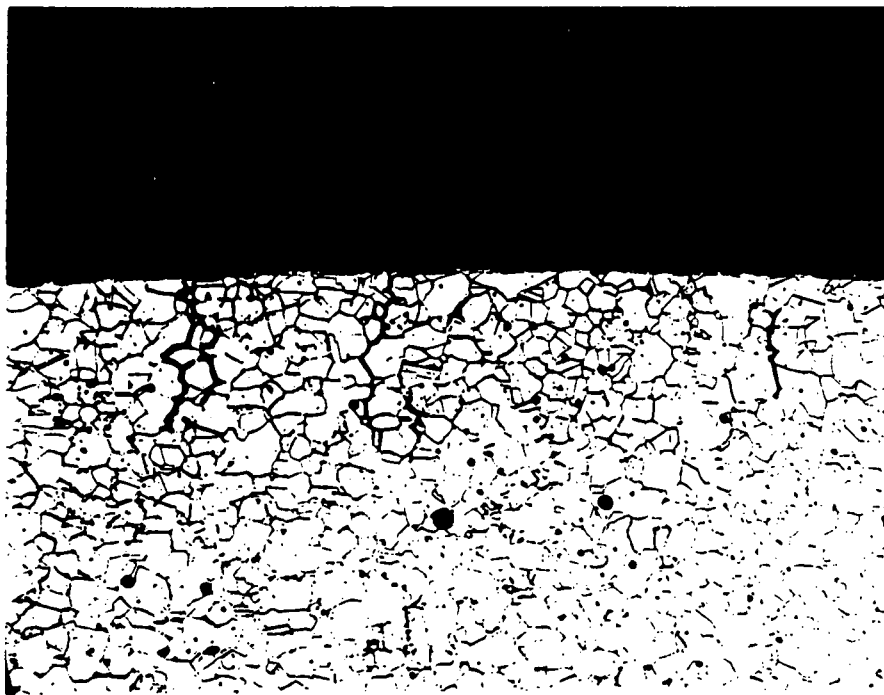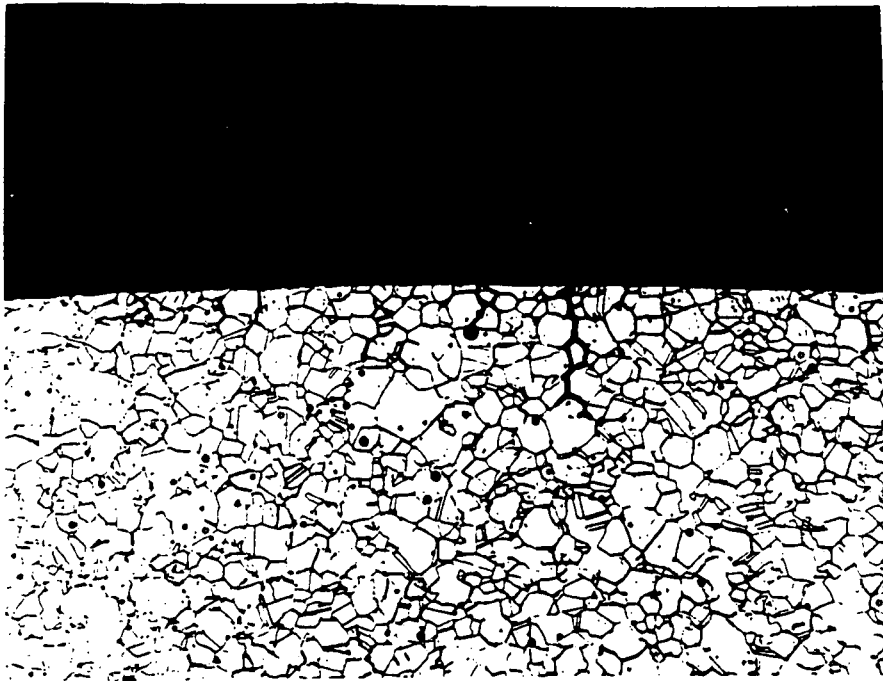
Figure 4-14   Tube R21-C58 from Plant D-2, first support plate region,
               transverse OD metallography (from a different section than
               the one shown in Figure 4-13), Mag. 100X.

Area D
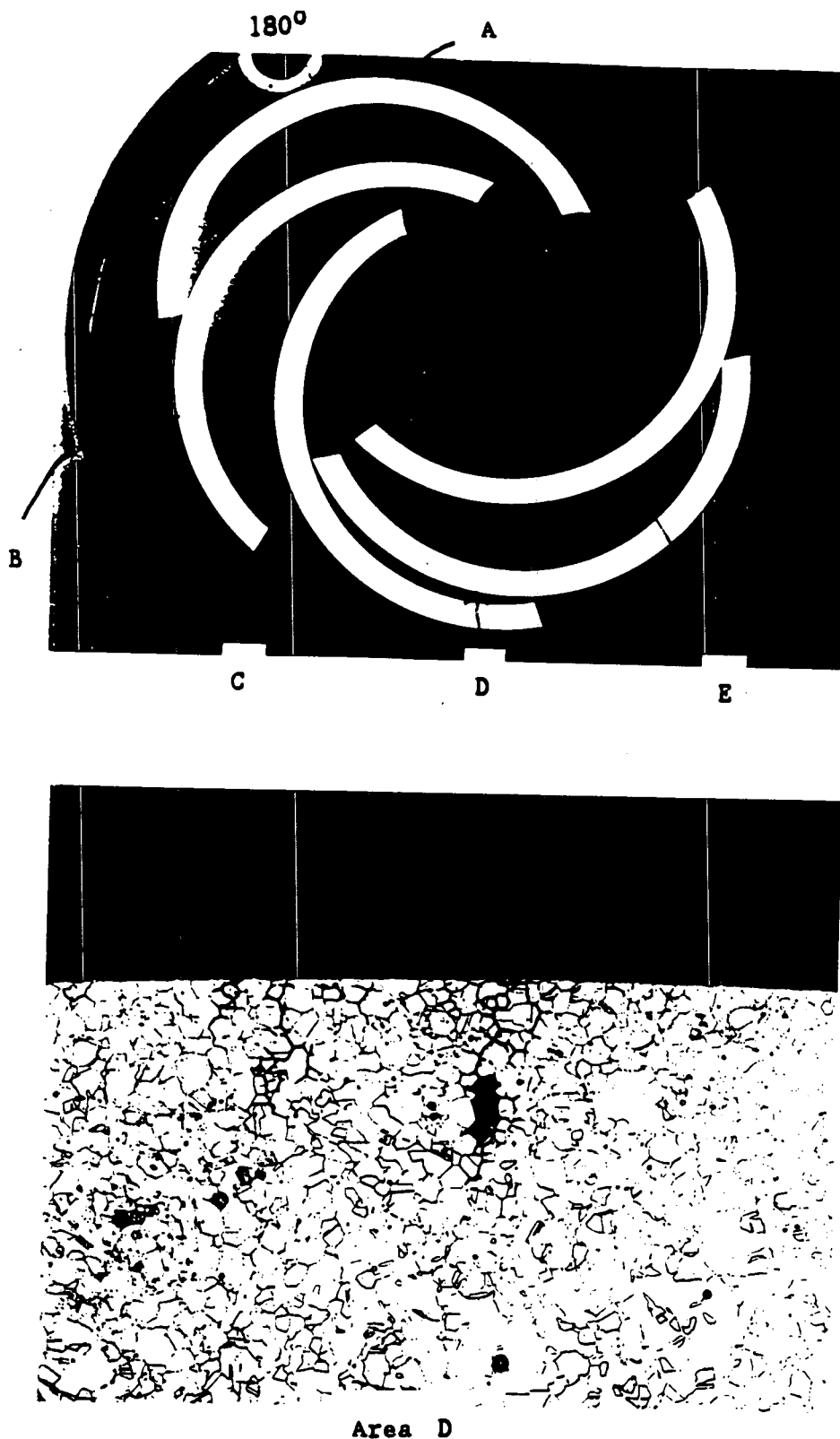
Figure 4-15   Tube R19-C55 from Plant D-2, first support plate region,
transverse OD metallography (bottom photo is one of many
areas with observed cracking on a series of transverse met.
sections different than those shown in Figures 4-13 and
4-14), Mag. 100X (bottom photo).
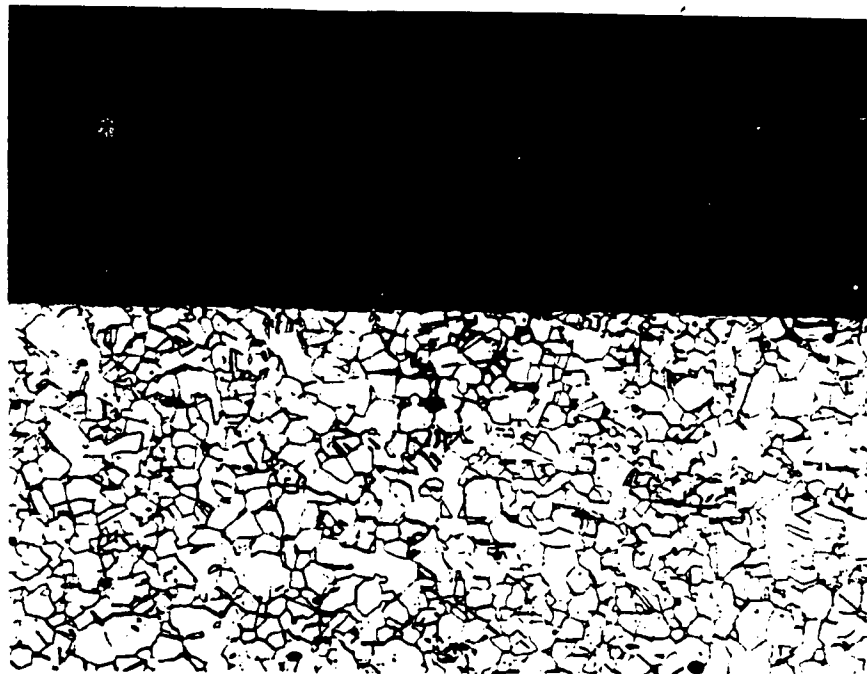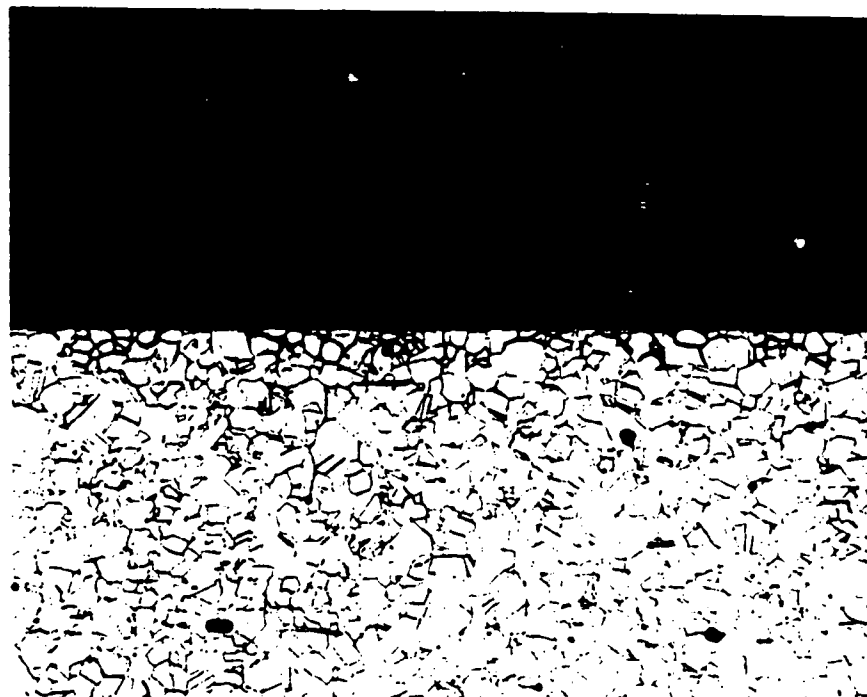
100X

100X

Figure 4-16   Tube R21-C58 from Plant D-2, first support plate region, longitudinal OD metallography, Mag. 100X.
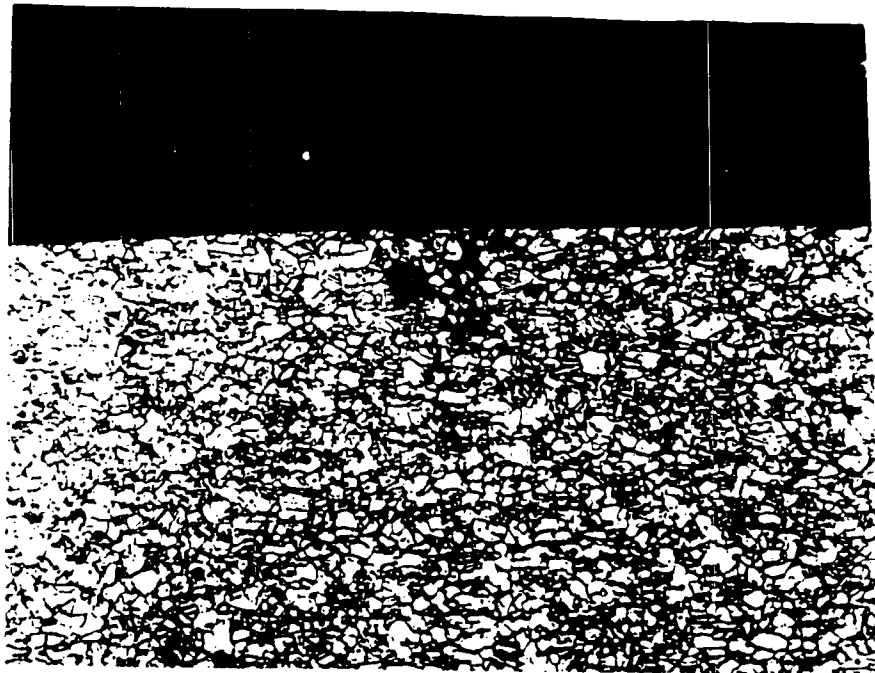
100X
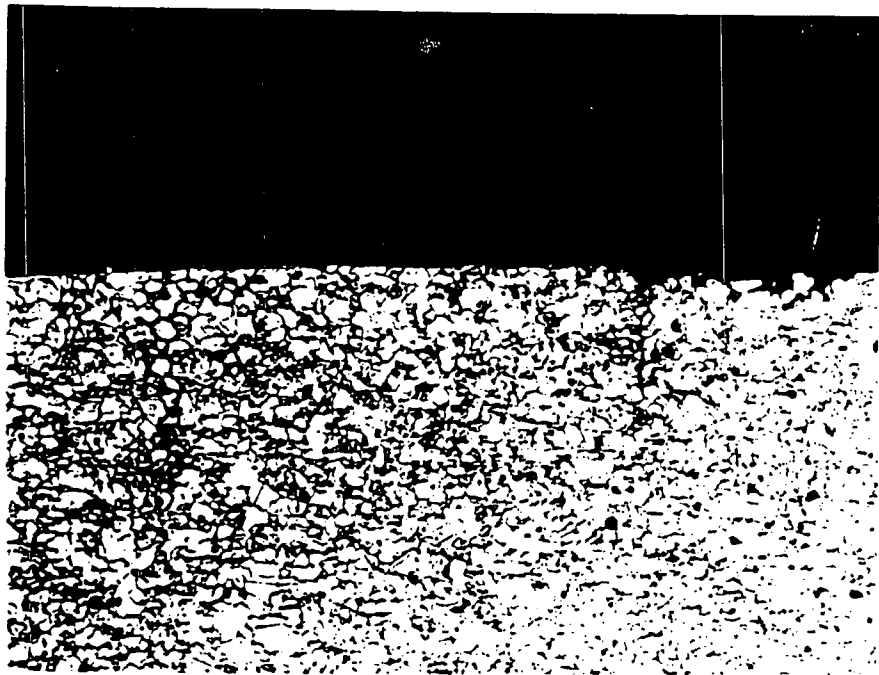
100X

Figure 4-17   Tube R16-C38 from Plant D-2 , first support plate region, transverse OD metallography, Mag. 100X.
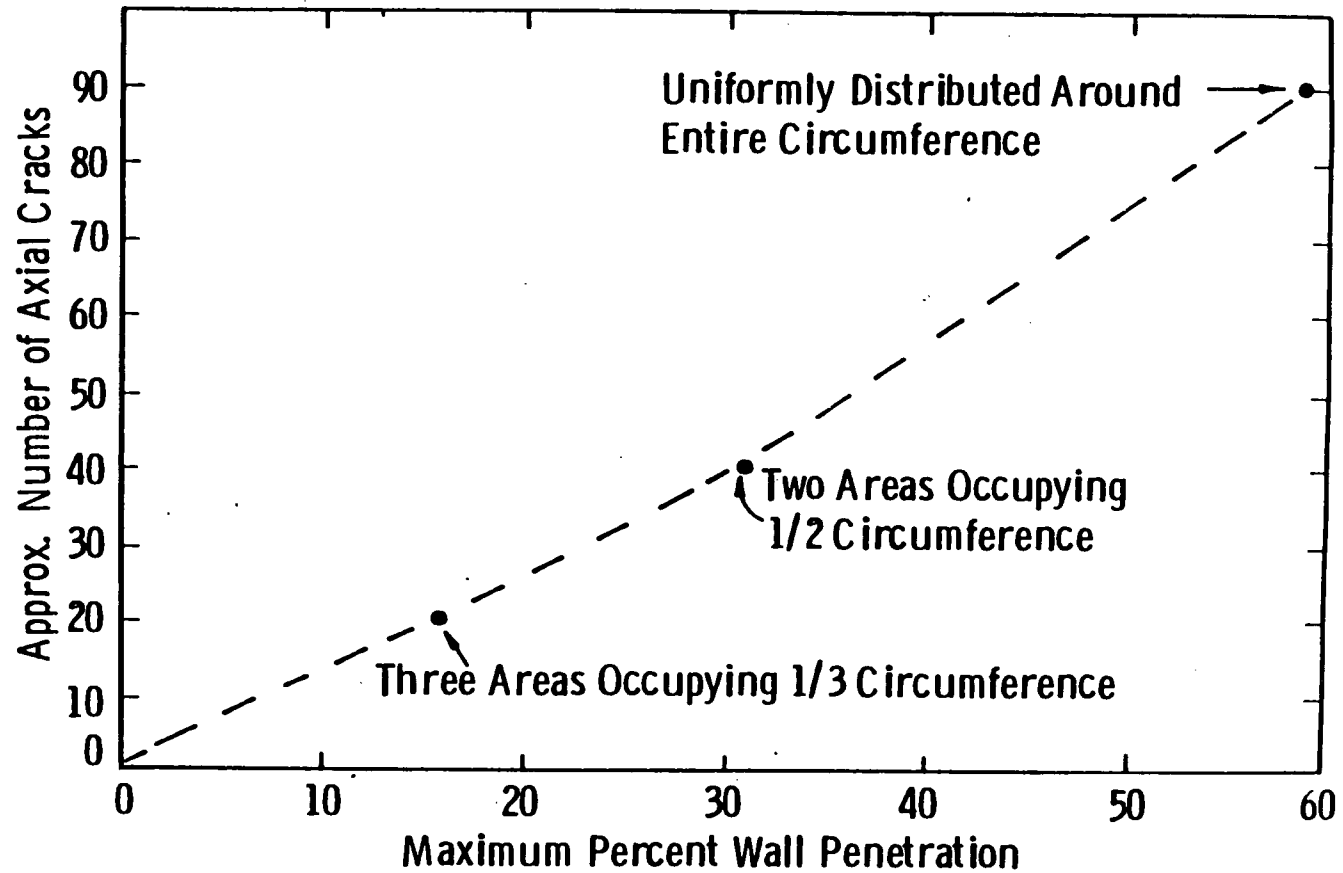
Figure 4-18   Plot of the number of cracks in a transverse plane versus maximum wall penetration for the first, second and third support plate region of tube R7-C38 from Plant D-2.
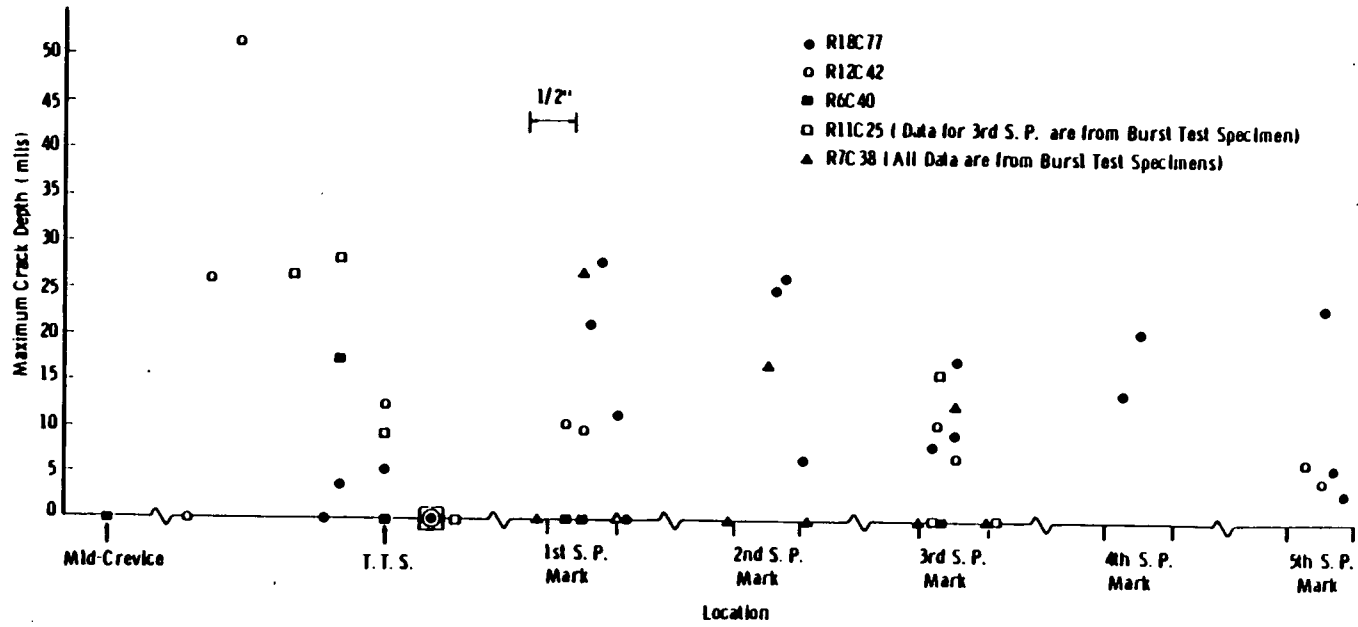
Figure 4-19   Maximum crack depth versus support plate elevation for steam generator tubes examined from Plant D-2.
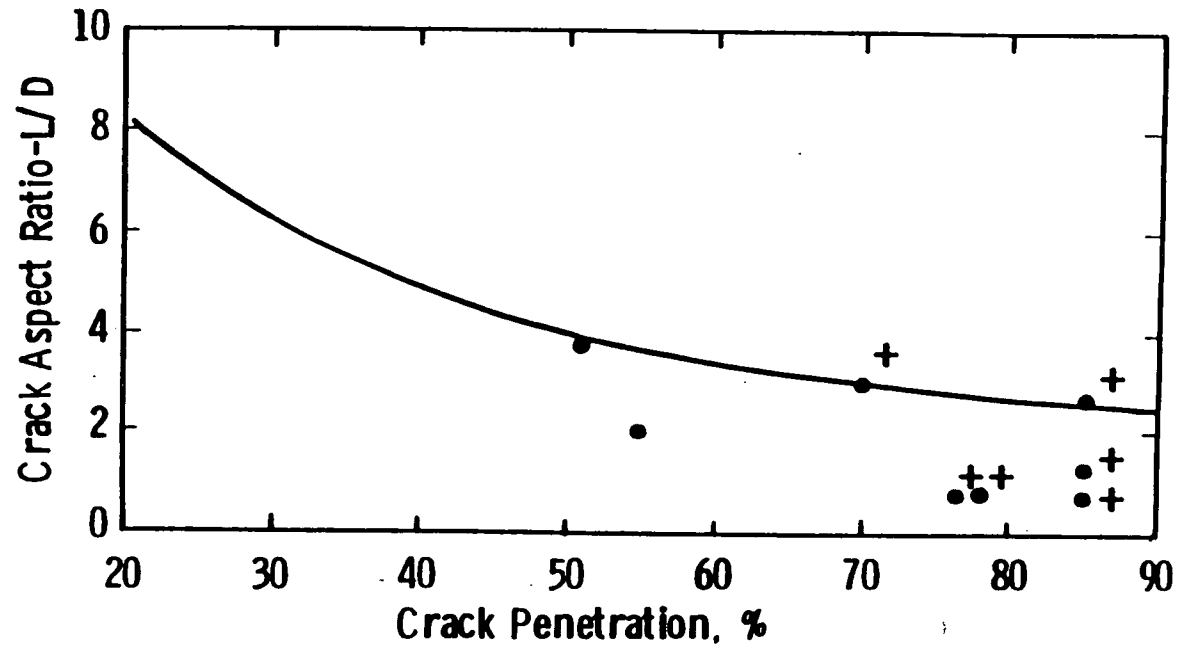
$^+$Appears to be 3 Cracks Which Linked Up Intergranularly

Figure 4-20   Plot of crack aspect ratios versus crack depth as measured
in Plant D-2 tuhe R12-C42.

Shear Ligament (L)

Case #1 : Aligned Cracks Linking
Head to Tail
('L'to L Spacing ~ Crack Length)

SCC #1   SCC #2

Shear Ligament (L)

SCC #1

Case #2: Parallel Cracks Linking
Head to Tail
(L to L Spacing ~ Crack Length)

SCC #2

SCC #1   Shear Ligament (L)

Case #3. Parallel Cracks Linking
Side to Side
(L to L Spacing < Crack Length)

SCC #2
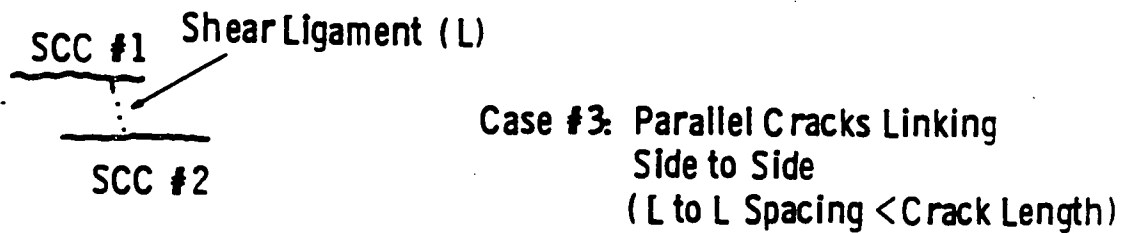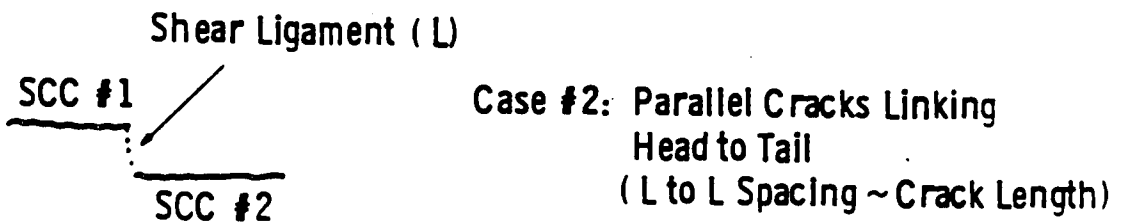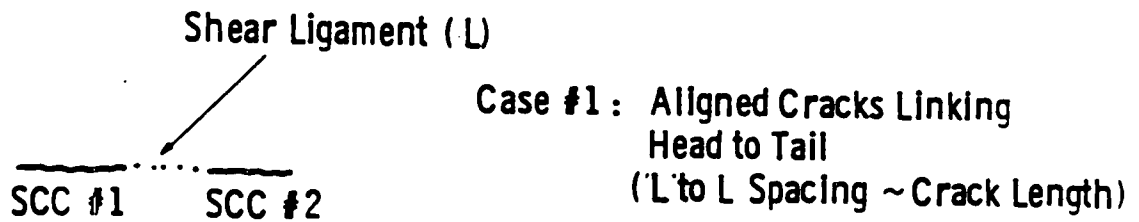
Figure 4-21   Sketch of the possible ways individual microcracks
interconnect by tensile tearing during a burst test.

4 - 62
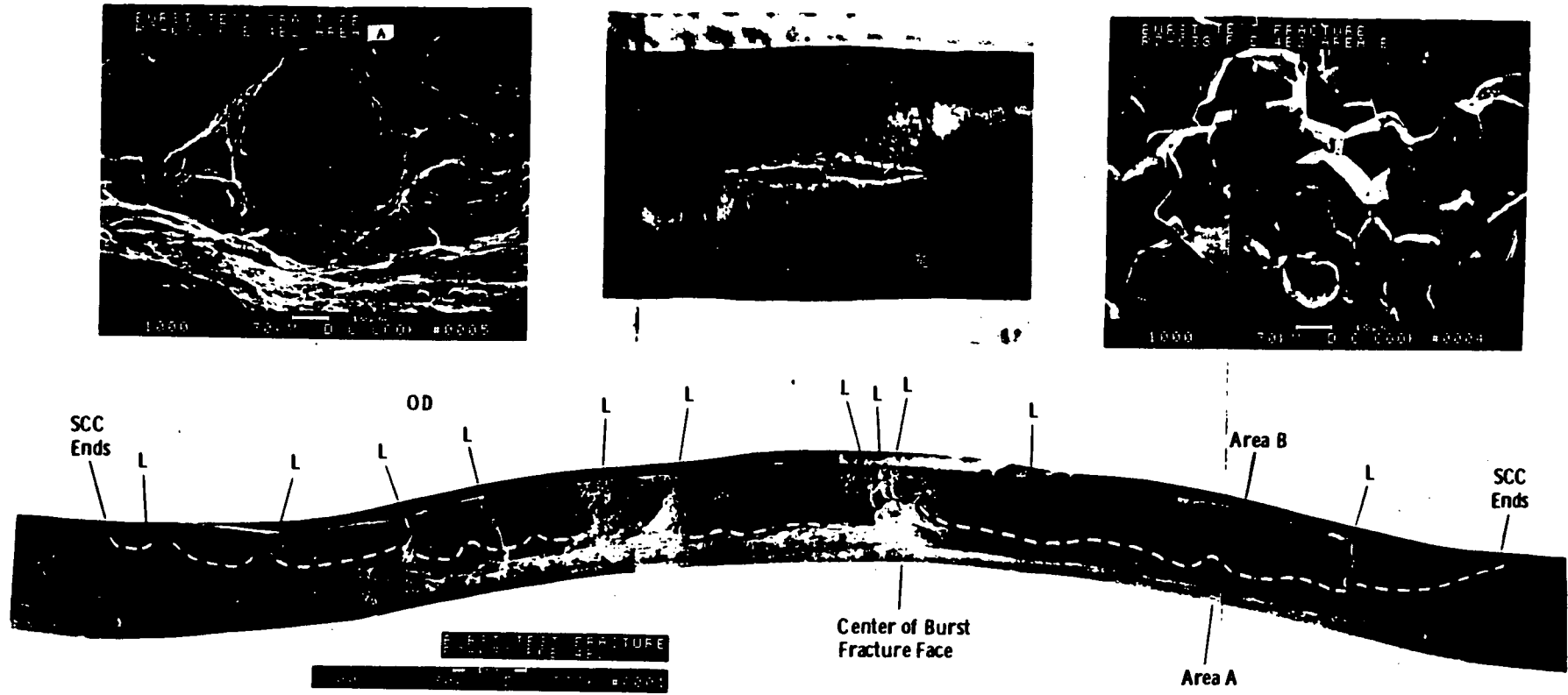
Figure 4-22 —SEM fractography of burst face of R7C 38, 1st support plate location. Top center photo shows burst face. Dotted line shows intergranular corrosion boundary in fractograph. "L" shows location of tensile torn ligament

0.010"
254 μm
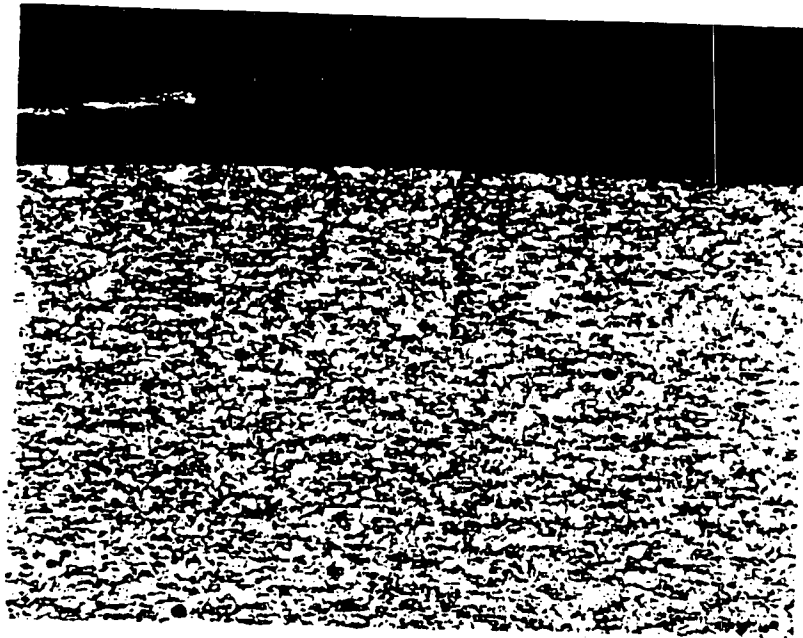
100 X

Figure 4-23   Tube R6-C40 from Plant D-2 , third support plate region,
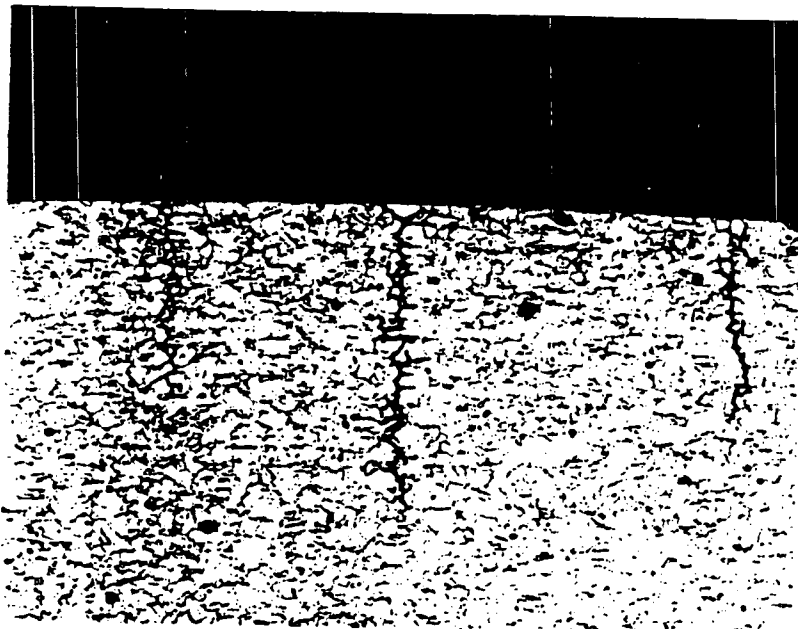transverse OD metallography, Mag. 100X.

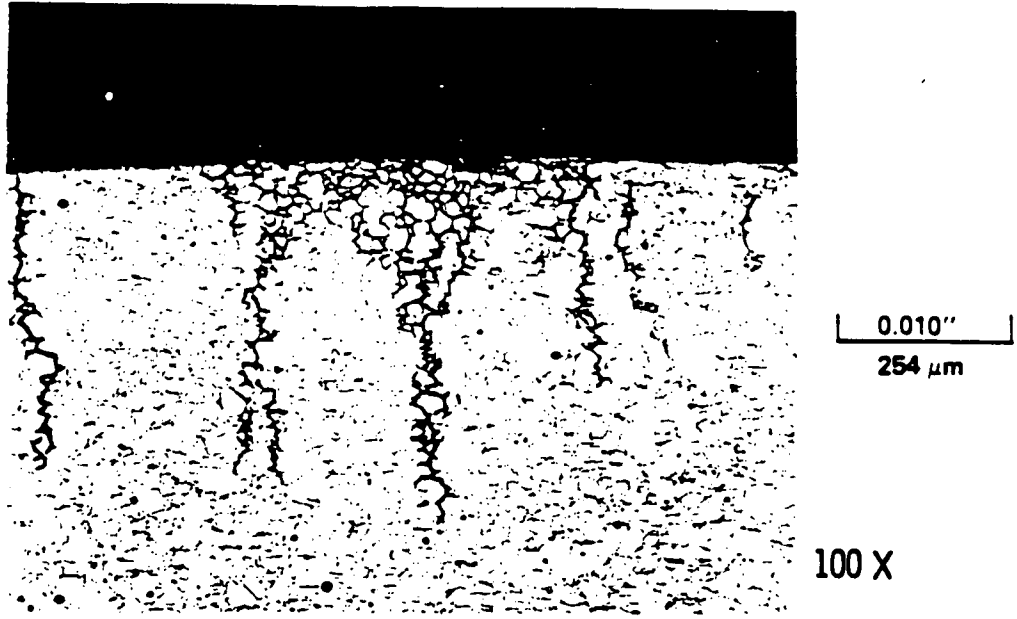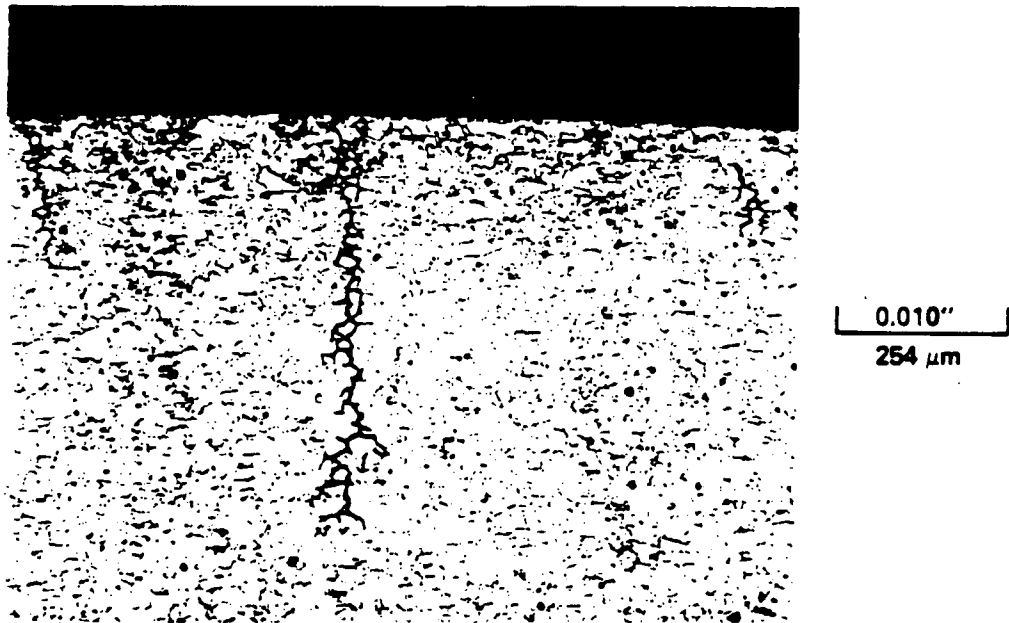(a) First Support Plate Crevice Region (Micro 1009, Photo D)
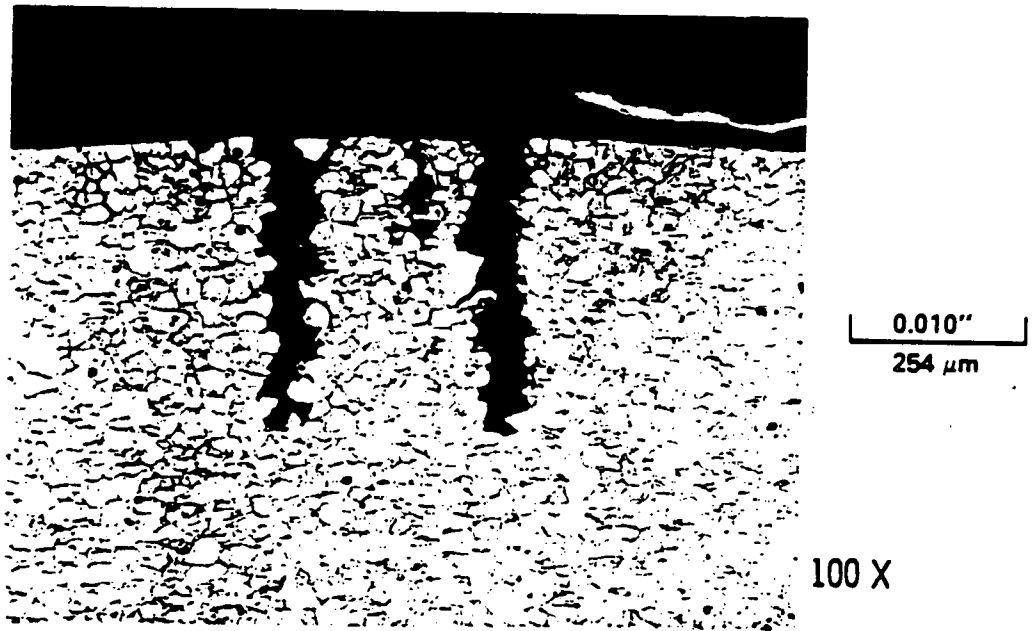
(b) Second Support Plate Crevice Region (Micro 1012, Photo B)

Figure 4-24   Tube R7-C38 from Plant D-2, first and second support plate regions, transverse OD metallography, Mag. 100X.
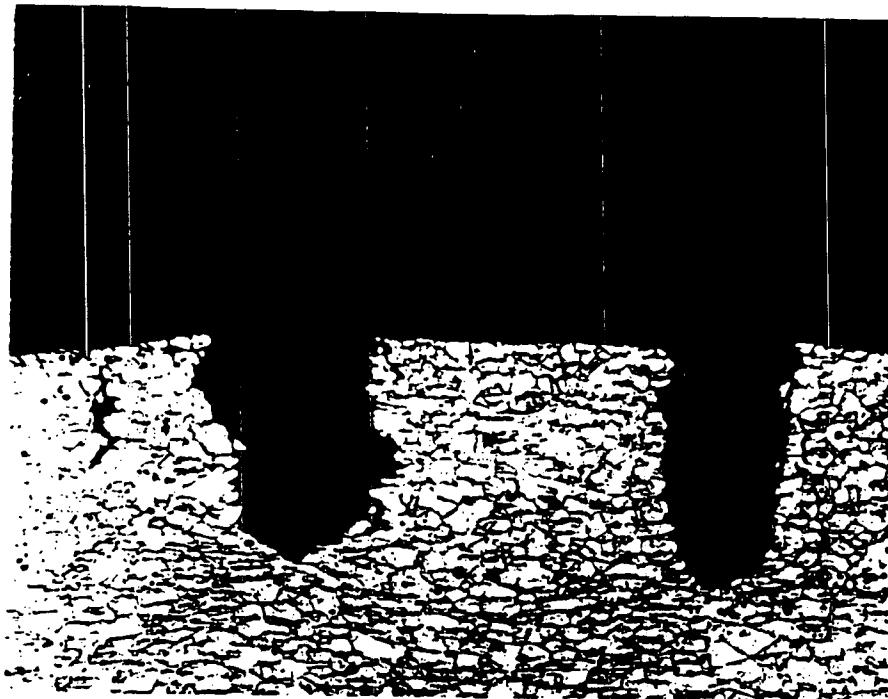
0.010"
254 μm

100 X

(c) Third Support Plate Crevice Region (Micro 1015,

Figure 4-25   Tube R7-C38 from Plant D-2, third support plate region,
transverse OD metallography, Mag. 100X.

4 - 66

0.010″
254 μm
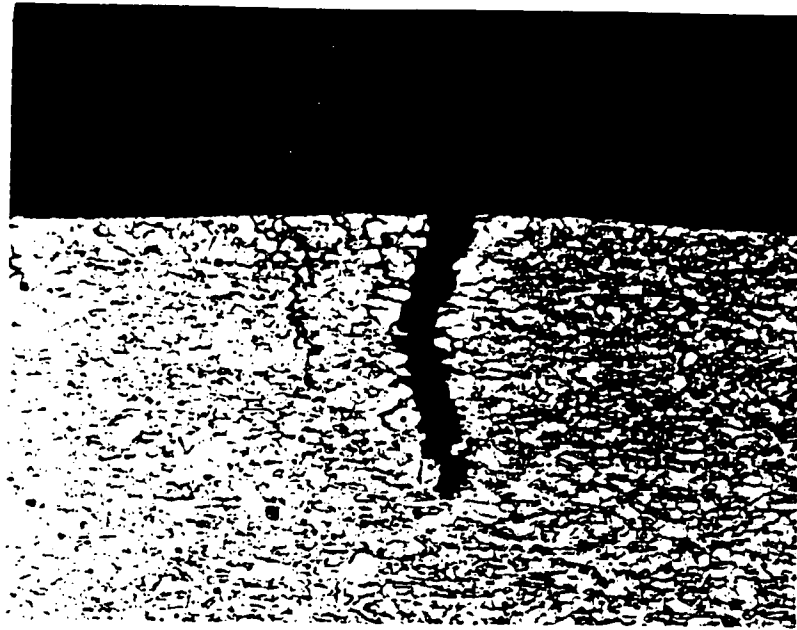
100 X

(b) Third Support Plate Crevice Region-Burst Test Specimen (Micro 1006, Photo D)

Figure 4-26   Tube R11-C25 from Plant D-2, third support plate region, transverse OD metallography, Mag. 100X.
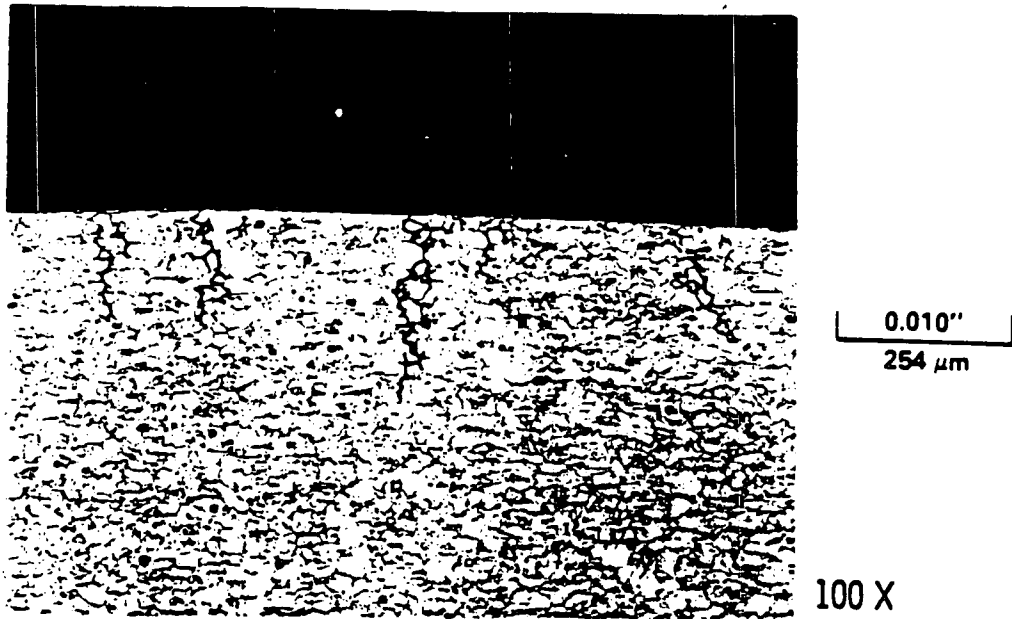
(b) First Support Plate Crevice Region (Micro 999, Photo B)
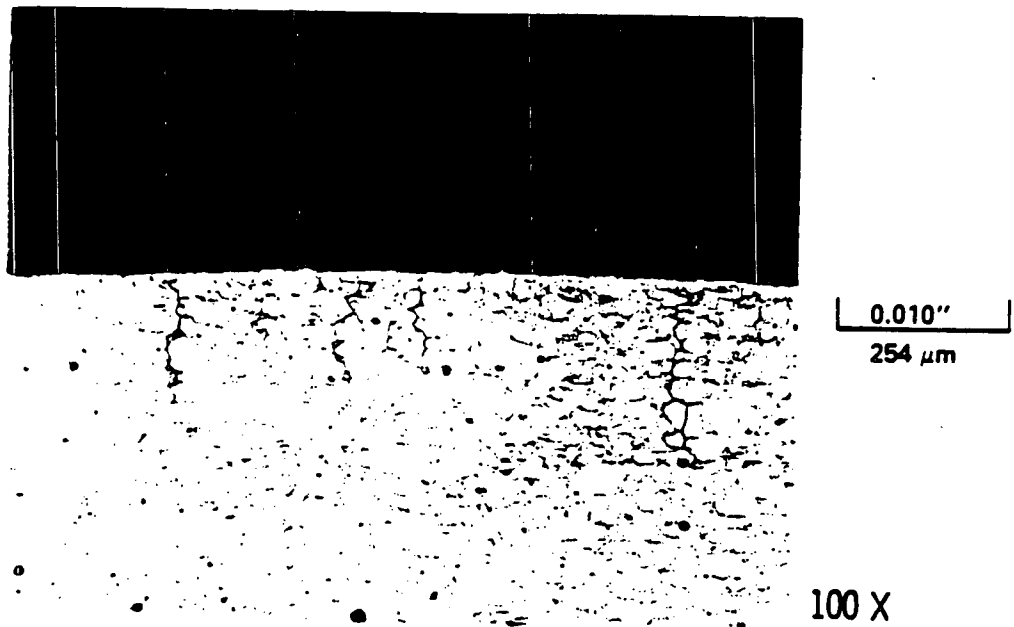
(c) Third Support Plate Crevice Region (Micro 997, Photo B)

Figure 4-27   Tube R12-C42 from Plant D-2, first and third support plate regions, transverse OD metallography, Mag. 100X.
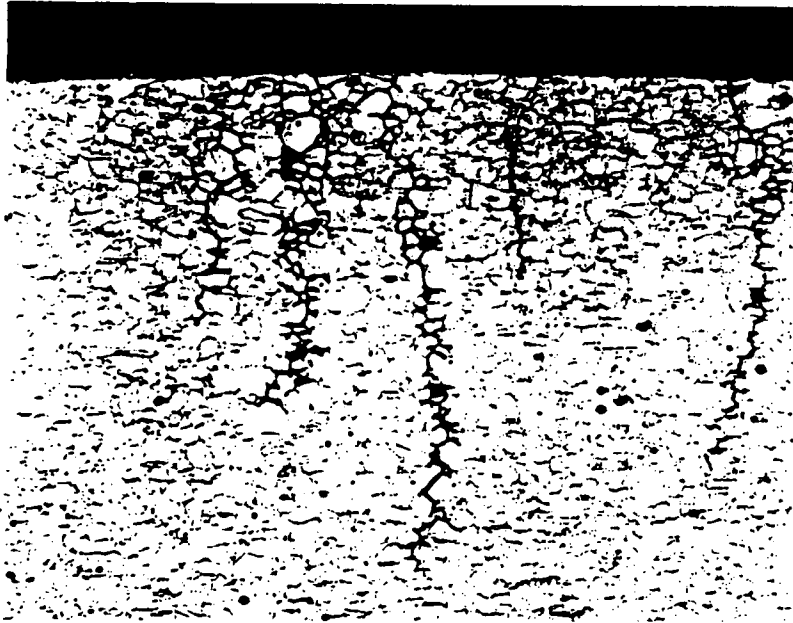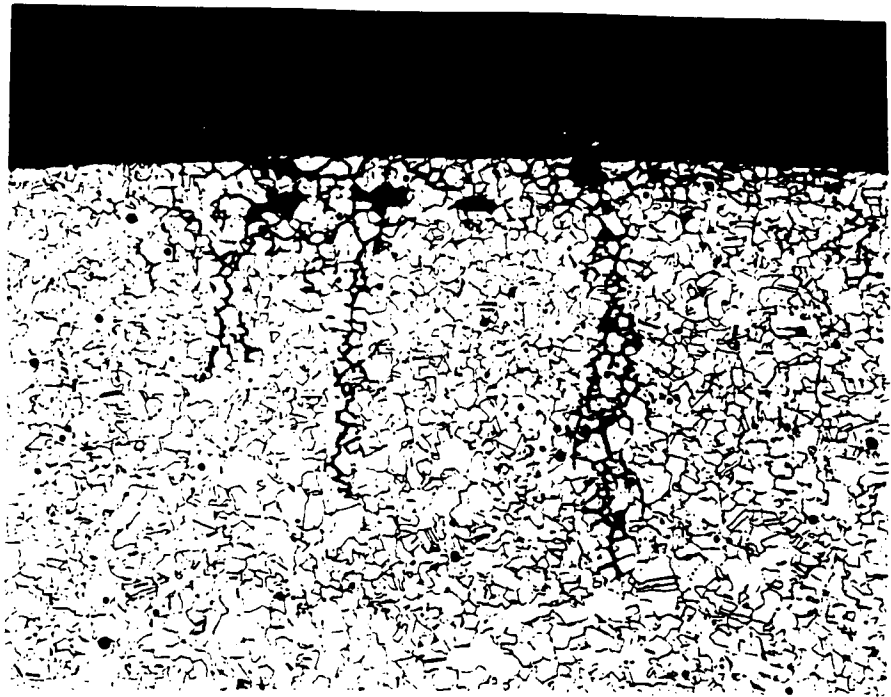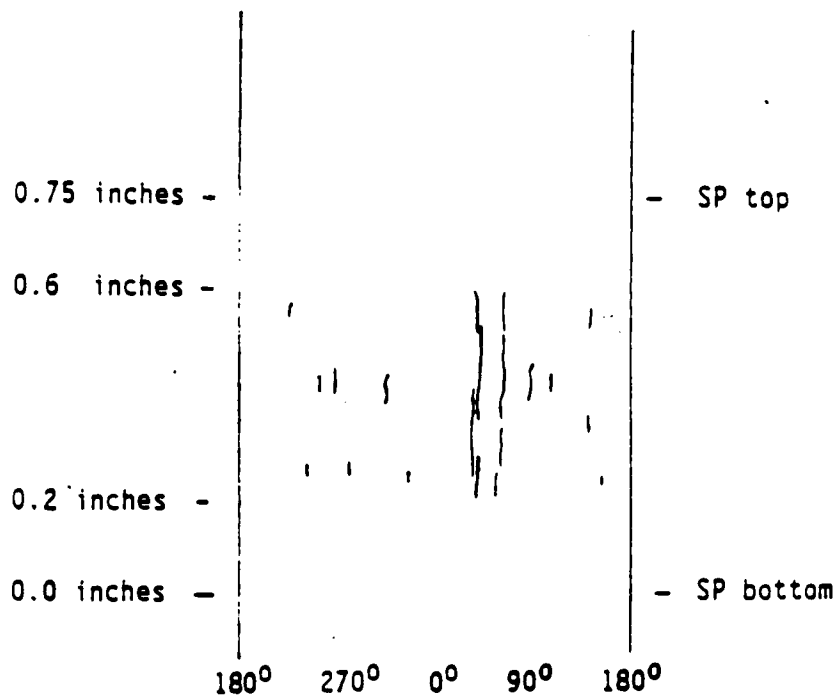
0.010"

254 μm

100 X

Figure 4-28   Tube R18-C77 from Plant D-2, first support plate region,
transverse OD metallography, Mag. 100X.

0.010″
254 μm

100 X

(d) Second Support Plate Crevice Region (Micro 979, Photo A)

0.010″
254 μm

100 X

(e) Third Support Plate Crevice Region (Micro 977, Photo C)

Figure 4 - 29   Tube R18-C77 from   Plant D-2, second and third support plate regions, transverse OD metallography, Mag. 100X.

0.010"
254 μm

100 X

(f) Fourth Support Plate Crevice Region (Micro 975,
Photo D)

0.010"
254 μm

(g) Fifth Support Plate Crevice Region (Micro 971,
Photo A)

Figure 4 - 30   Tube R18-C77 from Plant D-2, fourth and fifth support
plate regions, transverse OD metallography, Mag. 100X.

OD

:D
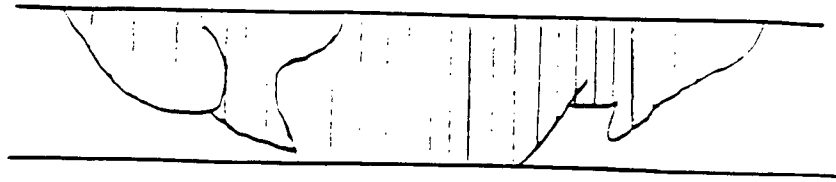
<u>Sketch of Burst Crack</u>

Macrocrack Length = 0.42 inches

Throughwall Length = 0.18 inches

Number of Microcracks = 4 (all ligaments with intergranular
features)

Morphology = Intergranular SCC with some IGA characteristics
(width of IGA 0.012 inches)

0.75 inches –   – SP top

0.6 inches –

0.2 inches –

0.0 inches –   – SP bottom

        180°   270°   0°   90°   180°

<u>Sketch of Crack Distribution</u>

Figure 4 - 31 Description of OD origin corrosion at the first support plate crevice
region of tube R4-C73.

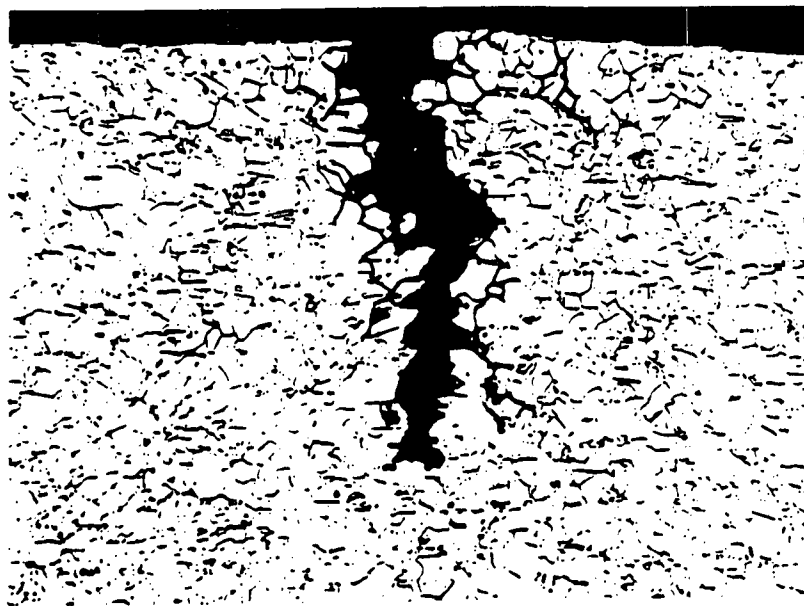4 - 72
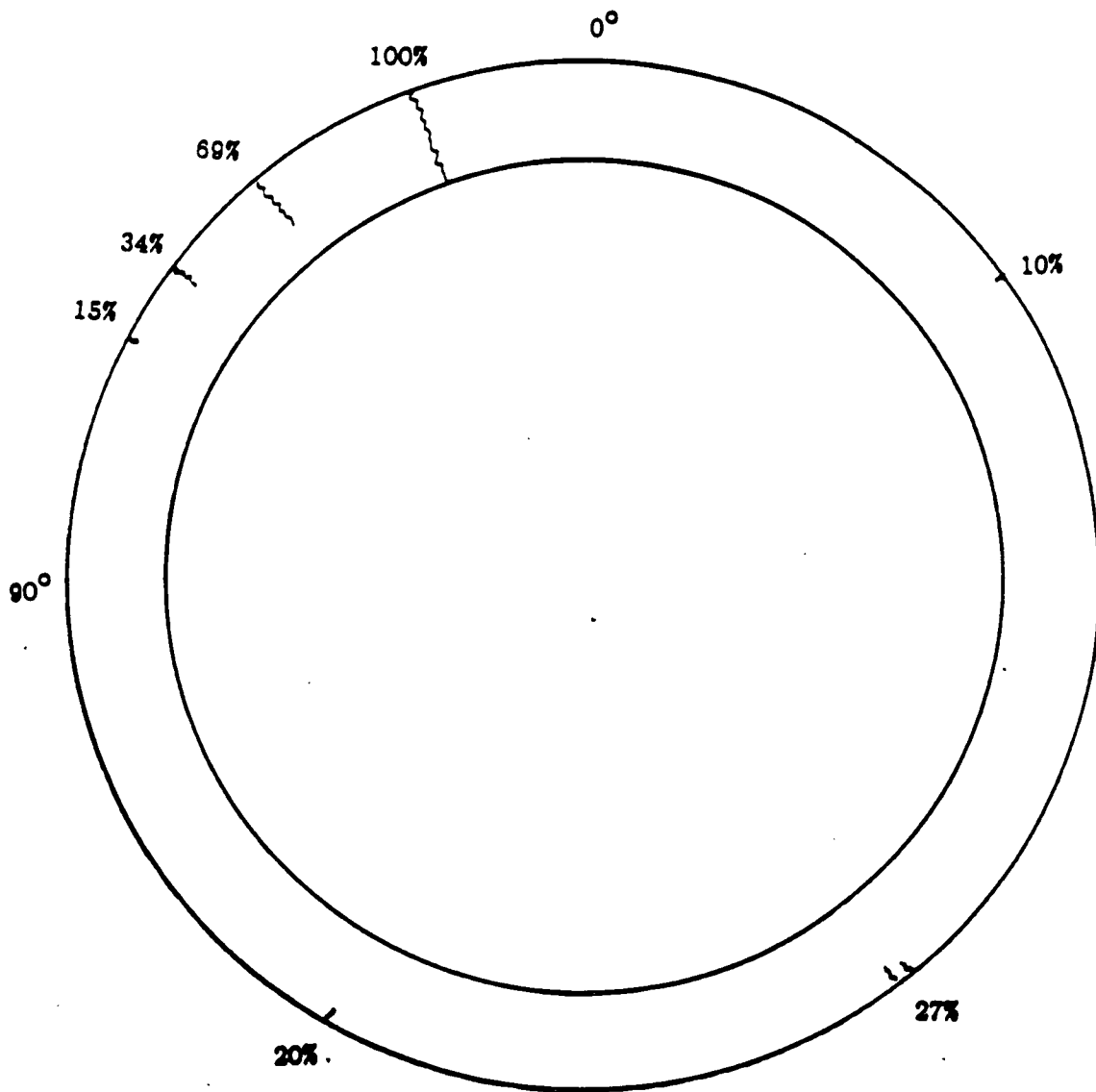
Figure 4 - 3 2 Sketch of crack distribution and depth within the center of the first support plate intersection in tube R4-C73.

Mag. 50X

Burst Opening Fracture
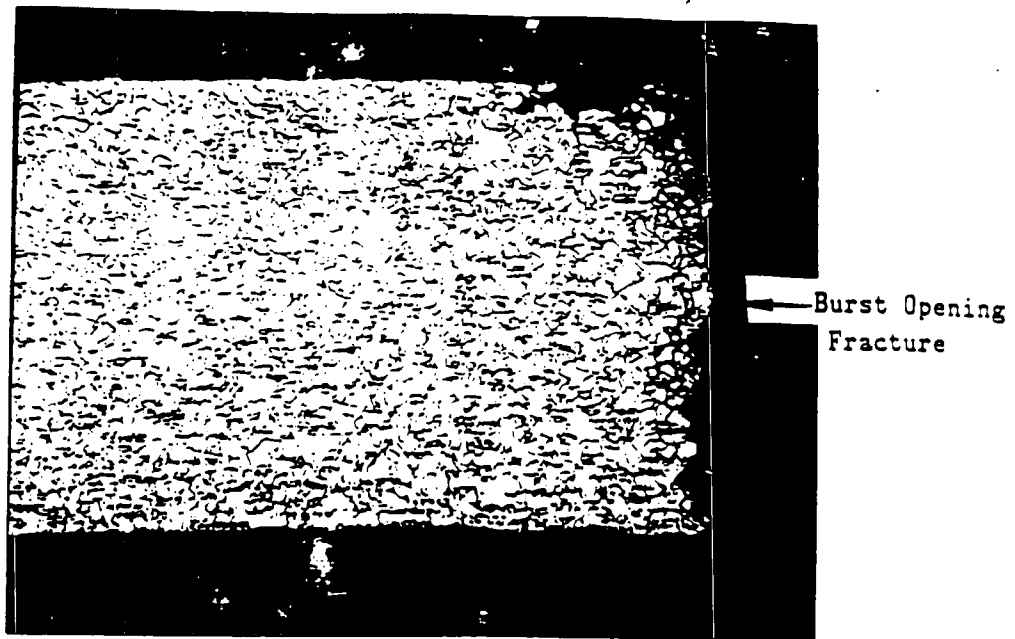
Mag. 100X

Figure 4 - 33 Top photomicrograph is from a transverse section through one half of the main burst crack. The crack morphology is that of IGSCC with some IGA characteristics (width of IGA is 0.006 inch on one side of the crack). Bottom micrograph is from a transverse section through a typical crack located near the burst crack. The morphology is that of IGSCC with only minor IGA characteristics. (Note: crack is opened wide by tube deformation).
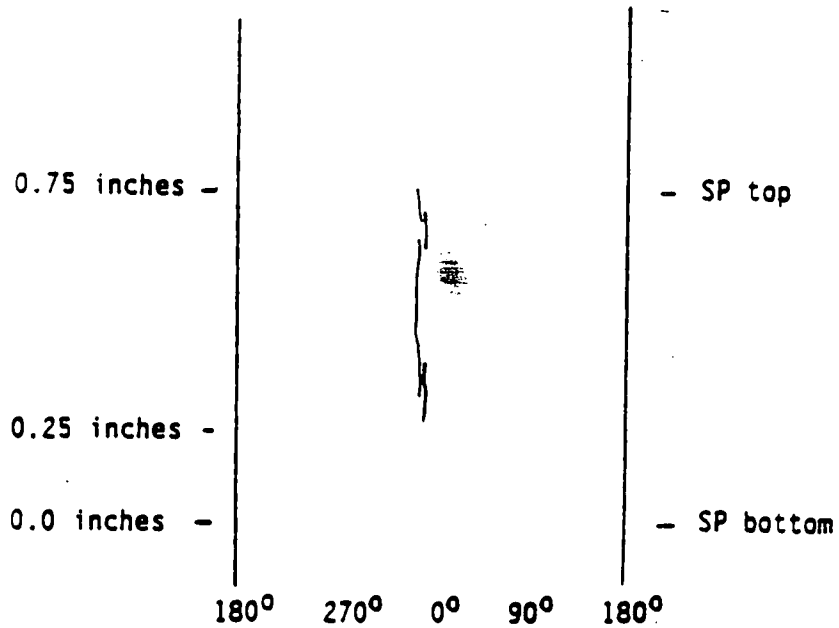
4 - 74

OD

CI
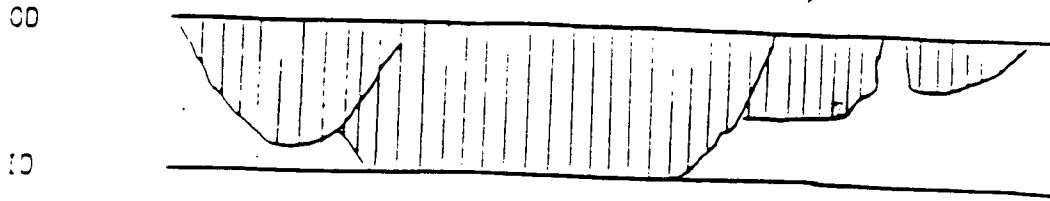
Sketch of Burst Crack

Macrocrack Length = 0.50 inches

Throughwall Length = 0.15 inches

Number of Microcracks = 4 (two ligaments with intergranular
features, one with ductile overload features)

Morphology = Intergranular SCC with significant IGA
characteristics (width of IGA 0.030 inches)

0.75 inches —		— SP top
0.25 inches -		
0.0 inches —		— SP bottom

180°   270°   0°   90°   180°

Sketch of Crack Distribution

Figure 4 - 34 Description of OD origin corrosion at the first support plate crevice
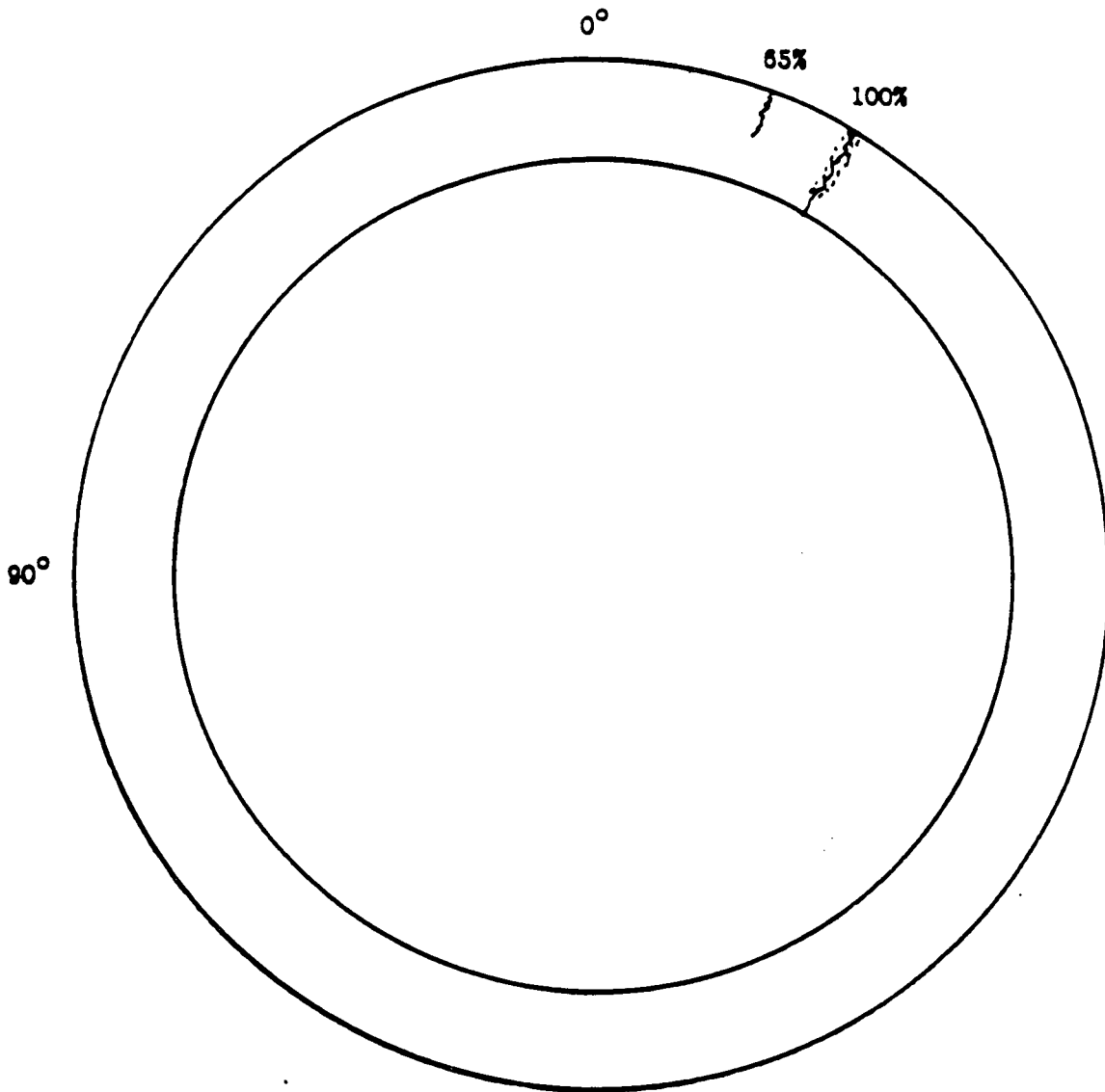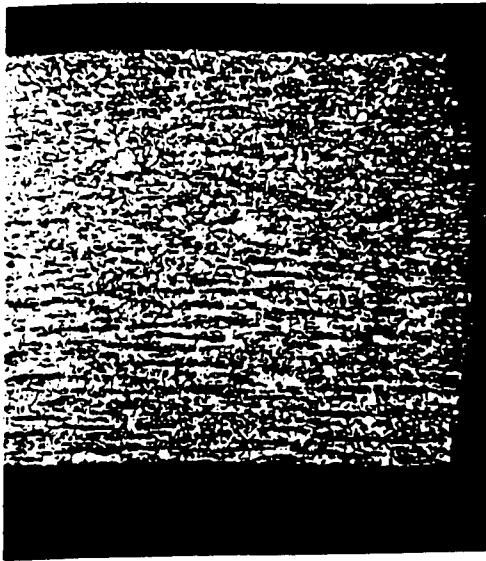region of tube R21-C22.

4 - 75

Figure 4 - 3 5 Sketch of crack distribution and depth within the first support plate crevice region in tube R21-C22.

Mag. 50X   Mag. 100X

Mag. 100X

Figure 4 - 36   Top micrographs are from a transverse section through one half of the main burst crack. The morphology is that of IGSCC with significant IGA characteristics (width of IGA is 0.015 inch on one side of the crack). Bottom micrograph is from a transverse section through the only other crack found in the crevice region. Its morphology is more that of IGSCC. (Note: crack has been opened wide by tube deformation).
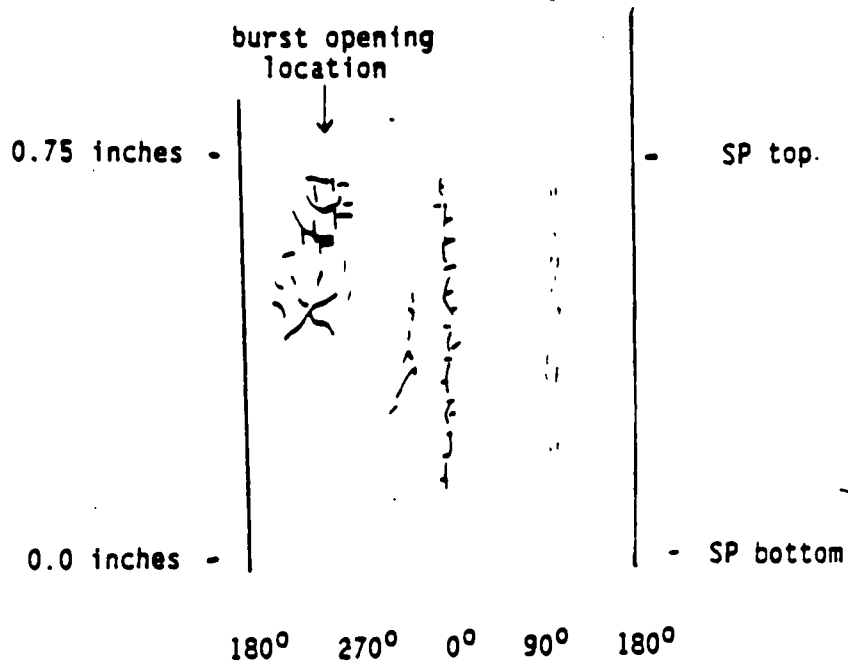
OD

IO
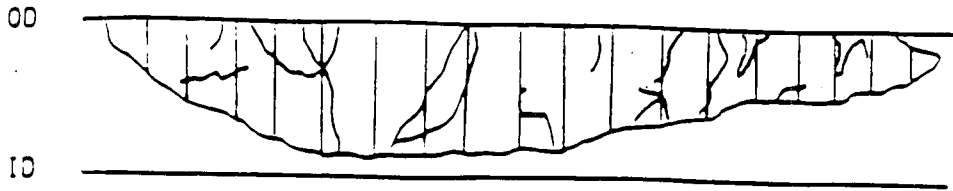
Sketch of Burst Crack

Macrocrack Length = 0.37 inches

Throughwall Length = 0 (78% throughwall)

Number of Microcracks = numerous (ligaments have intergranular features)

Morphology = Intergranular SCC with minor IGA features (Unusual spider-shaped crack distribution)

burst opening
location

0.75 inches -   - SP top.

0.0 inches -   - SP bottom

180°   270°   0°   90°   180°

Sketch of Crack Distribution

Figure 4 - 37   Description of OD origin corrosion at the first support plate crevice region cf tube R38-C46.
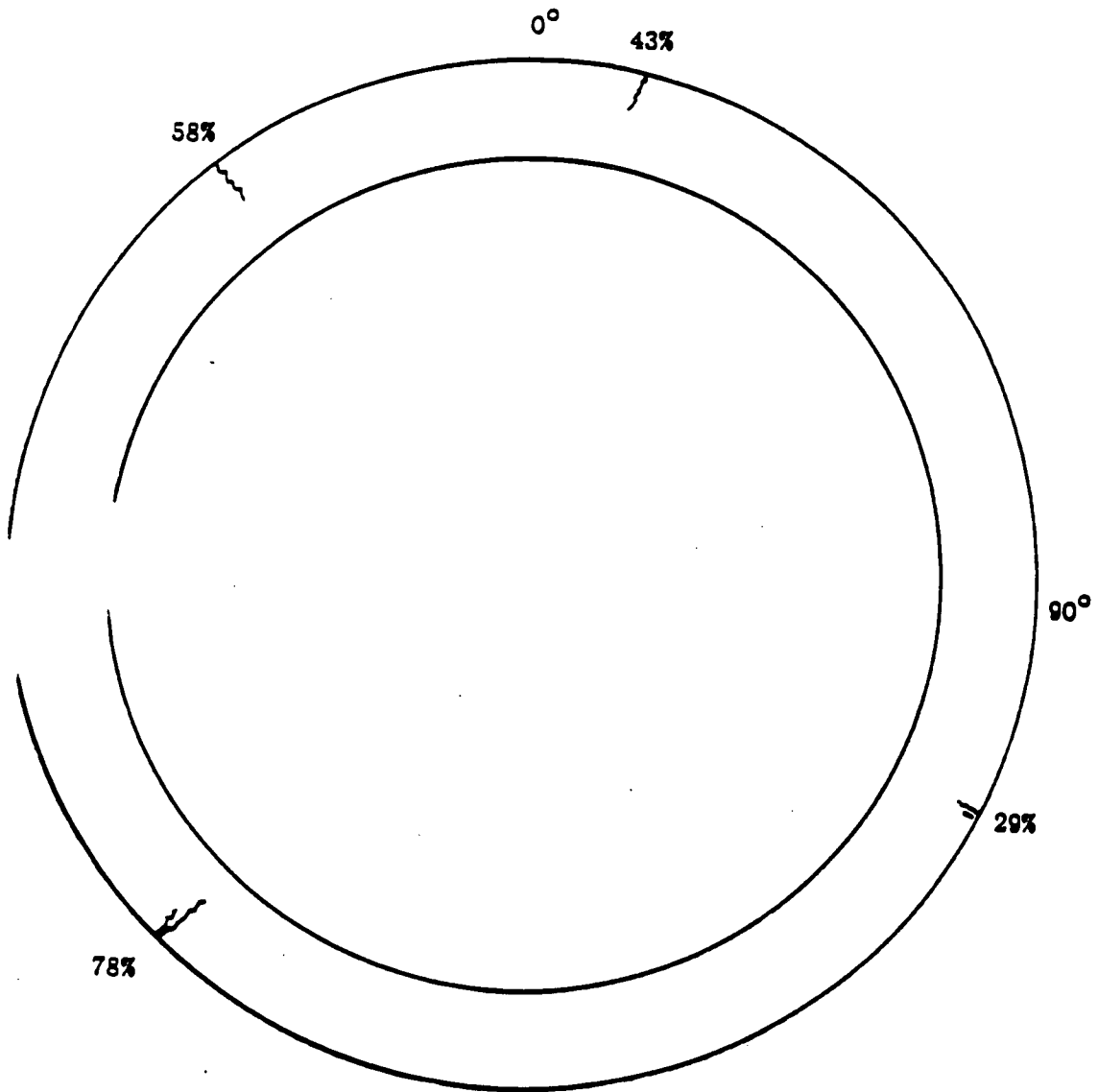
Figure 4 - 38 Summary of distribution and maximum depth of cracks found within the first support plate crevice region of tube R38-C46.
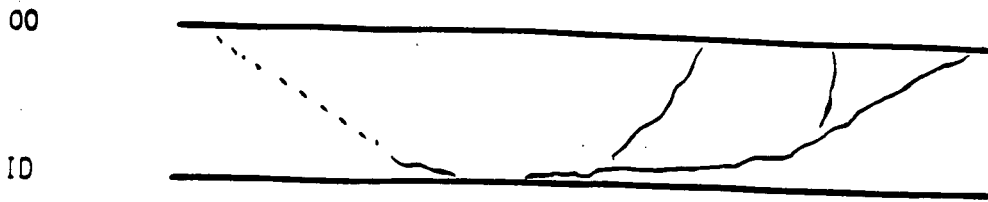
Area B

Area C

Figure 4 - 39 Photomicrographs of a transverse metallographic section through the first
support plate crevice region of tube R38-C46. The crack morphology is that
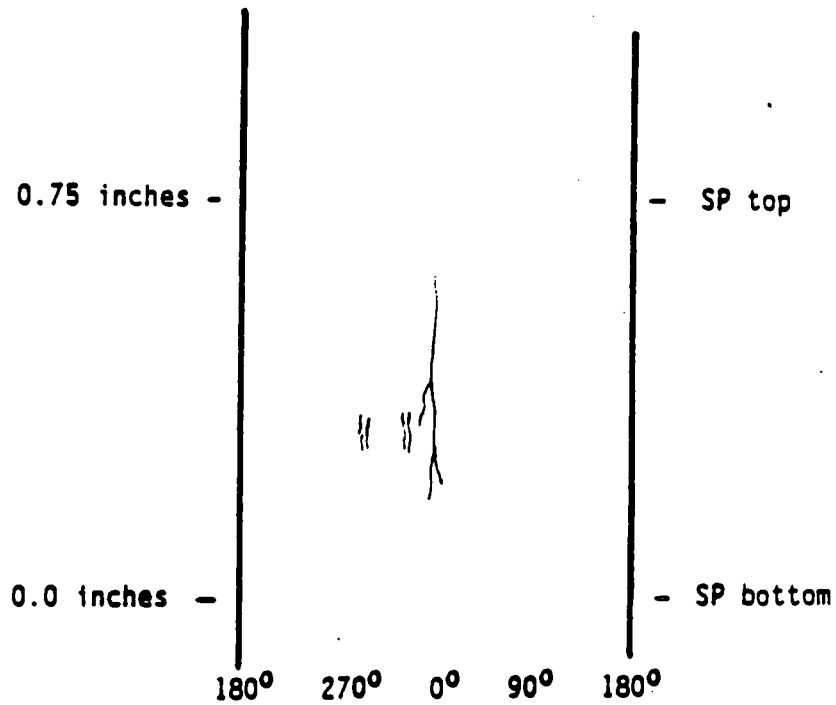of IGSCC with minor IGA characteristics. Mag. 100X.

OO

ID

Sketch of Burst Crack

Macrocrack Length = 0.52 inch

Throughwall Length = 0.02 inch

Number of Microcracks = at least 3

Morphology = IGSCC with moderate IGA components

0.75 inches –   – SP top

0.0 inches –   – SP bottom

180°   270°   0°   90°   180°

Sketch of Crack Distribution

Figure 4 - 4 0   Summary of crack distribution and morphology observed on the first support plate crevice region of tube R31-C46.

46%

22%

22%

OD Surface

0.010"

254 um

ID Surface
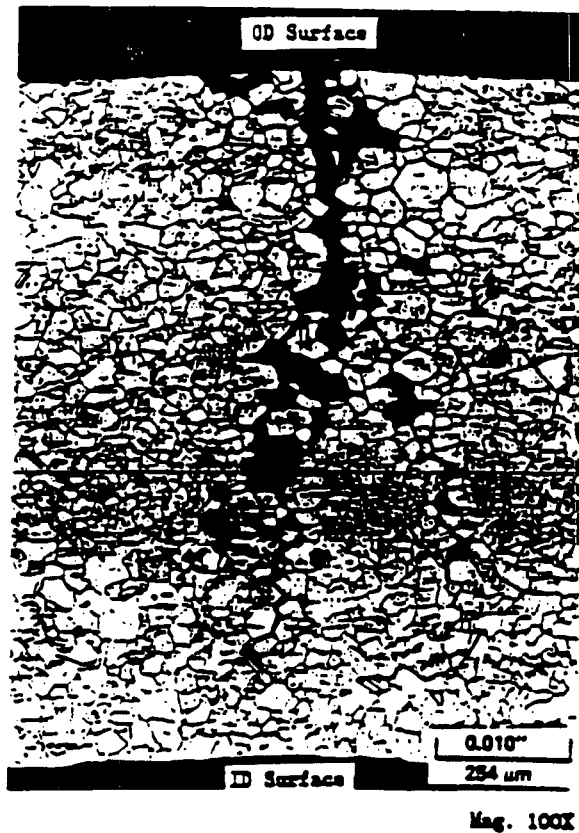
Mag. 100X
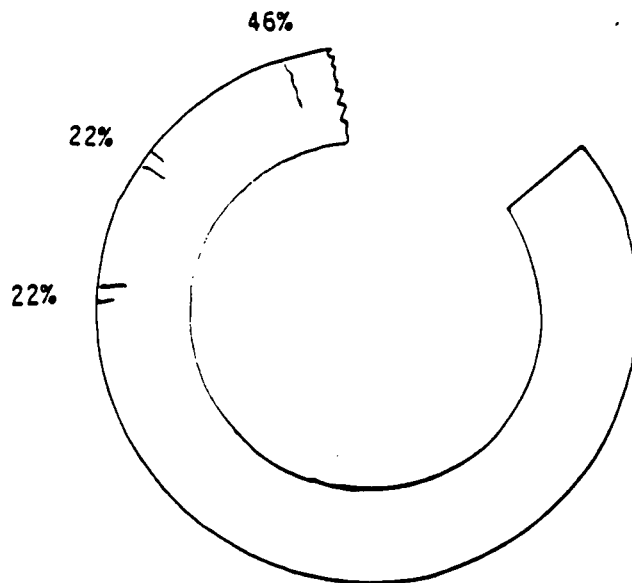
Figure 4 - 41 Secondary crack distribution and a photomicrograph of one of the cracks in a transverse metallographic section of the first support plate crevice region of tube R31-C46. The crack morphology is that of IGSCC with moderate IGA components.
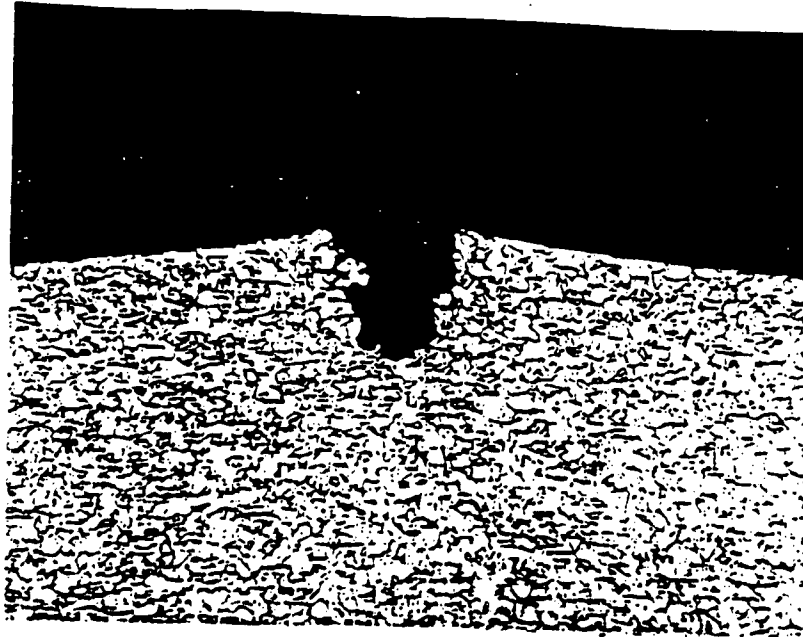
Figure 4 - 42   Cracks at the OD surface of tube R16-C50 at the first tube
                 support plate crevice. Mag. 100X.

H

I

J

Figure 4 - 43 Photomicrographs of a transverse section from the first support plate
crevice region of tube R16-C53. Mag. 100X.
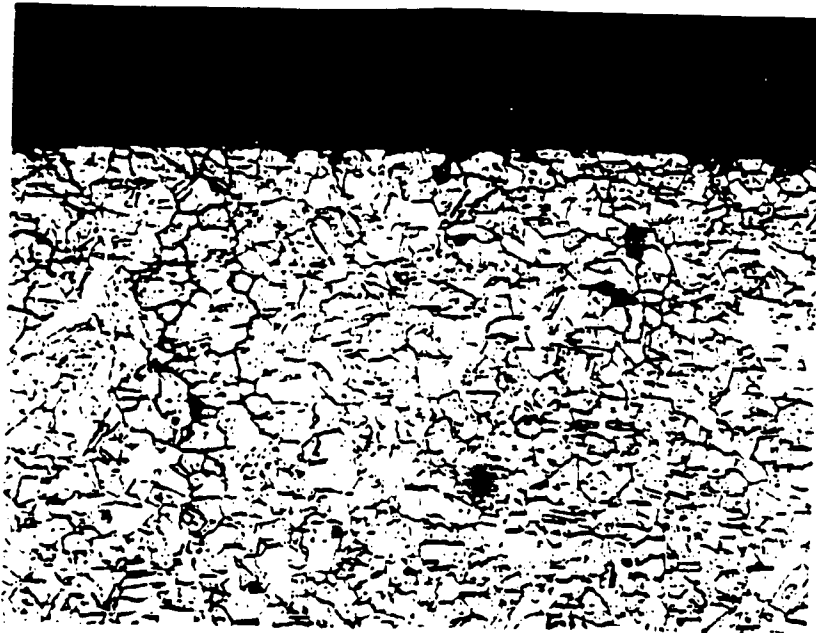
F

G

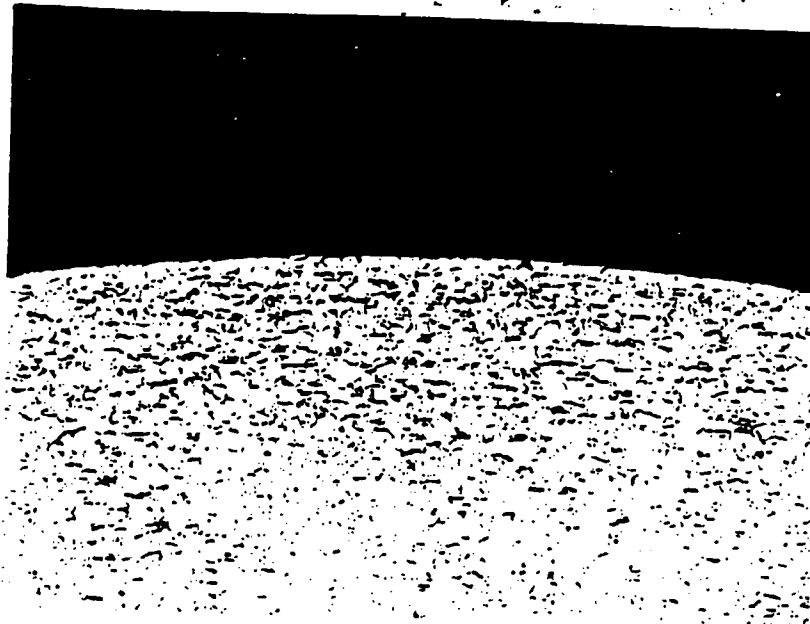Figure 4 - 4 4   Additional micrographs from the same transverse section shown in
Figure 4-43 tube R16-C53. Mag. 100X.

	Max Depth Near 90° (% Throughwall)	Max Depth Near 270° (%)
Minor OD Axial Cracks	< 10	
SP Top	10	7
	42	22
		47
		62
	32	45
		50
		52
SP Bottom	25	40
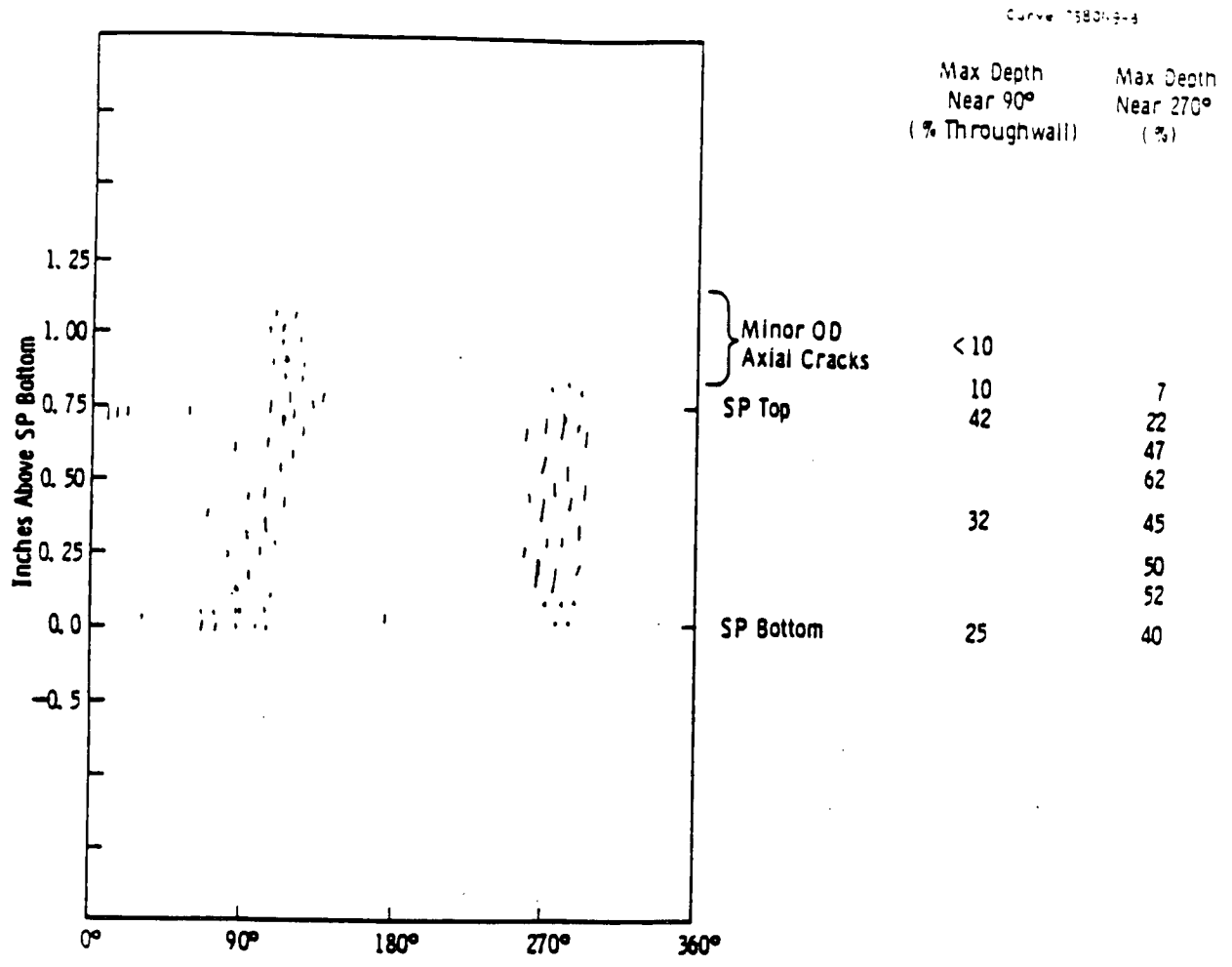
Figure 4 - 4 5   Crack network location at first support plate region on tube R20-C26 HL.

4 - 86

Figure 4 - 46 Transverse metallographic section through tube R20-C26 HL at the mid-point of the first support plate crevice region (90° deformed half) with crack details in Areas A and B.
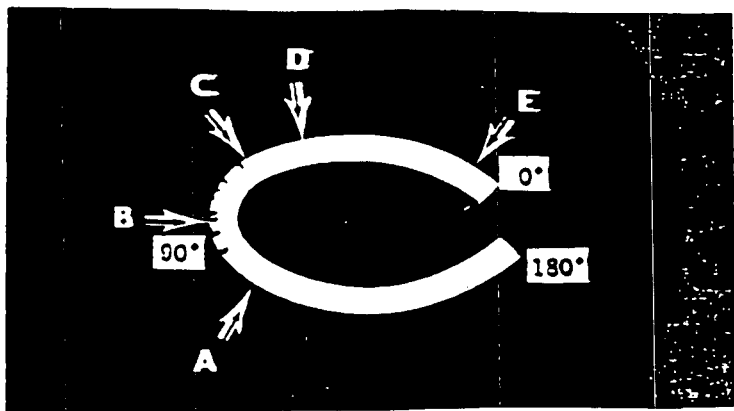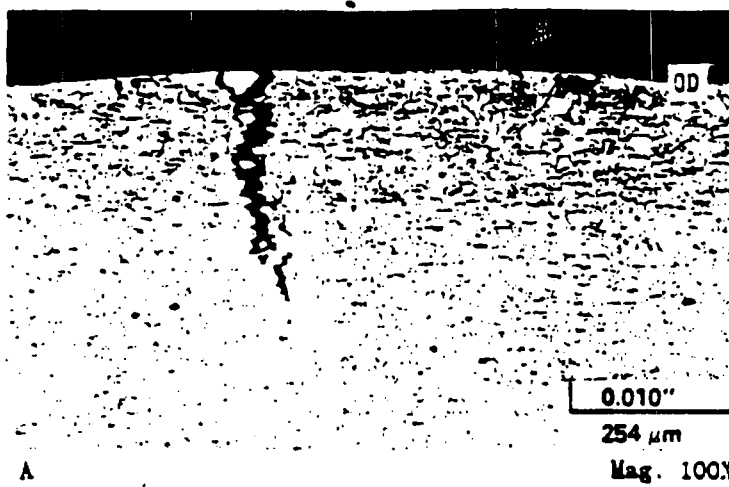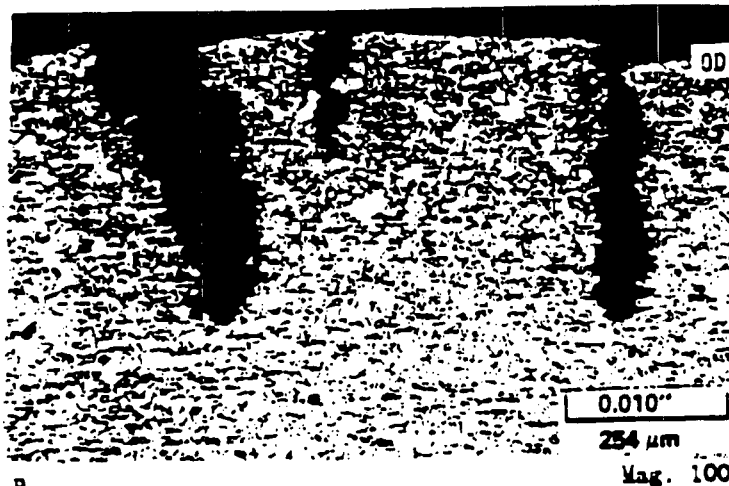
Figure 4 - 4 7   Transverse metallographic section through Plant A tube R20-C26 HL
at the first support plate crevice region (90° deformed half) below the
support plate crevice top with crack details in Areas A and B.
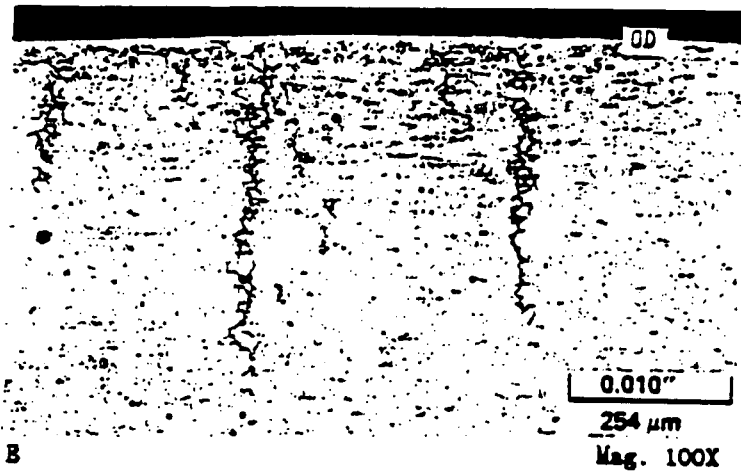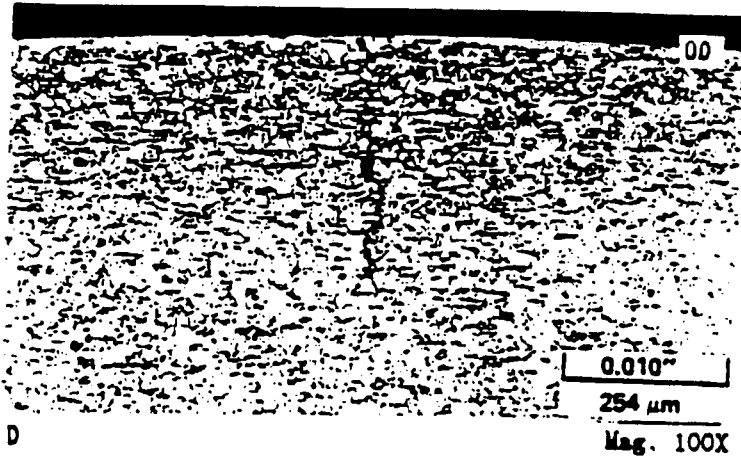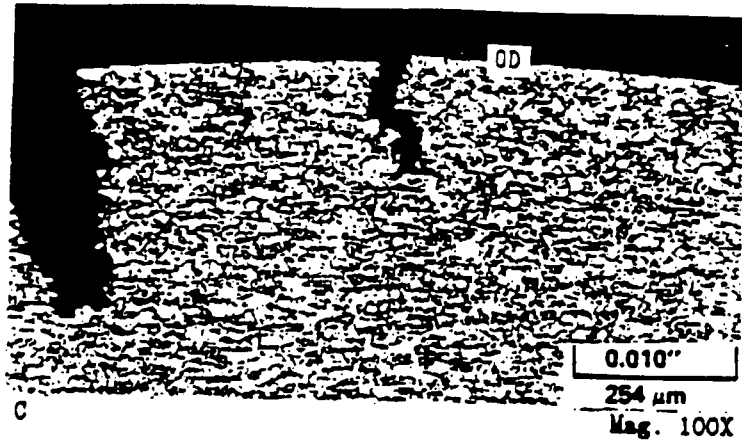
Figure 4 - 4 8   Crack details in Areas C, D, and E of metallographic cross section shown in previous figure, tube R20-C26 HL, Plant A.
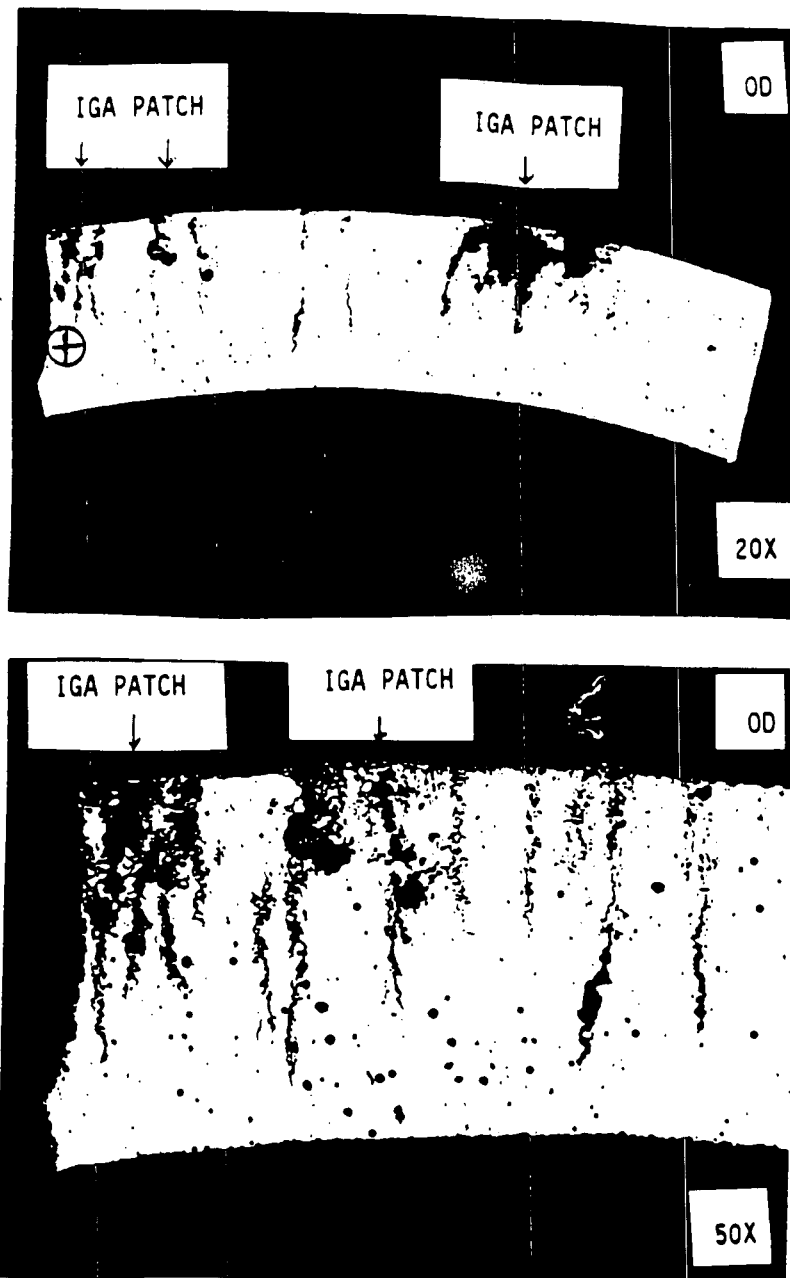
Figure 4 - 49   Transverse optical micrographs obtained just below the circumferential
fracture at the canter of the support plate. The circumferential location is
that where the deepest corrosion was found. The deepest axial IGSCC is 85%
through wall and three IGA patches are observed: one 43% through wall and
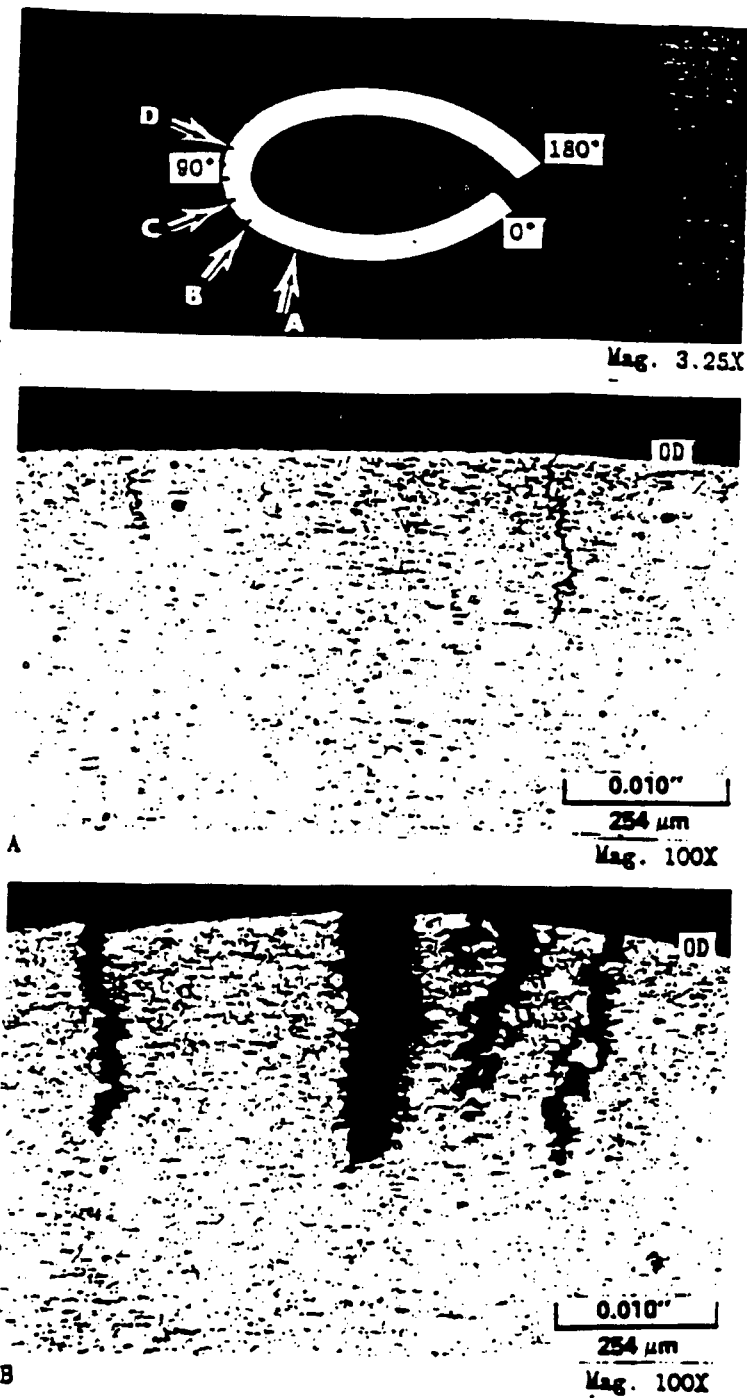0.015 inch long, one 33% through wall and 0.05 inch long, and one 28%
through wall and 0.015 inch long. The axial IGSCC had IGA aspects to
individual cracks. These aspects can be characterized by ratios comparing
the crack length (depth from OD surface) to IGA width at the mid-crack
location. L/W ratios vary from 6 to 18. Plant L, R12C8
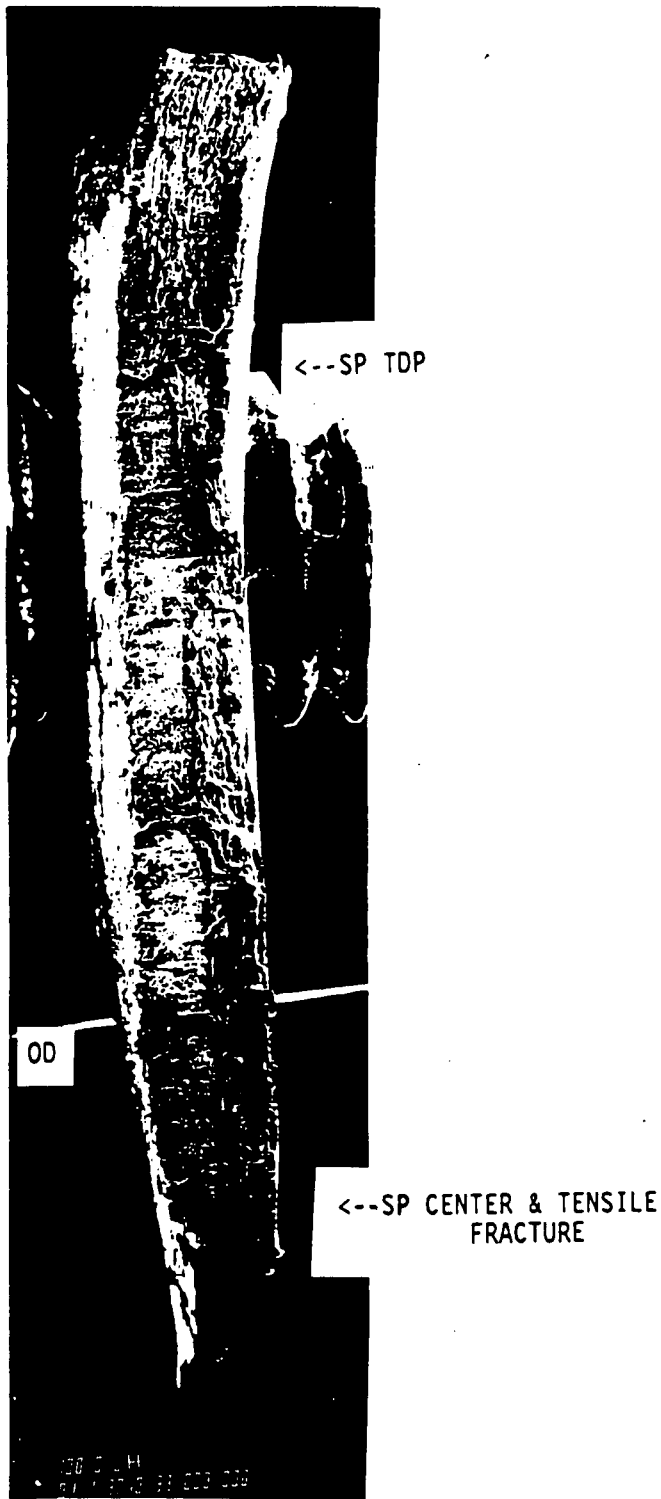
Figure 4 - 50 SEM photograph of axial fracture face from the first support plate center region to just above the top edge at a region believed to have the deepest corrosion. OD intergranular corrosion was observed continuously within the crevice region. Ledges were clearly observed separating individual microcracks. The depth of corrosion ranged from 41% through wall at the top edge of the crevice to 55% through wall 0.1 inch below the top edge of the crevice.
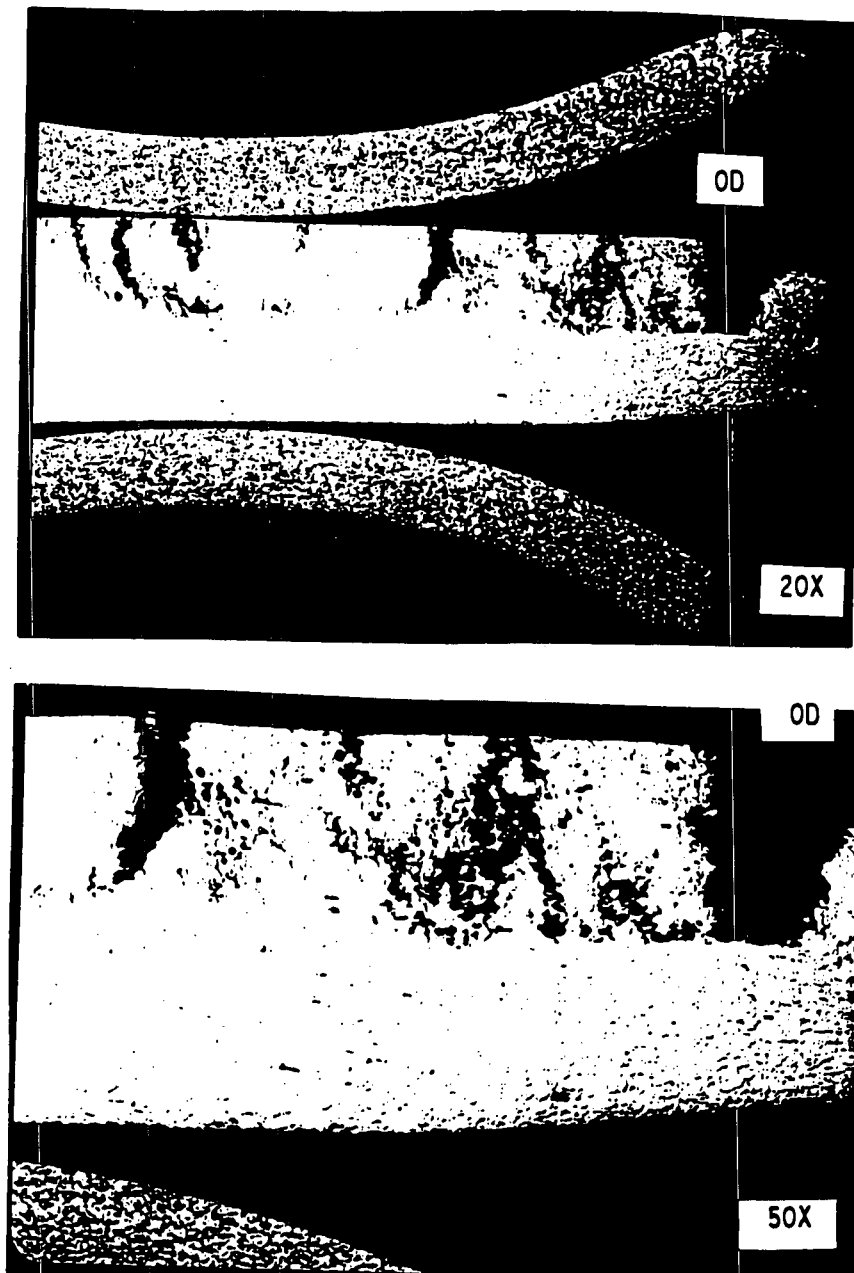
Figure 4 - 51 Axial optical micrographs obtained from the center of the support plate crevice region to the bottom edge of the crevice at a location where the deepest corrosion is believed to exist. A uniform corrosion front, approaching half way through wall, is observed within the crevice region. The section is believed to cut through a region composed of numerous axial microcracks.

4 Mils Deep

11 Mils Deep

Axial Direction
-------------------->

21 Mils Deep

Mag. 11.5X
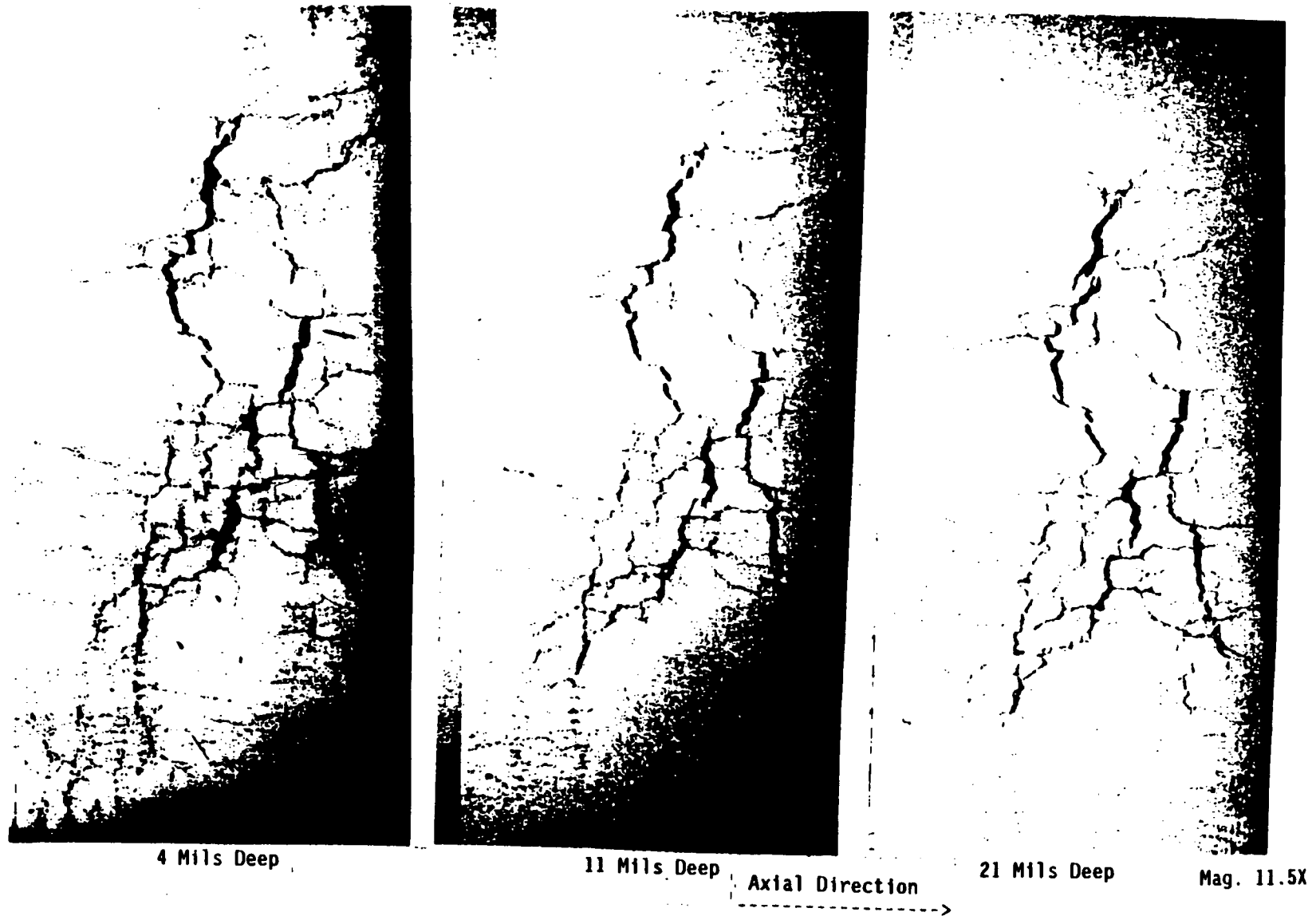
Figure 4 - 52   Photomicrographs of radial metallography performed on a region with
axial and circumferential degradation on tube R16-C74, support
plate 1. Cellular IGA was found with little change in the cell
shape and cell wall thickness at depths of 4, 11 and 21 mils below
the OD surface. Note that the cut section was flattened,
preferentially opening the circumferential wall of the cells.
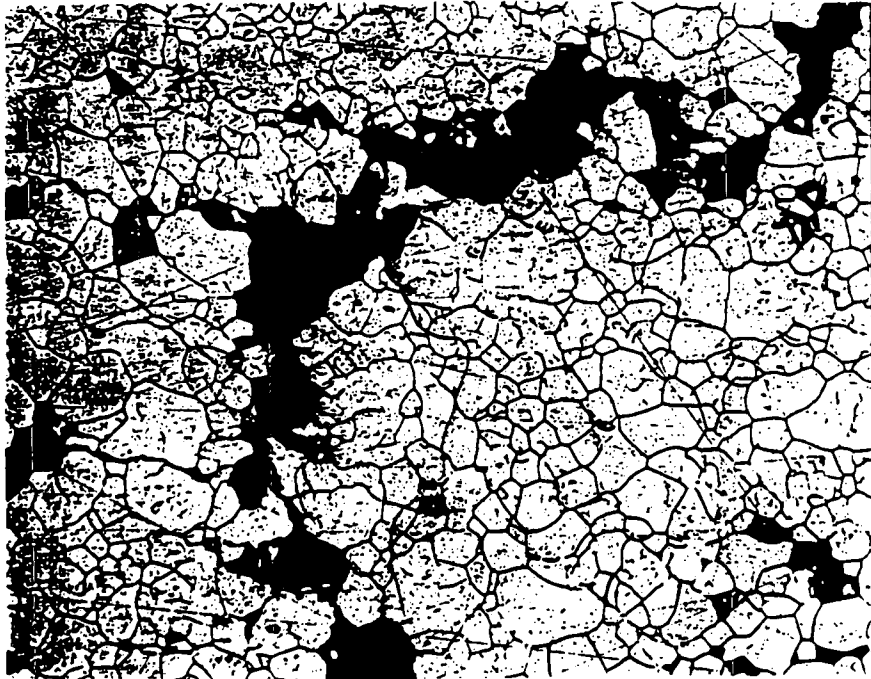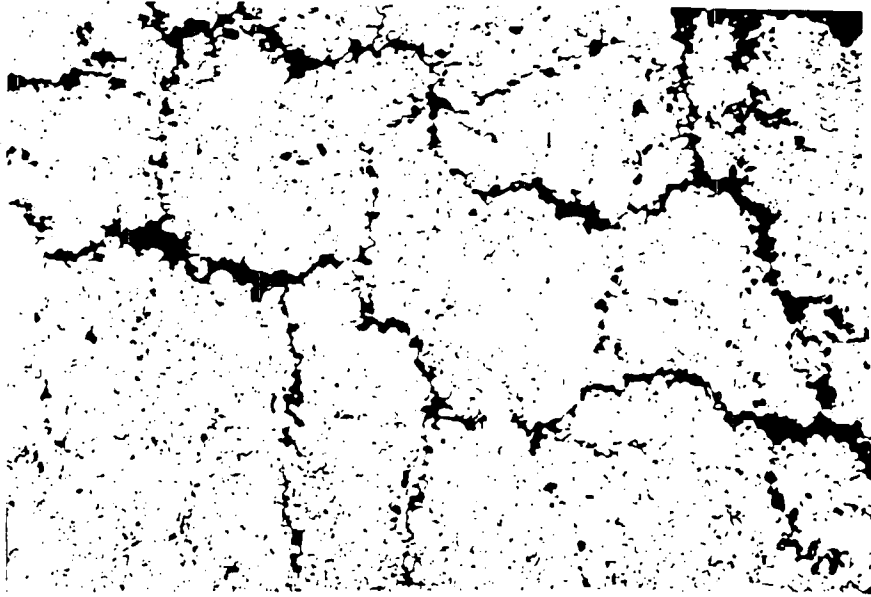
Figure 4 - 53   Higher magnification photomicrographs of the radial section shown in the previous figure. Top photo 50X, bottom 200X

Axial Direction ----->

50X

Figure 4 - 54 Radial metallographic section through a portion of the third
support plate crevice region of tube R19-C35 from Plant
E-4. A cellular IGA/SCC structure is observed. The depth
of the section was not specified.
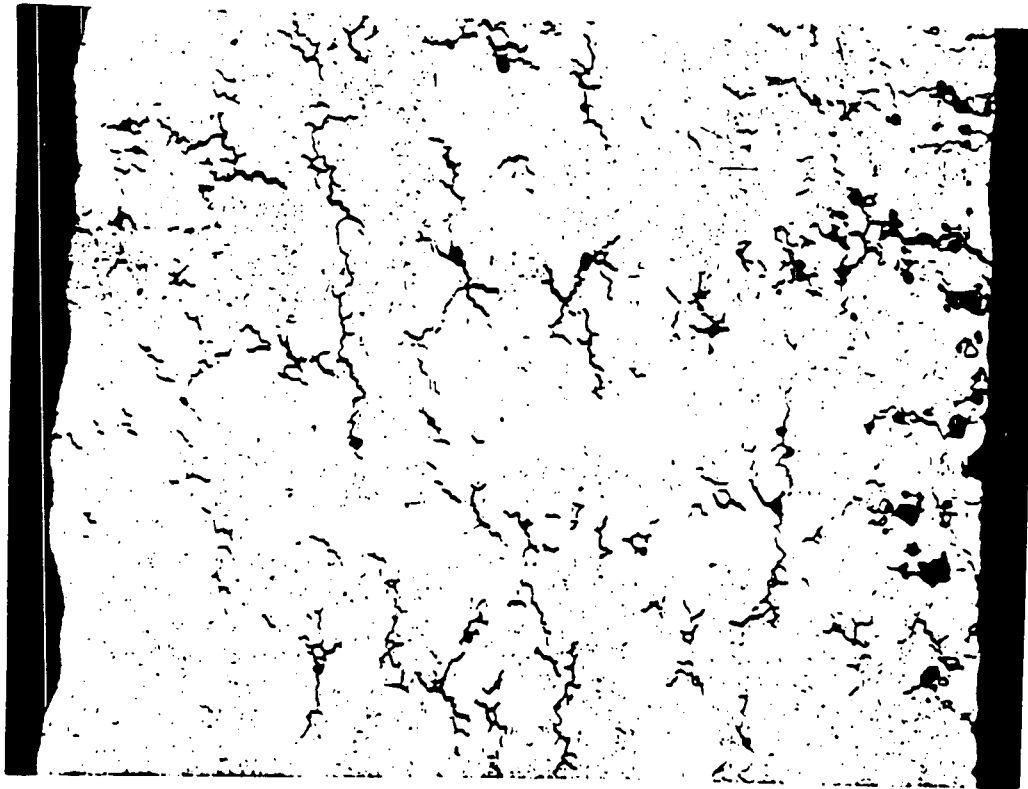
Axial Direction ---->

50X

Figure 4 - 55 Radial metallographic section through a portion of the fourth support plate crevice region of tube R19-C35 from Plant E-4. A cellular IGA/SCC structure is observed. The depth of the section was not specified.

OD

ID

Sketch of Burst Crack

Macrocrack Length = 0.4 inch

Throughwall Length = 0.01 inch

Number of Microcracks = 7 (all ligaments have predominantly
intergranular features)

Morphology = IGSCC with some IGA aspects (circumferential cracking
has more IGA characteristics)

0.75 inches — — SP top

0.0 inches — — SP bottom

180°   270°   0°   90°   180°
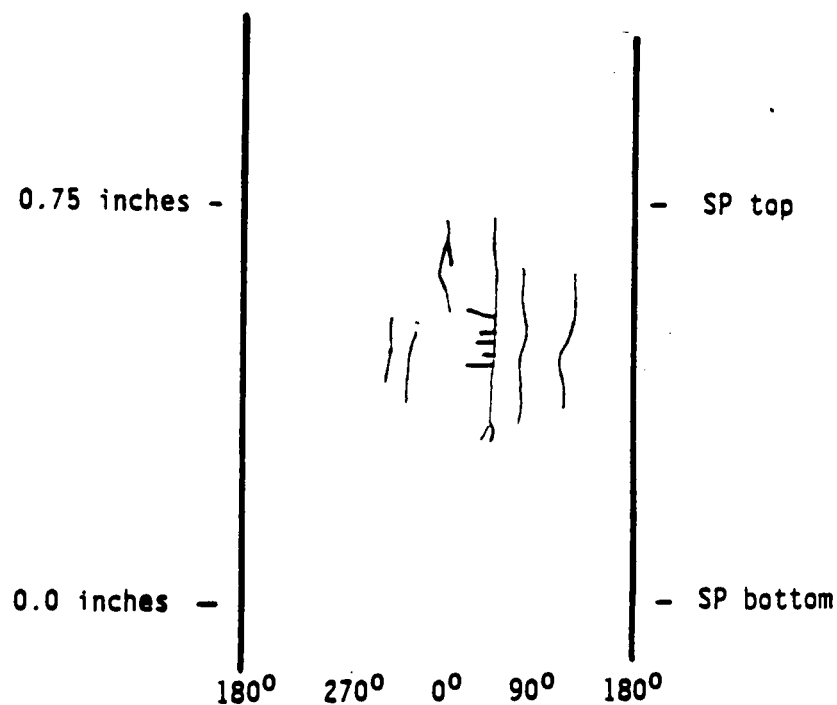
Sketch of Crack Distribution

Figure 4 - 5 6 Description of OD origin corrosion at the fifth support plate crevice region of
tube R4-C61, Plant B-1

Axial Direction →

Fracture
Face of
Axial
Crack
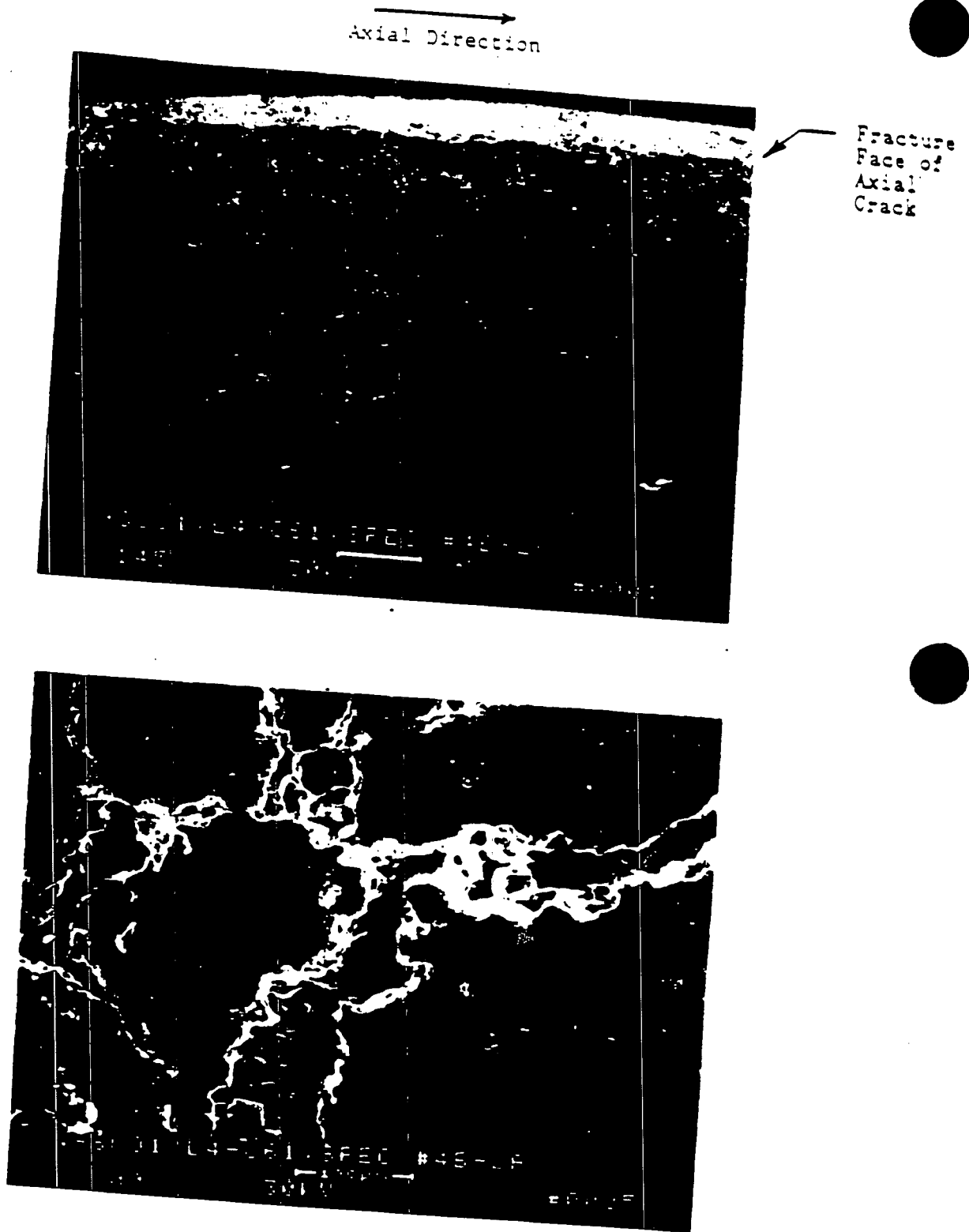
Figure 4 - 57 Network of small, mostly circumferentially oriented OD
surface cracks observed in the 5th support plate region,
Tube R4-C61.
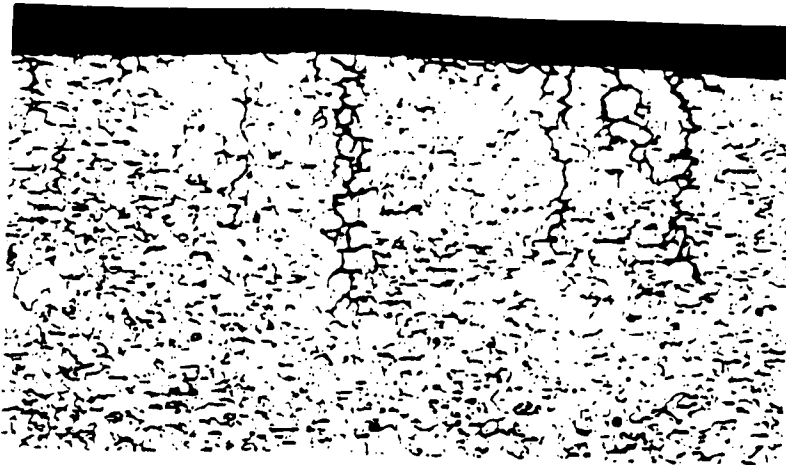
Mag. 100X
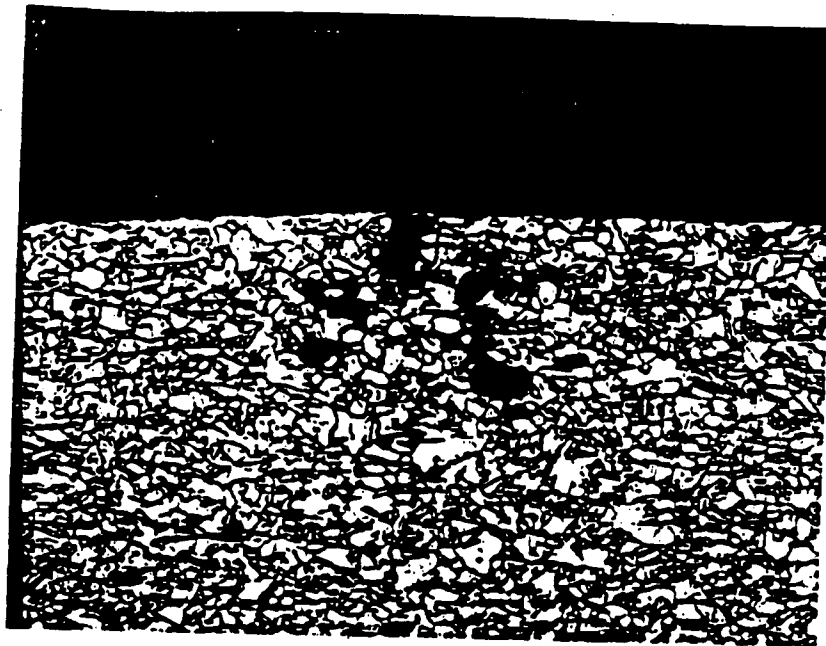
Mag. 100X

Figure 4 - 58 Photomicrographs of tube R4-C61 corrosion degradation. Top photo shows axial crack morphology (transverse section) at the eighth support plate location (no transverse metallography was performed at the fifth support plate region). Bottom photo shows circumferential crack morphology (axial section) at fifth support plate region.
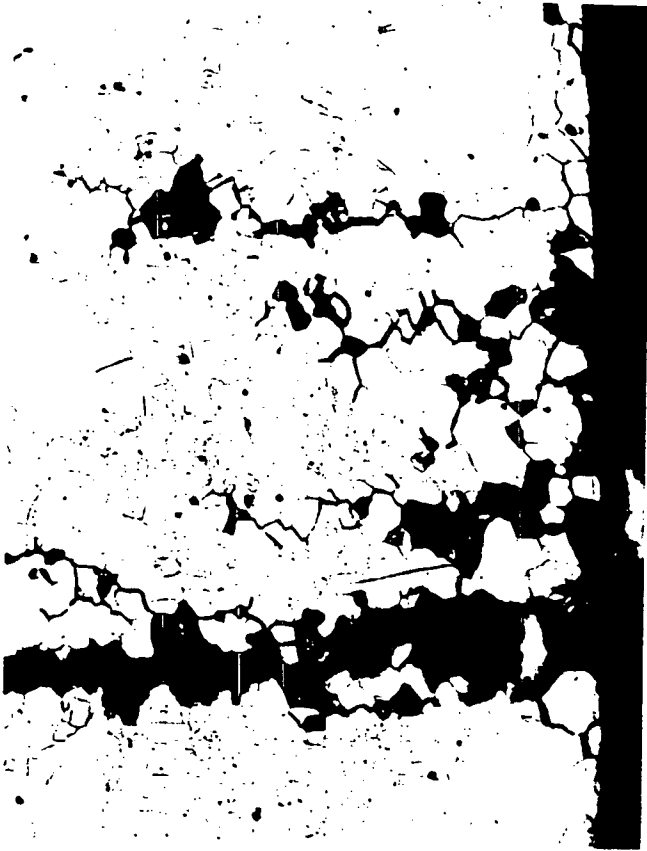
98079   200X   98080   200X
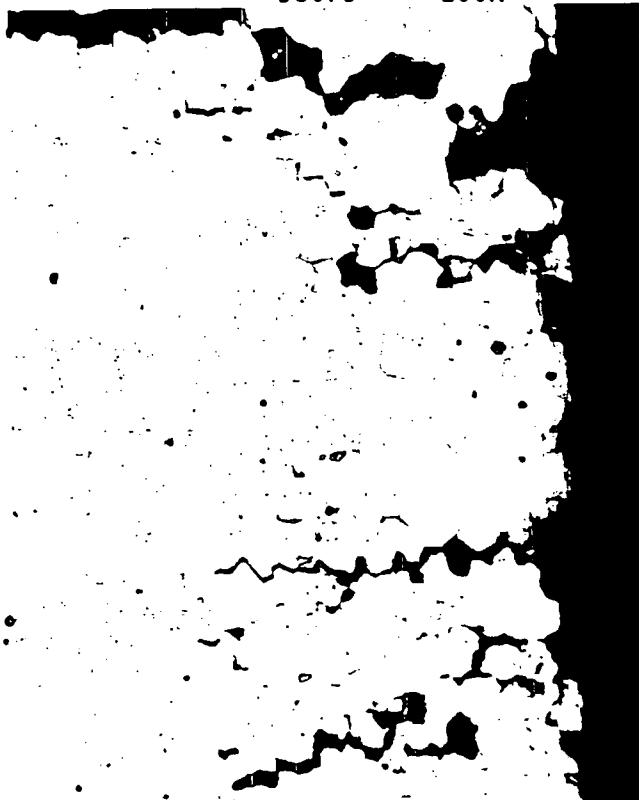
98081   200X   98076   200X

Figure 4-59   Transverse View of Top of TSP Region of R16C60
TSP #1 - Plant P

98514   200X
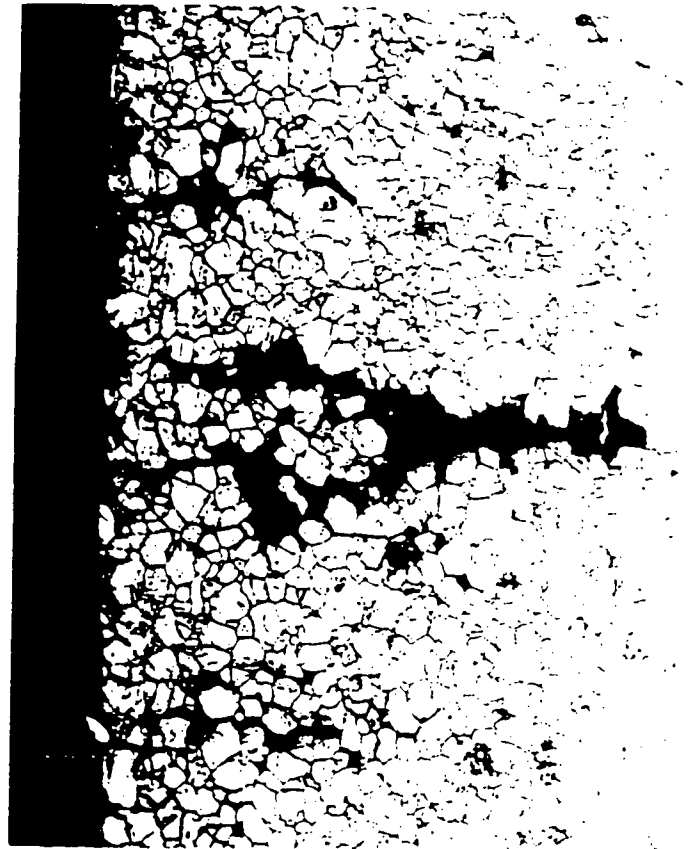
98515   200X
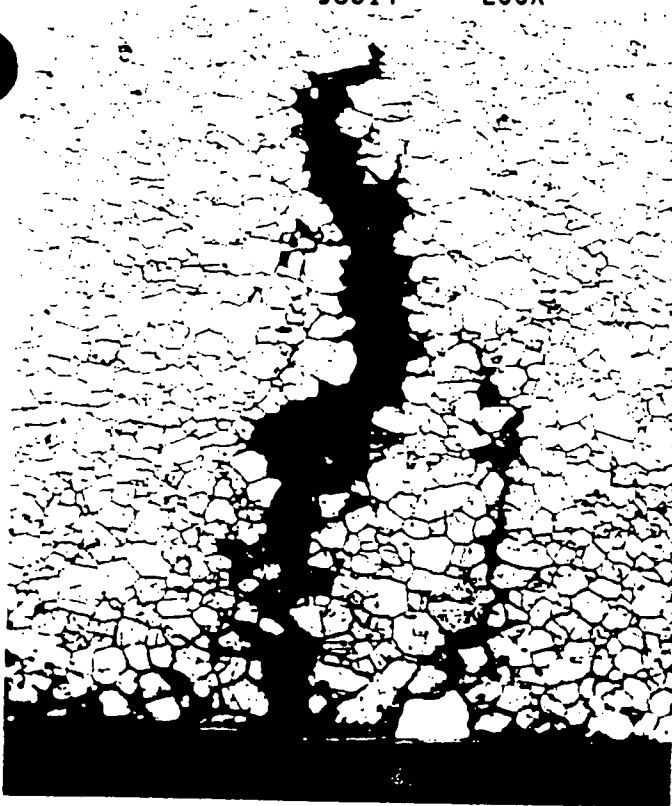
98516   200X
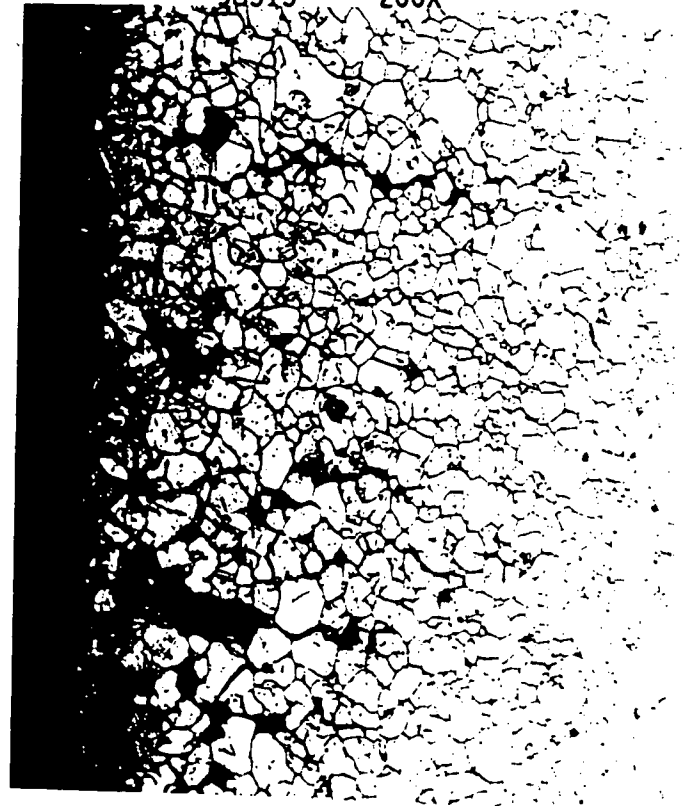
98517   200X

Figure 4-60   Transverse View of Mid-Plane Region of R16C60
                      TSP #1 - Plant P

Figure 4-61   Axial Crack Profile of R16C60 TSP#1 Mid-Plane
- Plant P
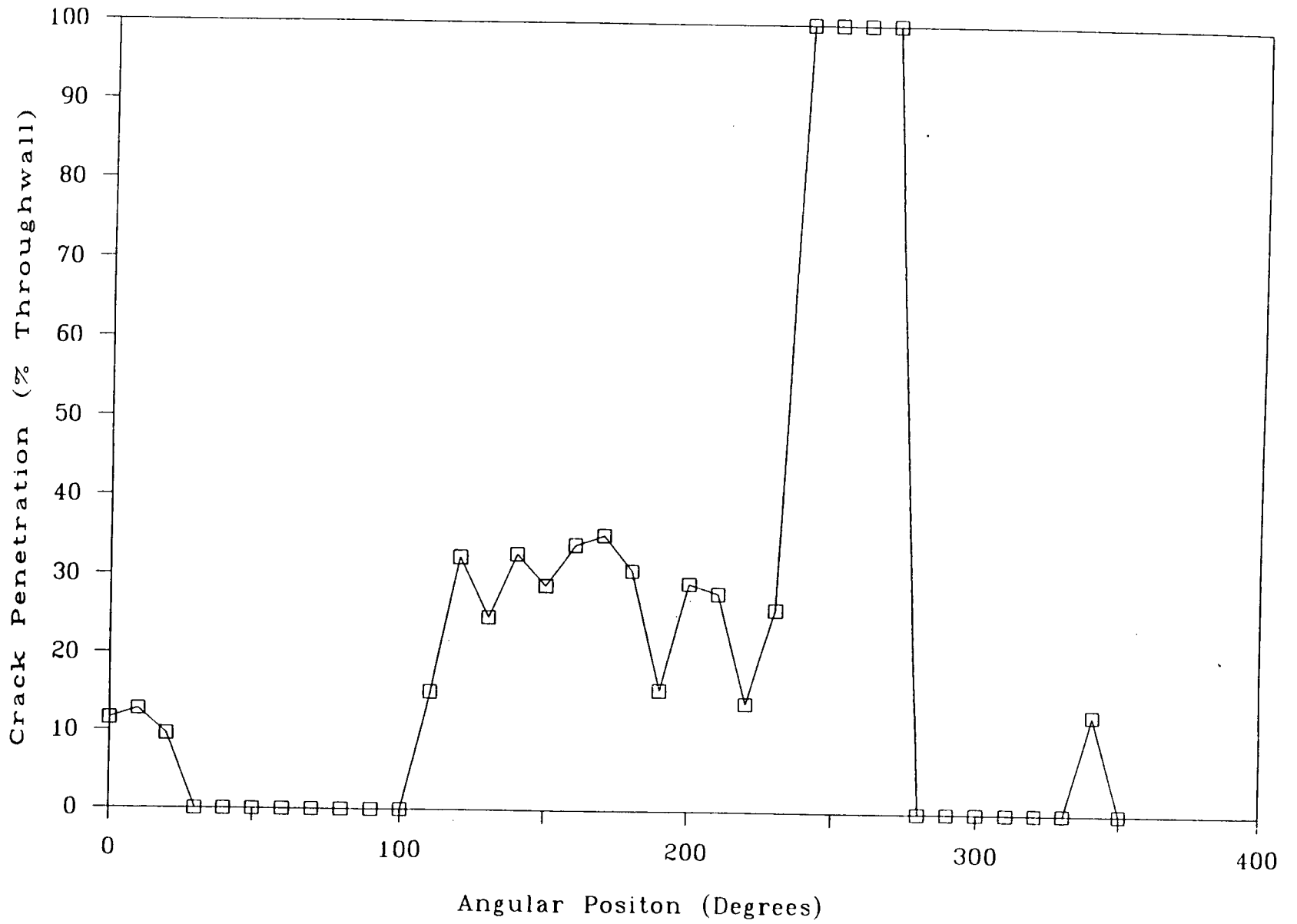
98903   200X
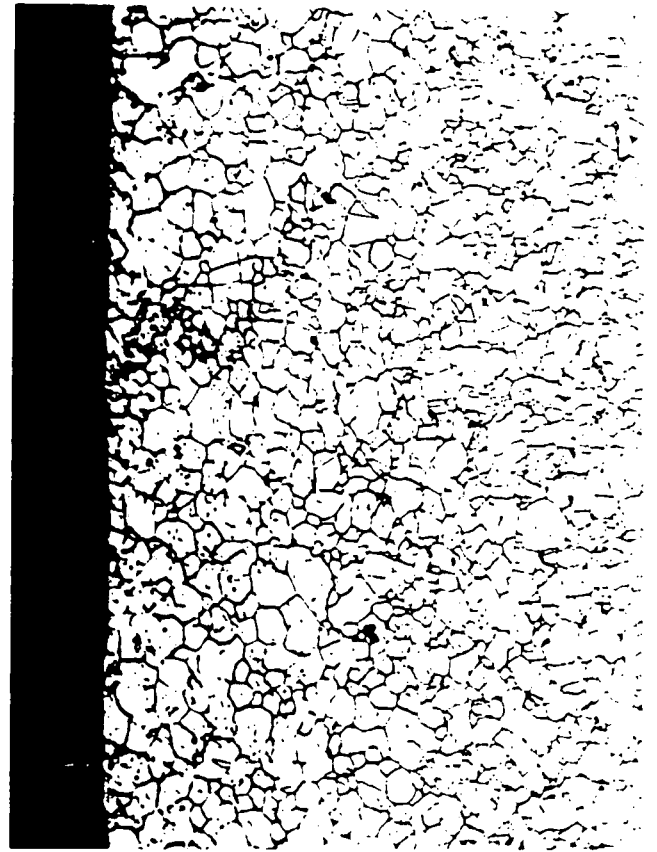
98904   200X
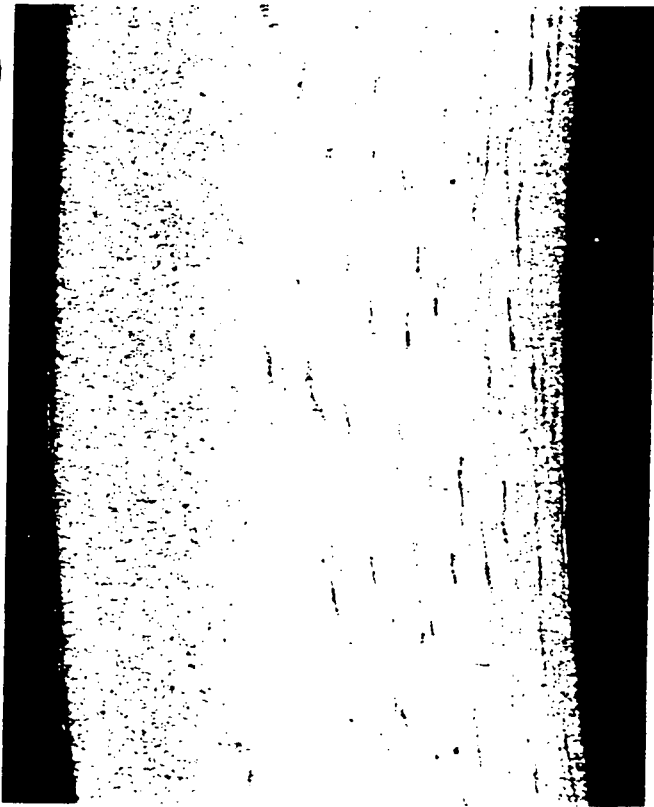
98905   50X
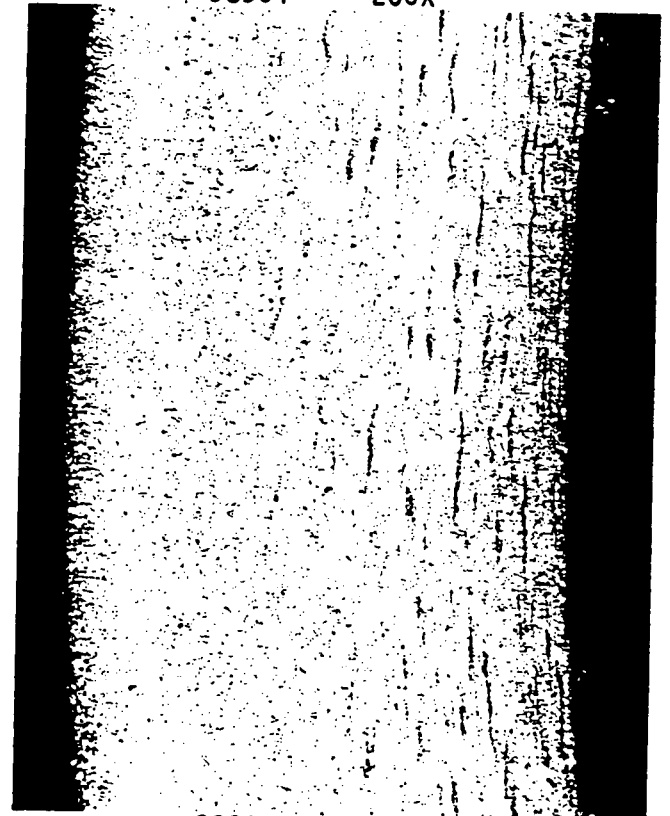
98906   50X

Figure 4-62   Transverse View of Bottom of TSP Region of R16C60
                    TSP #1 - Plant P

98979 200X

98982 200X
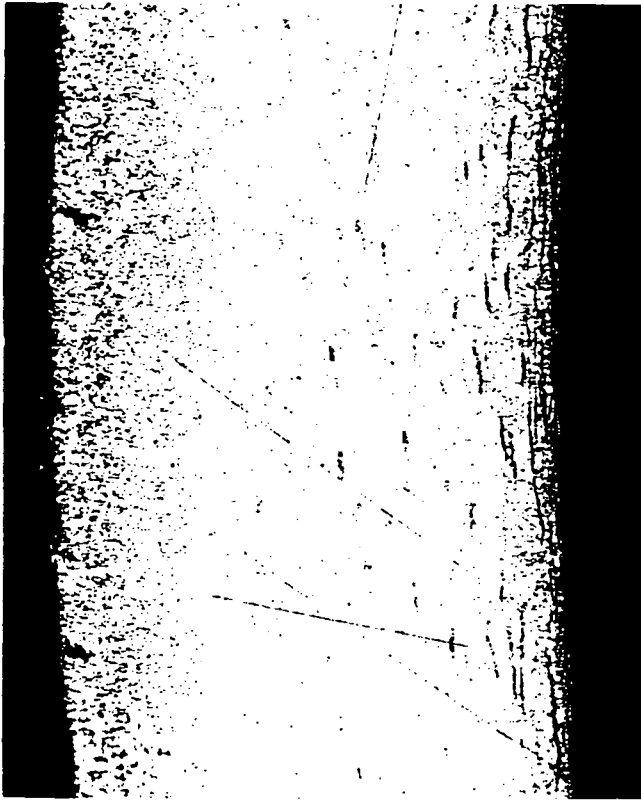
98983 50X
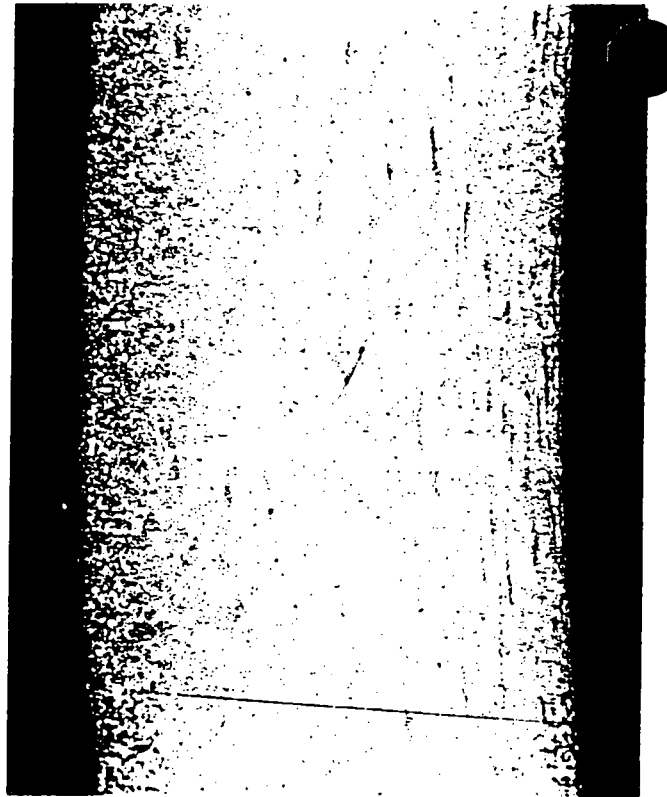
98985 50X

Figure 4-63 Transverse View of Top of TSP Region of R16C60
TSP #2 - Plant P
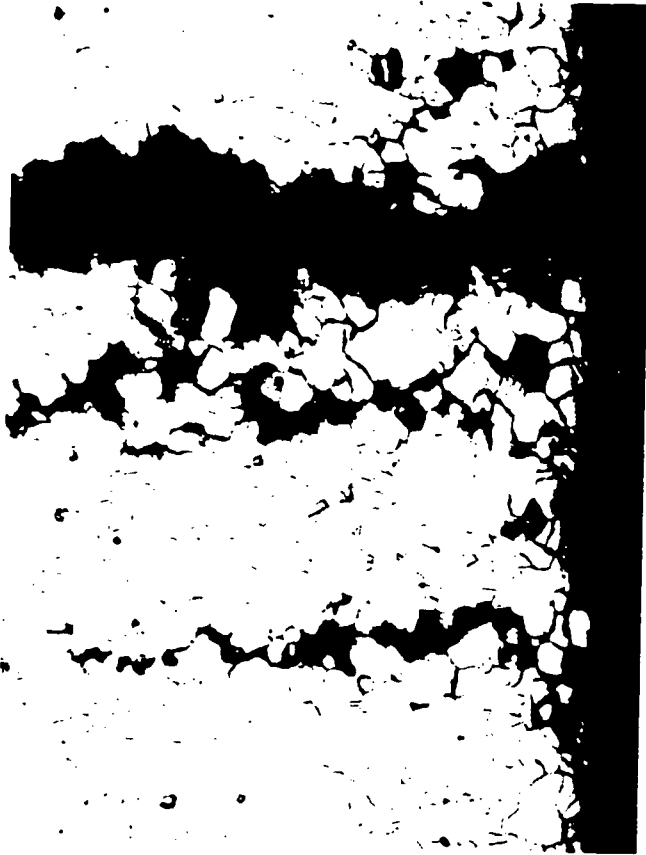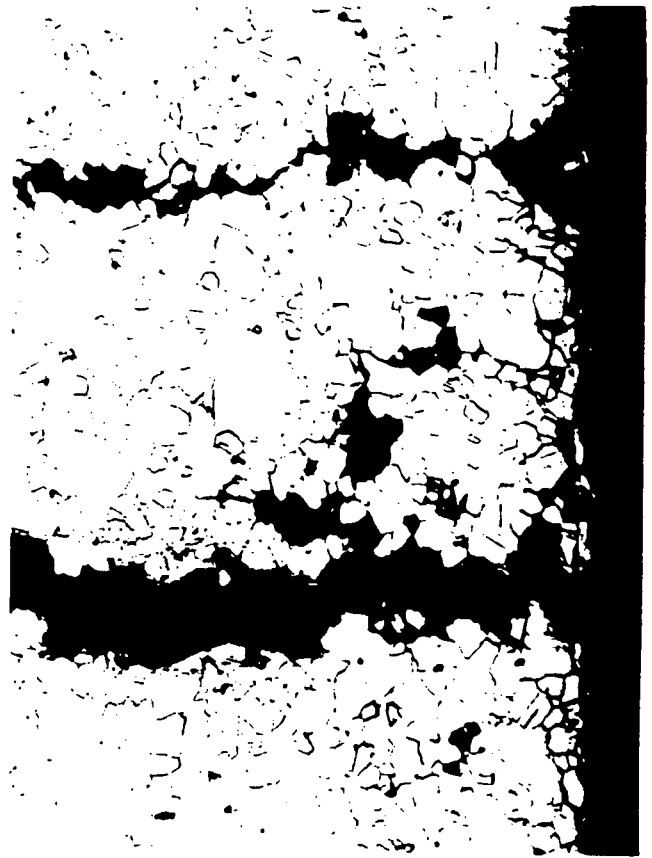
98834   200X   98835   200X

98836   200X   98837   200X

Figure 4-64   Transverse View of Mid-Plane Region of R16C60
TSP #2 - Plant P
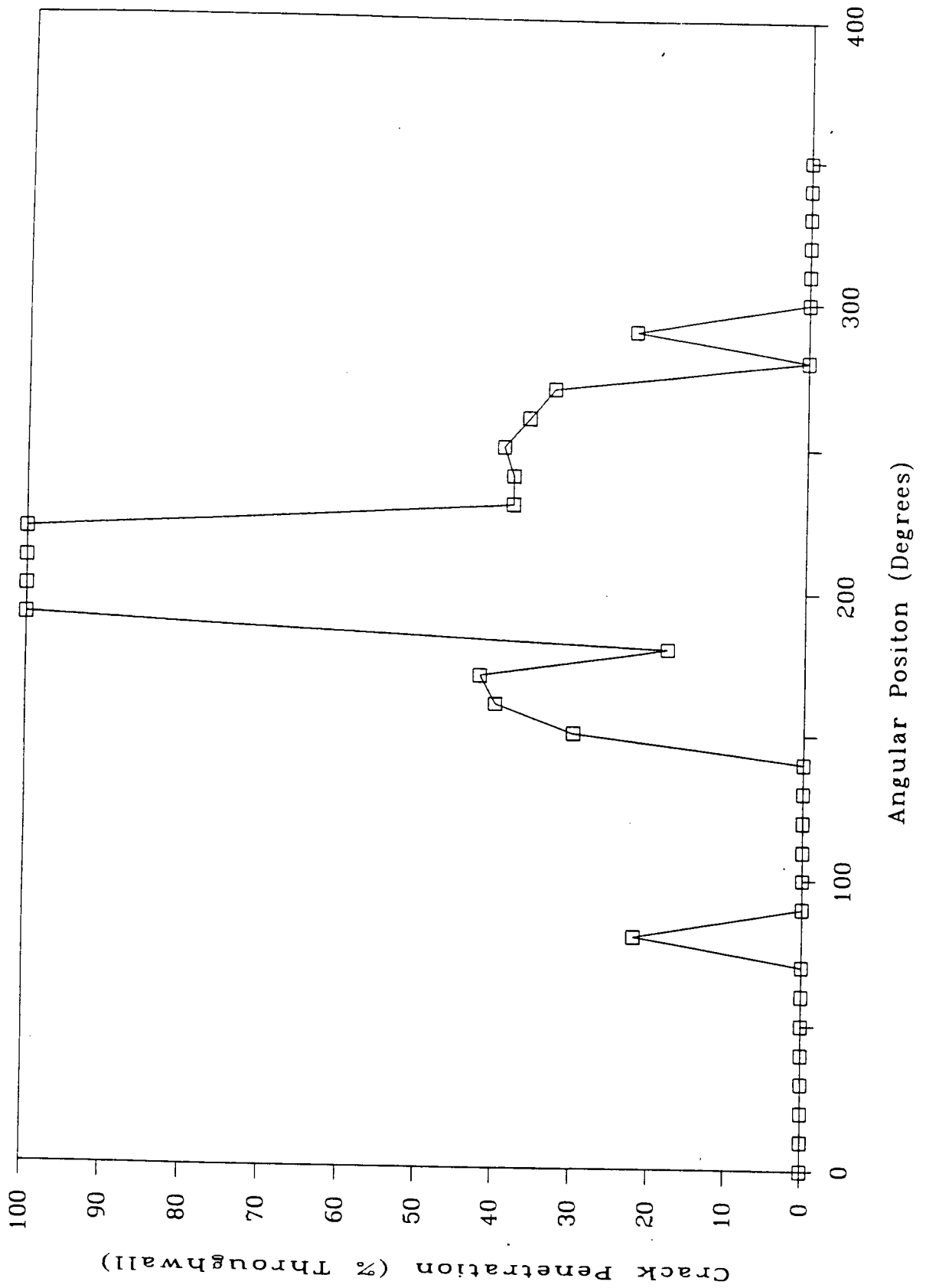
Figure 4-65   Axial Crack Profile at the Mid-Plane of R16C60
TSP #2- Plant P
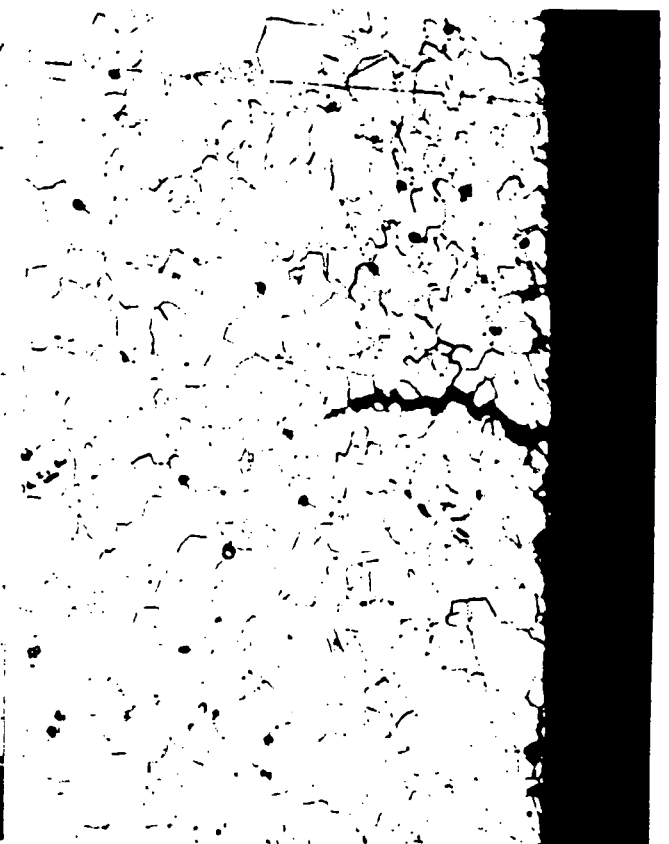
98546   200X   98547   200X
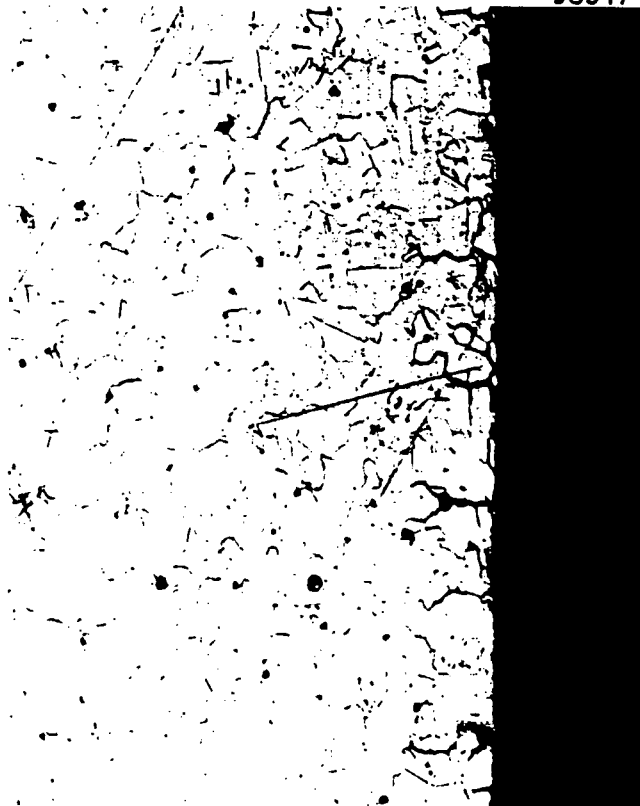
98548   200X

Figure 4-66   Transverse View of Top of TSP Region of R11C48
TSP #1 - Plant P

4 -107
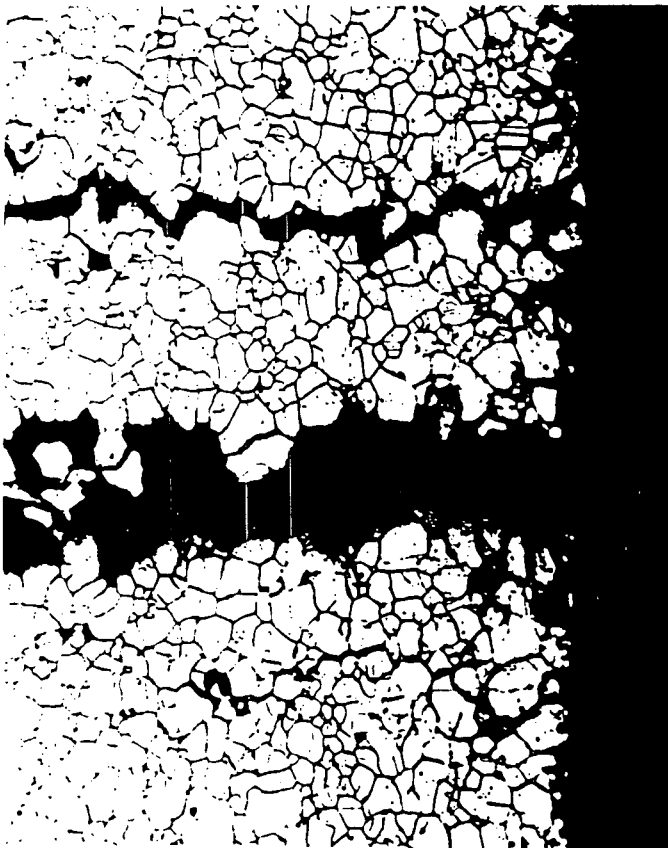
98513   200X
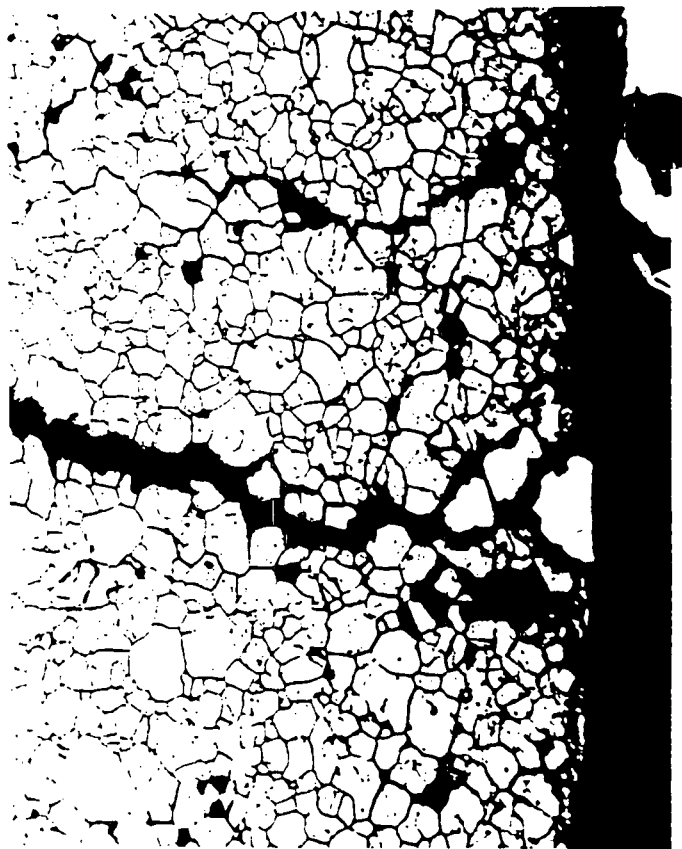
98512   200X
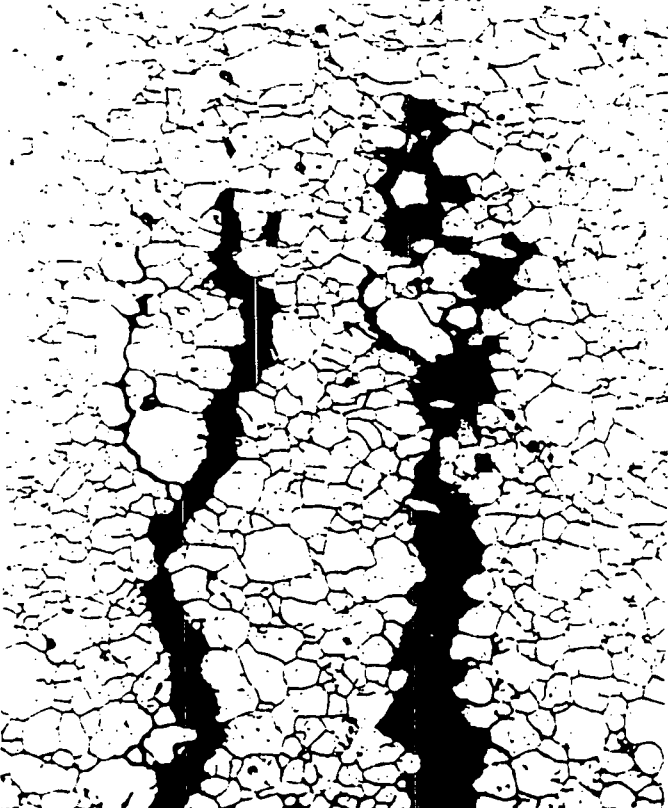
98510   200X

98511   200X

Figure   4-67   Transverse View of Mid-Plane Region of R11C48
                         TSP #1 - Plant P

4 -108
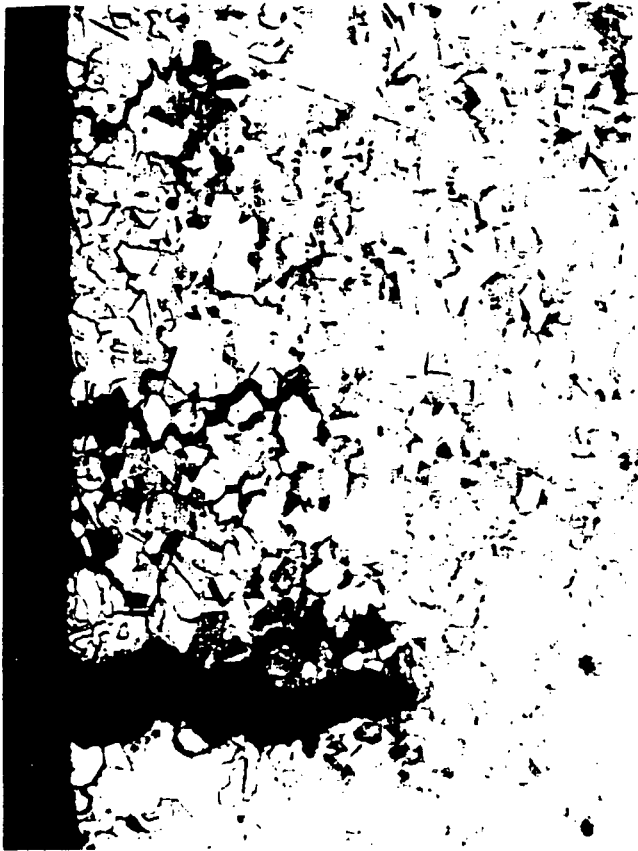
98940   200X

98938   200X
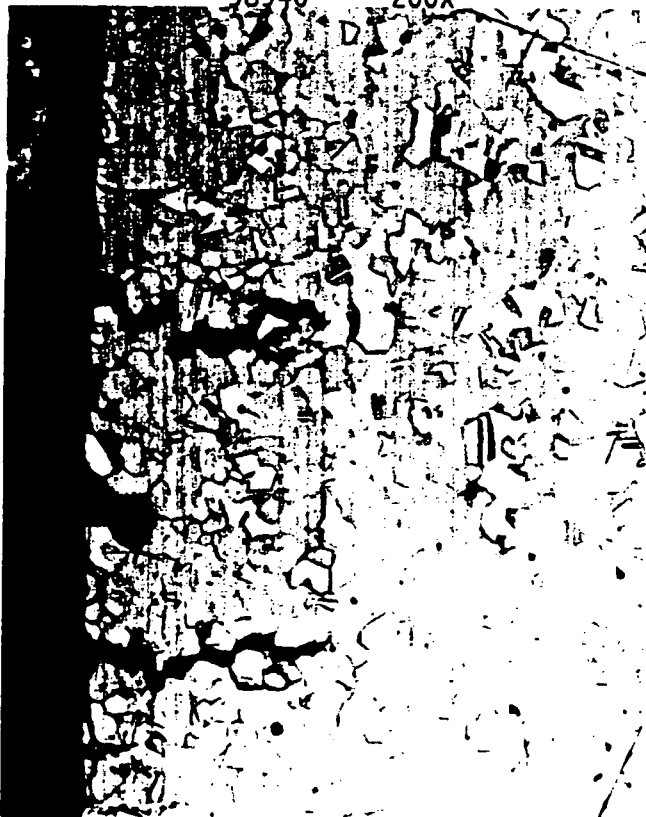
98936   200X

98937   200X

Figure 4-68   Transverse View of Bottom of TSP Region of R11C48
TSP #1 - Plant P
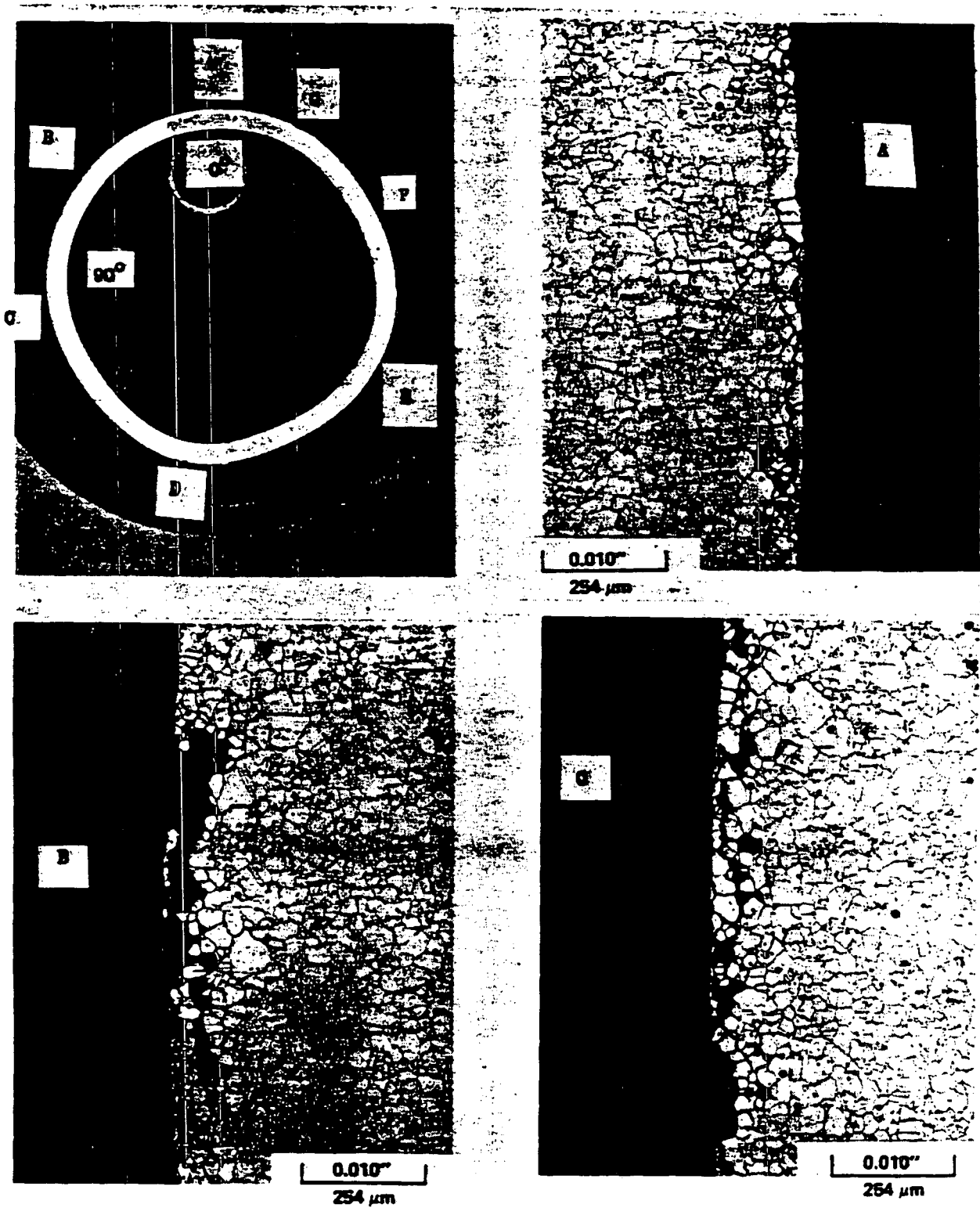
Figure 4-69   **Transverse metallography at 0.2 inches above first support plate bottom edge showing almost continuous OD IGA around circumference. Maximum depth is 24%.**

Tube R29-C46 CL, Plant M-2

4 - 110
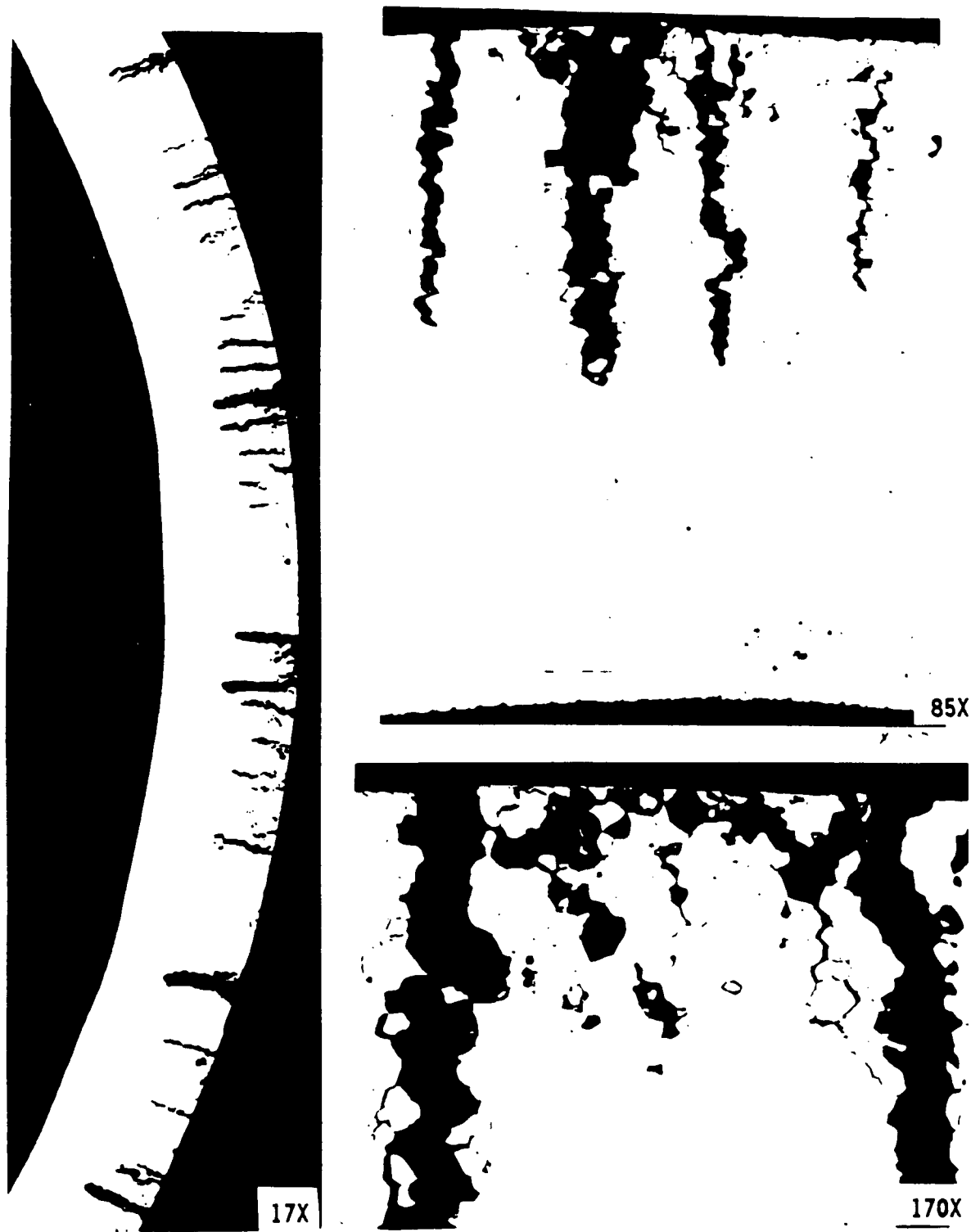
Figure 4-70   Transverse photomicrographs of intergranular corrosion at the second support plate region of tube L8-C74 from Plant J-1

5.0   NON-DESTRUCTIVE EXAMINATION (NDE)

An extensive NDE program was implemented to characterize the laboratory cracked specimens and to assess the sensitivity associated with application of the bobbin coil voltage limits for the tube plugging criteria.

The test program included tests to address some of the variables associated with field characterization of degradation as follows:

1.   Bobbin probe voltage sensitivity to the length of the cracks, depth of the cracks, presence of ligaments in the cracks and parallel cracks.

2.   Multiple probes to address probe-to-probe variations utilizing probes from Echoram and Zetec.

3.   Influence of tube to TSP crevice condition on bobbin coil response including open crevices, packed crevices, incipient denting and fully developed denting.

4.   Bobbin probe voltage sensitivity to probe wear to establish field inspection requirements for acceptable NDE uncertainties.

5.   Variability among calibration standards, and normalization of the frequency mix.

6.   Eddy current analyst variability in evaluating bobbin voltage signals.

7.   Use of RPC to augment bobbin probe inspections, although the RPC data are not considered essential to the development of the plugging criteria of this report.

The NDE results for the laboratory specimens are utilized in later sections to establish the relation of eddy current voltage response to potential leakage and burst pressure as the basis for the tube plugging criteria.

Establishing a relationship between the bobbin coil response and tube integrity (leakage, burst considerations) is important to inspection planning. A relationship helps determine the importance of detecting degradation with a small amplitude; that is, justification that "small" indications can be left in service and have negligible consequences for safe operation.

The morphology of the intergranular corrosion can explain the lack of an eddy current response for small cracks. The field degradation, as observed in the tube examinations, consists of multiple short OD cracks coupled with intergranular cellular corrosion which includes IGA in the regions adjacent to the crack faces. This allows paths for the eddy currents to pass uninterrupted through the degradation. An appreciation for why this phenomenon can account for the lack of an eddy current response has come from the use of liquid metal modeling techniques. Using this technique, degradation is simulated as inserts in liquid metal, and degradation morphologies that are difficult or impossible to machine can be easily simulated. The difference in response between "real" cracks and notches have been modeled by varying the contact between the faces of the crack. In that work, interfacial contact of 50% reduced the eddy current response by a factor of 5. An example of this behavior was found for the doped steam specimens cracked with high applied hoop

stresses. These specimens were found to have lower voltages than expected for the crack sizes present in these tubes. This result is judged to be the consequence of crack face contact as a result of removing the applied stress. Similarly, the voltage sensitivity tests reported here show large voltage increases as ligaments between cracks are lost. The presence of crack ligaments and partially degraded grain boundaries provides an explanation for the lack of eddy current response associated with field induced degradation. Further, the presence of these ligaments and the low instance of primary coolant leakage associated with this degradation mode suggests that there is residual strength associated with these ligaments. Thus, significant degradation depths may result in less severe loss of strength than was assumed in determining the plugging limits based only on crack depth. For this reason, plugging criteria are based on voltage responses correlated to tube integrity through the voltage versus burst pressure and leakage correlations.

5.1 Voltage Sensitivity to Crack Morphology

A series of eddy current tests were performed to establish voltage trends with crack morphology to characterize voltage as a measure of tube integrity. In most cases, machined specimens were used to simulate degradation features. This section describes using simulated cracks and volumetric indications. In addition, voltage measurements for laboratory specimens and pulled tubes with IGA degradation are summarized to assess detectability of IGA.

Voltage Sensitivity Using Slits in Copper Foil

To establish the general trends of bobbin coil voltage amplitude to crack morphology, sensitivity tests were performed using slits in a cylindrical copper foil to simulate varying crack lengths, ligaments and parallel cracks around the tube circumference. The copper foil was placed around a plastic tube. The various crack morphologies simulated by the slits in the copper foil , and the associated voltage responses are shown in Figure 5-1. For each combination of simulated cracks in Figure 5-1, the total crack network length is equal to the TSP thickness of 0.75 inch. The connecting cuts between the parallel axial cracks simulate loss of ligaments between cracks.

The voltage trends of Figure 5-1 show that the voltage increases with:
* Increasing crack length
* Increasing number of cracks around the tube circumference, and
* Loss of ligaments between cracks.

Voltage Sensitivity Tests Using Slots in Inconel 600 Tubing

Additional information on the functional dependence of bobbin signal voltage on length and depth of axial cracks was obtained using EDM slots in 7/8 inch OD, 50 mil wall alloy 600 tubing as shown in Figure 5-2. The signal voltages for the slots represent the upper bound for the signal voltages expected for actual cracks of similar length. For the 100% deep slots, the signal voltage increases steeply with slot length up to about 0.5 inch and continues to increase up to one inch, after which it tends to level off. For the 50% deep OD slots, the signal amplitude increases with slot length up to about 0.250 inch after which it levels off. The signal amplitude increases by a factor of about 50 for 100% deep slots as the slot length increases from 0.03 inch to 1.0 inch; it increases by a factor of about 4 for the 50% deep OD slots over the same range of crack length. It may further be noted that for longer slots, there is a greater increase in the signal voltage as the depth increases from a shallow depth to 100%. For example, for 1/4" slots, the voltage increases by a factor of about 50 as the depth increases from 50% to 100%, where as for a 60 mil long slot the voltage increases by only a factor of 10 for the same range of depth change.

Voltage increases in an exponential manner with depth for a given slot length. For example, the voltage for a 1/4" slot increases from about 5 volts at 80% depth to 40 volts at 100% depth. Overall, the voltage amplitude is particularly sensitive to deep wall penetration and crack length; this is the desired dependence for voltage as a severity index for tube integrity.

Figure 5-2 also shows the data for three slots with depth varying along slot length. The central 1/3 of each slot had 100% depth which tapered off to 0% at the ends. The signal amplitudes for these slots with tapered ends are, as expected, higher than for the through wall rectangular slots when plotted against the through wall slot lengths. Figure 5-3 shows a plot of percentage increase in signal amplitude above that for a uniform through wall slot resulting from the tapers as a function of the 100% deep portion of the slot length. As the through wall length increases, the influence of the partial depth slot decreases such that for lengths greater than about 0.25 inch, the partial depth slot length has negligible influence on the voltage amplitude.

Figure 5-4 shows the signal amplitudes for the axial slots obtained by using the rotating pancake probe with a 125 mil diameter coil. This data is qualitatively similar to the bobbin data of Figure 5-2. Figure 5-5 gives a plot of bobbin voltage vs. RPC voltage for the slots showing a correlation between the signal amplitudes expected from the two types of probes. It may be noted that for both the bobbin and the RPC probes, the amplitudes are dominated by the deepest part of the slots. A well defined correlation between bobbin and RPC voltages is seen for the single slot data.

The effect of ligament within the crack length on the eddy current signal voltage was studied by varying the axial distance between two 0.125 inch long 100% deep axial slots. The results are shown in Figure 5-6. The bobbin signal voltage drops by approximately a factor of 2 when a ligament as thin as 8 mils is placed in the middle of the two slots. The bobbin signal voltage is relatively insensitive to any significant increase in the spacing beyond 16 mil. RPC voltage is also seen to decrease with increasing ligament size although the rate of decrease for small ligaments is less than for the bobbin coil. Since the small 16 mil ligaments within a crack cannot be distinguished by eddy current, the voltage increase with loss of ligaments supports voltage as a severity index for tube integrity.

A variation in bobbin signal amplitude is expected in the case of parallel, multiple axial cracks, spaced around the circumference of the tube. This effect can again be studied using EDM slots in the Alloy 600 tubing. Figure 5-7 shows the effect on the signal amplitude of varying the spacings between four throughwall axial slots. The signal amplitude increases by a factor of about three as the spacing between parallel slots increases from a few mils to 700 mils. Closely spaced parallel slots do not show an increase in voltage above that of a single slot. The signal phase angle decreased by about 10 degrees at 400 kHz for this entire range of spacing. Qualitatively, a similar result was found for 50% deep OD axial slots.

The positioning of degradation near the end of the TSP can potentially influence the responses, with the principal contribution due to the mix residual that occurs at these locations. This response is typically small compared to the voltage plugging limits so that the amplitude of significant degradation will not be influenced by this residual. To demonstrate the TSP edge effects, bobbin coil measurements were made on 1/4-inch EDM slots of 50% and 100% depth. Measurements were made for the slot at the center of the TSP and at the inside and outside edges of the TSP. Results of these measurements are given in Table 5-1. It is seen that the voltage values for the crack within the TSP are essentially the same at the center and at the inside edge of the TSP. Variations in voltage with the slot inside the TSP are <2% for both 50% and 100% deep notches, while moving the slot outside the TSP increased voltages by 5%-10%. The bobbin coil indicated depth changed by 29% as the 50% slot was moved from the center to the outside edge of

the TSP. These results support the conclusion that amplitude responses to degradation on the order of the 3-4 volt plugging limits will not be significantly impacted by the location of a crack within the TSP.

General conclusions from this eddy current evaluation of axial slots are:

- Both bobbin and RPC voltage amplitudes increase sharply with axial crack length up to about one inch for 100% deep slots.

- The voltage increase is much smaller for partial depth OD axial slots and voltage does not increase significantly with length for slots greater than about 1/4" long.

- Signal amplitude is dominated by the 100% deep portion of the slot.

- Bobbin coil signal voltage is a function of spatial separation between parallel axial slots. Very closely spaced slots show an insignificant increase in the voltage over that of a single slot.

- A correlation exists between RPC and bobbin voltages for single slots. However, bobbin voltages increase for parallel slots while RPC voltage can be isolated to a single slot provided slots are adequately separated to permit resolution of each slot.

- The presence of a small ligament between two axial slots reduces the signal voltage.

- Amplitude reponses to degradation on the order of the voltage plugging limits are not significantly influenced by the location of a slot (crack) within the TSP.

- Both bobbin and RPC voltage amplitudes from slots represent an upper bound for the voltages expected from cracks of similar length and depth.

These results demonstrate the use of the voltage amplitude as a crack severity index for tube integrity assessments. Voltages increase with increasing crack length, with increasing depth particularly near through wall penetration and with loss of ligaments between cracks.

The general concept of relating voltage to burst pressure can be demonstrated by combining data for voltage vs. slot length with burst pressure vs. slot length data. Figure 5-8 demonstrates the resulting voltage/burst correlation. Voltages for slots are not typical of cracks but the general trend and slope are similar to that later developed in Section 8 from burst testing of cracked tubes. As intuitively expected and shown even for machined specimens, a given voltage amplitude does not define a unique crack morphology. Thus a spread in burst pressures for a given voltage is expected. This spread is accommodated in the plugging criteria by using a voltage/burst correlation at the lower 95% confidence band of the test data. Various crack morphologies involving variables such as length, depth, ligaments, multiple cracks, etc. influence the spread of the data and thus the resulting tube plugging limit.

Voltage Sensitivity to Volumetric (Non-Crack) Indications

It is desirable to compare voltage amplitudes for volumetric indications to those associated with plugging levels for ODSCC cracks. Given defect specific plugging criteria for ODSCC at TSPs, these comparisons help to guide the importance of distinguishing ODSCC from other types of degradation. The plugging criteria of this report establish a bobbin voltage threshold above which

RPC inspection is required to facilitate identification of ODSCC from other types of degradation. These voltage comparisons provide guidance on setting the bobbin voltage threshold for RPC inspection.

Typical bobbin coil voltage amplitudes were developed from laboratory simulations of volumetric degradation as developed below and summarized in Table 5-2:

Wastage: Flat rectangular shaped flaws of different depths were machined to simulate tube wastage: the bobbin signal amplitudes as a function of maximum OD depth for 1/4" and 1/8" long machined flaws are shown in Figure 5-9. In addition, tapered flaws were machined to simulate the tube wastage shapes observed at some plates. Figure 5-9 shows the bobbin signal voltage as a function of maximum OD depth for tapered flaws.

Fretting: Flaw shapes somewhat similar to the tapered flaws shown in Figure 5-9 are observed from fretting. Thus, the data of Figure 5-9 can be used to assess the voltages expected from fretting.

Pitting: Figure 5-10 shows the bobbin signal amplitude vs. diameter of machined through wall holes simulating 100% deep pits. Pitting observed in operating SGs occurs as multiple pits for which voltages are significantly higher. The data from ASME flat-bottom holes of partial depths may be used for estimating the signal voltages expected from partial depth OD pits.

Cold Leg Thinning: Pulled tube data from two different plants with cold leg thinning were reviewed and are summarized as follows. In one case, a flaw at the second TSP in the cold leg with a maximum wall penetration of 48% had a bobbin amplitude of 4 volts. Figure 5-11 shows a photograph of the OD surface at the degraded location. In the second example, which was also at the second TSP in the cold leg, a maximum wall penetration of 59% yielded a bobbin amplitude of 4.9 volts. Examination of the pulled tubes showed no cracks in these tubes and the degradation was identified as "cold leg thinning."

The data of Table 5-2 and supporting figures indicate that bobbin voltages would exceed about 2 volts, as limiting by pitting degradation, before being a concern for tube integrity. A single pit, simulated by 30 and 60 mil through wall holes would have voltages of about 2 and 7.5 volts, respectively. Pitting typically occurs as multiple pits in operating SGs, with higher voltage levels. Cold leg thinning at 50% depth will yield a bobbin amplitude of over 4 volts.

Based upon the above noted voltage levels, volumetric indications with bobbin voltage amplitudes exceeding about 2 volts should be inspected using RPC probes to aid characterization of the causative mechanism. Volumetric indications less than this voltage amplitude would be expected to be acceptable for continued service and separation of the causative mechanism from ODSCC would not be critical to assure tube integrity.

IGA Detectability

Limited laboratory specimens and pulled tubes at TSP intersections with significant IGA are currently available for assessments of detectability and tube integrity. Available laboratory IGA specimens were prepared as long (4 to 6 inches), uniform IGA to assess detectability in unexpanded regions of tubesheet crevices. Data from three domestic plants, including tube to TSP intersections from Plant L , one from Plant M-2 (see Section 4), and three from

non-Westinghouse Plant N are available. Some French and Belgian data for TSP indications are also assessed. The general morphology of the French indications is similar to the Plant L tube R12C8 morphology. The Belgian data shows more extensive cellular corrosion than found at a few patches in Plant L tubes.

Three sets of laboratory IGA specimens are available for NDE assessments. Two are Westinghouse samples and the third represents samples prepared by Westinghouse under EPRI sponsorship (EPRI NP-5503). The two Westinghouse sets of specimens represent laboratory IGA under accelerated conditions and provide uniform wall penetration IGA over 4 to 6 inch lengths. Bobbin coil detection for these specimens is shown in Figure 5-12. Figure 5-12a represents specimens prepared using sensitized tubing and shows very high bobbin coil amplitudes. Figure 5-12b shows bobbin coil responses using non-sensitized material. The non-sensitized material shows much lower amplitudes. Methods of sample preparation were refined for the EPRI program to further improve comparisons with field experience.

The EPRI specimens were prepared using a 50% caustic and 12% chromium oxide environment at 650°F for up to 10,000 hours. Temperatures in some cases were increased to 700 °F to accelerate the corrosion rate such that 21% penetration was obtained in 35 days. Even under the accelerated laboratory conditions, the times to create IGA are very long compared to preparation of ODSCC specimens. Specimens in the range of 2 to 30% nearly uniform wall penetration were obtained in this program. Figure 5-13 shows typical NDE results for 29% deep IGA. The bobbin coil differential tests reveal the uniform IGA whereas the RPC results are not particularly revealing. Voltage amplitudes are not available for the samples that were destructively examined. Bobbin coil measurements of library samples were performed with the results given in Table 5-3. These samples show voltage amplitudes of about 1-2 volts where the IGA depth is expected to be <30% deep and are NDD where depths of a few percent are expected. Deep cracks within the samples were detected with amplitudes of 4-40 volts. These samples are more representative of field IGA than the Figure 5-12 samples although limited pulled tube data for uniform IGA are available for direct comparisons.

As described in Section 4, a pulled tube from Plant M-2 shows IGA with cracks up to 26% depth. This tube had a voltage amplitude of 1.8 volts, which is high compared to tubes with principally ODSCC at comparable depths as shown in Figure 6-9. The signal amplitude is comparable to the laboratory specimens of Table 5-3, although lower than the specimens of Figure 5-12.

Three pulled tube results from Plant N-1 with egg crate supports are also shown in Figure 6-9. These data for IGA degradation also support IGA detectability at voltage levels comparable or higher than that for ODSCC with minor IGA.

The pulled tube (R12C8) indications from Plant L were detected by pre-pull bobbin coil inspection. Table 6-2 and Figure 6-9 show the voltage and maximum depth for the three Plant L indications of R12C8 that were found to have significant IGA involvement as compared to other pulled tube results including Plant L data with negligible IGA involvement. It is seen that the Plant L voltage levels are typical of the rest of the population of pulled tubes with less IGA involvement than the Plant L tube R12C8 crack morphology, which shows patches of IGA with IGA/SCC cracks.

Figure 6-9 also shows voltage amplitudes for tube to TSP intersections removed from French units. The French data show voltage responses toward the high range of the data. The French crack morphology is IGA + SCC as shown in Figure 6-8. The Plant L, Plant M and Plant N morphologies also show IGA + SCC.

Tube removal analyses performed in Belgian Plant E during 1991 showed ODSCC with shallow IGA at all support plate intersections examined. Again the affected areas were located entirely within the TSP intersections, mainly at mid-height. The affected circumference was small when shallow depths prevailed, and reached nearly 360° in strongly affected intersections; at shallow depths, many initiation sites with multi-directional cracking were visible; in strongly affected areas, axial cracking was predominant, with only shallow associated IGA. For tube R19C35-2H, the burst cracks, developed with a loose fitting TSP collar, were axial in direction, showing 100% intergranular depth. Several tube sections broke upon pulling; the maximum corrosion penetration was 60% in a dense array of axial cracks, with shallow IGA in some places.

Figure 4-19 illustrates the cellular morphology of the Belgian tubes and Figure 5-14 shows the EC traces collected in the field for the corresponding location prior to pulling. The 2.27 volt signal recorded at 300 kHz, when converted to US voltage calibration in accordance with Section 6.6, corresponds to approximately 11 volts, well in excess of any voltage-based alternate criteria under consideration in this report. The stated reporting threshold for TSP ODSCC in Belgium is 0.2 volts at 300 kHz, or approximately 1 or more volts at U.S. voltage calibration. Many tubes plugged in the U.S. for TSP ODSCC would escape reporting under the Belgian criteria.

Since Belgian practices are based on the absence of safety implications for ODSCC/IGA contained within the TSPs, only the most severe degradation is plugged and many indications are not recognized. Since the Plant E tubes are pilgered in the manufacturing process, the periodic noise in the tubing complicates detection of minor degradation; thus the relatively high reporting threshold is consistent with the S/N limitations in the EC data.

In summary, the conditions which went "unreported" in the Belgian tubes were not simple IGA, which is easily identified as the U.S. field and lab data show; rather the voltage calibration and reporting threshold combined to create the impression that cracking and associated shallow IGA, comprising the cellular degradation observed in the lab, had not been detectable. In the U.S. NDE calibration system, these are prominently visible and pose no challenge to evaluation.

Overall, the available pulled tube results show comparable voltage responses relative to maximum depth with no quantifiable dependence on IGA involvement within the broad scatter of the data. As shown in Figure 6-9, indications with significant IGA and cellular corrosion tend toward the higher voltage responses as a given maximum depth. The laboratory uniform IGA samples show significant voltage responses at 30% depth. The available pulled tubes with significant IGA levels show IGA with cracks and have been found to be detectable indications.

5.2 Probe Comparisons

To address issues that the results of the study might be limited to a specific probe, probes from different eddy current probe vendors, Echoram (Er) and Zetec (Zt), were used. Both probes were nominally 0.720 inch in diameter and incorporated the latest technology for centering. The coils on each probe were nominally 0.06 inch wide and were spaced by 0.06 inch. Initially each of the probes was used with two different sets of frequencies duplicating typical field inspection configurations. The first set of frequencies (configuration I) was 400, 200, 100 and 10 kHz. The second (configuration II) was 600, 400, 100, and 10 kHz. Review of the data indicated no significant differences in the results from the different probes for the different frequency configurations.

Comparisons were made between the data obtained from probe Er and probe Zt for the cracked tube specimens. The probes have different frequency response characteristics: Probe Zt gives a greater response at 100 kHz , while probe Er has a larger response at 600 kHz since it is designed for higher frequency operation than the Zt probe. This difference is not a significant issue and is noticeable only as a consequence of the way in which the voltage calibrations have been derived. Table 5-4 gives the voltage measured by probe Zt divided by the voltage measured by probe Er for the EDM calibration notches. As can be observed for each frequency, the difference between the probe responses is a constant factor for all notches. This apparent variation between the probes can be eliminated by calibrating each of the frequencies individually rather than using the 400 kHz calibration factor, or by calibration at the planned mix frequency. The latter approach is recommended as a part of the plugging criteria of this report.

The results for the 400/100 kHz Mix channel were fortuitous. Plots of the measured voltage for various indications from probe Zt versus the voltage from probe Er indicate a one to one correspondence for both amplitude and depth (Figures 5-15 to 5-17). The correspondence between the mix channels of the two probes is due to the fact that the 400 kHz channel is being used both as the "primary" mix frequency and to set the calibration factor. If another frequency is used as the primary mix frequency (i.e., 100 kHz) the apparent mix amplitudes will differ. Table 5-5 gives the measurement of the ASME holes using a 100/400 kHz mix for the two different probes. As can be seen the results from the two probes differ by a constant multiplier. As with the individual frequencies, this factor can easily be accommodated by using a different calibration procedure.

The bobbin coil inspections were supplemented by two RPC examinations, also with probes from the two eddy current probe vendors noted above. However only one set of frequencies (400, 200, 100, and 10 kHz) was used for both RPC probes. The data gathered during this phase of the program were used primarily as a qualitative tool in assessing the extent of the degradation.

5.3   Influence of TSP Crevice Condition

For some specimens, the crevice between support and the tube was packed with magnetite and the sample was inspected again with the bobbin coil. Table 5-6 compares the data from the two inspections. With the exception of sample BW-11 the amplitude of the responses from the samples changed by approximately 10 %. Sample BW-11 showed a 50 % increase in amplitude. When the support was removed from the sample the degradation response had indeed increased, indicating that the presence of magnetite in the crevice did not cause the increase in response, rather the process of packing the crevice had mechanically deformed the sample causing further loss of ligaments and a subsequent increase in response. Additional evidence for the minimal impact of the presence of magnetite in the crevice is derived from the comparison of the data from corrosion samples with tight packed crevices. A comparison of the samples prior to support removal and after magnetite removal with the packed support ring (Figure 5-18) in place show a 5% increase in response with the magnetite present with a scatter of approximately 10%.

As part of the test program, 6 fatigue crack and 3 doped steam corrosion crack samples were leak tested to determine the influence of the dented support plate crevice condition. Table 5-7 summarizes the results of the eddy current inspection of these samples before and after denting (note samples FAT 1, 2, and 3 had been leak tested previously). Denting resulted in a significant change in the amplitude of the fatigue crack eddy current responses. Prior to denting, all but one of the fatigue cracks had amplitudes which approached that of the through wall EDM notch (80 volts). After denting, two of the fatigue cracks could not be distinguished from the response of the

dents, despite the fact that the dent response was an order of magnitude smaller than the initial fatigue crack response. Initially the corrosion cracks produced smaller responses than the fatigue cracks. However, their responses on average, could be detected in the presence of the dent. However, these results represent large indications in the presence of small dents. In field applications, small to moderate indications typically cannot be separated from dent signals that exceed the amplitude of the indication.

The difference in the behavior of the two crack types (and further within the fatigue samples) in the presence of denting is a consequence of the heavier oxide coating on the crack faces of the corrosion samples and the leak tested fatigue cracks. Under the compressive loads of denting, the crack faces are forced together. The presence of the oxides on the corrosion crack faces prevents interfacial contact and therefore results in a minimal change in the crack response. On the other hand, the faces of a virgin fatigue crack, being free of oxides, come into intimate contact permitting the eddy currents to flow unimpeded across the crack, significantly reducing the response. The significant loss in response of the fatigue cracks demonstrates that interfacial contact does indeed result in a reduced eddy current response. However, it is not expected that service-induced degradation will respond to denting as have the fatigue cracks. Rather, it is expected that the compressive stresses from denting would not play a direct role in providing interfacial contact such that field induced cracking would respond as did the doped steam samples, with little change in amplitude. However, it is recognized that bobbin coil detection of cracks at dented intersections is unreliable when the degradation amplitude is smaller than the dent amplitude and both signals are at the same elevation, such as the edge of the TSP.

5.4 Sensitivity to Probe Wear

Eddy current test parameters can exist over which there is little systematic control and which may vary between tubes or along the length of a tube. The centering of the eddy current probe as it passes the degradation poses the greatest concern of this type. This study has shown that probe centering can vary the amplitude of a signal, in the worst case, by a factor of two. The laboratory study used field probes which had excellent centering characteristics. At the beginning of a field inspection sequence, the probe centering characteristics would mimic those found in the laboratory. As the inspection continues the probe is expected to wear and its centering capability to degrade. The time frame for this to occur is unknown because it is a complex function of inspection extent, tube geometry, the presence of oxides, etc.

A means of assessing the probe's centering capability is through the use of an appropriate verification standard as illustrated in Figure 5-19. Such a standard can be as simple as four holes drilled in a segment of tubing. The holes are displaced axially in different planes with each spaced 90 degrees around the circumference from its neighbor. The amplitude ratio between the holes then determines the degree of centering of the probe. A standard of this type would be implemented during inspections to periodically verify probe centering during the inspection.

The bobbin probe centering mechanism wears with usage. This could affect the eddy current signal. The effect of wear on signal voltage was evaluated using a "4-hole standard." The four holes were 67 mils in diameter, 100% deep, 90 degrees apart circumferentially, and 1.5 inches apart, axially. A 0.720 inch diameter probe fabricated by Echoram was used for this evaluation. The centering mechanism in this probe consists of three sets of spring loaded plastic buttons (hemispherical) 120 degrees apart and protruding approximately [ ]a mils from the probe body. The test runs were made with the tubes in a vertical position. The tubes were rotated 90 degrees after each run to provide for the randomness in the probe to tube orientation expected in

5 -9

the field. For the new probe, the standard deviation for the voltages obtained from the four identical holes for repeated test runs was [   ]a of the average voltage amplitude.

The centering buttons of the probe were worn by repeatedly running the probe through a tube with an abrasive tape on the tube ID. The data from the 4-hole standard were collected for different levels of probe wear. At the level of probe wear represented by a 50% reduction in height of the centering plastic buttons (ie, about [   ]a mils radial reduction), the standard deviation in the voltage for the four holes was found to be within [   ]a. Increasing the probe wear beyond this level resulted in rapid deterioration of the quality of the data. The results of the tests are shown in the upper part of Figure 5-20. The 50% reduction in height of the centering buttons appears to envelope typical field wear between probe changeouts during an inspection. Thus, even for a worn probe, the variation in voltage measurements can be represented by a standard deviation of 10%. These data can be used to estimate the NDE uncertainty associated with probe wear. Since acceptable field measurements would be made for probe wear between 0 and about 20 mils radial material loss, all the data for 0 to 20 mils wear can be combined to define the NDE uncertainty. Probe wear approaching the 27 mil wear data of Figure 5-20 is minimized by field application of the probe wear standard requiring probe replacement if the worn probe voltage for any hole differs from the new probe voltage for the same hole in the wear standard by more than 15%. Combining the data of Figure 5-20 from 0 to 20 mils wear yields an average voltage difference of 8.38 volts with a standard deviation of 0.59 volts or 7.0% of the mean difference in voltage, as shown in the upper part of Figure 5-21. Thus, the uncertainty allowance for probe wear can be represented by a standard deviation of 7.0%. The remaining concerns over probe centering are the impact of tube to tube variations in diameter and ovality. Neither of these are anticipated to be major sources of variability.

Channel head mockup tests were performed to evaluate field implementation of the probe wear standard of Figure 5-19. During field implementation of the probe wear standard, the wear standard must be utilized essentially in line with an ASME calibration standard and both located within the channel head below the tubesheet. This application introduces the effects of bends in the probe leads, as well as probe wear, on the variation in voltages between new and worn probes as measured against the holes in the wear standard. The effects of bending the probe leads can be a function of the location of the eddy current fixture in the channel head. A probe pusher, 100 foot cable extension and a robot fixture for tube location were used in these tests. This testing was performed at 9 tube locations using both Echoram and Zetec new and simulated worn probes as summarized in Figure 5-20. This figure also shows the approximate location of the standard, which rested on the bottom of the channelhead pointed away from the manway. Moving the eddy current fixture between tube locations can potentially move the location of the standard. Ten repeat voltage measurements were made at 4 tube locations and two measurements were made at 5 locations. For field application of the probe wear standard (see Appendix A), probe wear acceptability requires that the change in voltage between a new and worn probe for each of the four holes be less than 15% of the new probe hole voltage. Four different probes from each manufacturer were used to represent a new probe and three levels of probe wear. Simulated probe wear was obtained by machining the centering devices to the material losses given in Figure 5-20. For the Echoram probes, the material loss represents the thickness removed at each of the three centering buttons, which represents a reduction in the probe radius. For the Zetec probes, the material loss represents the radial reduction in the centering petals. The bobbin voltages were normalized to a 4 hole ASME standard at tube location R23C44 following the pull of the probe for each probe diameter tested. The voltage normalization for these tests was different than used for the probe wear tests described above, such that the voltages are not directly comparable. The data from these tests can be compared with the above described tests by comparing the standard deviation of the results as a percentage of the mean voltage.

5 -10

The mockup test data were evaluated to assess the fraction of the wear standard measurements, as a function of probe wear, that would exceed the 15% allowable change in the hole voltage measurements. For example, with 10 repeat tests at each probe wear value, there are 100 probe wear measurement combinations. Each of the 10 measurements for a new probe is compared with all 10 measurements on a worn probe. If the voltage difference for any one of the four holes between new and worn probes changes by >15%, the occurrence would be considered to require probe replacement. The results are summarized in Table 5-8. It is seen that very few Echoram probe replacements would be required up to probe wear of 11 mils. These replacements represent premature probe replacement, as the standard deviation on voltage variations is only 6% at this wear level. This is consistent with the prior test for the vertical wear standard, as shown in Figure 5-20, for which the voltage variations did not increase substantially until 27 mils radial wear was reached. The results for the Zetec probe show more dependence on tube location, with relatively high fractions (30%-91%) of measurements exceeding 15% voltage changes at probe wear values of 5 and 7.5 mils. Overall, the Echoram probe with its spring loaded centering buttons appears to have only minor sensitivity to the location of the probe fixture for the range up to 11 mils radial wear that was tested. The Zetec probe, with fixed centering petals, appears to show more sensitivity to fixture locations, particularly at locations (R8C92, R2C88, and R23C44) adjacent to or behind the end of the wear standard (see Figure 5-22).

The standard deviation of 5%-6% for the Echoram probe in the horizontal wear standard tests is the same as that found for the vertical wear standard tests for 0 to 15 mil radial wear (Figure 5-22). Thus, there does not appear to be a significant dependence on orientation of the standards and probe over this range of probe wear. The Zetec probe, with fixed diameter centering petals, shows the standard deviation increasing from 4.7% at zero wear to 9.7% at 5 mils radial wear, and to 12.3% at 7.5 mils radial wear. Combining these results with the overall likelihood of probe replacement from Table 5-8, the probability of probe replacement is about 30% at wear levels resulting in about 10% voltage variability and about 90% at wear levels with about 12% voltage variability. Thus, applying the probe wear standard with a limit of a 15% voltage change between new and worn probes effectively limits the voltage variability due to probe wear to about 15% for worn probes. Only a small fraction of indications measured with a given probe would be made at this stage of probe wear.

Since the wear standard measurements are not a strong function of the measurement location, the data can be used as an additional assessment of the NDE uncertainty associated with probe wear. Figure 5-20 shows the signal amplitude variations as a function of probe wear for both the Echoram and Zetec probes for the measurements taken with the wear standard horizontal in the channelhead. The Echoram probe does not show a strong function of probe wear up to the 11 mils of wear tested for this case. This result is consistent with the upper figure given in Figure 5-20 which indicates substantial voltage variability only at about 27 mils of probe wear. The Zetec probe shows increasing amplitude variability at 5 mils or larger wear, with significant variability (~12%) at 7.5 mils wear. At 15 mils wear, there is a significant likelihood that probe replacement would be required for field applications of the wear standard based on one of the 4 hole voltages differing by 15% from the new probe value as shown above.

The data of Figure 5-20 show that the trends in voltage variability with wear are similar for both the Echoram and Zetec probes. Prior to wear values for which probe replacement is likely (~27 mils for the Echoram probe, ~7.5 mils for the Zetec probe), the voltage variability is similar for both probes and the same NDE uncertainty for probe wear can be used for both probes. This similarity is further shown in Figure 5-21, where distributions of voltage variability can

5 -11

be compared for Zetec and Echoram probes. The standard deviation is 0.31 volts (~5.1%) for the Echoram probe and 0.33 volts (~6.2%) for the Zetec probe. If the 7.5 mil wear data is included in the voltage variability distribution for the Zetec probe, the standard deviation increases from 6.2% to 9.1%.

The field application of the wear standard requires probe replacement when the voltage difference between that measured for a new probe (at time of probe replacement) and subsequent measurements changes by more than 15% of the new probe voltage for any of the 4 holes in the standard. As discussed earlier in this section, this occurred in the tests a few times at an Echoram probe wear of 11 mils or a Zetec probe wear of 5 mils and in most tests for a Zetec probe wear of 7.5 mils. These results correspond to a few premature probe replacements where voltage variability is 5%-6% (standard deviation) and nearly 100% chance of probe replacement where voltage variability is >12%. Thus, the NDE uncertainty for probe wear, when the wear standard is implemented for field applications can be represented by a normal distribution with a mean of zero, and a standard deviation of 7% with a cutoff on the distribution at an error of 15%.

5.5 Eddy Current Inspection and Analysis Practices

To lay the foundation for field application of the results of the tests, the data collection and analysis procedures were made as close to those used in the field as possible, while conducted under laboratory conditions. A formal procedure for instrument calibration, data acquisition and analysis was developed. The key point to note from the procedure is that the analysis of the bobbin coil data was conducted from a 400/100 kHz mix data channel. The mix was established by eliminating the response from the support ring on the calibration tube. The voltage for all channels was calculated from the conversion factor found by setting the response of the 20% ASME calibration holes at 400 kHz to 4 volts (save/store mode). This corresponds to setting the 400/100 kHz mix channel voltage of the 20% holes to 2.75 volts. A similar procedure, in which the 400 kHz response of a 0.25 inch through wall EDM notch was set to 20 volts and the voltage of all other channels established using the Save/Store mode, was used to calibrate the RPC probes.

Because each calibration standard is potentially unique, a system to assure consistency of the data must be established. Currently, the field data is tied to the calibration tube used during an inspection and the correlation between that standard and all others used in the industry is through the certification provided by the manufacturer of the standard. Typically, the controlled parameters of the standards are the depth of the calibration holes and whether the phase response of the machined holes is within acceptable tolerance. The amplitudes of the hole responses are not controlled parameters. Small changes in tube dimensions, hole placement and other subtleties can cause variations in the hole response and therefore systematic offsets in the measured degradation response with respect to the data obtained in this study. An examination of a limited number of field standards has found a variation in the 20% hole response as large as 18% above that of the standard used in the laboratory work. The variability between standards can be minimized by requiring the ASME allowable 20% hole tolerance of 0.003" be reduced to 0.001". It is recommended that the field ASME standards be cross-calibrated against the laboratory standard either directly or through a transfer standard which has been calibrated against the laboratory standard.

5.6 Alternate Inspection Methods: Rotating Pancake Coil (RPC)

The primary objective of this program was to arrive at inspection and plugging criteria based

upon the bobbin coil inspection. However supplemental RPC data was also acquired from the test samples. This data served two objectives: (1) to establish a data base that if needed could be used to augment the bobbin coil data in establishing tube plugging criteria, and (2) to gather information that might be used as additional support for the current practice of using RPC data as the final arbiter for determining tube plugging.

It is believed that combinations of deposits and other spurious conditions can result in bobbin coil responses that have degradation-like characteristics. To minimize plugging tubes with such responses, the philosophy of using the bobbin coil as a screening tool and the RPC as a confirmatory tool has developed. For the samples that were leak checked, indications were present in both the bobbin and RPC data. Table 7-10 contains a comparison of the bobbin coil and RPC results respectively for the leak tested model boiler samples. It is noted that the samples with the largest bobbin responses generally had large multiple RPC responses. It can be noted that specimen 568-4 had a crack length greater than the 0.75 inch TSP thickness. In this case, the crack extended below the TSP into a teflon spacer used to support the TSP in the test. Figure 5-23 shows examples of RPC traces for typical model boiler specimens at 12.7, 26.5, and 57.2 volts (bobbin coil). It can be seen that for bobbin coil voltages above about 25 volts, multiple axial cracks of comparable amplitudes are found. Specimen 542-4 (57.2 volts) shows closely spaced, long axial cracks with large RPC amplitudes.

An example of an apparently spurious bobbin response, similar to those observed in pulled tubes, was identified in the model boiler tests (model boiler 568). During interim inspections these samples displayed the characteristic of having bobbin coil indications without showing discrete RPC indications. The bobbin coil mix response had amplitudes on the order of one volt, with depths based upon phase measurements on the order of 80% through wall. However, the phase of the indications did not change as a function of frequency consistent with that of the calibration tubes. Rather, as the frequency was decreased the phase remained essentially constant such that the apparent depth of the indication decreased. RPC inspection in the helicoil scan mode did not confirm 80% flaws and gave a response indicating a band of material with electromagnetic properties different from that of the remaining portion of the tube but with no discrete indications. When the pancake probe was pulled axially through the band, a response was obtained which behaved similar to the bobbin coil response. That is, as the inspection frequency is decreased the apparent depths of the indications appeared shallower. The underlying mechanism which causes this shift in the tubing's electromagnetic properties has not been identified. Ultimately the samples showed both significant bobbin coil responses and discrete RPC indications. Post-burst examination of the samples showed no apparent degradation apart from that identified in the RPC results. This example tends to lend support for the RPC probe as an arbiter of bobbin coil indications for identifying discrete crack responses and to avoid plugging of undegraded tubes with electromagnetic property changes.

5.7 Field Considerations

Proper implementation of the tube plugging criteria depends on consistent data acquisition between the field and the laboratory. Although field NDE procedures were utilized in the laboratory, the test program yielded the following modifications to the field eddy current procedures which are necessary to assure proper control of the uncertainties in the data acquisition:

1. The 20% ASME hole (Section XI, Article IV-3220) should be used for field voltage normalizations. However, hole diameter and depth tolerance should be ±0.001 inch rather

than the ASME value of 0.003 inch. Field standards should be cross calibrated against the reference laboratory standard to define the appropriate voltage adjustment for each field standard.

2.   An additional standard should be used during inspections, along with the ASME standard, to limit the effect of probe wear (probe centering) on the field data. Use of this standard indicates when data uncertainties due to probe wear become greater than acceptable for the tube plugging criteria, requiring use of a new probe.

3.   The calibration should be normalized to 2.75 V for the 400/100 kHz mix channel for the 20% ASME holes or by calibration to 4 V for the 400 kHz channel and carrying over the conversion factor for the mix channels. The 400 kHz channel calibration should be applied only if the field probes provide the laboratory probe/standard ratio of 0.69 within about 5% for the 400/100 kHz mix relative to the 400 kHz value.

4.   The NDE data acquisition and analysis guidelines of Appendix A should be implemented to enhance consistency and repeatability of the inspection data.

5.8   Eddy Current Uncertainties for Tube Plugging Criteria

In most prior evaluations, SG NDE uncertainty is determined as the difference between bobbin coil indicated depth versus actual depth from destructive tube examinations. This is not the case for voltage measurements such that the NDE uncertainties for voltage do not have such a unique interpretation. For voltage plugging criteria based upon voltage versus burst pressure correlations, the NDE voltage "uncertainties" affect both the voltage measurement and the spread or uncertainty in the burst pressure correlation. The goal for the voltage measurements is to minimize the uncertainty on repeating a measurement so that the uncertainty on the burst correlation is reduced to the extent practical. The remaining voltage measurement uncertainties end up as part of the burst correlation uncertainty. For example, assume that a number of perfectly identical samples were prepared such that burst pressures would be identical. If voltage measurements were then made with different probe diameters, calibration standards, open crevices, packed crevices, copper deposits in crevices, etc., the voltage measurement variability would then result in a spread in the voltage versus burst correlation. Clearly the goal is to minimize the burst correlation uncertainty (lower 95% confidence limit used for plugging criteria) by controlling the voltage variability. The voltage measurement procedures must be consistent between laboratory and field implementation to apply the laboratory specimen NDE/burst data for developing plugging limits. Inclusion of field voltage measurements for tubes pulled prior to implementating the procedures to improve measurement repeatability tend to increase the spread in the burst correlation. The NDE voltage uncertainty is defined as the uncertainty in voltage repeatability emphasizing differences between the laboratory and the field measurements.

As applied for the plugging limit development, the variables affecting the burst correlation are split into NDE uncertainties for determining voltage and burst correlation uncertainties as given in Table 5-9. The potential contributors to the NDE repeatability uncertainty are probe centering (principally probe wear), calibration standards, probe design differences, eddy current analysis variability and eddy current system variability. Eddy current system variability results from noise due to instrumentation and cabling. This contributor is on the order of 0.1 V and can be ignored when combined with the probe wear uncertainty for applications to plugging limits above a few volts.

Probe design differences are eliminated by requiring that only bobbin coil probes with 0.06 inch coils and 0.06 inch spacing between coils be used for voltage measurements. These values are commonly used by nearly all probe vendors. The voltage amplitude is a function of coil to coil spacing. For differential responses and a center to center coil spacing of 0.12 inch, the influence of small changes in coil spacing such as associated with manufacturing tolerances is small. This sensitivity is shown in Figure 5-24. The data base for the voltage/burst correlation includes magnetic bias and non-magnetic bias bobbin probe data. Most of the pulled tube data, were obtained with magnetic bias probes while the model boiler data were obtained with non-magnetic bias probes. In either case, the differences in voltage measurements between these probe types is negligible. A systematic comparison of magnetic and non-magnetic bias probes was performed by B&W in evaluating pulled tube data from Plant R. Eddy current data were obtained with both probe types on 8 pulled tube indications and various machined hole standards. The differences between probe types was <4%, which is less than the analyst variability of 10% as developed below. Thus, either probe type is acceptable for application of the plugging limits of this report.

The calibration uncertainty results from dimensional tolerances in fabricating the standards. The effects of dimensional tolerances in SG tubing result in a spread of the voltage/burst correlation as the tolerances may affect both voltages and burst pressure and thus are not categorized as an NDE uncertainty. The calibration standard variability for Kewaunee SG applications is eliminated by requiring that the field standards be calibrated against the laboratory standard.

The probe centering uncertainty is limited by requiring probe replacement if individual hole voltages for an axially staggered, four through wall hole wear standard vary by more than a probe wear allowance between the initial or new probe values and subsequent measurements. Thus this uncertainty is limited by field data collection requirements. The probe wear allowance includes voltage repeatability uncertainties (found to be ~ 5% as shown in Figure 5-20) for a new probe and a wear allowance for additional repeatability variation. NDE uncertainties due to probe wear were developed in Section 5.4 as a standard deviation of 7% with a cutoff on the distribution of 15%. At 90% cumulative probability, which is applied for the NDE uncertainty in establishing the Kewaunee SG repair limits, the probe wear uncertainty would be about 10%. Probe replacement is required by Appendix A at a 15% voltage change between the new and worn probe for any of the four holes in the probe wear standard.

Table 5-9 identifies variables which led to spread or uncertainties in the voltage/burst correlation. Crack morphology variations are the principal contributor to spread in the burst correlation. Voltage amplitude does not define a unique crack morphology but rather a range of morphologies and associated burst pressures with the empirical relationship established by the voltage/burst correlation. The correlation relates the EC sensitivity and burst pressures to the degradation morphology. To date, emphasis in developing the burst correlation has been placed on axial ODSCC with crack branching and limited IGA which represents the Plant L tubes active prior to tube pulling and many other plants based upon pulled tube examinations. Assessments of increased IGA involvement will be performed as data become available. The crack morphology for previously active Plant L pulled tubes shows limited IGA involvement such that the model boiler generated ODSCC specimens are representative of Plant L SG tube degradation. The large number of Plant L pulled tube intersections (21 data points) help to define the voltage/burst correlation below a few volts. Currently available data for increased IGA involvement indicates that the current burst correlation tends to envelope IGA and IGA/SCC modes of degradation. Section 5.1 shows comparable voltage responses, Section 8 includes Plant L data with IGA/SCC in the burst correlation.

Data analysis guidelines for voltage amplitudes are given in Appendix A to minimize the human factor variability in interpreting signal amplitudes. Some uncertainty will remain and becomes reflected in the spread of the voltage/burst correlation. For conservatism, the eddy current analyst variability is also included in the NDE voltage uncertainty. However, this issue is less significant for application of the voltage plugging limits than for 40% depth limits, for which indications are evaluated at or near the detection threshold such that many of the indications have a poor signal to noise ratio. Under these circumstances, it is expected that the human factor plays a greater role in determining the accuracy of the inspection. The voltage limits move the amplitude of concern for tube plugging to generally higher signal to noise ratios so that human factors and details of interpretation guidelines become less significant.

To assess analyst variability on voltage measurements, an assessment was performed by comparing voltage measurements from six analysts evaluating the largest indications (592 included in the evaluation) at TSP intersections found in the 1991 Plant L inspection. The steps included in this assessment of analyst variability included:

o   Preparation of eddy current analysis guidelines similar to Appendix A including Plant L examples.

o   Preparation of tapes of bobbin data for the largest indications found in the last inspection. A total of 592 indications were used in the evaluation.

o   Selection of six eddy current analysts including primary vendor analysts and subcontracted analysts typically used in Plant L inspections.

·o   Discussion of the Plant L guidelines with the six analysts utilizing a Westinghouse analyst having previous experience with the guidelines to explain the guidelines using Plant L examples.

o   Independent evaluation of the 592 Plant L bobbin indications to obtain 592 x 6 = 3552 data points to evaluate the eddy current analyst variability and define the associated NDE uncertainty.

Figure 5-25 shows the distribution of voltage amplitudes for the 592 indications obtained as the average of the six independent evaluations for each indication. The voltages ranged from about 0.6 volts to 3.8 volts with an average amplitude of 1.41 volts. Figure 5-26 shows the distribution of analyst differences from the mean for each of the 592 indications. The mean of the difference is 0.0 voltage with 1904 of the 3552 data points between -0.05 and +0.05 volts. The distribution is narrower than a normal distribution and shows exponentially decreasing trends from the zero voltage difference peak of the distribution. At 90% cumulative probability, the analyst variability is 0.13 volts or 9.2% of the 1.41 average voltage. Based on this evaluation, a 10% uncertainty at 90% cumulative probability was derived and is applied for the Kewaunee eddy current analyst variability as part of the NDE uncertainty. This result is the same as found in a similar study for two units at another plant (WCAP-12871, Rev. 2).

It can be noted that a similar analyst variability study was performed following the 1991 Plant L outage. In this case, the eddy current analyses were performed with no major emphasis on voltage measurements and no specific guidelines for voltage interpretation. This study performed on 925 indications yielded an analyst variability of 27% (differences between two analysts for each indication) at 90% cumulative probability. The reduction of the associated NDE uncertainty from 27% to 10% (differences of six analysts from the mean) demonstrates the benefits of analysis guidelines such as Appendix A in developing consistency and repeatability of voltage measurements.

As noted in Table 5-9, the use of field voltage measurements for pulled tubes obtained prior to implementing the present voltage calibration requirements contributes to the spread or

uncertainty in the burst correlation. Uncertainties associated with field crevice conditions, like the human factors, are more significant at the low amplitudes near detection thresholds than at the voltage plugging limits. This has been the experience in Plant L SGs where distorted indications have been primarily low amplitude indications. Again, the larger amplitudes near voltage plugging limits provide more reliable quantification of the indications than associated with current experience with depth limits for tube plugging. This is supported by the 10% eddy current analyst variability uncertainty developed from the larger Plant L indications as described above.

An uncertainty in the burst correlation that adds conservatism to the correlation is the effect of tube pull forces on crack morphology and potential reduction in burst pressures. Although not a major concern for axial indications, effects of the tube pull such as loss of ligaments can occur. Since pre-pull field voltage amplitudes rather than post-pull values are used in the burst correlation, the pull force effects add conservatism. Post-pull voltages are commonly higher than pre-pull values, particularly for indications that tend toward lower burst pressures on the voltage/burst correlation. For example, Plant L tube R8C69 had post-pull voltages for both bobbin and RPC probes that were higher than pre-pull voltages by a factor of two or more.

Based on the above, the contributions to the NDE uncertainty at 90% cumulative probability are 9% for probe wear and 10% for analyst variability. These contributors can be considered independent variables and combined as square root-sum-of-squares (SRSS) to obtain the net NDE uncertainty of 14%. For probabilistic SLB leak rate and tube burst evaluations, as required for the tube plugging criteria of Section 13, a distribution for the NDE uncertainty is required. The probe wear uncertainty with a standard deviation of 7% (Section 5.5) is bounded at 15% by the probe replacement requirement. The cumulative probability distribution of Figure 5-25 is used for the NDE uncertainty due to analyst variability. Fcr analyses in Section 13 demonstrating the Monte Carlo methods, the upper bound on the total NDE uncertainty distribution is estimated at about 25% representing the SRSS of 15% for probe wear and 20% for analyst variability. The distribution for the NDE uncertainty for these demonstration analyses is then represented by a standard deviation of 11% with a distribution cutoff at 25%.

Overall, the NDE uncertainty reflects measurement repeatability and is dominated by probe wear allowances which can be limited to 10-15% by field implementation of a probe wear standard. Burst correlation uncertainties are dominated by crack morphology variations which are accounted for by application at the lower 95% uncertainty on the burst correlation for tube plugging limits.

5.9   Conclusions

1.   The use of probes from Echoram or Zetec has negligible influence on the data acquisition for the tube plugging criteria.

2.   For indications with amplitudes greater than 2 volts the presence of the tube support causes only small changes in indication response for the ODSCC specimens.

3.   Small indications, where their amplitude approaches the size of the mix residual, can be influenced by the presence of the support.

influenced by the presence of the support.

4. The eddy current response is essentially unaffected (~5%) for a packed tube to tube support plate crevice as compared to an open crevice.

5. Large amplitude cracks which are likely to have oxide coating on the crack surfaces remain detectable by eddy current in the presence of minor denting. Small amplitude cracks and cracks with clean crack surfaces (i.e., fatigue generated cracks) may be masked by the dent signal for dented intersections.

6. Probe centering characteristics, related to probe wear, can contribute to the uncertainty of the eddy current signal. This uncertainty was found by probe wear test simulations to be about [   ]^a to envelope typical field probe replacements. Probe wear influence on the signal uncertainty can be controlled by the use of an appropriate wear standard. The staggered 4-hole standard will be applied at Kewaunee to limit the voltage amplitude uncertainties from probe wear to [   ]^a for the 720 mil diameter probe.

7. Use of ASME standards cross calibrated against the reference laboratory standard and calibration of the voltages at the 400/100 kHz mix channel for the 20% ASME hole are recommended for application of the tube plugging criteria. Calibration at the mix frequency is recommended to minimize effects of variations in frequency response between probes. Calibration at 400 kHz can be performed if, for the probes used in the inspection, the ratio of the mix to 400 kHz voltage is the same as obtained for the laboratory probes (0.69) within about 5%.

8. NDE uncertainties contribute to the spread or uncertainty in the voltage vs. burst pressure correlation and tend to lower the structural limit for tube burst which is based on the lower 95% confidence interval. The use of reference calibration standards, frequency mixes, etc. are directed toward minimizing the NDE uncertainties associated with voltage measurement repeatability. Other NDE considerations remain as part of the burst correlation uncertainty although the principal variable in the burst uncertainty is crack morphology differences.

9. Eddy current analyst variability was evaluated for 592 Plant L indications (from the 1991 outage) utilizing six analysts typical of personnel utilized at Plant L inspections. Evaluation of the bobbin voltage differences between the six analysts and the average amplitude from the six analysts' data leads to a bobbin voltage uncertainty of 9.2%. Utilization of the Appendix A eddy current analysis guidelines to reevaluate the data in this analysis reduced the bobbin voltage variability from the 27% value obtained without the guidelines.

10. At 90% probability, the bobbin voltage NDE uncertainty is 14%. This is based on SRSS averaging of 9% for probe wear and 10% for analyst variability.

11. For EOC voltage projections and SLB leak rate analyses, the NDE uncertainty distribution can be represented by a standard deviation of 7% with a distribution cutoff at 15% together with the cumulative probability distribution of Figure 5-25 for analyst variability.

Table 5-1

Effect of Flaw Location on Bobbin Coil Measurements*

Flaw Location	50% Deep Slot		100% Deep Slot	
	Voltage	Depth	Voltage	Depth
1. Slot centered in TSP	0.95	43%	47.4	100%
2. Slot extending from TSP edge inside TSP	0.95	72%	48.1	100%
3. Slot extending from TSP edge outside of TSP	1.07	36%	49.3	99%
4. Slot without a TSP	1.07	49%	48.7	99%

_____

* Measurements for 0.25 inch long EDM slot in 0.75 inch diameter tubing.

Table 5-2

Typical Voltage Amplitude for Volumetric Types of Degradation

Type of Degradation	Voltage Examples	Comments
Wastage		
o Characterized by machined rectangular flaws	~4.5-7.5 volts @60% depth[1]	Data of Figure 5-9
Fretting		
o Characterized by machined, tapered flaws	~10 volts @60% depth[1]	Data of Figure 5-9
Pitting		
o Single drilled hole simulation	~7.5 volts for 60 mil dia., 100% deep	Data of Figure 5-10
	~5.3 volts for 109 mil dia., 60% deep	Data of Table 6-4 of WCAP-13129 Rev. 1
	~2 volts for 30 mil dia., 100% deep	Data of Figure 5-10
o Multiple pits	~2 volts multiple indications for multiple pits up to 60 mils in diameter and 64% deep	Pulled tube example

Note 1. Typical limiting depths for continued service allowing 10% for EC uncertainty and about 5% for growth between inspections.

Table 5-3

Bobbin Coil Detectability of EPRI IGA Samples[*]

Specimen No.	Differential B. C.		Absolute B. C.		Comments
	Volts	Depth	Volts	Depth	
1-3	1.07*	11%	2.48	34%	
	2.33*	17%	2.78	22%	
	40.0	95%	33.3	91%	Crack
1-4	1.57*	12%	2.6	13%	
	4.0	72%	5.7	72%	Crack
	9.0	80%	4.1	70%	Crack
1-5	0.8*	0%	0.9	8%	
	0.7*	0%	0.9	15%	
1-8	1.0*	8%	2.3	14%	
	2.0*	6%	2.6	14%	
1-15	0.9*	6%	1.4	6%	
	0.85*	0%	1.0	13%	
1-17	0.4*	0%	0.45	0%	
	0.6*	0%	0.7	0%	
1-18	NDD		NDD		
1-19	NDD		NDD		
1-20	0.65*	0%	0.67	0%	
	0.42*	0%	0.45	0%	

---

[*] Voltage measurements represent the peak at the start or end of the IGA. Peak to peak differential voltages would be about twice the single peak values for comparisons with the absolute voltages and for comparisons or correlations with ODSCC degradation at TSPs.

Table 5-4

**Comparison of the EDM Notch Amplitude Response of Probe ZT and Probe ER
(Ratio Probe ZT /Probe ER)**

Notch Depth	400 kHZ	200 kHz	100 kHz	Mix 400/100 kHz
100 %	1.07	1.70	1.94	1.01
80 %	0.98	1.67	1.93	0.94
60 %	1.05	1.67	1.90	0.94
40 %	1.04	1.70	1.87	0.91

Table 5-5

**Comparison of ASME Hole Amplitude Response of Probe ZT and Probe ER
(Ratio Probe ZT/ Probe ER)**

Hole Depth	Response Ratio 100/400 kHz Mix
100 %	1.58
80 %	1.54
60 %	1.55
40 %	1.53

Table 5-6

Comparison of Tight (Magnetite Packed) and Open Crevices
for Probe ZT and Probe ER
(Ratio Tight/Open)

Sample	400/100 kHz Mix	
	Probe Zt	Probe Er
BW-8	1.05	1.08
BW-10	1.01	1.03
BW-11	1.51*	1.54*
BW-14	0.95	0.97
BW-17	0.96	0.94
BW-12	0.91	0.93

* Caused by process of packing the crevice as verified by comparing the pre-packed response with the tube response after removal of the magnetite packing.

Table 5-7

Influence of Denting on Indication Response

Sample	400/100 Mix Amplitude		Dent Size
	Before Denting volts	After Denting volts	volts
Fatigue			
FAT-1	61.5	18.6	7.39
FAT-2	14.6	5.42	6.09
FAT-3	NT	2.39	12.1
FAT-4	59.0	NDD	12.08
FAT-7	NT	1.24	9.43
FAT-8	69.0	NDD	17.4
Doped Steam			
BW-1	8.9	18.0	14.7
BW-3	12.5	3.97	6.27
BW-9	4.21	4.9	6.36

NT   No Test
NDD   No Detectable Degradation

Table 5-8

Channelhead Mockup Probe Wear Standard Test Results

Tube Location	Number Test Repeats	No. Probe Replacement Chances(1)	Number of occurrences of Voltage Difference > 15% from New Probe (2)					
			Echoram Probe(3)			Zetec Probe(3)		
			.005	.0075	.011	.0025	.005	.0075
R8C92	10	100	0	0	0	0	82	96
R2C88	2	4	0	0	0	0	2	4
R33C47	10	100	0	0	3	0	0	88
R3C45	2	4	0	0	0	0	0	4
R10C45	2	4	0	0	0	0	0	4
R23C44	10	100	0	0	0	0	40	100
R30C36	2	4	0	0	0	0	0	4
R3C16	2	4	0	0	0	0	0	4
R20C15	10	100	0	0	1	0	0	80

Notes:

1. Number of tests permitting comparisons of 4-hole voltages between worn and new probes.

2. An occurrence of voltage difference > 15% is each occurrence that absolute [(Vworn-Vnew) / Vnew] is 15% for at least one of the 4 holes.

3. Dimensions (0.005, etc.) are reductions in radius (inches) of the probe centering devices.

Table 5-9

Variables Influencing NDE Voltage and Burst Correlation Uncertainties

NDE Voltage Uncertainties (Voltage Repeatability)

o   Probe centering: probe diameter and wear considerations[1]
o   Calibration standards: dimensional tolerances[2]
o   Probe design differences[3]
o   Human factors affecting voltage repeatability that are not adequately controlled by data analysis guidelines

Burst Correlation Uncertainties

o   Crack morphology (length, depth, ligaments, multiple cracks, IGA involvement) variability for same voltage amplitude
o   Tubing dimensional tolerances[4]
o   Variations in field crevice conditions (open, packed, deposits, TSP corrosion, small dents, etc.)[5]
o   Effects of tube pull forces on crack morphology and associated burst pressures[6]
o   Utilization of voltage measurements for pulled tubes obtained prior to implementing voltage measurement standards of this report[7]

<u>Notes</u>:

1. Minimized in the field during APC implementation by use of a 4-hole probe wear standard.

2. The influence of dimensional tolerances of the calibration standards on voltage normalization is eliminated by calibrating the field standards to the laboratory reference standard.

3. Uncertainty minimized by specifying coil to coil spacing (coil centers are separated by 120 mils).

4. The influence of tubing dimensional tolerances as they affect burst pressure are inherently included in the spread of burst pressures from pulled tubes and laboratory specimens.

5. The influence of field crevice conditions as they affect burst pressure are inherently included in the spread of burst pressures from pulled tubes.

6. Results as pre-pull field measured voltages rather than post-pull voltages are used in burst correlation.

7. The use of field voltage measurements for pulled tubes obtained prior to implementing the voltage calibration requirements contributes to the spread or uncertainty contained in the burst correlation.

Figure 5-1

Voltage Sensitivity to Simulated Crack Network Morphology
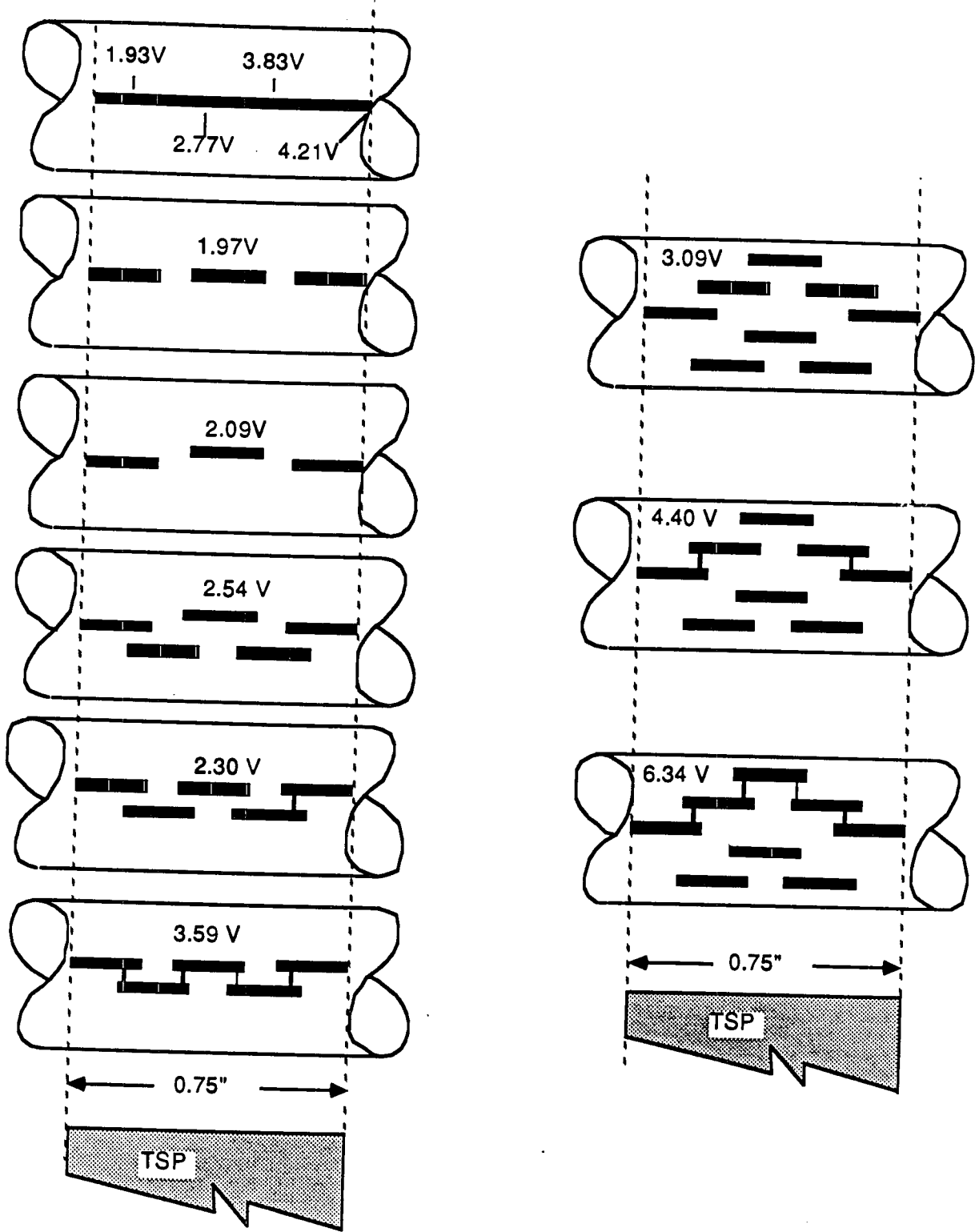
Figure 5-2

Bobbin Coil Voltage Dependence on Slot Length and Depth
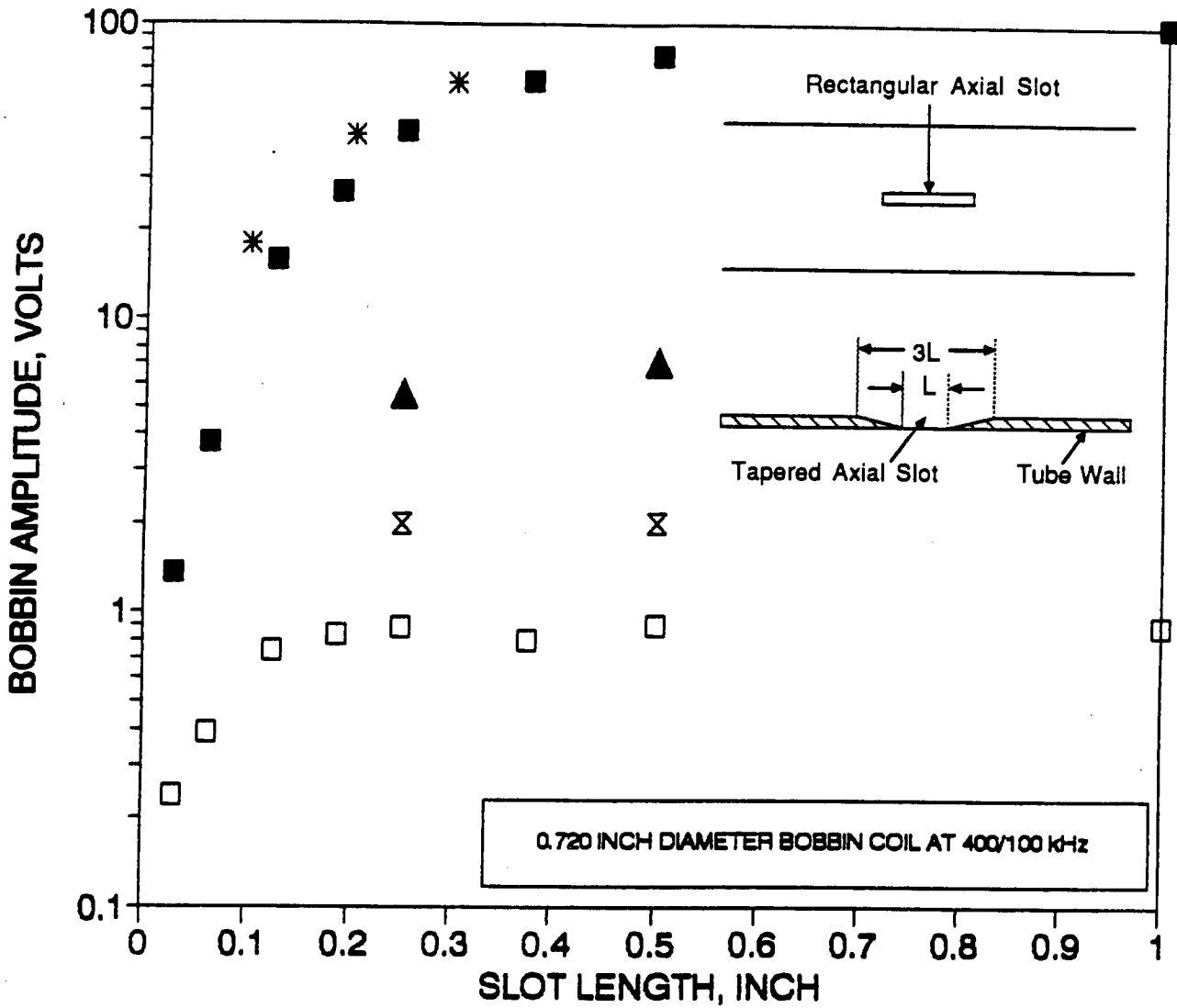
Figure 5-3

Bobbin Coil Voltage Increase due to Tapers at Ends of Through Wall Axial Slots
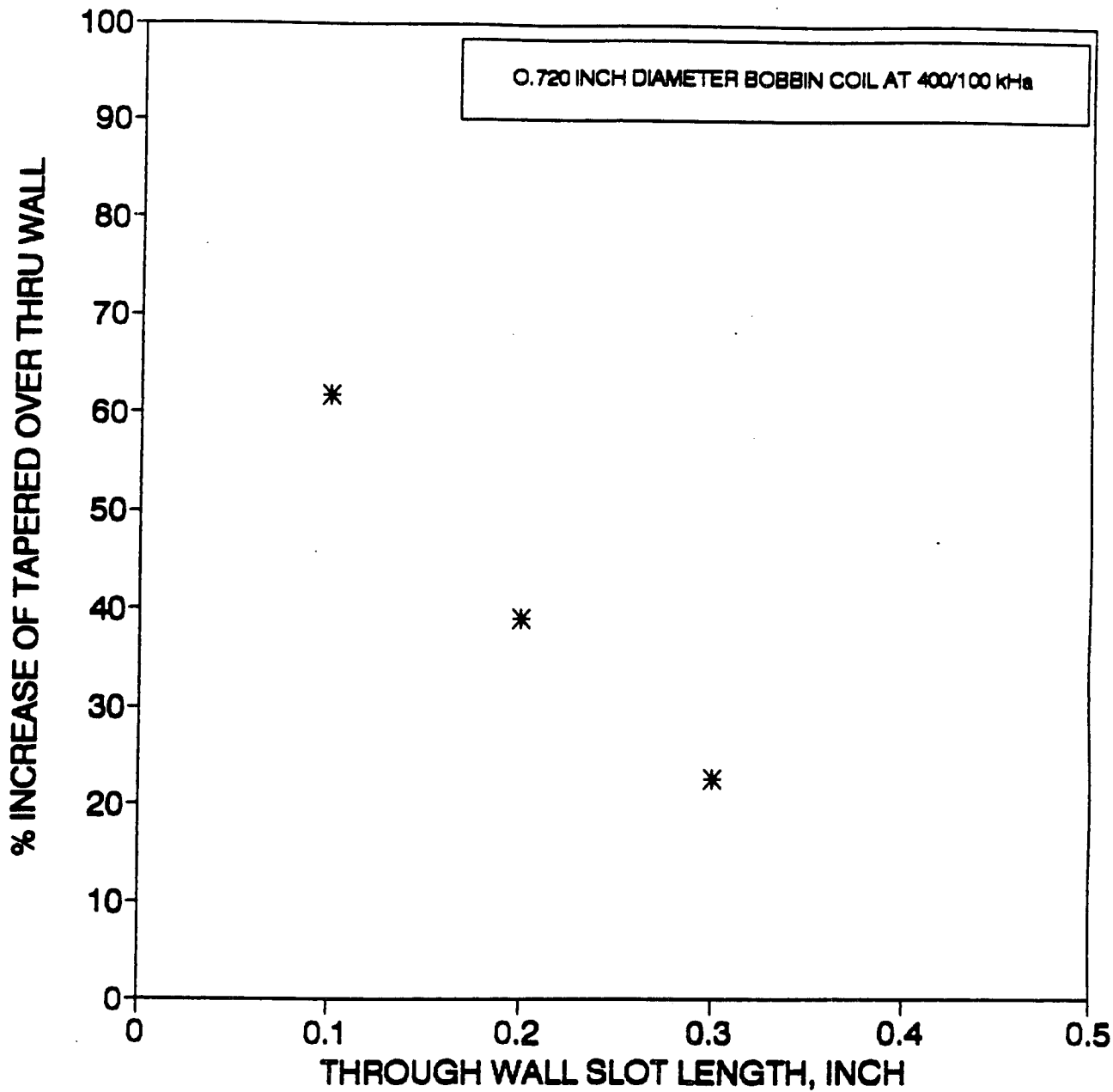
Figure 5-4

RPC Voltage Dependence on Slot Length and Depth

0.125 INCH DIAMETER RPC COILS AT 400 kHz

■ THRU-WALL □ 50% DEEP * TAPERED
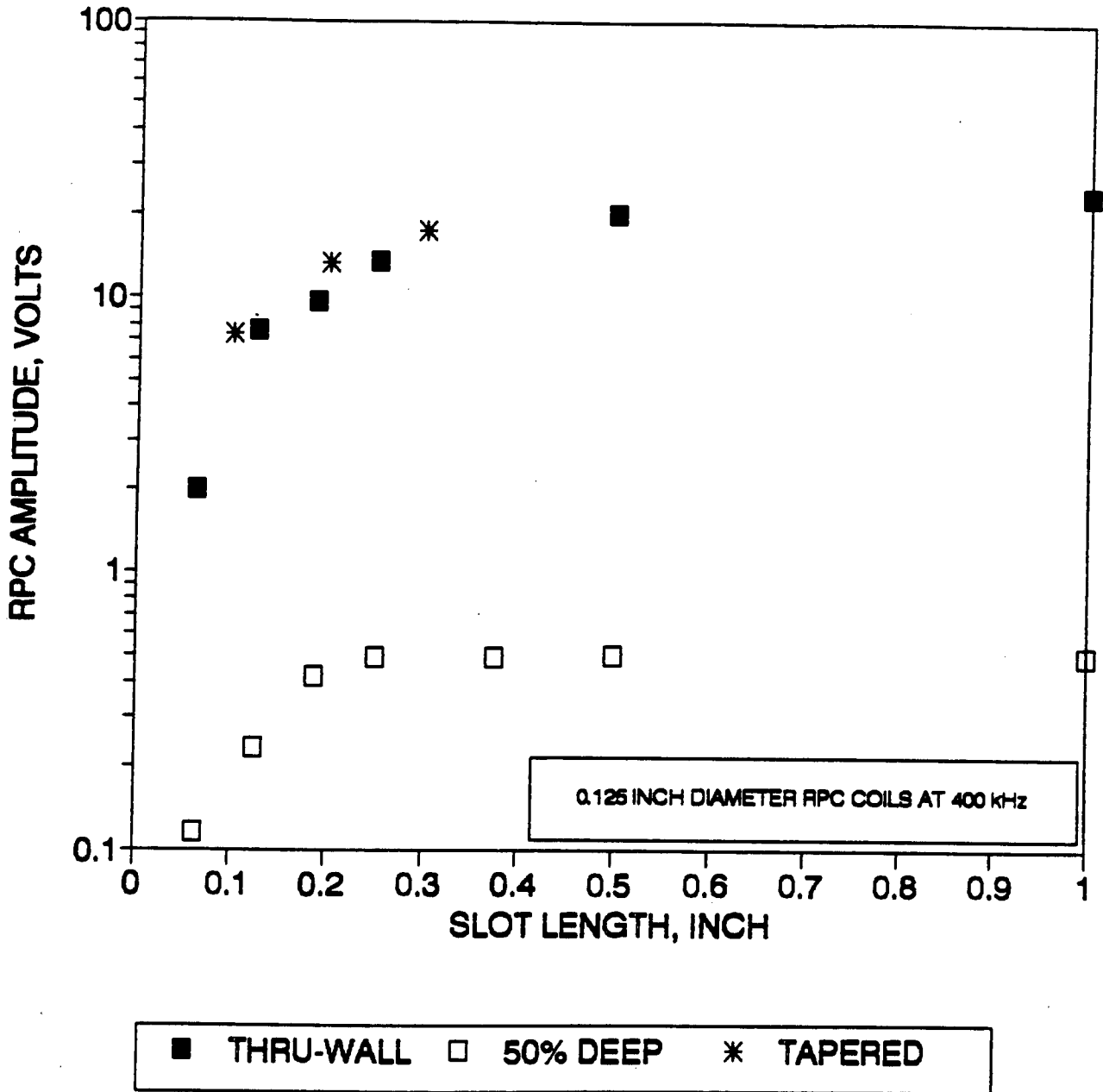
Figure 5-5

Correlation of Bobbin Coil to RPC Voltage
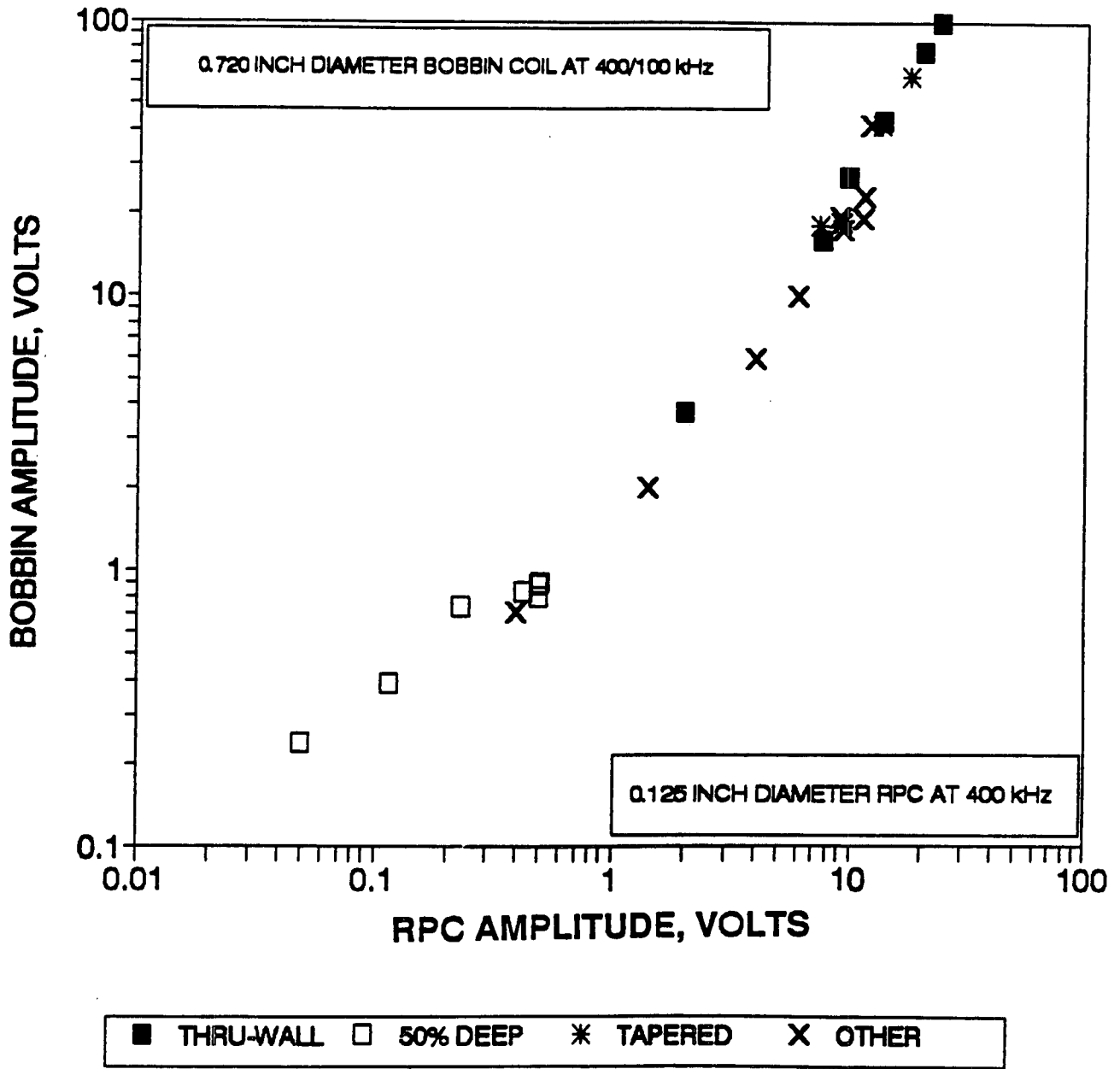
Figure 5-6

Voltage Dependence on Ligament Size Between Axial Slots
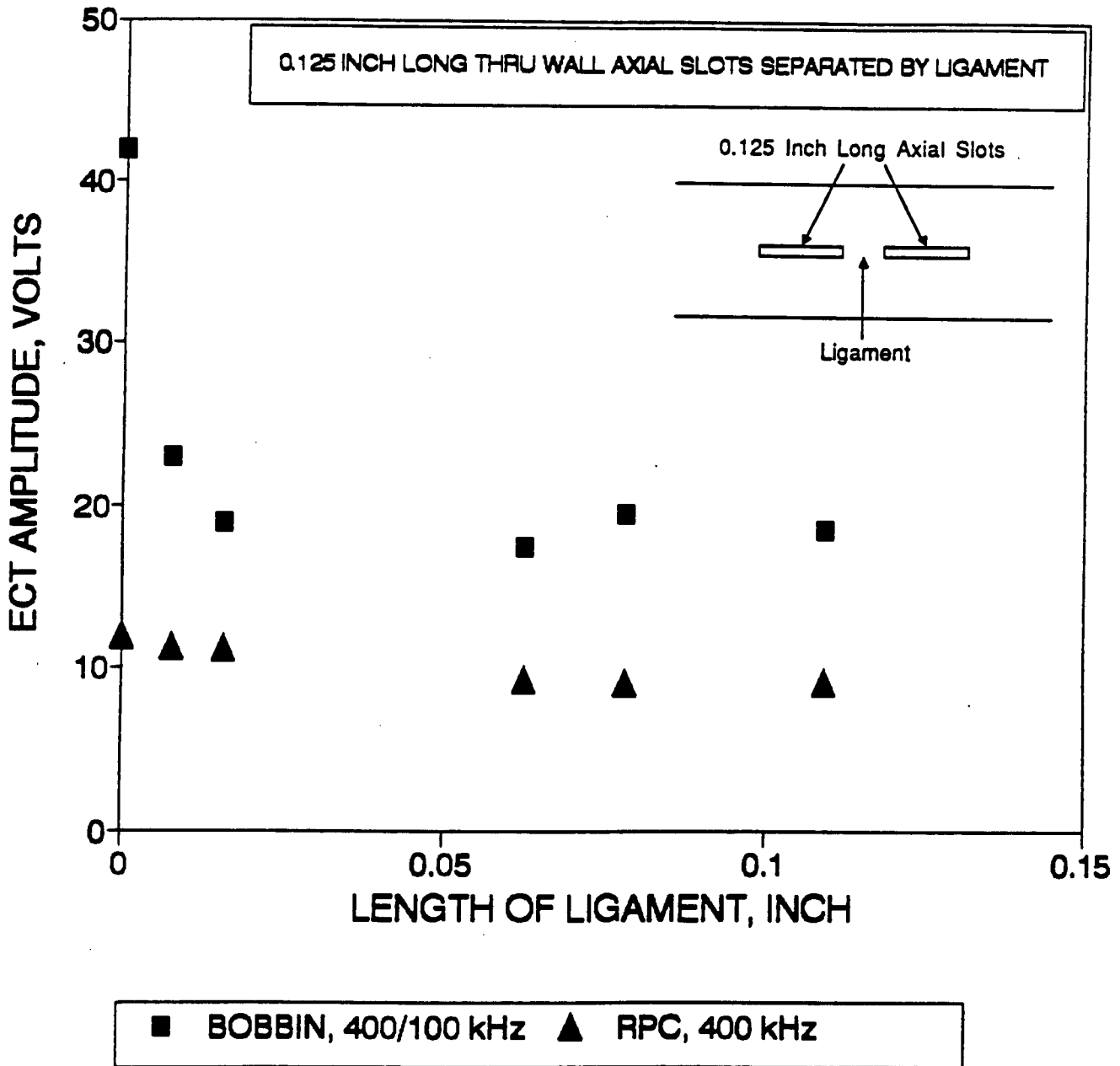
Figure 5-7

Bobbin Coil Voltage Dependence on Circumferential Spacing Between Axial Slots
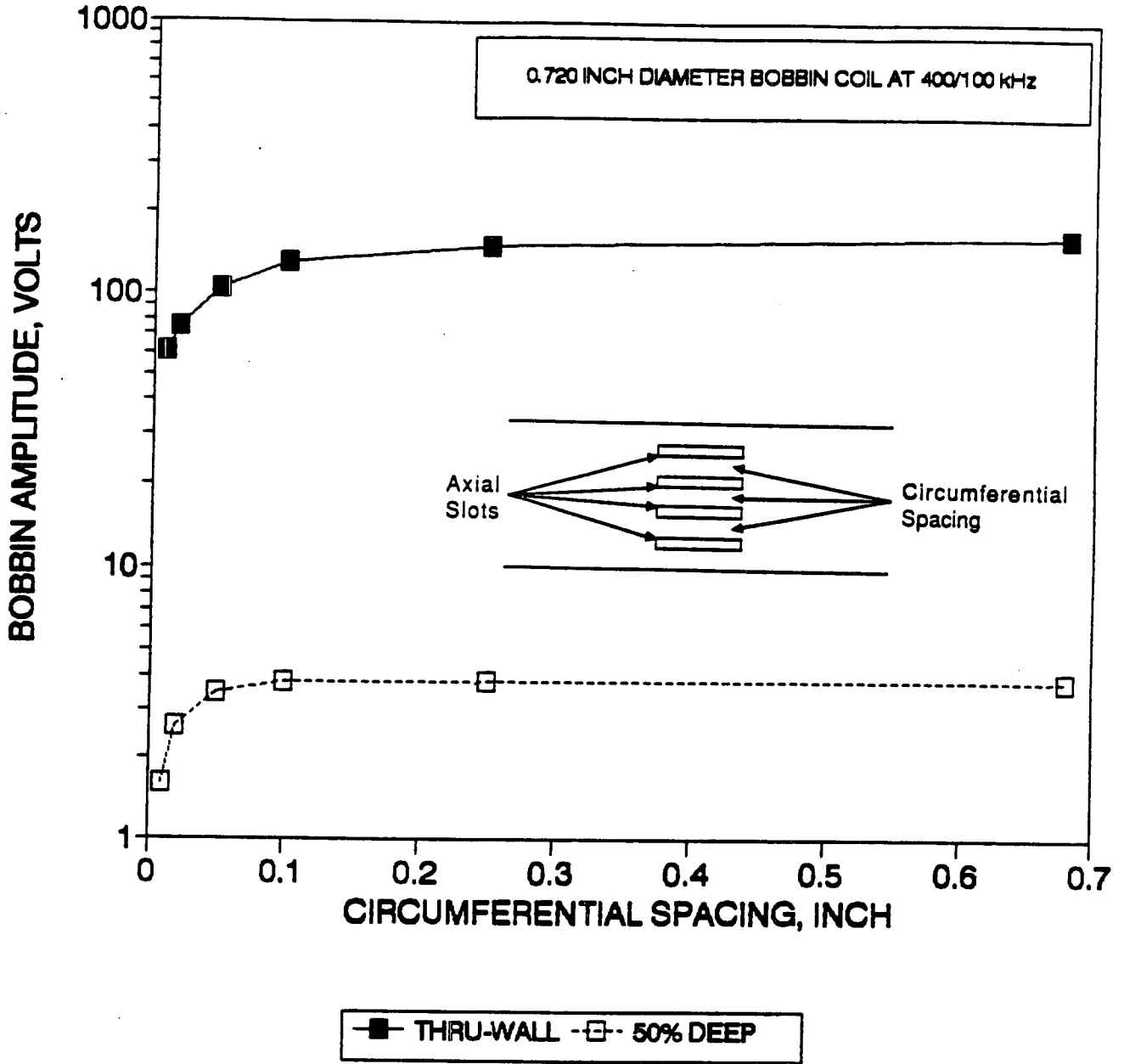
Figure 5-8

Burst Pressure vs. Voltage for EDM Slots

Burst Pressure Vs Bobbin Voltage
Thru-wall Slots
(7/8X0.05" Tubing)
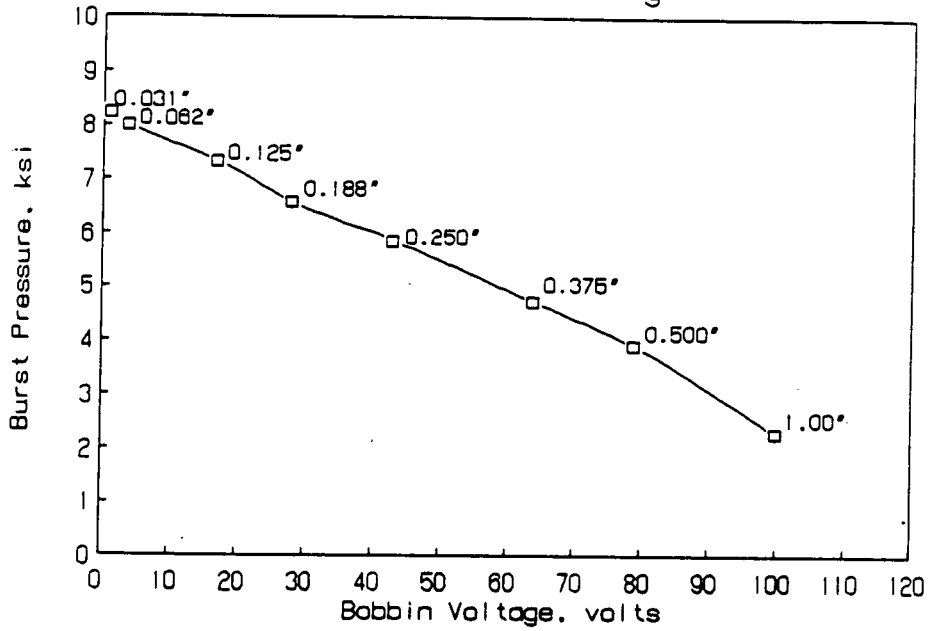
Burst Pressure Vs Bobbin Voltage
Partial Wall Slots
(7/8X0.05" Tubing)
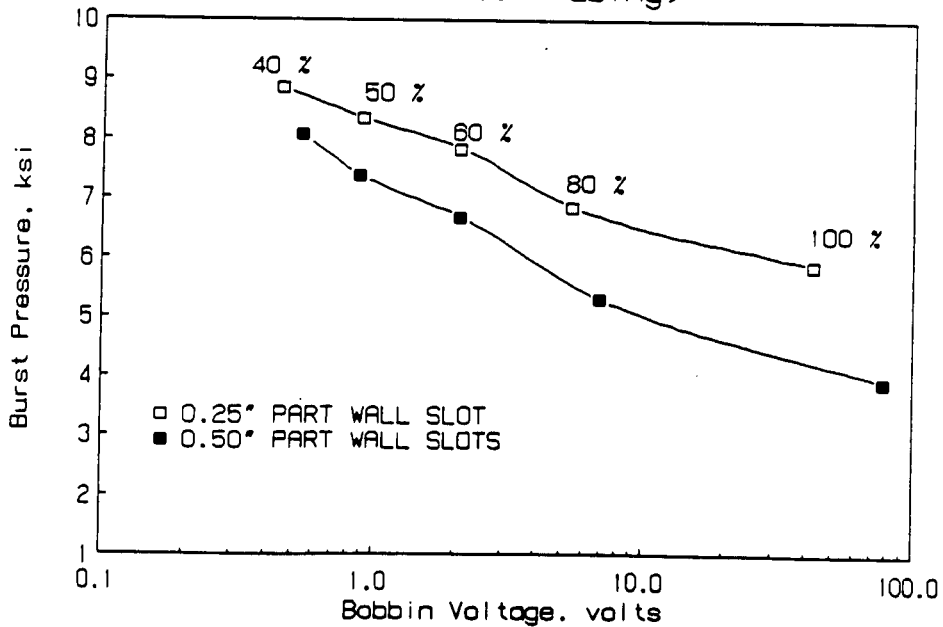
Figure 5-9

Typical Bobbin Coil Voltage vs Depth for Simulated Volumetric Tube Degradation
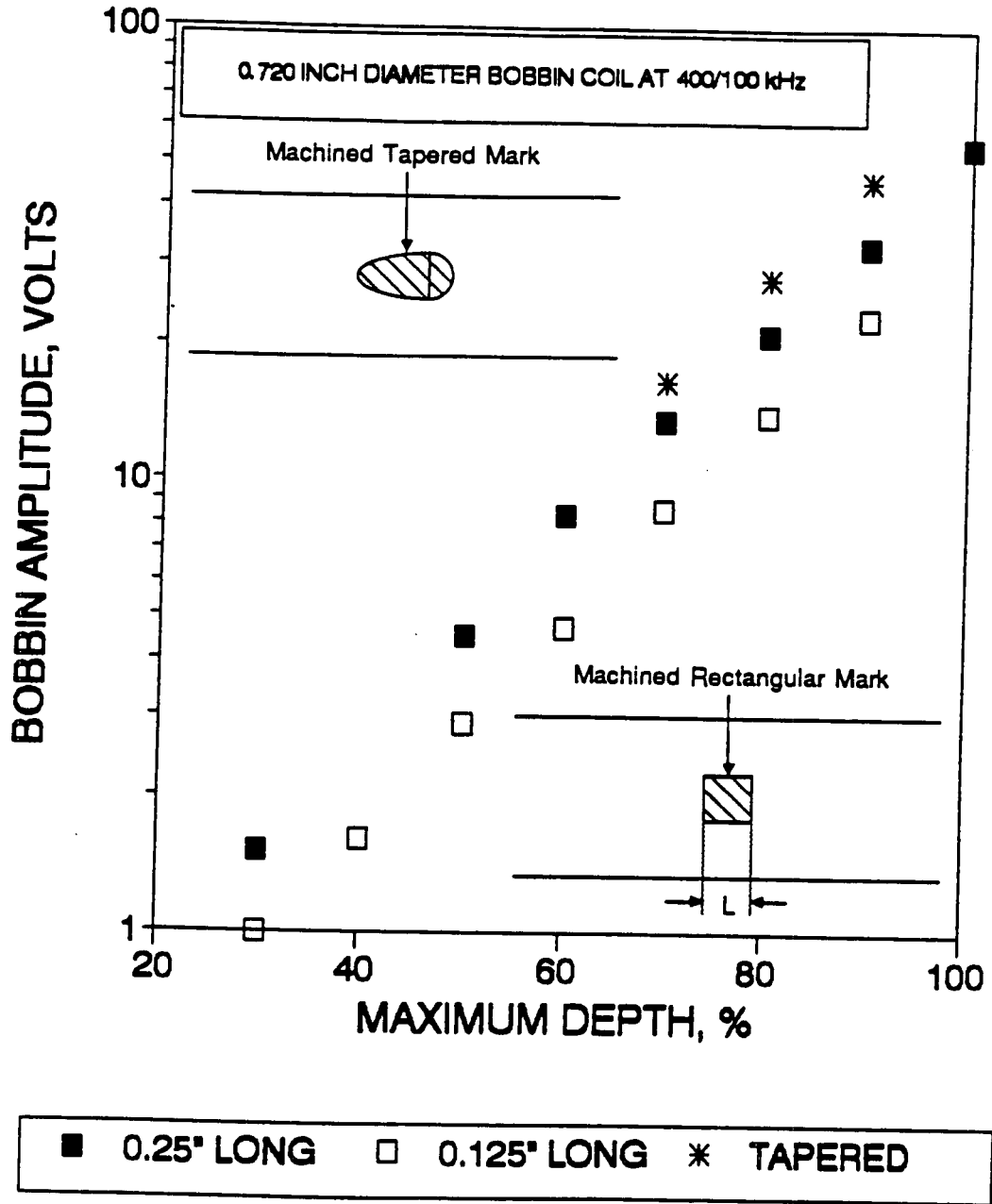
Figure 5-10

Bobbin Coil Voltage Dependence on Diameter of Through Wall Holes
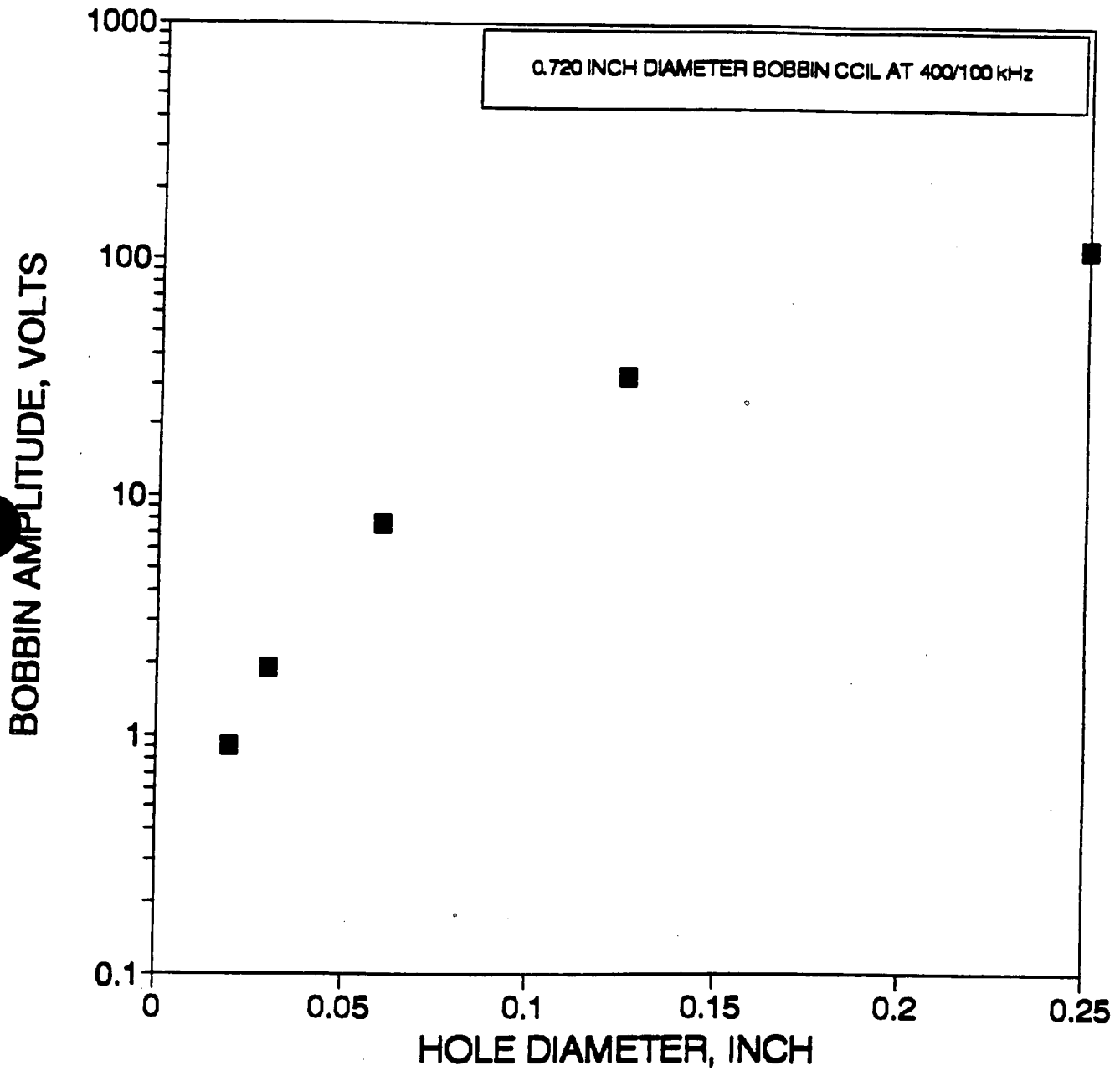
Figure 5-11

Photograph of the OD Surface of a Pulled Tube With Cold Leg Thinning
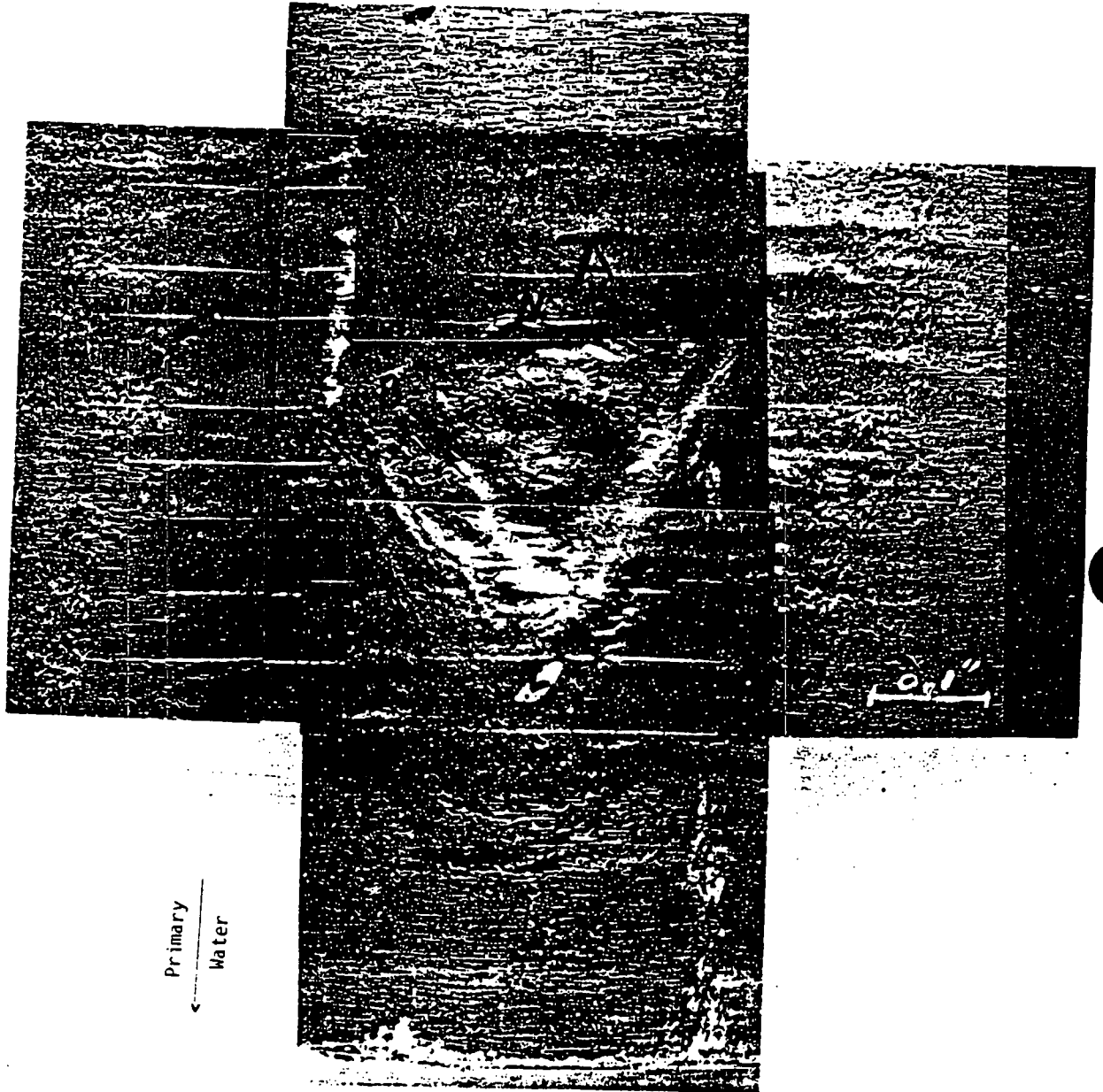
Figure 5-12a

Bobbin Data and Typical Metallographic Sections of Simulated
IGA Specimens Using Sensitized Alloy 600MA Tubing
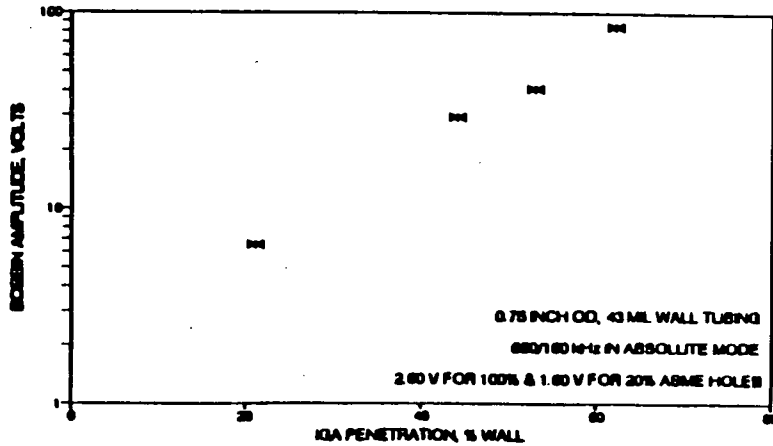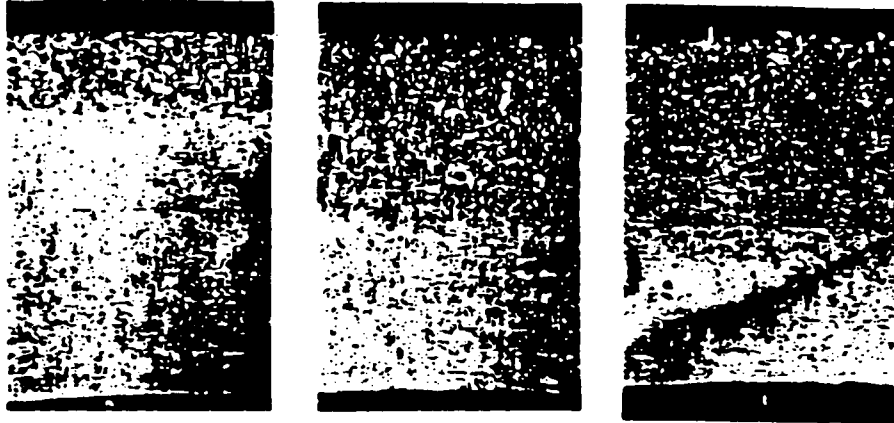
Figure 5-12b

Bobbin Data from Simulated IGA Specimens
Using Non-Sensitized Alloy 600MA Tubing
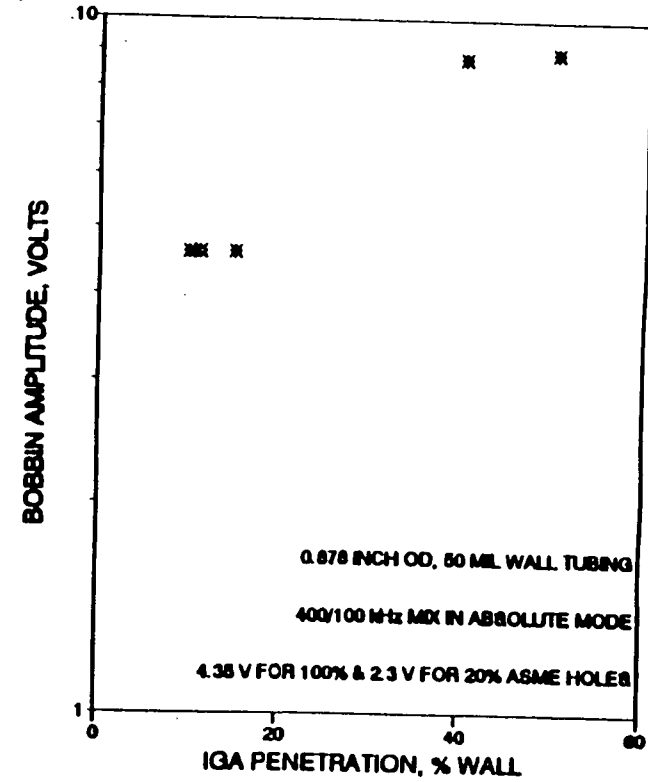
Figure 8-12. Bobbin Coil Results for Laboratory IGA Specimens

Microstructural   29% Thru Wall

Single Ball X-Ray

Dye Penetrant

RPC (ID)
(differential)

RPC (OD)
(differential)

Bobbin Probe Results (Differential)

Figure 5-13a   NDE Results for a Type 1 (IGA) Sample
(Dye Penetrant and X-Ray)

Figure 5-13b   NDE REsults for Type 1 (IGA) Damage
(Eddy Current)

Figure 8-13. Inspection Results for Laboratory IGA Samples from EPRI Program

Figure 5-14

Field EC Traces for Third TSP Crevice Region of Belgian Tube R19C35
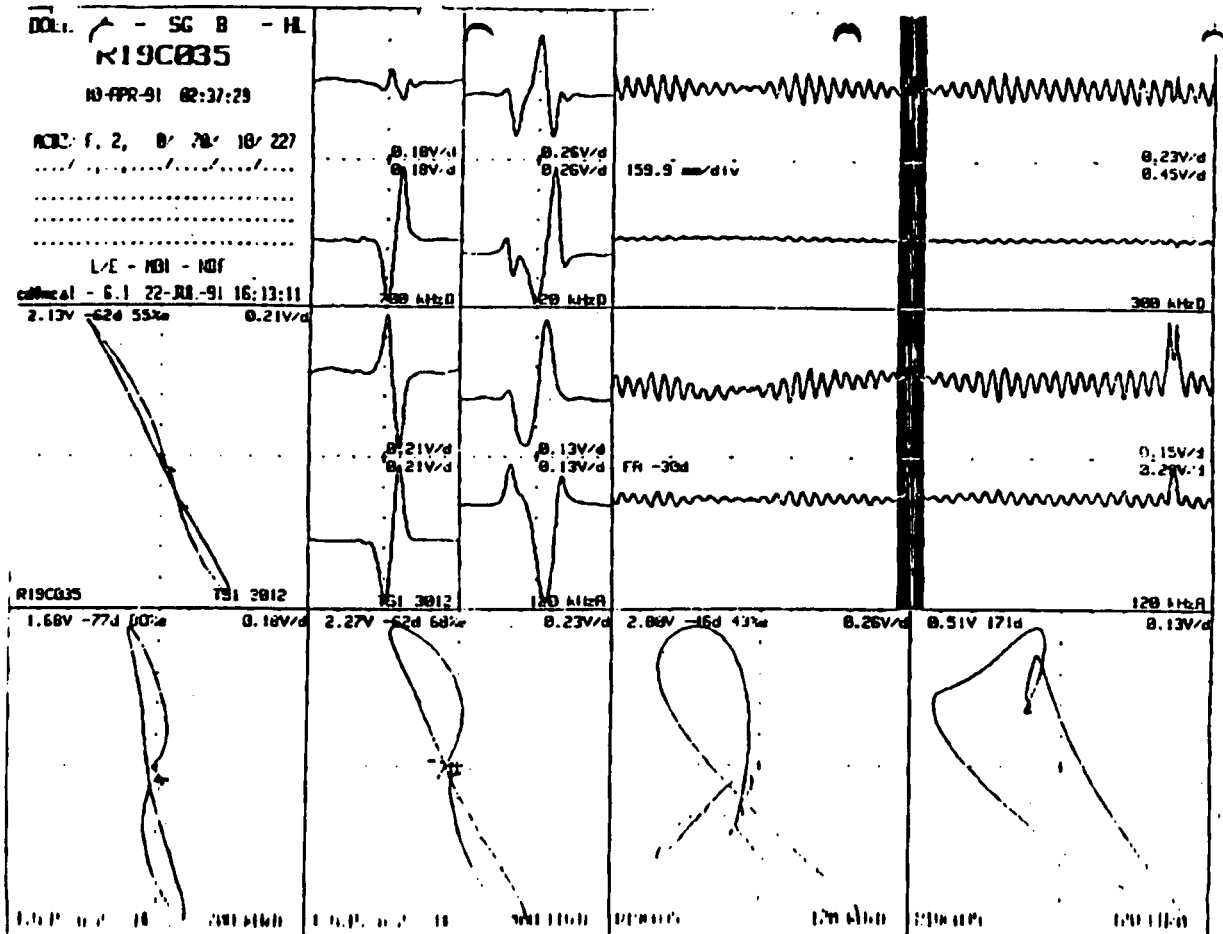
Figure 5-15

Voltage Comparison of Indications Found With Two Eddy Current Probes
(400/100 kHz Mix)

PROBE 1 VOLTAGE VERSUS PROBE 2 VOLTAGE

PROBE 2 VOLTAGE, VOLTS
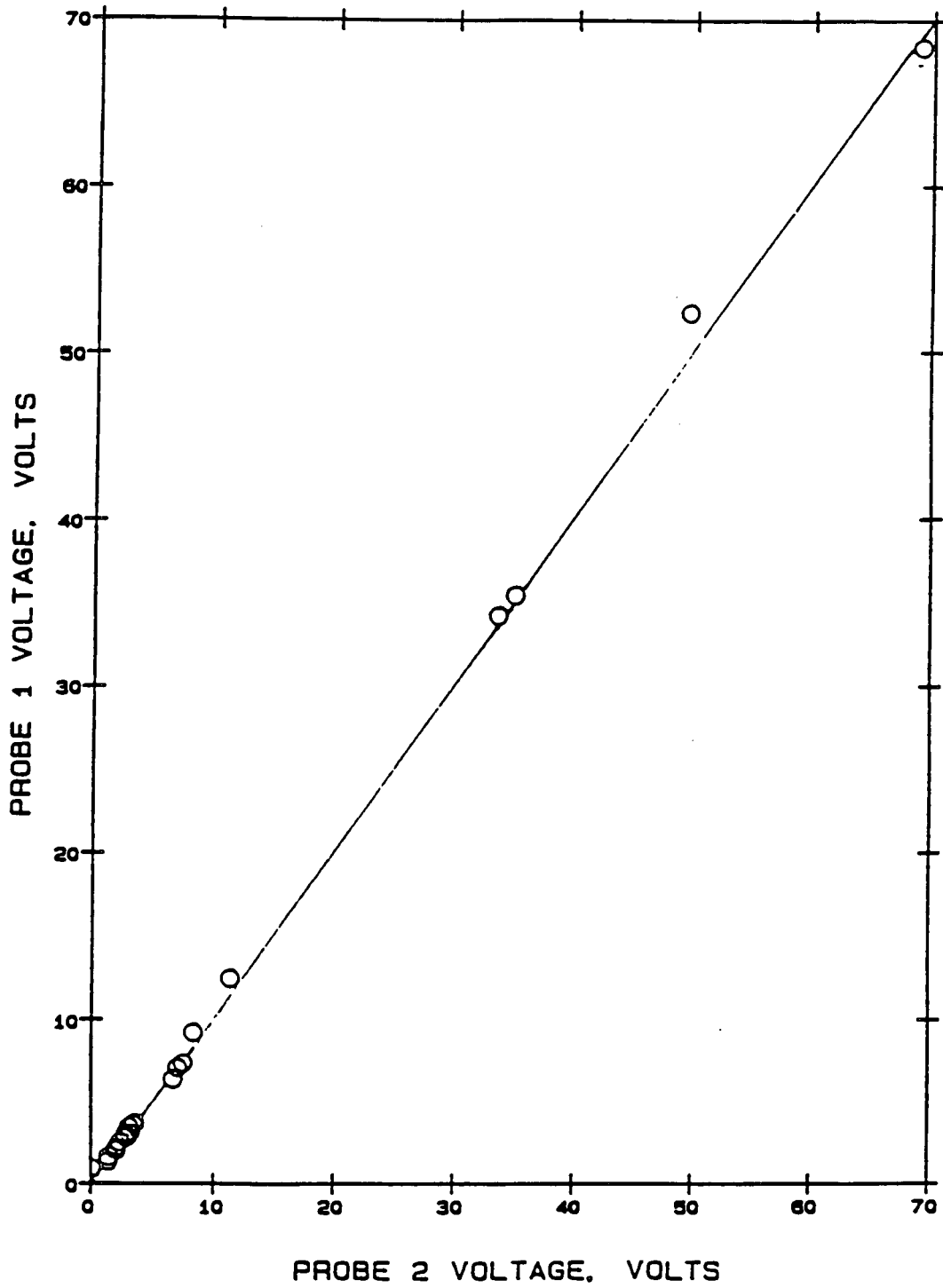
Figure 5-16

Comparison of 400/100 kHz Mix Amplitude Response from Two Probes (Model Boiler Sample)

EDDY CURRENT PROBE COMPARISON

PROBE 2/PROBE 1
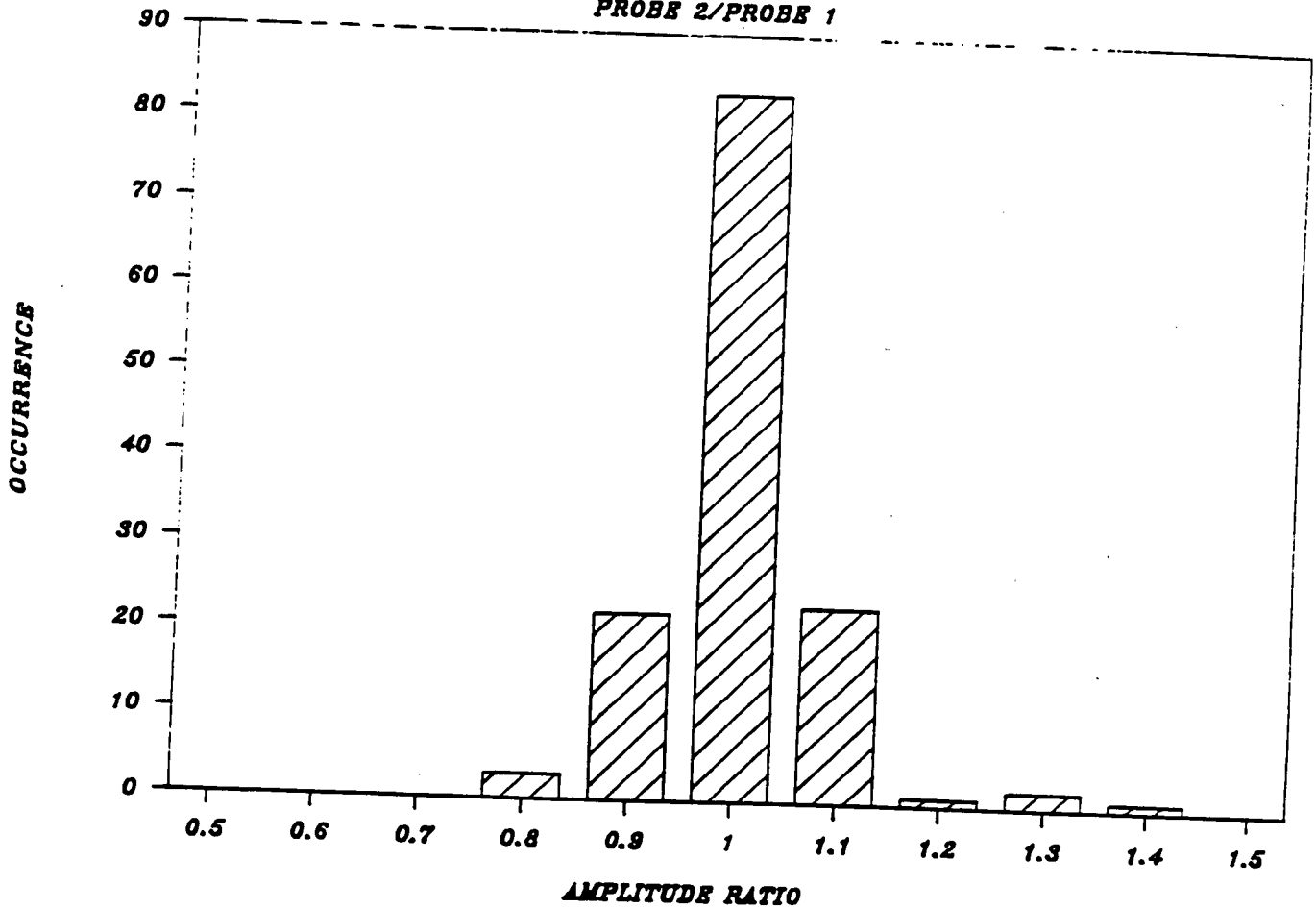
Figure 5-17

Comparison of 400/100 kHz Mix Phase Response from Two Probes (Model Boiler Sample)

EDDY CURRENT PROBE COMPARISON
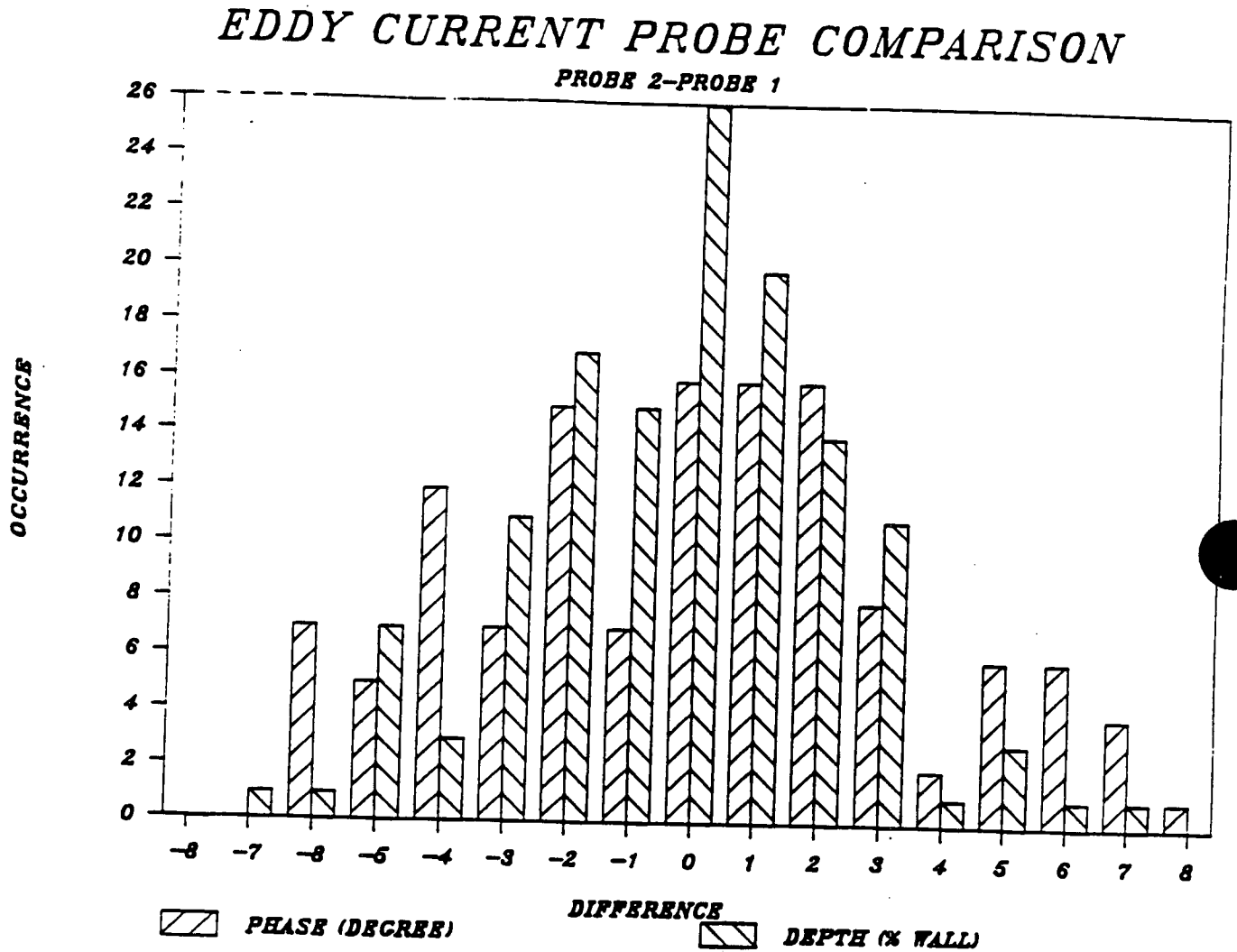
Figure 5-18

Comparison of Tight and Open Crevice Indication Response

INDICATION RESPONSE
TIGHT/OPEN CREVICE

RATIO TIGHT/OPEN CREVICE
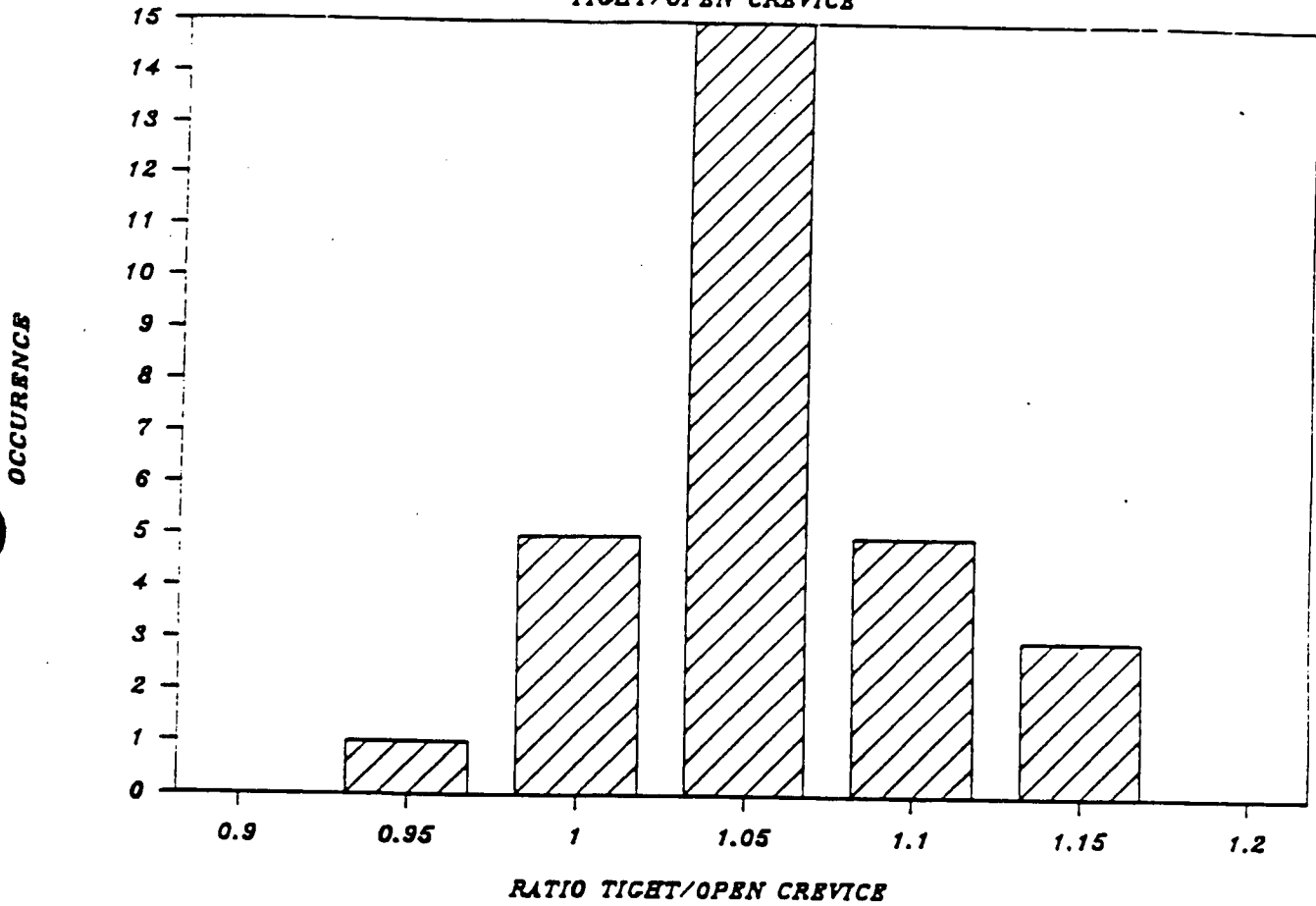
Figure 5-19

Probe Wear Calibration Standard
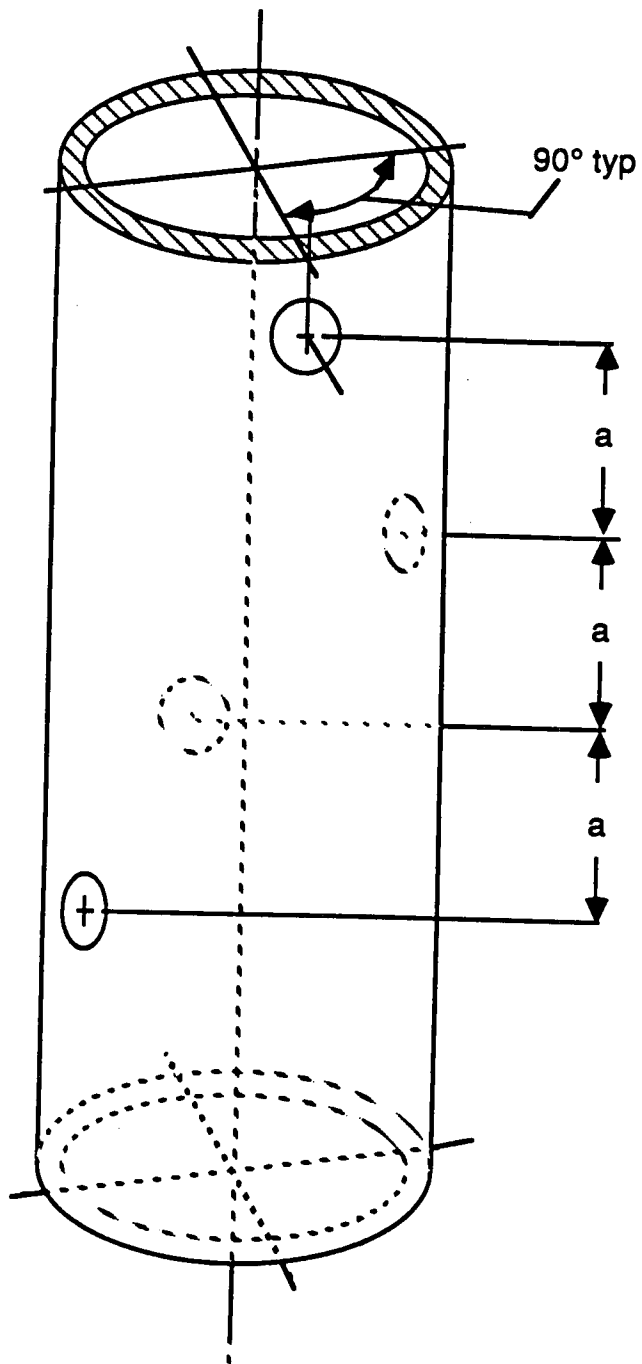
Figure 5-20

Bobbin Coil Amplitude Dependence on Probe Wear

Echoram Probe
Wear Standard in Vertical Tube Location

Echoram Probe
Wear Standard Horizontal in Channelhead

Zetec Probe
Wear Standard Horizontal in Channelhead
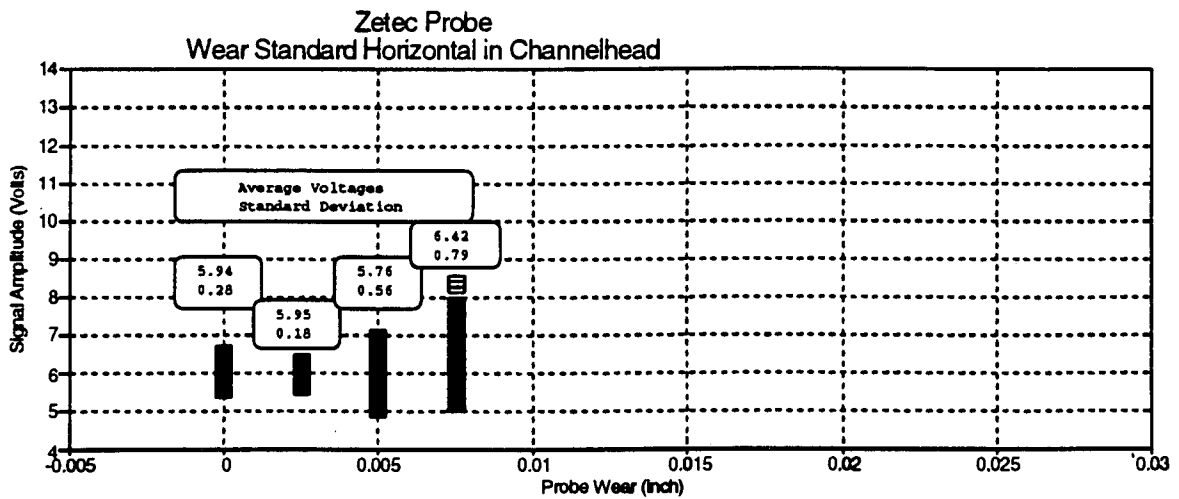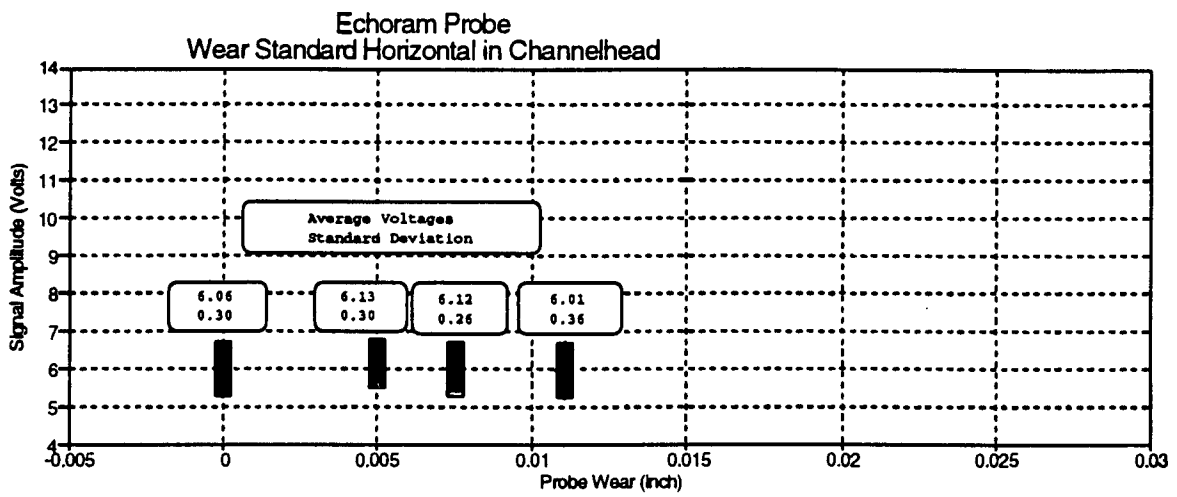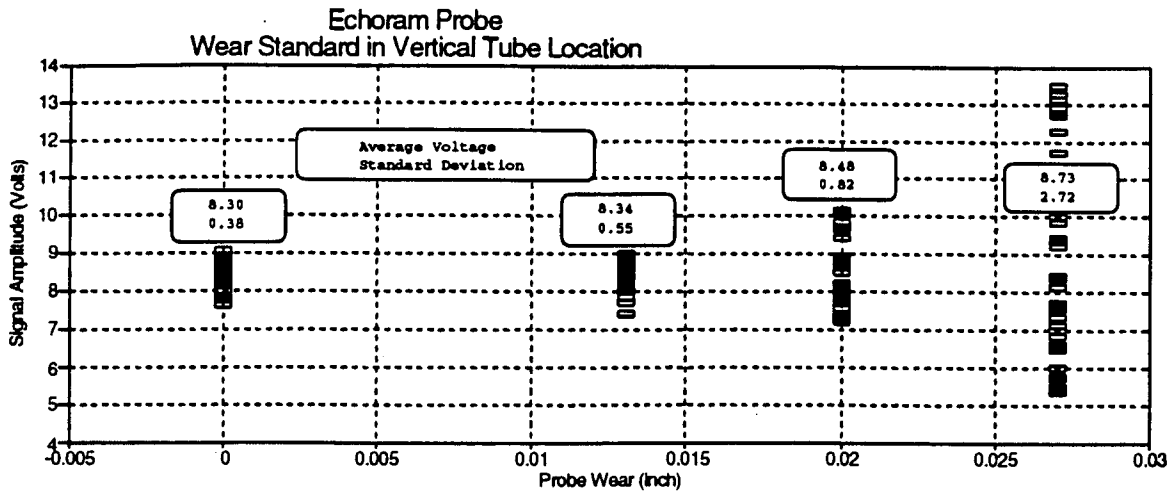
Figure 5-21

Voltage Variability Due to Bobbin Probe Wear

5-46
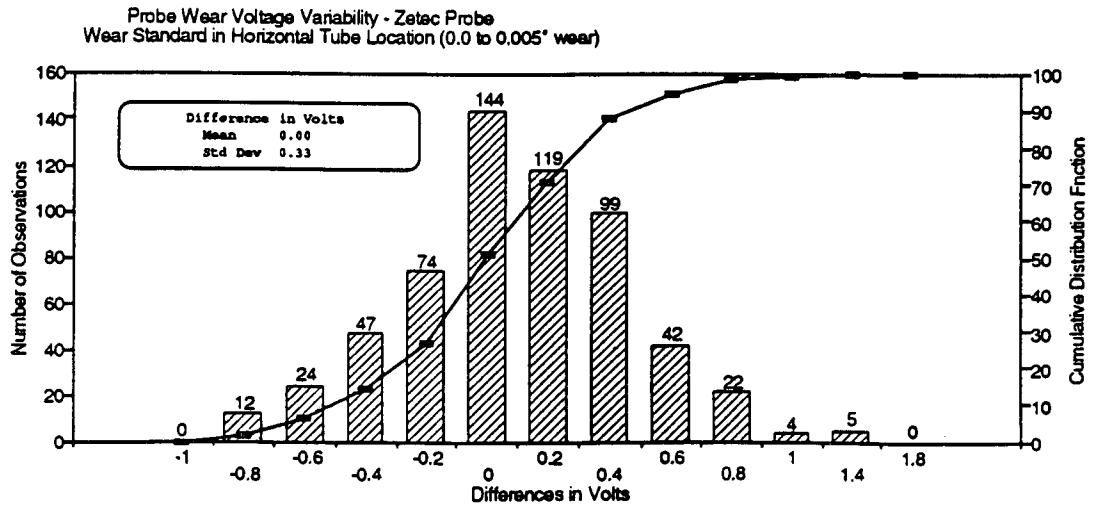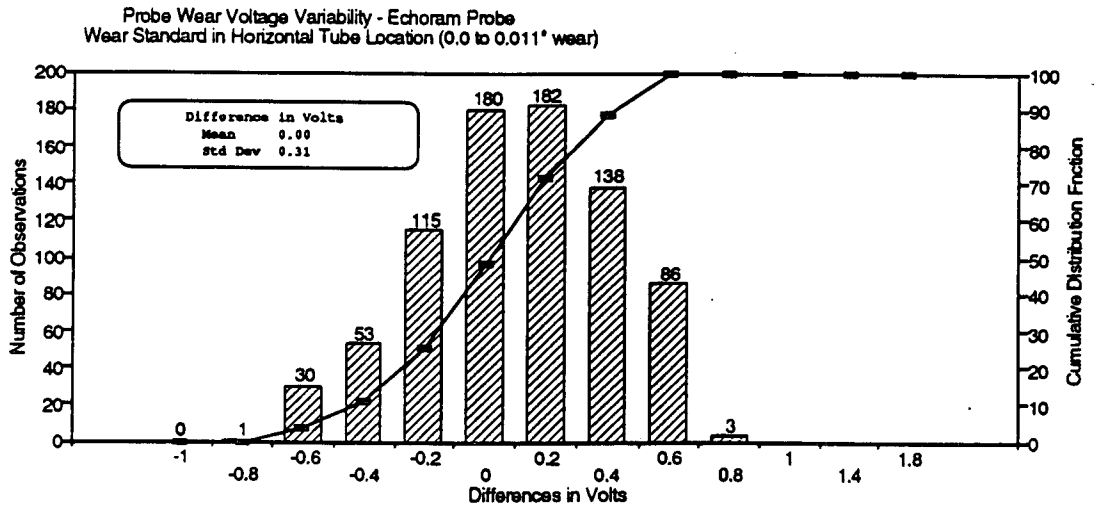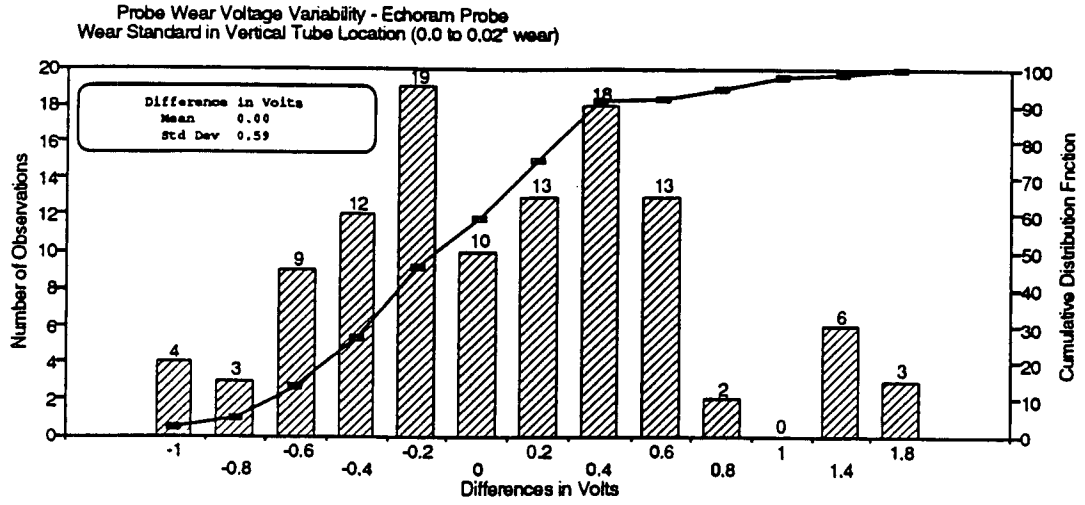
Figure 5-22

Tube Locations for Channelhead Mockup Probe Wear Tests
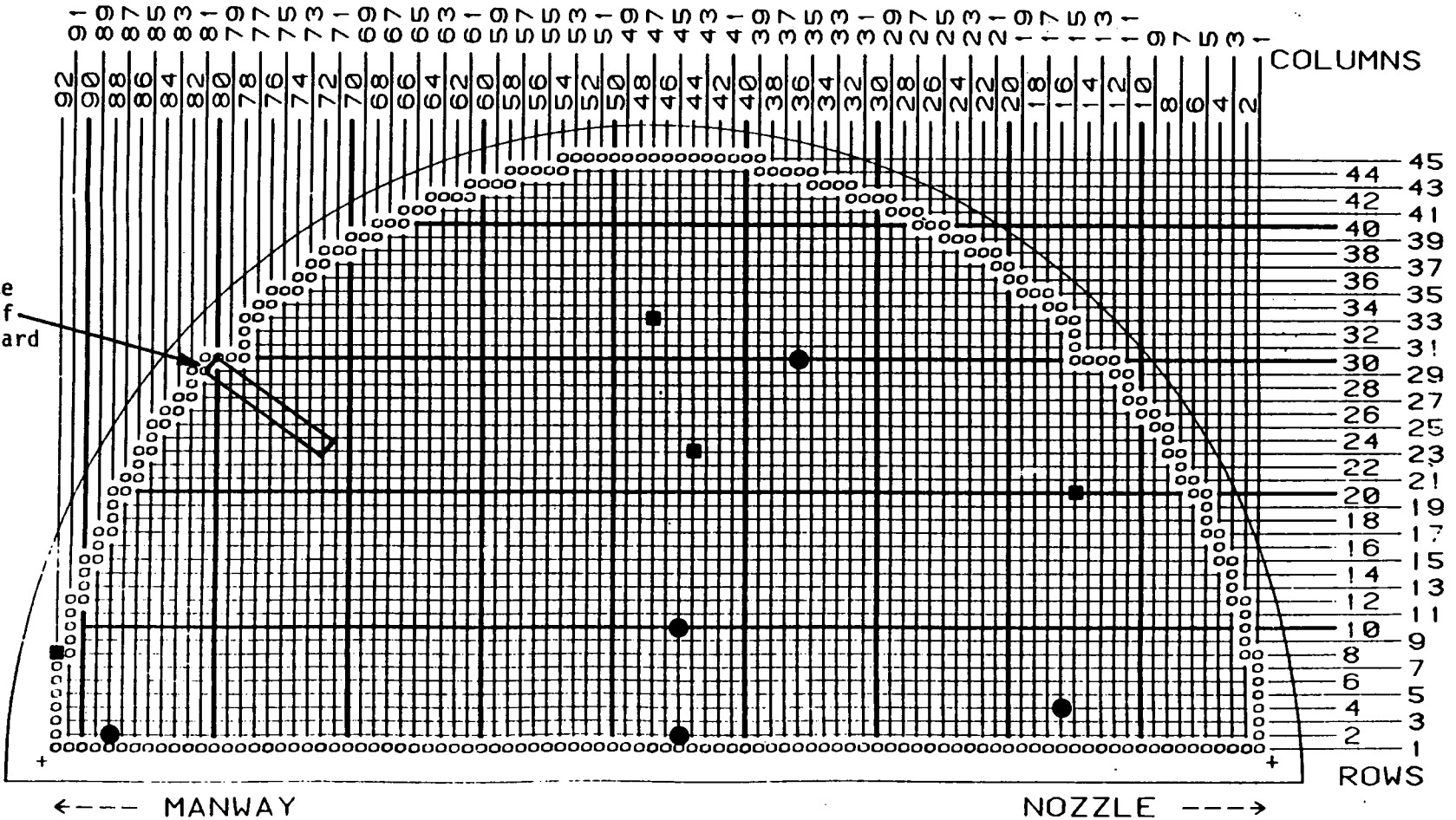
Figure 5-23

RPC Traces of Typical Model Boiler Specimens

574-4
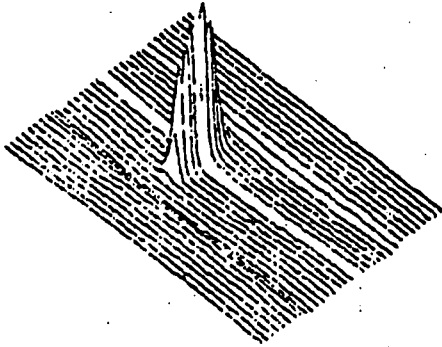
568-2
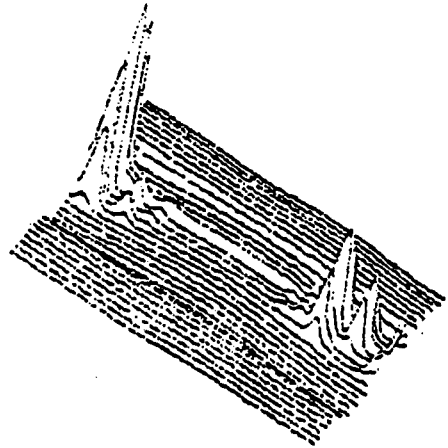
542-4
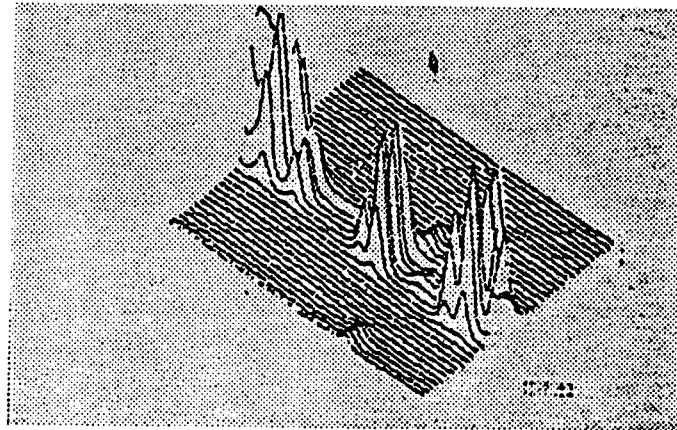
Figure 5-24

Signal Amplitude (Arbitrary Units) vs. Center-to-Center Coil Spacing

Center-to-Center Coil Spacing (d)

Chart Amp vs Coil Spacing 10/10/91
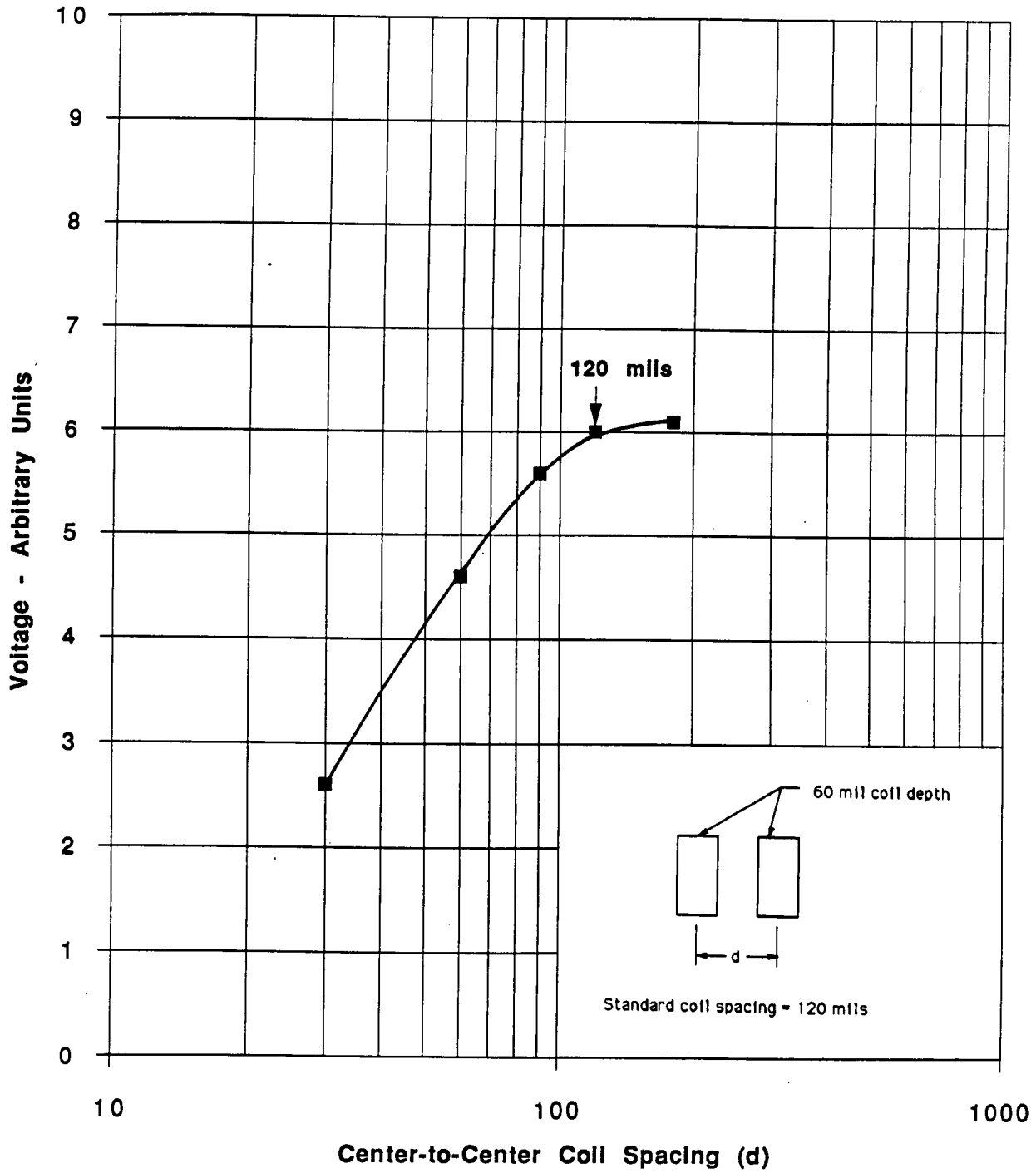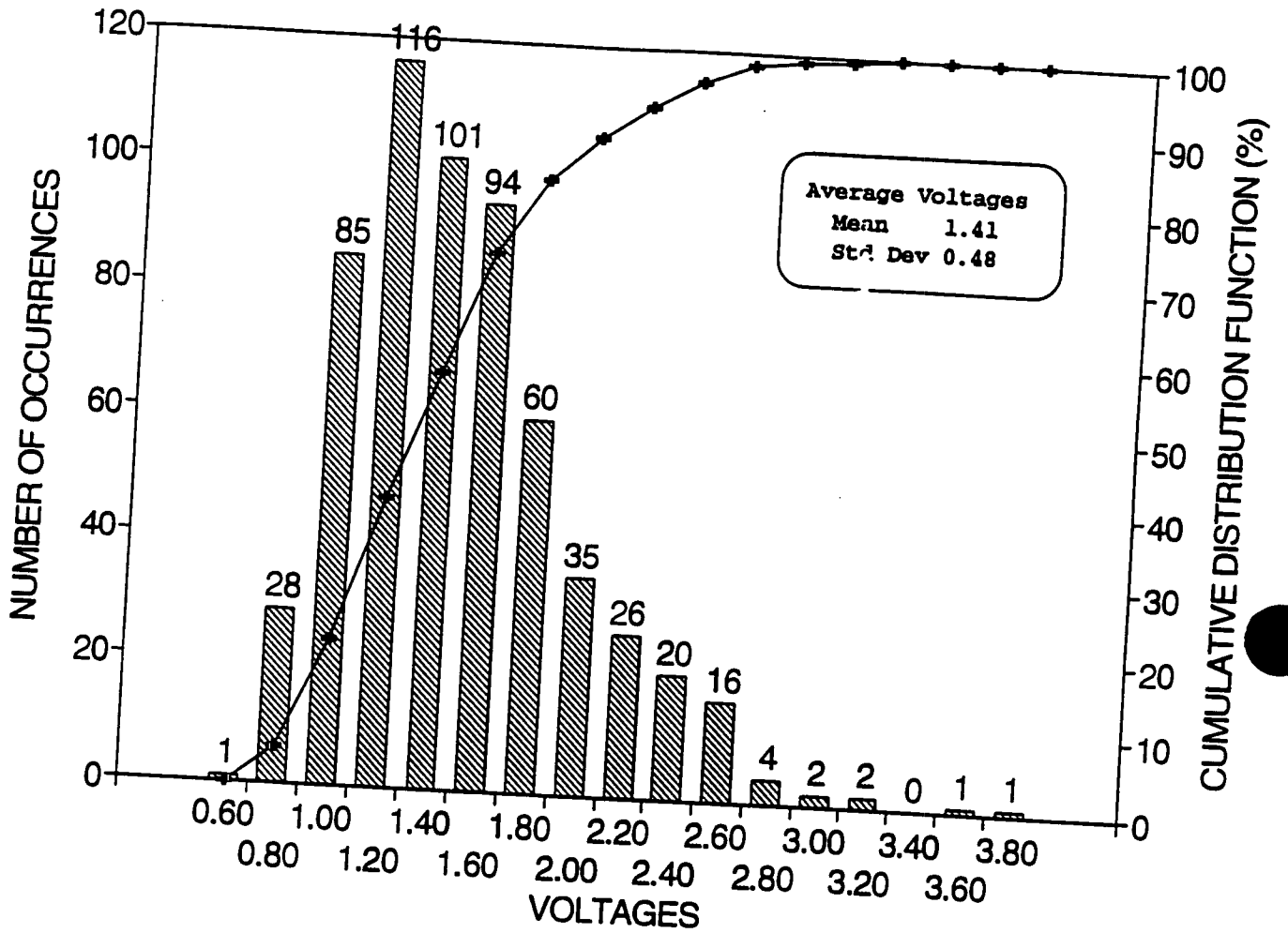
Figure 5-25

Figure 5-25. Distribution of Plant L Voltage Indications Used for
EC Analyst Variability Evaiuation
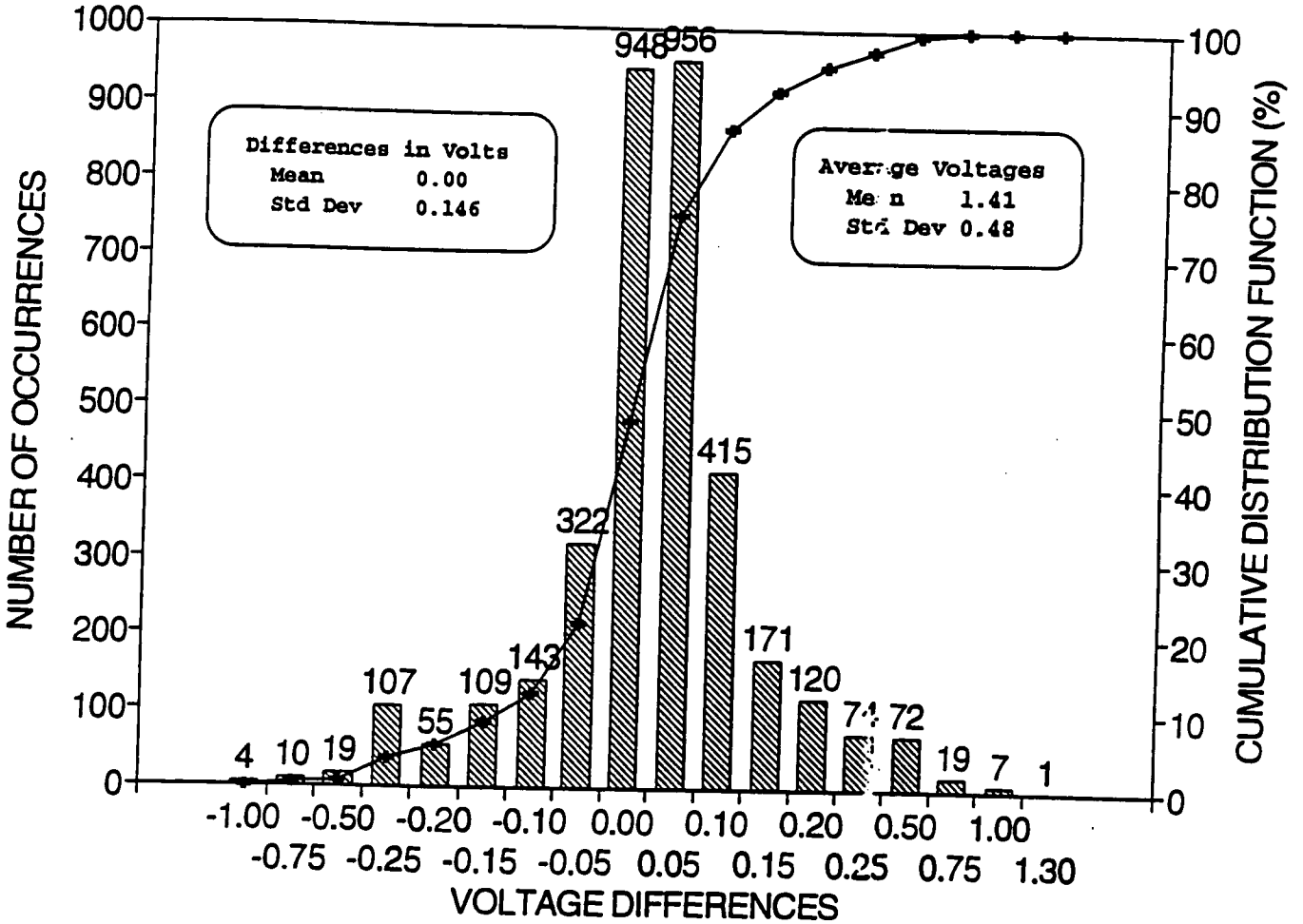
Figure 5-26

Figure 5-26. Distribution of Voltage Differences Between Individual Analysts and Mean Values

6.0   FIELD EXPERIENCE SUMMARY (Pulled Tube, Plant Leakage and Inspection Data)

This section identifies the field experience data from certain operating SGs that are utilized in the development of tube plugging criteria for ODSCC at TSPs. The field data utilized include pulled tube examination results, occurrences of tube leakage for ODSCC indications at support plates and field inspection results for relatively large crack indications with no identifiable leakage.

6.1   Utilization of Field Data in Tube Plugging Criteria

Operating SG experience represents a preferred source of data for the plugging criteria. Where the available operating data are insufficient to fully define plugging criteria, data developed from laboratory induced ODSCC specimens were used to supplement the field data base. Table 6-1 summarizes the utilization of field and laboratory data to develop the tube plugging criteria. The field data utilized for the plugging criteria are identified in this report section. Sections 7 to 11 describe the development of the laboratory data. The field and laboratory data are combined in Sections 9 and 12 to develop the tube plugging limits.

The overall approach to the tube plugging criteria is based upon establishing that R.G. 1.121 guidelines are satisfied. It is conservatively assumed that the tube to TSP crevices are open and that the TSPs are displaced under accident conditions such that the ODSCC generated within the TSPs becomes free span degradation under accident conditions. Under these assumptions, preventing excessive leakage and tube burst under SLB conditions is required for plant safety. Tube rupture under normal operating conditions is prevented by the constraint provided by the drilled hole TSPs with small tube to TSP clearances (typically ~ 16 mil diametral clearance for open crevices). For the plugging criteria, however, the R.G. 1.121 criteria for burst margins of 3 times normal operating pressure differentials are applied to define the structural requirements against tube rupture.

In addition to providing margins against tube burst, it is necessary to limit SLB leakage to levels based on FSAR evaluations for radiological consequences under accident conditions. Thus SLB leakage models are required for the plugging criteria in addition to tube burst data.

Based on the above considerations and the plugging criteria objective of relating tube integrity to NDE measurements, the primary data requirements for the plugging criteria are the correlation of burst pressure capability and SLB leak rates with bobbin coil voltage. For plant operational considerations, it is desirable to minimize the potential for operating leakage to avoid forced outages. Thus an additional objective is to relate bobbin coil voltage to operating leakage. The field data of this section indicate low leakage potential for ODSCC at TSPs even at voltage amplitudes much higher than the plugging limits.

Within the above overall approach, field data are utilized as follows:

A.   Pulled Tube Data

Four tubes pulled from Plant A-2 and three from Plant A-1 support application of the alternate repair criteria to the Farley SGs. Four of the Plant A indications have the highest bobbin voltage indications (2.8 to 9.9 volts) of domestic plants. French Plant J-1 also provides a burst data point at 4.4 volts and two leakage points at 17 and 30 volts. Two tubes were pulled from Plant P-1 in support of application of alternate repair criteria. Two indications burst tested showed high burst pressures of 9,350 and 10,200 psi for bobbin voltages of 2.7 and 0.9 volts, respectively. The eight Plant L pulled tubes with 21 TSP intersections burst tested contribute significantly to the pulled tube data base. The test results for pulled tubes having had leak rate and burst tests performed are used directly in

supporting the plugging limits. If metallographic data on the crack morphology is available but leak/burst tests were not performed, the crack depths and lengths were evaluated to assess the potential for leakage. Only tubes with measured burst pressure are used in the voltage/burst pressure correlation. The pulled tube data base is discussed in Section 6.2.

B. Plant Leakage Experience for ODSCC at TSPs

Domestic and international data for operating leakage within certain Westinghouse plants was reviewed for identification of occurrences of leakage attributable to ODSCC at TSPs. No occurrences of identifiable leakage due to ODSCC at TSPs were found in domestic units reviewed. Three occurrences were identified in European units reviewed. The latter data (see Section 6.3 below) together with field inspection data are used to assess the potential for operating leakage at plugging limits that meet tube burst and SLB leakage requirements.

6.2 Pulled Tube Data Base

The available pulled tube data base for ODSCC at TSPs in Westinghouse and licensee SGs in the data base includes 57 pulled tubes for which more than 115 tube-to-TSP intersections have both NDE and destructive examination results. None of the pulled tubes have been reported as leaking during plant operation. The data base includes tubes with both 7/8 and 3/4 inch tube diameters. Only 7/8 inch tubing data is used in the burst and leak rate correlations of this report. The 3/4 inch data is used qualitatively to compare voltage response and leakage potential with 7/8 inch tubing.

Table 6-2 provides the leak rate and burst pressure data for 23 pulled tubes (46 intersections) for which leak rate and/or burst tests were performed. Eight tubes pulled from Plant L in 1991 provide the most extensive free span burst pressure data; of the 24 Plant L intersections (3 intersections per tube), 21 were burst tested and 23 were destructively examined. The leak rate and burst tests were conservatively performed as free span (without collars) tests. None of the Plant L indications were found to leak at normal operating or SLB conditions, which is consistent with the destructive examination results which showed that none of the intersections had throughwall corrosion cracks. The burst pressures for the Plant L intersections ranged from 5900 psi to 10,600 psi, which compares to a range of about 10,500 psi to 11,600 psi for undegraded tubing. The Plant L pulled tube data were reevaluated to the eddy current data analysis guidelines of of Appendix A of this report.

In addition to the Plant L data, Table 6-2 provides data for 15 pulled tubes (23 TSP intersections) for which leak rate and/or burst tests were performed. The burst pulled tubes in Table 6-2, with up to 10 volt indications, all show burst pressures for the test conditions (room temperature, as-built material properties) in excess of 4470 psi, 3 times the normal operating pressure differential (adjusted to room temperature, the 3 times normal operating pressure differential equivalent is about 5300 psi).

The crack morphologies were reviewed for TSP intersections having no leakage or burst test measurements. This review indicates that no leakage would be expected for these tubes even under SLB conditions and that the burst pressures would exceed 3 times normal operating conditions. The field eddy current data for all pulled tubes were reviewed for voltage normalization consistent with the standard adopted (see Section 8 and Appendix A) for the plugging criteria development. Voltages for plants with 3/4" tubing are adjusted for comparisons with 7/8" tubing data as described in Section 6.6.

The pulled tube NDE data from eight plants are shown in Figure 6-1 as bobbin coil voltage versus indicated depth. All pulled tube results at normal operating pressure differential

represent no leakage conditions while two small leakers at SLB conditions were found from Plant A-2. Figure 6-2 shows the same data plotted as voltage versus actual depth from destructive examination.

Correlations of the bobbin coil phase angle based depth estimates with the maximum depths from destructive examinations have shown an uncertainty of 15% for the depth indications. The pulled tubes have typically shown one dominant axial crack network with multiple, small cracks around the tube circumference. With multiple, large axial crack networks around the tube circumference, the bobbin coil depth uncertainty can be larger than 15%.

Figure 6-2 shows that below 2.5 volts the maximum depths are predominantly less than 80% with a few indications up to 98% depth. An occasional, very short, 100% through wall indication, could potentially occur at these low voltage levels although the pulled tube examination results indicate that the associated crack length can be expected to be too short for any measurable leakage at normal operating or SLB conditions. Between 3 and 10 volts, the limited pulled tube data indicate the potential for throughwall cracks with negligible leakage at normal operating conditions and very small leaks at SLB conditions.

6.3   Operating Plant Leakage Data for ODSCC at TSPs

Table 6-3 summarizes the available information on three suspected tube leaks attributable to ODSCC at TSPs in operating SGs in the data base. The three leakage occurrences have been in 3/4" diameter tubing. Bobbin voltages for these indications are given for 3/4" tubing and as adjusted (Section 6.6) to equivalent 7/8" tube diameters. These leakers occurred in European plants, with two of the suspected leakers occurring at one plant in the same operating cycle. In the latter case, five tubes including the two with indications at TSPs were suspected of contributing to the operating leakage. Leakage for the two indications at TSPs was obtained by a fluoresceine leak test as no dripping was detected at 500 psi secondary side pressure.

For the Plant B-1 leakage indication, other tubes also contributed to the approximately 63 gpd total leak rate. Helium leak tests identified other tubes leaking due to PWSCC indications. Using relative helium leak rates as a guide, it was judged that the leak rate for the ODSCC indication was less than 10 gpd.

These leakage events indicate that limited leakage can occur for indications above about 7.7 volts for 3/4" tubing and about 10 volts for 7/8" tubing. No leakage at Kewaunee has been found that could be attributable to ODSCC at TSPs.

6.4   RPC Data Considerations

Per the proposed alternate plugging criteria, RPC inspections are required for bobbin indications above 1.5 volts (see Section 12) to support the continued presence of ODSCC as the dominant degradation mechanism. In addition, the data obtained would support further development of SLB leakage models which may utilize leak rate correlation with RPC data as the independent parameter. The RPC inspection results can be optionally applied to verify the presence of the bobbin coil indication.

6.5   Voltage Renormalization for Alternate Calibrations

To increase the supporting data base, it is desirable to be able to renormalize available data to the calibration values used in this report. When 400/100 kHz mix or 400 kHz data normalized to an ASME standard are available, the renormalization is a straight forward ratio of the calibration voltage values. However, when different frequencies are used, the

6 - 3

normalization ratio is phase angle or depth dependent and this normalization has been evaluated as described below.

The voltage normalizations applicable to the APC calibrations used in this report are:

7/8 Inch Diameter Tubing:

ASME 4-hole, 20% deep, 0.187 ± 0.001 inch dia. = 2.75 volts at 400/100 kHz
ASME 4-hole, 20% deep, 0.187 ± 0.001 inch dia. = 4.00 volts at 400 kHz

3/4 Inch Diameter Tubing:

ASME 4-hole, 20% deep, 0.187 ± 0.001 inch dia. = 2.75 volts at 550/130 kHz
ASME 4-hole, 20% deep, 0.187 ± 0.001 inch dia. = 4.00 volts at 550 kHz.

The 3/4" frequencies are obtained by scaling considerations from the 7/8" frequencies. For scaling, frequencies are inversely proportional to the square of the tube diameter. Probe diameters of 0.720" for 7/8" tubing and 0.610 for 3/4" tubing are linearly scaled. Probe coil sizes and spacing have not been scaled but are judged to have a minor influence on voltage equivalence between tube sizes. However, the ASME calibration standard hole diameters for the 20% deep flaws are not scaled between tube diameters. For appropriate scaling, the hole dimension should also be scaled. The 3/4" flaw diameter should be reduced by the 7/8" to 3/4" diameter ratio of 1.167. Wall thickness is scaled for the 20% deep flaws. Alternately, the calibration voltage could be increased if the hole size is not scaled. The adjusted voltage would be proportional to hole volume increase or the square of the hole diameter ratio. Thus, for appropriate voltage, scaling between 3/4" and 7/8" tubing, the 3/4" voltages should be increased by $1.167^2 = 1.36$. Calibration standard voltages have been compared between a 0.033" hole in 7/8" tubing and the scaled 0.028" hole in 3/4" tubing. When both standards are normalized to the above recommended values at 2.75 volts for the 20% flaw, the ratio of the 7/8" to 3/4" hole voltages was found to be 1.28 which is consistent with the theoretical 1.36 within hole tolerances. For comparisons of the 3/4" pulled tube and field voltages with the 7/8" data, the 3/4" voltages are adjusted in this report by the factor of 1.36.

In France and Belgium, 240 kHz differential inspections are applied for TSP intersections with 7/8" diameter tubing. The French normalization is to 1.3 volts for four throughwall 1.0 mm diameter holes, while the Belgium normalization is 2.0 volts for four throughwall 1.25 mm diameter holes. By both hole volume scaling and direct measurements, the French and Belgian normalizations are equivalent within 1% to 2%. Thus a U.S. APC voltage to French/Belgian voltage renormalization can be obtained from either or both French and Belgian data.

French to U.S. voltage renormalization has been evaluated using comparisons between calibration standards and model boiler specimens with both U.S. and French probes and equipment. Table 6-4 summarizes voltage ratios based on calibration standards. U.S. Zetec and Echoram probes were applied with the U.S. calibration standards and equipment, and French and Echoram probes were used with the French calibration standards and equipment. The Zetec and Echoram probes, when normalized to the 20% hole, yield about 10% differences in voltages for the four throughwall holes using U.S. equipment, with the Echoram probe showing the larger voltage increase between 20% and 100% holes. With the French equipment, the Echoram probe shows a smaller voltage than the French probe between 20% and 100% holes. The appropriate French to U.S. voltage renormalization and French equipment would utilize U.S. equipment for the U.S. normalization and French equipment for the French normalization. However, the results of Table 6-4 show insignificant differences

between choice of equipment for the French normalization. The results show U.S./French voltage renormalization factors of about 3.3 at 20% to 4.0 at 40% and 7.5 at 100%.

Laborelec has performed measurements in Plant K-1 SGs using U.S. equipment/probes/ standards for the APC voltage measurements and Belgian equipment/probes/standards for the Belgian voltage measurements. The APC voltage measurements were obtained using Zetec equipment, an Echoram probe and an ASME standard cross-calibrated to the reference standard. Voltage data were obtained for 52 indications up to 3 Belgian volts. Data have also been obtained on 10 model boiler specimens using Zetec equipment, a French probe, the reference ASME standard and a standard with four throughwall 1.0 mm diameter holes for the French voltage normalization. These 10 data points range up to 9 French volts with 4 points overlapping the Belgian data up to 3 volts. To develop a correlation for renormalizing Belgian/French voltages to the U.S. calibration, the Belgian and model boiler data were combined and the overlapping data up to 3 volts were used as shown in Figure 6-3(a). The y-axis intercept is negative for the overall fit as the large slope associated with the deeper, higher voltage indications dominates the data. For this reason, a constant renormalization factor of 4.0 (typical of that found for 40% depth ASME holes) is suggested below 0.36 Belgian/French volts. The correlation of Figure 6-3(a) can be acceptably used to convert Belgian and French data for use in the voltage/burst and voltage/leakage correlations. Currently available data from Plant J-1 are given in Table 6-2. The fitted correlation of Figure 6-3(a) is compared with the higher voltage, six model boiler data points in Figure 6-4. It is seen that the correlation tends to underestimate the U.S. voltages at the higher voltage range. This is consistent with the ASME standard data of Table 6-4 which shows a throughwall ratio of 7 to 8 for the U.S./French normalizations compared to the asymptotic value of 6.69 obtained for the data up to 3.0 volts. A polynomial could be fit to the total voltage range to improve the overall fit. However, the region of interest for APC applications is up to about 3.0 French/Belgian volts (~2.0 U.S. volts) so the simpler linear regression is being applied for the voltage renormalizations.

A Belgian study was performed on 3/4" tubing to develop the Belgian to U.S. voltage renormalization utilizing field indications. Over 50 indications were first measured using the Belgian equipment and a Belgian probe, with voltage measurements at 300 kHz normalized to 2.0 volts for a four throughwall, 1.25 mm hole standard. The indications were then measured using Zetec analysis equipment using both 550/130 kHz normalized to the APC calibration of 2.75 volts for the 20% ASME hole. Data were also taken at 300 kHz with the Belgian normalization. All data were taken using the Belgian bobbin probe. Based on measurements of ASME calibration standards fabricated in the U.S. with drilled holes and in Belgium with EDM holes, an ASME cross-calibration factor of 1.70 was developed. That is, the voltages measured with the Belgian ASME standard must be increased by a factor of 1.70 for cross-calibration to the reference laboratory standard. Figure 6-3(b) shows the correlation developed for renormalizing the Belgian 300 kHz data (Belgian automated analysis equipment) to the APC 550/130 kHz mix. Below 0.3 volts (200 kHz), it is suggested that a factor of 4.0 be applied to the 300 kHz data as shown in Figure 6-3(b). All the data of Figure 6-3(b) were independently evaluated by Westinghouse and the 550/130 kHz data were found to be in excellent agreement (R squared = 0.999) with the Belgian evaluation. Thus the Belgian methods for calling bobbin voltages are considered to be equivalent to the APC guidelines of Appendix A.

The APC 550/130 kHz -to-Belgian 300 kHz voltage ratio was also evaluated using ASME and Belgian 3/4" calibration standards. Both the laboratory ASME standard and a transfer standard were used with an Echoram bobbin probe. The results given in Table 6-3 indicate a U.S.-to-Belgian voltage ratio ranging from about 4 to 9. This ratio is very close to that obtained from the field data evaluation shown in Figure 6-3(b).

6.6 Growth Rate Trends

Of particular interest to establishing the plugging limits of this report is voltage growth rate as a function of the voltage amplitude. Current domestic plugging limits result in little data on growth rates in the range of voltage amplitudes being evaluated for the plugging limits of this report. The larger voltage amplitudes of the European data provide guidance on growth rate progression. Figure 6-5 shows growth rate data for Plant H-1 both as voltage amplitude and percentage growth as a function of voltage amplitude. The data of Figure 6-5 tend to indicate percentage growth rates are not a strong function of absolute voltage amplitude. As generally expected, the spread in the data at low amplitudes is greater than for larger voltages due to the greater influence of voltage uncertainties and measurement repeatability at low amplitudes.

Figures 6-6 and 6-7 compare the percentage growth rates per cycle between domestic plants Kewaunee, Plant A-1 and Plant A-2 with that for Plant H-1. Figure 6-6 shows the individual data points; the lower part of the figure is a magnification of the lower left hand corner of the upper figure. Figure 6-7 compares average growth rates and standard deviations. The averages are displayed for different ranges of the initial amplitude. The first range is 0 to 0.75 volts, the second range is 0.75 to 2.5 volts and the third is for initial amplitudes greater than 2.5 volts. In the case of the U.S. plants In the data base there Is very little data above 2.5 volt amplitude; hence such data is included in the second range. The French data (Plant H-1) Indicate percent growth rate nearly independent of initial amplitude whereas the domestic units display percent growth rates decreasing with increase In initial amplitude. The domestic in the data base plants dominate the growth rate data of Figures 6-6 and 6-7 for low amplitudes, with the French data extending to larger amplitudes.

6.7 Field Data Conclusions

The following conclusions can be drawn from the field data described above:

1. Burst tests performed on pulled tubes, which to date include signal levels up to 10 volts, show burst pressures exceeding 3 times normal operating pressure differential, adjusted for operating temperature effect on material properties.

2. The pulled tube, leak rate test results indicate the potential for low [

    ]9. A French pulled tube with an 18 volt indication showed a SLB leak rate of 8.3 l/hr.

3. Pulled tube examination results indicate that through wall cracks can potentially occur below 10 volts but that the associated crack lengths are short with no measurable leakage at operating conditions.

4. Leakage at operating conditions has not been identified for bobbin coil voltage below [   ]9 volts for 3/4" tubing (equivalent to ~10 volts for 7/8" tubing), with only 1 indication of leakage below the 7/8" tubing equivalent voltage of 10 volts.

5. Negligible leakage is expected from ODSCC at TSPs based on domestic experience as well as European experience with voltage amplitudes higher than the domestic operating experience.

6. Percent growth in voltage amplitude tends to be approximately independent of voltage amplitude for the available French data while decreasing with amplitude for the

domestic plants. Assuming growth in voltage is independent of amplitude appears to be very conservative for the Kewaunee SGs.

To supplement the above field data to define tube plugging limits, laboratory tests were performed with the following areas of emphasis:

- Improved definition of tube burst capability as a function of bobbin coil voltage to better define voltage levels that meet Reg. Guide 1.121 guidelines for burst pressures of 3 times normal operating pressure differentials.

- Improved resolution of leak rate potential for normal operating and SLB conditions above about 2 volt signal amplitudes.

- Determining NDE uncertainties associated with application of voltage plugging limits.

Table 6-1

Field and Laboratory Data Utilized for Tube Plugging Criteria Development

Tube Burst Capability: Burst Pressure vs Voltage Correlation
- Pulled Tube Data
- Model Boiler Specimens

SLB Leakage Model
- Pulled Tube Data
- Model Boiler Specimens
- Plant Inspection Results
  - ODSCC Indication Distributions
  - Growth Rates

Operating Leakage Assessment
- Pulled Tube Data
- Operating SG Leakage Occurrences
- Field Inspection Data for Tubes Without Identified Leakage
  - Larger (>1 volt) Indications
- Model Boiler Specimens

NDE Evaluation: Specimen Characterization, Inspection Sensitivity/Uncertainties
- Model Boiler Specimens
- Pulled Tube Data
- Machined Defect Simulations

Influence of Tube Denting on Leakage
- Fatigue Specimens
- Doped Steam Specimens

Effects of SLB Loads on TSP Displacement
- Pull Tests on Laboratory Dented Specimens
- Thermal-Hydraulic and Structural Analyses

Table 6-2

Pulled Tube Leak Rate and Burst Pressure Measurements

Plant	Row/Col.	TSP	Bobbin Coil Volts(4)	Depth	RPC Volts	Destructive Exam Max.Depth	Length)(1) (in.)	Leak Rate(l/hr) Normal Oper.	SLB	Burst Pressure (psi)

7/8-Inch Diameter Tubing

g

Table 6-2 (continued)

Puiled Tube Leak Rate and Burst Pressure Measurements

Plant	Row/Col.	TSP	Bobbin Coil Volts[4]	Depth	RPC Volts	Destructive Exam Max.Depth Length)[1] (in.)		Leak Rate(l/hr) Normal Oper.	SLB	Burst Pressure (psi)

7/8-Inch Diameter Tubing (continued)

g

Table 6-3

Field Experience: Suspected Tube Leakage for ODSCC AT TSPs[1]

Plant	Inspection	Bobbin Coil Volts		Depth	Comments
		3/4" Tubing	7/8" Equiv. Volts[3]		
B-1	Outage following suspected leak				g
E-4	Outage following suspected leak				
	Outage following suspected leak				

Notes:

1. Field experience noted is for nominal 0.750" OD tubing with 0.043" wall thickness. No data are known to be available for tubes with 0.875" OD.

2. Equivalent volts for 7/8" tubing = 1.36 x (Volts for 3/4" tubing). See Section 6.6.

3. Field voltages of 1.4 and 4.2 volts, as given In parentheses, were obtained at 300 kHz with Belgian normalization. Voltages converted to 3/4" tubing normalization of this report utilizing Figure 6-5.

Table 6-4

Comparisons of Voltage Amplitudes for 7/8" Tubing
Between U.S.-ASME and European Standards

| | | ASME Standard | | | | Four Throughwall Holes | | |
| | | | | | | ASME | French 1.0mm | Belgian 1.25mm |
Probe	Frequency	20%	40%	60%	80%	0.032	0.039"	0.049"
U.S. Calibration, U.S. Equipment								
Zetec	400/100 kHz	2.62(1)	2.91	3.24	4.52	6.29	9.14	14.46
Echoram	400/100 kHz	2.62(1)	3.17	3.83	5.45	7.05	10.26	16.1
French Calibration, U.S. Equipment								
Zetec	240 kHz	0.84	0.72	0.65	0.74	0.90	1.30	2.03
Echoram	240 kHz	0.74	0.67	0.66	0.78	0.90	1.30	2.03
French Calibration, French Equipment								
Echoram	240 kHz	0.95	0.84	0.75	0.84	0.90	1.30	2.04
French	240 kHz	0.80	0.73	0.70	0.80	0.89	1.30	2.05
Ratio: U.S. Calibration/French Calibration								
U.S. Equipment Only								
Zetec/Zetec	(400/100)/240	3.12	3.46	4.32	5.38	6.99	7.03	7.09
Echo./Echo.	(400/100)/240	3.54	4.73	5.80	6.99	7.83	7.89	7.93
U.S. Equipment/French Equipment								
Zetec/French	(400/100)/240	3.28	3.99	4.63	5.65	7.06	7.03	7.05
Echo./French	(400/100)/240	3.28	4.34	5.47	6.80	7.92	7.89	7.85
Echo./Echo.	(400/100)/240	2.76	3.77	5.11	6.49	7.83	7.89	7.89

Note 1: Transfer standard used in analysis yielded 2.62 volts for 20% flaw when cross calibrated against reference laboratory standard at 2.75 volts.

Table 6-5

Comparisons of Voltage Amplitudes for 3/4" Tubing
Between U.S.-ASME and Belgian Standards

| | | ASME Standard | | | | Four Throughwall Holes | |
| | | | | | | ASME | Belgian ~1.25mm |
Standard	Frequency	20%	40%	60%	20%	0.027"	0.048"
U.S. Calibration							
Lab	550/130 kHz	2.75	2.51	4.15	4.81		
Transfer	550/130 kHz	2.68	3.18	4.23	5.63	5.52	18.6
Beigian Calibration							
Lab	300 kHz	0.68	0.51	0.62	0.62		
Transfer	300 kHz	0.62	0.60	0.65	0.72	0.63	2.0
Ratio: U.S. Calibration/Belgian Calibration							
Lab	(550/130)/300	4.05	4.92	6.69	7.76		
Transfer	(550/130)/300	4.32	5.30	6.50	7.82	8.76	9.3

Figure 6-1

Pulled Tube Data: Bobbin Coil Voltage and indicated Depth

g

Chart Fig 6-1 7/13/92

Figure 6-2

Pulled Tube Data: Bobbin Coil Voltage and Depth from Destructive Exam

g

Chart Fig 6-2 7/13/92

6 - 15
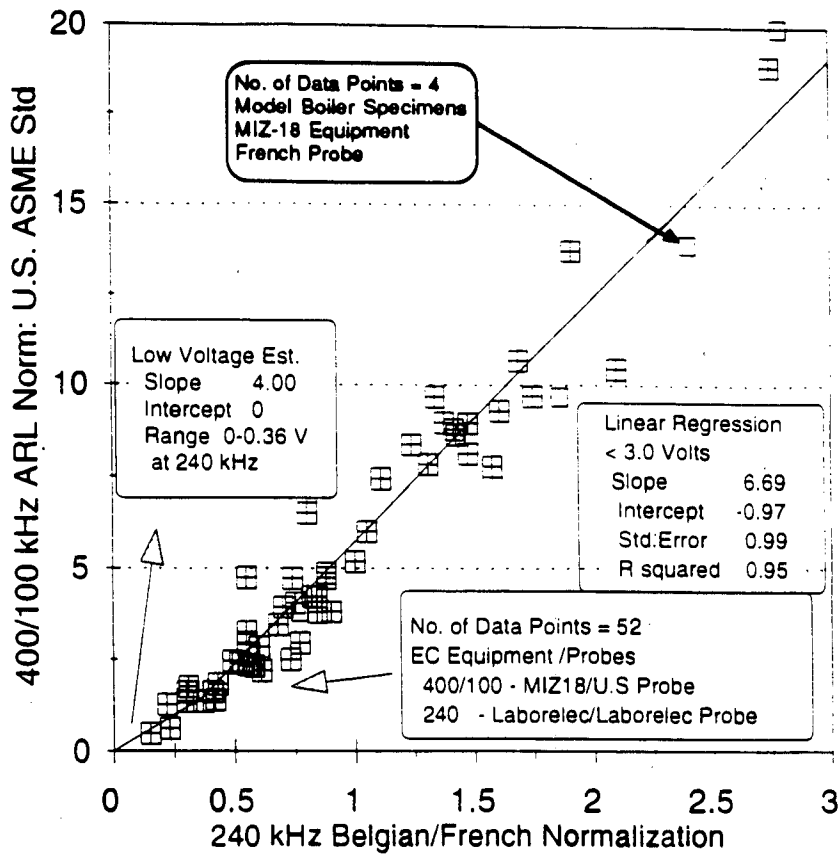
Figure 6-3(a) Belgian/French Voltage (3/8" Tubing) Renormalization to U.S. APC Calibration for Belgian Plant K-1 (1992 Data) and Model Boiler Data Below 3.0 Volts
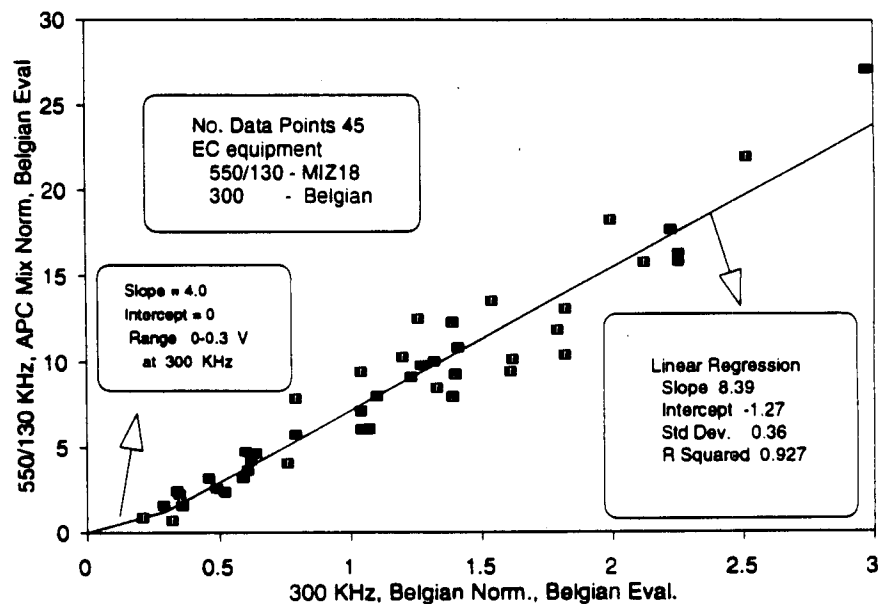
Figure 6-3(b) Belgian (3/4" Tubing) Voltage Renormalization to U.S. APC Calibration for Plant E-4 1992 Voltage Indications at Tube Support Plates
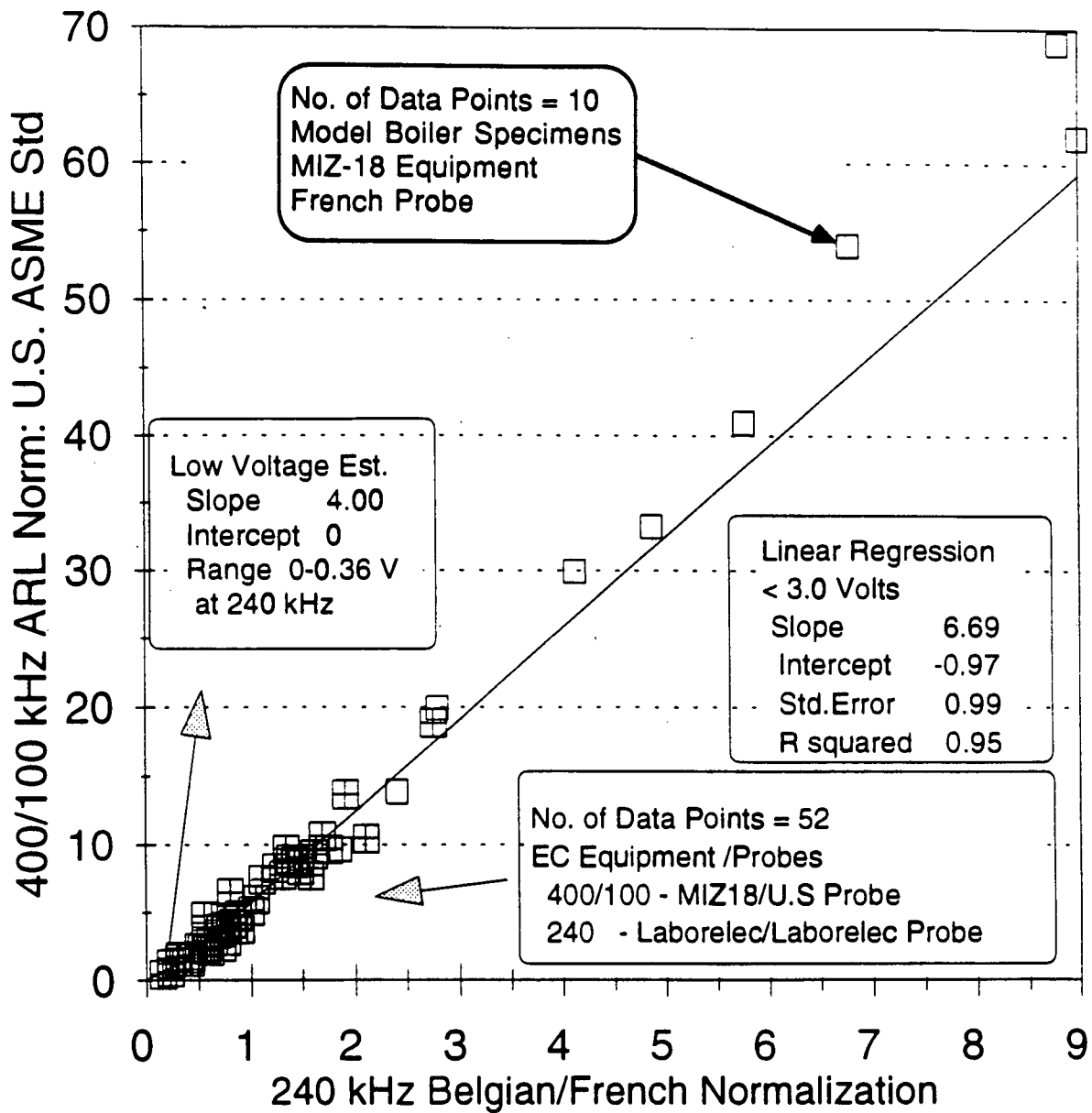
Figure 6-4   Belgian/French Voltage Renormalization (7/8" Tubing) to U.S. APC Calibration - Comparison of Correlation with Model Boiler Data above 3.0 Volts

Figure 6-5

TSP Indication Voltage Growth Rates for Plant H-1
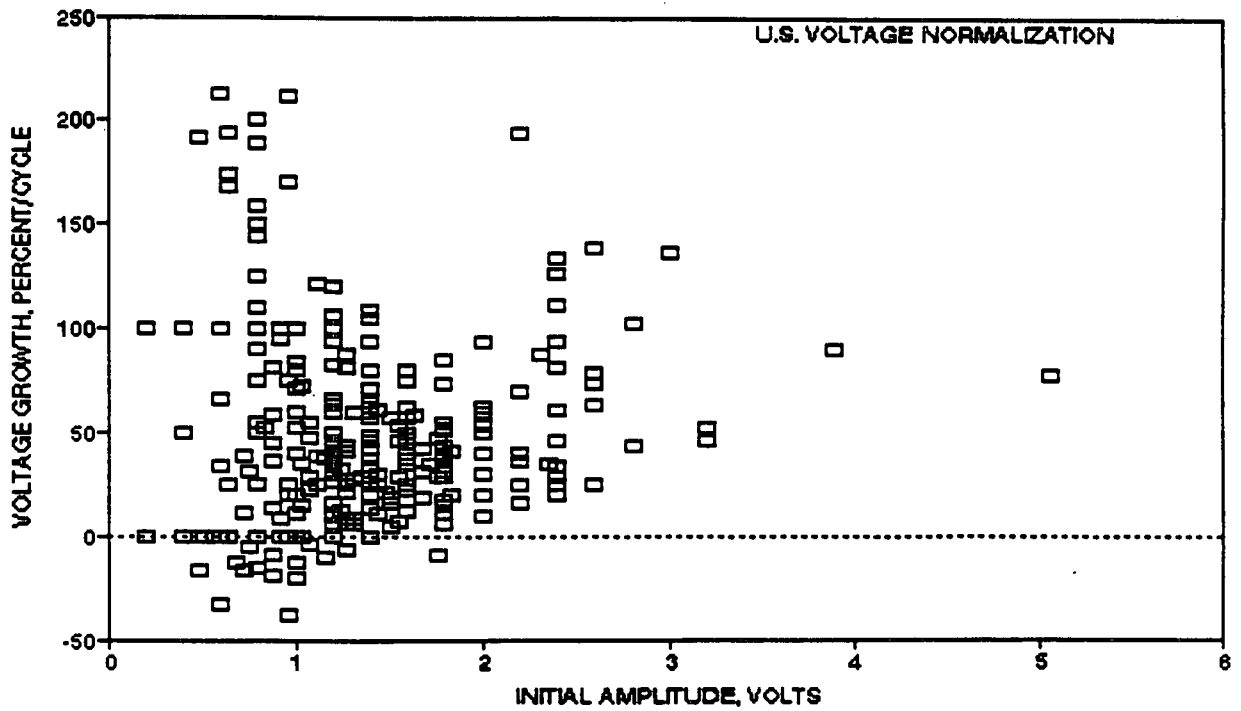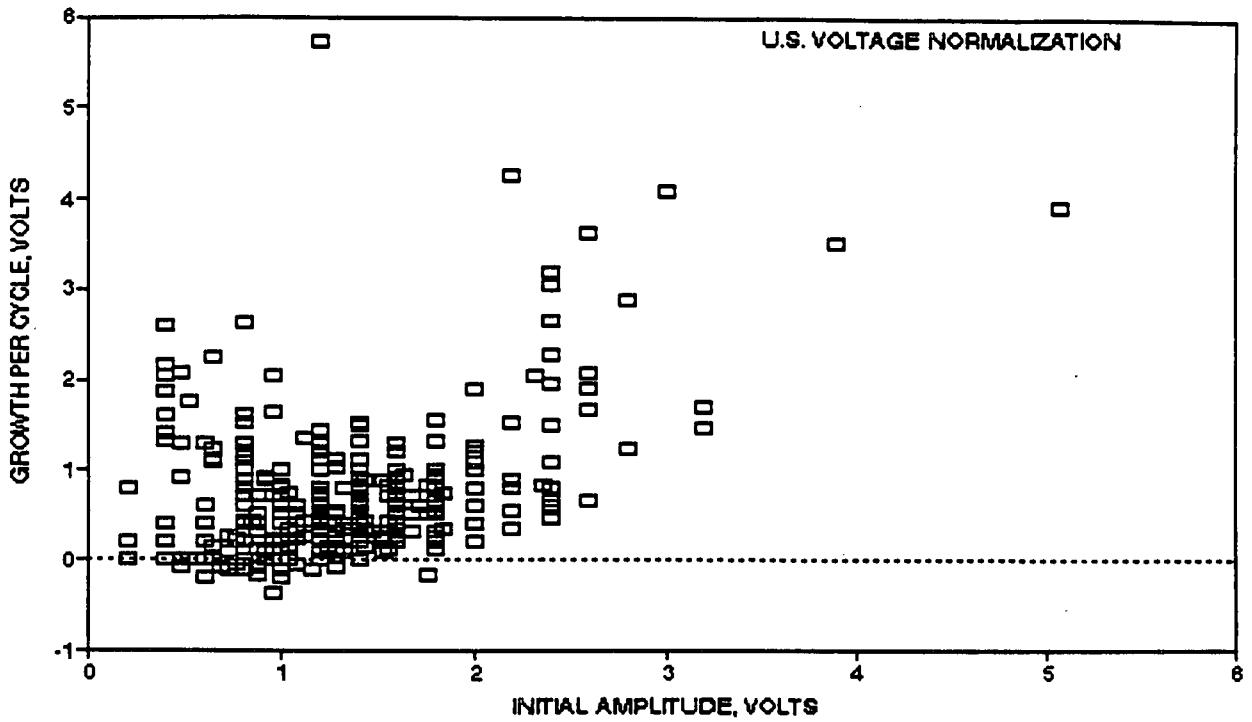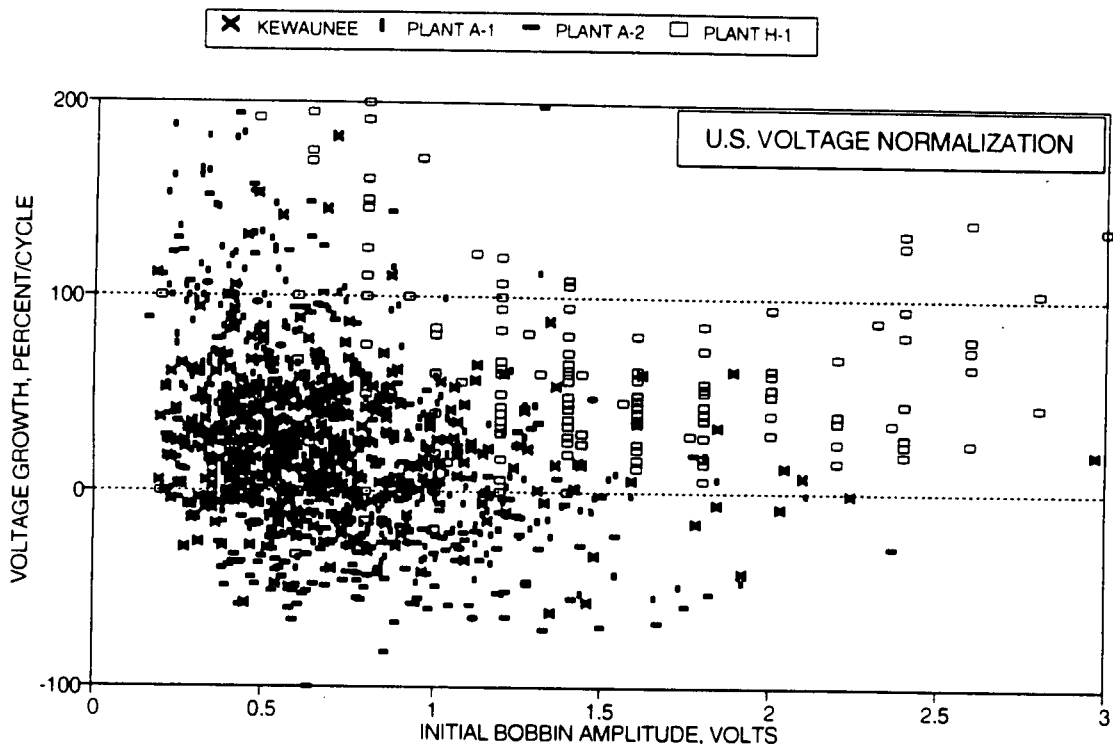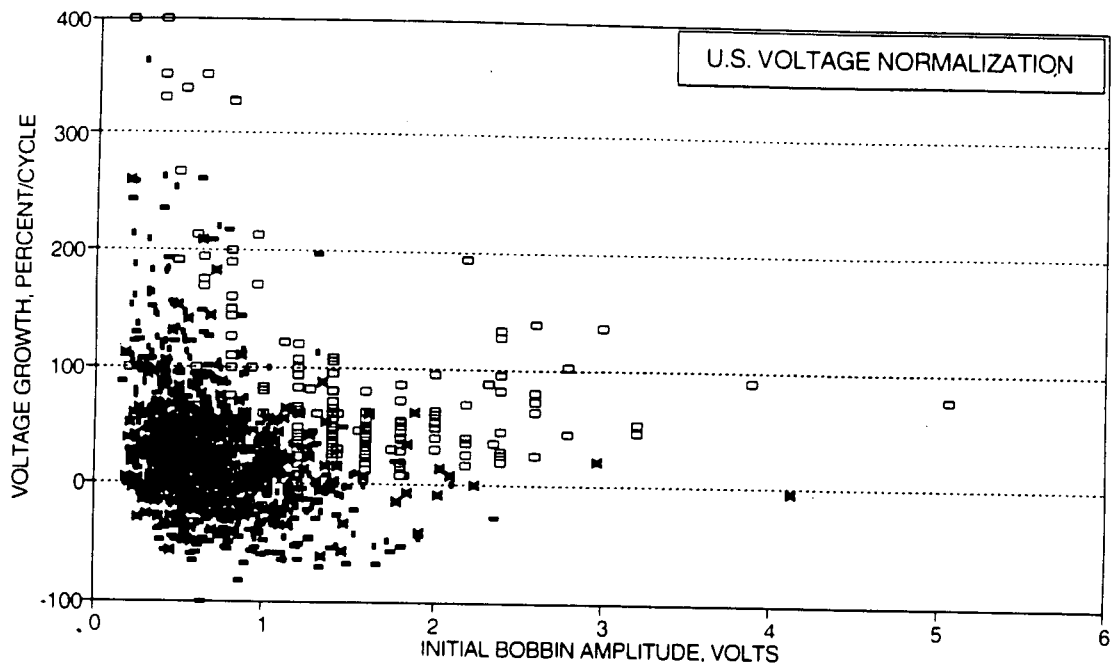
Figure 6-6   Growth Rate Data for Kewaunee, Plant A, and Plant H-1
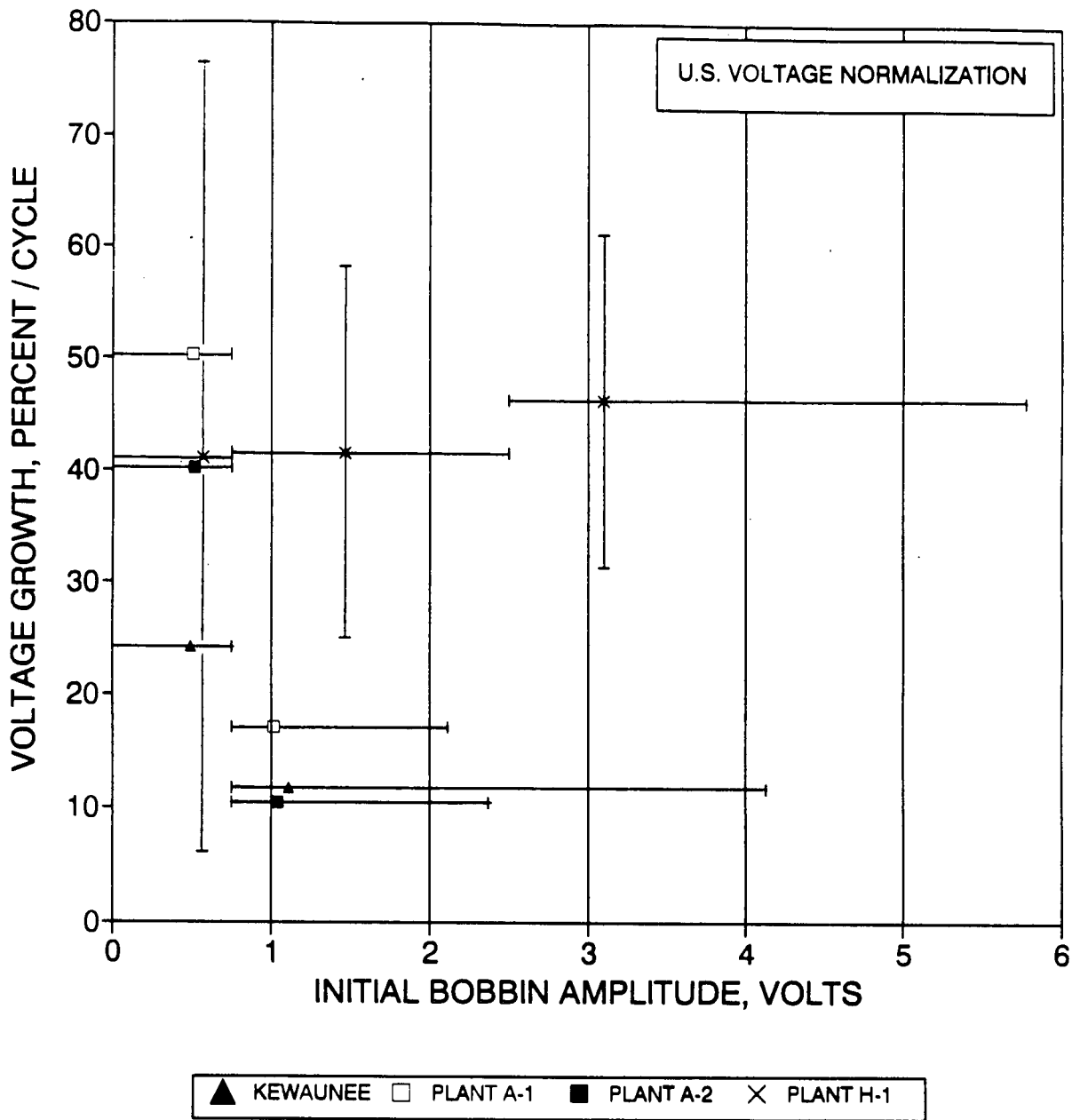
Figure 6-7 Average Percent Voltage Growth Rates for Kewaunee, Plant A, and Plant H-1

7.0   LABORATORY SPECIMEN PREPARATION AND TESTING

7.1   Model Boiler Specimens

The Forest Hills Single Tube Model Boiler test facility consists of thirteen pressure vessels in which a forced flow primary system transfers heat to a natural circulation secondary system. Test specimens are placed around the heat transfer tube to simulate steam generator tube support plates. One to six tube support plate crevice assemblies are typically included in a given test. A schematic of the test facility is presented in Figure 7-1, and typical thermal and hydraulic specifications are presented in Table 7-1. As indicated in the table, these specifications are representative of those in a pressurized water reactor steam generator.

Six series of Single Tube Model Boiler tests have been performed to provide test pieces having ODSCC for subsequent nondestructive examination, leak rate measurements, and destructive examination. The first series consisted of 19 archive crevice assemblies which were produced in previous Westinghouse-funded testing; the second and third series each consisted of eight crevice assemblies; the fourth series contained 45 crevice assemblies, while the fifth and sixth each contained eight assemblies. The later test series were performed to provide additional specimens, with an emphasis on producing specimens having lower voltage eddy current signals. Series 6 tests attempted to promote intergranular attack (IGA), as well as stress corrosion cracking.

Series 1 Tests: Of the 19 archive crevice assemblies which comprised the Series 1 tests, several had no detectable cracks or were not used due to having voltages which were larger than those observed in pulled tubes. The archive test pieces used for this program are summarized in Table 7-2. The test pieces are listed by their tube designation and their location on the tube. The sludge type refers to the manner in which sludge was placed in the tube support plate crevices. Chemically consolidated sludge is formed by baking a mixture of sodium hydroxide, sodium silicate and sodium phosphate with the sludge; mechanically consolidated sludge is formed by hydraulically pressing the sludge into the tube support plate, drilling a hole in the sludge, and sliding the tube through the hole; the fritted design uses an Inconel sinter at each end of the crevice to hold the sludge in place. The test containing an eccentrically mounted tube support plate, in which the sludge was removed from the crevice, was used to simulate chemical cleaning. All tests utilized simulated plant sludge, consisting of approximately 60% magnetite, 32% copper, 5% copper oxide, 2% nickel oxide, and 1% chromium oxide.

The cracks were produced in what is termed the reference cracking chemistry, consisting of either a 600 ppb (1X) or a 6 ppm (10X) sodium carbonate solution in the makeup tank. Because of hideout in the crevices, the boiler concentration is typically about 75% of the makeup tank concentration. Hydrazine and ammonia are also added to the makeup tank for oxygen and pH control, respectively.

The tubing used for the tests was taken from Heat 2675. This heat of mill annealed Alloy 600 was fabricated by Westinghouse and has been used extensively in other stress corrosion cracking programs. The tubing has a 0.875 inch outside diameter.

Series 2 Tests: The initial program test pieces consisted of eight crevice simulants which were mounted on two tubes. These tests were specified to produce rapid throughwall cracking, so that the 10X reference cracking chemistry was utilized. Heat 2675 was also used for these tests. One test utilized chemically consolidated simulated plant sludge (tube 543), while the other used

mechanically consolidated sludge (tube 542). The sludge filled the entire crevice volume. Primary to secondary leakage was noted in the chemically consolidated test after 10 days of boiler operation, and in the mechanically consolidated test after 24 days of operation. During the subsequent nondestructive examination (NDE), indications were identified adjacent to the Teflon collars used to support the tube support plates, as well as within the support plates. The bobbin probe voltages were found to be higher than those typically encountered in plant eddy current examinations. As a consequence, subsequent tests were designed to produce smaller cracks.

Series 3 Tests: Since the NDE of the archive and Series 2 test pieces produced higher voltages than are measured in steam generator tube support plate crevices, the sludge configuration of the Series 3 tests was modified to produce shorter cracks. Two tests were specified, with each containing four test specimens. Both tests utilized chemically consolidated sludge, with the sludge occupying a 60° arc and half of the 0.75 inch height of the tube support plate crevice. As in the Series 1 tests, Westinghouse heat 2675 was used for the tubing.

Tube 557 utilized simulated plant sludge and was treated with the 10X reference cracking chemistry, in order to produce accelerated SCC. Tube 558 utilized chromium oxide for crevice packing and was treated with the 1X cracking chemistry. Previous testing has found that using chromium oxide rather than simulated plant sludge promotes IGA rather than SCC. It was believed that field experience with IGA produces lower bobbin probe voltages than does SCC. The 1X chemistry was specified because it was hypothesized that it would produce less grain boundary corrosion, and therefore lower voltages.

Through wall cracking of tube 557 was produced after 16 days of operation. NDE of the tube indicated the voltages to be generally lower than in the previous tests, but still well above what is typically found in the field in TSP crevices.

Operation of tube 558 continued with the 1X chemistry for 56 days, at which time the specification was changed to the 10X chemistry in order to accelerate the corrosion rate. The test was then operated for an additional 52 days, at which time a primary to secondary leak occurred. Eddy current inspection identified a throughwall crack at the bottom tube support plate elevation, with the crack producing a 6.5 volt signal and a 69% indicated depth. The voltage is typical of field indications of throughwall cracks, while the indicated depth is shallower than what is typically found in the field. Following inspection, the remaining three tube support assemblies were returned to test. Testing continued for an additional 50 days, extending beyond the scheduled program completion date.

Although not originally included in the Series 3 tests, one test piece produced as part of EPRI Program S408-06, "Alloy 690 Qualification: Corrosion Under Prototypic Heat Flux and Temperature Conditions", was subsequently transferred to this program. Test piece 555-3 utilized mill annealed Alloy 600 tubing from heat 2675, and contained a cylindrical hole tube support plate crevice. As in some of the Series 1 tests, the crevice was filled with simulated plant sludge, which was held in place with porous Inconel frits located at both ends of the crevice. The test piece developed a through wall crack following 23 days of operation with the 1X cracking chemistry.

Series 4 Tests: This test series was undertaken after it was found that the test specimens produced in doped steam environments exhibited high leak rates compared to those found in tests of tubes pulled from the field. The high leak rates of the specimens produced in doped steam were attributed to the plastic deformation of the tubing required to obtain accelerated corrosion.

Consequently, the Series 4 tests were intended to produce both bobbin probe voltages and leak rates representative of those expected to be found in the field.

The Series 4 tests contained 45 specimens, mounted on eight tubes. 23 of the specimen collars were fabricated from Teflon, while the remaining 22 were fabricated from carbon steel. Teflon collars were utilized because the cracks located beneath the Teflon collars in the Series 2 tests typically produced lower bobbin probe voltages than did the cracks located adjacent to the collars.

Unlike the Series 2 and 3 tests, the Series 4 tests used tubes supplied to Westinghouse by the EPRI NDE Center. Tubing Heat 96834, lot 6, was originally fabricated by another NSSS vendor, and is the same as was used in the doped steam testing (see Section 7.2). The heat of material was changed because the doped steam testing found that this heat produced more accelerated corrosion than did the Westinghouse heat.

The design of the test specimens was also modified in order to reduce the magnitude of the eddy current voltages. These modifications are outlined in Table 7-3. The specimens in Series 4, Test 1 were configured to fit snugly around the tube (as did the Teflon collars in the Series 1 tests), but the height of the collars was varied between 0.25 and 0.7 inch. The expectation is that the shorter collars should limit the length of the cracks which can be produced.

The inside face of the specimens in Series 4, Test 2 were machined to produce a grid pattern to limit the crevice area between the tube and the collar. Six holes were first drilled around the periphery of the inside face of the specimen, so that the crevice would have an approximate 40° arc width. Two rings were milled on the face of three of the specimens. The rings had a width of 0.125 inch, so that the face was divided into three contact regions, with the outer regions having a 0.125 inch width and the central region having a 0.25 inch width. A helical pattern was machined into the face of the remaining three specimens, with the width of the helix being 0.125 inch and the pitch of the helix being 0.25 inch.

The specimens in Series 4, Test 3 all had a 0.75 inch height, but the diametral gap width was varied between a snug fit (as in Series 4, Test 1), a 10-mil gap, and a 20-mil gap. The gap width was varied because previous testing has found that the gap width affects the rate and location of corrosion.

Tests 4 and 5 of Series 4 both utilized chemically consolidated simulated plant sludge located adjacent to carbon steel tube support specimens. Two sets of specimens having thicknesses of 0.25, 0.50, and 0.75 inch were used in each test. The sludge was consolidated over a 40° arc width within the crevice. The 0.25 inch specimens contained one sludge region, which occupied essentially the full thickness of a specimen; the 0.5 inch specimens contained two sludge regions, separated by a 100-mil wide band at the center; the 0.75 inch specimens contained three sludge regions, separated by two bands.

Test 6 of Series 4 contained carbon steel specimens having the same range of thicknesses as in Tests 4 and 5. Instead of using simulated plant sludge, however, the crevices remained empty, with the specimens being held in place with porous Inconel sinters located at each end of the crevice. This design has been used to produce accelerated intergranular corrosion in previous tests.

The 10X reference cracking chemistry was specified for use in Tests 1 through 6 of Series 4. Because of concern that this specification may produce excessive grain boundary corrosion and therefore high bobbin probe voltages, two additional tests (7 and 8) were specified to utilize the 1X chemistry. Test 7 of Series 4 utilized five Teflon specimens, while Test 8 utilized four carbon steel specimens. The specimens utilize a range of designs selected from Tests 1 through 6 of Series 4.

The eight Series 4 tests accumulated between 96 and 328 days of operation, depending upon the test. Throughwall cracks had been produced in five test pieces, with a few additional test pieces containing partial throughwall cracks. The designs of the test specimens having throughwall cracks are presented in Table 7-4. As indicated in the table, three of the throughwall cracks were produced adjacent to Teflon simulants in Test 3, while the other two throughwall cracks were produced adjacent to carbon steel simulants. The only common feature of the crevice configurations which produced the cracks is that the crevice length was always 3/4 inch, perhaps suggesting that the shorter crevices could not produce sufficient superheat to promote accelerated corrosion.

Series 3 Tests: Two additional tests were conducted when it became apparent that accelerated corrosion was not being produced in Series 4 tests. The test specifications are summarized in Table 7-5. Both tests utilized tubing from heat 2675, the same heat used in the first three series, rather than heat 96834, which had been used in Series 4. Test 575 of Series 5 contained four tube support simulants having the same fritted design used in the Series 1 tests. The test was conducted because the test piece had been assembled for a previous program, but had not been used. Since this design was known to produce accelerated corrosion, it was hoped that the test could also provide additional crevice assemblies having small indications. While throughwall cracking was produced after 25 days of boiler operation, the associated eddy current signals were on the order of 20 volts, so that no further evaluation of the crevice assemblies was performed.

Test 576 of Series 5 was configured to produce small cracks, as was the intention of the Series 4 tests, while maintaining local crevice superheats in the same region as in the tests which produced accelerated corrosion. The crevices contained two sludge regions: a larger outer region of chromium oxide and a smaller inner region of simulated plant sludge. The expectation was that the cracking would be confined to the inner region, while the outer region would increase the superheat to values comparable to those in the early tests. Two of the crevice assemblies were specified to have the simulated plant sludge occupying the center of the top half of the chromium oxide region, while the other two crevice assemblies were specified to have the simulated plant sludge centered in the chromium oxide. In both cases, the inner region had a width of 0.125 inch and a height of 0.375 inch.

The test operated for 49 days with the 1X reference cracking chemistry, plus an additional 56 days with the 10X chemistry, when it was shut down because of a primary to secondary leak. Subsequent eddy current evaluation identified indications at two locations, as outlined below:

Location	Voltage	Depth
576-2	8.41	80%
576-4	8.43	86%

Both locations correspond to crevice configurations in which the simulated plant sludge was centered both axially and circumferentially with respect to the chromium oxide. An RPC evaluation identified three cracks; two were in the simulated sludge, while the third was in the chromium oxide. These results suggest that the two-region sludge configuration is a potential means of producing smaller cracks in model boiler specimens.

<u>Series 1 Tests:</u> Three model boiler tests were conducted in an effort to achieve accelerated intergranular corrosion. The test pieces were included in the program after through wall corrosion was obtained in two of the tests. The test specimens which underwent leak and burst testing are listed in Table 7-6. Modifications made to the test specifications to promote intergranular corrosion included using mechanically consolidated chromic oxide sludge (i.e., a nonoxidizing sludge), increasing the secondary pressure, and increasing the bulk concentration. These modifications were intended to reduce tubing stresses and promote uniform corrodent accumulation within the crevices.

7.2   Doped Steam Specimens

Axial stress corrosion cracks and crack networks were produced in 30 mill-annealed Alloy 600 tubes through exposure to a doped steam environment. The steam was produced from water containing 30 ppm each of chloride, fluoride, sulfate and nitrate anions as salts of sodium. The steam pressure was 3000 psi at a temperature of 750° F. Individual specimens were eight inches in length. Stressing was accomplished by clamping the tube at mid length between two flat steel plates, as shown in Figure 7-2. Ovalization of the tube resulted in outer fiber tensile yielding on the OD surface of the tube at the maximum diameter. The tube ends were sealed to permit internal pressurization of the tube during the autoclave exposure. The OD surface of the clamped tube was exposed to the 3000 psi doped steam environment in a one gallon autoclave. Nitrogen gas was used to pressurize the inside of the tube to 4500 psi producing a differential pressure across the tube wall of 1500 psi. The development of throughwall cracking was detected by a drop in the internal pressure of the tube.

Table 7-7 summarizes the specimens tested in the doped steam environment. Two heats of mill annealed Alloy 600 tubing were used, Heat 2675 and Heat 96834L. The width of the clamp in contact with the tube was typically 0.25 inch but larger clamp widths were also used in an attempt to vary the crack morphology. All of the tube displacements were sufficient to cause outer fiber yielding. These displacements ranged from 0.030 to 0.005 inch. In general, the smaller displacements resulted in shorter crack lengths and an increase in the test exposure time. The eddy current voltages listed in Table 7-7 are preliminary values used to help decide the disposition of the tube and should not be confused with the eddy current results provided in Section 8 for the same samples using representative field inspection procedures. The crack lengths shown in Table 7-7 are from optical measurements on the tube OD surface obtained at low magnification and may differ significantly from later destructive examinations. Some attempt to control the length of crack initiation sites was made on the last 7 specimens listed in Table 7-7. Selected portions of these specimens were grit blasted. This procedure had no discernible effect on crack initiation. Selected specimens from Table 7-7 were forwarded for full NDE examination, leak and burst testing as described later.

7.3   Fatigue Precracked Specimens

Throughwall axial fatigue precracks were developed in 12 mill annealed Alloy 600 tubes by cyclic internal pressurization. A starter flaw was spark machined half way through the wall of

the 0.050 inch thick by 0.875 inch diameter tubing with a length of 0.25 inch. Cyclic internal pressurization then was used to grow the crack throughwall. A soft plastic bladder seal was then inserted in the tube and cracks up to 0.70 inch in length were grown by a fatigue process. The pressure was adjusted during fatigue precracking to maintain the maximum applied stress intensity factor below 25 ksi-√in.. The maximum plastic blunting of the crack tip was thus kept below 0.0003 inch. Table 7-8 lists the fatigue precracked specimens, crack lengths and number of cycles. The fatigue precracked samples have well characterized leak rates from previous evaluations, although the leak rates are large compared to those for ODSCC cracks. These samples were used in studies of the effect of denting at tube support plate intersections on leak rates through cracked tubes.

7.4   Chemically Dented Tubes

Fatigue precracked tubes and tubes with stress corrosion cracks were used to simulate cracked tubes in tube support plates which are also dented. Carbon steel collars were used to simulate tube support plates. These collars were drilled with the nominal clearance hole for 0.875 inch diameter tubing. The collars were then packed with magnetite using a hydraulic press. The pressed magnetite was drilled out to a tight fit hole for insertion of a precracked tube. The final configuration was a carbon steel collar with an inside diametral clearance of 0.016 inch, a pressed 0.014 inch layer of magnetite and then the tube wall. The ends of these specimens were sealed and the specimens were exposed to a 0.2 M cupric chloride solution in an autoclave at 572°F.

Corrosion of the carbon steel and a smaller reaction layer with the Alloy 600 tubing resulted in corrosion products which tightly packed the tube-tube support plate crevice and led to a small amount of denting of the tube. Table 7-9 lists the dented specimens, the eddy current dent voltage and the average estimated radial dent size.

A section through the tube and collar of specimen Trial-1 is shown in Figure 7-3. The packed magnetite and the corrosion products in the crevice are clearly evident. A scanning electron photograph of the polished section in Figure 7-3a shows several layers of corrosion products along with the starting layer of packed magnetite. The EDS nickel and iron maps of Figure 7-4 show that the corrosion product adjacent to the Alloy 600 tube is enriched in nickel and somewhat depleted in iron. The corrosion product adjacent to the carbon steel collar appears to have the same iron content as the packed magnetite layer. The corrosion product layers in general appear to be relatively dense and any leakage path would be highly tortuous.

7.5   Crack Morphologies

Plugging criteria which are partially based upon eddy current characterization, leak rate and burst strength testing of laboratory specimens depend upon a reasonable simulation of actual service produced cracks. The crack morphologies of service tubes, doped steam test specimens and model boiler test specimens are presented in this section. An intergranular mode of cracking is common to cracks produced in these three environments. Figure 7-5 illustrates this fact with scanning electron fractographs. A further illustration of intergranular cracking is provided by the metallographic details shown in Figure 7-6.

Stress corrosion cracking patterns on the OD of Alloy 600 tubes at tube support plate intersections range from a few to many axial cracks distributed around the circumference of the tube. The model boiler test specimens also show this characteristic. Figure 7-7 shows several

arrays of cracks and a larger single crack. The cracks in the doped steam specimens tend to be either a single axial network or axial cracks 180 degrees apart. This is due to the nature of loading of the doped steam specimens. Clamping of the tube leads to a 180 degree symmetry of stresses, bending across the wall thickness and outer fiber bending stresses beyond the yield point. In model boiler specimens, as in actual tube support plate intersections, the stresses are uniform around the circumference of the tube and the occurrence of single or multiple axial cracks is controlled by the crevice conditions. The differential pressure hoop stress is relatively low, about 12 ksi. Hence the model boiler specimens experience essentially prototypic loading while the doped steam specimens experience stresses far beyond actual service conditions. The doped steam environment is substantially less aggressive than that produced in the model boiler tests and thus clamping loads are required in addition to the pressure stress to produce cracking in reasonable lengths of time. The high stress clamped condition of the doped steam specimens led to a higher degree of throughwall cracking for a given total axial crack network length and hence higher leak rates at a given eddy current bobbin coil voltage. Another complicating factor is the fact that relaxation of the throughwall bending stresses when the clamping fixture is removed can lead to contact across the faces of the crack. This would provide an eddy current path and reduce the bobbin coil voltage relative to a crack with non-contacting faces, as in the model boiler specimens. The above considerations indicate that the clamped test condition of the doped steam specimens produced non-prototypic stress corrosion cracks, particularly as they relate to any correlation between bobbin coil voltage, leak rate and burst strength. Therefore, only the model boiler specimen test results were added to the data base used to develop tube plugging criteria.

7.6   Nondestructive Examination (NDE) Results

The model boiler specimens were eddy current tested in the laboratory using both the bobbin coil probe and the RPC probe. The bobbin coil voltages were measured in accordance with the analysis guidelines used for the EPRI APC program. In the case of the 7/8-inch diameter tubing, the bobbin coil results reported here are for the 400/100 kHz mix frequency. The reference calibration was performed with the 20% holes in the ASME standard set to 2.75 volts in the differential mix channel. The RPC test results are for the 400 kHz frequency with the voltage normalization of 20 volts for the 0.25 inch long through-wall EDM (electric discharge machining) slot in the ASME calibration standard. Table 7-10 presents a summary of the NDE data for the model boiler specimens. The NDE data of Table 7-10 are obtained as received from the model boilers with TSPs in place and packed crevices. A few cases are given for which the NDE measurements were reported following a leak test at normal operating conditions and after removal of the packed crevice condition to obtain an open crevice. In these cases, the force required to remove the TSPs is expected to have changed the crack morphology, such as by tearing ligaments, to result in higher bobbin voltages for the subsequent open crevice measurements. The 7/8-inch tubing analysis guidelines used in the evaluation of the laboratory specimens are consistent with the Kewaunee analysis guidelines.

7.7   Leak and Burst Test Objectives

The objective of the leak rate tests is to determine the relationship between eddy current characteristics and the leak rates of tubes with stress corrosion cracks. Leak rates at normal operating pressure differentials and under steam line break conditions are both of interest, since leakage limits are imposed under both circumstances. The SLB leak rate data are used to develop a formulation between leak rate and bobbin coil voltage.

Crevice condition is another important factor. Tightly packed or dented crevices are expected to impede leakage through cracked tubes. Since denting is readily detectable by non destructive means while crevice gaps cannot be readily assessed, the emphasis is placed upon open crevices and dented crevices as the limiting cases.

Given the assumption that significant support plate displacements cannot be excluded under accident conditions, burst tests of tubes with stress corrosion cracks are conducted in the free span condition and burst pressure is correlated with bobbin coil voltage. This burst pressure correlation is then applied to determine the voltage amplitude that satisfies the guidelines of Reg. Guide 1.121 for tube burst margins.

7.6   Leak Test Procedure

Leak testing of cracked tubes is accomplished as follows. The ends of the tube are plug welded. One end has a fitting for a supply of lithiated (2 ppm Li), borated (1200 ppm B) and hydrogenated (1 psia) water to the tube inner diameter. The specimen is placed in an autoclave and brought to a temperature of 616°F and a pressure of 2250 psi. The pressure on the outer diameter is brought to 1000 psi. A back pressure regulator on the secondary side maintains the 1000 psi pressure. Any leakage from the primary side of the tube tends to increase the secondary pressure because of the superheated conditions. The back pressure regulator then opens, the fluid is released, condensed, collected and measured as a function of time. This provides the measured leak rate. The cooling coil is located prior to the back pressure regulator to prevent overheating and to provide good pressure control. Typical leakage duration is one hour unless leak rate is excessive and overheating of the back pressure regulator occurs. Pressure is controlled on the primary side of the tube by continuous pumping against another back pressure regulator set at 2250 psi. The bypass fluid from this regulator is returned to the makeup tank.

To simulate steam line break conditions the primary pressure is increased to 3000 psi by a simple adjustment of the back pressure regulator and secondary side is vented within one to three minutes to a pressure of 350 psi. The pressure differential across the tube is thus 2650 psi. Temperature fluctuations settle out in several minutes and the leakage test period lasts for approximately 30 minutes.

7.9   Leak Test Results

A summary of leak test results is provided in Table 7-11. The first series of leak rate tests were conducted at the normal operating pressure differential. Some of the model boiler specimens had tightly packed crevices as a result of corrosion product buildup. These specimens were tested as is. Following this first series of leak rate tests, the welded end plugs were cut from the leak specimens. Because of the crack location and short length of some specimens additional leak rate testing could not be performed. Specimens with tight collars were subjected to extensive eddy current testing. This required removal of the tight collars to obtain data comparing packed and open crevice eddy current response. Hence all repeat testing of the first series of test specimens was performed under open crevice conditions. Repeat testing led to higher leak rates either as a consequence of the open versus packed crevices, handling or forceful removal of tight collars. Only in one case did a non-leaker become converted into a leaker as a result of retesting. This case, 533-4, is one of forceful removal of a tight collar.

From Table 7-11, tight crevices are seen to be sometimes of benefit in reducing leak rates.

Specimen 542-4 had a very high eddy current voltage and a low leak rate of [   ]9, while specimen 543-2 had a high voltage and a leak rate of [   ]9. The four other tight crevice specimens were non-leakers. Three of these remained non-leakers after removal of the tight collars. Damage during removal of the tight collar is suspected as the reason the fourth non-leaker became a leaker. Tight crevices can be of benefit in reducing leak rate but cannot be relied upon. Further, pending future developments, eddy current techniques have not been shown to be able to confidently distinguish between open and tight crevices although the presence of magnetite can often be detected in the crevice.

Eddy current inspection techniques are very sensitive to denting at tube support plate intersections. Dents of a fraction of a mil are easily detectable. Specimens with large through wall cracks which were then dented to less than one mil have not leaked significantly either at operating pressure or under steam line break conditions. A tight through wall fatigue crack 0.50 inch in length will leak at more than the typical tech spec limit of 0.35 gpm. From Table 7-11 it is evident that a small dent has turned such a cracked tube into a non-leaker. [

]9.

The data of Table 7-11 that are used for APC development are given in Table 7-12. All bobbin voltages applied are obtained prior to removal of the TSPs, i.e., for the tight crevice condition. The crevice condition given in Table 7-11 applies to the condition for the leak rate tests and not for the voltage measurement except where both tight and open crevice voltages are given. All leak rates of Table 7-12 are for open crevice conditions.

7.10   Burst Test Procedure

Given the assumption that significant support plate displacements cannot be excluded under accident conditions, burst tests of tubes with stress corrosion cracks are conducted in the free span condition and burst pressure is correlated with bobbin coil voltage. This burst pressure correlation is then applied to determine the voltage amplitude that satisfies the guidelines of Reg. Guide 1.121 for tube burst margins.

Burst tests were conducted using an air driven differential piston water pump at room temperature. Pressure was recorded as a function of time on an X-Y plotter. Sealing was accomplished by use of a soft plastic bladder. Burst tests of tubes with stress corrosion cracks were done in the free span condition. No foil reinforcement of the sealing bladders was used since the crack location which was to dominate the burst behavior was not always readily apparent. Some of the maximum openings developed during burst testing were not sufficient to cause extensive crack tearing and thus represent lower bounds to the burst pressures. The openings were large enough in all cases to lead to large leakage.

7.11   Burst Test Results

Burst test results are summarized in Table 7-11. Figure 7-8 illustrates a plot of burst pressure versus bobbin coil voltage for specimens from model boiler and pulled tube tests which are considered reasonably representative of the range of field observations of ODSCC of tubes at tube support plate intersections. Note that some of the burst data points are lower bound estimates since extensive crack tearing did not develop. In these cases the crack openings were large enough to cause large leakage events in service. From Figure 7-8 it is seen that burst pressures remain above about [   ]9. As discussed later,

7 - 9

reasonable limits on bobbin coil voltage contributes to maintenance of required burst pressure margins with respect to both operating and accident pressure differentials.

The burst test data used for APC applications are given in Table 7-12. As noted previously, the bobbin voltages used to correlate with burst pressure were obtained with the TSPs present and with packed crevices as obtained from the model boilers.

7.12 Destructive Examination of Laboratory Specimens

The objective of this task was to characterize the size, shape, and morphology of the laboratory created corrosion in alloy 600 tube specimens which have been leak rate and burst tested. Examination methods include visual examinations, macrophotography, light microscopy and/or SEM (scanning electron microscopy) examinations, SEM fractography, and metallography. The crack morphology is also to be compared generally to the corrosion morphology observed in tubes pulled from operating power plant steam generators. Section 7 of EPRI Report NP-7480-L, Volume 1, provides a description of the results of destructive examinations performed on the 7/8-inch laboratory tube specimens. Table 7-12 provides measured crack lengths for the burst cracks from the destructive examinations.

7.13 Comparison with Pulled Tube Crack Morphology

Section 4.0 of this report described the crack morphology observed on tubes pulled from operating steam generators. Most of the support plate cracking was OD origin, intergranular stress corrosion cracking that was axially orientated. Most cracks had minimal IGA features in addition to the overall stress corrosion features. Even when the IGA was present in significant amounts, it usually did not dominate over the overall SCC morphology. Large macrocracks were composed of numerous short microcracks (typically < 0.1 inch long) separated by ledges or ligaments. The ledges could have either intergranular or dimple rupture features depending on whether or not the microcracks had grown together during plant operation.

The laboratory-generated corrosion cracks are observed to have the same basic features as the support plate crevice corrosion from pulled tubes. The laboratory specimens frequently had somewhat lower crack densities, but individual cracks usually had similar IGA aspects. The laboratory specimens possibly had even less of a tendency to develop IGA components to the overall stress corrosion crack features. The observed differences in corrosion morphology between the model boiler specimens and the pulled tubes is believed to be insignificant.

7.14 Model Boiler Database Summary

As described in the above subsections, model boiler specimens have been fabricated and tested to augment the pulled tube database at support plate intersections. Thirty-five (35) laboratory specimens have been prepared using 7/8-inch OD tubing. The specimens were subjected to eddy current examination. Degradation at simulated tube support plate intersections have ranged from 0.12 to 68 volts in bobbin coil amplitude. All of these specimens have been burst tested, with the results displayed in Table 7-12. All specimens were also been leak tested. Further, several of the samples were destructively examined to determine degradation characteristics and crack morphology. The currently available maximum and through wall crack length data obtained for many of these specimens from the destructive examinations are also listed in Table 7-12. The model boiler database is combined with the pulled tube database and the total used for determining leak rate and burst correlations.

Table 7-1

MODEL BOILER THERMAL AND HYDRAULIC SPECIFICATIONS

Primary loop temperature	327°C (620°F)
Primary loop pressure	13.8 MPa (2000 psi)
Primary boiler inlet temperature	324°C ± 3°C (610°F ± 5°F)
Primary boiler outlet temperature	313°C ± 3°C (595°F ± 5°F)
Secondary T_{sat} at 5.5 MPa (800 psi)	271°C ± 3°C (520°F ± 5°F)
Steam bleed	8 cm^3/min (continuous)
Blowdown	1 cm^3/min (8 hr/day)
Nominal heat flux	16.28 x 10^4 kcal/m^2-hr (60,000 Btu/ft^2-hr)

Table 7-2

MODEL BOILER TEST SPECIMEN SUMMARY FOR SERIES 1, 2, AND 3
7/8" Diameter Tubing

SPECIMEN	INITIAL SLUDGE TYPE	DAYS IN TEST	THRU WALL	HYDRO TESTED*
Series 1 - Archive Test Pieces				
500-1	Mech. Cons.	56	No	Yes
509-2	Frit	10	Yes	No
509-3	Frit	10	Yes	No
510-1	Frit	8	Yes	No
525-1	Frit	148	No	Yes
528-1	Chem. Cons.	7	Yes	No
528-2	Chem. Cons.	7	Yes	No
530-1	Chem. Cons.	8	Yes	Yes
532-1	Frit	31	Yes	No
532-2	Frit	31	Yes	No
533-4	Mech. Cons.	12	Yes	Yes
535-1	Mech. Cons.	73	No	No
536-1	Eccentric	73	No	Yes
Series 2 Test Pieces				
542-1**	Mech. Cons.	24	Yes	Yes
542-2**	Mech. Cons.	24	No	No
542-3**	Mech. Cons.	24	No	Yes
542-4	Mech. Cons.	24	Yes	Yes
543-1	Chem. Cons.	10	Yes	Yes
543-2	Chem. Cons.	10	Yes	Yes
543-3**	Chem. Cons.	10	No	Yes
543-4	Chem. Cons.	10	No	Yes
Series 3 Test Pieces				
557-1	Chem. Cons.	16	No	Yes
557-2	Chem. Cons.	16	Yes	Yes
557-4	Chem. Cons.	16	No	Yes
558-1	Chromium Oxide	116	Yes	Yes
558-2**	Chromium Oxide	166	No	No
558-3**	Chromium Oxide	166	No	No
558-4**	Chromium Oxide	166	No	No

*   Indicates if a hydrotest was performed prior to NDE.

** Specimens not leak or burst tested after NDE for use in APC data base.

Table 7-3

SUMMARY OF SERIES 4 TEST SPECIFICATIONS

Test	Tube	Collar Material	No. of TSP's	Thick. (in.)	Crevice * Configuration	Chemistry
1	569/1	Teflon	2	0.25	Snug Fit	10X
			2	0.5	Snug Fit	
			2	0.75	Snug Fit	
2	567/9	Teflon	3	0.75	Mach'd Rings	10X
			3	0.75	Mach'd Helix	
3	568/12	Teflon	2	0.75	Snug Fit	10X
			2	0.75	10 Mil Gap	
			2	0.75	20 Mil Gap	
4	570/2	C. Steel	2	0.25	Sim. Plant	10X
			2	0.5	Sim. Plant	
			2	0.75	Sim. Plant	
5	571/4	C. Steel	2	0.25	Sim. Plant	10X
			2	0.5	Sim. Plant	
			2	0.75	Sim. Plant	
6	572/5	C. Steel	3	0.25	Frits, Empty	10X
			3	0.5	Frits, Empty	
7	573/6	Teflon	2	0.25	Snug Fit	1X
			1	0.5	Snug Fit	
			1	0.75	Snug Fit	
			1	0.75	Mach'd Rings	
8	574/3	C. Steel	2	0.75	Sim. Plant	1X
			1	0.25	Frits, Empty	
			1	0.75	Frits, Empty	

*   Where a sludge type is listed, the sludge is chemically consolidated over a 40 to 60 degree arc width within the crevice; the machined rings are formed by dividing the tube support plate circumferentially into six land regions, and axially into two rings having a 1/8 inch thickness; the machined helix is formed by dividing the tube support plate circumferentially into six land regions, and axially into a helical pattern having a 1/8 inch thickness and a 1/4 inch pitch.

Table 7-4

SUMMARY OF SERIES 4 TEST PIECES HAVING EDDY CURRENT SIGNALS
7/8" Diameter Tubing

Test	Tube	Collar Material	Thick. (in.)	Crevice Conf'guration	Thru wall Leak	Days in Test	Hydro Tested*
3	568-1-1	Teflon	0.75	Snug Fit	Yes	30	Yes
	568-2-1	Teflon	0.75	10 Mil Gap	Yes	38	Yes
	568-4-1	Teflon	0.75	Snug Fit	Yes **	47	Yes**
	568-6-1	Teflon	0.75	20 Mil Gap	No	152	No
5	571-1-1	C. Steel	0.75	Sim. Plant	Yes	61	Yes
8	574-2-1***	C. Steel	0.75	Sim. Plant	No	32	No
	574-4-1	C. Steel	0.75	Frits, Empty	Yes	64	Yes

*   Indicates If a hydrotest was performed prior to NDE.

**   Separate cracks were identified at the top and bottom ends of the crevice. Both cracks were included in the leak test.

***   Specimen not leak or burst tested after NDE for use in APC data base.

Table 7-5

SERIES 5 TEST SPECIMENS

Test Specimen	Crevice Configuration	Sludge Type	Throughwall Leak
575-1	Frit	Sim. Plant	Unknown
575-3	Frit	Sim. Plant	Yes
576-2	Dual Chem. Cons.	Chr. Ox. + Sim. Pl.	Yes
576-4	Dual Chem. Cons.	Chr. Ox. + Sim. Pl.	Yes

Table 7-6

SERIES 6 TEST SPECIMENS

Test Specimen	Crevice Configuration	Sludge Type	Throughwall Leak
605-2	Mech. Cons.	Chr. Ox.	Yes
605-3	Mech. Cons.	Chr. Ox.	Yes
606-3	Mech. Cons.	Chr. Ox.	No
607-3	Mech. Cons.	Chr. Ox.	Yes
607-4	Mech. Cons.	Chr. Ox.	No

Table 7-7

Summary of SCC Behavior in Doped Steam at 750°F

Specimen[a] Number	Alloy Heat	Clamp Width (in)	OD min Deflection (in)	TW SCC (hours)	Crack Network Lengths (in)	Bobbin Mix Voltage
SL-FH-1	2675	0.75	0.030	143.1	1.20	5.7
SL-FH-2	2675	2.0	0.030	93.3[b]	2.67; 2.96	0.48; 0.27
SL-FH-3	2675	0.25	0.020	169.9	0.90	0.95; 8.5; 1.1
SL-FH-4	2675	0.25	0.010	261.3	0.63	7.4; 3.2
SL-FH-5	2675	0.25	0.010	170.5	0.47	4.0
SL-FH-6	2675	0.25	0.005	98.2	1.45	5.2; 7.5; 1.6
SL-FH-7	2675	0.25	0.005	175.0	1.22	6.1
SL-FH-8	2675	0.25	0.005	207.8[c]	0.27; 0.34	1.5; 0.44
SL-FH-9	2675	0.25	0.005	118.0	0.97; 1.15	1.3; 3.9; 2.0
SL-FH-10	2675	0.25	0.005	118.0	1.20; 1.16	0.69; 1.7; 1.8
SL-FH-11	2675	0.25	0.005	119.9	0.50; 1.10	2.3; 5.7
SL-FH-12	2675	0.25	0.005	119.9	0.57; 1.63	1.9; 0.48
SL-FH-14	2675	0.25	0.005	307.8	0.67	2.2; 5.2
SL-BW-1	96834L	0.75	0.030	95.1	0.72; 0.85	5.4; 1.5
SL-BW-2	96834L	2.0	0.030	35.3	1.65	6.0
SL-BW-3	96834L	2.0	0.020	58.0	0.78	7.4
SL-BW-4	96834L	0.25	0.020	64.5	1.10; 1.44	7.5; 4.1; 4.3
SL-BW-5	96834L	0.25	0.020	164.4[c]	0.37; 0.50	0.48; 0.53
SL-BW-6	96834L	0.25	0.030	71.0	2.07; 2.35	8.0; 7.2
SL-BW-7	96834L	0.25	0.010	93.8	0.72	4.2
SL-BW-8	96834L	0.25	0.005	132.8	0.28	2.6
SL-BW-9	96834L	0.25	0.005	334.0	0.65	4.3
SL-BW-10	96834L	0.25	0.005	424.0	0.62; 0.17; 0.28	7.0
SL-BW-11	96834L	0.25	0.005	213.0	0.34	2.2
SL-BW-12	96834L	0.25	0.005	693.0[d]	e	2.5
SL-BW-13	96834L	0.25	0.005	87.0	0.63	3.2; 3.4; 7.6
SL-BW-14	96834L	0.25	0.005	64.0	0.33	4.6
SL-BW-15	96834L	0.25	0.005	667.0[d]	e	1.2; 2.3
SL-BW-16	96834L	0.25	0.005	500.0	0.20	4.9; 7.7; 4.6
SL-BW-17	96834L	0.25	0.005	146.0	0.14	1.8; 1.3; 2.8
SL-BW-18	96834L	0.25	0.005	366.0[d]	e	NDD[f]
SL-BW-19	96834L	0.25	0.005	480.0[d]	e	NDD[f]
SL-BW-20	96834L	0.25	0.005	257.0[d]	e	NDD[f]
SL-BW-21	96834L	0.25	0.005	243.0[d]	e	NDD[f]

a   SL-FH-13 rejected because of baseline NDE indication.
b   Leaked at 750°F; did not leak at room temp.; but had visible OD cracks.
c   Did not leak at 750°F. Test periodically shut down till OD cracks visible.
d   Did not leak at 750°F.
e   No OD cracks visible at termination.
f   No detactable degradation.

Table 7-8

Fatigue Precracked Specimens

Specimen	Crack Length	Number of Cycles
FAT-1	0.500	323,700
FAT-2	0.299	85,000
FAT-3	0.300	26,100
FAT-4	0.697	1,278,000
FAT-5	0.300	22,600
FAT-6	0.302	110,000
FAT-7	0.509	410,000
FAT-8	0.707	710,000
FAT-9	0.513	370,000
FAT-10	0.701	726,000
FAT-11	0.499	226,000

Table 7-9

Summary of Dented Specimens

Specimen	Dent Voltage	Average Radial Dent (inches)	Exposure Time (hours)
Trial-1	-	-	24
FAT-1	7.39	0.00037	24
FAT-2	6.09	0.00030	24
FAT-3	12.11	0.00061	48
FAT-4	12.0	0.00061	58
FAT-5	4.55	0.00023	6
FAT-6	0.00	0.0	6
FAT-7	9.43	0.00047	24
FAT-8	17.42	0.00087	48
FAT-9	3.40	0.00017	6
FAT-10	2.50	0.00012	6
FAT-11	2.75	0.00014	6
BW-1	14.67	0.00073	24
BW-3	6.27	0.00031	24
BW-9	6.38	0.00032	48
BW-14	7.03	0.00035	48

Table 7-10

Laboratory Specimen NDE Summary[1]

Sample Number	Probe Type	Flaw Amplitude (V)	Phase (°)	Flaw[4] Depth (%)	Flaw[4] Length(in)	No. of Flaws

g

---

(1)   As received Specimens, Prior to Leak Test. Data are average results for Echoram EE-720-FsbM-UF and Zetec A-720-ULC(775) Bobbin Probes and Echoram EB-720-2XSRPC and Zetec 720-MRPC Pancake Probes.

(2)   Specimen had multiple axial indications.

(3)   Second NDE after initial leak testing.

(4)   RPC depth is for the deepest crack and length for the total crack network.

Table 7-10   (continued)

Laboratory Specimen NDE Summary[1]

Sample Number	Probe Type	Flaw Amplitude (V)	Phase (°)	Flaw[4] Depth (%)	Flaw[4] Length(in.)	No. of Flaws

g

_____

(1)   As received Specimens, Prior to Leak Test. Data are average results for
Echoram EE-720-FsbM-UF and Zetec A-720-ULC(775) Bobbin Probes and
Echoram EB-720-2XSRPC and Zetec 720-MRPC Pancake Probes.

(2)   Specimen had multiple axial indications.

(3)   Second NDE after initial leak testing.

(4)   RPC depth is for the deepest crack and length for the total crack network.

Table 7-10 (continued)

Laboratory Specimen NDE Summary[1]

Sample Number	Probe Type	Flaw Amplitude (V)	Phase (°)	Flaw[4] Depth (%)	Flaw[4] Length(in.)	No. of Flaws

g

_____

(1)   As received Specimens, Prior to Leak Test. Data are average results for Echoram EE-720-FsbM-UF and Zetec A-720-ULC(775) Bobbin Probes and Echoram EB-720-2XSRPC and Zetec 720-MRPC Pancake Probes.

(4)   RPC depth is for the deepest crack and length for the total crack network.

Table 7-10   (continued)

Laboratory Specimen NDE Summary[1]

Sample Number	Probe Type	Flaw Amplitude (V)	Phase (°)	Flaw[4] Depth (%)	Flaw[4] Length(in.)	No. of Flaws
						g

---

(1)   As received Specimens, Prior to Leak Test. Data are average results for Echoram EE-720-FsbM-UF and Zetec A-720-ULC(775) Bobbin Probes and Echoram EB-720-2XSRPC and Zetec 720-MRPC Pancake Probes.

(4)   RPC depth is for the deepest crack and length for the total crack network.

Table 7-11

Summary of Leak and Burst Teat Reaults

g

Table 7-12

7/8-Inch Diameter Model Boiler Specimens: Test Data Summary

No.	Model Boiler Spec. #	Bobbin Coil Volts	% Depth	RPC Volts	# Cracks	Leak Rate (l/hr) N. Op. ΔP	SLB ΔP	Burst Press. - psi	Destructive Exam. Length - inch Max	Thruwall*

g

---

*   For specimens without throughwall penetration, maximum depth of penetration is listed.

** Destructive examination and review of RPC data shows that only 1 crack has a significant response that contributes to the bobbin signal.

*** Tube not burst tested due to physical limitation of specimen.
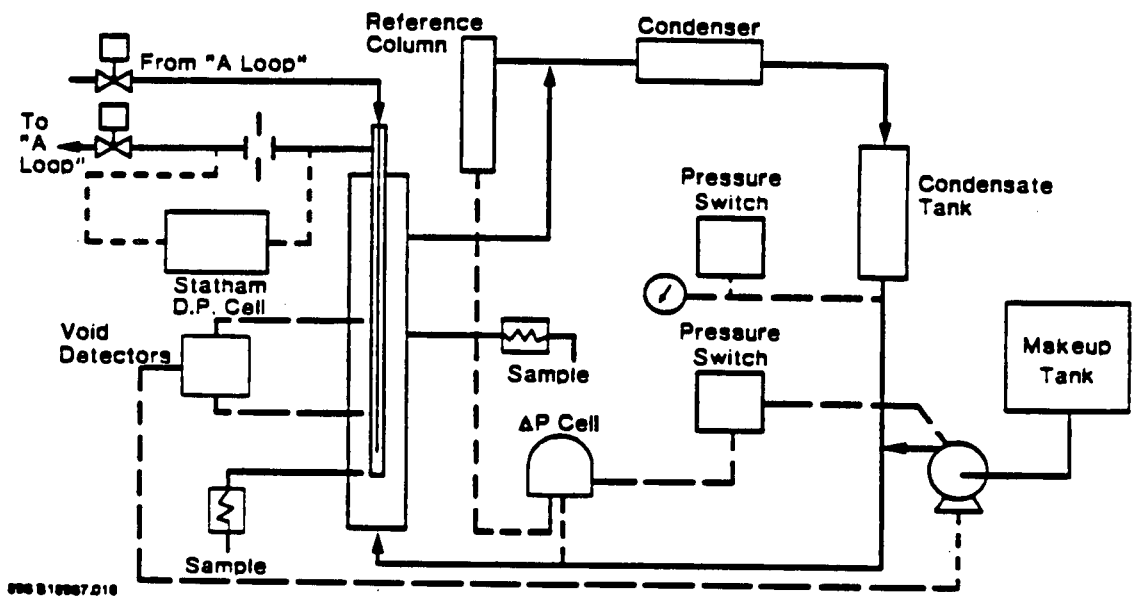
Figure 7-1. Schematic of Model Boiler Facility
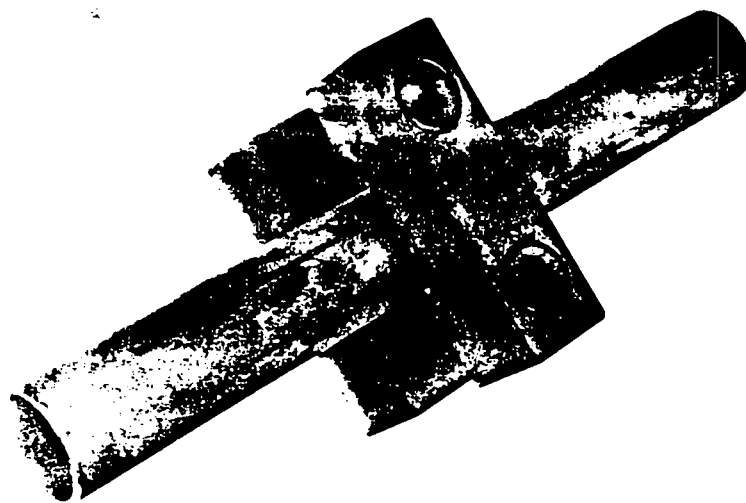
Figure 7-2. Clamped Specimen Used For Doped Steam Test

Specimen Trial-1

Alloy 600 Tube

Carbon
Steel

Prepacked Magnetite

Alloy 600 Tube

Carbon
Steel

Corrosion
Product

Corrosion
Product

×254   30kV   100μm   #0004
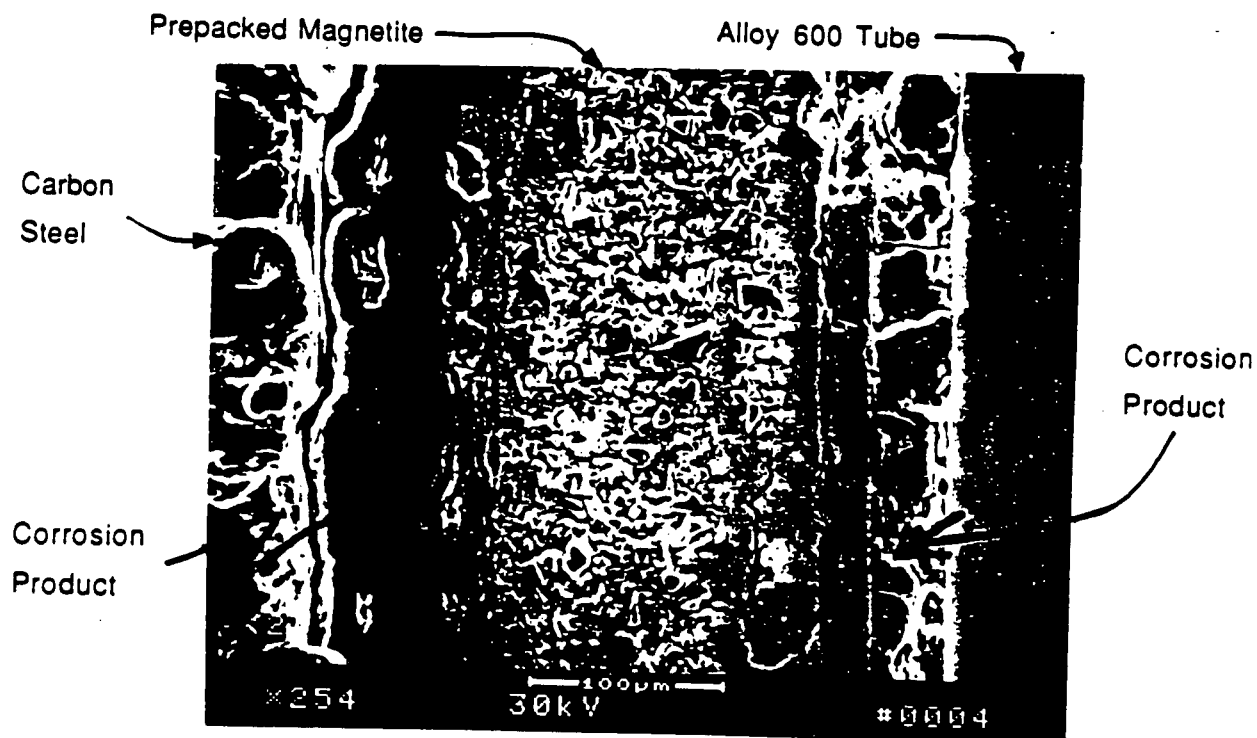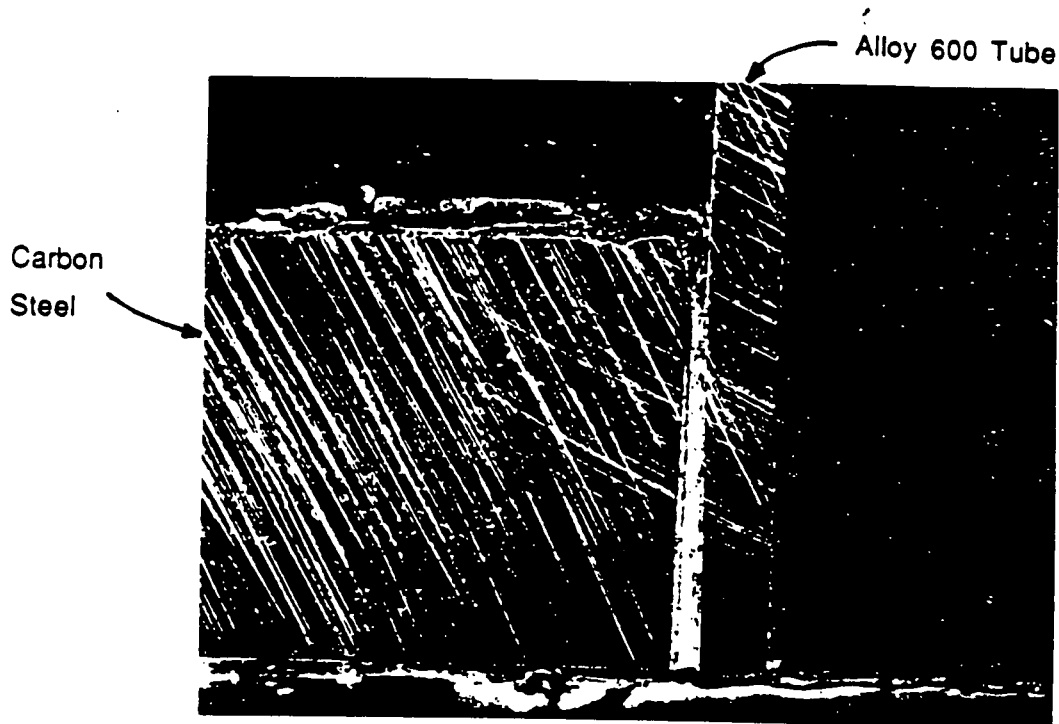
Figure 7-3. Section Through a Dented Tube Support Plate Intersection

NI Map

Corrosion Product

Alloy
600
Tube

×250   ━━100μm━━→
30kV   #0004

Fe Map

×250   ━━100μm━━
30kV   #0004
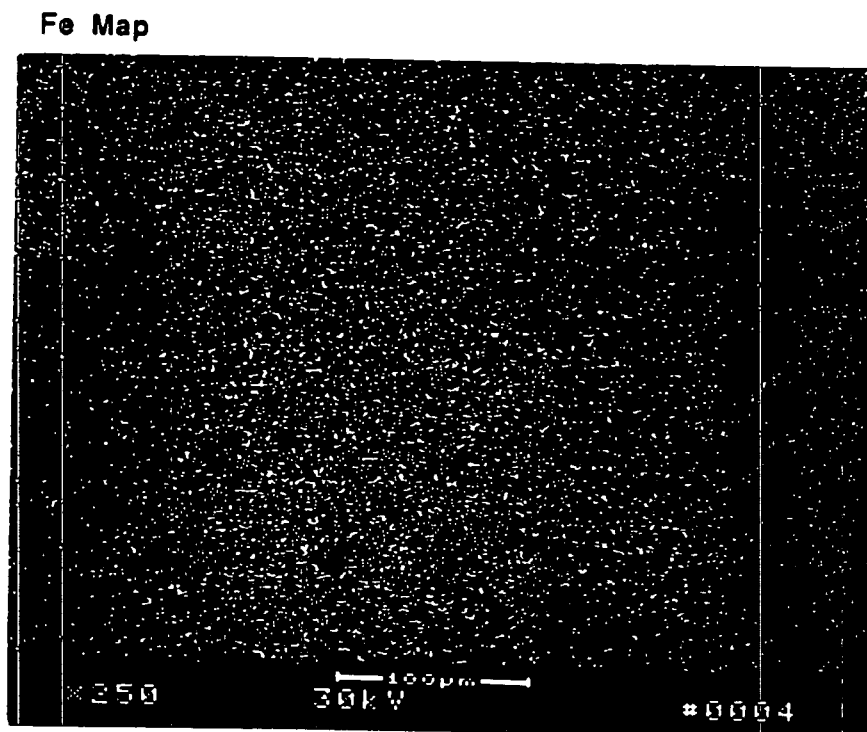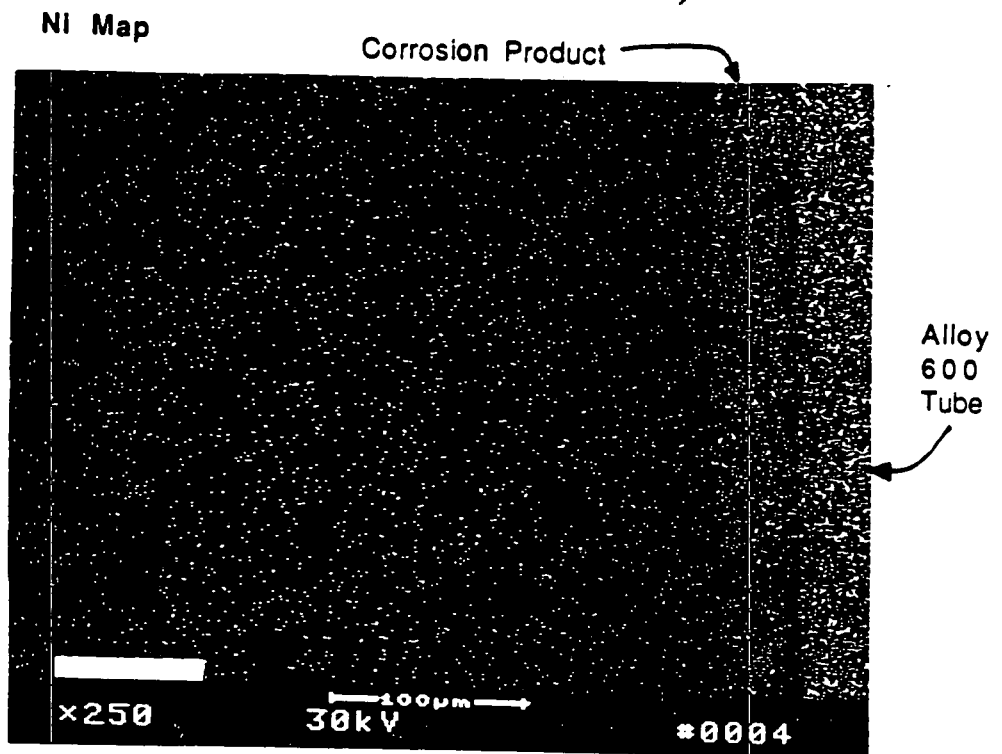
Figure 7-4 . EDS Elemental Maps Across a Dented Crevice; Specimen Trial-1
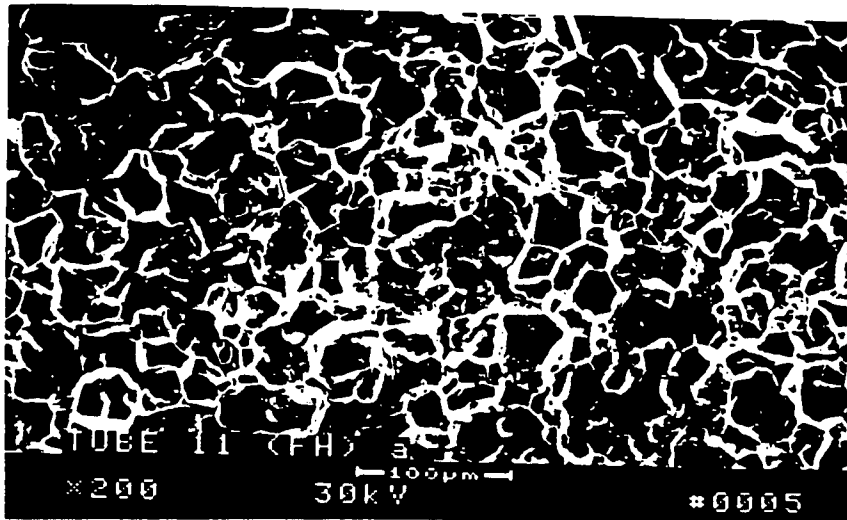
Doped
Steam
Specimen

200X
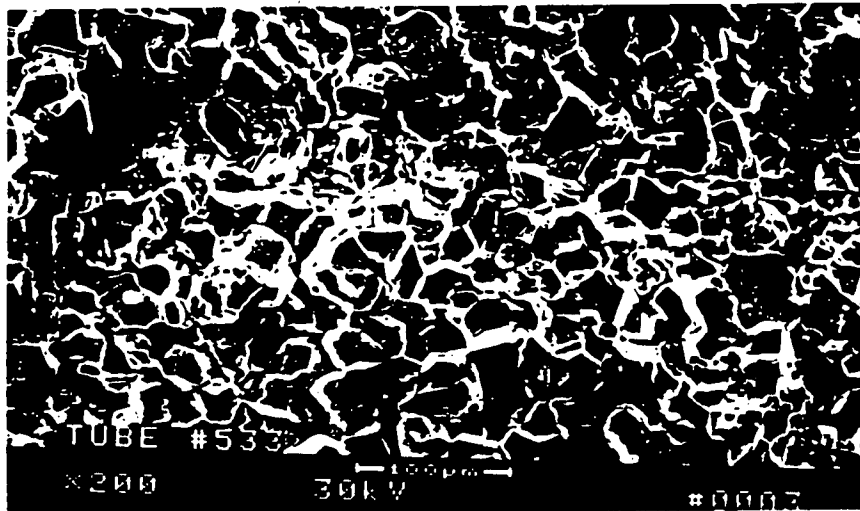
Model
Boiler
Specimen

200X
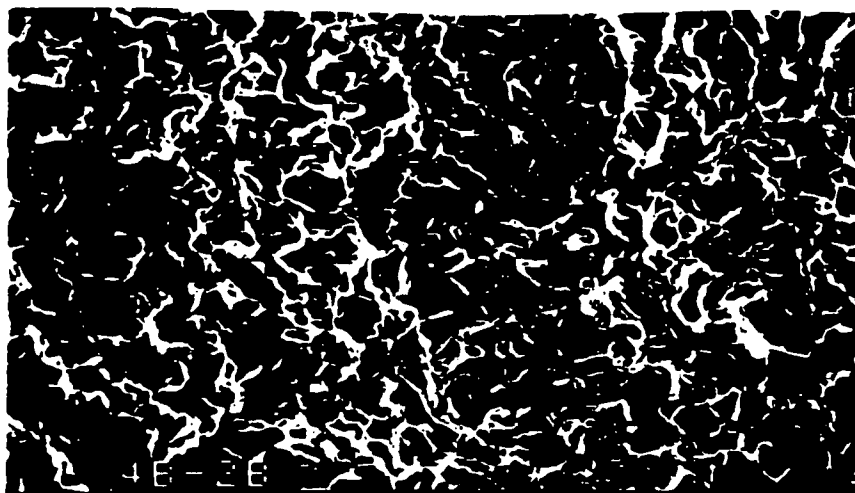
Pulled
Tube
(Field)

200X

Figure 7-5. SEM Fractographs of Cracks in Doped Steam Specimen,
Model Boiler Specimen and Service Tube
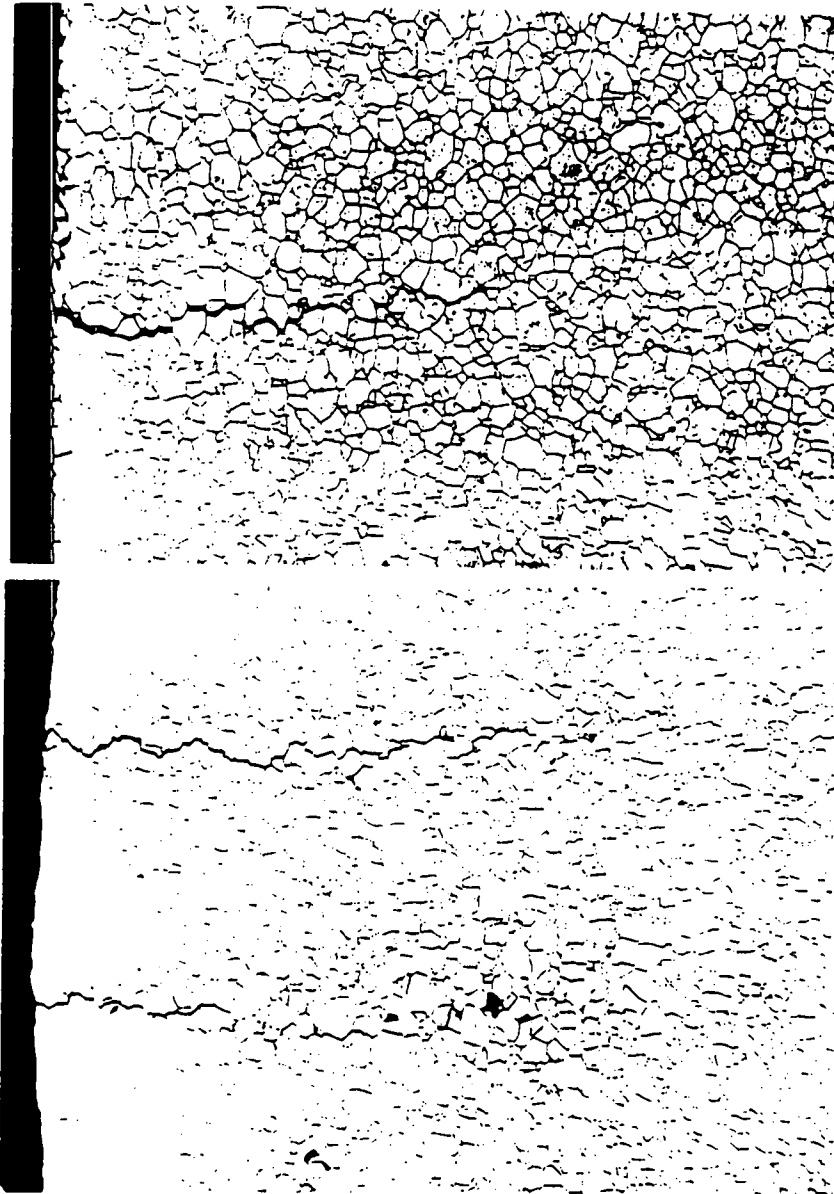
Doped
Steam
Specimen

100X

Model
Boiler
Specimen

100X

Figure 7-6. Metallograph of Cracked Specimens
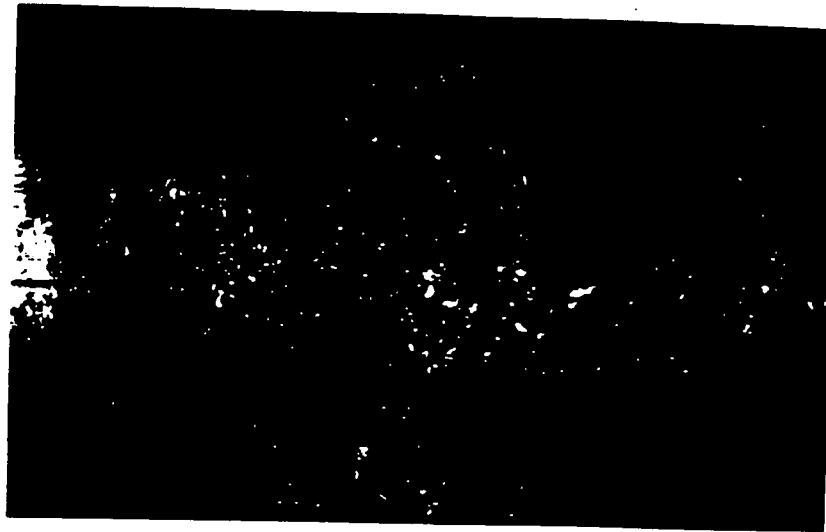
Axial
Crack
Network

Distributed
Cracks Under
Steel Collar

Large Cracks
Under Teflon
Spacer Pins

Single
Large
Crack

Figure 7-7. Cracks in Model Boiler Specimens

8.0   BURST PRESSURE CORRELATION

8.1   Introduction

This section uses the model boiler (Section 7) and pulled tube (Section 6) data to develop the correlation of burst pressure vs bobbin voltage. An enhanced statistical procedure was implemented as described below and in Appendix C. This methodology has been reviewed and accepted by the EPRI APC Committee and an independent EPRI consultant. All normalization of eddy current data has been reviewed and has been accepted by the EPRI Committee. Thus the data, methodology, and correlation provided in this section provide confidence in the results.

8.2   Database for Burst Pressure Correlation (7/8 Inch Tubing)

The database used for the development of the burst correlation (burst pressure vs bobbin coil voltage amplitude) for 7/8 inch diameter tubing is derived from model boiler specimens and pulled tubes. All of the data were derived from Alloy 600 tubing with 7/8 inch OD and 0.050 inch nominal wall thickness. The model boiler test results for 7/8 inch tubing are described in detail in Section 7. All bobbin coil measurements on model boiler specimens are reported from the 400/100 kHz mix frequency with the 20% holes in the reference ASME standard normalized to 2.75 volts.

The pulled tube data included in the database is obtained from Plants A-2, D-1, D-2, J-1, L, and P-1 . The bobbin voltages for Plants A-2, D-1, D-2, L, and P-1 were field measured prior to the tube pulls at a frequency mix the same as the model boiler specimens. The bobbin data from Plant J-1 pulled tubes were measured at 240 kHz using the Belgian NDE procedures. This data has been normalized to correspond to the APC database using the process described in Section 6.6. The pulled tube results are described in Section 6.

The burst pressures of all the room temperature data are normalized to a reference flow stress of 75 ksi to provide a consistent data base. This value is close to the 77 ksi mean flow stress for the mill annealed Alloy 600 tubing at room temperature (WCAP-12522). The resulting burst pressure database is summarized in Table 8-1 for both the model boiler specimens and the pulled tubes. The database includes 33 model boiler specimens and 35 pulled tube intersections.

8.3   Burst Pressure Voltage Correlation

The bobbin coil voltage amplitude and burst pressure data of Table 8-1 were used to determine a correlation between burst pressure and bobbin voltage amplitude. This is not to say that a "formal" functional relationship, in the sense of one variable being dependent on the other, exists between the variables since the burst pressure is not caused by the bobbin voltage and vice versa. The burst pressure and bobbin voltage variables considered are mainly functions of a third variable, i.e., the crack morphology. While the variation in crack morphologies is essentially infinite, suitable descriptions can be effected based on the depth, average depth, profile description, etc. However, the characterization of the morphology is not essential to this analysis since a relationship is being independently established between two offspring variables. Although the correlation analysis does not establish a causal relationship between the

variables, it does, however, establish a "working" relationship that can be employed for the prediction of one variable from the other. The data considered are shown on Figures 8-1 and 8-2 along with the results of correlation analyses (discussed later).

The analysis performed considered the scale factors for the coordinate system to be employed, i.e., logarithmic versus linear, the detection and treatment of outliers, the order of the regression equation, the potential for measurement errors in the variables, and the evaluation of the residuals following the development of a relation by least squares regression analysis.

In summary, it was concluded that the optimum linear, first order relation could be achieved by considering the burst pressure relative to the common logarithm (base 10) of the bobbin amplitude voltage (Section 8.3.1). For this relationship it was determined that a bobbin voltage value of 0.1 volt could be ascribed to the burst data where degradation was not detected, i.e., no detectable degradation (NDD). This is necessary to include NDD specimens in the database since the burst pressure should be a continuous function to the point of no existing degradation. A linear, first order equation relating the burst pressure to the logarithm of the bobbin amplitude was developed. The correlation coefficient from the regression analysis was found to be significant at a >99.9% level. Analysis of the residuals from the regression analysis indicated that they are normally distributed, thus verifying the assumption of normality inherent in the use of least squares regression.

8.3.1 Selection of Coordinate System

Since the measured bobbin coil voltage and measured burst pressure are expected to have independent variances, the method of least squares (LS) curve fitting was employed. The simplest functional form is a linear relationship of the type

$$y = a_0 + a_1 x \qquad (8-1)$$

where the variables x and y may be individually linear or logarithmic, and the coefficients of the relation, a_0 and a_1 are to be determined from the analysis. In addition, the choice of the regressor variable is not pre-determined. Both variables are assumed to be subject to random fluctuations which are normally distributed about the mean of the variable or the logarithm of the variable with a mean of zero and some unknown, but reasonable variance. It is also assumed that this variance is constant, or uniform, over the range of interest of the variables. In practice this may not be the case; however, any non-uniformity present would not be expected to significantly affect the analysis outcome.

Analyses were performed to determine the optimum nature of the variable scales, i.e., linear versus logarithmic, and the appropriate selection of the regressor variable. It was concluded that the most meaningful correlation could be achieved by considering the log of the voltage as the regressor and the burst pressure as the response. Thus, the functional form of the correlation is

$$P_B = a_0 + a_1 \log(V) \qquad (8-2)$$

where P_B is the burst pressure and V is the bobbin voltage amplitude. The basis for selection of the form of the variables was based on performing least squares regression

analysis on each possible combination and examining the square of the correlation coefficient (the index of determination) for each case. The selection of the regressor variable does not affect the calculation of the index if the calculations are performed on the transformed data. The results of the calculations for 3/4 inch tubes were presented in Section 10.3 of WCAP-13522, and are applicable to 7/8 inch tubing.

The results clearly showed an advantage in treating the voltage on a logarithmic scale and the burst pressure on a linear scale. Given this choice of axes scales, the burst pressure should be regressed on the logarithm of the voltage amplitudes. The rationale for this is that the residual error bands will be reduced with this selection relative to performing the regression in the opposite direction.

It is noted that the data contain some results for specimens in which there was no detectable degradation from the non-destructive examination. The inclusion of this data is necessary in order to predict burst pressures for indications with very low bobbin amplitudes. Two methods were considered for inclusion of the data in the analysis. The first method consists simply of assigning a low bobbin voltage amplitude to the data. This was done for the determination of the best choice of scales for the coordinates of the plot. The value assigned was 0.1 volt for the NDD specimens. The second method consists of modifying the prediction model to include a voltage offset variable to be determined from the data, i.e., the prediction equation becomes

$$P_B = a_0 + a_1 \log(V + V_0) \qquad (8-3)$$

where V_0 is the additional parameter to be determined from the data. V_0 represents a voltage offset at which the NDD are included in the regression at V=0. Since the equation is now non-linear in the parameters the application of least squares techniques is not appropriate. However, if an assumed value is assigned to the offset term the equation is once again linear and least squares can be applied to find the values for the other two coefficients. Analysis was performed in Section 10.3 of WCAP-13522 (3/4 inch tube correlation) for a variety of offset values with the result that the index of determination was a maximum of 79% for $V_0 = 0.24$ volt. This is slightly less than the maximum value found for determining the best selection of the coordinate scales. It was thus concluded that the complication of including a voltage offset in the prediction model is not necessary to account for the NDD specimens. Additional analysis was performed to determine if a value less than 0.1 volt would be appropriate for NDD specimens. It was found that the index of determination becomes a maximum if the NDD specimens are assigned a voltage level of 0.15 V. However, the improvement was significant only in the third decimal place. Since this level of amplitude was present in the data for a confirmed indication it was judged to be inappropriate as an assigned value for NDD specimens. Likewise, reduction of the assigned value from 0.1 volt was considered inappropriate since it would reduce the fit of the burst regression curve artificially.

An additional consideration for the analysis of the data was to increase the order of the prediction equation. This would allow for the assignment of a lower value for the NDD specimens. Under this consideration the model would be

$$P_B = a_0 + a_1 \log(V) + a_2 [\log (V)]^2 \qquad (8-4)$$

The results of this analysis are shown on Figure 8-1. The results indicate no improvement in the index of determination and the introduction of a second order term provides no improvement in the model. Thus, a linear (first order) model was retained for the analysis.

8.3.2 Regression Analysis for the Identification of Outliers

The data contained in Table 8-1 were analyzed to identify any potential outlying data points using a robust regression technique based on minimizing the the median of the squares of the residuals. The method, known as the least median of squares method, is described in Appendix C. Six specimens, two from the Model Boiler (Specimens 535-1 and 525-1) and four from Plant D (specimens D-1-02, D-1-01, D-1-03, and D-1-05) were found to have residual to scale ratios indicating that their burst pressures do not conform with the rest of the data. These values are shown as solid symbols on Figure 8-1.

A discussion of the physical basis for outliers is appropriate in reviewing the outliers. For the six specimens identified at outliers above, all had high burst pressures relative to the indicated voltages. These specimens tended to have more RPC indications than other specimens. The bobbin voltage increases with the number of indications around the tube circumference, while the burst pressure is limited by the limiting single crack. Thus specimens with multiple indications (high voltages relative to burst pressure) are expected to contribute to the high (non-conservative) burst pressure tail of the burst/voltage correlation, and the six specimens mentioned above are deleted accordingly. Although no low burst pressure outliers were excluded in this analysis, in contrast, the low burst pressure outliers have a different physical basis (crack morphology). The low burst pressure outliers are seen for burst cracks having one or more relatively large, ductile (uncorroded) ligaments separating deep microcracks that comprise the overall macrocrack. Thus the physical basis for high and low outliers are distinctly different and the extreme tails of the distribution could be different. Only high outliers were excluded from the regression analysis. The low outliers are retained to provide conservatism in the regression fits. It is seen by later analysis that the retained data follow a normal distribution.

8.3.3 Error-in-Variables Analysis

A general assumption in performing a least squares regression analysis to establish a correlation is that both of the variables, i.e., burst pressure and bobbin voltage, are subject to random fluctuations about their respective mean values (or their respective log mean values). If there are significant uncertainties in the measurement of one or both of the variables the slope of the LS correlation line will be biased. There is no significant measurement error in the burst pressure values; however, no such evaluation was made relative to the reported bobbin coil voltage amplitudes. Thus, it was assumed that measurement error could present itself in one of the two variables, but not both. This means that the variance of the variable, X, with the measurement error, as estimated from the data, consists of two parts, the intrinsic variation of the variable, σ_x, and the variation due to measurement error, σ_m, i.e.,

$$\sigma_X^2 = \sigma_x^2 + \sigma_m^2 \qquad (8-5)$$

This results in the expected value of the slope of the regression line, b_1, being

$$E(b_1) = \beta / [1 + (\sigma_m)^2 / (\sigma_x)^2] \qquad (8-6)$$

where β represents the slope of the true relation, if any. Thus, the regression performed always underestimates the slope of the true relation. Since the omission of correction for measurement error results in an under prediction of the slope of the correlation, predicted burst pressures for voltages below the centroid of the data will likewise be less than a prediction based on consideration of the measurement error. For voltage values greater than the centroid of the data, the correlation slightly overpredicts the burst pressure. If the measurement error variance or the ratio of variances is known, the effect of the error on the slope of the regression line can be evaluated directly. An alternative evaluation of the potential effect can be performed based on an examination of the data per the partitioning procedure developed by Wald and subsequently improved by Bartlett. A Wald-Bartlett evaluation of the data was performed and it was concluded that the presence of measurement error would not have a significant effect on the slope of the correlation line. These results were presented in Section 10.3 of WCAP-13522.

8.3.4 Burst Pressure Correlation for 7/8 inch Diameter Tubing

The final fit of the data is shown on Figure 8-2. The correlation line is given by

$$[\qquad\qquad\qquad\qquad\qquad\qquad\qquad]^{a,g} \qquad (8-7)$$

where the burst pressure is measured in ksi and the bobbin amplitude is in volts. A one-sided 95% simultaneous confidence band and a 95% one-sided prediction band were also calculated. These are also shown in Figure 8-2. Following the determination of the prediction band, it was further reduced to a level corresponding to the 95% lower tolerance limit for the material properties of the tubes. A second order fit of bobbin amplitude to differential pressure was performed for the purpose of determining lower bound voltage amplitudes as a function of the applied pressure differential.

$$[\qquad\qquad\qquad\qquad\qquad\qquad\qquad]^{a,g} \qquad (8-8)$$

Using this result the voltage amplitude corresponding to a differential pressure of 4.620 ksi would be [ ]^{a,g} volts, and the amplitude corresponding to a differential pressure of 2.335 ksi would be [ ]^{a,g} volts.

8.3.5 Analysis of Residuals

The results of the analysis of the residuals for the 7/8 inch burst correlation are provided on Figures 8-3 and 8-4. The initial analysis consists of plotting the residual burst pressure values against the regression (predicted) burst pressure values. Since no correlation is expected, the scatter plot should exhibit non-descript characteristics. An examination of the data plotted on Figure 8-3 demonstrates that no correlation exists between the residual values and the predicted values. If the residuals are normally distributed with a mean of zero they should plot as a straight line with the zero value of the residual burst pressure at the 50 percent value. Examination of Figure 8-4

demonstrates that the amplitudes plot as an approximate straight line with a mean value of 0.1 to 0.2 ksi. This value approximates zero relative to the range of the residual burst pressures involved. The conclusion of the examination of the residuals is that the assumptions inherent in the least squares analysis are verified.

The data considered as outliers for the analysis are also shown on the plots. For the scatter plot the outliers do not violate the non-descript nature of the plot, and thus do not indioate a correlation. On the cumulative probability plot the outlying data plot to the right of the included data in the upper portion of the plot. This may tend to confirm the outlying nature of those data points, however, their departure from the rest of the data is slightly exaggerated due to their omission from the least squares analysis.

Table 8-1

**7/8-Inch Diameter Pulled and Model Boiler Tube Leak Rate
and Burst Pressure Measurements**

Plant	Specimen No. or Row/Col.	TSP	Bobbin Coil Volts[4]	Depth	RPC Volts	Destructive Exam Max.Depth	Length[1] (in.)	Leak Rate(l/hr)[3] Normal Oper.	SLB	Burst Pressure Meas. (psi)	Adj.[14] (psi)

(See notes at bottom of next page)

Table 8-1 (cont'd)

Plant	Specimen No. or Row/Col.	TSP	Bobbin Coil Volts[4]	Depth	RPC Volts	Destructive Exam Max.Depth	Length[1] (in.)	Leak Rate(l/hr)[3] Normal Oper.	SLB	Burst Pressure Meas. (psi)	Adj. (psi)

g

Figure 8-1: Burst Pressure vs. Bobbin Amplitude
7/8" x 0.050" Alloy 600 Tubes, Model Boiler & Field Data

a,g

Burst Pressure, ksi

8 - 9

Bobbin Amplitude, Volts

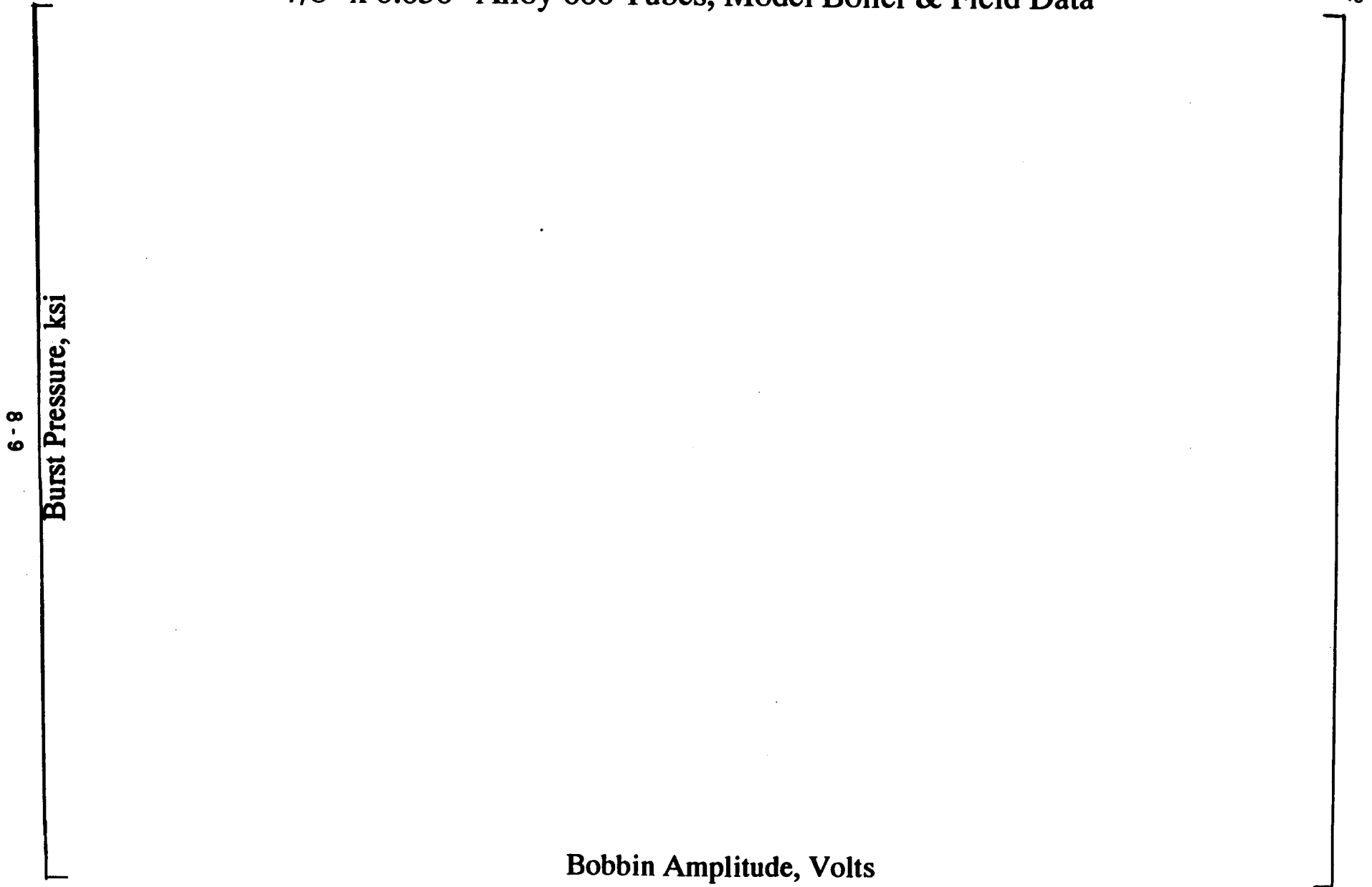# Figure 8-2: Burst Pressure vs. Bobbin Amplitude
7/8" x 0.050" Alloy 600 Tubes, Model Boiler & Field Data

a,g

Burst Pressure, ksi
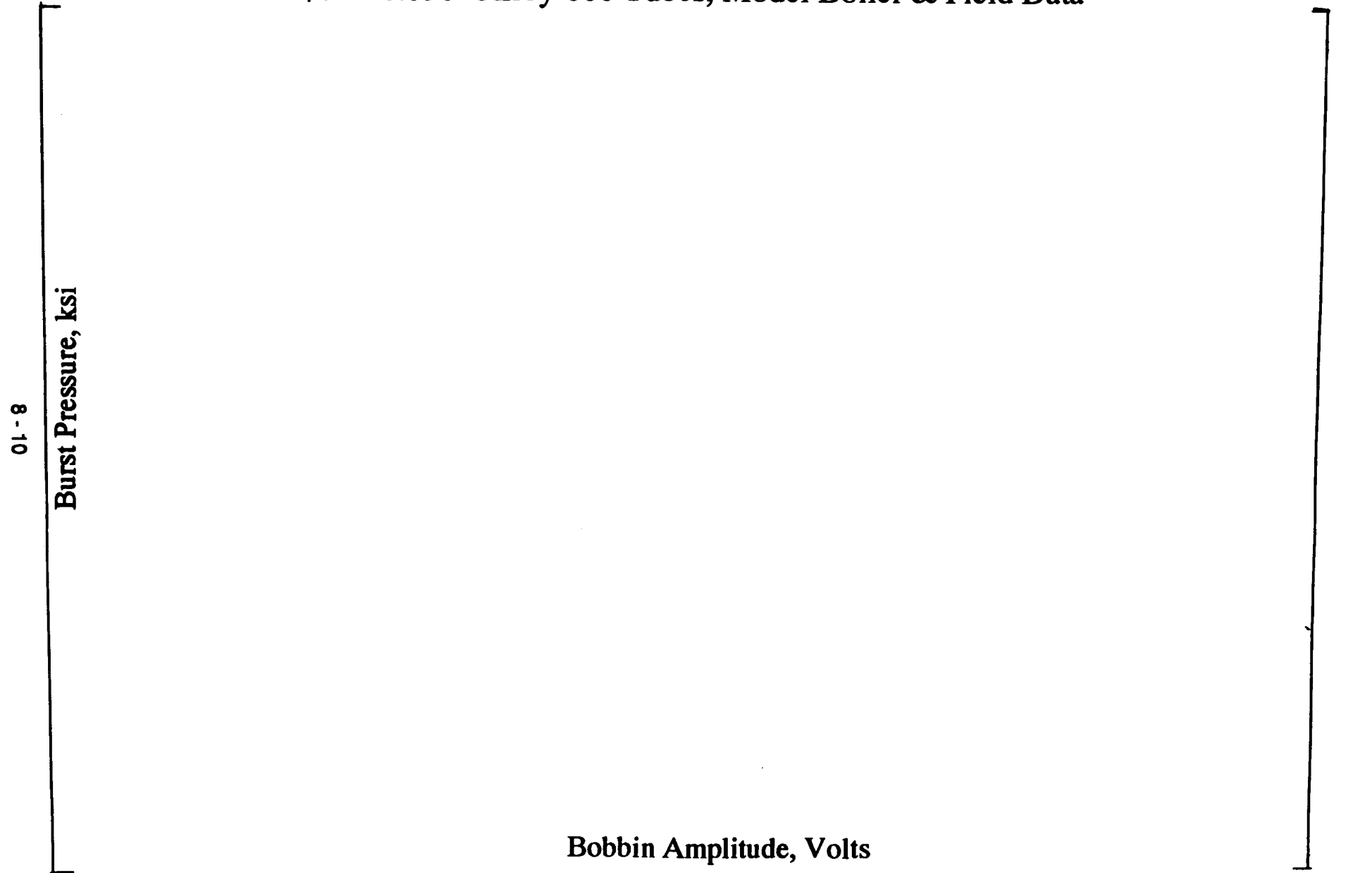
Bobbin Amplitude, Volts

8 - 10

78PBVLTS.SP5

Figure 8-3: Residual vs. Predicted Burst Pressure
7/8" x 0.050" Alloy 600 Tubes, Model Boiler & Field Data

a,g

Residual Burst Pressure (ksi)

9.0 SLB LEAK RATE CORRELATION

9.1 Introduction

This section uses the model boiler (Section 7) and pulled tube (Section 6) data to develop a correlation of SLB leak rate (primary to secondary leak rate under steam line break conditions) vs bobbin voltage. An enhanced statistical procedure was implemented as described below. All renormalization of eddy current data has been reviewed in detail and resolved by the EPRI APC Committee. Data from non-leaking tubes are not included in the leak rate correlation. However, a separate correlation has been developed for probability of leakage using all available data from 7/8 inch tubing, as described in Section 9.4 below.

The developed probability of leakage (Section 9.4) as a function of voltage provides a statistically based estimate of the leakage threshold. Alternate leakage threshold assessments are given in Section 9.3 to estimate a threshold for significant leakage. To assess trends expected for leak rate vs. voltage correlations, a combination of analytical calculations of leakage as a function of crack length and field crack length vs. voltage data are presented in Section 9.5. These trend analyses help to guide selection of the bounding leak rate correlation in Section 9.6.

9.2 Database for SLB Leak Rate Correlation (7/8 Inch Tubing)

The database used for the development of the SLB leak rate correlation (primary to secondary leak rate under SLB conditions vs bobbin coil voltage amplitude) for 7/8 inch diameter tubing is derived from model boiler specimens and pulled tubes. All of the data were derived from Alloy 600 tubing with 7/8 inch OD and 0.050 inch nominal wall thickness. The model boiler test results for 7/8 inch tubing are described in detail in Section 7. All bobbin coil measurements on model boiler specimens were reported from the 400/100 kHz mix frequency with the 20% holes in the reference ASME standard normalized to 2.75 volts.

The pulled tube data included in the database is obtained from Plants A-2 and J-1. The bobbin data from Plant J-1 pulled tubes were obtained from the APC 400/100 kHz mix and voltage normalized to U.S. voltages. These data include cross-calibration of ASME standards to the reference laboratory standard, as described in Section 5.6. This process involved significant and detailed efforts by two independent parties (Laborelec and Westinghouse) and review by the EPRI APC Committee such that there is negligible uncertainty in the renormalization procedure. The pulled tube results are described in Section 6.

The SLB leak rate data are normalized to primary pressures of 2350 and 2665 psia and to the secondary side pressure of 15 psia (atmospheric) at operating temperature. Renormalization from the measured leak rate conditions for SLB leak rates (as described in Section 7.4) is developed in Appendix B. The resulting SLB leak rate database is summarized in Table 8-1 for both the model boiler specimens and the pulled tubes. The leak rate data from French plant J-1 are not included in the SLB leak rate correlation. The measurements were performed at room temperature and neither a description of the experimental methods nor the facility is currently available to adequately review the measurements. The SLB leak rate measurement for model boiler specimen 535-1 is not considered reliable since the measured leak rate decreased between the normal operating pressure differential of 1500 psid and the SLB 2650 psid. Similarly, the leak rate for specimen 542-4 increased by only 8% between normal operating and SLB conditions. It

is expected that the crack openings for specimens 535-1 and 542-4 became plugged by deposits at the SLB test conditions and these specimens are not included in the leak rate correlation. The Plant J-1 tubes and specimen 542-4 also have a large number of cracks around the tube circumference which tends to yield high bobbin voltages for the associated throughwall crack length and low leak rates for the resulting bobbin voltage. Statistical analyses for outliers (see Section 9.2) identify Plant J-1 tube R8C74 and model boiler specimen 542-4 as the largest outliers in the database, which is consistent with the aforementioned reasons for not including these indications in the correlation. Specimen 535-1 would be marginally an outlier while Plant J-1 tube R22C36 is consistent with the database. Data from non-leaking tubes are not included in the leak rate correlation. The resulting leak rate database includes 20 model boiler specimens and 2 pulled tube intersections.

9.3   Leak Rate Threshold Assessment

As a crack is initiated and grows to a certain size (in depth and length) it becomes detectable through eddy current inspection. Such a crack indication would have a signal amplitude associated with it. As the crack grows, so does its signal amplitude. When the crack becomes throughwall, it would have a significant voltage amplitude signal. Although extremely short cracks may be construed to have small amplitudes, in practice, a throughwall corrosion crack will have some minimum signal amplitude. It is not known explicitly what minimum voltage amplitude may be associated with such a crack.

In order for a crack to result in leakage across the tube wall, the crack must be throughwall. Further, for an OD initiated throughwall crack to leak, it must have some minimum length at the tube ID. The estimated bobbin voltage threshold for leakage based on throughwall crack length considerations is discussed in Section 9.3.4 A voltage threshold for leakage is also supported by the scarcity of leak rate test results for bobbin coil amplitudes below 3 volts. Thus it may be concluded that there would be an eddy current voltage threshold below which corrosion cracks would not cause leakage. A voltage threshold for SLB leakage is assessed below from the body of available data.

9.3.1   Threshold Based on Destructive Exam Depth of Pulled Tubes

Figure 9-1 is a plot of bobbin voltage versus maximum depth of cracks in pulled tubes from operating steam generators with 7/8 inch diameter Alloy 600 tubing. There are 63 pulled tube specimens from seven different plants, both domestic and European. Due to the differences in crack morphology among the various pulled tube specimens, the plotted data is scattered as expected. However, an increasing trend between bobbin voltage and maximum throughwall depth from destructive examination is visible. On the semi-log plot, a linear relationship between the voltage and destructive examination depth is broadly indicated. Figure 9-1 shows a regression fit to the data for depths <100%. This regression fit can then be extrapolated to 100% depth to estimate the expected voltage for a crack just penetrating throughwall. The best estimate voltage for a throughwall indication is about 2.4 volts and the lower 90% confidence on the mean regression line is about 1.7 volts. All of the data for throughwall cracks fall above this voltage as may be noted in Figure 9-1. Since a crack must be throughwall to cause leakage, it follows that the minimum bobbin voltage threshold for leakage in 7/8 inch tubing is expected to be about 2.4 volts.

Figure 9-2 is a similar plot for pulled tubes of 3/4 inch diameter. There are 45 pulled tube specimens from five different plants, both domestic and European. A trend similar to the 7/8 inch data may be observed. The data is scattered and a linear relationship on

9 - 2

the semi-log plot is displayed. Extrapolation of a regression fit of the partial depth cracks suggests a bobbin amplitude of about 1.7 volts for a crack in 3/4 inch diameter tubing to reach throughwall depth. Again almost all of the pulled tube data from throughwall cracks lie above this value (higher voltage amplitudes than 1.7 volts).

9.3.2   Threshold Based on Leakage Data

A considerable amount of data exists on the leak rate of ODSCC flaws in pulled tubes and model boiler specimens. This database includes both 3/4 inch and 7/8 inch diameter tubing. The database consists of 77 model boiler specimens and 109 pulled tube intersections. The data from 7/8 inch tubing is reported from the 400/100 kHz differential mix with the 20% holes in the ASME standard normalized to 2.75 volts in the mix. Similarly, the 3/4 inch tubing data is normalized to 2.75 volts for the 20% holes in the ASME standard at the 550/130 kHz differential mix.

In order to combine the data from the 7/8 inch and 3/4 inch specimens, a conversion factor equal to the square of the diameter ratios is applied. This factor results from the fact that the ASME standard hole size is the same for 3/4 and 7/8 inch tubing. Thus, to convert the 3/4 inch data to the same basis as the 7/8 inch data, the voltage amplitudes from the 3/4 Inch data (at 550/130 kHz) were multiplied by the factor 1.36. The results were then combined with the 7/8 inch database.

The leak rates were, for most (150 of 186) cases, the direct result of measurements in the laboratory under SLB conditions. For the other (36) cases, laboratory data on leak rate measurement was not available and the likelihood of leakage was inferred from crack morphology (throughwall depth and length) obtained from destructive examination.

The data was classified into leaking and nonleaking specimens. A frequency distribution of voltage amplitudes (corresponding to the 7/8 Inch data normalization) in each classification was determined. This is shown in Figure 9-3 as a stacked bar chart. The number of leaking specimens in each voltage range out of the total number in that range is also shown listed at the top of each bar in the figure.

The ratio of the number of leaking specimens in a voltage range (bin) to the total number of specimens in the bin was calculated from the above frequency distribution of voltage amplitudes. This result, probability of leakage, within each voltage range is plotted as a bar chart in Figure 9-4.

The above results (Figures 9-3 and 9-4) were developed using data from both the 7/8 and 3/4 inch diameter tubing. If the 3/4 inch data is excluded and only the SLB leak rate data from 7/8 inch tubing is used, the results are not changed significantly. This is displayed in Figures 9-5 and 9-6.

For the 7/8 inch tubes, the data supports no leakage under SLB conditions for indications up to 2.8 volts and a low probability of leakage between 2.8 and 6 volts.

9.3.3 Threshold Based on Bobbin Voltages of Non-leaking Specimens

A voltage threshold for SLB leakage is derived using data from non-leaking specimens. All available data for corrosion cracks with throughwall or near throughwall indications is used in this evaluation. Specimens with crack depths greater than 90% (from destructive examination) which exhibited no leakage during the leak test are listed in Table 9-1. It may be noted that, in the case of 7/8 inch tubing, these flaws had signal

amplitudes in the range of 1.0 to 10.8 volts. These data suggest an SLB leakage threshold of about 3.9 volts, although the standard deviation is large which indicates that this estimate may not be reliable.

9.3.4 Threshold Based on Throughwall Crack Length

The threshold for SLB leakage can also bo assessed by evaluating the lowest bobbin voltages resulting in leakage at SLB conditions and by evaluating the throughwall crack length generally required for measurable leakage. If the throughwall crack length assoolated with measurable leakage can be defined, the voltage versus crack length relationship developed for 3/4 inch tube in WCAP-13522 (Section 11.5.1) can be used to assess the voltage threshold for leakage. The crack length method for estimating a voltage threshold for leakage provides a more physical insight into the threshold estimate.

The leakage threshold can be assessed by examining crack length data. Table 9-2 shows specimen throughwall crack lengths for no leakage, leakage <1.0 liter/hr and leakage between >1.0 and 6.0 liter/hr. In the case of 7/8 inch diameter tubing, no leakage was found for throughwall cracks up to 0.16 inch. The smallest throughwall crack length for which even small leakage (<1 liter/hr) is detected is 0.11 inch. Specimen 535-1 had a 0.11 inch throughwall corrosion crack (0.28 inch total crack length) with a leak rate of 0.07 liter/hr at SLB conditions. Pulled tube R4C73 from Plant A-2 had a 0.18 inch throughwall crack (0.42 inch total crack length) with a leak rate of <0.001 l/hr at normal operating conditions and 0.17 l/hr at SLB conditions. Overall, the data of Table 9-2 indicate that throughwall crack lengths >0.1 inch are generally required for SLB leakage. The bobbin voltage associated with a throughwall crack length of 0.1 inch is expected to be >2.5 volts.

9.3.5 Voltage Threshold Considerations for SLB Leakage (7/8 inch Tubing)

In the above sections, the SLB leakage threshold was evaluated from different perspectives: voltage indications required for throughwall cracks (2.4 volts), voltage threshold from leak rate data (2.8 volts), voltages of non-leaking tubes with throughwall and near throughwall degradation (3.9 volts), and crack lengths required for leakage (>2.5 volts). In all cases, the data show that the bobbin amplitude threshold for zero leakage is expected to exceed about 2.4 volts whereas the threshold for significant leakage (≥ 0.3 liter/hr or ~10^{-3} gpm) in a 7/8 inch diameter tube, based on Table 9-2, is about 6 volts.

Based on the above, leakage rates (bobbin volts) should be related to a threshold leak rate. The threshold for zero leakage is expected to exceed 2 volts, while the threshold for meaningful leakage (~0.3 liter/hr or ~10^{-3} gpm) is expected to exceed 6 volts. The SLB leak rate methodology and analysis for Kewaunee is intended to be conservatively applied. Therefore, a leakage threshold of 2.0 volts is applied for Kewaunee. That is, all indications above 2.0 volts have a probability of leakage as developed in Section 9.4 (Figure 9-7) and a conservative leak rate (Figure 9-8) for indications in the range of APC applications.

The best fit or maximum likelihood estimate for probability of leakage given in Figure 9-7, developed below in Section 9.4, supports a 2.0 volt leakage threshold. The upper 95% bound of Figure 9-7 shows a low probability of leakage of less than 12% below the 2.0 volt limit. This lower voltage estimate is inconsistent with the threshold estimates developed above and is judged to result from the limited database in the range of 2 to 6

volts. In either case, both the 2.0 volt probability of leakage at +95% confidence (<12%) and the SLB leak rate at +95% confidence (1 l/hr) are very low such that the 2.0 volt threshold can be applied with negligible error in the SLB leak rate.

9.4   Probability of SLB Leakage Versus Bobbin Voltage

It is seen from the above discussion and the supporting data that even when the voltage amplitude of a corrosion crack exceeds the leakage threshold, there is a likelihood of no leakage. In order to quantify this fact, probability of SLB leakage as a function of voltage is derived in this section.

9.4.1 Database for Probability of Leakage

The current evaluation of probability of SLB leakage is limited to 7/8 inch diameter tubing. Hence, the database used here is limited to the 7/8 inch specimen results shown in Figure 9-7. Figure 9-7 includes pulled tube results for which leak or burst tests were not performed. The data set for this analysis consists of pairs of test results for which leakage test results are available, or for which it could be verified from destructive exam results that leakage would not occur at a pressure less than or equal to the postulated SLB differential pressure. When leak tests were not performed, the maximum crack depths were evaluated to define the indications as either non-leaking tubes or leaking tubes. An example would be for a very small bobbin amplitude wherein a large burst pressure was observed during burst testing (e.g., for a burst pressure test in which no leakage was observed to a pressure in excess of about 3100 psi at room temperature for a tube with a material flow stress of 75 ksi). The database consists of 22 model boiler specimens and 4 pulled tubes specimens for which SLB leak rates are known from direct measurement. In addition, there are pulled tube specimens for which leak rate tests were not performed. For these specimens, leakage was assessed on the basis of the crack morphology from the destructive examination.

9.4.2 Statistical Evaluation for Leakage Probability

An analysis was performed to establish an algebraic relationship that could be used to predict the probability of leakage during a postulated SLB as a function of bobbin voltage. Two approaches were considered for the analysis. The first approach would be to segregate the results into a series of discrete bobbin amplitude ranges, or bins, based either on the actual voltage observed or on the logarithm of the bobbin voltage. This would be followed by the preparation of a cumulative histogram of the results, e.g. Figure 9-4, and the fitting of a smooth polynomial, or a cumulative normal distribution type curve through the results. There are, however, two significant drawbacks associated with this type of an approach. The first drawback is that the shape of the plotted histogram is dependent on the number of subdivisions used to segregate the data range. The second drawback is that there would be no direct way of establishing confidence bounds on the model, although binomial limits could be calculated for each bin.

To consider the second drawback further we note that the probability of leakage must be limited to a range of 0 to 1. A correlating equation to fit the data could be achieved by employing the method of least squares (LS) or maximum likelihood (ML) to estimate the parameters of the equation. If the expression was based on correlating probability as a function of leakage, the upper confidence band for the resulting expression would exceed unity for some voltages. Likewise, for lower voltages the lower confidence band would yield probabilities less than zero.

In general, the criteria for a good estimator are that it be unbiased, consistent, efficient, and sufficient. The parameters of a correlation curve from either LS or ML analysis will satisfy the above requirements if the requirements for performing the analysis are met. However, for the probability of leakage, the estimating curve will not be strictly consistent for a sample size less than infinitely large due to variability inherent in establishing the subdivision size. It is noted that although the objections of the second drawback might be overcome by correlating voltage to probability, the requirement for a consistent estimator might not be met. It was therefore decided, that the first analysis approach would not be pursued.

The second approach to the analysis stems from the observation that the data may be considered as samples from a dichotomous population. This means that the data are categorical, and that the number of categories is two, i.e., either no leak or leak. However, for an analysis treating the data in this manner, a linear correlation model of the type

$$P(\text{leak} \mid \text{volts}) = a_0 + a_1 f(\text{volts}) + \varepsilon \qquad (9\text{-}1)$$

where f(volts) is either volts or log(volts), is not appropriate since normally distributed errors, ε, do not correspond to zero (no leak) or one (leak) responses.

It is appropriate to analyze the data in this situation by non-linear regression analysis (logistic regression in particular) since the data are dichotomous. Letting P be the probability of leak, and considering a logarithmic scale (based on the range of the data) for volts, V, the first order logistic expression is

$$P = 1/\{1 + e^{-[a_0 + a_1 \log(V)]}\} \qquad (9\text{-}2)$$

This can be rearranged as

$$\ln[P/(1-P)] = a_0 + a_1 \log(V) \qquad (9\text{-}3)$$

where the logit transform is defined to be

$$\text{logit}(P) = \ln[P/(1-P)]. \qquad (9\text{-}4)$$

The model considers that there is a binomial probability of leak for each voltage value. The objective of the analysis was to find the values of the coefficients, a_0 and a_1, that best fit the test data. Since the outcomes of the leakage tests are dichotomous, the binomial distribution, not the normal distribution, describes the distribution of model errors. It would, therefore, be inappropriate to attempt an unweighted LS regression analysis based on equation (9-3). The appropriate method of analysis is based on the principle of maximum likelihood. The application of ML leads to estimates of the equation parameters, i.e., a_0 and a_1, such that the probability of obtaining the observed set of data is a maximum. The results of applying ML to the dichotomous outcomes are the likelihood equations,

$$\sum_{i=1}^{n} [P_i - P(v_i)] = 0 \qquad (9\text{-}5)$$

and

$$\sum_{i=1}^{n} v_i \, [P_i - P(v_i)] = 0 \qquad\qquad (9\text{-}6)$$

Here, P_i is a test outcome and $P(v_i)$ is an expected outcome based on the input value of the voltage, using equation (9-2), where $v_i = \log(V_i)$. Since these equations are non-linear in the coefficients a_0 and a_1, an iterative solution must be determined.

Two evaluations of the parameters were performed, one using a commercially available statistics program with logit fitting capability, and a second based on manually trying to iterate to a solution based on weighted least squares. The purpose was to provide an independent verification of the results from the commercial program. The accepted measure of the goodness of the solution is the deviance,

$$D = 2 \sum_{i=1}^{n} \{ P_i \ln[P_i/P(v_i)] + (1-P_i)\ln[(1-P_i)/(1-P(v_i))] \}. \qquad (9\text{-}7)$$

The deviance is used similar to the residual, or error, sum of squares in linear regression analysis, and is equal to the error sum of squares (SSE) for linear regression. For the probability of leak evaluation, P_i is either zero or one, so equation (9-7) may be written

$$D = -2 \sum_{i=1}^{n} \{ P_i \ln[P(v_i)] + (1-P_i)\ln[(1-P(v_i)] \}. \qquad (9\text{-}8)$$

Both evaluations provided similar deviance values and the final solution obtained was

$$[\qquad\qquad\qquad\qquad\qquad\qquad\qquad\qquad]^{a,g} \qquad (9\text{-}9)$$

Asymptotic confidence limits for each individual logit(P_i) are found as

$$\text{logit}(P_i) \pm Z_{\alpha/2} \, \sigma \, [\, \text{logit}(P_i) \,] \qquad\qquad (9\text{-}10)$$

where $100(1-\alpha)\%$ is the associated probability for a two-sided confidence band.

The standard error of logit(P_i) is found for each voltage level as

$$\sigma \, [\text{logit}(P_i)] = \lfloor 1, \, \{\log(V_i)\}^{T} \rfloor \, V_a \lfloor 1, \, \{\log(V_i)\}^{T} \rfloor^{T} \qquad (9\text{-}11a)$$

or $\qquad \sigma \, [\text{logit}(P_i)] = V_{11} + 2V_{12} \log(V_i) + V_{22} \, [\log(V_i)]^2 \qquad (9\text{-}11b)$

where V_a is the estimated variance -covariance matrix of the parameter estimates, and V_{11}, V_{12}, and V_{22} are the matrix coefficients for a first order equation.
Letting

$$\eta_i = \text{logit}(P_i) \qquad\qquad\qquad (9\text{-}12)$$

the upper and lower $100(1-\alpha/2)\%$ one-sided confidence limits are

$$1/\{1 + e^{-[\eta_i \pm Z_{\alpha/2} \sigma(\eta_i)]}\} \qquad (9\text{-}13)$$

The upper bound values were calculated for each voltage/leak pair. The results are shown graphically in Figure 9-7.

9.5 General Trends for SLB Leak Rate Correlation

An evaluation has been completed that provides results supporting the recommended correlation methodology employed for SLB leak rate versus bobbin voltage. The evaluation establishes leak rate versus voltage from:

1) Formulation of a throughwall (TW) crack length (L) versus voltage (v) correlation from available data using regression analysis $\{L=f_1(v)\}$.

2) Calculation of leak rate (Q) as a function of L using the CRACKFLO computer code. Formulate a simplified relationship of Q as a function of L through regression analysis of CRACKFLO predictions $\{Q=f_2(L)\}$.

3) Development of a correlation between Q and v from the above. Substitute the formulation $L=f_1(v)$ into $Q=f_2(L)$ to get $Q=f_3(v)$. Compare $Q=f_3(v)$ to the direct correlations.

This evaluation is described in Section 11.5 of WCAP-13522.

9.6 SLB Leak Rate Versus Voltage Correlation

The bobbin coil and leakage data of Table 8-1 were used to determine a correlation between SLB leak rate and bobbin voltage amplitude. This is not to say that a "formal" functional relationship, in the sense of one variable being dependent on the other, exists between the variables since the amount of leakage is not caused by the bobbin voltage and vice versa. Both of the variables considered are mainly functions of a third variable, the crack morphology. While the variation in crack morphologies is essentially infinite, suitable descriptions can be effected based on the depth, average depth, profile description, etc. However, the characterization of the morphology is not essential to this analysis since a relationship can be independently established for two offspring variables. Since both bobbin voltage and leakage are offspring variables the results of the correlation analysis do not establish a formal relationship between the variables, however, the results do establish a "working" relationship that can be employed for the prediction of one variable from the other.

9.6.1 Selection of Coordinate System

In order to establish a correlation between the two variables, which are paired, but expected to have independent variances, the method of least squares (LS) curve fitting was employed. The simplest functional form is a linear relationship of the type

$$y = a_0 + a_1 x \qquad (9\text{-}14)$$

where the variables x and y may each be considered to be linear or logarithmic. In addition, the choice of the regressor variable is not pre-determined. Both variables are assumed to be subject to random fluctuations which are normally distributed about the mean of the variable or the logarithm of the variable with a mean of zero and some unknown, but reasonable, variance. It is also assumed that this variance is constant, or uniform, over the range of interest of the variables. In practice this may not be the case; however, any ncn-uniformity present would not be expected to significantly affect the analysis outcome, and can be tested at the conclusion of the analysis.

Analyses were performed tc determine the cptimum nature of the variable scales, i.e., linear versus logarithmic, and the appropriate selection of the regressor variable. It was initially concluded that the most meaningful correlation could be achieved by considering the log of the leak rate as the regressor and the log of the voltage as the predicted variable. Thus, the functional form of the correlation is

$$\log(V) = a_0 + a_1 \log(L) \qquad (9-15)$$

where L is the leak rate and V is the bobbin voltage. The final selection of the form of the variable scales was based on performing least squares regression analysis on each possible combination and examining the ccrrelation coefficient for each case, and has been reported in WCAP-13522.

An attempt was made to determine the appropriate choice of the regressor variable based on the knowledge, from CRACKFLO analyses, of the approximate value of the slope of the relationship. The CRACKFLO results were somewhat inconclusive. Although the slope of the log(v) on log(O) regression line more closely matches the CRACKFLO results relative to selecting the best regression direction, the results indicate the potential for a slope change between about 8 and 10 volts. It was concluded, therefore, that both regression lines would be determined and the higher of the two for any voltage level would be taken as the upper bound leakage.

9.6.2 Correlation Analysis and Identification of Outliers

In order to determine if the parameters of the relationships were being biased by the presence of unduly influential data points, a least median of squares regression analysis was performed on the entire data set for both regression directions. As discussed in Section 9.2, four data points were not included in the leak rate correlation based on non-statistical considerations. For the data included in the regression analysis, four additional points (pulled tube Plant A-2 R21C22, model boiler specimens 568-4, 576-4 and 605-2) are indicated as marginal outliers for both regression directions. However, there is no physical basis for excluding these data points from the correlation and they are retained in the final regression analysis.

9.6.3 Error-In-Variables Analysis

The potential effect of measurement errors in the regressor were discussed in Section 8 relative to bobbin amplitude. It was noted that the variance of a variable, say σ_X, with measurement error, as estimated from the data, consists of two parts, the intrinsic variation of the variable, σ_x, and the variation due to measurement error, σ_m, i.e.,

$$\sigma_X^2 = \sigma_x^2 + \sigma_m^2 \qquad (9-16)$$

A Wald-Bartlett type of analysis was performed for each direction of regression. Considering the leak rate as the regressor resulted in a line indistinguishable from the standard regression line. Considering the bobbin amplitude as the regressor resulted in a line with a slightly larger slope than the standard fit. This was to be expected since the previous use of the technique for the burst pressure correlation indicated that measurement errors for the bobbin amplitude were not significant. Since the decision was made to proceed using both regression lines (leak rate on bobbin amplitude and vice versa), the results of these analyses become moot. This is because the two lines cross at the centroid of the data. Therefore, omitting the consideration of errors results in a larger prediction of leakage for all levels of bobbin amplitude.

9.6.4   SLB Leak Rate Correlation for 7/8 Inch Diameter Tubing

The final fits of the data are shown on Figures 9-8 and 9-9 for SLB pressure differences of 2335 and 2650 psi, respectively. The correlation lines are given by

$$\log(L) = a_0 + a_1 \log(V),\qquad(9-17)$$

and

$$\log(V) = b_0 + b_1 \log(L).\qquad(9-18)$$

The coefficients for the above equations are shown below.

Regression Coefficients for SLB Leak Rate
to Bobbin Amplitude Correlation

$$\left[\rule{0pt}{6em}\qquad\qquad\qquad\qquad\right]^{a,g}$$

In addition to the least squares regression lines, the upper 95% one-sided, simultaneous confidence bound, upper 95% prediction bound, and upper 99% prediction bounds were determined. Each is shown on Figures 9-8 and 9-9.

The expected, or arithmetic average, leak rate, Q, corresponding to a voltage level, V, from the above expressions was also determined. Since the regression was performed as log(Q) on log(V) the regression line represents the mean of the log of the leak rate at each level of bobbin amplitude. Thus the expected Q for a given V is provided by:

$$E\{Q\,|\,V\} = 10^{a_0 + a_1 \log V + \frac{\ln 10}{2}\sigma^2}$$

$$(9-19)$$

where σ^2 is the estimated variance of log(Q) about the regression line. A plot of the expected leak rate is provided in Figure 9-10. Examination of the figure indicates that below a voltage level of ~7 volts the upper 95% confidence band on log(Q) is conservative relative to the expected mean leak rate.

The statistical analyses indicate that the correlation of voltage on leak rate is the preferred regression fit, although both fits are conservatively applied to bound the leak rate vs. voltage for the Kewaunee APC. The slope of leak rate vs. voltage based on the regression analysis of voltage vs. leak rate at 2335 psi is

$$1/b_1 = [\qquad]^{a,9}$$

which is consistent with the trend analysis of Section 9.5 and the general dependence of leak rate on crack length.

9.6.5   Analysis of Residuals

Additional verification of the appropriateness of the regression is obtained by analyzing the regression residuals, i.e., the differences between the actual variable value and the predicted variable value. There are a variety of plots that can be used for the analysis of residuals. A frequency plot of the residual values should appear to be similar to a normal distribution. A plot of the residual values against the predicted values should be nondescript since the residuals and predicted values should not be correlated. A plot of the ordered residuals on normal probability paper should approximate a straight line. Any of these plots may be used to verify that the regression residuals are normally distributed. The normal probability plot offers the advantages that it can easily be used to determine if the mean is approximately zero, and a reasonable estimate of the standard deviation of the residuals may be read directly.

To prepare the cumulative normal probability plot, the residuals are sorted in ascending order and then plotted against an ordinate cumulative percent probability value given by $100^{(i-0.5)}/n$, where n is the number of data points used in the regression and i is an index ranging from 1 to n. If a small number of outliers have been omitted from the regression analysis, but the depiction of their residuals is desired, n may be taken as the total number of data points and the residuals of the outliers included accordingly. This has the effect of compressing the spread of the outliers along the probability axis, but generally will not affect the conclusions relative to the linearity of the plot. The rationale for the cumulative probability values used is if the unit area under the normal curve is divided into n equal segments, that it can be expected (if the distribution is normal) that one observation (residual) lies in each section. Thus, the ith observation in order is plotted against the cumulative area to the middle of the ith section. The factor of 100 is used to convert the scale to percent probabilities.

If the plotted residuals approximate a visually fitted straight line, it may be concluded that they are normally distributed. The residual value where the line crosses 50% probability is a good estimation of the mean of the residuals and can be used to verify that the mean is approximately zero. The residual distance from the 50% point to the 84% point is an approximation for the standard deviation of the residuals. If the residuals for the outliers have been included in the plot they will distort the results obtained for the mean and standard deviation, with the mean value being less affected. For this type of plot, the outliers in the data, if any, will tend to appear on the far left in the lower half of the residual normal plot and on the far right in the upper half, i.e., large negative and positive residual values. The results from the normal probability plot may be used to determine the need for performing any of the other plots, i.e., it may be apparent that no additional information would be available from a scatter plot.

Normal probability plots of the residuals for two of the regression analyses performed for the leak rate (at a SLB ΔP of 2335 psi) to bobbin amplitude correlation were prepared, as shown in Figure 9-11. The upper plot of Figure 9-11 considers the residuals from the log(Q) on log(V) regression while the lower plot considers the residuals from the log(V) on log(Q) regression. For both, the residuals approximate a straight line and would not be considered to depart significantly from normality. The voltage residuals exhibit a better fit, because the range of the log voltages (two decades) is significantly less than that of the log leak rates (four decades). In addition, the outliers of the data are better illustrated on the voltage residuals plot. Since the outliers occur at only one end of the residuals data they tend to pull the mean value of the visually fitted line in their direction. This effect is small and it is seen that the mean of the residuals on both plots is approximately zero. Based on these results it was concluded that frequency plots and scatter plots of the residuals were not necessary. In addition, the plots were not repeated for the SLB ΔP of 2650 psi since similar results would be expected. The conclusion is that the residuals are approximately normally distributed with a mean of zero for either direction of the regression.

Table 9-1

Non-Leaking 7/8 Inch Specimens with Throughwall or Near Throughwall Cracks [1]

Specimen	Bobbin Amplitude, volts	a,g

Note 1: Maximum depth > 90% from destructive exam.

Table 9-2

Dependence of SLB Leakage on Throughwall (TW) Crack Length

TW - No Leakage			TW - <1 liter/hr			TW >1 liter/hr. & < 6 l/hr		
No.	Bobbin Volts	TW Length	No.	Bobbin Volts	TW Length	No.	Bobbin Volts	TW Length

g

Notes:
1. Not leak tested - judged to be non-leaker at SLB based on short throughwall length and crack morphology.
2. Bathtub flaw (thin OD ligament) reasonably expected to open crack at SLB ΔP.
3. Judged to be non-leaker based on no detectable loss in pressure at SLB ΔPs during burst test without a bladder and on overall crack morphology.

Figure 9-1: Bobbin Coil Voltage vs. Maximum Examination Depth
7/ 8" Pulled Tubes Data, Destructive Examination

a,g

9 - 15

Figure 9-2: Bobbin Coil Voltage vs. Maximum Examination Depth
3/4" Pulled Tubes Data, Destructive Examination

a,g

9 - 16

34VLTDE
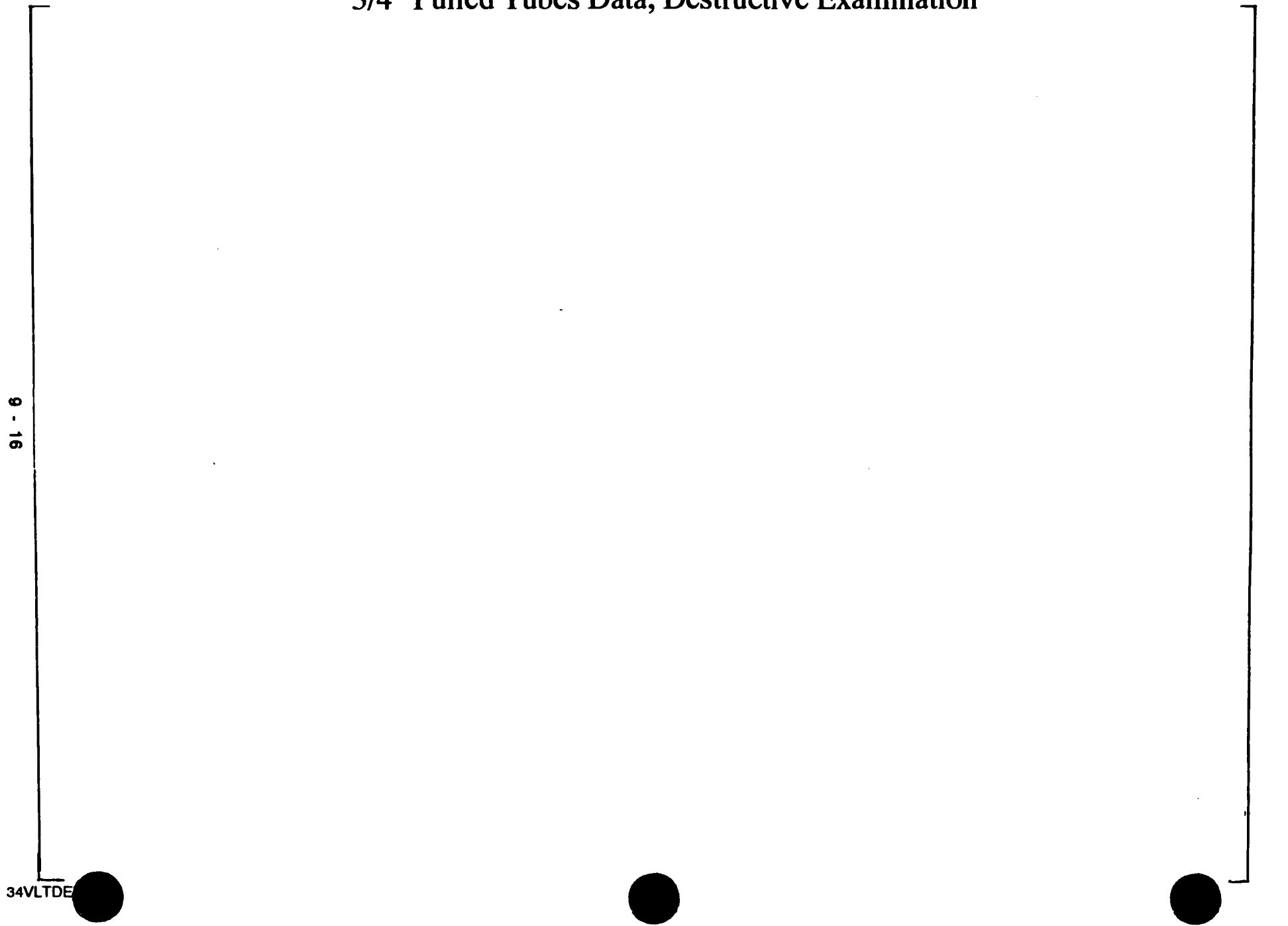
Figure 9-3

SLB LEAKAGE - VOLTAGE DISTRIBUTION
COMBINED DATA (7/8 INCH NORMALIZATION)

g
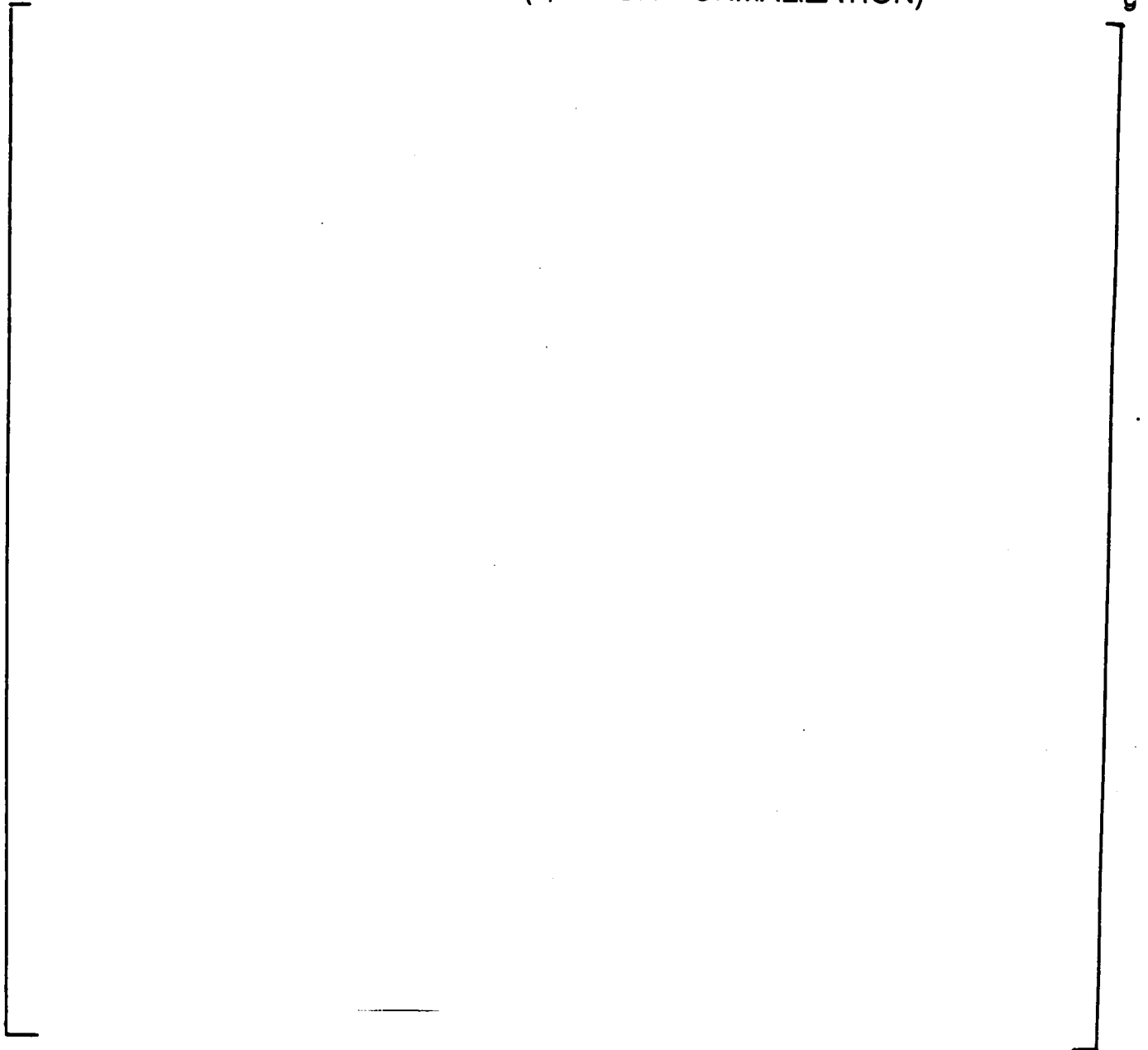
Figure 9-4

SLB LEAKAGE PROBABILITY
COMBINED DATA (7/8 INCH NORMALIZATION)

g
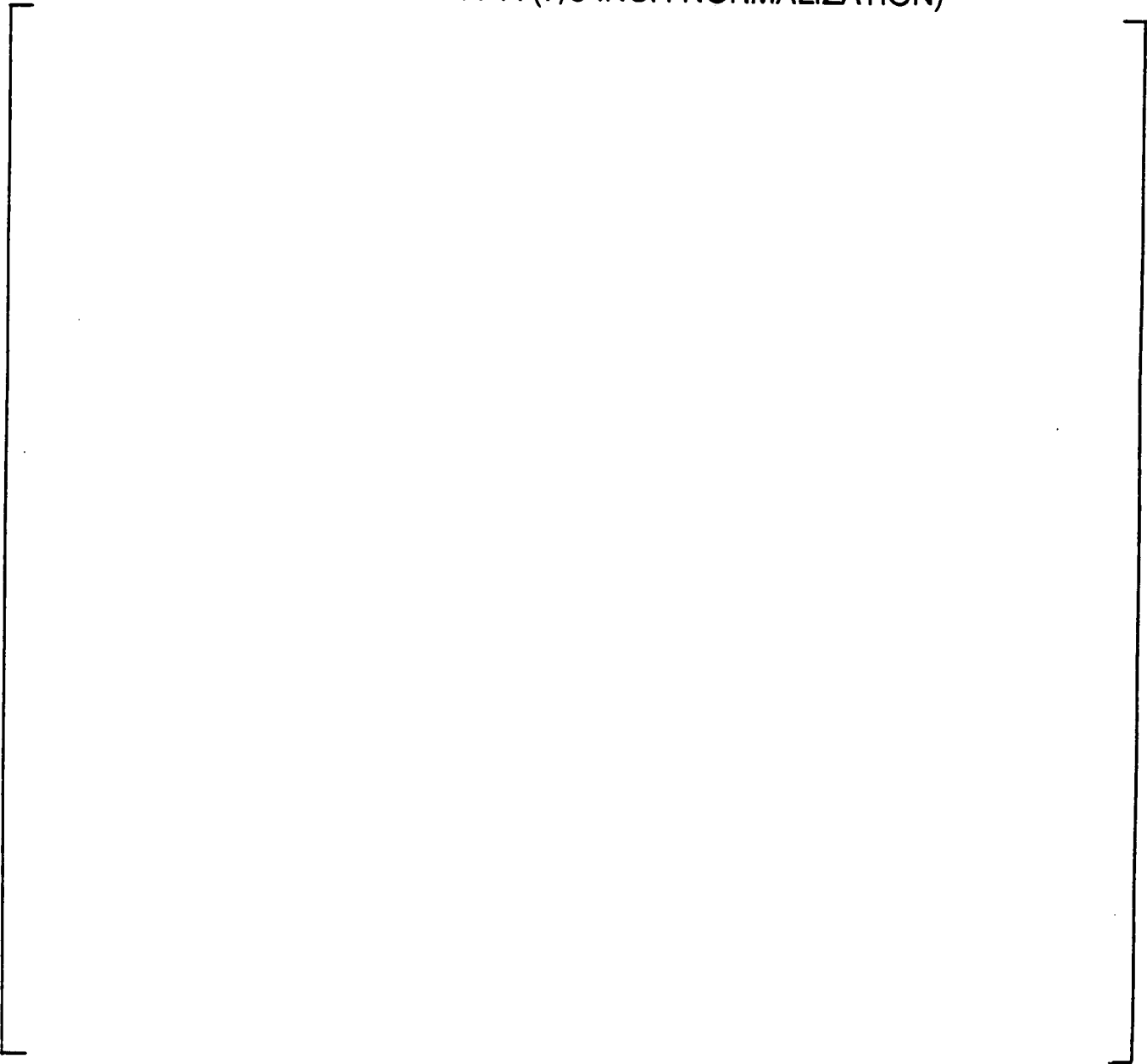
Figure 9-5

SLB LEAKAGE - VOLTAGE DISTRIBUTION
7/8 INCH TUBING DATA

g
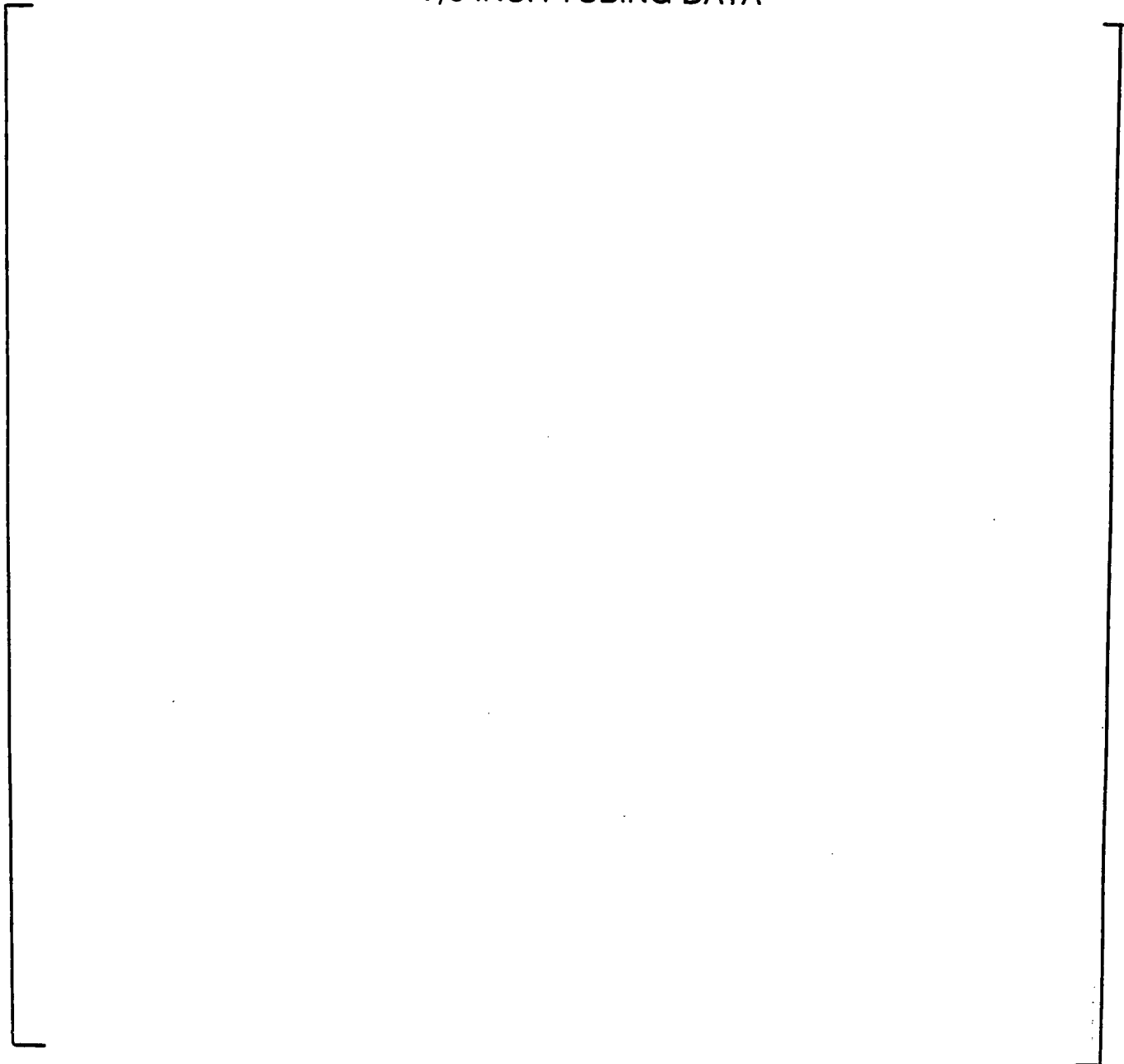
Figure 9-7: Probability of Leak vs. Bobbin Amplitude
7/8" Tubes, Model Boiler & Field Data

a.g

9 - 21

Figure 9-8: 2335 psi SLB Leak Rate vs. Bobbin Amplitude
7/8" Tubes, Model Boiler & Field Data

Leak Rate at SLB Pressure (l/hr)

9 - 22

9

78LK2337.GP5

Figure 9-9: 2650 psi SLB Leak Rate vs. Bobbin Amplitude
7/8" Tubes, Model Boiler & Field Data

a,g

Leak Rate at SLB Pressure (l/hr)

9 - 23

78LK2652.SP5

Figure 9-10: 2335 psi SLB Leak Rate vs. Bobbin Amplitude
7/8" Tubes, Model Boiler & Field Data

a,g

Leak Rate at SLB Pressure (l/hr)

9 - 24

Figure 9-11: Examination of Regression Residuals
7/8" Tubes, Model Boiler & Field Leak Rate Data

a.9

10.0   GUIDELINES FOR ACCIDENT CONDITION ANALYSES

This section develops guidelines for the pressure differential to be used in SLB leak rate and tube burst analyses and the confidence levels or probabilities to be applied for the analyses. Probabilistic safety analyses (PSA) results are used to assess the frequencies associated with the sequence of actions that result in a given primary-to-secondary pressure differential for an SLB event. The results of NUREG-0844 analyses together with the event sequence frequencies are used to define guidelines for the confidence levels to be applied to SLB leak rate analyses and for an acceptable tube rupture probability.

10.1   Limiting Accident Condition

The most limiting accident condition for containment bypass (potential radiation release to the public) is a steam line break (SLB) in the piping between the containment and the main steamline isolation valve (MSIV). The SLB event also envelopes the feedline break (FLB) event with regard to sequence frequencies as obtained from a probabilistic safety analyses.

For most Westinghouse plants, a value of 2600 psid bounds the maximum pressure differential during a limiting secondary system pipe break. This value is determined by applying a maximum uncertainty of 4% of the safety valve setpoint, which includes allowances for setpoint uncertainty, valve accumulation and setpoint shift (setpoint shift of 1% maximum is applied to plants with pressurizer loop seals). For Kewaunee, since there is a pressurizer loop seal, the maximum uncertainty would be about 3% and the maximum primary pressure would be limited to 2575 psia. Therefore, with atmospheric pressure on the secondary side, the limiting primary to secondary pressure differential for Kewaunee would be 2560 psia.

Westinghouse has typically conservatively bounded the FLB ΔP at 2650 psi and, for simplicity in analyses, applied this ΔP also for the SLB event. To obtain an upper bound FLB ΔP, a long term reactor coolant system (RCS) heatup event was postulated with the pressurizer assumed to go water solid during the event. The bounding RCS pressure was obtained assuming water relief through the pressurizer safety valves at 110% of design pressure (~2750 psia). The secondary pressure in the faulted SG was 100 psia to obtain a 2650 psid across the SG tubes.

A large ΔP during SLB is dependent on assuming no operator action to terminate safety injection and failure of the PORVs to open. As described in Section 10.2, these assumptions lead to a low probability (~1×10^{-6}) for primary pressure exceeding the PORV relief pressure of 2350 psi and hence a SG tube ΔP of 2335 psi is the appropriate ΔP for the SLB analyses. In the case of the FLB, for the event to become of concern for atmospheric release, it also requires that the check valve in the feedline fail to close; hence the frequency would be further reduced. Typical variations of pressure with time for the SLB and FLB events are described below.

Steam Line Break (SLB) Event Description

Figure 10-1 shows a typical dependence of the primary pressure as a function of time in a SLB event. The primary pressure variation of Figure 10-1 assumes no operator action on safety injection and that the PORVs fail to open. The primary pressure and SG tube ΔP initially decrease below the normal operating pressure differential (ΔP_{NO}) for about the initial 3 minutes of the event. Safety injection then increases primary pressure until the plant operator acts to terminate safety injection. If a reduction in safety injection is not initiated within about 20-25 minutes, the primary pressure reaches the PORV pressure setting of 2350 psi. Only if the PORVs fail to open would the pressure continue to increase to 2575 psi. Thus the typical SLB event would have the SG tube ΔP decrease and postulated tube leakage would not increase

above normal operation for about the first 6 minutes of the event. Thereafter, postulated tube leakage would increase above that for normal operation as dependent on operator action to terminate safety injection with maximum leakage at the PORV relief pressure of 2350 psi.

Feedline Break (FLB) Event Description

During a postulated FLB event, it is assumed that the feedwater pipe undergoes a double-ended guillotine break. Whether the break occurs inside or outside the building, the feedwater isolation valves, located outside of the containment, will perform their intended function. For pipe breaks upstream (beyond valve relative to containment) of the isolation valve, the valve would restrict the backflow of the secondary coolant. Feedwater line check valves located inside containment would prevent steam release with subsequent containment bypass. Containment bypass can occur only assuming failure of the check valve (to close) and FLB downstream of the isolation valve, between the isolation valve and the containment.

Although the Kewaunee licensing basis does not require the postulation of a FLB, a FLB scenario as discussed above was analyzed to support this probabilistic assessment. The assumed guillotine feed line pipe break results in a break area of 1.06 ft^2. A SI signal occurs at 11.1 seconds into the event on low steam line pressure -- reactor trip on SI signal, 2 seconds for rod motion, -- turbine trip on reactor trip (feedwater isolation and feedwater pump trip also occurs on an SI signal.) Approximately 15 seconds into the event, a turbine trip signal results in closure of the turbine inlet valves and isolation of the steam lines. Secondary system pressure on the intact steam generator will rise to the steam generator safety setpoint of 1089 psia coincident with increasing RCS pressure (no credit is taken for secondary PORV or steam dump operation to assist RCS cooldown). At about 50 seconds the faulted loop pressure is assumed to have dropped to atmospheric pressure (assuming a break on SG side of the check valve within containment or failure of the check valve to close.) At about 200 seconds the primary system pressure reaches the PORV setpoint resulting in a maximum primary-to-secondary differential of 2335 psi.

For Kewaunee, Figure 10-2 shows reactor coolant system pressure and steam pressure as a function of time for a FLB event. For this analysis, no credit was taken for PORV or RCP operation, and RCS system pressure is eventually elevated to approximately 2400 psi. Upon reactor trip, primary system pressure drops to a minimum (for the first portion of the event) of approximately 2160 psi at about 40 seconds, and then increases due to coolant expansion caused by the reduced heat transfer in the steam generators. As the RCS returns to normal operating pressure, the shutoff head of the safety injection pumps (nominally 2250 psia) prevents continued inventory addition to the RCS. At approximately 500 seconds, decay heat generation decreases to less than the heat removal capability of the intact SG, and RCS temperatures and pressures begin to decrease. If offsite power is available, credit for PORV operation can be assumed, in which case RCS pressure will be limited to approximately 2350 psi. AFW initiation is delayed 10 minutes to simulate operator response time to isolate AFW to the faulted loop and align to the intact loop. SG level recovers after 10 minutes.

For considerations of tube rupture at TSP locations during a FLB event, it can be noted that tube burst would be prevented by the constraint of the TSPs. The SLB event results in a rapid loss of SG pressure, resulting in a pressure drop across the TSPs and potential TSP displacement to uncover potential indications at TSPs under normal operating conditions. The steam pressure changes in an FLB are slow and result in minimal loads to displace the TSPs. Potential offsite dose consequences for the feedline break are bounded by the SLB event. The postulated SLB event leads to containment bypass and pressure differentials across the tube which are equal to or greater than those for the FLB event. Offsite dose for the FLB is postulated to occur due to steam

relief from the non-faulted loops. Upon implementation of the APC/IPC, the reduction in allowable primary to secondary leakage from 500 gpd to 150 gpd leads to reduced offsite doses.

Primary Coolant Leakage Assumptions During Steam Line Break Used in Dose Analysis

For a SLB event, negligible leakage would occur until the primary pressure increased above the normal operation ΔP. The postulated limiting tube in the SG could then conceptually rupture if safety injection was not terminated. The single tube rupture for the limiting tube would tend to reduce the rate of RCS pressure increase or decrease the pressure. This effect reduces the likelihood of large cumulative leakage and multiple tube ruptures in a SLB event. In contrast, the SLB leakage analyses and burst probability analyses assume primary pressure reaches the PORV relief pressure of 2350 psi.

In accordance with the Safety Evaluation for Kewaunee Nuclear Power Plant, a continuous primary to secondary leak rate of 5.0 gpm was assumed for the calculation of 0-2 hour site boundary doses and low population zone entire accident duration dose estimates. As described in the Kewaunee USAR, primary system pressure drops upon reactor trip, and the pressure differential across the steam generator tubes is not expected to surpass the normal operating value of about 1300 psi. Upon initiation of Safety Injection (SI) the reactor coolant system pressure is reestablished. The normal operating ΔP is re-established at approximately 6 minutes into the event. Primary system pressure equal to the pressurizer PORV setpoint is achieved at about 23 minutes, and is only obtainable if the operator fails to terminate SI. Therefore, actual volumes of released coolant could be reduced to a fraction of that assumed in the Kewaunee Safety Evaluation, to as much as 100%, based upon operator action.

The Kewaunee Safety Evaluation uses the guidance of 10CFR100, Reactor Site Criteria, in establishing the extent of the protected area. In accordance with 10CFR100, 0 to 2 hour doses at the site boundary are limited to 25 Rem whole body, 300 Rem thyroid. These values, however, are not used as acceptable limits for individual accident scenarios, but establish maximum limits for emergency conditions. NUREG-0800, Standard Review Plan, establishes acceptable doses during Design Basis Accidents, based on a percentage of these limits. For IPC/APC SLB analyses, the two hour duration that establishes allowable limits for SLB leakage can occur only if the operator fails to terminate SI, so the probability of reaching the allowable leakage limit must include the probability of failing to terminate SI.

The dose estimates are calculated based on primary coolant activity levels of 1.0 microcuries per gram of dose equivalent I-131. An increase in the coolant activity to 500 microcuries per gram (iodine spike) is assumed due to the reactor trip. The 1.0 microcurie per gram value is a Technical Specification maximum limit. If this limit were reduced, dose estimates would be reduced by a nearly proportional level. Residual activity in the secondary system due to primary to secondary leakage during normal operation adds to the dose estimate. In the case of the APC, allowable primary to secondary leakage is reduced from 500 gpd to 150 gpd. This reduction will have an overall effect to lower dose estimates in the event of a postulated SLB. Also, the operating history of Kewaunee has shown that measured coolant activity levels (generally less than 0.1 microcurie per gram) are far below the allowable Technical Specification limit. These factors all have an overall effect of lowering actual doses compared to the calculated values. Lowering of the allowable coolant activity, such as through administrative controls on operation, would permit an increase in the allowable SG leak rate as measured in gpm.

10.2   Event Sequence Probabilities

Probabilistic Safety Analysis (PSA) results can be used to assess the probability cf SLB event sequences leading tc varicus pressure differentials acrcss the SG tubes. Kewaunee PSA results for this event are given in Table 10-1 and compared with the assessment given In NUREG-0844. The event evaluated is a pipe break between containment and the MSIV, which leads to containment bypass. The pipe break frequencies cf Table 10-1 apply to this section of piping. The highest probability sequence (Sequence 1; 6.8×10^{-4}/RY) Includes the cperators terminating safety Injection, which would resuit in a $\Delta P <2335$ psid. As Indicated in Figure 10-1, the SLB pressure differential initially decreases and operator action can be initiated before primary pressure reaches the PORV setpoint. The time in the event at whioh operator action is taken to terminate safety injection determines whether cr nct the ΔP reaches 2335 psid. If the operator fails to terminate safety Injection (Sequence 2), the SLB ΔP remains at 2335 psid but at a much lower probability of 4.8×10^{-7}/RY. If the PORV fails to open (Sequence 3), the ΔP could increase to 2560 psid at an even lower probability of 1.4×10^{-10}/RY.

10.3   NUREG-0844 Analysis

From Table 10-1, it can be noted that NUREG-0844 conservatively obtained a 2.5×10^{-3}/RY probability of reaching a ΔP of 2600 psid. This is a factor of about 5×10^3 higher than the Kewaunee estimate (Sequence 2) for obtaining a ΔP of 2335 psid.

The probability cf a tube rupture at 2600 psid was estimated as 2.5×10^{-2} in NUREG-0844. Thus, the probability of a SLB event with a ccnsequential tube rupture in NUREG-0844 was 6.3×10^{-5}/RY. This rupture probability is a factor of 100 greater than the Kewaunee Sequence 2 prcbability of reaching or maintaining a ΔP of 2335 psid, not ccnsidering the probability of a consequential tube rupture event. The NUREG-0844 analyses result in a 2.5×10^{-8} per reactor year probability of a core melt In combination with the SLB event and consequential single tube rupture. This core melt frequency would be a factor of at least 100 greater than what would be estimated for Kewaunee.

The NUREG-0844 evaluations led the NRC staff to conclude that the increment in risk associated with a single tube rupture event Is a small fraction of the accident and latent fatality rlsks to which the general public is routinely exposed (i.e., the associated risk of early and latent fatalities were found to be zero and 1.1×10^{-5}/RY, respectively). This conclusion Indicates that the 6.3×10^{-5} probability fcr an SLB with a tube rupture results in negligible Incremental risk to the public. This probability Is a factor of 100 greater than the Kewaunee Sequence 2 frequency of 4.8×10^{-7}/RY for a pressure differential of 2335 psid, not considering the probability of a consequential tube rupture event.

For APC applications, SLB leakage Is limited to satisfy a small fraction of 10CFR100 dose over a 2 hour time frame. Appiying average SLB ieak rate analyses at 2335 psid for Kewaunee yields a probability of $<10^{-6}$ of exceeding a small fraction of 10CFR100 limits. This probabillty is less than the probability of a single steam generator tube rupture found in NUREG-0844, which as noted above, is concluded by the NRC staff to result in only a small incremental risk to the public. Consequentiy, the use of a 95% confidence limit on the mean regression fit to SLB leak rate is conservative to determine SLB leakage. Appiication of the 95% confidence level on the mean regression fit to SLB leak rate yields a probability

($<4.8 \times 10^{-7}$) of satisfying a small fraction cf 10CFR100 limits less than was determined to be acceptably low for the large leakage associated with a single tube rupture event as discussed in NUREG-0844.

10.4   SLB Analysis Guidelines

10.4.1   SLB Pressure Differential

Based on the low probability ($<10^{-6}$) for SLB event sequences leading to a ΔP of 2335 psid, a 2335 psid ΔP is adequate for the SLB leak rate and tube burst analyses in support cf the alternate plugging criteria. The probability fcr exceeding SLB leak rate limits or obtaining a tube rupture will be higher for the 2335 psid of Sequence 2 (see Table 10-1) than for the 2560 psid of Sequence 3. This results as the differences in leak rates between 2335 and 2560 psid are about 25% while the difference in sequence prcbabilities (Sequence 2 versus Sequence 3) is a factor of >1000. The contribution of Sequence 3 to leak rate can be ignored as it would contribute negligibly to the total leak rate prcbability.

10.4.2   Guidelines for Tube Burst Analyses

Although the NUREG-0844 analyses show small incremental risk tc the public for a single tube rupture at a conditional probability of 2.5×10^{-2}/RY, the analyses supporting implementation of APC require significant confidence levels to support the NUREG-0844 probabilities. Maintaining the NUREG-0844 tube burst probability in combination with the Kewaunee Sequence 2 probabilities provides a net probability of a combined SLB and tube rupture event of a factor of about 10^3 lower than NUREG-0844. Thus a 2.5×10^{-2}/RY rupture probability represents a conservative goal for Kewaunee. For deterministic analyses of SLB burst margins, the analyses should be performed at a plus 99% uncertainty level. When Mcnte Carlo analyses are performed for tube burst, the predicted burst probability should be less than 2.5×10^{-2}/RY. Applying the 2.5×10^{-2} to APC applications permits the 10^3 Kewaunee margin to cover other potential causes of a rupture such as loose parts, etc.

In applying the R.G. 1.121 guidelines for tube repair criteria, tube burst capability at three times normal operating pressure differentials ($3\Delta P_{NO}$) is found to be most limiting for Kewaunee (Section 8). Satisfying the $3\Delta P_{NO}$ requirement provides margins against burst at SLB conditions. The tube burst correlation is evaluated at the lower 95% prediction interval to provide a high confidence of burst capability exceeding $3\Delta P_{NO}$. The Kewaunee SLB tube burst margin analyses of Section 13 show that an indication at the repair limit based on $3\Delta P_{NO}$ (at the -95% interval) results in a much lower probability of burst at SLB conditions than the $\sim10^{-2}$ guideline established above.

10.4.3   Confidence Levels for SLB Leak Rate Analyses

The NUREG-0844 analyses and the low sequence probabilities for Kewaunee indicate that a single consequential tube rupture coincident with an SLB event does not result in significant risk to the public. As noted in Section 10.3, the probability of SLB leakage exceeding a small fraction of 10CFR100 limits should be permitted to be smaller than that associated with the 2.5×10^{-5}/RY rupture probability found to have negligible incremental risk to the public. For Kewaunee, the Sequence 2 probability for reaching cr maintaining 2335 psid in a SLB

event is 4.8×10^{-7}/RY. Safety injection could be terminated by the operators prior to reaching the PORV relief pressure leading to 2335 psid across the tubes. In either case, safety injection would be terminated in less than the 2 hour period used for dose analyses of the leak rate at the site boundary. Thus, use of a leak rate at 2335 psid is conservative for the leak rate analyses to satisfy the allowable leak limit developed for the 0 to 2 hour dose at the site boundary. The probability of 4.8×10^{-7}/RY, which assumes operator failure to terminate SI, for reaching or maintaining 2335 psid is thus also conservative for the 0 to 2 hour dose estimate. The use of average values for SLB leak rate analyses at a SLB pressure differential of 2335 psid result in $<10^{-6}$ probability of radiological consequences which exceed a small fraction of 10CFR100 limits. These consequences at a 10^{-6} probability are conservatively bounded by the NUREG-0844 analyses of a single tube rupture coincident with an SLB. Therefore, it is judged that a 95% confidence limit on the mean regression fit for SLB leak rate analyses provides adequate conservatism for event sequence probabilities comparable to the NUREG-0844 SLB consequential tube rupture event probability.

In this report, the Kewaunee SLB leak rate calculations are conservatively performed using deterministic analyses starting with a BOC voltage value and adding allowances at 95% cumulative probability for NDE uncertainty and growth to obtain a corresponding EOC voltage value. The SLB leak rate is obtained by evaluating the SLB probability of leakage and leak rate correlations at +95% confidence on the mean regression fit at the EOC voltage value. The leak rates are evaluated at a ΔP_{SLB} of 2335 psid which is the highest pressure differential expected at probabilities of $>10^{-7}$/RY.

Table 10-1

SLB Event Sequence Frequencies and
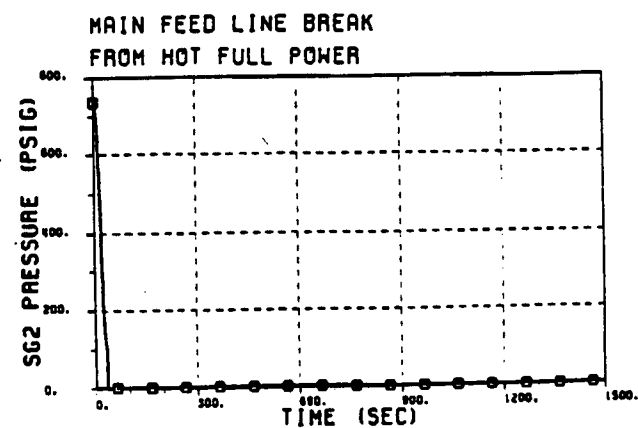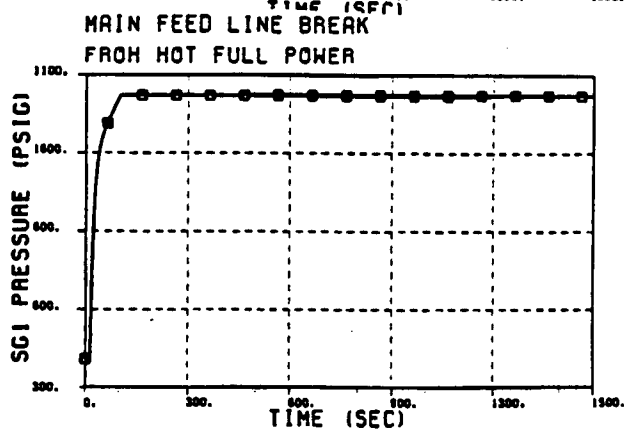## Resulting Pressure Differentials

| | NUREG-0844 | Kewaunee | | |
		Sequence 1	Sequence 2	Sequence 3
Sequence Initiator	$SLB=2.5 \times 10^{-3}/RY$	SLB Between Containment and MSIV $6.8 \times 10^{-4}/RY$	SLB Between Containment and MSIV $6.8 \times 10^{-4}/RY$	SLB Between Containment and MSIV $6.8 \times 10^{-4}/RY$
Action 1	NA	Operators Terminate SI 0.999	Operators Fail to Terminate SI 7.1×10^{-4}	Operators Fail to Terminate SI 7.1×10^{-4}
Action 2	NA	NA	Pressurizer PORV Relieves Pressure ~1.0	Pressurizer PORV Fails to Relieve Pressure[1] 2.8×10^{-4}
Total Sequence Frequency	$2.5 \times 10^{-3}/RY$	$6.8 \times 10^{-4}/RY$	$4.8 \times 10^{-7}/RY$	$1.4 \times 10^{-10}/RY$
Pressure Differential Across Tubes	Assumed 2600 psid	<2335 psid	2335 psid[2]	2560 psid[3]

Notes:

1) PORV failure rate includes failure of the PORV to open, failure to restore instrument air and unavailability of the PORV due to isolation by the block valve.

2) PORV relief pressure of 2350 less atmospheric pressure in SG.

3) Pressurizer safety valve set pressure plus 3% for valve accumulation less atmospheric pressure in SG.

Figure 10-2

Main Feedline Rupture With Offsite Power
Pressurizer and Steam Generator Pressures vs. Time

MAIN FEED LINE BREAK
FROM HOT FULL POWER

MAIN FEED LINE BREAK
FROM HOT FULL POWER

MAIN FEED LINE BREAK
FROM HOT FULL POWER
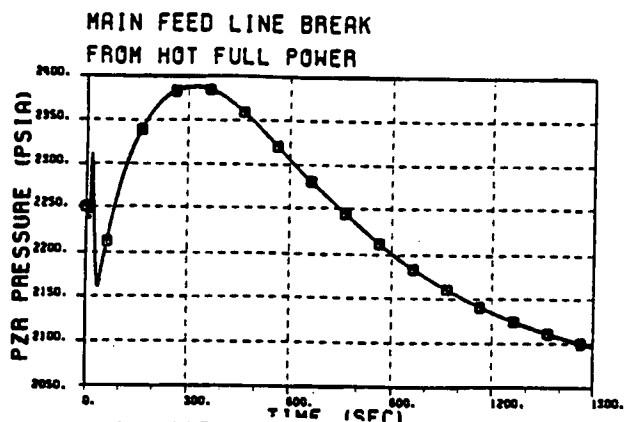
11.0 ACCIDENT CONDITION STRUCTURAL ANALYSIS

This section gives consideration to the limiting accident conditions and their implications relative to tube plugging criteria applications. If the TSP displacements from normal operation positions are large compared to the crack lengths which can lead to burst during an SLB event, then the benefit of the TSP to prevent tube rupture could be lost. Assuming uniform through wall cracks (not typical of ODSCC) approaching the TSP thickness, displacement of the TSP during the SLB event exceeding approximately 0.75 inch would expose sufficient length of the crack with the possibility that burst margins would not be met. TSP displacements were evaluated using non-linear, dynamic time history analyses to assess the potential for crack exposure, assuming an open crevice.

A combined accident condition for LOCA + SSE (loss of coolant accident + safe shutdown earth quake)is evaluated to identify potentially deformed tubes, if any, at specific locations in the S/G which will be excluded from the proposed plugging criteria.

11.1 Tube Support Plate Displacement Under SLB Loads

The potential for TSP displacement under SLB loading conditions has been evaluated for open crevices, for small gaps and for corroded TSP conditions of incipient denting which lead to contact forces between the tube and the hard magnetite in the crevices. These evaluations were performed to assess the potential for uncovering of the ODSCC under SLB conditions.

Analyses for TSP displacements with crevice gaps in an SLB event were performed using finite element, dynamic time history analysis methods. Conservative analysis assumptions, such as no friction, which ignores the TSP to wedge to wrapper contact forces, lead to overestimates of the TSP displacements. Given these assumptions, analyses for open, as manufactured crevices indicate potential displacements yielding plastic deformation at the upper five TSPs. The analyses for the lowest two TSPs show no local yielding of the plates and these plates would recover to their original positions relative to the elevation of cracking in the tubes. The dynamic loading on the plates occurs early in the SLB event and well before the increase in the pressure differential across the tubes. The TSP constraint at the elevation of the degradation for the lower two TSPs would prevent burst in an SLB event, even under the zero friction, open crevice assumptions. For these results, it could not be assured that the TSPs would envelope the ODSCC at the times of increasing primary to secondary pressure differentials in an SLB event. The incipient denting and dented conditions at TSP intersections prevent TSP displacement under SLB conditions. TSP displacement analyses for varying crevice gaps show that even if the TSP corrosion resulted in up to [ ]^a mil gaps at the most limiting plate, the TSP displacements would not uncover the ODSCC.

With corroded TSP conditions, the maximum SLB loads on the TSPs would be less than the forces resulting from tube to TSP contact pressures. To support this conclusion, pull tests were performed to determine the force required to pull the tube from incipient denting and dented crevice conditions. The results show that the ODSCC at TSPs would continue to be enveloped by the TSPs even under accident conditions if even minor crevice packing is present. Since crevice packing has not been demonstrated at the predominance of the TSP intersections of the Kewaunee SGs, the plugging criteria are conservatively based upon free span ODSCC under accident conditions.

11.2 Combined Accident Considerations

This section deals with combined accident condition loadings in terms of tube deformation and the effects on tube burst pressure. The most limiting accident conditions relative to these concerns are seismic (SSE) plus loss of coolant accident (LOCA) for tube deformation, and SSE plus steamline/feedline break (SLB/FLB) for tube burst. Details of the analysis methods used in calculating tube stresses and tube support plate loads for these loading conditions are also provided.

11.2.1 SSE Analysis

Seismic (SSE) loads are developed as a result of the motion of the ground during an earthquake. A seismic analysis specific to Series 51 steam generators has been completed. Response spectra that umbrella a number of plants with Series 51 steam generators, including the Kewaunee plant, have been used to obtain tube support plate (TSP) loads and the displacement time history response of the tube bundle. A nonlinear time-history analysis is used to account for the effects of radial gaps between the secondary shell and the TSPs, and between the wrapper and shell.

The seismic excitation defined for the steam generators is in the form of acceleration response spectra at the steam generator supports. In order to perform the non-linear time history analysis, it is necessary to convert the response spectrum input into acceleration time history input. Acceleration time histories for the nonlinear analysis are synthesized from El Centro Earthquake motions, using a frequency suppression/raising technique, such that each resulting spectrum closely envelopes the corresponding specified spectrum. The three orthogonal components of the earthquake are then applied simultaneously at each support to perform the analysis.

The seismic analysis is performed using the WECAN computer program. The mathematical model consists of three-dimensional lumped mass, beam, and pipe elements as well as general matrix input to represent the piping and support stiffnesses. In the nonlinear analysis, the TSP/shell, and wrapper/shell interactions are represented by a concentric spring-gap dynamic element, using impact damping to account for energy dissipation at these locations.

The mathematical model which is used is shown in Figure 11-1. The tube bundle straight leg region on both the hot and cold leg sides of the bundle is modeled by two equivalent beams. The U-bend region, however, is modeled as five equivalent tubes of different bend radii, each equivalent tube representing a group of steam generator tubes. In addition, a single tube representing the outermost tube row is also modeled. Continuity between the straight leg and U-bend tubes, as well as between the U-bend tubes themselves, is accomplished through appropriate nodal couplings. Note that the five equivalent tube groups are extended down two support plates before the single tube representation begins. This allows dissipation of tube response differences due to the variation in U-bend stiffnesses.

For reasons that will be discussed later, tube deformation calculations are performed for three TSP groupings, TSP 1, TSP 2-6, and TSP 7. The highest seismically induced TSP forces are 82 kips for TSP 1, 102 kips for TSP 2-6, and 78 kips for TSP 7.

11.2.2 LOCA Analysis

LOCA loads are developed as a result of transient flow, and temperature and pressure fluctuations following a postulated main coolant pipe break. For the 51 series S/Gs in another plant, LOCA loads are developed for five different pipe break locations. These include three primary pipe breaks and two minor pipe breaks. The primary pipe break locations include the steam generator inlet and outlet lines, and the reactor coolant pump outlet line, while the minor pipe breaks include the pressurizer surge line and the accumulator line.

Prior qualification of the Kewaunee steam generators for leak before break requirements for the primary piping results in the limiting LOCA event being either the accumulator line break or the pressurizer surge line break. Bounding LOCA loads calculations for Kewaunee for the accumulator or pressurizer surge line are not available, however. Therefore, as a conservative approximation, the LOCA loads for the prior primary piping breaks are used to bound the Kewaunee smaller pipe breaks. As the results presented later in this section will show, the large pipe breaks are several times larger than the smaller pipe breaks, and thus, these loads form a conservative basis for the small pipe breaks for Kewaunee.

As a result of a LOCA event, the steam generator tubing is subjected to the following loads:

1) Primary fluid rarefaction wave loads.

2) Steam generator shaking loads due to the coolant loop motion.

3) External hydrostatic pressure loads as the primary side blows down to atmospheric pressure.

4) Bending stresses resulting from bow of the tubesheet due to the secondary-to-primary pressure differential.

5) Bending of the tube due to differential thermal expansion between the tubesheet and first tube support plate following the drop in primary fluid temperature.

Loading mechanisms 3) through 5) above are not an issue since they are a non-cyclic loading condition and will not result in crack growth, and/or result in a compressive membrane loading on the tube that is beneficial in terms of negating cyclic bending stresses that could result in crack growth.

11.2.2.1 LOCA Rarefaction Wave Analysis

The principal tube loading during a LOCA is caused by the rarefaction wave in the primary fluid. This wave initiates at the postulated break location and travels around the tube U-bends. A differential pressure is created across the two legs of the tube which causes an in-plane horizontal motion of the U-bend. This differential pressure, in turn, induces significant lateral loads on the tubes.

The pressure-time histories to be input in the structural analysis are obtained from transient thermal-hydraulic (T/H) analyses using the MULTIFLEX computer code. A break opening time of 1.0 msec to full flow area (that is, instantaneous double-ended rupture) is assumed to obtain conservative hydraulic loads. A plot of the tube model for a typical T/H model for determining LOCA pressure time histories for the tubes is shown in Figure 11-2. Pressure time histories

are determined for three tube radii, identified as the minimum, medium, and maximum radius tubes. For the structural evaluation, the pressures of concern occur at the hot and cold leg U-bend tangent points. Plots of the hot-to-cold leg pressure drops for the limiting major and minor pipe breaks, the steam generator inlet break and the accumulator line break, are provided in Figures 11-3 and 11-4, respectively, for each of the three tubes considered. These results show that significantly higher pressure drops occur for the primary pipe break than for the minor pipe break.

For the rarefaction wave induced loadings, the predominant motion of the U-bends is in the plane of the U-bend. Thus, the individual tube motions are not ccupled by the anti-vibration bars. Also, only the U-bend region is subjected to high bending loads. Therefore, the structural analysis is performed using single tube models limited to the U-bend and the straight leg region over the top two TSPs. The LOCA rarefaction pressure wave imposes a time varying loading condition on the tubes. The tubes are evaluated using the time history analysis capability of the WECAN computer program. The structural tube model consists of three-dimensional beam elements. The mass inertia is input as effective material density and includes the weight of the tube as well as the weight of the primary fluid inside the tube, and the hydrodynamic mass effects of the secondary fluid. The geometry of the three tube models used for the LOCA analysis are shown in Figure 11-5, with the node numbers identified.

To account for the varying nature of the tube/TSP interface with increasing tube deflection, three sets of boundary conditions are considered. For the first case, the tube is assumed to be laterally supported at the top TSP, but is free to rotate. This is designated as the "continuous" condition, in reference to the fact that the finite element model for this case models the tube down to the second TSP location. As the tube is loaded, it moves laterally and rotates within the TSP. After a finite amount of rotation, the tube will become wedged within the TSP and will no longer be able to rotate. The second set of boundary conditions, therefore, considers the tube to be fixed at the top TSP location, and is referred to as the "fixed" case. Continued tube loading causes the tube to yield in bending at the top TSP and eventually a plastic hinge develops. This represents the third set of boundary conditions, and is referred tc as the "pinned" case.

Using the pressure time histories from the T/H analyses, lateral loads are calculated for each tube length at each time point and the dynamic response of the tube is calculated. The analysis shows the continuous set of boundary ccnditions to give the largest TSP loads for the minimum and medium tubes. For the maximum radius tube, the fixed ccndition is found to be most representative due to its increased flexibility and higher tube rotations at the top TSP. Each of the dynamic solutions results in a force time history acting on the TSP. These time histories show that the peak responses do not occur at the same time during the transient. For the Kewaunee analysis, however, it is assumed that the maximum reaction forces occur simultaneously. Using the results for these three tubes, a TSP load corresponding to the overall bundle is then calculated.

Summaries of the resulting TSP forces for the Inlet break and the Accumulator line break are shown in Table 11-1. Based on the plots shown, a bi-linear representation is assumed for the peak amplitudes as a function of tube radius. Summaries of the overall TSP forces are provided in Tables 11-2 and 11-3 for the top TSP for the Inlet and Accumulator line breaks, respectively. Note that for tube rows 1-6, the peak response is assumed to be constant and equal to the Row 6 response. Shown in Figure 11-6 is the distribution of TSP load for the Inlet break for the top TSP. A summary of the resulting TSP loads for each of the breaks for the top TSP and for the TSP below the top TSP is provided in Table 11-4.

11.2.2.2 LOCA Shaking Loads

Concurrent with the rarefaction wave loading during a LOCA, the tube bundle is subjected to additional bending loads due to the shaking of the steam generator caused by the break hydraulics and reactor coolant loop motion. However, the resulting tube stresses from this motion are small compared to those due to the rarefaction wave induced motion.

To obtain the LOCA induced hydraulic forcing functions, a dynamic blowdown analysis is performed to obtain the system hydraulic forcing functions assuming an instantaneous (1.0 msec break opening time) double-ended guillotine break. The hydraulic forcing functions are then applied, along with the displacement time-history of the reactor pressure vessel (obtained from a separate reactor vessel blowdown analysis), to a system structural model, which includes the steam generator, the reactor coolant pump and the primary piping. This analysis yields the time history displacements of the steam generator at its upper lateral and lower support nodes. These time-history displacements formulate the forcing functions for obtaining the tube stresses due to LOCA shaking of the steam generator.

Past experience has shown that LOCA shaking loads are small when compared to LOCA rarefaction loads. For this analysis, these loads are obtained from the results of a prior analysis for a Model D steam generator. To evaluate the steam generator response to LOCA shaking loads, the WECAN computer code is used along with the seismic analysis model discussed previously. The steam generator support elements are removed, however, because the LOCA system model accounts for their influence on the steam generator response.

Input to the WECAN model is in the form of acceleration time histories at the tube/tubesheet interface. These accelerations are obtained by differentiation of the system model displacement time histories at this location. Acceleration time histories for all six degrees of freedom are used. The resulting LOCA shaking loads used for the this analysis are 17.1 kips for TSP 1-6 and 15.5 kips for TSP 7 for the large break LOCA, and 7.75 kips for all TSP for the minor breaks. The small break loads are scaled from the large break loads based on a comparison of support displacements from system analyses for the two types of breaks.

11.2.3 Combined Plate Loads

In calculating a combined TSP load, the LOCA rarefaction and LOCA shaking loads are combined directly, while the LOCA and SSE loads are combined using the square root of the sum of the squares. The overall TSP load is transferred to the steam generator shell through wedge groups located at discrete locations around the plate circumference.

For the Series 51 steam generators, there are six wedge groups located every 60° around the plate circumference (see Figure 11-7). The distribution of load among wedge groups is approximated as a cosine function among those groups reacting the load, which corresponds to half the wedge groups. Except for the bottom TSP, the wedge groups for each of the TSPs are located at the same angular location as for the top TSP. Thus, if TSP deformation occurs at the lower plates, the same tubes are affected as for the top TSP. For the top TSP, however, the wedge groups have a 10 inch width, compared to a 6 inch width for the other plates. This larger wedge group width distributes the load over a larger portion of the plate, resulting in less plate and tube deformation for a given load level. For the bottom TSP, the wedge group width is 6 inches, and the wedge groups are rotated 36° relative to the other TSPs. The distribution of load among the various wedge groups for the LOCA load, which can only act in the plane of the U-bend, is shown in Figure 11-8 for TSP 2-7. Although, the wedges are rotated for TSP 1, the rotations

are such that the same load factors result. For seismic loads, which can have a random orientation, the maximum wedge load is 2/3 of the maximum TSP load.

Summaries of the resulting TSP and wedge loads for the Inlet and Accumulator line breaks are provided in Tables 11-5 and 11-6, respectively.

11.2.4 Tubo Deformation

[

11.2.5 Effect on Burst Pressure (SSE + FLB/SLB)

Since the tube support plates provide lateral support to tube deformation that may occur during postulated accident conditions, tube bending stress is induced at the TSP intersections. This bending stress is distributed around the circumference of the tube cross section, tension on one side and compression on the other side, and is oriented in the axial (along the tube axis) direction. Axial cracks distributed around the circumference will therefore either experience tension stress that tends to close the crack or compressive stress that tends to open the crack. The compressive stress has the potential then to reduce the burst capability of the cracked tube due to the crack opening.

[

11.3 Allowable Leak Rate for Accident Conditions

A calculation has been completed to determine the maximum permissible steam generator primary-to-secondary leak rate during a steam line break outside-containment for the Kewaunee steam generators. The calculation considered accident initiated and pre-accident iodine spikes. The accident initiated iodine spike resulted in the limiting leak rate. Based on a 30 rem thyroid dose at the site boundary, a leak rate of 13.8 gpm (9.2 gpm at room temperature) was determined to be the upper limit for the total allowable primary to secondary leakage in both loops. The SG in the intact loop is assumed to have primary to secondary leakage of 150 gpd each (approximately 0.1 gpm), which is the maximum value defined by the proposed technical specification. Thus, the allowable leak rate for the SG in the faulted loop is 13.7 gpm (9.1 gpm at room temperature). Although the leakage in any of the SG's may be distributed among tubesheet and tube support plate (TSP) locations, the calculation that was performed conservatively assumed that the leakage is all at TSP locations (above the mixture level).

Thirty rem was selected as the dose acceptance criteria for the accident initiated iodine spike case based on the guidance of Standard Review Plan (NUREG-0800) Section 15.1.5, Appendix A. The SRP further states that the acceptance criteria for SGTR with a pre-accident iodine spike is the 10 CFR 100 guideline. In this case, 150 rem was considered to be appropriately within the 300 rem guideline of 10 CFR 100, and, thus, was selected as the dose acceptance criteria. Only the release of iodines and the resulting 2 hour site boundary thyroid dose was considered in the leak rate determination. Whole-body doses due to noble gas immersion have been determined, in other evaluations, to be considerably less limiting than the corresponding thyroid doses.

The salient assumptions used in the evaluation follow.

Initial primary coolant iodine activity:

Accident initiated iodine spike: 1 μCi/gm of dose equivalent I-131

Pre-accident iodine spike: 60 μCi/gm of dose equivalent I-131

Accident initiated spike iodine appearance rate:

500 X the iodine release rate that corresponds to the 1 μCi/gm equilibrium primary coolant activity level.

The release rate from the fuel to the coolant (Curies/sec) for each iodine nuclide is as follows:
I-131: 0.78
I-132: 1.72
I-133: 1.85
I-134: 2.47
I-135: 1.79

Failed fuel, percent of core: 0, applicable with or without offsite power

Initial secondary coolant activity: 1.0 μCi/cc of dose equivalent I-131 (Tech. Spec. LCO)

Offsite power: not available

Turbine condenser: not available, all activity is released directly to the environment

Steam released to the environment (0 to 2 hours): from the SG in intact loop - 209,000 lb (plus p/s leakage), from faulted loop - 99,300 lb (plus p/s leakage) (the entire initial SG water mass - does not include aux. feedwater addition)

Iodine partition coefficients:

SG in intact - 1.0 for primary to secondary leakage loops since leakage is assumed to be above the mixture level (conservative for leaks at the tube sheet)

0.1 for steam release

SG in faulted loop - 1.0 due to dry SG - for both p/s leakage and steam release - leaks can be at any location .

Atmospheric dispersion factor: 0 to 2 hour at the site boundary, 2.23 E-4 sec/cu meter

Thyroid dose conversion factors (rem/curie): Regulatory Guide 1.109

The radioactivity released to the environment due to a main steam line break can be separated into two distinct releases: the release of the initial iodine activity contained in the secondary coolant and the release of primary coolant iodine activity that is transferred by tube leakage. Based on the assumptions stated previously, the release of the iodine activity initially contained in the secondary coolant (2 SGs) results in a site boundary thyroid dose of approximately 8.6 rem. This is independent of both the leak location and iodine spiking assumptions.

The dose contribution due to primary-to-secondary leakage, from both the faulted loop SG and the intact loop SG, regardless of the leak location, is as follows:

accident initiated iodine spike - 1.55 rem/gpm
pre-accident iodine spike - 2.22 rem/gpm

The total allowable leak rate is as follows:

accident initiated iodine spike (30 rem limit) - 13.8 gpm
pre-accident iodine spike (150 rem limit) - 63.7 gpm.

The allowable leak rate for the SG in the faulted loop is as follows:

accident initiated iodine spike - 13.7 gpm
pre-accident iodine spike - 63.6 gpm.

Based on these results, the accident initiated spike results in the limiting leak rate.

Because of the potential for steam generator tube uncovery, treatment of leakage is different depending on the location of the leak. Following a reactor trip, the mixture level in the steam generator can drop below the apex of the tube bundle. For the SG in the intact loop, leakage that occurs in the tube sheet region is assumed to remain covered by water and mix with the secondary coolant (partition coefficient associated with steaming is 0.1). Leakage that occurs at a support plate is assumed to transfer directly to the environment without mixing or

partitioning since the leakage site is assumed to be above the mixture level. Although less than approximately 4 feet of the bundle is expected to be above the mixture level, any support plate leak is assumed to remain uncovered for the duration of the accident recovery. The SG in the faulted loop is assumed to steam dry (no mixture level). Hence, leakage to this SG is also assumed to transfer directly to the environment regardless of the location of the leak.

The accidents that are affected by primary to secondary leakage are those that include, in the activity release and offsite dose calculation, modeling of leakage and secondary steam release to the environment. The reasons that the steam line break is limiting are 1) the steam line break primary to secondary leak rate in the faulted loop is assumed to be many times greater than the operating leak rate because of the sustained increase in differential pressure and 2) leakage to the faulted steam generator is assumed to be released directly to the environment, i.e., no mixing with the secondary coolant or partitioning of activity is assumed, since the steam generator in the faulted loop is subject to dryout. Depending on the elevation of the degradation (at the tubesheet region versus a TSP), for other accidents in which there is a secondary side steam release, the secondary sides of all SG's are assumed to be intact, hence, a prolonged increase in the primary to secondary leak rate is not predicted because there is not a sustained increase in the primary to secondary differential pressure. Also, there may be justification for mixing or iodine partitioning in the steam generators following the potential initial uncovery of the top of the tube bundle after the reactor trip. These factors significantly reduce the release of iodine to the environment for accidents other than steam line break.

As noted above, mixing and iodine partitioning are dependent upon the elevation of the degradation. For non-SLB accidents in which there is a secondary side steam release, there is justification for mixing and partitioning if the primary to secondary leakage is at the tubesheet region (below the SG water level). If the degradation is at a TSP, such that reactor coolant could bypass the secondary coolant and directly enter the steam space, the radioactivity release path is assumed to be directly to the environment, just as it is for the SG in the faulted loop following an SLB.

Table 11.1

Summary of TSP Forces - Top TSP
Dynamic Time History Analysis
LOCA Rarefaction Pressure Wave Loading

a

Table 11.2

Summary of Total TSP Force - Top TSP
LOCA Rarefaction Pressure Wave Loading
Steam Generator Inlet Bresk

a

Table 11.3

**Summary of Total TSP Force - Top TSP
LOCA Rarefaction Pressure Wave Loading
Accumulator Line Break**

a

Table 11.4

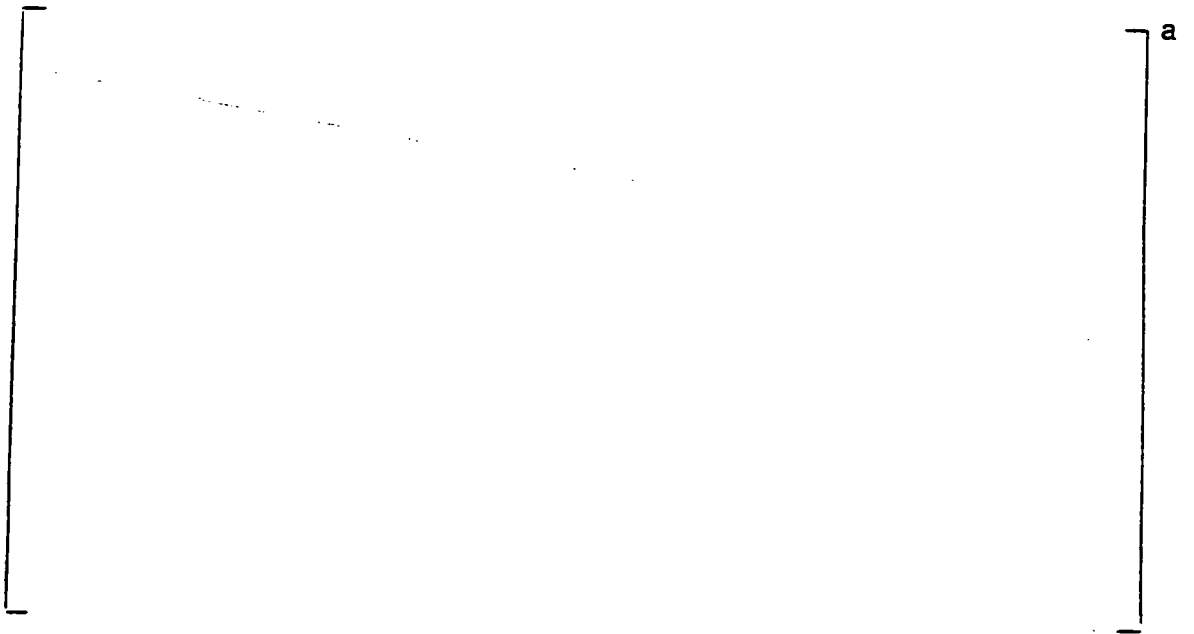Summary of TSP Forces

LOCA Rarefaction Pressure Wave Loading

$$\begin{bmatrix} & & \end{bmatrix}^a$$

Table 11.5

Summary of Wedge Loads
Combined LOCA + SSE Loading
Steam Generator inlet Break

a

Table 11.6

Summary of Wedge Loads
Combined LOCA + SSE Loading
Accumulator Line Break

Table 11.7

Summary of Calculations to Determine Area Under Force/Deflection Curve

Crush Test No. 2

a,b

Table 11.8

Summary of Number of Deformed Tubes as a Function of Load
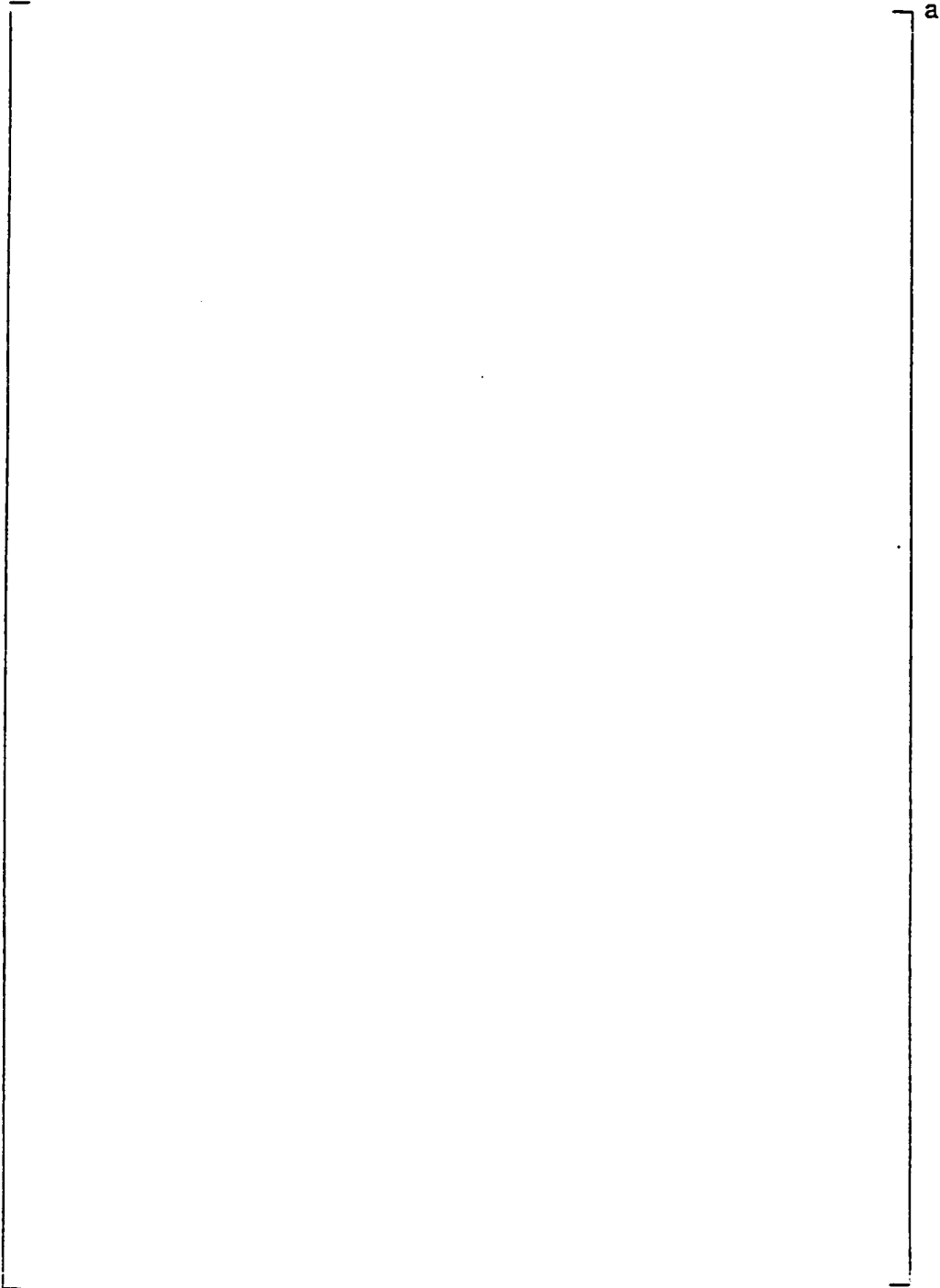
a,b

Table 11.9

Summary of Number of Deformed Tubes at Wedge Locations

TSP 1
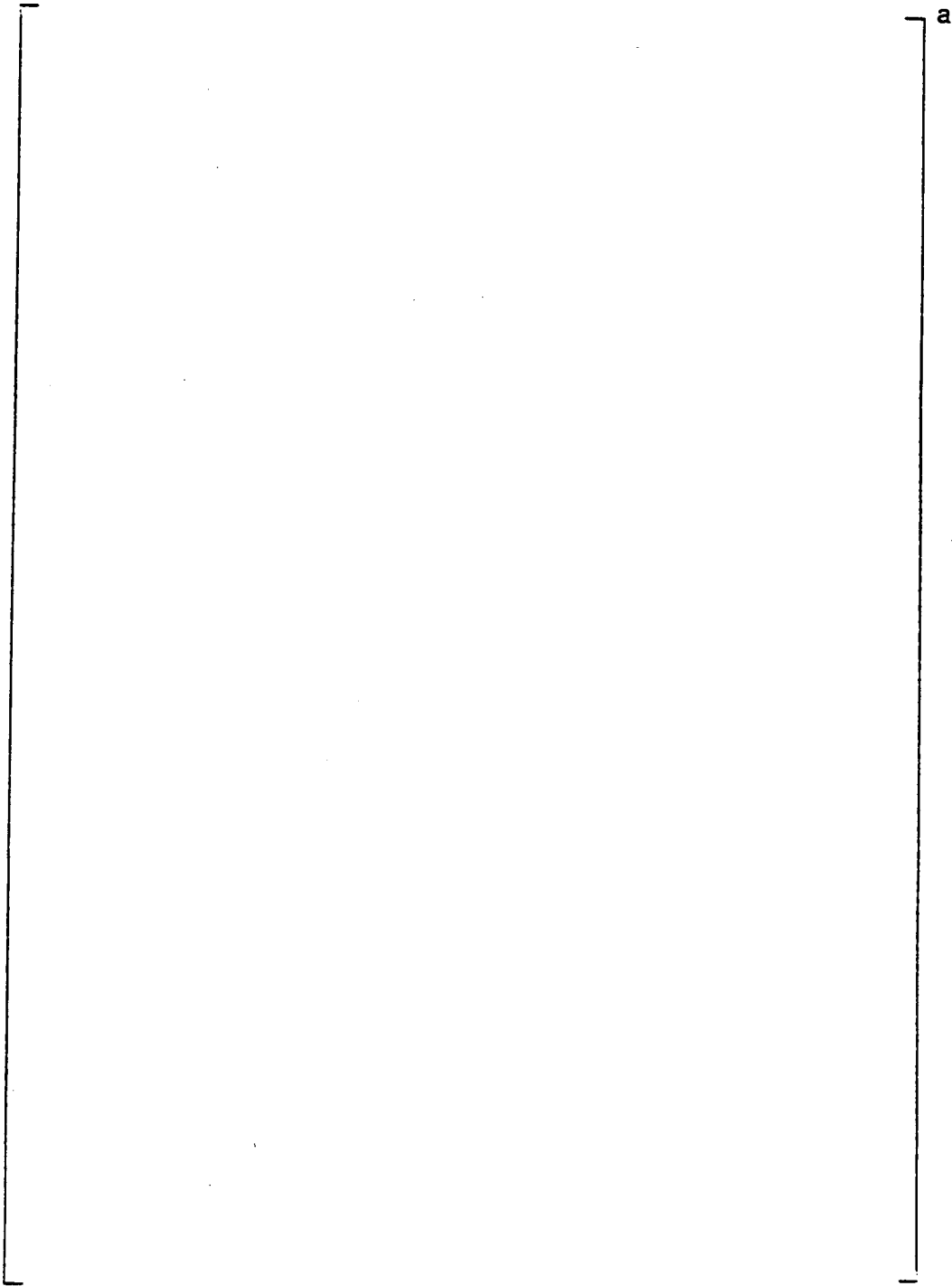
a

Table 11.10

Summary of Number of Deformed Tubes at Wedge Locations

TSP 2-6

$$\begin{array}{c} \quad \end{array}$$

a

Table 11.11

Summary of Number of Deformed Tubes at Wedge Locations

TSP 7

a

Table 11.12

Applicability of Test Results to Wedge Locations

a,b
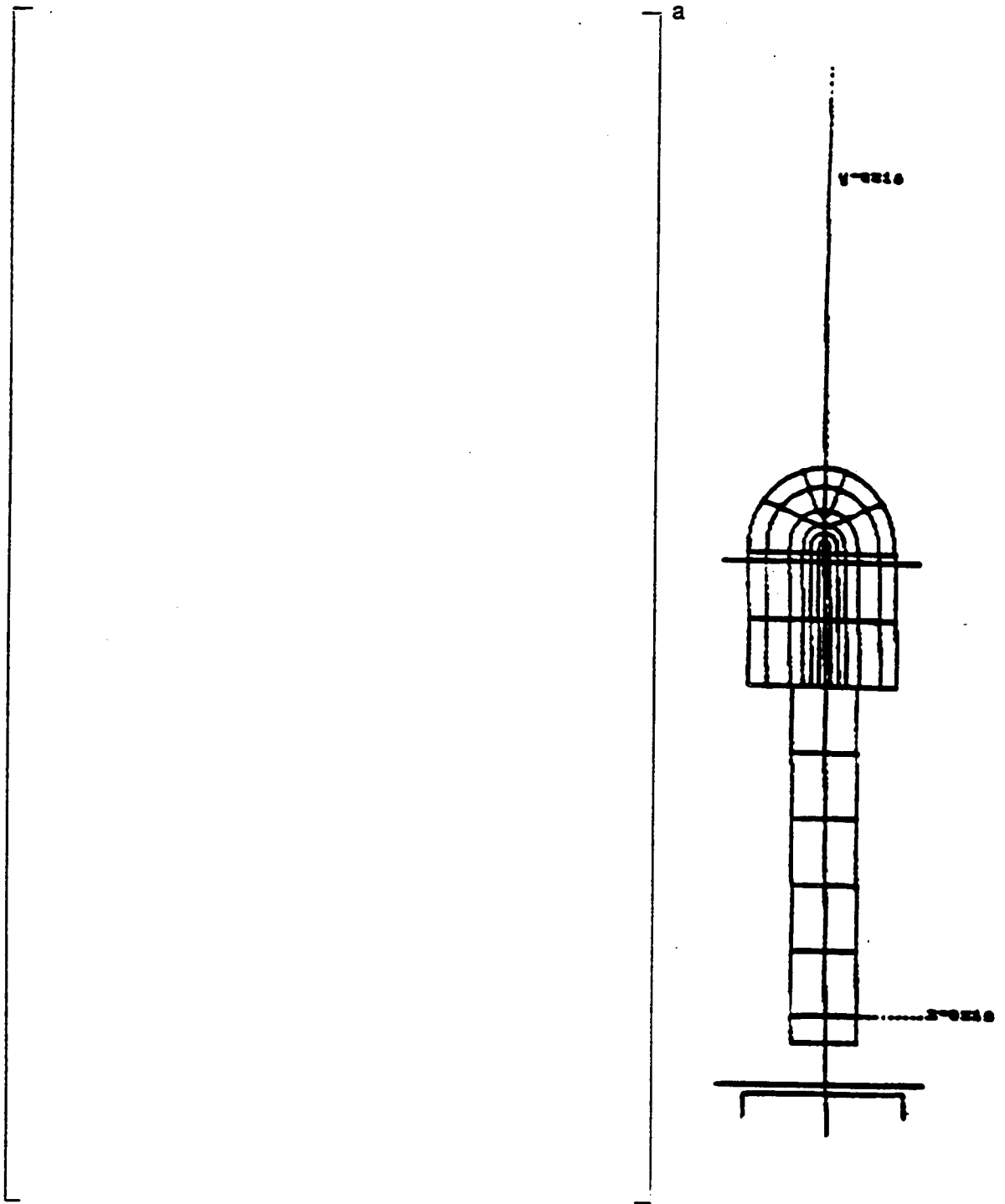
Figure 11-1. Series 51 Seismic Finite Element Model Geometry
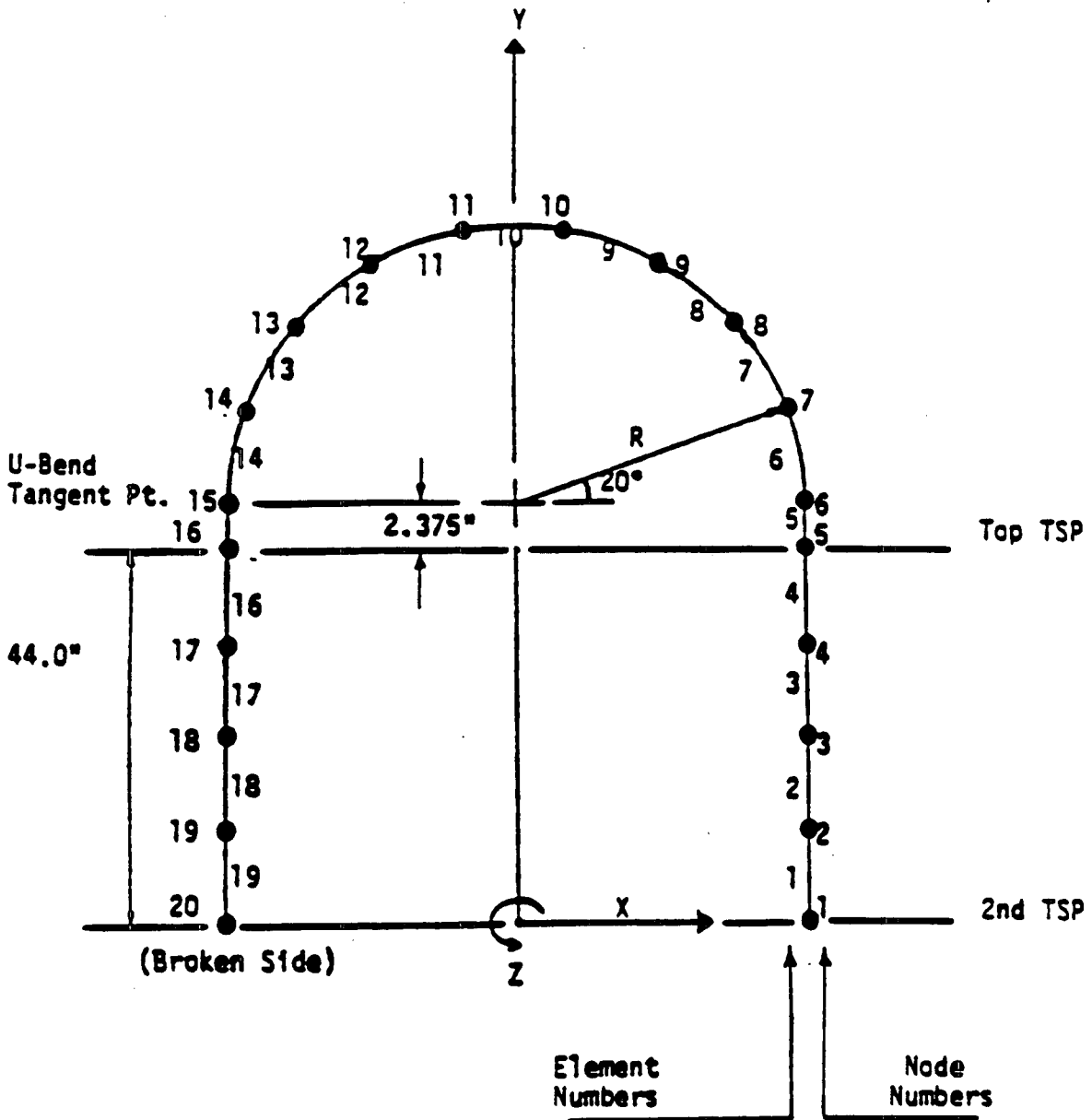
Figure 11-2. T/H Tube Model for LOCA Rarefaction Wave Analysis

a
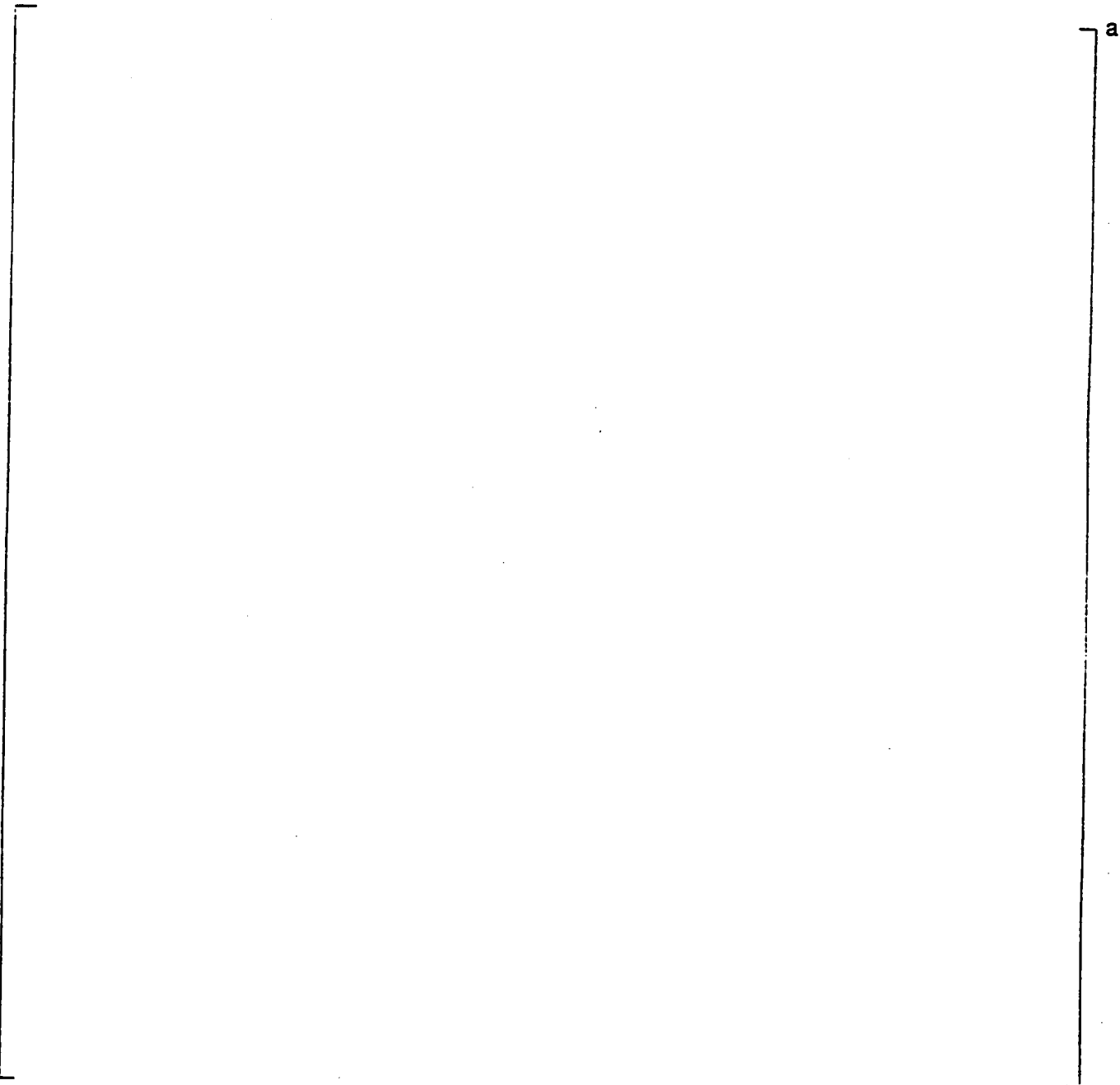
Figure 11-3. LOCA Pressure Differentials for S/G Inlet Break
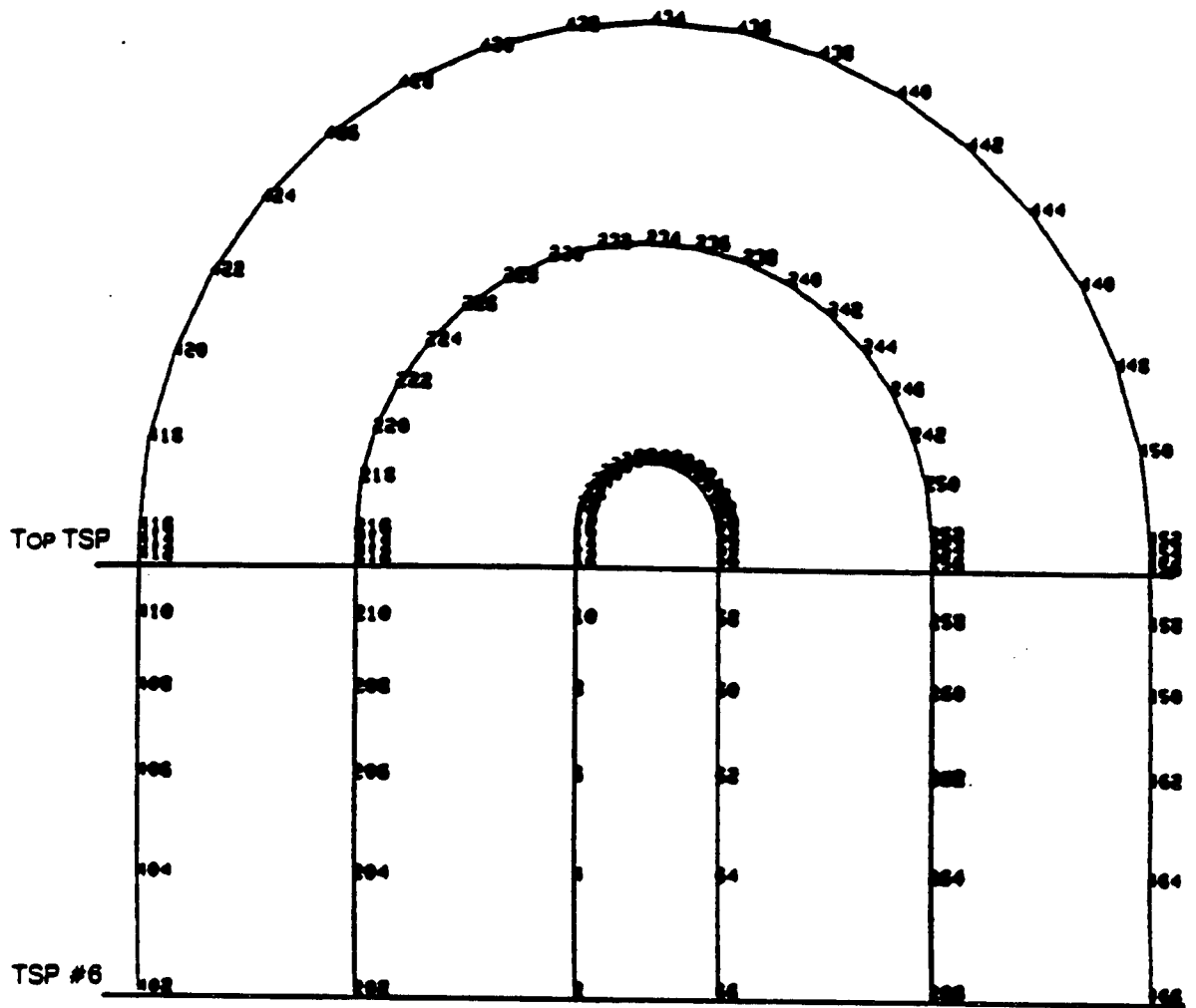
Figure 11-5. Finite Element Model for Structural LOCA Time History Analysis

a
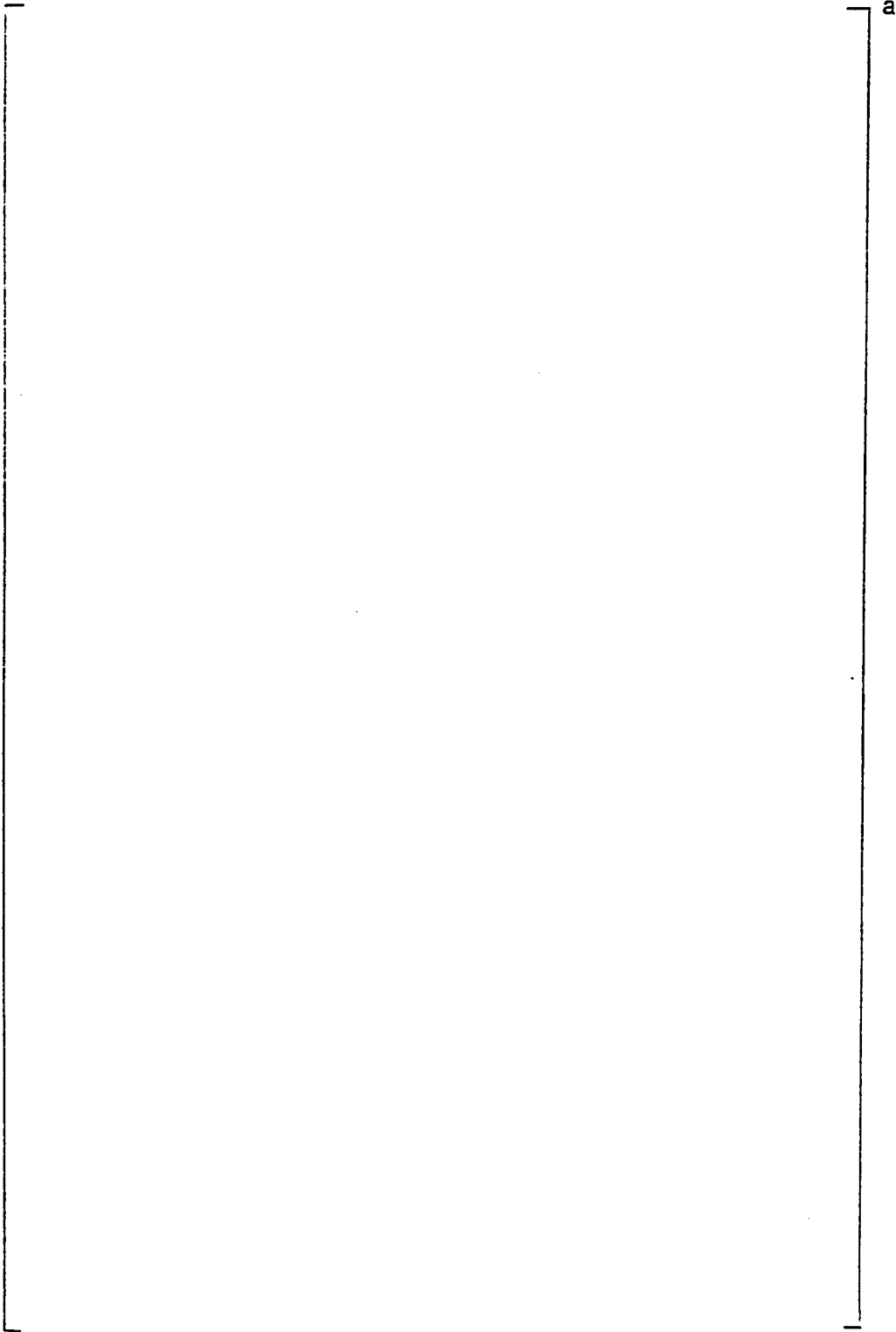
Figure 11-6. LOCA Rarefaction Force Distribution for S/G Inlet Break

a
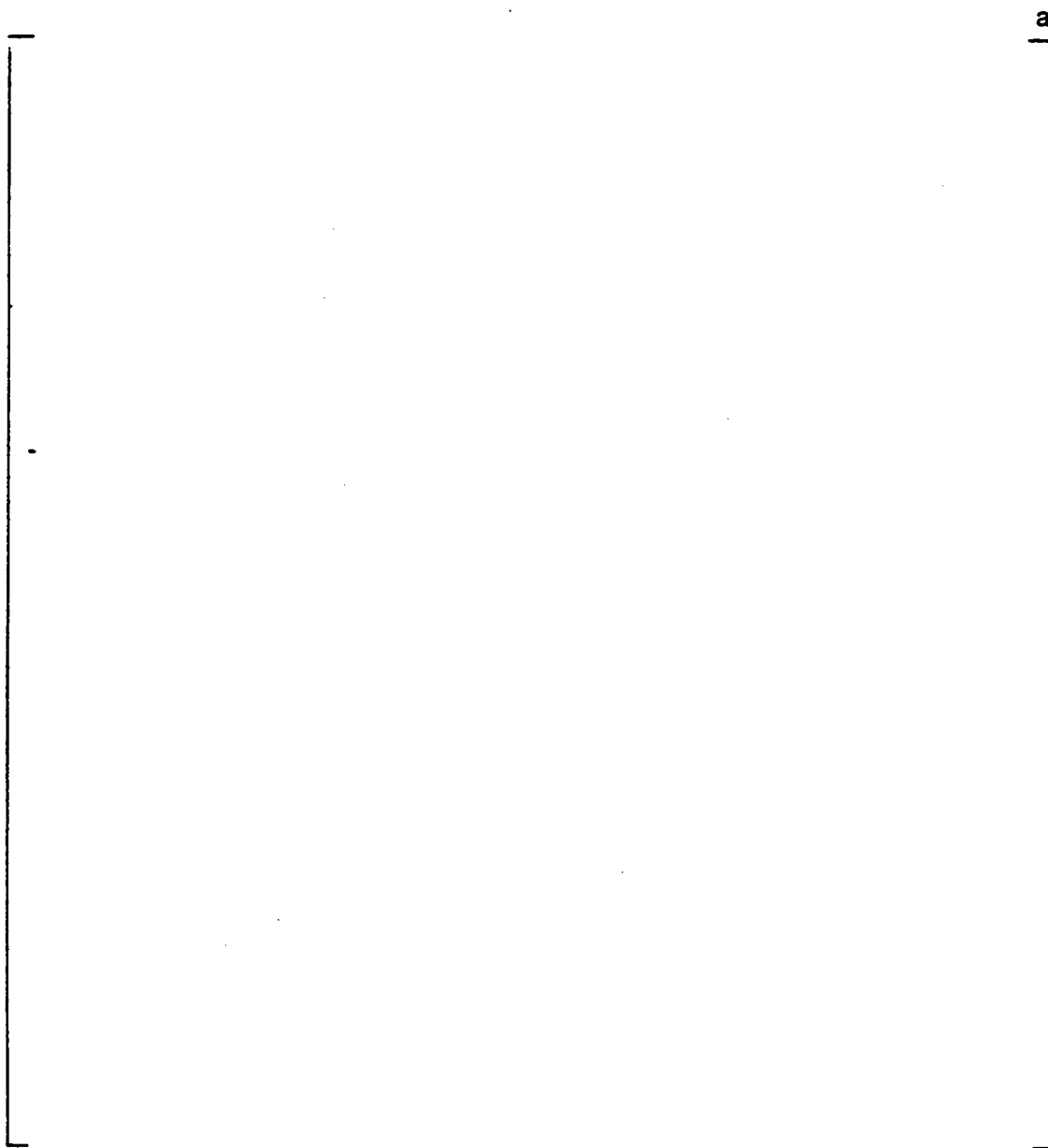
Fifgure 11 -7. Wedge Group Orientation Looking Down on TSP

11 - 31

a,b
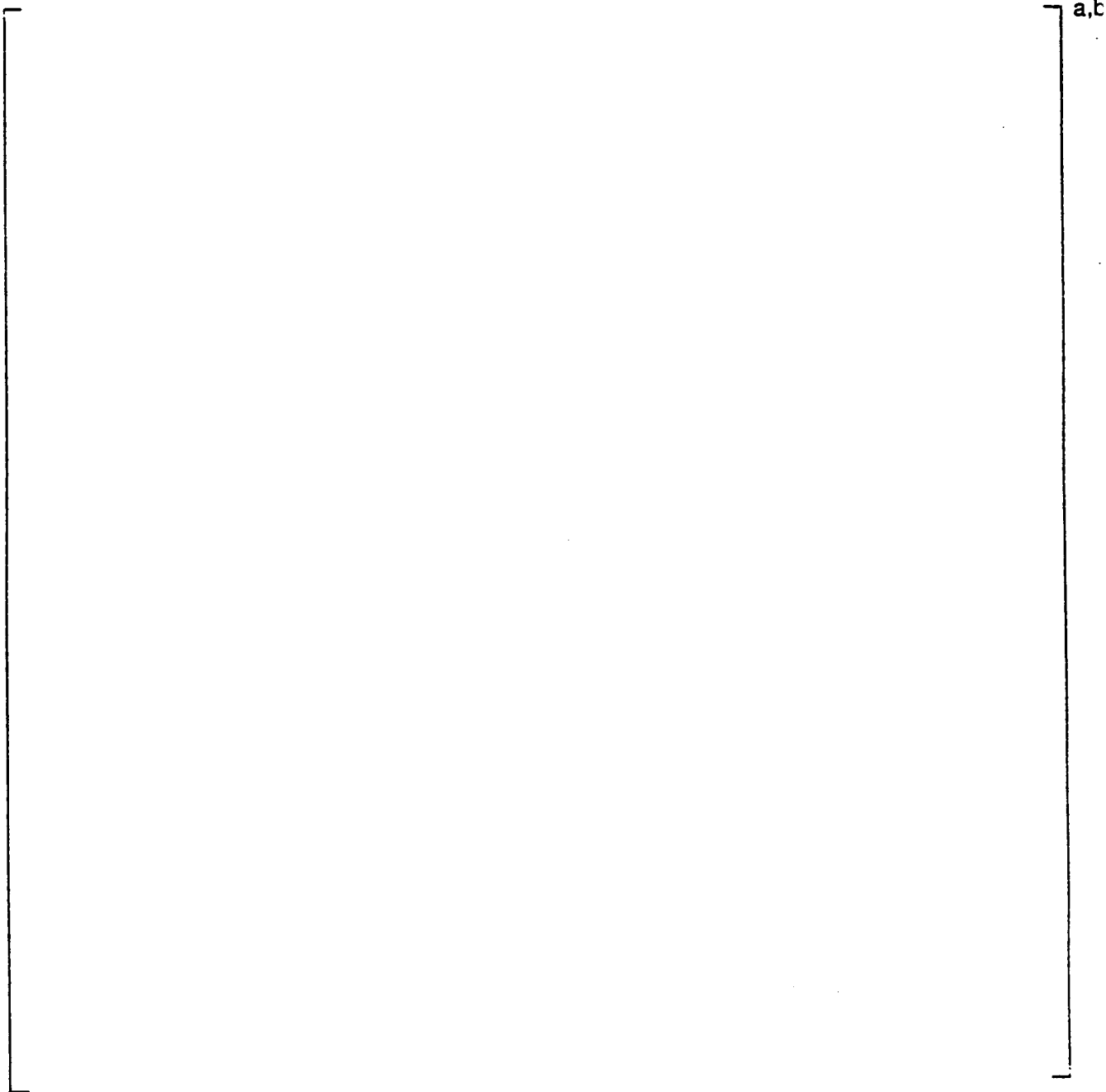
Figure 11-9. Crush Test Results - Force vs Deflection
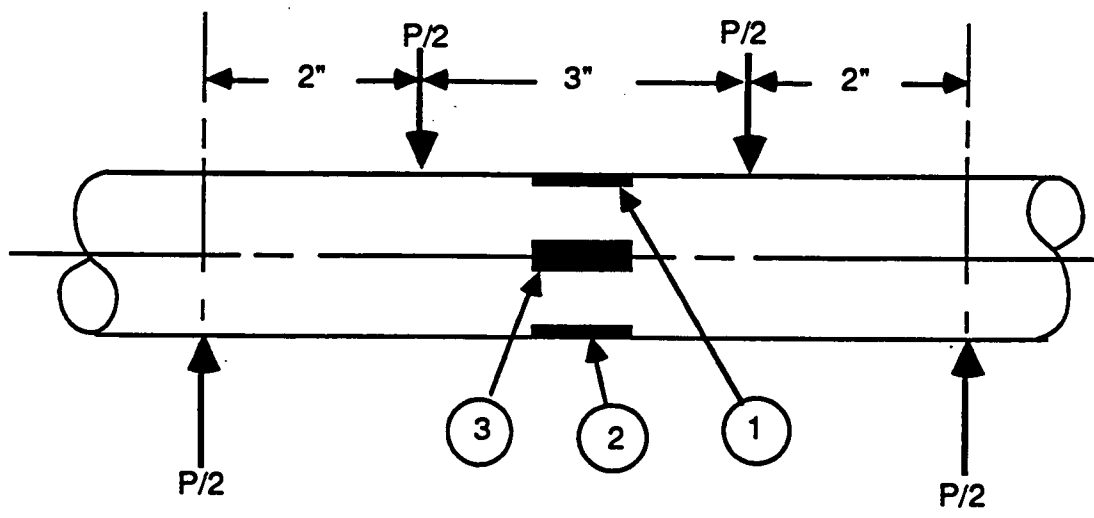
Figure 11-11. Externally Applied Bending Load and Locations of Through Wall Slots

12.0   KEWAUNEE INSPECTION RESULTS

12.1   March 1992 Inspection

A scheduled inspection of the Kewaunee steam generators was conducted during the refueling outage in March, 1992. All tubes in service were inspected by bobbin coil eddy current tests. Over 400 indications at the tube support plate (TSP) locations were reported as a result of the inspection. These flaw signals were reevaluated off site and particular attention was paid to obtaining accurate voltage amplitudes needed to estimate growth in indication voltage. Eddy current data from the 1991 inspection of these tubes were also reevaluated with the primary objective of estimating voltage growth rates during the last cycle. Eddy current data tapes from a few tubes could not be readily converted in format to allow a timely evaluation. A few indications from the 1992 outage were NDD (no detectable degradation) in the 1991 inspection. This reevaluation is the sole source of the results described in this section, i.e., no use was made of the field data analysis results. The following is a summary of the results relating to ODSCC indications at TSP locations.

EC results were obtained for both the 1991 and 92 outages for 382 indications at TSP locations. This population was used for growth rate calculation and projection. The TSP indications were distributed among the two steam generators as follows. There were 108 indications in steam generator A and 274 in S/G-B. Indications were reported at all TSP locations; many of the indications were in the cold leg. Figure 12-1 displays the frequency distribution of TSP indications by support plate locations. The upper figure shows the number of indications at a TSP while the lower figure shows the percent of all TSP indications falling within a given support plate location. In the figure, the TSP locations are listed in the order of primary coolant flow direction. 1H refers to the first (lowest) TSP in the hot leg, 2H the second TSP in the hot leg, etc. all the way to 1C which is the lowest TSP in the cold leg. It may be noted that no trend exists in the variability of the number of indications among the TSPs.

The bobbin voltage amplitudes of these TSP indications during the 1992 inspection ranged from 0.19 to 4.00 volts with an average value of 0.81 volts. A frequency distribution of the 1992 bobbin coil voltage amplitudes from the TSP indications is displayed in Figure 12-2. The upper ends of the voltage range bins are shown on the X-axis scale. Thus the first bar at 0.2 volts represents indications of amplitudes between 0.0 and 0.2 volts. The cumulative percent frequency is also plotted and is shown as a curve. 75% of the indications had amplitudes less than 1 volt (400/100 kHz mix channel) and over 97% had amplitudes less than 2 volts. There were two indications exceeding 3 volts, the largest being 4.00 volts. A histogram of the bobbin voltages in each steam generator is shown in Figure 12-3. As in Figure 12-2, the X-axis scale displays the upper ends of the voltage ranges. It may be noted that the voltage distribution of the TSP indications is quite similar in the two steam generators.

12.2   Voltage Growth Evaluation

The reevaluation included a review of the eddy current inspection results from the March 1991 inspection conducted at Kewaunee. The objective of the review was to assess the progression of ODSCC in the Kewaunee steam generators. The indications from the 1992 inspection were traced back to the prior inspection to assess whether they may be observed in light of the 1992 data and

if so, to obtain the bobbin signal evaluation. The results of this review are used to obtain growth rates of the TSP Indications.

The bobbin signal amplitudes are dependent on the calibration standards used during each of the inspections. The ASME standard for flaw depths specifies a tolerance of ± 3 mils or 20% whichever is less, whereas the diametral tolerance is ± 10 mils. This leads to possible diametral variations of ± 15% and ± 5%, respectively, for the 100% and 20% deep ASME holes assuming that the machined standard is within the specifications. The engineering drawing of the calibration standard used during an Inspection provides the exact as-built (measured) depths of the machined flaws, but does not give the as-built diameters of the flaws. Further, the accuracy of depth for the through-wall hole is absolute. Thus while the standard may have been well suited for depth estimates with high degree of confidence, the signal amplitude estimates tend to be less reliable due to the variation In hole diameters in the standard. This uncertainty is inherent in the voltage results from the 1991 and 1992 inspections as well as all prior inspections.

The bobbin voltage amplitudes of these TSP indications during the 1991 inspection ranged from 0.18 to 4.13 volts with an average value of 0.69 volts. It may be noted that virtually all of these indications remalned In service during the operatlng cycle since they could be found In the 1991 eddy current inspection data (only 3 of the 436 indications reported in 1992 were NDD in the 1991 EC data). Since these indications were present in 1991, they are not newly formed flaws, but rather, indications which existed previously.

Growth in amplitude during the last operating cycle was determined from the 1991 and 1992 data. Grcwth estimates were calculated only for the cases where bobbin signal voltage data were available for both inspections; I.e., no assumption about the signal voltage for prior year was made if a flaw indication was not available. Growth estimates were not made for the 3 Indications which were NDD in 1991 and for the 5 Indications which had "bad data" from the 1992 inspection (all 8 were In steam generator A). 1992 eddy current results for 46 indications In steam generator B could not be reassessed due to the difficulty encountered in data conversion. As a result, growth estimates for the 1991-92 cycle were made for 382 indications.

A frequency distribution (in percent cf each steam generator indications) cf voltage growth in each of the two steam generators during the 1991-92 operating cycle is shown in Figure 12-4. It may be noted that the growth rate distribution is substantially similar among the two steam generators. The mode (interval of highest frequency) of the amplitude growth is the range of 0.0 to 0.1 voit.

Figure 12-5 shows a plot of the growth In amplitude from 1991 tc 1992 as a function of the 1991 amplitude for the TSP indications in each of the steam generators. It may be noted that the amplitude growth ranged from -0.84 to +1.46 volts. The negative growths (and possibly some of the higher positive growth values) result from the uncertainties in the eddy current inspection and data evaluation discussed above. Overali, the distribution of amplitudes and their growths appear reasonable, based on experience with data from other plants.

Figure 12-6 shows a frequency distribution of voltage growths during the 1991-92 cycle. The upper ends of the ranges are displayed on the X-axis. The cumulative frequency distribution in percent is also displayed in the figure, as an "S" curve. It may be noted that most of the indications had growth rates between 0.0 and 0.2 volt per cycle. Only 4 of the 382 growth rates were greater than 1 volt/cycle and all (100%) of the indications had growth rates less than 1.46 volts per cycle.

The average growth in amplitude for indications in each steam generator was calculated for the 1991-92 cycle. This is displayed in Table 12-1 along with the overall average which includes both steam generators. The number of indications used in the calculation of the average is also shown in the table. Some of the variation in the growth rates is attributable to the uncertainty in the voltage indications from prior inspections. The overall average growth rates of TSP indications during the 1991-92 cycle was 0.12 volt. The standard deviation associated with the overall average growth rate is 0.26 volt. As discussed before, part of the scatter results from the uncertainty in the eddy current tests and the data evaluation and the remaining from the variability in growth between indications. Overall, the average amplitude growth is low, being in the range of 0.1 to 0.2 volt per cycle.

12.3   Percent Growth in Voltage Amplitude

As discussed in Section 12.2, the growth in amplitude during the last fuel cycle ranged from -0.84 to +1.46 volts. Experience with the data from one European plant indicates that the percent growth in amplitude tends to be stable, i.e., independent of amplitude (however, this is not supported by data from several other domestic units). The European data suggests that the small amplitude indications grow by smaller voltages and that large amplitude signals are more likely to grow by a larger amplitude during the subsequent cycle. Percent growth rate is calculated by taking the ratio of the growth in amplitude during an operating cycle and the amplitude of the signal during the prior inspection. Figure 12-7 shows a plot of the percent growth in amplitude vs BOC bobbin voltage for the cycle. The high percent growth rates are observed only at low amplitudes. Two factors contribute to this: 1) at low signal amplitudes, the uncertainty in the signal analysis may be higher, and 2) since the BOC amplitude is in the denominator in the percent growth calculation, the percent growth value is magnified for the low amplitude (BOC) indication.

The average percent growth rate of all the indications were calculated for Kewaunee. This is displayed in Table 12-2. For the 1991-92 operating cycle, the average growth rate of TSP indication voltage was 18%.

It was noted before that the percent growth rate of amplitude is lower at higher BOC amplitudes (see Figures 12-7). This observation is typical of all domestic plants evaluated by Westinghouse to date. Thus an overall average of percent growth rate may have a strong upward bias due to the small amplitude signals. To assess the impact of this factor, average percent growth rates were calculated for two different BOC amplitude ranges: above and below 0.75 volts. The results are displayed in Table 12-2. For BOC amplitudes below 0.75 volts, the average percent growth rate was 24% whereas the average for BOC amplitudes equaling or exceeding 0.75 volts was 12%. This significant difference must be noted as additional conservatism in the development of the plugging criteria. The standard deviations associated with the averages are listed in Table 12-2.

12.4   Influence of TSP Location

Initiation and progression of ODSCC could be affected by, among other factors, the temperature of the local environment, particularly the temperature of the tubing. Since the primary coolant temperature decreases as it flows up through the tube on the hot leg side, the local tube wall temperature decreases with increase in support plate number (number 1 being the lowest TSP in the hot leg). Hence initiation and progression of ODSCC can vary with TSP location. In other

plants, strong correlation could be observed between the number of indications and TSP location. However, such a relation is not apparent in the Kewaunee frequency distribution of indications by TSP location shown in Figure 12-1. Nevertheless, an assessment of the growth rates by TSP location was made.

The average growth in amplitude was calculated for each of the support plate locations in the Kewaunee data (382 tube-to-TSP intersections reviewed). The results are presented in Table 12-3. The number of growth values used in calculating the average in each case is also shown in the table. The average growth rates of indications appear to be scattered among the TSP elevations. No dependency is evident either with TSP elevation or between hot leg and cold leg. The same conclusion appears to hold for the percent growths in amplitude. Thus the growth rate data suggest no trend between growth rates and TSP locations. This is consistent with observations at several other plants.

12.5 Voltage Growth Projection for Future Cycles

Voltage growth rates calculated above for the 1991-92 cycle cannot be used directly as indicators of growth in future cycles. The growth rates have to be corrected for any potential changes in cycle operating durations. The operating length of the 91-92 cycle was 292.9 effective full power days (EFPD). Typical duration of future cycles is projected to be 305 EFPDs. In order to obtain projection of future growth rates, the calculated growth rates from the last cycle were multiplied by the ratio of EFPDs (305/292.9). A cumulative frequency distribution of the resulting growth rate projection is shown in Figure 12-8. The negative growth rates from the last cycle were treated as zero growths. This growth rate distribution is used in the calculations described in Section 13. The maximum change in voltage from 1991 to 1992 was 1.46 volts which becomes 1.52 volts adjusted to 305 EFPD.

12.6 Voltage Growth During Prior Cycles

In 1991, a review of the past eddy current inspection results was conducted to assess the progression of ODSCC in the Kewaunee S/Gs. That analysis used tubes plugged during 1990 for support plate indications (34 tubes from S/G-A and 13 tubes from S/G-B) and the TSP indications in these tubes as the population to be evaluated. For these tubes, the available eddy current test results in four consecutive inspections (from 1987 through 1990) were reviewed to trace the indication growth and to evaluate the growth rate. There were other tubes with "distorted indications" (DI) at the support plates; however, only the data from the plugged tubes were reevaluated in the study and hence is likely to be conservative (large growth rates). Some of the tubes had indications at more than one tube support plate (TSP) intersection and hence the number of total indications reviewed exceeds the number of plugged tubes.

Several of the indications could be traced back to each of the four inspections. For others, the indications were not detectable from one or more prior eddy current inspections. When an indication was detectable in two consecutive inspections, the corresponding signal voltages were used to calculate voltage growth rates. The average growth in amplitude for all indications was calculated for each of the three cycles for both S/Gs. The results of the analysis are summarized in Table 12-4. It may be noted from this table, that the average voltage growth rate has been very low and stable during these three cycles. It may also be noted that the average growth rates calculated for the last (1991-92) cycle are quite comparable to those calculated for the three cycles between 1987 and 1990. The maximum voltage growth for 187 indications between

12 - 4

1990 and 1991 was 1.1 volts which compares well with the value of 1.46 volts for 382 indications from 1991 to 1992.

Table 12-4 also shows the average growth rate during the 1990-91 cycle. These are based on TSP indications reported during the March 1991 outage. Average growth rates calculated for this population was negative. Unlike the data from the other prior cycles and the 1991-92 cycle, reanalysis of the eddy current results per Appendix A analysis guidelines was not performed for the 1990-91 cycle; growth rates were calculated from indication voltages reported in the field during the 1990 and 1991 inspections. Further, the ASME standards used in the 1990 and 1991 inspections were different. These factors explain why the growth rates estimated for the 1990-91 cycle were different from those in the other cycles. Thus the 1990-91 cycle growth rates listed in Table 12-4 are not considered to be reliable and are not used in the development of the plugging criteria.

12.7 RPC Inspection Results

During the 1992 Kewaunee outage, RPC inspection was performed on several tubes in each steam generator. In general, RPC test results confirmed bobbin coil indications. The review of the RPC data suggests that the TSP signals are due to axial ODSCC. They are comprised of both single and multiple axial indications. Most of the RPC traces could be easily interpreted. However, interpretation of the signal is difficult in a few cases as a result of noise or other complexity in the RPC results.

Samples of the RPC traces are shown in Figures 12-9 and 12-10. Figure 12-9 shows RPC traces from four different support plates in S/G-A, all from the hot leg. These traces are clearly attributable to axial indications. The first (12-9a) was in tube R8C71 at the 7th TSP in hot leg (7H). It is a single axial indication. The reevaluation of the bobbin coil test data for this location from the 1992 inspection as discussed in Section 12.2 showed a signal amplitude of 0.84 volt (400/100 kHz mix). The next trace (12-9b) is from R43C30 at location 3H; this is also a single axial indication and had a bobbin amplitude of 0.70 volt. The trace 12-9c is from the second TSP in the hot leg (2H) in tube R42C29. This is also a single axial indication and had a bobbin amplitude of 0.51 volt. The last trace, 12-9d, is from tube R5C12 at location 1H. This is clearly seen to be an axial indication; however, whether it is a single crack or represents multiple cracks is not very clear. This indication had a bobbin amplitude of 0.65 volt.

Figure 12-10 shows RPC traces from S/G-B. Two of the four traces in Figure 12-10 are from the hot leg and the others from the cold leg. All of these traces are attributable to axial ODSCC indications. The first (12-10a) was in tube R35C77 at 1H. It is a single axial indication. The next trace (12-10b) is from R32C17 at location 5H; this is predominantly a single axial indication and had a bobbin amplitude of 0.45 volt. The two lower traces in this figure are from the cold leg and show multiple axial indications. Figure 12-10c shows a trace from R25C12 at the support plate 6C. This is a multiple axial indication which had a 4.00 volt bobbin signal from the 1992 inspection. Of all the TSP indications evaluated, this indication had the highest bobbin amplitude from the 1992 eddy current data. The last (12-10d) is from R24C75 at 6C. This is a multiple axial indication. It had the second highest bobbin amplitude from the last inspection, 3.58 volts.

These are examples of the RPC traces from the 1992 Kewaunee inspection. Review of the overall RPC data suggests that the support plate indications are axial ODSCC signals.

Table 12-1

Voltage Growth Per Cycle for Kewaunee S/Gs

| S/G | Number [1] | BOC Indication Voltage | | Voltage Growth per Cycle | |
		Average	Std. Dev.	Average	Std. Dev.
A	108	0.67	0.36	0.10	0.33
B	274	0.69	0.43	0.13	0.23
All	382	0.69	0.41	0.12	0.26

Notes

1. Number of indications included in the calculation of the statistics (average and standard deviation).

Table 12-2

Percent Voltage Growth Per Cycle for Kewaunee[1]

| | Number of [2] Indications | BOC Voltage | | Voltage Growth | | Average % |
		Average	Std. Dev.	Average	Std. Dev.	Growth/Cycle
1991 to 1992						
Entire voltage range	382	0.69	0.41	0.12	0.26	18%
$V_{BOC} < 0.75$ volt	261	0.49	0.15	0.12	0.22	24%
$V_{BOC} \geq 0.75$ volt	121	1.11	0.46	0.13	0.33	12%

Notes

1. Percent voltage growth per cycle determined as $(V_{EOC} - V_{BOC}) / V_{BOC} * 100$.

2. Number of indications in the calculation of the growth statistics.

Table 12-3

Voltage Growth Per Cycle by TSP Location

TSP Location	Number of [1] Indications	Average BOC Voltage	Average Voltage Growth	Average Percent Growth
1H	37	0.77	0.19	24%
2H	10	0.86	0.04	5%
3H	6	0.74	0.20	28%
4H	5	0.66	0.01	2%
5H	12	0.52	-0.03	-6%
6H	5	0.49	0.11	22%
7H	17	0.57	0.10	17%
7C	52	0.77	0.14	19%
6C	66	0.81	0.09	11%
5C	26	0.71	0.16	23%
4C	17	0.59	0.06	10%
3C	16	0.58	0.06	10%
2C	57	0.59	0.14	23%
1C	56	0.62	0.16	27%

Notes

1.   Number of indications in the calculation of the growth statistics.

Table 12-4

Comparison of Voltage Growth During Prior Cycles

Cycle	Number of [1] Indications	Average BOC Voltage	Average Voltage Growth	Average Percent Growth
1987-88	20 [2]	0.87	0.11	13%
1988-89	35 [2]	0.93	0.13	14%
1989-90	52 [2]	0.95	0.14	15%
1990-91	187 [3]	1.20	- 0.24	- 20%
1991-92	382 [4]	0.69	0.12	18%

Notes

1. Number of indications included in the calculation of the average.

2. Based on reevaluation (consistent with Appendix A analysis guidelines) of TSP Indications in tubes plugged in 1990.

3. TSP indications reported in the 1991 inspection.

4. Based on reevaluation (consistent with Appendix A analysis guidelines) of TSP indications reported In the 1992 inspection.

KEWAUNEE TSP INDICATIONS
LOCATION OF 1992 INDICATIONS
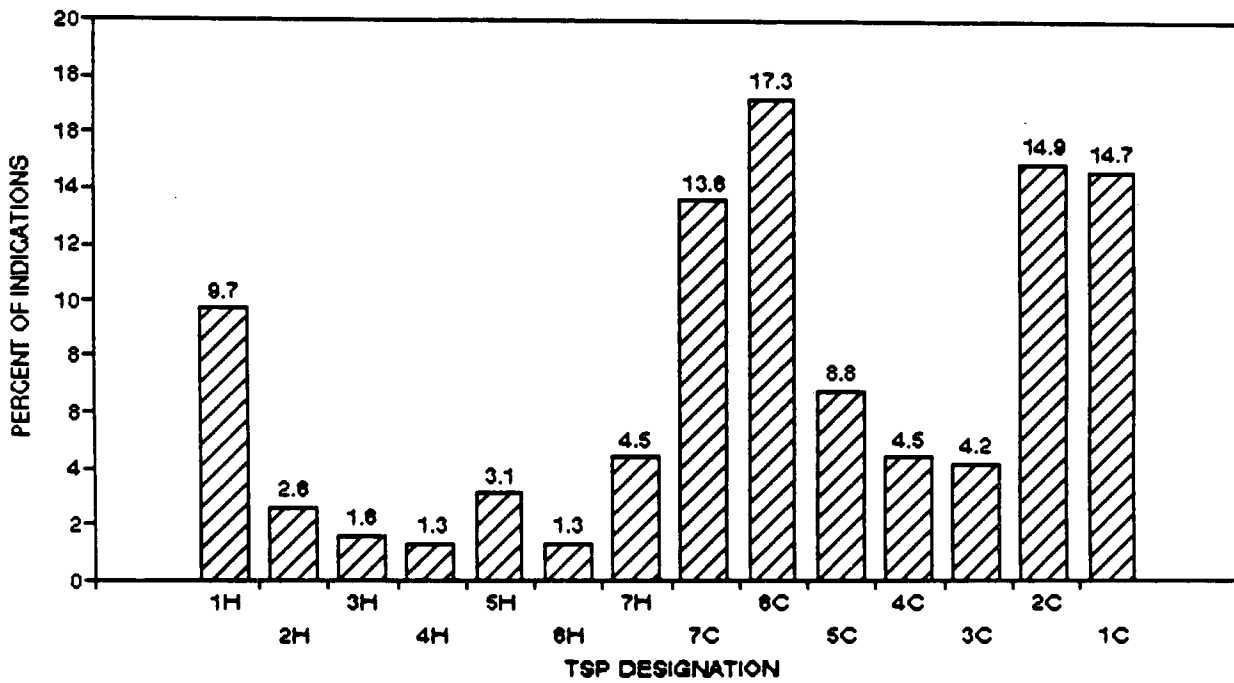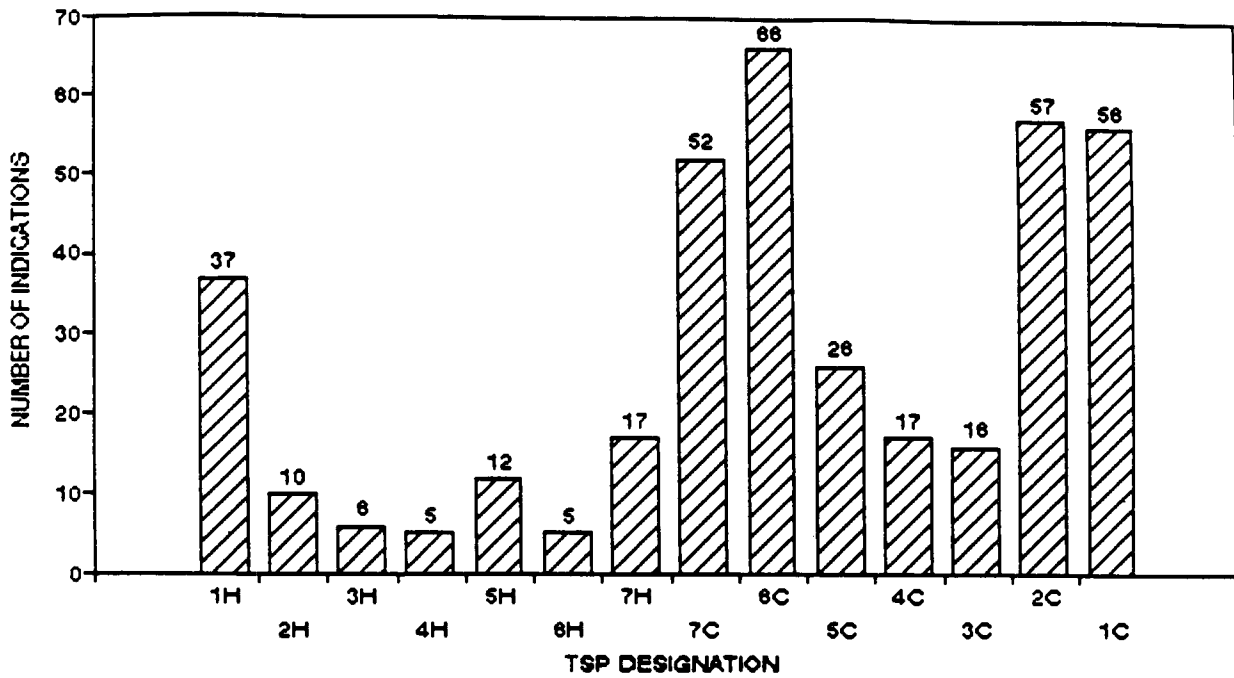
Figure 12-1. Frequency Distribution of TSP Indications by Location (1992 Inspection)
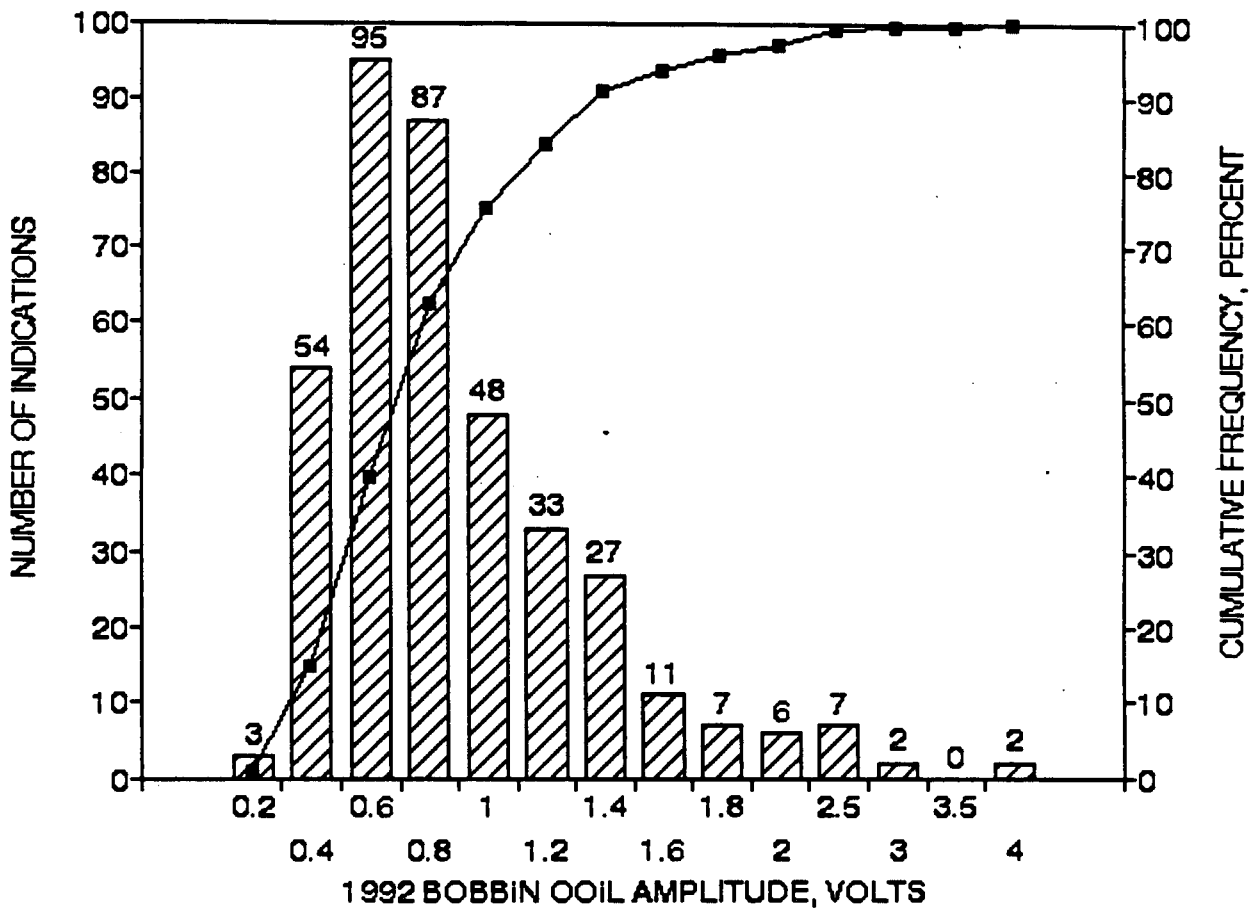
Figure 12-2. Frequency and Cumulative Percentage Distribution of Bobbin Amplitudes
(TSP Indications from the 1992 Inspection)
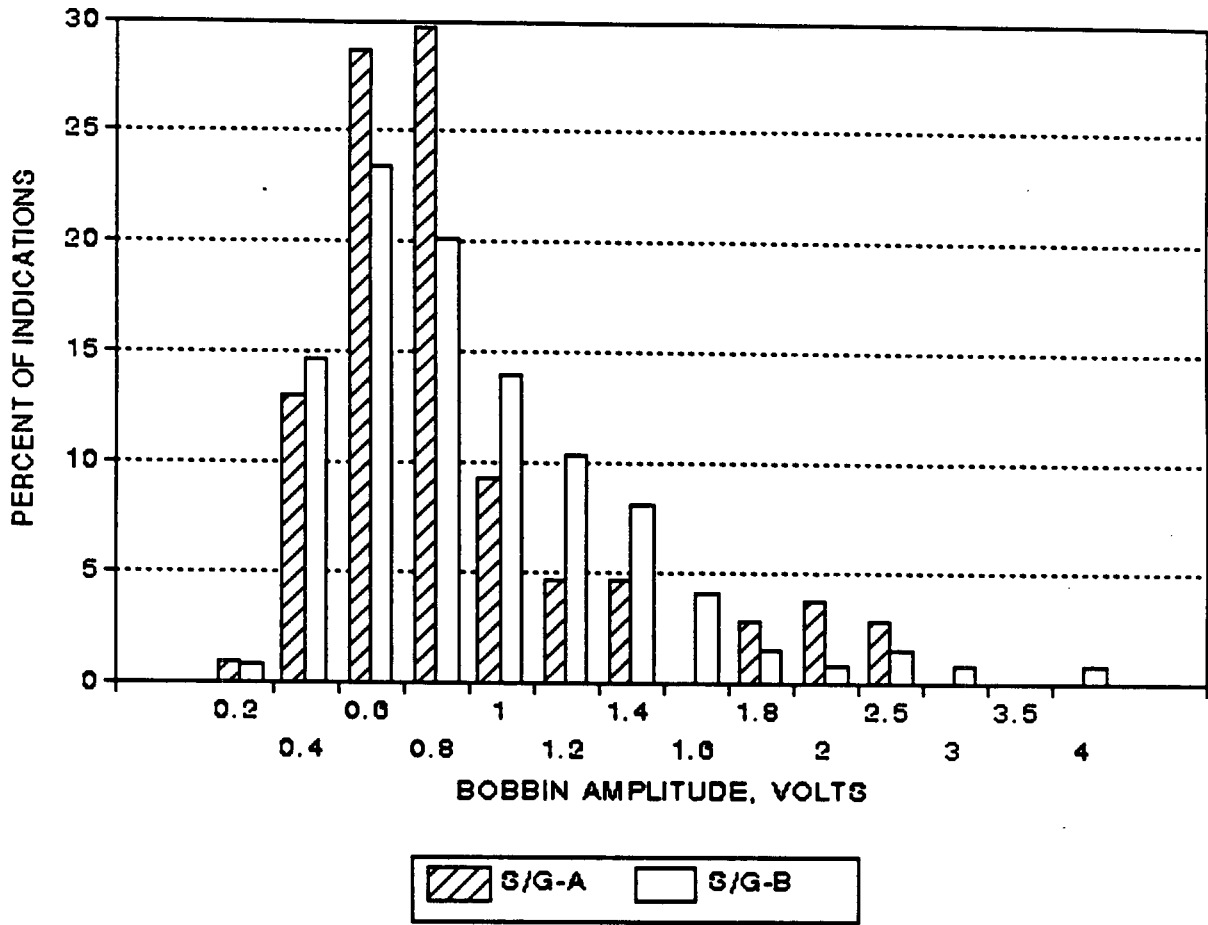
Figure 12-3. Histogram of Bobbin Voltage Distribution in each Steam Generator
(1992 Inspection)

KEWAUNEE TSP INDICATIONS
1991-92 VOLTAGE GROWTH DISTRIBUTION
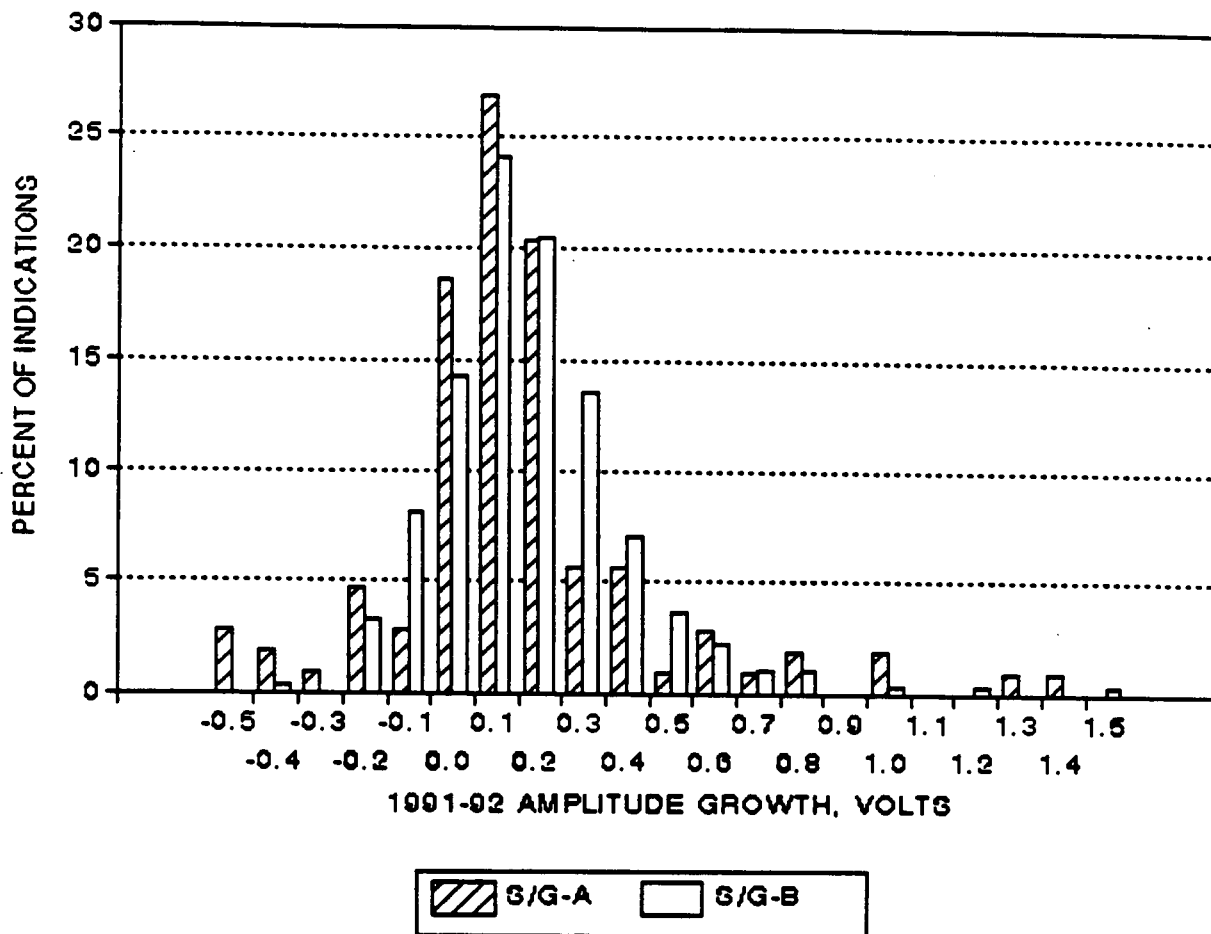
Figure 12-4. Percentage Distribution of Voltage Growths in each Steam Generator
(1991-92 Cycle)
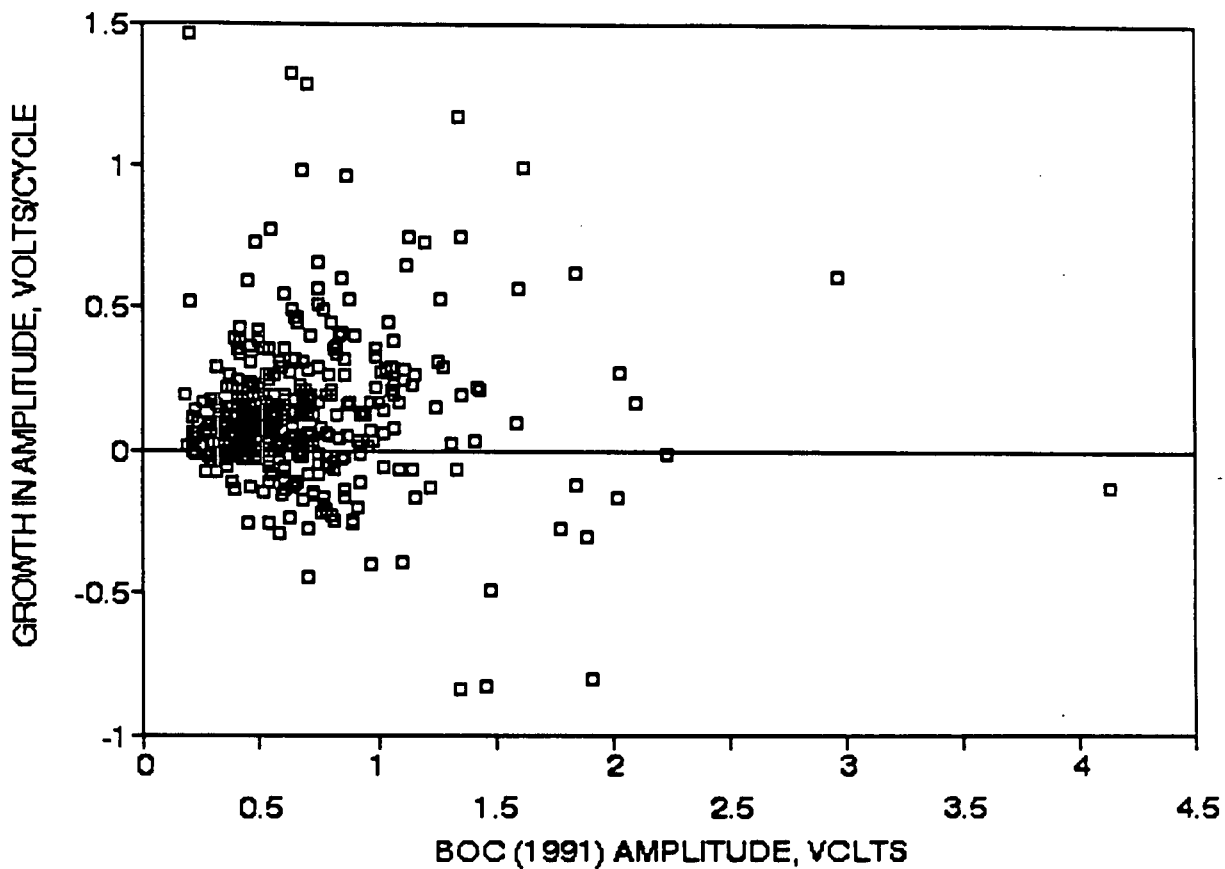
Figure 12-5. Growth in Bobbin Amplitudes During the 1991-92 Cycle

KEWAUNEE TSP INDICATIONS
1991-92 VOLTAGE GROWTH DISTRIBUTION
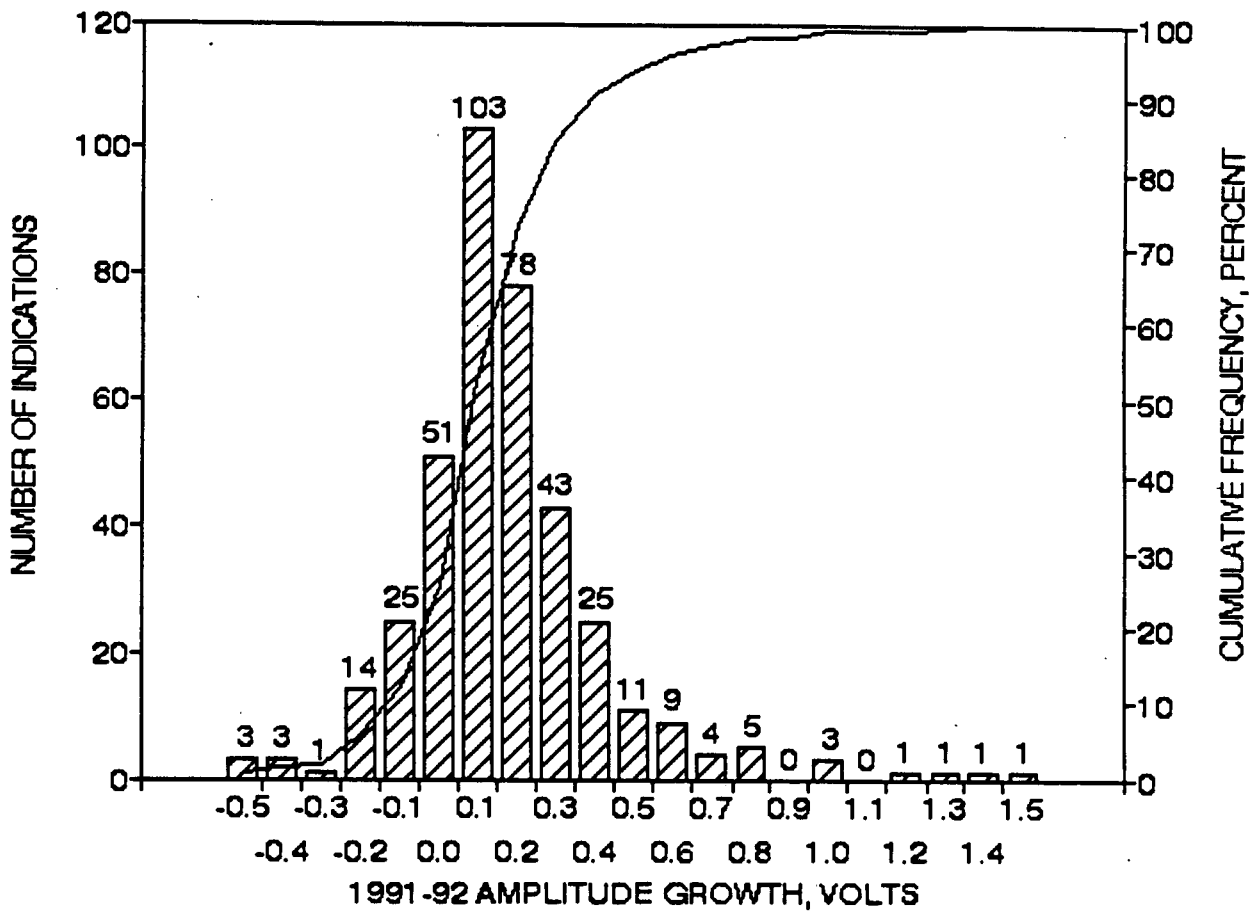
Figure 12-6. Histogram and Cumulative Probability Distribution of Voltage Growth
During the 1991-92 Cycle

KEWAUNEE TSP INDICATIONS
1991-92 VOLTAGE GROWTH RATES
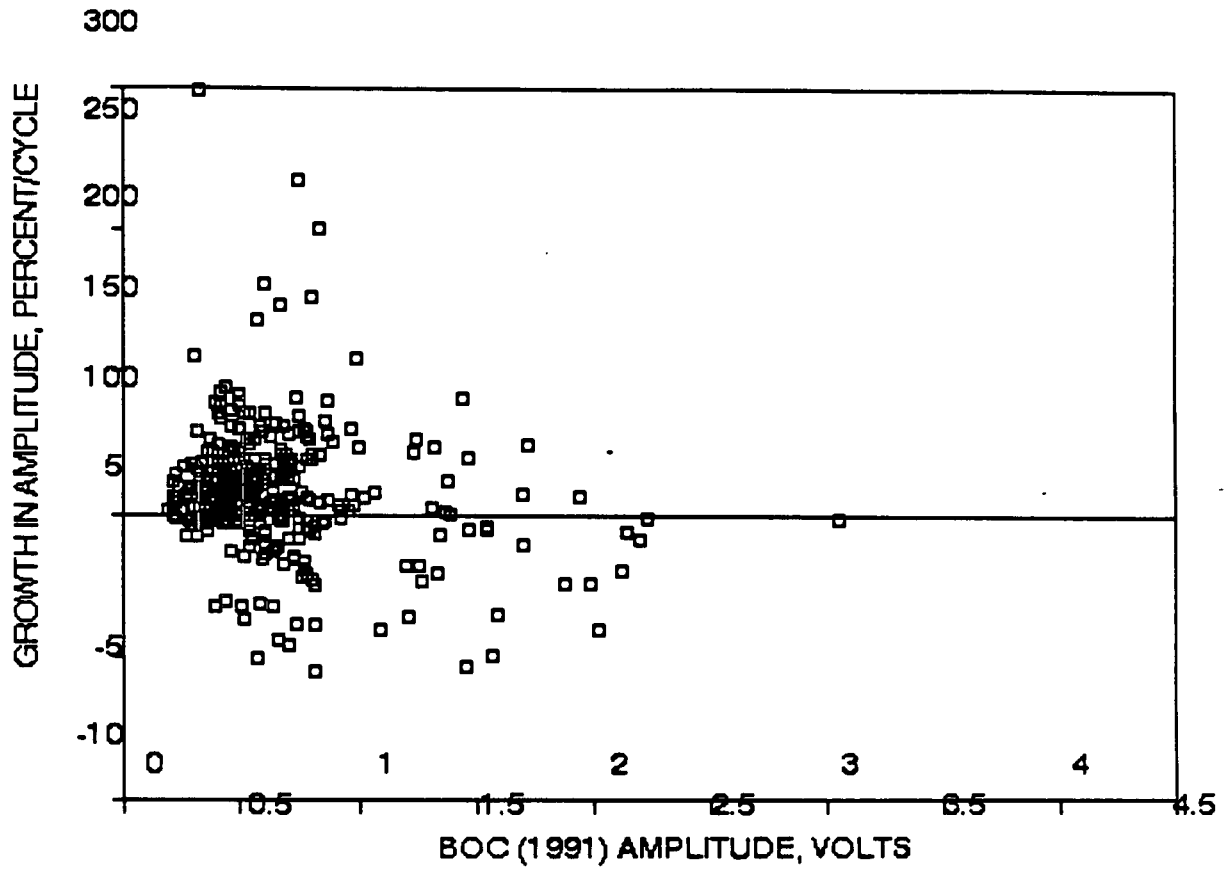
Figure 12-7. Percent Growth in Bobbin Amplitudes During the 1991-92 Cycle

KEWAUNEE TSP INDICATIONS
PROJECTED VOLTAGE GROWTH DISTRIBUTION
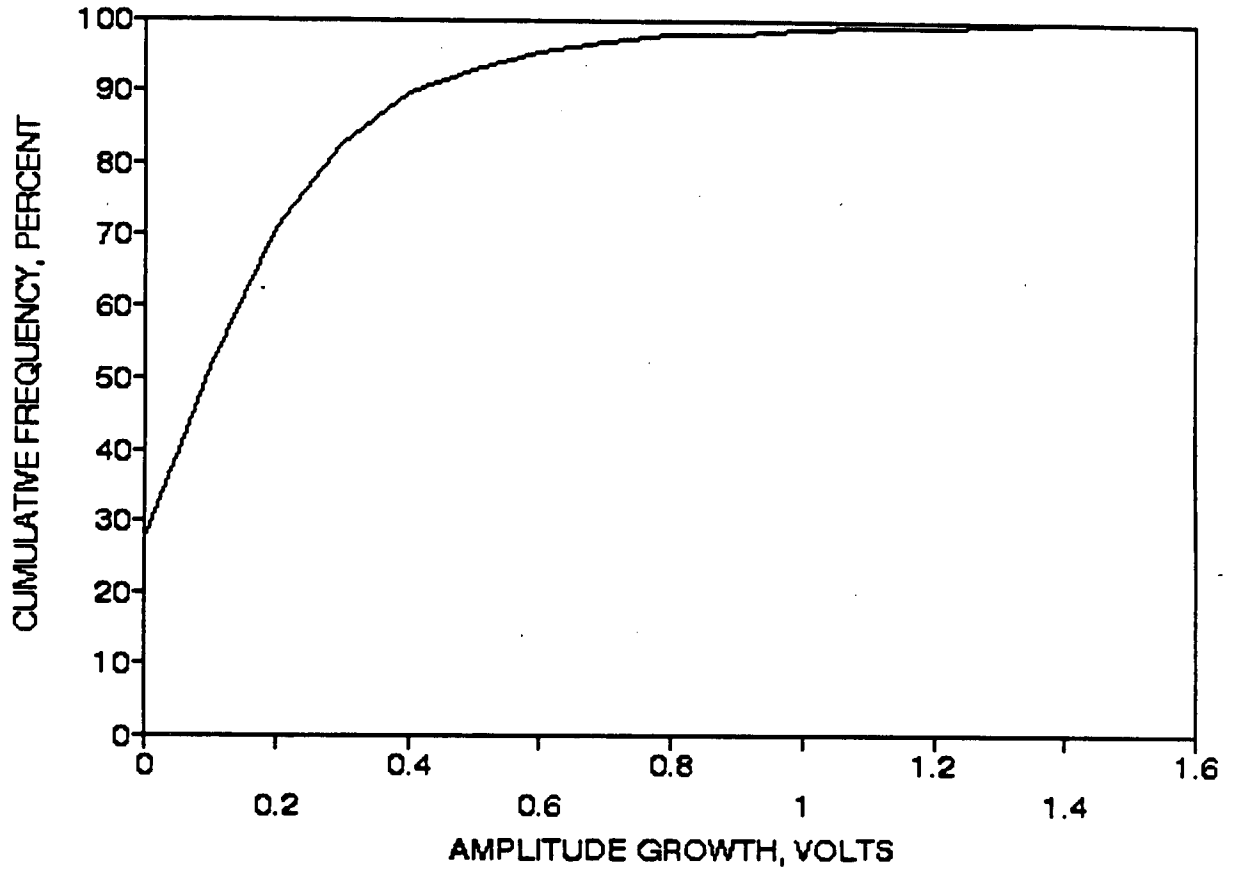
Figure 12-8. Cumulative Probability Distribution of Projected Voltage Growth
for Future Cycles
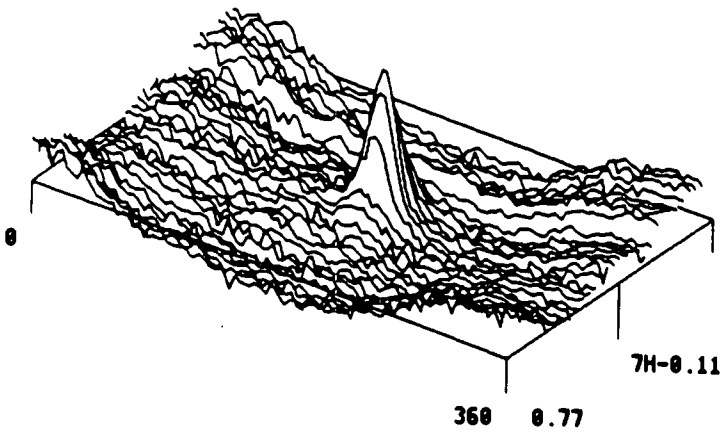
a) R8 C71, Location 7H
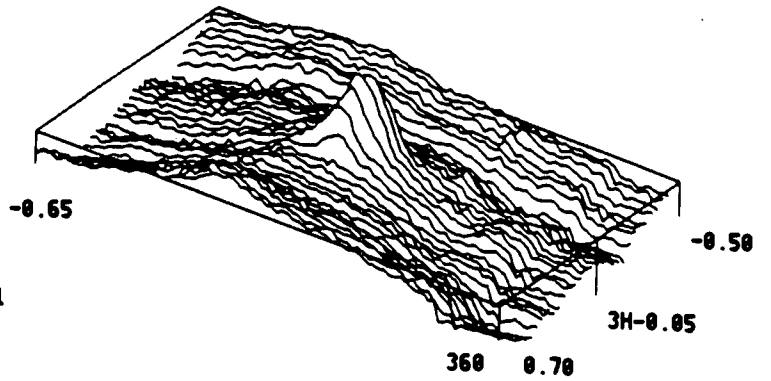
b) R43 C30, Location 3H
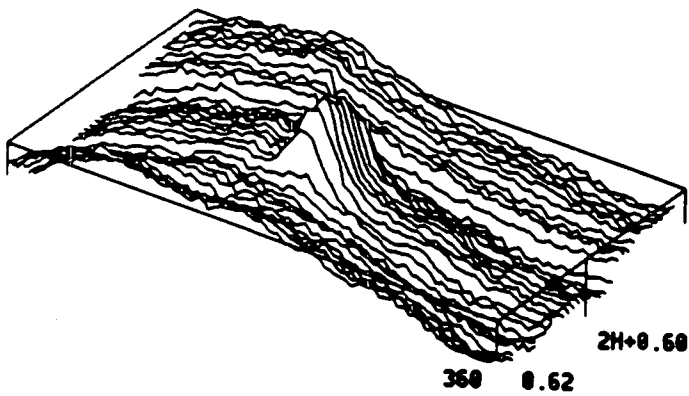
c) R42 C29, Location 2H
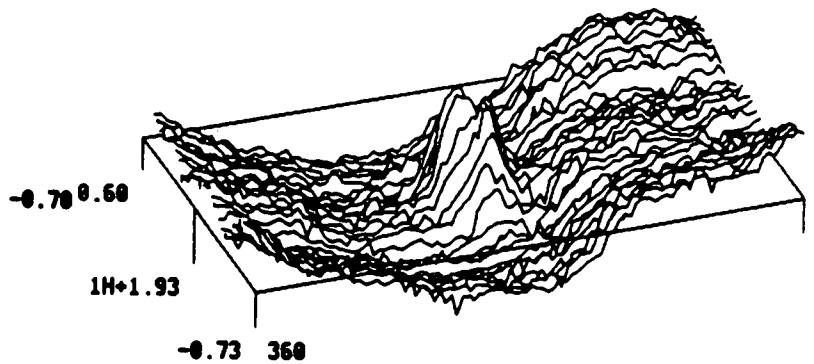
d) R5 C12, Location 1H

Figure 12-9. Example RPC Traces from Hot Leg Support Plate Locations in S/G-A
(1992 Inspection)
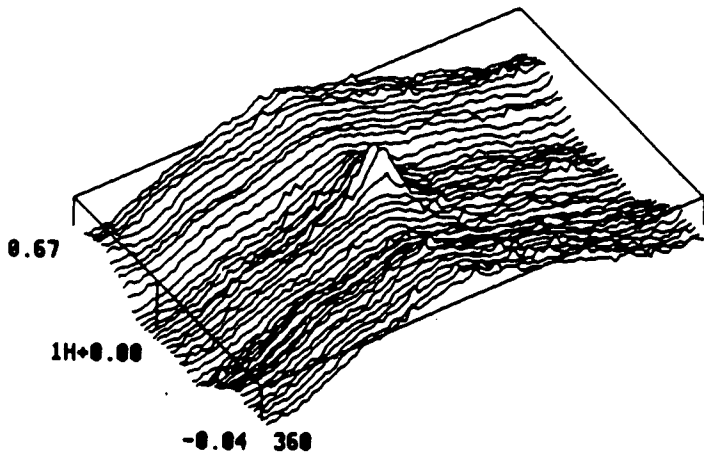
a) R35 C77, Location 1H
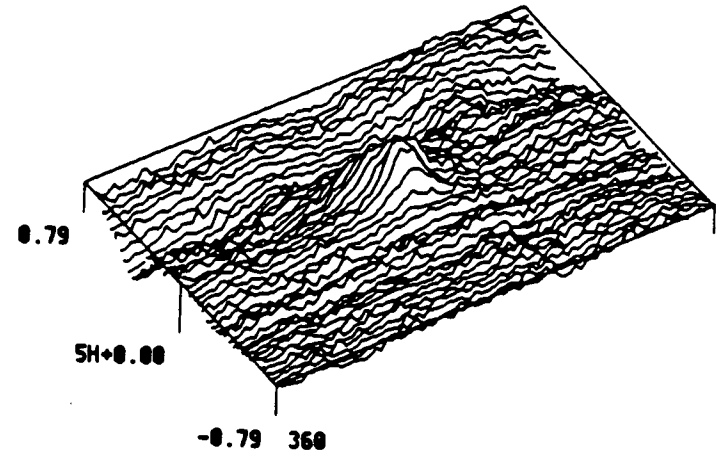
b) R32 C17, Location 5H
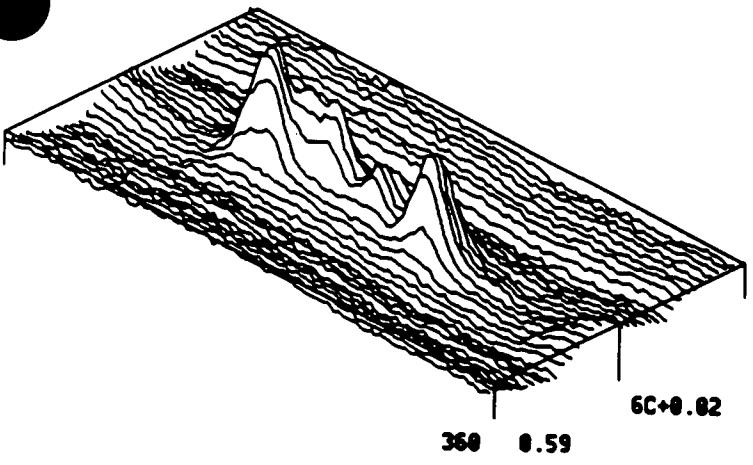
c) R25 C12, Location 6C
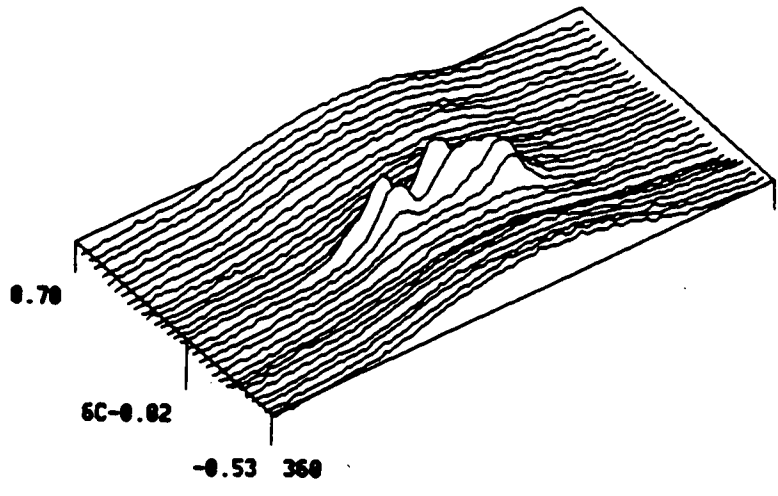
d) R24 C75, Location 6C

Figure 12-10. Example RPC Traces from Hot Leg Support Plate Locations in S/G-B
(1992 Inspection)

13.0 TUBE PLUGGING CRITERIA FOR ODSCC AT TSPS

This section integrates the results obtained from the prior sections to develop the technical basis for the Kewaunee tube plugging criteria for ODSCC at TSPs.

13.1 General Approach to Plugging Criteria

The general approach taken to develop the tube plugging criteria for the Kewaunee steam generators includes:

1) Specifying conservative burst correlations based on free span (uncovered) ODSCC under accident conditions to demonstrate structural integrity.

2) Conservatively assuming open crevice conditions to maximize leakage potential.

3) Satisfying the R.G. 1.121 structural guidelines for tube burst margins by establishing a conservative structural limit on voltage amplitude that assures 3 times normal operating pressure differential for tube burst capability.

4) Satisfying the USAR requirements for allowable leakage under accident conditions by demonstrating that the dose rate associated with potential leakage from tubes remaining in service is a small fraction of 10 CFR 100 limits.

5) Including considerations for crack growth and NDE uncertainties in both the structural assessment and leakage analysis.

6) Specifying a requirement to perform 100% bobbin coil inspection for all hot leg TSP intersections and all cold leg intersections down to the lowest cold leg TSP where ODSCC indications have been identified.

13.2 Test and Field Data Summary

The model boiler test data supporting the plugging criteria were discussed in Section 7. To clarify the application of the laboratory data, the laboratory burst pressure and leak rate data used for the criteria development are given in Table 8-1. Table 8-1 includes all burst data normalized to a flow stress of 75 ksi and leak rates adjusted to ΔP_{SLB} = 2335 psi. The as-measured model boiler data are given in Table 8-1. The leak rate adjustment procedure and adjusted values for the ΔP_{SLB} are also given in Appendix B. All bobbin voltages for model boiler specimens are measurements prior to removal of the TSPs with packed crevices and were obtained directly after removal of the tube from the model boiler. All bobbin voltages for pulled tubes are field data obtained prior to the tube pulling operations by laboratory re-evaluation of the field eddy current tapes. The re-evaluation of pulled tubes is performed to provide consistency of the bobbin voltages with the Appendix A guidelines.

Field data supporting the criteria are given in Table 8-1 as normalized for the burst (75 ksi flow stress) and leakage (2335 psi) correlations. Table 6-3 provides occurrences of operating leakage, and Figure 6-1 demonstrates pulled tube bobbin coil voltage as a function of depth. Only

the data of Table 8-1 are used In the voltage versus burst pressure and SLB leak rate correlations. The voltage/burst correlation is given in Section 8.3. The SLB leakage and probability of leakage correlations are developed in Sections 9.6 and 9.4, respectively. These data, together with the Kewaunee growth rates given in Sections 12.2 and 12.3, and the NDE uncertainties developed In Section 5.8, define the data base used to develop the Kewaunee tube plugging criteria for ODSCC at TSPs.

The actual in-service leakage from ODSCC at TSP intersections has been very limited on a world wide level. No leakage from ODSCC has been reported for U.S. plants with nondented tubes. This experience is consistent with a 40% depth repair policy, even if deeper defects cannot be precluded and may exist. Other countries following a policy similar to that currently used In the United States have reported only one leakage event. This event occurred at a Spanish plant and resulted from a pluggable indication that was missed during the previous outage.

In European countries with no repair criteria to prevent through-wall defects at TSP Intersections, reported leakage events are low. In Belgium, no leakage has been observed at Plant K-1 (where all 3 steam generators are known to have been affected by ODSCC for a number of years). A 1990 leakage event reported for plant E-4 cannot be quantitatively correlated with the two detected leakers at the TSP level because of three leaking tubes attributed to primary water stress corrosion cracking (PWSCC) in the expansion zones of roll transitions. In France, units with ODSCC at TSP intersections have been operating for a significant period without reported leakage.

This Insignificant in-service leakage from TSP ODSCC, even when no criteria are set to prevent through-wall defects, is likely to result from a combination of the following factors:

- The crack morphology is such that wall penetration is not readily achieved (relatively long cracks are prevented from leaking by a thin ligament on the ID side and, even after penetration, the ID length remains substantially less than the OD length). Also, unbroken ligaments between the crack faces often tend to restrict the leakage path.

- The small opening areas of through-wall cracks can get clogged easily by circulating corrosion products, Impurities, or precipitates.

- The crevice chemistry may block the leak path, either by corrosion product accumulation (leading to "packed crevices"), or by tube denting from the corroded TSP.

While this experience indicates that leakage from TSP ODSCC should not be an operational concern, consideration is given In Section 13.5 to tube leak-before-break (LBB) to deal with possible unanticipated leaks or cracks that might grow at a greater than expected rate and thus challenge the adequacy of the structural repair limit. Using the LBB methodology to reduce the probability of tube break to a negligible level also addresses the issue of a single large leaker (outside the predicated range) during postulated faulted loads.

13.3 Tube Plugging Criterion for Margins Against Tube Burst

The tube plugging criteria are developed to preclude free span tube burst if it is postulated that TSP displacement would occur under accident conditions. The plugging limits that satisfy R.G. 1.121 tube burst margins are developed in this section.

13.3.1 Voltage Limit for Structural Requirement

The recommended correlation between burst pressure and bobbin voltage, as adjusted for temperature and minimum material properties, is developed in Section 8.3. At the lower 95% prediction interval, a bobbin voltage of 3.5 volts corresponds to a differential pressure of $3\Delta P_{NO} = 4620$ psi. Similarly, a bobbin voltage of 40.8 volts corresponds to the SLB ΔP of 2335 psi. Therefore, the burst pressure capability requirements of Reg. Guide 1.121 are satisfied by a limit of 3.5 volts for the bobbin coil amplitude.

13.3.2 Allowance for NDE Uncertainty

The allowance for NDE uncertainties was developed in Section 5.8 as a net 14% uncertainty at 90% cumulative probability. The 14% is applied at the voltage limit requiring tube plugging. To support this uncertainty, voltage calibration standards normalized to the reference laboratory standard as well as probe wear standards will be utilized for Kewaunee SG inspections applying the plugging criteria of this report. In addition, Appendix A provides data collection and analysis guidelines to be implemented for consistent application of the plugging criteria.

Application of the probe wear standard per Appendix A leads to probe replacement if the voltage difference between a new probe and subsequent measurements for one or more of the four holes exceeds 15%. As developed in Section 5.5, the overall standard deviation on voltage measurements made prior to probe replacement is 7%, which corresponds to about 9% at 90% cumulative probability. The eddy current analyst variability was developed in Section 5.8 as 10% at 90% cumulative probability. A square-root-sum-of-the squares (SRSS) combination of the 9% and 10% contributions to the NDE uncertainty leads to a 14% uncertainty.

13.3.3 Allowance for Crack Growth

Voltage growth rates for the Kewaunee S/Gs are developed in Sections 12.2 and 12.3. Growth rates are defined in terms of percent growth per cycle and are applied at the voltage amplitude requiring tube plugging. The Kewaunee growth rates in percent per cycle are compared with other plant data in Figure 6-6. The percent growth rates for Kewaunee and other domestic plants are shown to decrease with increasing BOC (beginning of cycle) amplitude, while data from a European plant indicates percent growth may be essentially independent of amplitude. It is thus conservative to assume percentage growth is independent of BOC amplitude and to use overall average growth from Kewaunee operating experience for the growth rate allowance in the plugging limits.

From Section 12.3 and Table 12-2, the average percent growth rate for all TSP indications for the 1991-1992 operating cycle was 18%. This also bounds the average percent growth rates for the last five cycles, as shown in Table 12-4. For indications with BOC amplitudes below 0.75 volt, the average percent growth rate was 24%, whereas the average for BOC amplitudes ≥ 0.75 volt was 12% (Table 12-2). Use of the average percent growth rate of 18% for all indications is therefore noted as an additional conservatism in the development of the tube plugging criteria.

It was shown in Section 12.4 that an additional adjustment for TSP location is not required. However, the voltage growth rates from the 1991-1992 cycle cannot be used directly without correction for any potential future changes in operating cycle length. An appropriate scale factor for cycle duration was developed in Section 12.5. Allowing for potential increases in cycle

length from 292.9 EFPD for the 1991-1992 cycle to 305 EFPD in future cycles, the average growth per cycle could increase to about 19%.

The average growth rates for Kewaunee have been essentially constant and small (<20%) over the last five operating cycles. Similarly, the maximum growth of any indication has been small, at 1.1 to 1.5 volts. Likewise, the growth differences between support plates are small (Table 12.3). Consequently, an increase in the growth allowance for the repair limits above historical growth data should not be necessary. However, to allow for some variations in future cycles, the average growth is increased from the highest historical value of 19% to a value of 30% for establishing the repair limit. Average growth rates are considered to provide an adequate allowance for growth in satisfying R.G. 1.121 structural guidelines for burst pressure capability of three times normal operating pressure differential. At normal operating conditions, $3\Delta P_{NO}$ burst capability is inherently satisfied by the TSP constraints which preclude burst for indications within the TSP. Repair criteria are required to prevent burst and unacceptable leakage at SLB conditions such that the faulted condition structural limit of $1.4\Delta P_{SLB}$ (3275 psid) could be considered more appropriate for indications at TSPs than the $3\Delta P_{NO}$ structural limit. Allowances for growth uncertainties are addressed by demonstrating large margins against burst at SLB conditions as described in Section 13.4.

13.3.4   Tube Plugging Criterion

The structural voltage limit must be reduced by the allowances for crack growth and NDE uncertainty to obtain the voltage limit for tube plugging or repair consistent with R.G. 1.121 guidelines for margins against tube rupture. This can be expressed as:

$$V_{RL} + V_{NDE} + V_{CG} = V_{SL} \tag{13-1}$$

where: V_{RL} = voltage limit for tube repair or plugging,
V_{NDE} = NDE voltage measurement uncertainty,
V_{CG} = voltage growth rate per cycle, and
V_{SL} = voltage structural limit from the burst pressure versus bobbin coil voltage correlation.

The NDE voltage uncertainty and voltage growth rate terms are provided as a percentage of measured BC voltage (% V_{NDE} and % V_{CG}). Using V_{RL} as the maximum measured BC voltage to be left in service, V_{NDE} and V_{CG} are:

$$V_{NDE} = V_{RL} \times \%V_{NDE}/100, \text{ and}$$

$$V_{CG} = V_{RL} \times \%V_{CG}/100.$$

Using these expressions for V_{NDE} and V_{CG}, Eq. (13-1) can be rewritten as:

$$V_{RL} = V_{SL}/(1 + \%V_{NDE}/100 + \%V_{CG}/100) \tag{13-2}$$

Values for V_{SL}, $\%V_{NDE}$ and $\%V_{CG}$ are given in Sections 13.3.1 to 13.3.3 above and are V_{SL} = 3.5 volts, $\%V_{NDE}$ = 14 and $\%V_{CG}$ = 30. Substituting these values into Equation 13-2 gives

$$V_{RL} = V_{SL}/1.44 = 2.5 \text{ volts} \qquad (13\text{-}3)$$

An alternate summary of the development of the tube plugging or repair voltage limit is given in Table 13-1. The criterion for tube plugging is that the measured bobbin coil voltage exceed 2.5 volts. This criterion is applied independent of the bobbin coil indicated crack depth.

13.4 Projected EOC Voltages

The maximum EOC voltage for IPC or depth based repair limits can result from: (1) indications left in service through IPC or APC application with BOC voltages less than the repair limit, (2) from bobbin indications found to have depths less than the repair limits or to be RPC NDD at the prior inspection, or (3) from new indications which were bobbin NDD at the prior inspection. The latter two sources of indications are independent of IPC/APC implementation, as they result from current inspection practices based on 50% depth repair limits. In fact, the IPC/APC application is more conservative than standard practice by requiring all bobbin flaw indications attributable to ODSCC >2.5 volts to be repaired, independent of depth or RPC confirmation. This section compares the three above sources of EOC indications to demonstrate that an IPC/APC repair limit of 1.0 to 2.5 volts results in lower comparable EOC voltages than found for sources (2) and (3) above, which are applicable to current inspections and IPC/APC applications. Use of Kewaunee inspection results from the last cycle are used to demonstrate this point. It can be noted, however, that sources (2) and (3) which are not detected by both bobbin and RPC probes would not contribute to EOC SLB leakage. This results as the indications not detected by both probes have a very low likelihood of progressing to a throughwall indication in one operating cycle. It should also be emphasized that bobbin indications ≤2.5 volts, even if confirmed by RPC as assumed for SLB leakage analyses, contribute negligibly to SLB leakage as shown in Section 13.6.

This section develops maximum EOC bobbin voltages using both deterministic and Monte Carlo analyses, based on BOC 1.0 to 2.5 volt indications left in service by APC applications. These voltages are compared to the bobbin voltages found at the last Kewaunee inspection which are typical EOC voltages for an outage following application of 50% depth repair limits. As a demonstration for projecting BOC voltage distributions to EOC distributions for use in SLB leakage analyses, example results are presented assuming an APC repair limit of 2.5 volts had been implemented for Cycle 18 operation. Upon implementation of the APC for Kewaunee, SLB leak rates are expected to be based on deterministic methods (Section 13.6), unless an unexpectedly large number (~1000) of indications are found at EOC-18. In the latter case, Monte Carlo methods as demonstrated in this section would be used to develop the EOC voltage distribution for the leakage calculation.

Deterministic and Monte Carlo Projections of Maximum EOC Voltages

To estimate the EOC voltage for an indication left in service at the IPC/APC repair limit of 1.0 /2.5 volts, deterministic and Monte Carlo analyses were performed. Allowances for NDE uncertainty and growth based on the NDE uncertainty distribution (standard deviation of 11% with 25% maximum) of Section 5.8 and voltage growth distribution (Figure 12-8) are added to the BOC voltage to project the EOC voltage. For deterministic analyses, the distribution values at a specified cumulative probability are used to obtain a specific EOC voltage. For Monte Carlo analyses, the distributions are repeatedly (10^5 samples in present analyses) sampled to develop a cumulative probability for EOC voltage. For an assumed number of BOC indications, an EOC

maximum voltage from Monte Carlo analyses can be defined as the voltage value for which the tail of the distribution integrates to one tube (i.e., cumulative probability of (N-1)/N for N Indications). To define a maximum EOC voltage for the Monte Carlo analyses, an assumed 300 Indications leads to a 99.7% cumulative probability for the maximum EOC voltage.

Table 13-2 summarizes the projected EOC voltages resulting from the BOC IPC/APC limit of 1.0/2.5 volts. The deterministic assessments include growth and NDE allowances at +90% cumulative probability for comparisons with $3\Delta P_{NO}$ tube burst capability and at +99% for comparisons with SLB burst requirements. The deterministic assessments for BOC 1.0/2.5 volts Indicate EOC voltages of 1.56/3.27 and 2.35/4.23 volts at +90% and +99% cumulative probabilities. The Monte Carlo results at 99.7% cumulative probability for an assumed 300 indications left Inservice at 1.0/2.5 volts yield an estimated maximum EOC voltage of 2.47/4.06 volts (within ~5% of the +99% deterministic estimate). Thus, the maximum EOC voltage for Indications left In service by IPC/APC implementation is expected to be between about 1.56 and 2.47 volts for an IPC repair limit of >1.0 volt and between 3.27 and 4.06 volts for an APC repair limit of >2.5 volts and statistically is dependent on the number of indications left in service. From Table 13-2 it Is seen that a 2.3 volt BOC signal yields 3.98 volts at EOC for +99% confidence. This voltage compares to 4.0 volts found at the last inspection with a 50% depth repair limit.

Table 13-3 summarizes the Monte Carlo estimated EOC volts as a function of cumulative probability and assumed BOC voltage amplitude. It can be noted that the 3.5 volts corresponding to $3\Delta P_{NO}$ burst capability at -95% prediction interval is not reached in 10^5 samples for BOC = 1.0 to 1.5 volt, reached at 99.7% probability for BOC = 2.0 volts, and reached at 97% probability for BOC = 2.5 volts. Thus, based on the historical growth rates for Kewaunee, a repair limit of about 1.8 volts precludes reaching the $3\Delta P_{NO}$ burst pressure at EOC conditions and ~97% cumulative probability is required to reach $3\Delta P_{NO}$ for the APC repair limit of 2.5 volts.

EOC Voltages Resulting from Current 50% Depth Repair Limit

Current Inspection practice for application of the 50% depth repair limit Is to Identify potential indications by bobbin Inspection, RPC inspect distorted indications and repair bobbin indications >50% depth and RPC confirmed distorted indications. This practice results as bobbin coil depth Indications are often distorted such that reliable depth estimates are not feasible. Since both bobbin and RPC detectability are high for indications >50% depth, this practice is consistent with the 50% repair basis. The RPC confirmation permits conservative bobbin calling criteria for distorted indications and helps to eliminate false bobbin calls. In some cases, a subsequent inspection leads to RPC confirmation of an indication that was RPC NDD at the prior inspection as well as growth of indications to >50% depth. The bobbin voltage at the time of RPC confirmation can be used as Indicative of maximum EOC voltages based on 50% depth criteria for comparison with the above projected maximum voltages based on APC implementation.

The bobbin data re-evaluation for growth rates was conducted to Appendix A analysis guidelines, such that voltages are typical of an inspection implementing an IPC/APC. There were 436 bobbin potential Indications (PIs) Identified in the 1992 Inspection. Of these Indications, 56 were RPC confirmed In 1992 cr had bobbin depths >50%. Only 3 of the 1992 bebbin PIs were NDD In 1991. Table 13-4 summarizes the largest bobbin Indications grouped as 1992 RPC confirmed or had bobbin depths >50%, 1992 RPC NDD or had bobbin depths <50% and new

Indications (Bobbin NDD in 1991). The largest of the RPC confirmed indications ranged up to 4.00 volts. These amplitudes are typical of recent SG inspections which occasionally show indications above 3 volts (2 found in Kewaunee inspection). The three new bobbin indications have a maximum of 0.73 volts. The largest bobbin PIs not confirmed by RPC or having bobbin depths < 50% show amplitudes ranging up to 2.61 volts. A fraction of this group of indications can be expected to become RPC indications at the next inspection and result is some of the larger amplitudes at the next inspection.

The voltage range up to 4.0 volts found in the 1992 inspection followed application of 50% depth repair criteria at the prior outage. These voltages are essentially the same as the range of 3.27 to 4.06 projected at EOC-18 following implementation of a 2.5 volt APC repair limit, and significantly exceed the 1.56 to 2.47 volts projected for a 1.0 volt IPC repair limit. Thus even the APC repair limit of 2.5 volts does not significantly increase the limiting indication compared to the 50% depth limit.

In summary, the Kewaunee maximum EOC bobbin voltages for indications left in service by an APC repair limit of > 2.5 volts are expected to range up to 4.06 volts. Based on prior Kewaunee inspection results, the APC repair limit of 2.5 volts results in approximately equal EOC voltages and limiting tube integrity margins as the 50% depth criteria.

Example of Monte Carlo EOC Voltage Distribution

Monte Carlo analyses were performed to project the estimated EOC-18 voltage distribution assuming indications found in the 1992 inspection below the APC repair limit of 2.5 volts were left in service. This analysis is provided as a demonstration of Monte Carlo projection results based on a BOC distribution of indications. The BOC-18 distribution, growth rate distribution and projected EOC-18 distribution are shown in Figure 13-1. The EOC-18 results for the 270 indications <2.5 volts show an estimated EOC-18 maximum voltage of about 2.8 volts. The maximum EOC voltage is based on evaluating the Monte Carlo cumulative probability distribution at 269/270 = 0.996, which is equivalent to integrating the tail of the distribution to one indication. If the same distributions were applied to a larger number of indications, the projected maximum voltage would increase. These results indicate that, statistically, a small sample of BOC voltages up to 2.5 volts (max. BOC in Figure 13-1) can result in a smaller EOC maximum voltage of about 2.8 volts than a larger sample (500 indications) of <2.5 volt indications which project to a maximum EOC voltage of about 3.0 volts.

The EOC distribution results of Figure 13-1 show about average growth per cycle for each indication. The maximum voltage has a probability of less than one tube to have an EOC voltage up to about 4.4 volts. As noted, the 2.8 volt maximum of Figure 13-1 results from defining the maximum by integrating the tail of the Monte Carlo distribution to one tube. From Table 13-3 for BOC indications of up to 2.5 volts, it would require about 300 indications (based on 99.7% cumulative probability) at 2.5 volts to expect a single EOC voltage of 4.06 volts. These results indicate that even if the full APC repair limit of 2.5 volts were implemented, the maximum EOC voltages would be within <0.5 volt of the 4.0 volt indication found in the 1992 inspection (Table 13-4) following the application of the 50% depth repair limit.

13.5 Tube Burst Margin Assessment

Application of the APC repair limit developed in Section 13.3 would result in meeting R.G. 1.121 criteria at EOC conditions. The objective of an IPC repair limit is to establish additional margins beyond that included in the equivalent APC repair limit. This section identifies the burst margins against $3\Delta P_{NO}$ and ΔP_{SLB} for BOC voltages of 1.0, 1.5, 2.0, and 2.5.

The limiting R.G. 1.121 criterion for Kewaunee is to satisfy the $3\Delta P_{NO}$ tube burst margin requirement. Thus additional margins can be expressed as burst pressure margin ratios relative to $3\Delta P_{NO}$. That is, the ratios of BOC and EOC burst pressures to $3\Delta P_{NO}$. The burst margin ratios are developed adding +90% cumulative probability on growth and NDE uncertainties to the BOC voltage and evaluating the resulting voltages at the lower 95% prediction interval of the burst/voltage correlation (Figure 8-2 for tube burst capability.) These uncertainty levels provide that only a few, if any, indications would exceed $3\Delta P_{NO}$ at EOC conditions. It is necessary to establish higher confidence levels to prevent tube burst at ΔP_{SLB}. The burst margin ratios relative to ΔP_{SLB} are therefore developed applying +99% cumulative probability on growth and NDE uncertainties to the BOC voltage and the lower 99% prediction interval of the burst/voltage correlation for tube burst capability.

Table 13-5 summarizes the tube burst margin assessment relative to $3\Delta P_{NO}$ for Kewaunee. At +90% cumulative probability on allowances for growth and NDE uncertainties, the projected EOC voltages range from 1.56 for BOC = 1.0 volt to 3.27 for BOC = 2.5 volts. The corresponding burst pressure margin ratios range from 1.16 for BOC = 1.0 volt to 1.01 for BOC = 2.5 volts. Thus, an IPC of 1.0 volt provides about a 15% or 680 psi higher EOC burst pressure margin compared to the APC repair limit of 2.5 volts.

The tube burst margin ratio assessment relative to ΔP_{SLB} is given in Table 13-6 for 1.0 to 2.5 volt BOC indications and for the deterministically projected EOC voltage range of 2.35 to 4.23 volts. The corresponding EOC margin ratios are found to range from 1.92 to 1.69 for Kewaunee. This demonstrates substantial margin against burst at SLB for EOC-18 conditions. As a supplemental demonstration of burst margins, the probability of tube burst at ΔP_{SLB} (2335 psi) was calculated for BOC indications up to 2.5 volts using Monte Carlo methods and found to be about $<10^{-5}$ as given in Table 13-3. Thus both the deterministic and probabilistic analyses show that large margins against burst at SLB conditions are provided by the Kewaunee IPC and APC.

The above assessment shows that the Kewaunee APC repair limit of >2.5 bobbin coil volts provides significant margins against R.G. 1.121 structural criteria for tube burst. These assessments utilized the voltage/burst correlation of Figure 8-2.

13.6 SLB Leak Rate Analyses

The APC require that potential leakage under SLB conditions at EOC be less than 9.1 gpm. For an IPC, the allowable SLB leakage is 1.0 gpm. This section provides the results of the leak rate analyses to demonstrate the methodology for satisfying this requirement for the Kewaunee IPC and APC repair limits of 1.0 and 2.5 volts. Two methods of analysis are described for evaluating potential EOC SLB leakage for Kewaunee. If, as expected, the number of indications left in

service is less than about a thousand indications in the limiting SG, a deterministic analysis can be applied. If a larger number of indications are found, a Monte Carlo analysis would be applied.

As described in Section 9.3.5, a leakage threshold of 2.0 volt is applied for Kewaunee. Below 2.0 volt, the probability of leakage is negligible (~2%) and leak rates are also small. All EOC indications above 1.0 volt are included in the leakage analysis. The threshold for significant leakage ($\geq 10^{-3}$ gpm per indication) is expected to be about 6 volts (Section 9.3). The SLB leak rate per indication is obtained as the probability of leakage from Figure 9-7 times the leak rate per leaking indication of Figure 9-8. For the low voltage range (<3 volts) of interest for APC applications, the leak rate correlation of Figure 9-8 was conservatively developed to bound the SLB leak rate. Guidelines for the SLB analyses are developed in Section 10.4. The analyses are performed for a SLB SG tube pressure differential of 2335 psi.

The reference SLB leak rate analyses are deterministic analyses performed at a +95% confidence level for EOC voltages >1.0 volt. The BOC voltages are increased by allowances for NDE uncertainties and growth at +95% cumulative probability to obtain corresponding EOC voltages. At the EOC voltage, the probability of leakage (P.O.L.) of Figure 9-7 is evaluated at the +95% level. The SLB leak rate of Figure 9-8 is evaluated at the +95% confidence level. The total SLB leak rate is obtained by summing the P.O.L. times the leak rate per indication over all EOC indications. This methodology conservatively assumes all indications grow at the +95% level and is generally more applicable to a single tube estimate rather than a sum over all indications. Analyses are given in this section for BOC indications in the range of 1.0 to 2.5 volts to bound the number of indications that can be left in service by IPC or APC implementation using deterministic analyses.

If a large number of indications are found at EOC-18, Monte Carlo analyses can be applied by two alternate methods to reduce the conservatism of the deterministic analyses. The first method is to use Monte Carlo to develop an EOC voltage distribution for which leakage is evaluated at each EOC voltage by applying P.O.L. and leak rates at the +95% level. The second and most accurate method is to apply Monte Carlo analyses for the leak rate calculation. With the Monte Carlo methods, many random samples (10^5 to 10^6) are made for each BOC voltage level. The NDE uncertainty distribution (standard deviation of 11% with maximum of 25% per Section 5.8) and projected growth distribution (Figure 12-8) are sampled to obtain an EOC voltage sample. The P.O.L. and leak rate distributions are randomly sampled for each EOC voltage sample. The Monte Carlo analyses lead to EOC voltage and SLB leak rate cumulative probability distributions. With the use of P.O.L. distributions, the Monte Carlo methods for calculating the cumulative probability distribution for leakage differ from prior APC reports such as WCAP-12871. For analyses of a single indication, the cumulative probability of no leakage is calculated as 1.0 minus the sum of all leakage probability samples divided by the total number of samples. That is, 1.0 minus the average probability of leakage. The cumulative probability for leakage >0.0 starts at the zero leakage probability and increases based on the leak rates obtained by sampling the leak rate distribution. For Monte Carlo analyses of a distribution, the random samples of P.O.L and leak rate are multiplied to obtain the effective leak rate per sample.

The EOC-18 voltage distribution of Figure 13-1 was obtained using Monte Carlo methods and the SLB leak rate is obtained in this section for this distribution. Monte Carlo analyses are also used in this section to estimate the cumulative probability associated with leak rates obtained by deterministic analyses.

13 - 9

SLB Leak Rate Per Indication

Deterministic analyses for the SLB leak rate per BOC 1.0 and 2.5 volt indications are given in Table 13-7. As described above, the reference SLB leak rate is based on evaluating the leak rate correlations at the +95% confidence level on the mean regression fit. The resulting leak rate is 0.00032 and 0.0023 gpm per 1.0 and 2.5 volt indication left in service, respectively. Thus, for a 1.0 gpm leakage limit, approximately 3125 and 435 indications per SG at 1.0 and 2.5 volts, respectively, could be left in service per SG applying this conservative analysis procedure. For a BOC = 2.3 volts indication, the potential leak rate is 0.0017 gpm per indication which corresponds to an acceptable 585 indications for a 1.0 gpm allowable limit. The reference leak rate calculation for a 1.0 volt BOC indication results in a 1.77 EOC voltage at 95% cumulative probability. This is less than the proposed 2.0 volt threshold for SLB leakage. The negligible leak rate calculated supports insignificant leakage for EOC voltages <2.0 volts. For a BOC = 2.5 volt indication, the leak rate of 0.0023 gpm/indication corresponds to about 98% cumulative probability from Monte Carlo analyses, such that only about 2% of the 2.5 volt indications would have this leak rate. The principal difference is that the deterministic analyses assume all indications simultaneously have +95% P.O.L. and leak rate while the Monte Carlo analyses independently sample these data. For the 9.1 gpm allowable SLB leak rate for APC applications, 3950 indications per SG at BOC 2.5 volts would meet the allowable leak rate. Based on these results, SLB leakage is not expected to represent a constraint on IPC or APC implementation at Kewaunee.

Even more conservative analyses are given in Table 13-7 to demonstrate that SLB leakage is not a concern for APC implementation at Kewaunee. Deterministic analyses are given for BOC 1.0 and 2.5 volt indications at the +95% and +99% prediction intervals. For these analyses, P.O.L. is evaluated at the +95% (as for reference case) and +99% bounds. The SLB leak rates are evaluated at the additionally conservative prediction interval bounds rather than the confidence on the mean regression line used for the reference analyses. These analyses provide upper bound estimates on the leak rate from the most limiting single indication. However, even if it is postulated that all BOC = 1.0 volt indications leak at the upper bound rate, the per indication leak rates of 0.00062 and 0.013 gpm permit 1600 (+95%) and 77 (+99%) indications per gpm of leakage. It is seen from the Monte Carlo results of Table 13-7 that only about 0.3% and 0.02% of the tubes would leak at the +95% and +99% estimates. While these levels of conservatism are not appropriate for comparing with the 1.0 gpm IPC allowable SLB leakage limit, it is clear that total SLB leakage from all indications would not approach leak rate levels of greater than 350 gpm associated with a single tube rupture (guillotine break). Conservatively postulating all BOC = 1.0 volt indications (rather than expected 0.3% and 0.02%) leak at the +95% and +99% prediction intervals, the number of indications left in service for 350 gpm would be about 560,000 and 22,050, respectively. Even at an assumed APC repair limit of 2.5 volts and all indications (rather than expected 0.1%) leaking at the +99% prediction interval, 6600 indications per SG at 2.5 BOC volts in service would be required to reach leakage associated with a guillotine rupture. Consequently, cumulative leakage from TSP indications approaching levels associated with a tube rupture is extremely unlikely.

The Monte Carlo leak rates per BOC indication are summarized in Table 13-3 at various cumulative probability levels. The cumulative probability per indication of zero leakage is also given in Table 13-3. For the 2.5 volts APC repair limit, there is a 93.2% probability of zero leakage or only 6.8% of the indications would have leakage greater than zero. These results represent an average of the P.O.L. distribution of Figure 9-7 over the distribution of potential EOC voltages for a given BOC voltage. For an IPC repair limit of 1.0 volts, there is only a 1.1%

probability that an indication at EOC would leak. If the P.O.L. curve was developed for leakage above a minimum level such as about 10^{-2} to 10^{-3} gpm, the probability of leakage above this level would be considerably smaller than obtained for the zero leakage threshold.

SLB Leak Rate for Distribution of EOC Voltages

As noted previously, the use of Monte Carlo analyses to develop an EOC voltage distribution can be used for SLB leakage rather than the bounding deterministic values. Figure 13-1 (upper figure) shows the 270 indications below the APC repair limit of 2.5 volts found in the more limiting SG, SG-B, during the 1992 inspection. Figure 13-1 (lower figure) shows the Monte Carlo EOC distribution for these 270 indications. The SLB leak rate can be calculated by applying P.O.L. and leak rate at the +95% confidence levels to the EOC indications of Figure 13-1. This leads to a cumulative SLB leak rate of 0.029 gpm for the 270 indications. If the deterministic reference method at +95% is also used to calculate EOC voltages from the upper figures of Figure 13-1, the estimated SLB leak rate would be 0.086 gpm as compared to the 0.029 gpm using Monte Carlo EOC voltages. This comparison demonstrates the conservatism in the reference, completely deterministic analyses. Applying complete Monte Carlo total leak analyses to the BOC distribution would yield even lower leak rates. The 0.029 gpm leak rate corresponds to 96% cumulative probability by Monte Carlo analysis.

Overall, it is concluded that the 2.5 volt APC repair limit with voltage growth rates comparable to that found last cycle at Kewaunee will not result in SLB leak rates exceeding 9.1 gpm. Even if >3900 indications per steam generator are found, the reference deterministic methods would result in <9.1 gpm leakage.

13.7   Operating Leakage Limit

R.G. 1.121 acceptance criteria for establishing operating leakage limits are based on leak before break (LBB) consideration such that plant shutdown is initiated if the leakage associated with the longest permissible crack is exceeded. The longest permissible crack is the length that provides a factor of safety of 3 against bursting at normal operating pressure differential. As previously discussed, a voltage amplitude of 3.5 volts for typical ODSCC cracks corresponds to meeting this tube burst requirement at the lower 95% confidence level on the burst correlation. Alternate crack morphologies could correspond to 3.5 volts so that a unique crack length is not defined by the burst pressure to voltage correlation. Consequently, typical burst pressure versus through wall crack length correlations are used below to define the "longest permissible crack" for evaluating operating leakage limits.

The CRACKFLO leakage model has been developed for single axial cracks and compared with leak rate test results from pulled tube and laboratory specimens. Fatigue crack and SCC leakage data have been used to compare predicted and measured leak rates. Generally good agreement is obtained between calculation and measurement with the spread of the data being somewhat greater for SCC cracks than for fatigue cracks. Figure 13-2 shows normal operation leak rates including uncertainties as a function of crack length.

The through wall crack lengths resulting in tube burst at 3 times normal operating pressure differentials (4620 psi) and SLB conditions (2335 psi) are about [   ]a, respectively, as shown in Figure 13-3. Nominal leakage at normal operating conditions for these crack lengths would range from about [

]a would cause undue restrictions on plant operation and result in unnecessary plant outages, radiation exposure and cost of repair. In addition, it is not feasible to satisfy LBB for all tubes by reducing the leak rate limit. Crevice deposits, presence of small ligaments and irregular fracture faces can, in some cases, reduce leak rates such that LBB cannot be satisfied for all tubes by lowering leak rate limits.

An operating leak rate of 150 gpd (~0.1 gpm) will be implemented in conjunction with application of the tube plugging criteria. As shown in Figure 13-2, this leakage limit provides for detection of [

]a. Thus, the 150 gpd limit provides for plant shutdown prior to reaching critical crack lengths for SLB conditions at leak rates less than a -95% confidence level and for 3 times normal operating pressure differentials at less than nominal leak rates.

The tube plugging limits coupled with 100% inspection at affected TSP locations provide the principal protection against tube rupture. The 150 gpd leakage limit provides further protection against tube rupture. In addition, the 150 gpd limit provides the capability for detecting a rogue crack that might grow at much greater than expected rates and thus provides additional protection against exceeding SLB leakage limits.

13.8 Supplemental Requirements for Implementation of the Plugging Criteria

Upon implementation of the tube plugging criterion and associated limits on operating SLB leakage, additional requirements as noted in this section are to be implemented.

A 100% bebbin coil inspection is required for all hot leg TSP intersections and for cold leg intersections down to at least the lowest TSP with ODSCC indications. This requirement provides confidence that all ODSCC indications which could contribute to SLB leakage are identified for the leak rate evaluation. If <100% inspection is performed below cold leg TSP intersections with previously identified ODSCC indications, and indications at TSPs are identified, the inspection must be extended to 100% of the affected TSP or the 50% depth limit for tube plugging must be applied for all indications.

An RPC inspection is required to establish that the principal indications can be characterized as ODSCC. For Kewaunee, the RPC inspection will be performed for all ODSCC indications left in service that exceed a 1.5 volt bobbin coil amplitude. The RPC results are to be evaluated to establish that the principal indications can be characterized as ODSCC. As discussed in Section 5.1, bobbin coil indications <1.5 volt for degradation other than ODSCC are not expected to impact tube integrity for potential tube degradation at Kewaunee. Thus, characterization of the type of degradation above 1.5 volts by RPC is adequate to determine appropriate plugging limits. If indications other than ODSCC are identified, these indications should be evaluated against a 50% depth requirement for tube plugging. The >1.5 volt bobbin coil amplitude for RPC inspection also is below the ~2.0 volt threshold below which SLB leakage is expected to be negligible as noted in Section 13.4. Once an indication at a TSP is confirmed to be ODSCC, reconfirmation by RPC inspection at alternate refueling outages is acceptable.

Circumferential cracks at TSPs have only been found in one Westinghouse plant that has significant denting at support plates. Dents at TSP intersections have not been found in the Kewaunee S/Gs. Further, no circumferential cracks have been found at the TSPs in the Kewaunee

SGs and none are expected based on operating experience. The RPC Inspections required for indications >1.5 volt are to continue to monitor for potential occurrence of circumferential cracks. RPC resolution is required to define separation between circumferential and axial cracks. It is not assumed to be necessary to resolve potential circumferential cracks between closely spaced axial cracks since circumferential cracking is not anticipated at Kewaunee. Any initial identification of circumferential cracks by RPC should be based upon a well defined circumferential indication as contrasted to inadequate RPC resolution. If a well defined circumferential indication should be identified at the TSPs in the Kewaunee S/Gs, guidelines for RPC interpretation would be reviewed at that outage.

13.9   Summary of Tube Plugging Criteria

As developed in the sections above, the full implementation of the alternate plugging criteria for ODSCC at TSPs can be summarized as follows:

Tube Plugging Criterion

Tubes with bobbin coil indications exceeding 2.5 volts will be plugged or repaired.

SLB Leakage Criterion

Predicted end of cycle SLB leak rates from tubes left in service must be less than 9.1 gpm for each S/G, including considerations for NDE uncertainties and ODSCC growth rates.

Inspection Requirements

A 100% bobbin coil inspection shall be performed for all hot leg TSP intersections and all cold leg intersections down to the lowest cold leg TSP with reported ODSCC indications.

Any TSP indication with bobbin coil amplitude exceeding 1.5 volts, if planned to be left in service, shall be inspected by RPC, unless it was it was inspected by RPC during the prior refueling outage. The RPC results shall be evaluated to support ODSCC as the dominant degradation mechanism. Subsequent RPC inspection of 1.5 volt indications shall be performed during alternate refueling outages for reconfirmation as ODSCC.

Operating Leakage Limits

Plant shutdown will be implemented if normal operating leakage exceeds 150 gpd per S/G.

Exclusions from Tube Plugging Criterion

Tubes with RPC indications not attributable to ODSCC and tubes with circumferential indications shall be evaluated for tube plugging based on a 50% depth limit.

If an interim plugging criteria (IPC) is implemented rather than a full APC, the following changes to the above APC apply:

Tube Plugging Criterion

Tubes with bobbin indications exceeding the IPC voltage repair limit and ≤ 2.5 volts will be plugged or repaired if confirmed as flaw indications by RPC inspection. Bobbin flaw indications >2.5 volts attributable to ODSCC will be repaired independent of RPC confirmation.

SLB Leakage Criterion

Predicted EOC SLB leak rates from tubes left in service must be less than 1.0 gpm for each SG.

Inspection Requirements

The 100% bobbin coil inspection requirement for an APC repair limit applies also for an IPC repair limit.

Any bobbin flaw indication greater than the IPC repair limit shall be RPC inspected.

The above APC requirements on operating leakage limits and exclusions from the tube plugging criterion apply also to an IPC repair limit.

As noted in Section 13.4, an IPC repair limit less than the APC repair limit of 2.5 volts is expected to result in a maximum EOC voltage less than or comparable to that obtained in the last cycle following implementation of the 50% depth repair limit. Even for a 2.5 volt repair limit, over 99% of the EOC indications would be less than the 4.0 volt indication found and repaired in the last inspection. For a 2.3 volt IPC, the maximum EOC voltage would be <4.0 volts (Table 13-2) and the SLB leak rate would be about 0.0017 gpm per 2.3 volt indication (Table 13-7). Thus about 585 indications per SG could be left in service without exceeding a 1.0 gpm SLB leak rate. Thus an IPC repair limit of 2.3 volts would be approximately equivalent to a 50% depth repair limit with comparable maximum EOC voltages of about 4.0 volts and would limit potential SLB leakage to <1.0 gpm.

Table 13-1

Tube Plugging Limits to Satisfy Structural Requirements

Item	Volts	Basis
Maximum Voltage Limit to Satisfy Tube Burst Structural Requirement	[ ]a	Figure 8-2, Burst Pressure vs. Voltage Correlation at -95% confidence level.
Allowance for NDE Uncertainty	-0.3 (14%)[1]	Section 5.8 shows development of 14% uncertainty at 90% cumulative probability.
Allowance for Crack Growth Between Inspections	-0.7 (30%)[1]	Table 12.4 shows average growth/cycle of <20% in tho last 5 cycles. Allowance increased to 30% of Tube Plugging Limit to provide conservative margin for variations in future cycles.
Tube Plugging Voltage Limit • Acceptable Limit to Meet Structural Requirement	2.5	

<u>Note</u>

1.   Voltage percentage allowances for NDE uncertainty and growth rate per cycle applied to Tube Plugging Voltage Limit of 2.5 volts.

Table 13-2

Maximum EOC Voltage Assessment

	Deterministic Assessments								Monte Carlo	
	90% Cum. Prob.		95% Cum. Prob.			99% Cum. Prob.				
BOC Volts	1.0	2.5	1.0	2.3	2.5	1.0	2.3	2.5	1.0	2.5
NDE Uncertainty	0.14	0.35	0.18	0.41	0.45	0.25	0.58	0.63	--	--
Growth	0.42	0.42	0.59	0.59	0.59	1.10	1.10	1.10	--	--
EOC Maximum Volts	1.56	3.27	1.77	3.30	3.54	2.35	3.98	4.23	2.47	4.06

Table 13-3

Monte Carlo Results for EOC Volts, SLB Leak Rate, and SLB Burst Probability per Indication

BOC Volts	EOC Volts (% = Cumulative Probability)					SLB Leak Rate (% = Cum. Probability)				SLB Burst Prob.
	90%	95%	99%	99.7%[2]	99.9%	Cum. Prob. for Zero Leak	gpm at 95%	gpm at 99%	gpm at 99.9%	
1.0	1.46	1.62	2.17	2.47	2.60	98.9%	0.0	~10^{-5}	0.0029	<10^{-5} [2]
1.5	1.99	2.16	2.68	2.99	3.16	97.7%	0.0	0.0005	0.0099	<10^{-5}
2.0	2.55	2.70	3.20	3.52	3.71	95.9%	0.0	0.0020	0.024	<10^{-5}
2.5	3.10	3.26	3.73	4.06	4.27	93.2%	0.0002	0.0052	0.050	<10^{-5}

Notes:
1.) 99.7% corresponds to definition of maximum EOC voltage for 300 indications.
2.) No occurrences of burst <ΔP_{SLB} in 10^5 samples.

Table 13-4

Summary of Largest Bobbin Voltage Indications from 1992 Inspection

			Bobbin Coil	
SG	Tube	'92 Location	'92 Volts	'91 Volts
Bobbin Pls Confirmed by **RPC or Bobbin Depth ≥50%**				
B	R25C12	6C	4.00	4.13
B	R24C75	6C	3.58	2.97
B	R17C57	7C	2.46	1.84
B	R24C63	7C	1.57	1.28
B	R16C88	7C	1.50	1.78
Bobbin Pls NOT Confirmed by **RPC or Bobbin Depth <50%**				
B	R16C29	1C	2.61	1.62
B	R38C52	7C	2.51	1.34
B	R38C49	5C	2.31	2.04
B	R38C51	7C	2.27	2.10
A	R14C16	1H	2.23	2.24
A	R11C23	1H	2.10	1.36
New Bobbin Pls; Bobbin NDD in Prior Outage				
A	R45C41	1C	0.73	NDD
A	R39C57	6C	0.55	NDD
A	R40C29	5C	0.47	NDD

Table 13-5

Kewaunee Tube Burst Margin Assessment for $3\Delta P_{NO}$

BOC Voltage	1.0	1.5	2.0	2.5
Allowances at + 90% Cum. Prob.				
• Voltage Growth	0.42	0.42	0.42	0.42
• NDE Uncertainty	0.14	0.21	0.28	0.35
EOC Volts	1.56	2.13	2.70	3.27
Tube Burst Capability (psi)				
• $3\Delta P_{NO}$ Requirement	4620	4620	4620	4620
• Capability at -95% Prediction interval				
- At BOC	5770	5400	5130	4930
- At EOC	5360	5080	4860	4680
Burst Capability Ratios to $3\Delta P_{NO}$				
• At BOC	1.25	1.17	1.11	1.07
• At EOC	1.16	1.10	1.05	1.01

Table 13-6

Kewaunee Tube Burst Margin Assessment for ΔP_{SLB}

| BOC Voltage	1.0	1.5	2.0	2.5
Allowances at + 99% Cum. Prob.				
• Voltage Growth	1.10	1.10	1.10	1.10
• NDE Uncertainty	0.25	0.37	0.50	0.63
Maximum Projected EOC Volts				
• Deterministic	2.35	2.97	3.60	4.23
• Monte Carlo	2.47	2.99	3.52	4.06
Tube Burst Capability (psi)				
• ΔP_{SLB} Requirement	2335	2335	2335	2335
• Capability at -99% Prediction Interval				
- At +99% EOC Volts	4490	4280	4100	3950
- At Maximum EOC Volts	4440	4270	4120	3990
Burst Capability Ratios to ΔP_{SLB}				
• At +99% EOC Volts	1.92	1.83	1.75	1.69
• At Maximum EOC Volts	1.90	1.83	1.76	1.71

Table 13-7

Deterministic EOC SLB Rates and Equivalent Monte Carlo Probability

	Reference SLB Leak Rate (gpm) per Indication[1]			Bounding Single Indic'n 95% Prediction Int.		SLB Leak Rate (gpm) 99% Prediction Int.	
BOC Volts	1.0	2.3	2.5	1.0	2.5	1.0	2.5
EOC Volts per Table 13-2	1.77	3.30	3.54	1.77	3.54	2.35	4.23
Probability of Leakage (P.O.L)	0.07	0.23	0.27	0.07	0.27	0.23	0.48
SLB Leak Rate (gpm)	0.0045	0.0075	0.0084	0.0088[2]	0.023[2]	0.055[2]	0.11[2]
Weighted SLB Leak Rate (gpm) (P.O.L. x Leak Rate)	0.00032	0.0017	0.0023	0.00062	0.0062	0.013	0.053
Equivalent Monte Carlo Cumulative Probability for Weighted Leak Rate[3]	~99.1%	–	~97.8%	~99.7%	~99.2%	~99.98%	~99.9%

Notes:

(1.) Obtained evaluating voltage growth, probability of leakage and leak rate at +95% confidence level from Figure 9-8.

(2.) Obtained evaluating leak rate at specified bound on prediction interval (Figure 9-8).

(3.) Obtained evaluating Monte Carlo cumulative probability distribution for a given BOC indication at the weighted leak rate from the deterministic analysis.
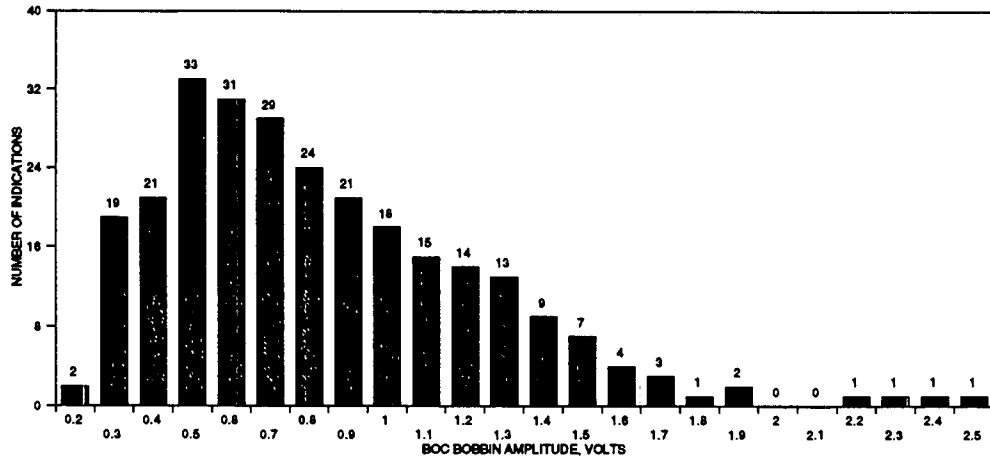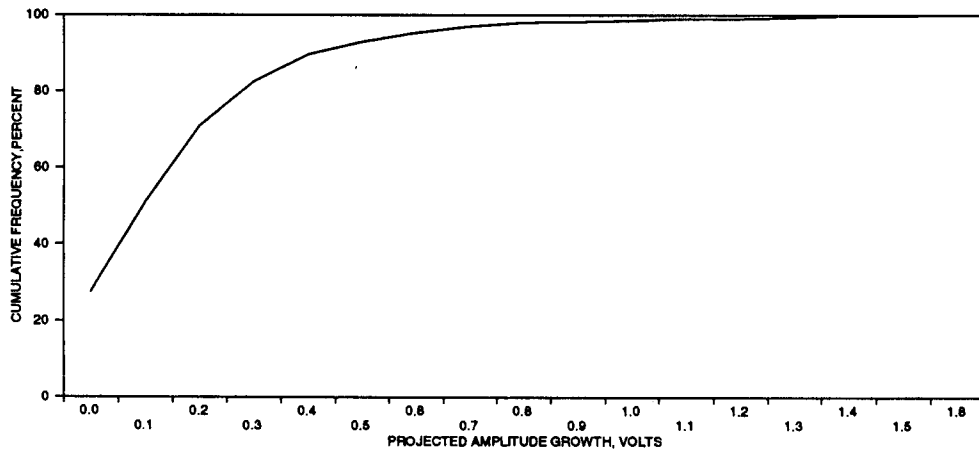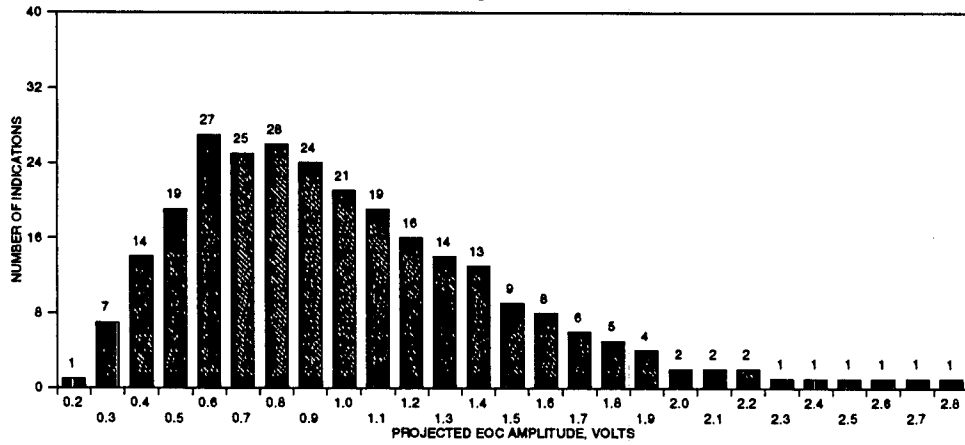
Monte Carlo Projection for EOC Voltages assuming 2.5 Volt Report Limit

FIGURE 13.1

NORMAL OPERATING CONDITIONS
LEAK RATE VS AXIAL CRACK LENGTH
7/8" TUBING AT 600F AND 1540 PSI

a

Figure 13-2. Normal Operation Leak vs. Axial Crack Length

BURST PRESSURE VERSUS CRACK LENGTH
7/8X0.050 INCH TUBING

a,g

Figure 13-3. Burst Pressure vs. Crack Length

Appendix A
NDE Data Acquisition and Analysis Guidelines

A.1   INTRODUCTION

This appendix contains guidelines which provide direction in applying the ODSCC alternate repair limits described in this report. The procedures for eddy current testing using bobbin coil and rotating pancake coil (RPC) techniques are summarized. The procedures given apply to the bobbin coil inspection, except as explicitly noted for RPC inspection. The methods and techniques detailed in this appendix are requisite for Kewaunee implementation of the alternate repair limit and are to be incorporated in the applicable inspection and analysis procedures. The following sections define specific acquisition and analysis parameters and methods to be used for the inspection of the steam generator tubing.

A.2   DATA ACQUISITION

The Kewaunee steam generators utilize 7/8" OD x 0.050" wall, Alloy 600 mill-annealed tubing. The carbon steel support plates are designed with drilled holes.

A.2.1   Probes

Bobbin Coil Probes

Eddy current equipment used shall be the ERDAU (Echoram Tester), Zetec MIZ-18 or other equipment with similar specifications. To maximize consistency with laboratory data, differential bobbin probes with the following parameters shall be used:

- All straight sections of tubing (including Rows 1-10) are to be tested with a 0.720" O.D. probe. U-bends may be tested with a 0.700" O.D. or smaller probe as required.
- two bobbin coils, each 60 mils long, with 60 mils between coils (coil centers separated by 120 mils)

In addition, the probe design must incorporate centering features that provide for minimum probe wobble and offset: the centering features must maintain constant probe center-to-tube ID offset for nominal diameter tubing.

Rotating Pancake Coil Probes

The pancake coil diameter shall be ≤0.125". While any multi-coil (i.e., 1, 2 or 3-coil) probe can be utilized, it is recommended that if a 3-coil probe is used, any voltage measurements should be made with the probe's pancake coil rather than its circumferential or axial coil. The maximum probe pulling speed shall be ≈0.2 in./sec for the 1-coil or 3-coil probe, or 0.4 in/sec. for the 2-coil probe. The maximum rotation speed shall be ≈300 rpm. This would result in a pitch of ≈40 mils for the 3-coil probe.

A.2.2 Calibration Standards

Bobbin Coil Standards

To provide APC implementation at Kewaunee consistent with the development and analyses of this report and with prior NRC-approved IPC applications, a probe wear standard to guide probe replacement and a transfer standard calibrated against the reference laboratory standard are to be utilized. The transfer standard is cross-calibrated against the laboratory standard, and permits currently acceptable Kewaunee standards to be utilized without modification.

The bobbin coil calibration standards shall contain:

- Four 0.033" diameter through wall holes, 90° apart in a single plane around the tube circumference. The hole diameter tolerance shall be ±0.001".
- One 0.109" diameter flat bottom hole, 60% through from OD
- One 0.187" diameter flat bottom hole, 40% through from the OD
- Four 0.187" diameter flat bottom holes, 20% through from the OD, spaced 90° apart in a single plane around the tube circumference. The tolerance on hole diameter and depth shall be ±0.001".
- A simulated support ring, 0.75" long, comprised of SA-285 Grade C carbon steel or equivalent.
- This calibration standard will need to be calibrated against the reference standard used for the APC laboratory work.
- A probe wear standard for monitoring the degradation of probe centering devices leading to off-center coil positioning and potential variations in flaw amplitude responses. This standard shall include four through wall holes, 0.067" in diameter, spaced 90° apart around the tube circumference with an axial spacing such that signals can be clearly distinguished from one another (see Section A.2.3).

RPC Standard

The RPC standard shall contain:

- Two axial EDM notches, located at the same axial position but 180° apart circumferentially, each 0.006" wide and 0.5" long, one 80% and one 100% through wall from the OD.
- Two axial EDM notches, located at the same axial position but 180° apart circumferentially, each 0.006" wide and 0.5" long, one 60% and one 40% through wall from the OD.
- Two circumferential EDM notches, one 50% throughwall from the OD with a 75° (0.57") arc length, and one 100% throughwall with a 26° (0.20") arc length, with both notches 0.006" wide.
- A simulated support segment, 270° in circumferential extent, 0.75" thick, comprised of SA-285 Grade C carbon steel or equivalent.

The center to center distance between the support plate simulation and the nearest slot shall be at least 1.25". The center to center distance between the EDM notches shall be at least 1.0". The tolerance for the widths and depths of the notches shall be ±0.001". The tolerance for the slot lengths shall be ±0.010".

A.2.3 Application of Bobbin Coil Probe Wear Standard

A calibration standard has been designed to monitor bobbin coil probe wear. During steam generator examination, the bobbin coil probe is inserted into the wear monitoring standard; the initial (new probe) amplitude response from each of the four holes is determined and compared on an individual basis with subsequent measurements. Signal amplitudes or voltages from the individual holes must remain within 15% of their initial amplitudes for an acceptable probe wear condition. If this condition is not satisfied for all four holes, then the probe must be replaced. If any of the last probe wear standard signal amplitudes prior to probe replacement exceed the +/- 15% limit, say by a value of x%, then any indications measured since the last acceptable probe wear measurement that are within x% of the plugging limit must be re-inspected with the new probe. For example, if any of the last probe wear signal amplitudes prior to probe replacement were 17% above or below the initial amplitude, then indications that are within 2% (17% - 15%) of the plugging limit must be re-inspected with the new probe.

A.2.4 Acquisition Parameters

The following parameters apply to bobbin coil data acquisition and should be incorporated in the applicable inspection procedures to supplement (not necessarily replace) the parameters normally used.

Test Frequencies

This technique requires the use of 400 kHz and 100 kHz test frequencies in the differential mode. It is recommended that the absolute mode also be used, at test frequencies of 100 kHz and 10 kHz. The low frequency (10 kHz) channel should be recorded to provide a positive means of verifying tube support plate edge detection for flaw location purposes. The 400 kHz channel or the 400/100 kHz mix are also used to assess changes in signal amplitudes for the probe wear standard as well as for flaw detection.

RPC frequencies should include 400 kHZ, 300 kHz and 100 kHz.

Digitizing Rate

A minimum bobbin coil digitizing rate of 30 samples per inch should be used. Combinations of probe speeds and instrument sample rates should be chosen such that:

$$\frac{\text{Sample Rate (samples/sec.)}}{\text{Probe Speed (in./sec.)}} \geq 30 \text{ (samples/in.)}$$

Spans and Rotations
Spans and rotations can be set at the discretion of the user and/or in accordance with applicable procedures.

Mixes
A bobbin coil differential mix is established with 400 kHz as the primary frequency and 100 kHz as the secondary frequency, and suppression of the tube support plate simulation should be performed.

A.2.5   Analysis Parameters

This section discusses the methodology for establishing bobbin coil data analysis variables such as spans, rotations, mixes, voltage scales, and calibration curves. Although indicated depth measurement may not be required to support an alternative repair limit, the methodology for establishing the calibration curves is presented. The use of these curves is recommended for consistency in reporting and to provide compatibility of results with subsequent inspections of the same steam generator and for comparison with other steam generators and/or plants.

400 kHz Differential Channel
Rotation: The signal from the 100% through wall hole should be set to 40° (±1°) with the initial signal excursion down and to the right during probe withdrawal.

Voltage Scale:

1) Bobbin - The peak-to-peak signal amplitude of the signal from the four 20% OD flaws should be set to produce a field voltage equivalent to that obtained for the EPRI lab standard. The EPRI laboratory standard normalization voltages are 4.0 volts at 400 kHz for 20% ASME holes and 2.75 volts at 400/100 kHz mix for 20% ASME holes.
The transfer/field standard will be calibrated against the laboratory standard using a reference laboratory probe to establish voltages for the field standard that are equivalent to the above laboratory standard. These equivalent voltages are then set on the field standard to establish the calibration voltages for any other standard. Voltage normalization to the standard specific calibration voltages at 400 kHz is the preferred normalization to minimize analyst sensitivity in establishing the mix. However, if the bobbin probes used at Kewaunee result in 400/100 kHz mix to 400 kHz voltage ratios differing from the laboratory standard ratio of 0.69 by more than 5% (0.66 to 0.72), the 400/100 kHz mix calibration voltage should be used for voltage normalization.

2) RPC - The RPC amplitude shall be set to 20 volts for the 0.5 inch throughwall notch at 400 kHz and 300 kHz.

Calibration Curve: Establish a curve using measured signal phase angles in combination with the "as-built" flaw depths for the 100%, 60%, and 20% flaws on the calibration standard.

400/100 kHz Differential Mix Channel
Rotation: Set the signal from the probe motion to be horizontal with the initial excursion of the 100% through wall hole signal going down and to the right during probe withdrawal.

Calibration Curve: Establish a curve using measured signal phase angles in combination with the "as-built" flaw depths for the 100%, 60%, and 20% flaws on the calibration standard.

A.2.6   Analysis Methodology

Bobbin coil indications at support plates attributable to ODSCC are quantified using the Mix 1 (400 kHz/100 kHz) data channel. This is illustrated with the example shown in

Figure A-1. The 400/100 kHz mix channel and other channels appropriate for flaw detection (400 kHz, 200 kHz) can be used to locate the indication of interest within the support plate signal. The largest amplitude portion of the lissajous signal representing the flaw should be measured using the 400/100 kHz Mix 1 channel to establish the peak-to-peak voltage as shown in Figure A-1. Initial placement of the dots for identification of the flaw may be performed from the raw frequencies as shown in Figures A-2 and A-3, but the final peak-to-peak measurements must be performed on the Mix 1 lissajous signal to include the full flaw segment of the signal. It may be necessary to iterate the position of the dots between the identifying frequency data (e.g., 400 kHz) and the Mix 1 data to assure proper placement of the dots. As can be seen in Figures A-2 and A-3, failure to do so can significantly change the voltage amplitude measurement of Mix 1 due to the interference of the support plate signal in the raw frequencies. The voltage measured from Mix 1 is then entered as the analysis of record for comparison with the repair limit voltage.

A.2.7 Reporting Guidelines

The reporting requirements identified below are in addition to any other reporting requirements specified by the user.

Minimum Requirements

At a minimum, flaw signals in the 400/100 mix channel at the tube support plate intersections whose peak-to-peak signal amplitude exceeds 1.5 volts, requiring RPC inspection, must be reported. Signals, however small, should also be reported for historical purposes and to provide an assessment of the overall condition of the steam generator(s).

Additional Requirements

For each reported indication, the following information should be recorded:

Tube identification	(row, column)
Signal amplitude	(volts)
Signal phase angle	(degrees)
Indicated depth	(%)[†]
Test channel	(ch#)
Axial position in tube	(location)
Extent of test	(extent)

[†] It is recommended that an indicated depth be reported as much as possible rather than some letter code. While this measurement is not required to meet the alternate repair limit, this information might be required at a later date and/or otherwise be used to develop enhanced analysis techniques.

RPC reporting requirements should include a minimum of: type of degradation (axial, circumferential or other), maximum voltage, phase angle, crack lengths, and location of center of crack within the TSP. The crack axial center need not coincide with the position of the maximum amplitude.

A.3 DATA EVALUATION

A.3.1 Use of 400/100 Differential Mix for Extracting the Bobbin Flaw Signal

In order to identify a discontinuity in the composite signal as an indication of a flaw in the tube wall, a simple signal processing procedure of mixing the data from the two test frequencies is used which reduces the interference from the support plate signal by about an order of magnitude. The test frequencies most often used for this signal processing are 400 kHz and 100 kHz where 50 mil wall Inconel-600 tubing is involved. The processed data is referred to as 400/100 mix channel data. This procedure may also eliminate the interference from magnetite accumulated in the crevices. Any of the differential data channels including the mix channel may be used for flaw detection (though the 100 kHz channel is subject to influence from many different effects), but the final evaluation of the signal detection, amplitude and phase will be made from the 400/100 differential mix channel. Upon detection of a flaw signal in the differential mix channels, confirmation from other raw channels is not required. The voltage scale for the 400/100 differential channel should be normalized as described in Section A.2.5.

The present evaluation procedure requires that there is no minimum voltage for flaw detection purposes and that all flaw signals, however small, be identified. The intersections with flaw signals ≥1.5 volts will be inspected with RPC in order to confirm the presence of ODSCC. Although the signal voltage is not a measure of the flaw depth, it is an indicator of the tube burst pressure when the flaw is identified as axial ODSCC with or without minor IGA.

The procedure using the 400/100 mix for reducing the influence of support plate and magnetite does not totally eliminate the interference from copper, alloy property change or dents. These are discussed below.

A.3.2 Amplitude Variability

It has been observed that voltage measurements taken from the same data by different analysts may vary, even when using identical guidelines. This is largely due to the analyst interpretation of where to place the dots on the lissajous figure for the peak-to-peak measurement for flaw identification. Figures A-4 and A-5 show the correct placement of the dots on the Mix 1 lissajous for the peak-to-peak voltage amplitude measurements for two intersections from Kewaunee. Figures A-4 and A-5 show different flaw directional excursions making flaw identification a judgment call. The placement of the dots should always correspond to the maximum amplitude voltage measurement.

In some cases, it will be found that little if any definitive help is available from the use of the raw frequencies. Such examples are shown in Figure A-6 and A-7. Consequently, the placement of the measurement dots must be made completely on the basis of the Mix 1 channel. The logic behind the placement of the dots on the Mix 1 channel is that sharp transitions in the residual support plate signals can be observed at the locations of both dots. In the following example, Figure A-8, this logic does not always apply inasmuch as there is no sharp, clearly defined transition. This is a conservative approach, in that the dot placement on Mix 1 is such that the dot placement in the raw frequencies are beyond what appears to be the flaw-like transition, and this approach should be taken whenever a degree of doubt as to dot placement exists.

The source of error becomes more noticeable when the data involves complicating factors or interferences which make the process of flaw identification more difficult; the contrast between tubes which exhibit signs of minor denting in the support plates and tubes which are essentially free from denting present such circumstances. How denting affects flaw detection is described in Section A.3.5.

It is noted that by employing these techniques, identification of flaws is improved and that conservative amplitude measurements are promoted. The Mix 1 traces which result from this approach conform to the model of TSP ODSCC which represents the degradation as a series of microcrack segments axially integrated by the bobbin coil; I.e., short segments of changing phase direction represent changes in average depth with changing axial position. This procedure is to be followed for reporting voltages for the plugging criteria of this report. This procedure may not yield the maximum bobbin depth call. If maximum depth is desired for information purposes, shorter segments of the overall crack may have to be evaluated to obtain the maximum depth estimate. However, the peak to peak voltages as described herein must be reported, even if a different segment is used for the depth call.

A.3.3   Copper Interference

In situations where significant copper interference in the eddy current data is noted, the eddy current technique basically becomes unreliable. This results from the unpredictability of the amount and morphology of copper deposit on the tubes which may be found in operating steam generators. The above observation is true both for bobbin and RPC or any other eddy current probe. Copper is not believed to be a significant issue for evaluating the support plate intersections of the tubing of the Kewaunee steam generators. This conclusion has also been reached for plants with significant plated copper deposits on the free span of the tubes. If copper interference is observed at Kewaunee, the existing rules and procedures for complying with the technical specification plugging limit based on depth of wall penetration and/or RPC confirmation of the indication will apply.

A.3.4   Alloy Property Changes

This signal manifests itself as part of the support plate "mix residual" in the 400/100 differential channel and as an offset in the 400/100 mix absolute channel. It has often been confused with copper deposit as the cause. Such signals are found often at support plate intersections of operating plants including Kewaunee, as well as in the model boiler test samples, and are not necessarily indicative of tube wall degradation. Six support plate intersections of Plant A judged as free of tube wall degradation on the basis of the 400/100 differential channel using the guidelines given in Section A.2.5 and A.2.6 of this document were pulled in 1989. Examples of the bobbin coil field data are shown in Figure A-9 to A-11. The mix residuals for these examples are between 2 and 3 volts in the 400/100 differential channel and no discontinuity suggestive of a flaw can be found in this channel. All of them have an offset in the 400/100 absolute channel which could be confused as a possible indication. These signals persisted without any significant change even after chemically cleaning the OD and the ID of these tubes. The destructive examination of these intersections showed very minor or no tube wall degradation. Thus, the overall mix residual of the 400/100 differential channel and the offset in the 400/100 absolute channel themselves are not an indication of tube wall degradation. One needs to examine the detailed structure of the "mix residual" (as outlined in Sections A.2.5 and A.2.6) in order to assess the possibility that a flaw signal is present in the residual composite. Similar offsets in the absolute channels have been observed at the top of the tubesheet in plants with partial length roll expansions; in such cases, destructive examination of sections pulled from operating plants have shown no indication of tube wall degradation.

A.3.5 Dent Interference

The 400/100 kHz (differential) support plate suppression mix eliminates the support plate and the magnetite signals, but the resulting processed signal may still be a composite of the dent, artifact, and the flaw signals. These composite signals represent vectorial combinations of the constituent effects, and as such they may not conform to the behavior expected from simple flaw

simulations as a function of test frequency. For the population of intersections analyzed that contained flaw-like indications, no denting has been observed in the Kewaunee steam generators.

The effect of the dent on the detection and evaluation of a flaw signal depends on both the relative amplitudes of the flaw and dent signals and the relative spatial relationship between them. If the flaw is located near the center of the dent signal, interference with flaw detection may become insignificant, even for relatively large dent to flaw signal amplitude ratios. The flaw signal in a typical support plate dent in this event occurs mid-plane -- away from the support plate edges where the dent signal has maximum voltage; thus the flaw in the middle section of the support plate shows up as a discontinuity in the middle of the composite signal. It can be observed from Figures A-12 to A-17, from another plant (Plant A), that one can readily extract a flaw signal when the signal to noise (S/N) ratio is less than unity. The question of S/N ratio requirements for the detection and evaluation of the flaw signal is answered by examination of Figures A-12 to A-17. The question of S/N ratio requirements necessary for flaw detection is not a number that can be readily determined; but as can be seen from these figures, even with ratios as low as 0.2, the flaw signal can be detected and evaluated.

The greatest challenge to flaw detection due to dent interference occurs when the flaw occurs at the peak of the dent signal. Detection of flaw signals of amplitude equal to or greater than 1.5 volts--the criterion associated with confirmatory RPC testing--in the presence of peak dent voltages can be understood by vectorial combination of 1.5 volt flaw signals across the range of phase angles associated with 40% (110°) to 100% (40°) throughwall penetrations with dent signals of various amplitudes. It is easily shown that 1.5 volt flaw signals combined with dent signals up to ~8 volts peak-to-peak will yield resultant signals with phase angles that fall within the Kewaunee flaw reporting range, and in all cases will exceed 1.5 volts. All such dent signals with a flaw indication signal will be subjected to RPC testing. To demonstrate this, one-half the dent peak-to-peak voltage (entrance or exit lobe) can be combined with the 1.5 volts flaw signal at the desired phase angle. The vector combination analysis shows that for moderate dent voltages where flaws occur coincident with dent entrance or exit locations, flaw detection at the 1.5 volt amplitude level is successful via phase discrimination of combined flaw/dent signals from dent only signals.

The vector addition model for axial cracks coincident with denting at the TSP edge is illustrated as follows:
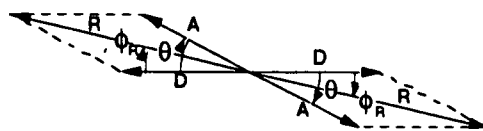
where,

R = Resultant Signal Amplitude
A = Flaw Signal Amplitude
D = TSP Dent Amplitude = one edge (Peak-to-Peak = 2D)

Θ = Flaw Signal Phase Angle (100% = 40°; 40% ~ 110°)

ϕ_R = Phase angle of Resultant Signal

and $R^2 = (D + A \cos\Theta)^2 + (A \sin\Theta)^2$

$\phi_R = \arctan^{-1} (A \sin\Theta/D + A \cos\Theta)^2$

For dents without flaws a nominal phase angle of 180° is expected. The presence of a flaw results in rotation of the phase angle to <180° and into the flaw plane. A phase angle of 170° (10° away from nominal dent signal) provides a sufficient change to identify a flaw. For dents with peak-to-peak amplitudes of 5 volts, D = 2.5v, and the minimum phase angle rotation (ϕ_R) for a 1.5v ODSCC flaw signal greater than 40% throughwall is predicted to be at least 15°, sufficiently distinguishable from the 180° (0°) phase angle associated with a simple dent.

Supplemental information to reinforce this phase discrimination basis for flaw identification can be obtained by examination of a 300/100 kHz mix channel; dent response would be lessened while the flaw response is increased relative to the 400/100 kHz mix. RPC testing of indications identified in this fashion will confirm the dependability of flaw signal detection. Intersections with dent voltages exceeding 8 volts, for which flaws ~1.5 volts may not be detectable, are candidates for RPC sampling of dented TSP intersections. In addition, dent indications that have phase angles less than 170° and whose amplitudes fall below the dent threshold value for RPC testing should be added to the RPC testing list.

A.3.6   RPC Flaw Characterization

The RPC inspection of the intersections with bobbin coil flaw indications >1.5 volts is recommended in order to verify the applicability of the alternate repair limit; this is based on establishing the presence of ODSCC with minor IGA as the cause of the bobbin indications.

The signal voltage for the RPC data evaluation will be based on 20 volts for the 100% deep, 0.5" long EDM notch at all test frequencies. The nature of degradation and its orientation (axial or circumferential) will be determined from careful examination of isometric plots of the RPC data. The presence of axial ODSCC at the support plate intersections has been well documented, but the presence of circumferential ODSCC at the support plate intersections has been established by tube pulls at a few plants. Figures A-18 to A-20 show examples of single and multiple axial ODSCC from Kewaunee. Figure A-21 gives an example of circumferential ODSCC from another plant at a tube support plate. If circumferential involvement results from circumferential cracks as opposed to multiple axial cracks, discrimination between axial and circumferentially oriented cracking can be generally established for affected arc lengths as small as 45°. RPC resolution is considered adequate for separation between circumferential and axial cracks. This can be supplemented by careful interpretation of 3-coil results.

The isometric graphs which are produced to illustrate the distribution of signals in a TSP may sometimes exhibit distributed extents of flaw content not readily identified with the discrete axial indications associated with cracks; this may occur with or without the presence of crack signals. The underlying tubing condition represented by volumetric flaw indications is interpreted in the context of the relative sensitivity of various flaw types (pits, wastage/wear, IGA, distributed cracks) potentially present.

The response from pits of significant depth is expected to produce geometric features readily identifiable with small area to amplitude characteristics. When multiple pits become so numerous as to overlap in the isometric display, the practical effect is to mimic the response from wastage or wear at comparable depths. In these circumstances the area affected is generally large relative to the peak amplitudes observed.

The presence of IGA as a local effect directly adjacent to crack faces is expected to be indistinguishable from the crack responses and as such of no structural consequence. When IGA exists as a general phenomenon, the EC response is proportional to the volume of material affected, with phase angle corresponding to depth of penetration and amplitude relatively larger than that expected for small cracks. The presence of distributed cracking, e.g. cellular SCC, may

produce responses from microcracks of sufficient individual dimensions to be detected but not resolved by the RPC, resulting in apparent volumetric responses similar to wastage and IGA.

For hot leg TSP locations, there is little industry experience on the basis of tube pulls that true volumetric degradation, i.e., actual wall loss or generalized IGA, actually occurs. All cases reviewed for the APC present morphologies representative of ODSCC with varying density of cracks and penetrations but virtually no loss of material in the volumetric sense. For cold leg TSP locations, considerable experience has accrued that volumetric degradation in the form of wastage has occurred on peripheral tubes, favoring the lower TSP elevations.

Therefore hot leg RPC volumetric flaw indications within the TSP intersections will be presumed to represent ODSCC, while only peripheral tube, lower TSP locations on the cold leg with RPC volumetric flaw indications will not be so characterized.

A.3.7 Confinement of ODSCC/IGA Within the Support Plate Region

In order to establish that a bobbin indication is within the support plate, the displacement of each end of the signal is measured relative to the support plate center. The field measurement is then corrected for field spread (look-ahead) to determine the true distance from the TSP center to the crack tip. If this distance exceeds half the support plate axial length (0.375"), the crack will be considered to have progressed outside the support plate. Per the repair criteria (Section 13), indications extending outside the support plate require tube repair or removal from service.

The measurement of axial crack lengths from RPC isometrics can be determined by the following EC interpretation practices. For the location of interest, the low frequency channel (e.g. 10 kHz) is used to set a local scale for measurement. Calibration of the distance scale is accomplished by setting the displacement between the 10 kHz absolute, upper and lower support plate transitions equal to 0.75 inch. By establishing the midpoint of the support plate response and storing this position in the 300 kHz and 400 kHz channels, a reference point for crack location is established.

At the analysis frequency, either 300 or 400 kHz, the ends of the crack indication are located using the slope-intercept method, i.e., the leading and trailing edges of the signal pattern are extrapolated to cross the null baseline. The difference between these two positions is the crack length estimate. Alternatively the number of scan lines indicating the presence of the flaw behavior times the pitch of the RPC provides an estimate of the crack length which must be corrected for EC field spread.
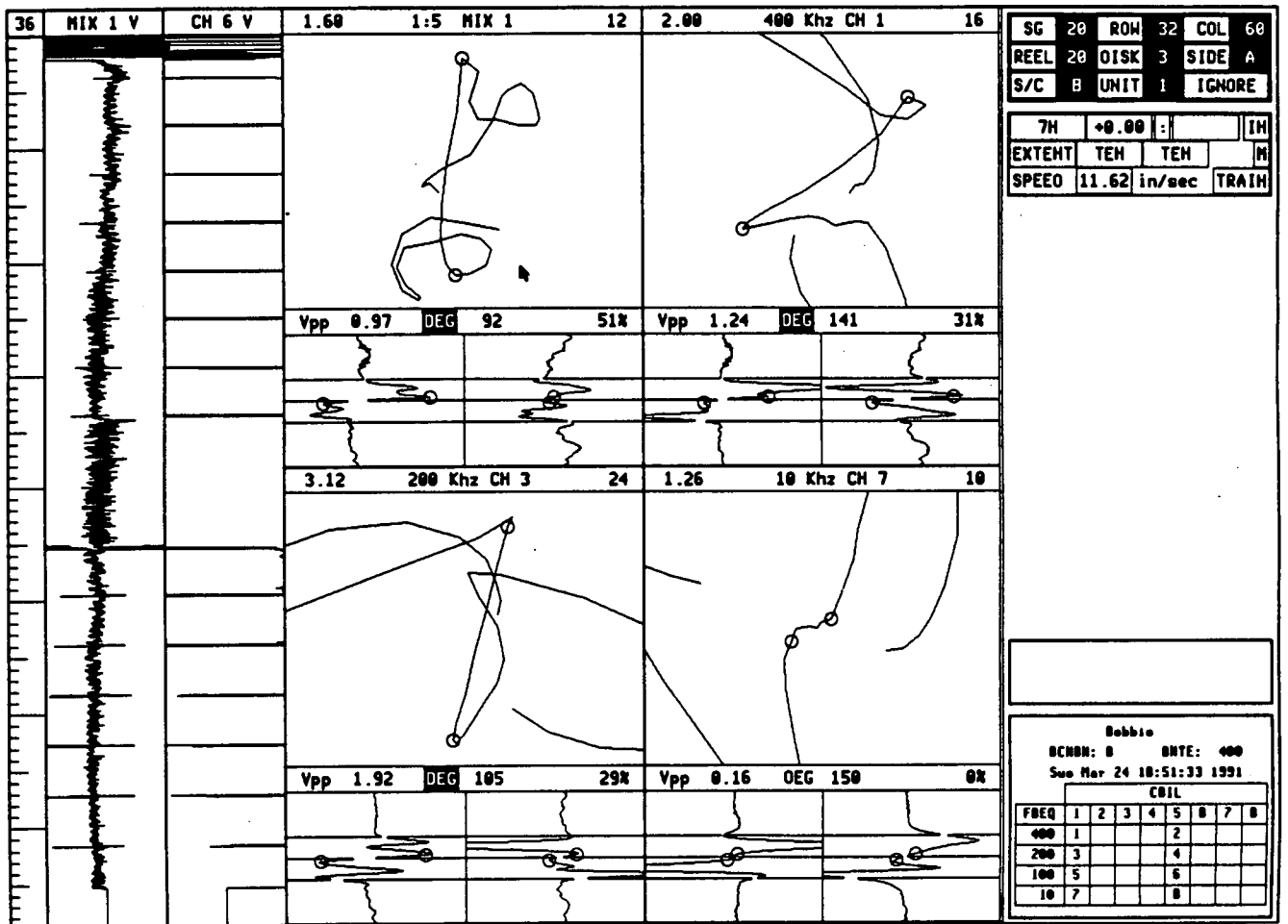
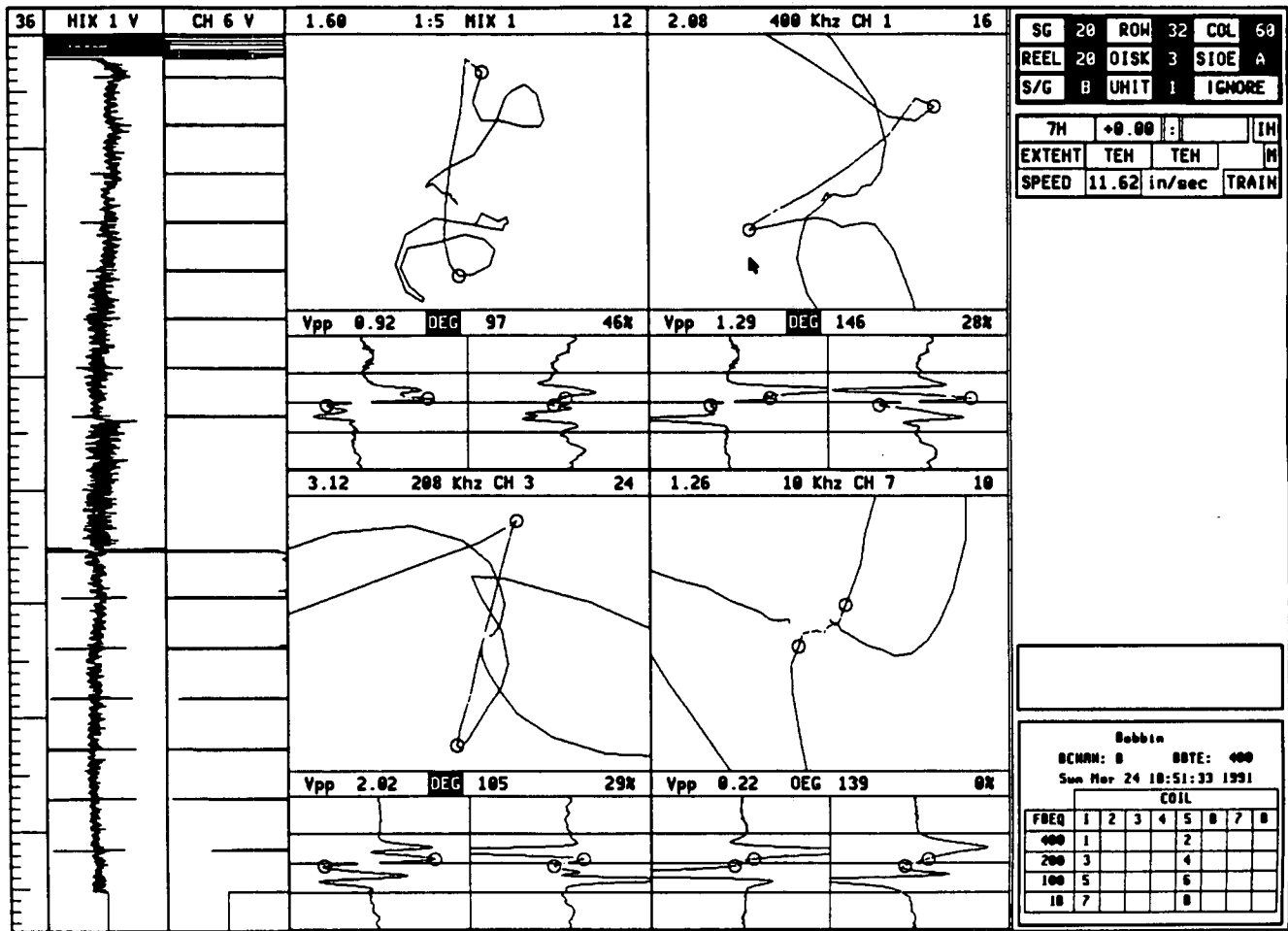Figure A-1   Bobbin Coil Amplitude of ODSCC at TSP

Figure A-2   Bobbin Coil Amplitude of ODSCC at TSP -
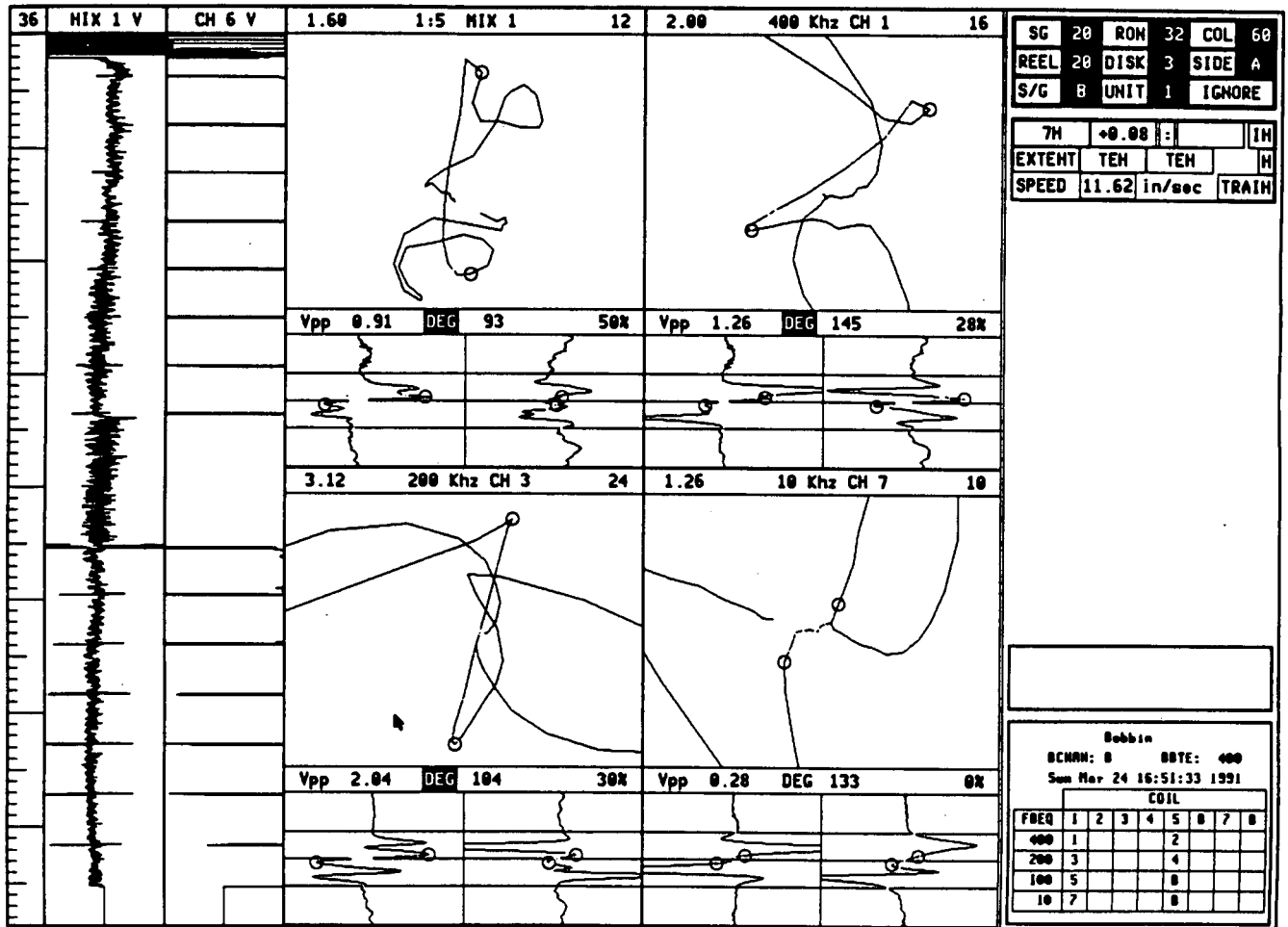Improper Identification of Full Flaw Segment

A - 12

Figure A-3   Bcbbin Coil Amplitude of ODSCC at TSP

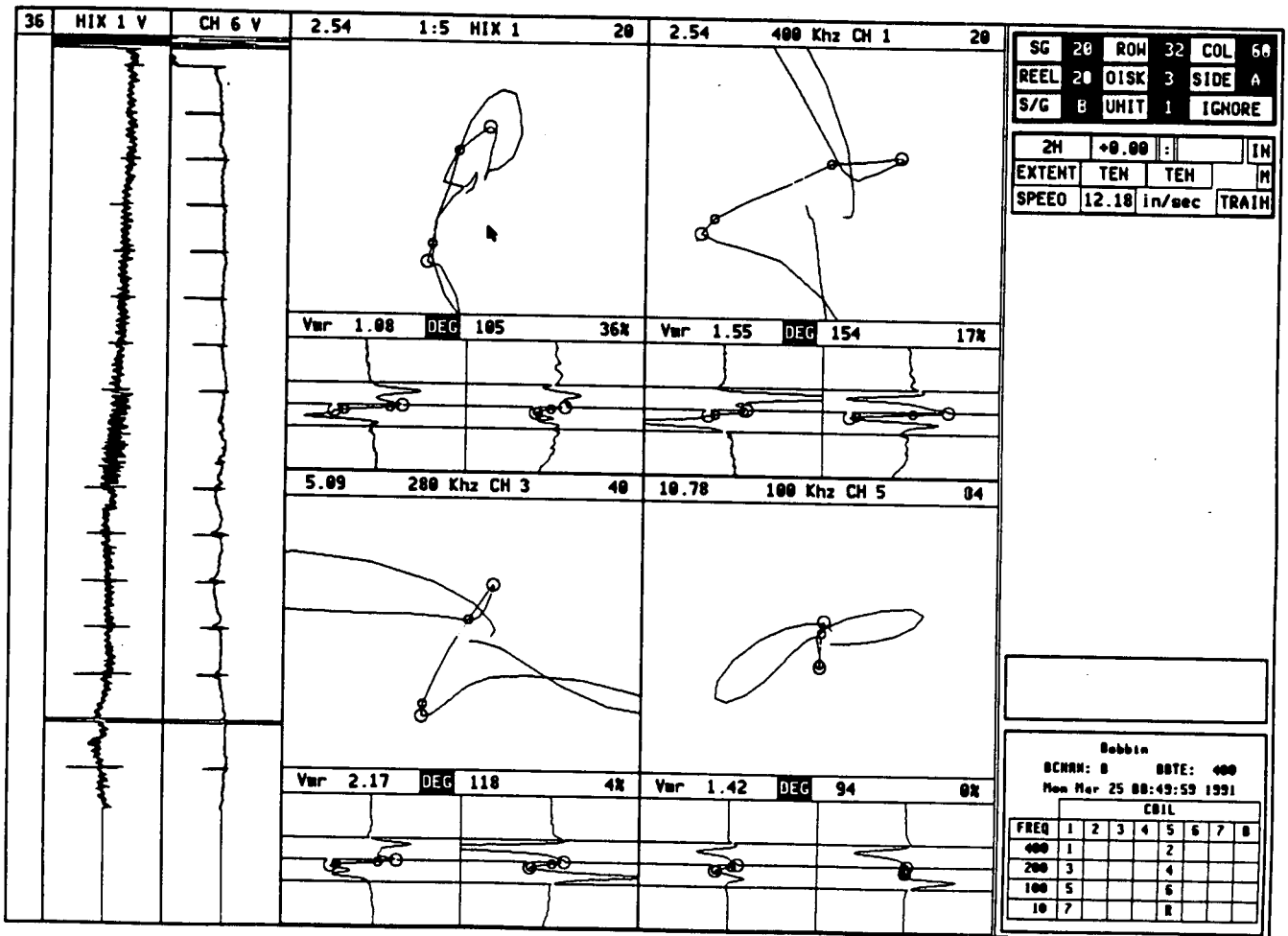Improper Identification of Full Flaw Segment

A - 13

Figure A-4   Bobbin Coil Amplitude Analysis of ODSCC at TSP
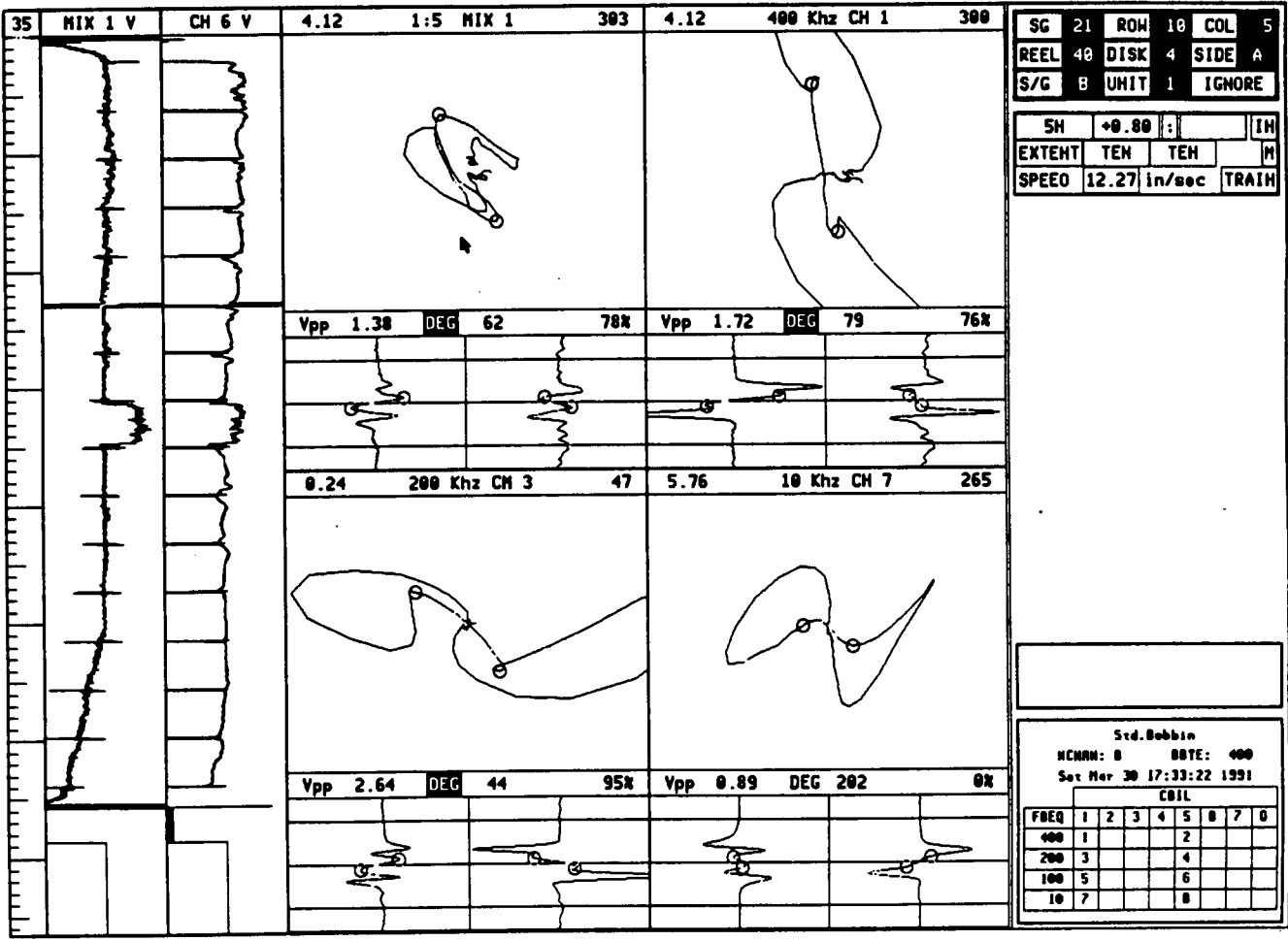Correct Placement of Dots on Mix 1

Figure A-5   Bobbin Coil Amplitude Analysis of ODSCC at TSP
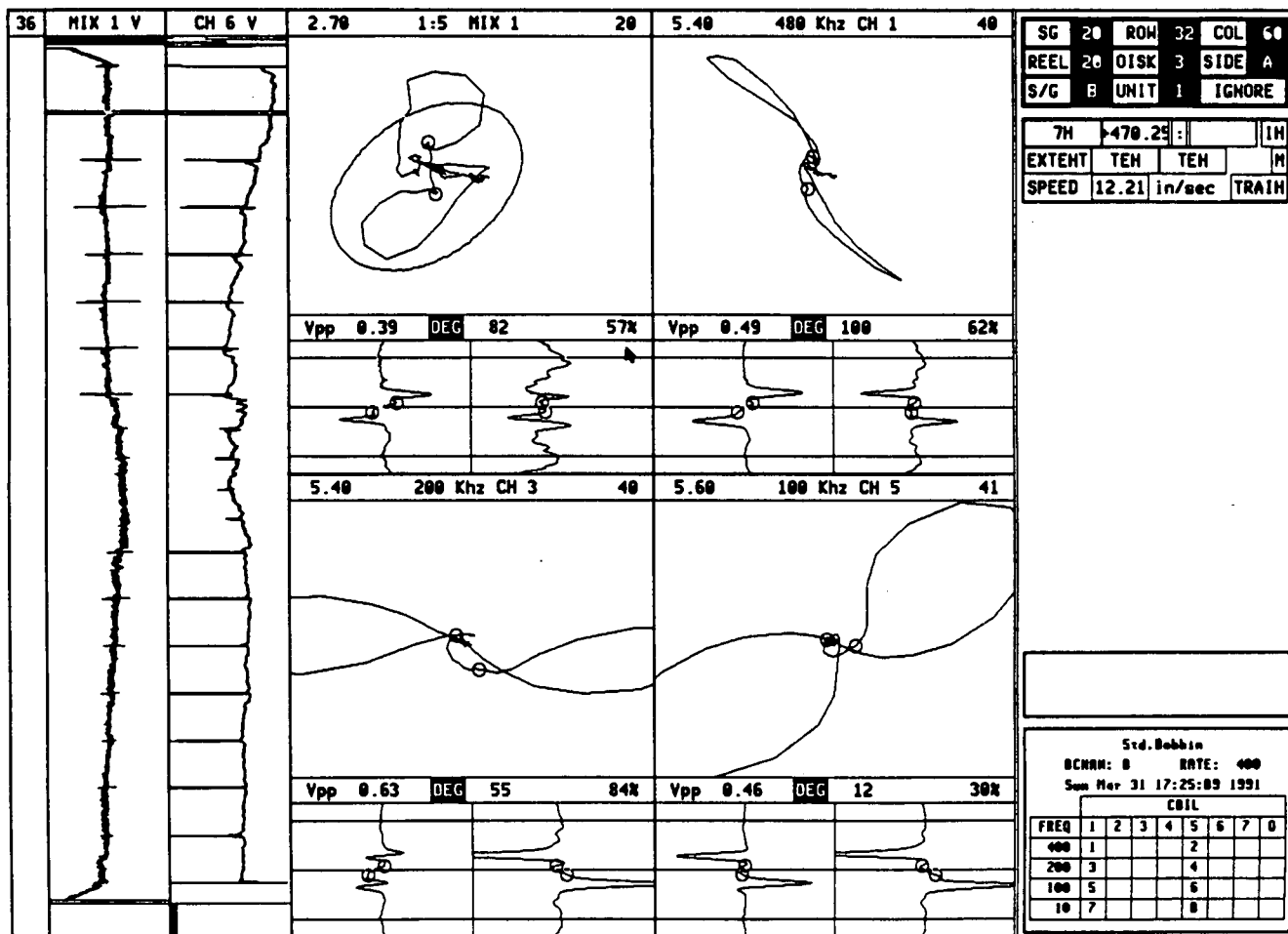Correct Placement of Dots on Mix 1

Figure A-6   Bobbin Coil Amplitude Analysis of ODSCC at TSP

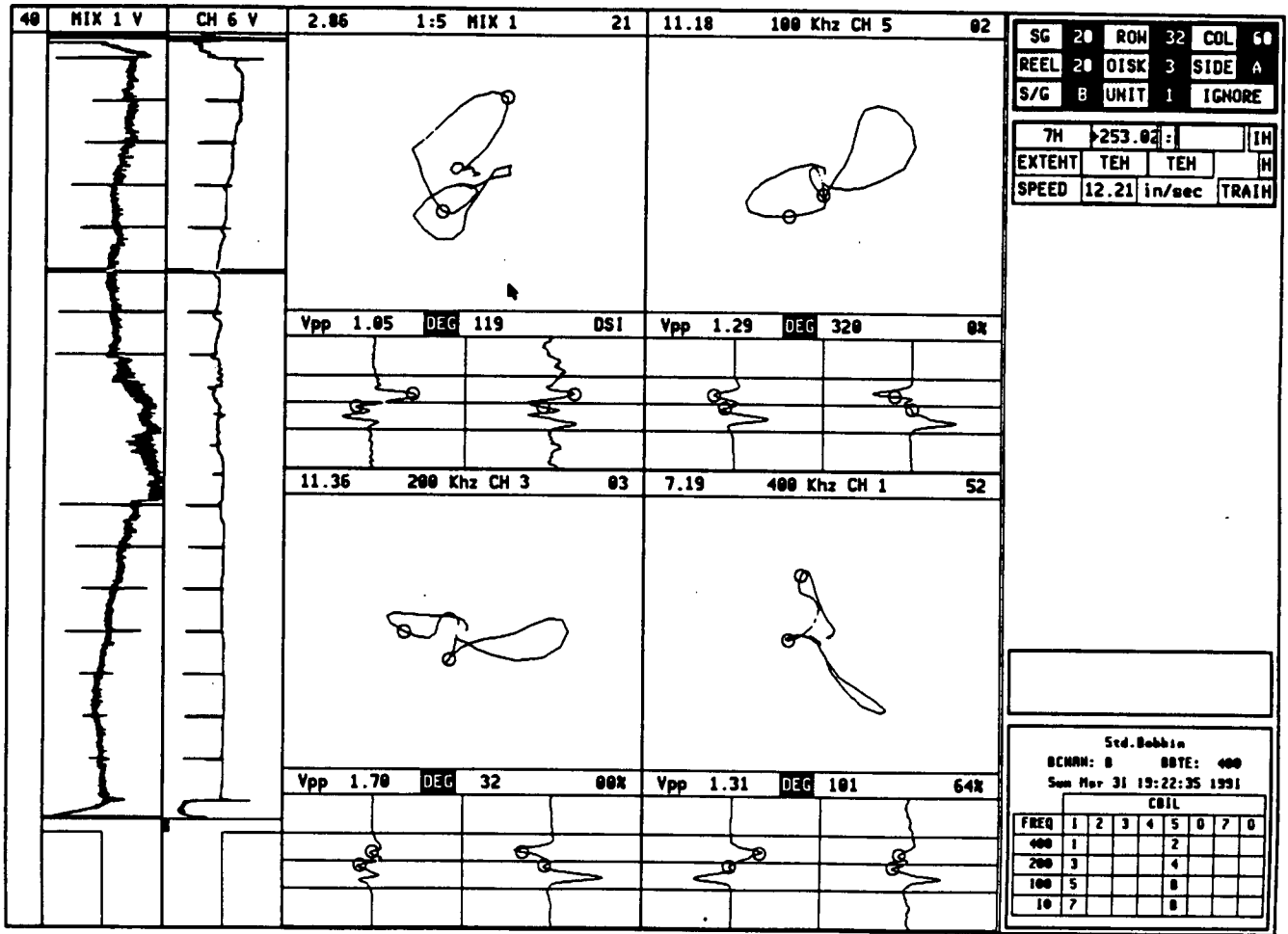Figure A-7   Bobbin Coil Amplitude Analysis of ODSCC at TSP
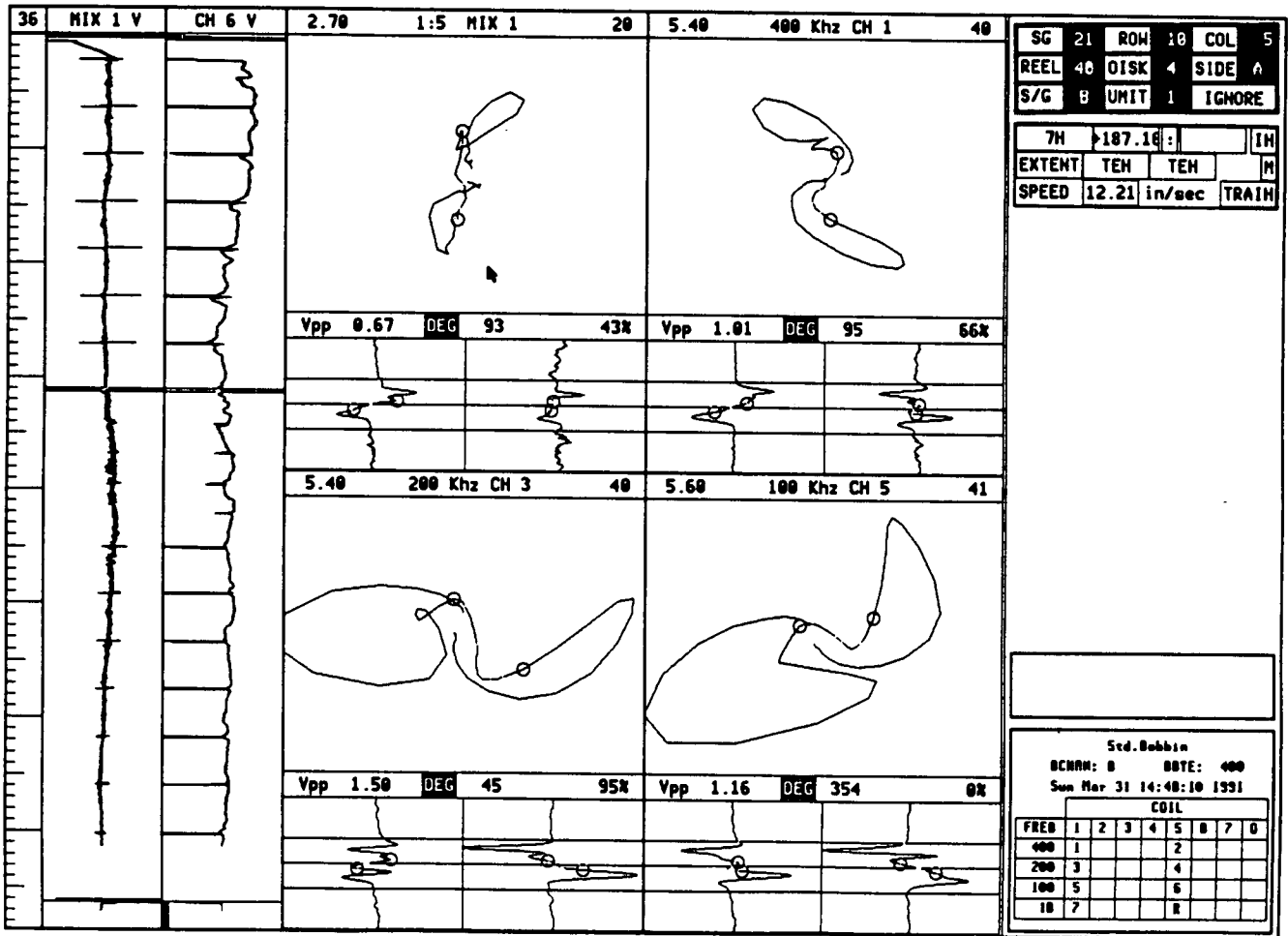
Figure A-8   Bobbin Coil Amplitude Analysis of ODSCC at TSP
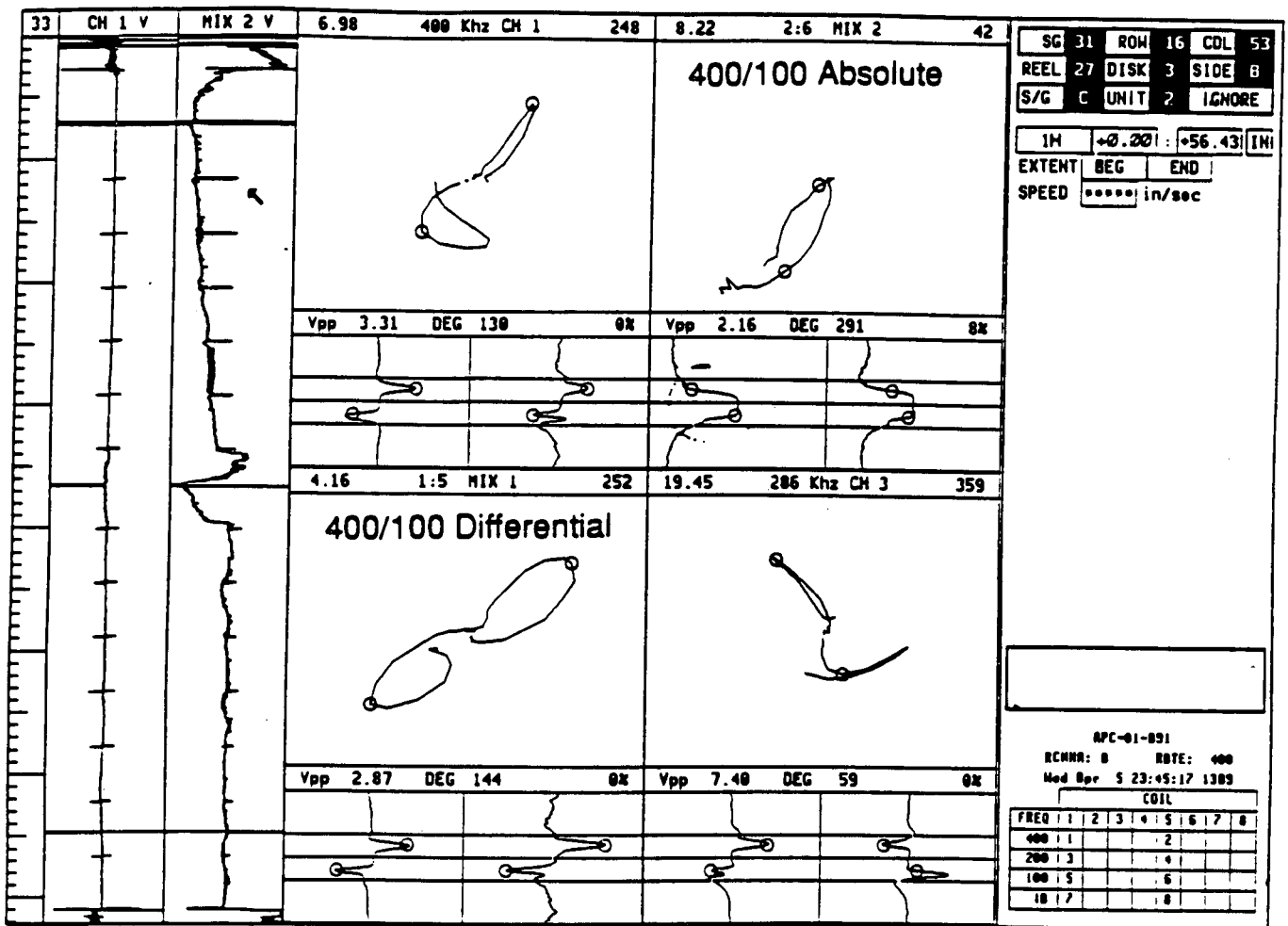
Figure A-9   Example of Bobbin Coil Field Data from Plant A - Absolute
Mix with No ODSCC
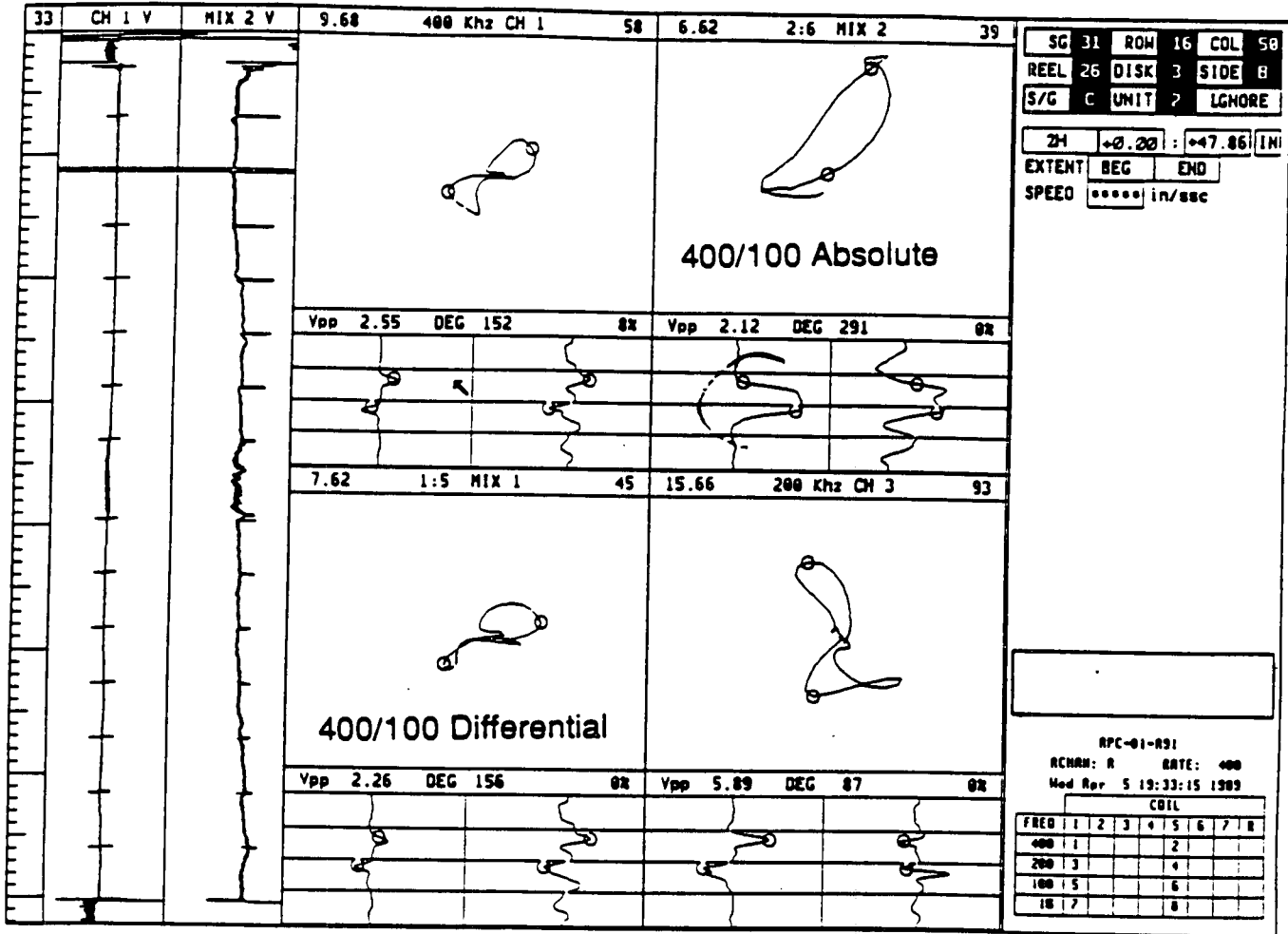
Figure A-10   Example of Bobbin Coil Field Data from Plant A - Absolute
              Mix with No ODSCC
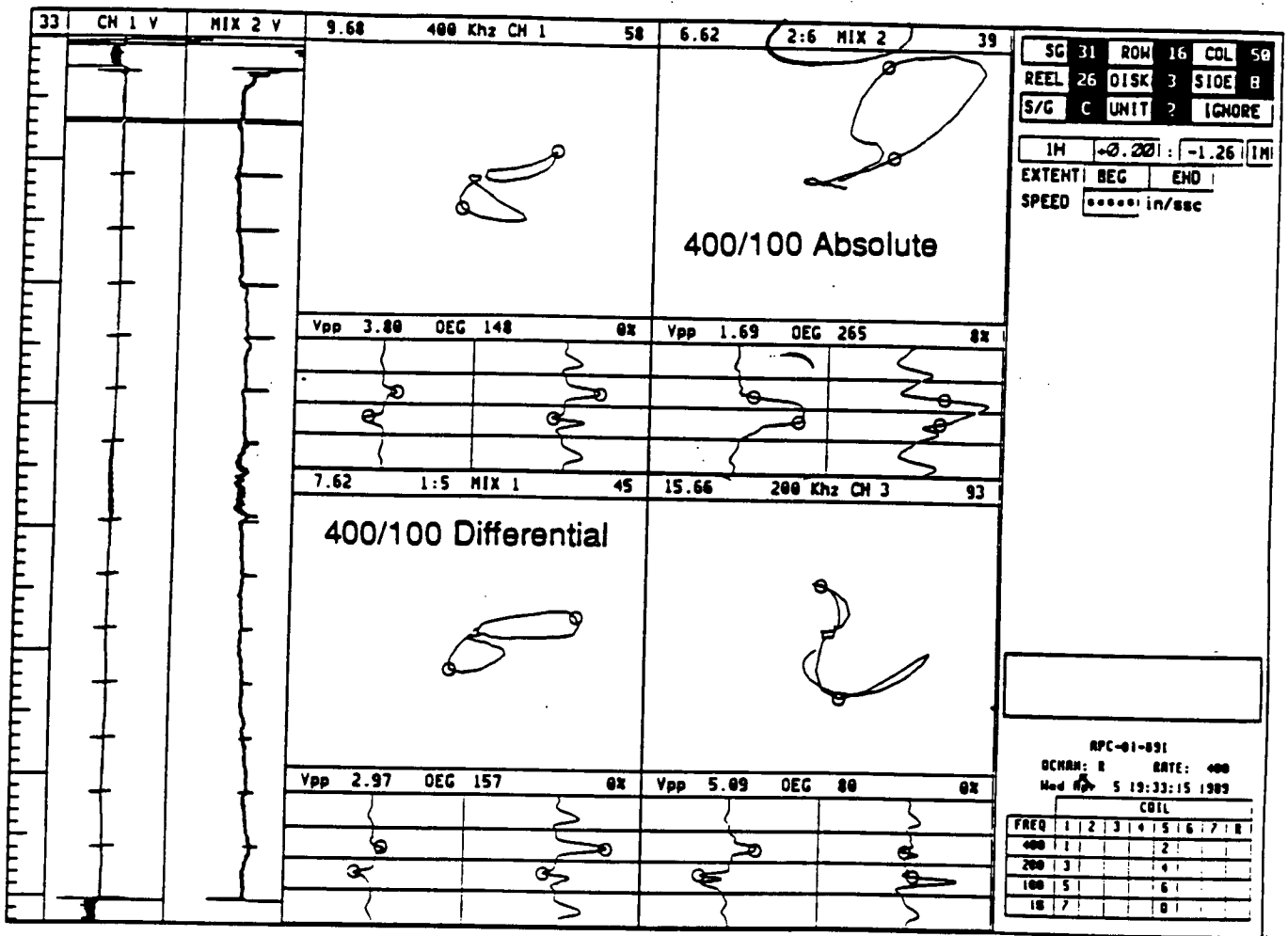
Figure A-11   Example of Bobbin Coil Field Data from Plant A - Absolute Mix with No ODSCC
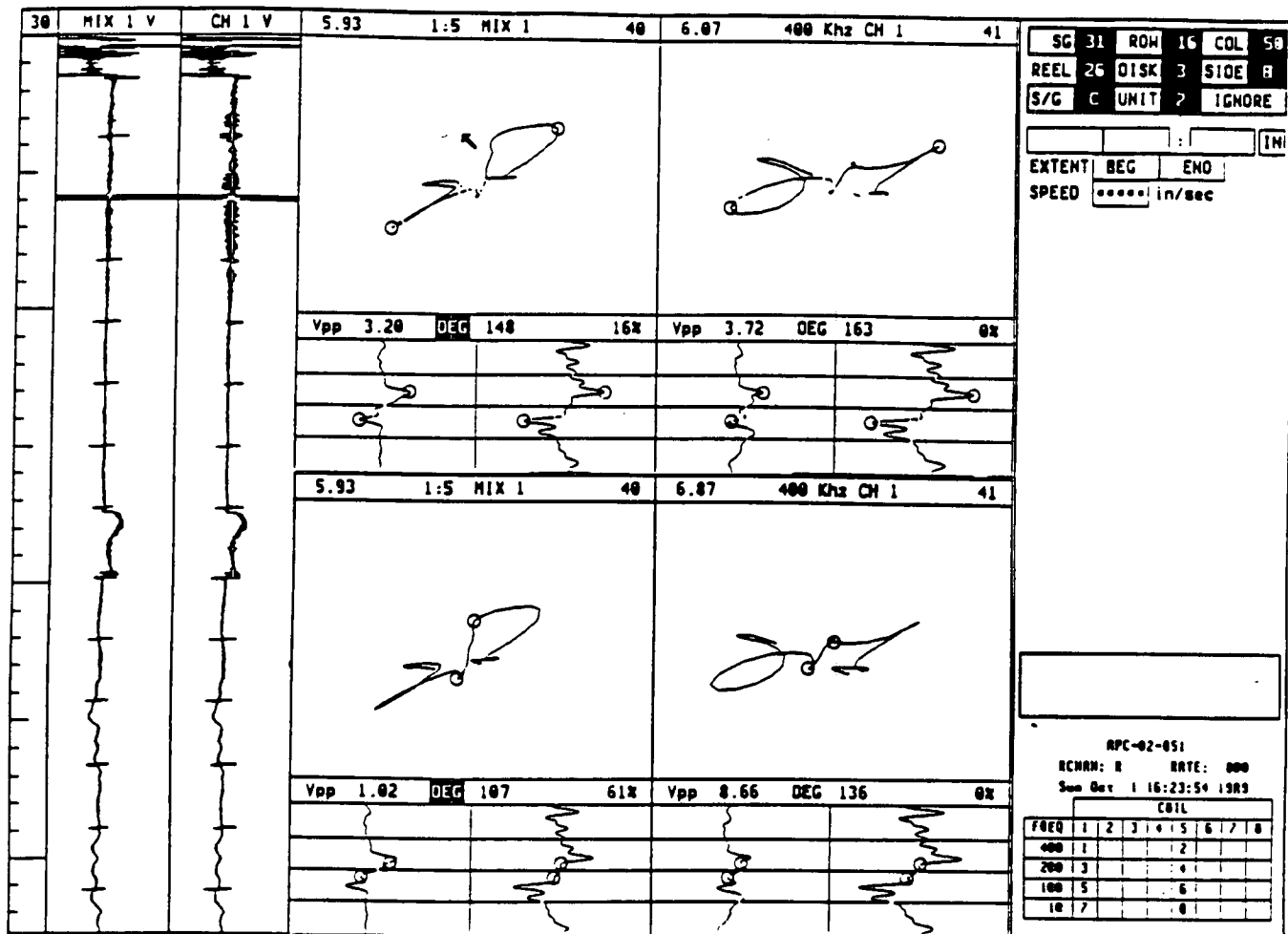
Figure A-12   Example of Bobbin Coil Field Data from Plant A
Flaw Signals of ODSCC at Dented TSP Intersection
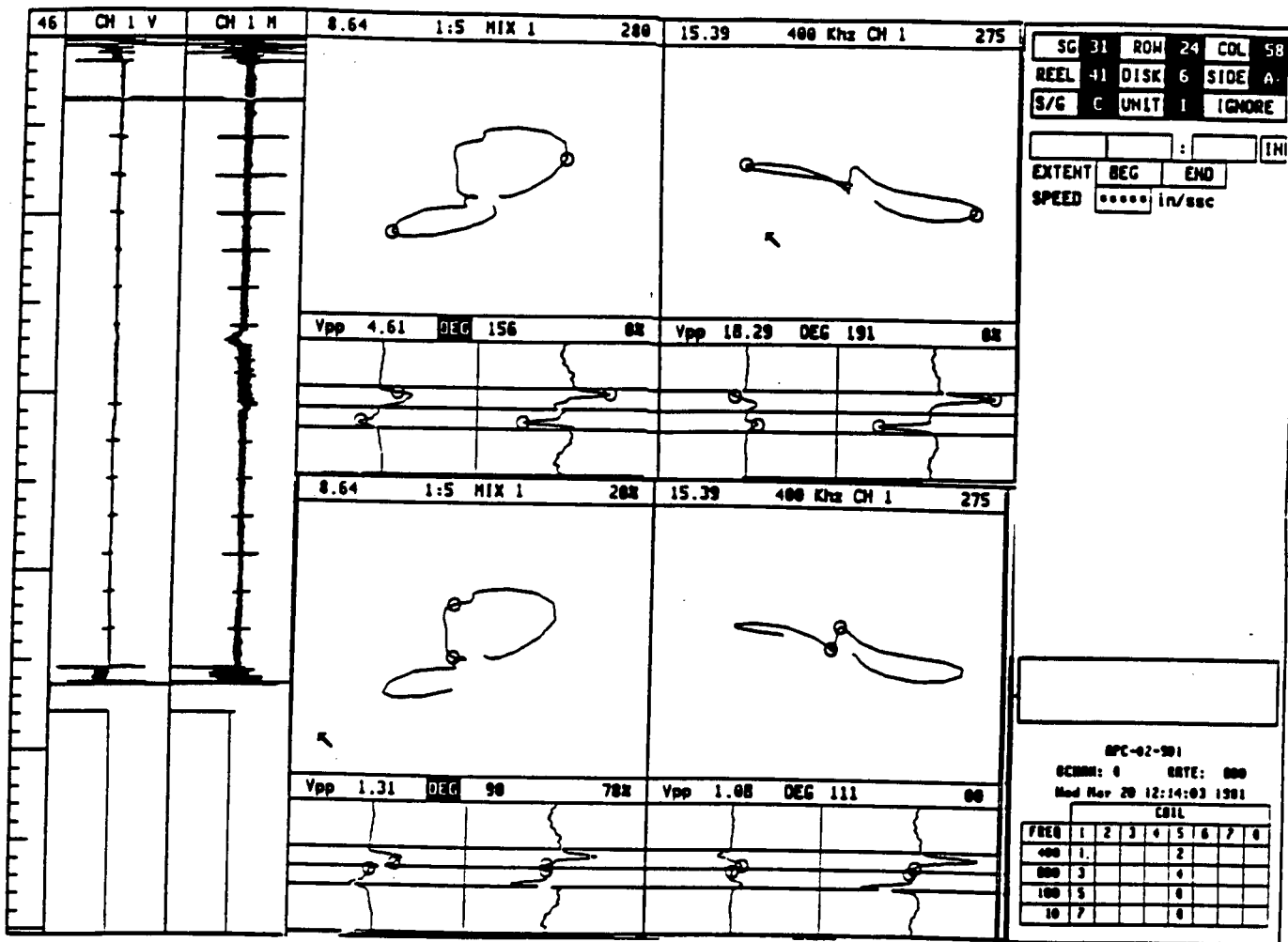
Figure A-13   Example of Bobbin Coil Field Data from Plant A
Flaw Signals of ODSCC at Dented TSP Intersection
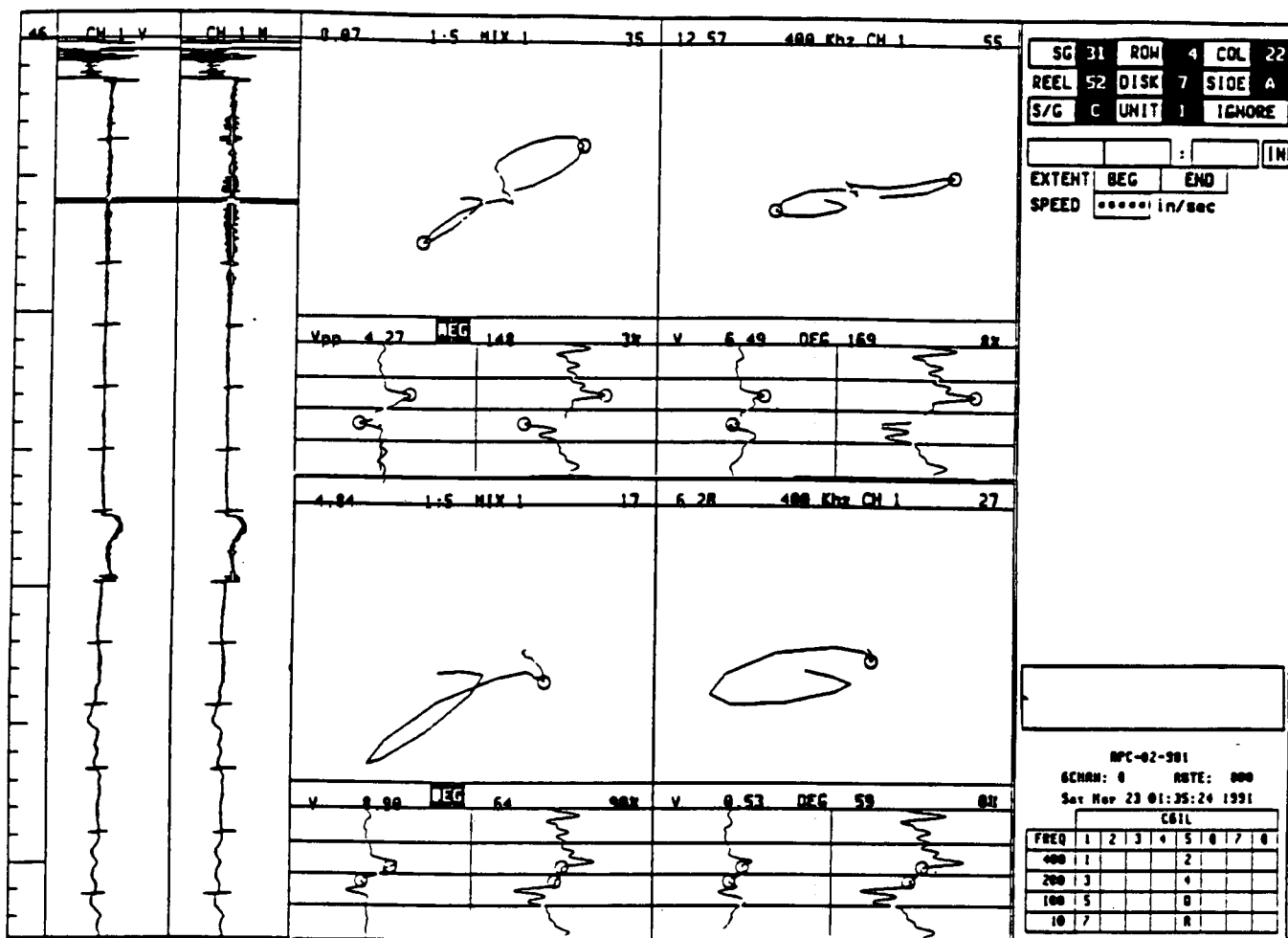
Figure A-14   Example of Bobbin Coil Field Data from Plant A
Flaw Signals of ODSCC at Dented TSP Intersection
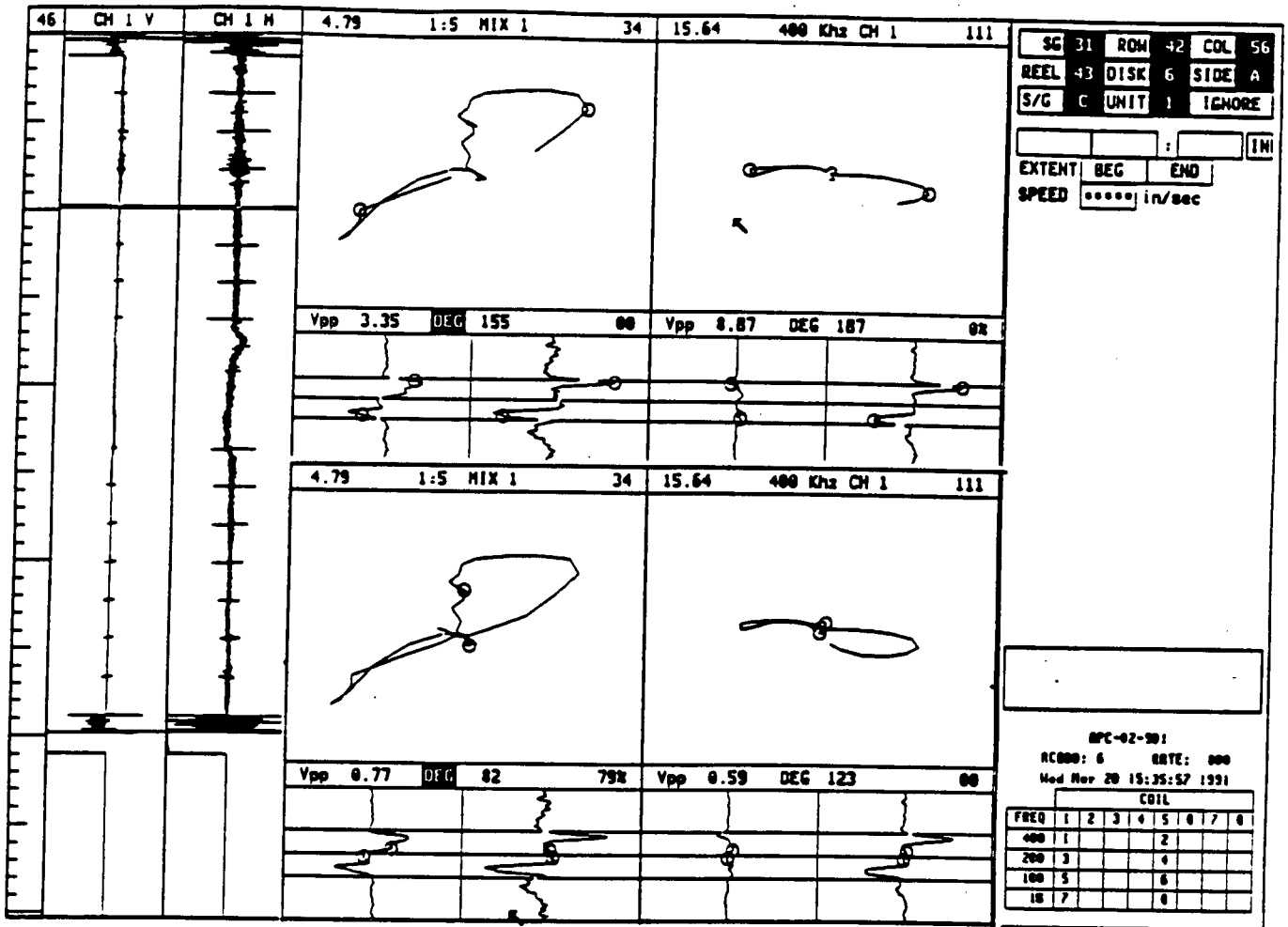
Figure A-15   Example of Bobbin Coil Field Data from Plant A
Flaw Signals of ODSCC at Dented TSP Intersection
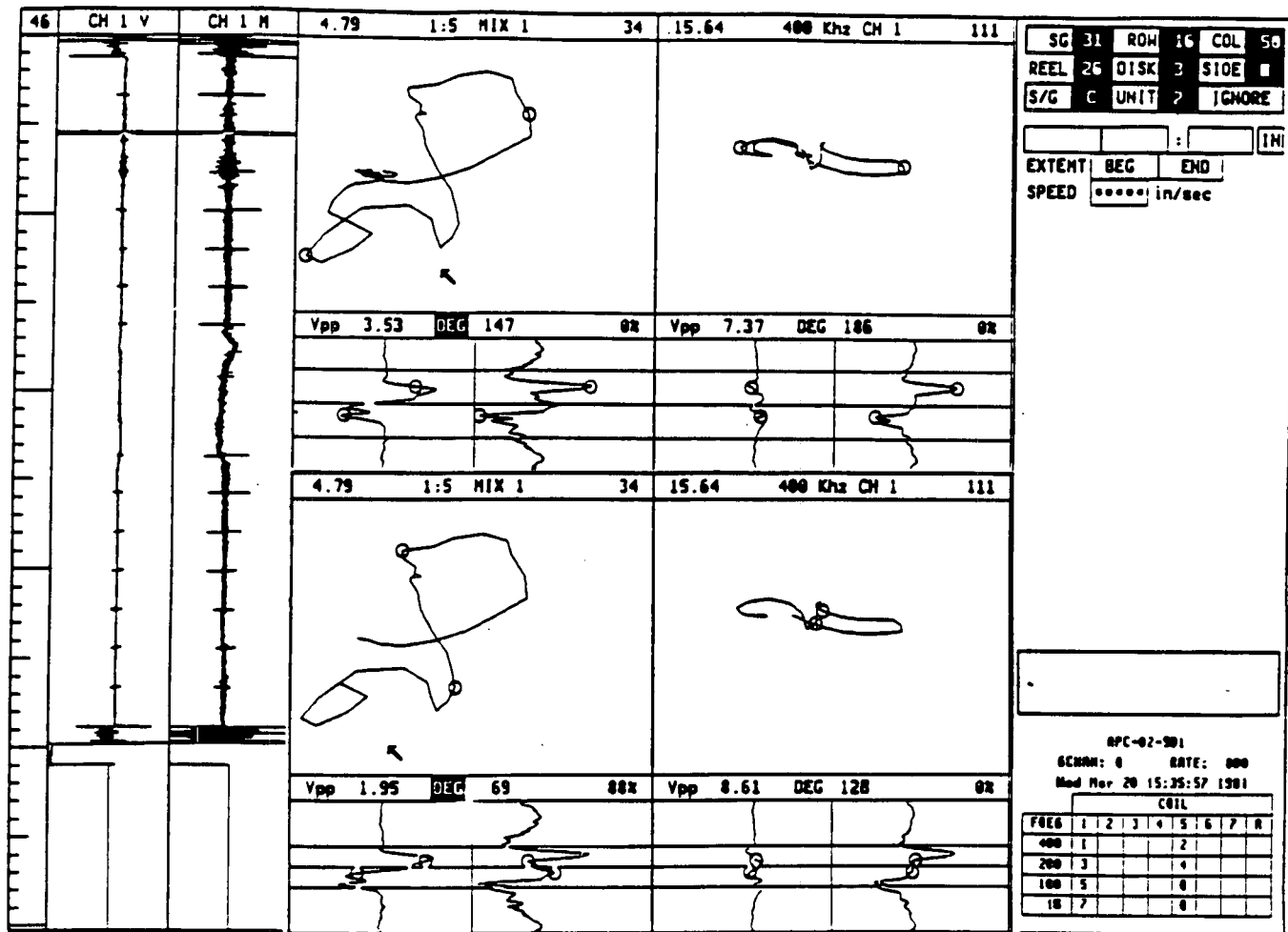
Figure A-16   Example of Bobbin Coil Field Data from Plant A
Flaw Signals of ODSCC at Dented TSP Intersection
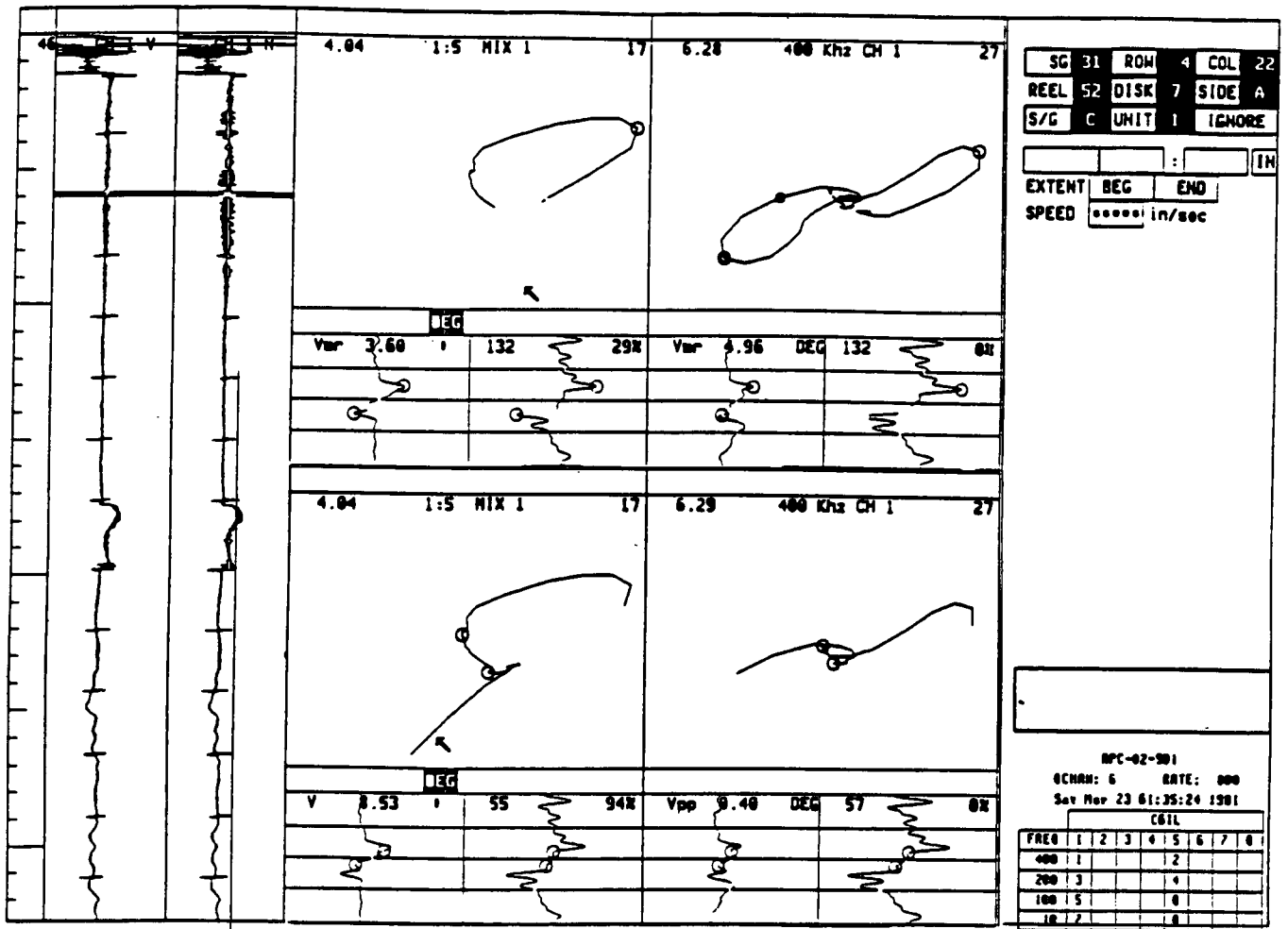
Figure A-17   Example of Bobbin Coil Field Data from Plant A
Flaw Signals of ODSCC at Dented TSP Intersection
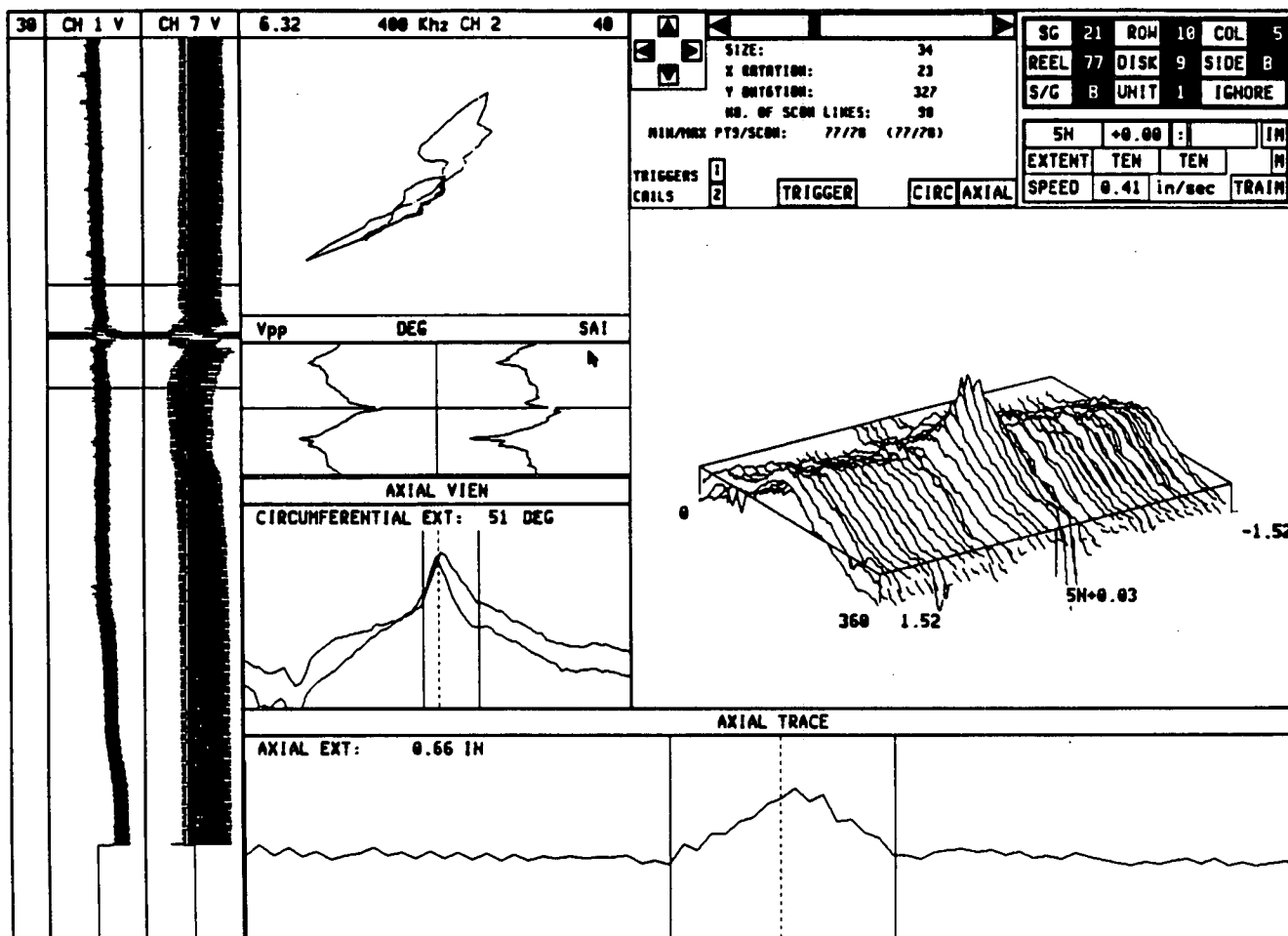
Figure A-18   Example of Rotating Pancake Coil Field Data
                Single Axial ODSCC Indication (SAI)
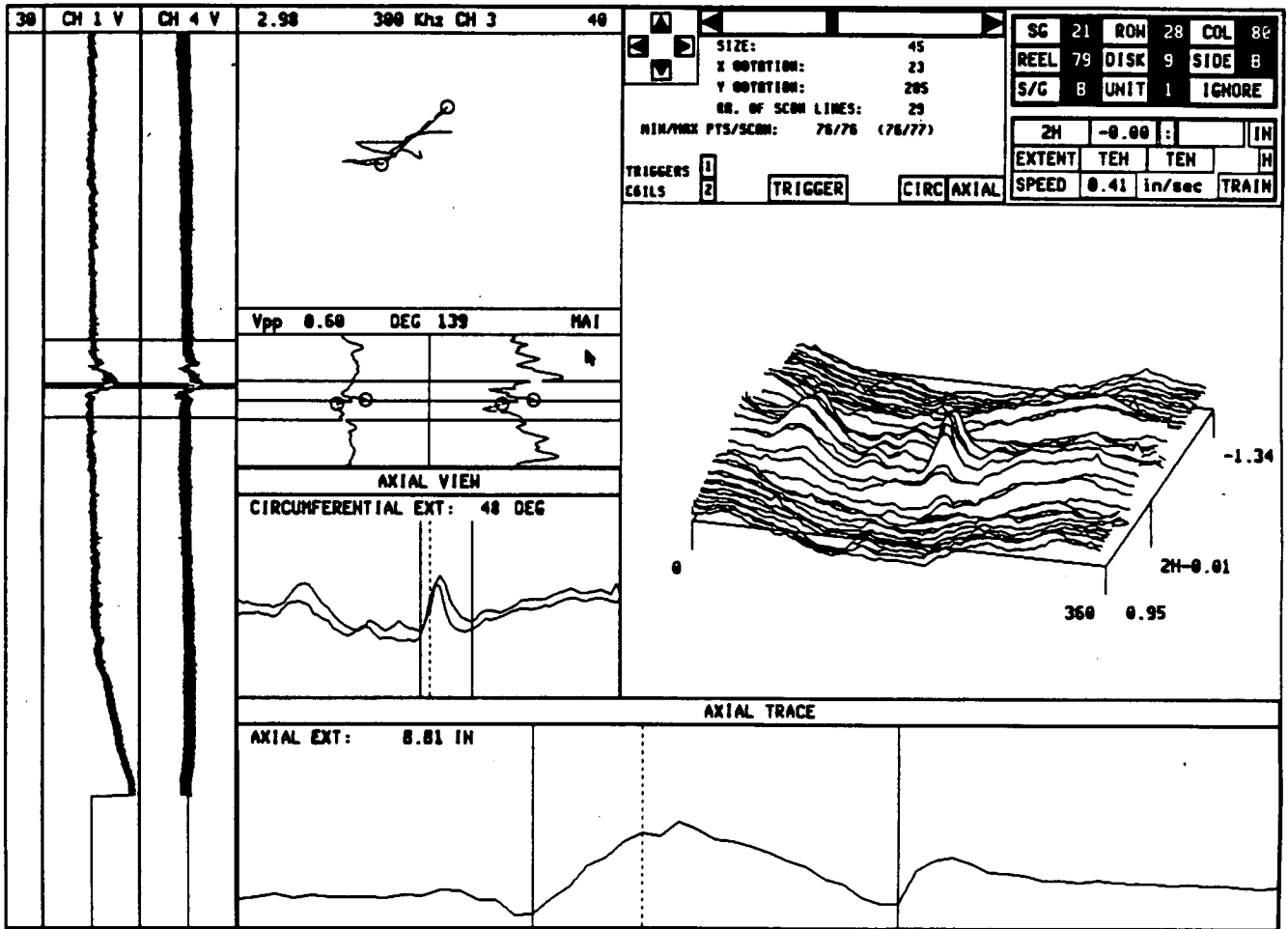
Figure A-19   Example of Rotating Pancake Coil Field Data
               Multiple Axial ODSCC Indication (MAI)
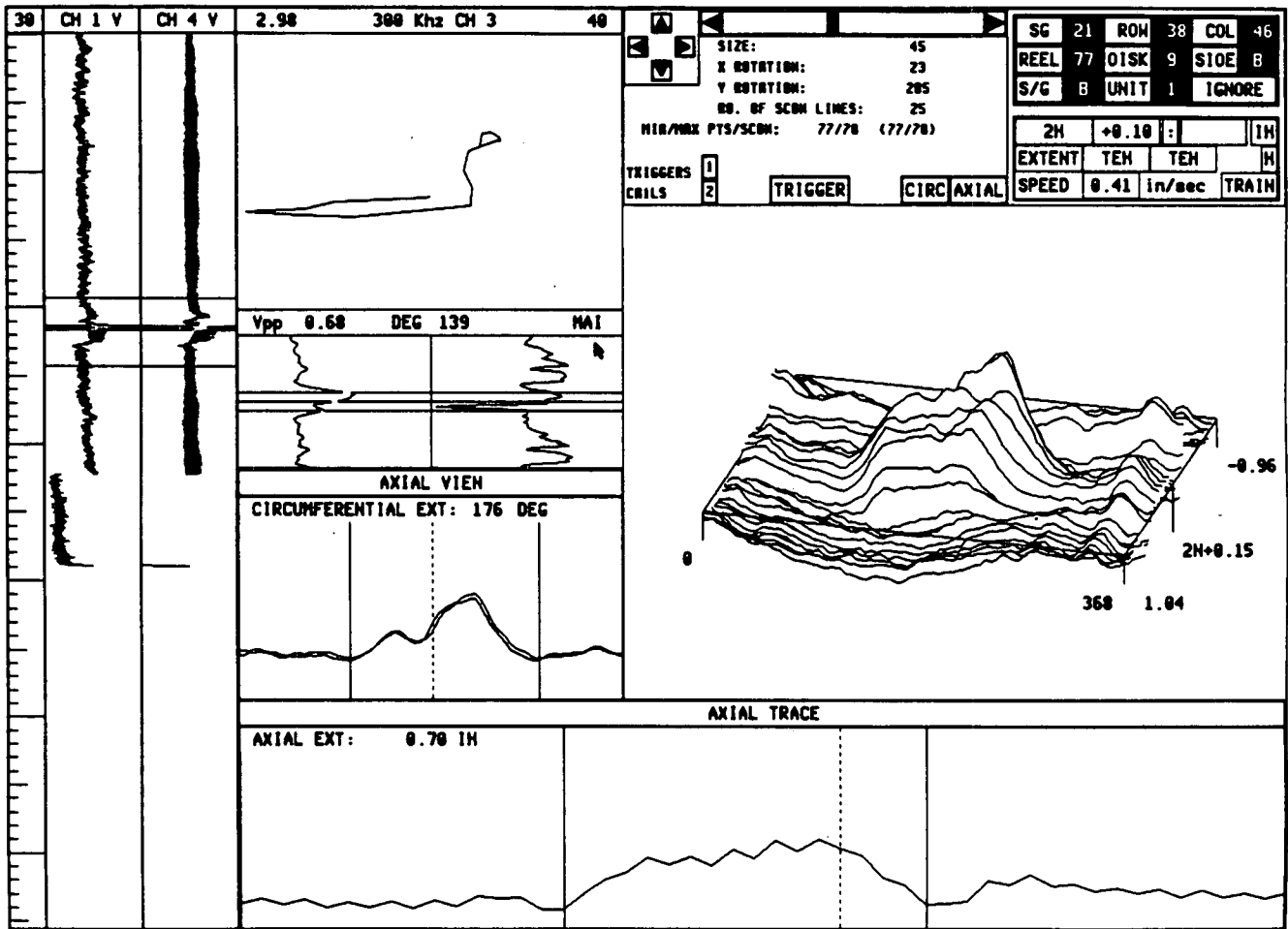
Figure A-20   Example of Rotating Pancake Coil Field Data
                     Multiple Axial ODSCC Indication (MAI)
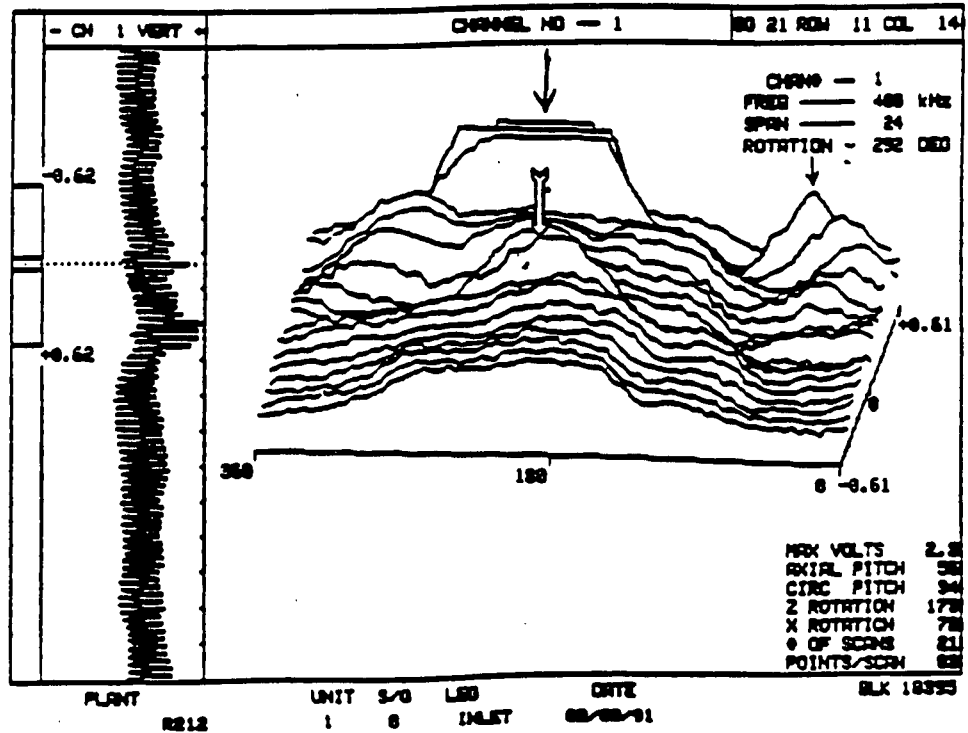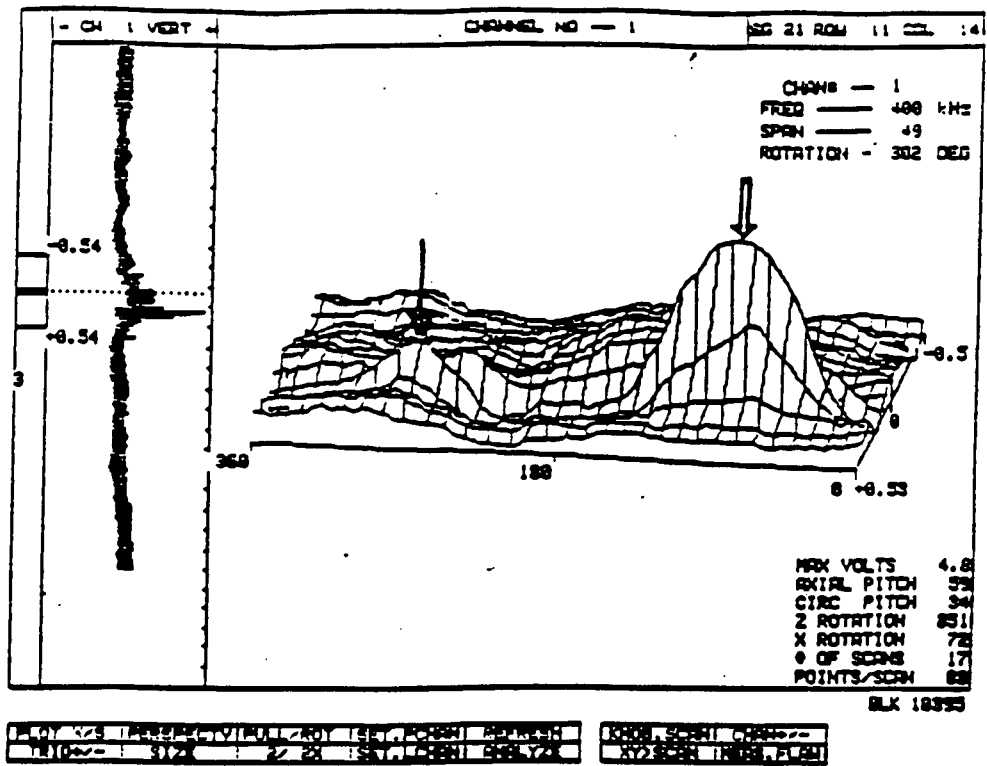
Figure A-21   Example of Rotating Pancake Coil Field Data from Plant A
Circumferential ODSCC Indication (COI)

B.1   Objectives

Test results from leak rate testing of 7/8 inch OD tubes with cracks were presented in Sections 6, for pulled tubes and Section 7, for laboratory prepared specimens. The tests were conducted under typical pressure differentials of normal power operation (NOP) and steam line break (SLB). However, it may not be identical to specific plant conditions. For instance, measurements at SLB conditions were obtained at a 2650 psi pressure differential but with a 350 psia secondary side pressure rather than a prototypic 15 psia pressure to improve the maintenance of constant test conditions in the measurement facility.

An adjustment procedure has been developed to scale the test conditions to specific plant conditions. The objectives of this appendix are as follows.

1. Adjust the French room temperature measurements of leak rate to operating temperature, and adjust to reference pressure differential from measured pressure differential.
2. Adjust Westinghouse meaurements at operating temperature from high primary pressure to realistic primary pressure during steam line break.
3. Adjust leak rates at temperature between measured and reference pressure differentials.

B.2   Leak Rate Adjustment Procedure

Paul Hernalsteen of Laborelec in Belgium has developed adjustment procedures to scale the Belgian data to operating temperature and pressures different from the measured ones. First, we define the leak rate as follows.

$$L = KA(\Delta p, T)\sqrt{\frac{2\Delta p}{\rho(T)}} \tag{1}$$

where

L = volumetric leak rate
K = discharge coefficient
A = leakage flow area; a function cf Δp and temperature T
ρ = water density; a function of temperature T
T = water temperature
Δp = pressure differential; $p_1 - p_2$ if no flashing or $p_1 - p_{1f}$ if flashing at p_{1f}
p_1 = upstream pressure, or primary side pressure
p_2 = downstream pressure, or secondary side pressure
p_{1f} = saturation pressure corresponding to upstream temeperature T_1

The pressure differential is the difference between upstream and downstream pressure of the cracked passage of the tube. During steam line break, the leak flow may flash on the secondary side. So the effective downstream back pressure is equal to the saturation pressure p_{1f} if it flashes at the saturation point of the upstream temperature T_1.

B.2.1 Adjustment under the Same Temperature

Let us consider the measurement conditions of leak rate at a reference temperature T_o. Now we can write

$$L(\Delta p_{mo}, T_o) = KA(\Delta p_{mo}, T_o) \sqrt{\frac{2\Delta p_{mo}}{\rho(T_o)}} \qquad (2)$$

$$L(\Delta p_o, T_o) = KA(\Delta p_o, T_o) \sqrt{\frac{2\Delta p_o}{\rho(T_o)}} \qquad (3)$$

where the subscript o indicates the condition at the reference temperature T_o, and the subscript m refers to measurement. In addition,

Δp_o = desired pressure differential at the reference temperature

Δp_{mo} = listed measurement pressure differential at the reference temperature

Both Eqs (2) and (3) describe the leak rate at the reference temperature but at different pressure differentials. Eq (2) is used for the test measurements. Eq (3) is for desired conditions, to which Eq (2) is to be adjusted. The leak rate is adjusted from the measured pressure differential Δp_{mo} to a desired pressure differential Δp_o under the same temperature T_o. by the following:

$$L(\Delta p_o, T_o) = \delta\, L(\Delta p_{mo}, T_o) \qquad (4)$$

where the coefficient δ is a function of pressure differential as follows:

$$\delta = \frac{A(\Delta p_o, T_o)}{A(\Delta p_{mo}, T_o)} \sqrt{\frac{\Delta p_o}{\Delta p_{mo}}}$$

This coefficient δ involves two parameters. The first one is the area of crack flow opening. The second one is the pressure differential. Rearranging the above expression as follows:

$$\delta = \frac{A(\Delta p_o^*, T_o)}{A(\Delta p_{mo}^*, T_o)} \sqrt{\frac{\Delta p_o^*}{\Delta p_{mo}^*}} \sqrt{\frac{\Delta p_o/\Delta p_o^*}{\Delta p_{mo}/\Delta p_{mo}^*}} \qquad (5)$$

where the following definition has been used:

$$\Delta p^* = p_1 - p_2$$

The asterisk (*) emphasizes the total difference of the upstream and downstream pressures, irregardless of whether water flashing taking place or not. When the Δp is used without the superscript * it can be $p_1 - p_2$ for non-flashing situation or $p_1 - p_{1f}$ for flashing situation. Explicit function of Eq (5) will be given later. Eqs (4) and (5) adjust the laboratory test data to any Δp_o to be analyzed at the same temperature.

B.2.2 Adjustments under Different Temperatures

Steam generator tube leakage occurs in general at operating temperatures T, of about 616°F. The Belgian data were measured at the room temperature. It is desired to scale the laboratory, room temperature data to the operating temperature. To accomplish this, the following equality is developed:

$$L(\Delta p, T) = L(\Delta p, T) \frac{L(\Delta p_o, T_o)}{L(\Delta p_o, T_o)} \tag{6}$$

Using Eq (4), Eq (6) becomes

$$L(\Delta p, T) = \delta\, L(\Delta p_{mo}, T_o) \frac{L(\Delta p, T)}{L(\Delta p_o, T_o)} \tag{7}$$

Using Eq (1), Eq (7) appears as follows:

$$L(\Delta p, T) = L(\Delta p_{mo}, T_o)\, \delta\, \frac{A(\Delta p^*, T)}{A(\Delta p_o^*, T_o)} \sqrt{\frac{\rho_o}{\rho}} \sqrt{\frac{\Delta p}{\Delta p_o}} \tag{8}$$

The above expression describes the procedure to adjust a measured leak rate at Δp_{mo} and T_o to an equivalent leak rate at Δp^*_o ($= \Delta p^*$) and T.

The leak rate $L(\Delta p, T)$ is the volumetric rate at operating temperature T. However, the leak rate detected in actual plant monitoring is collected at room temperature T_o. Laboratory tests of leak rate under the operating temperature are generally collected at room temperature, also. An equivalent room temperature, volumetric leak rate, say $L(\Delta p, T)_{T_o}$ can be obtained from

$$\rho L(\Delta p, T) = \rho_o L(\Delta p, T)_{T_o} \tag{9}$$

Using Eqs (8) and (9), the following is obtained

$$L(\Delta p, T)_{T_o} = L(\Delta p_{mo}, T_o)\, \delta\, \frac{A(\Delta p^*, T)}{A(\Delta p_o^*, T_o)} \sqrt{\frac{\rho}{\rho_o}} \sqrt{\frac{\Delta p}{\Delta p_o}} \tag{10}$$

Rewriting the above equation as follows:

$$L(\Delta p, T)_{T_o} = \alpha\, \beta\, \gamma\, L(\Delta p_{mo}, T_o) \tag{11}$$

where,

$$\alpha = \frac{A(\Delta p_o^*, T_o)}{A(\Delta p_{mo}^*, T_o)} \sqrt{\frac{\Delta p_o^*}{\Delta p_{mo}^*}} \tag{12}$$

$$\beta = \frac{A(\Delta p^*, T)}{A(\Delta p_o^*, T_o)} \sqrt{\frac{\rho}{\rho_o}} \qquad (13)$$

$$\gamma = \sqrt{\frac{\Delta p / \Delta p_o^*}{\Delta p_{mo} / \Delta p_{mo}^*}} \qquad (14)$$

The α factor involves a ratio of flow area of the crack opening as a function of Δp^*_{mo} and Δp^*_o under the same upstream temperature T_o. The α factor captures a mechanical effect of total pressure differential on crack opening area. The β factor adjusts the temperature effect on the leak rate through a flow area change and upstream water density variation under the same total pressure differential (i.e., $\Delta p^*_o = \Delta p^*$). The g factor takes care of the hydraulic effect of pressure differential on the leakage flow rate.

B.2.1 The Mechanical Factor α

According to the report by Hernalsteen of Laborelec, significant tearing has been observed during tube pulling. The measured leak rates in Table B-1 represent the behavior of significant tearing of crack length. For each of the eight leaking tubes, the leak rates have been plotted as a function of pressure differential on a semi-logarithmic paper. There are usually four data points per test tube and they reasonably align along a straight line. According to the straight line fitting of leak rate, Hernalsteen developed the following correlation for scaling measured leak rate from one pressure differential to another one at same room temperature.

$$\alpha = 10^{(\Delta p_o - \Delta p_{mo})/725} \qquad (15)$$

where the pressure differentials are in psi. This correlation cf the mechanical adjustment faotor α fits the Belgian pulled tubes data of Table B-1. Behavior of the pressure adjustment factor may vary from one pulled tube to another.

B.2.2 The Temperature Factor β

The flow opening area of the crack is approximately (as confirmed by CRACKFLO analyses) inversely proportional to the product of flow stress σ_f and Young's modulus E of the tube metal. Both flow stress and Young's modulus are functions of temperature. Therefore, it follows that

$$\beta = \frac{E_o \, \sigma_{fo}}{E \, \sigma_f} \sqrt{\frac{\rho}{\rho_o}} \qquad (16)$$

where ρ is the water density corresponding to upstream temperature T_1 and pressure p_1. The ρ_o refers to a T_1 at room temperature, say 70°F.

B.2.3 The Hydraulic Factor γ

The γ factor describes the effect of pressure differential on leakage flow rate. When there is no water flashing at T_o and T, $\Delta p = \Delta p^*_o$ and $\Delta p_{mo} = \Delta p^*_{mo}$, so $\gamma = 1$. When there is water flashing the effective pressure differentials for Δp and Δp_{mo} must be used. The γ factor can be

rewritten as follows:

$$\gamma = \sqrt{\frac{(p_1 - C_p p_{1f})/\Delta p_o^*}{(p_{mo1} - C_{pmo}p_{mo1f})/\Delta p_{mo}^*}} \quad \text{for flashing at } T_o \text{ and } T$$

$$= \sqrt{(p_1 - C_p p_{1f})/\Delta p_o^*} \quad \text{for flashing at } T \text{ only}$$

$$= 1 \quad \text{for non-flashing at } T_o \text{ and } T \tag{17}$$

where C_p is a parameter to correlate the effective flashing pressure. For an isentropic process of water choking (or flashing), the flashing takes place at the saturation pressure corresponding to the upstream water temperature T_1 (e.g., T_1, T_{o1}). So $C_p = 1$ is for an isentropic process. If a real process deviates significantly from an isentropic one, the parameter C_p will be less than unity.

B.3.0   The Mechanical Factor α

B.3.1   Belgian Factor α and   Leak Rate Adjustment for Plant E-4 Data

Table B-1 presents measured leak rates for the pulled tubes from Plant E-4 steam generators. The leak rate tests were done at room temperature (70°F). There are eight pulled tube samples which were tested. These data have been used to establish Eq (15) for the mechanical adjustment factor α.

CRACKFLO has been developed based on Westinghouse fatigue crack and pulled tube data. The CRACKFLO pressure adjustment factor is different than the Belgian. The difference is believed due to minimal ligament tearing used in the CRACKFLO model compared to significant tearing in the Belgian pulled tubes. The next subsection will discuss the mechanical adjustment factor for minimal ligament tearing.

B.3.2   General Mechanical Factor α and Leak Rate Adjustment for Minimal Ligament Tearing

A mechcanical adjustment factor a for minimal ligament tearing is proposed as follows.

$$\alpha = e^{(\Delta p_o - \Delta p_{mo})/725} \tag{18}$$

For the Plant E-4 data, the constant (725 psi) in Eq (15) principally varied from 725 to 940 with one indication at about 1450. The larger constants tended to occur when there was increased evidence of damage from tube pulling effects which would likely lead to higher than expected leak rates at low pressure differentials such as normal operating conditions. Leak rate at higher pressure differentials such as SLB conditions would be less influenced by ligament tearing in tube pulling operations as some ligaments would likely tear away at the higher pressure differential. For this reason, Laborelec has recommended the constant of 725 psi for all Plant E-4 tube intersections.

Eq (18) is similar to Eq (15), except the base is e (=2.718) rather than 10. The applicability of Eq (18) with the CRACKFLO code is verified below. Table B-2 presents the CRACKFLO code results of leak rate at different crack lengths under a variety of pressure differentials during

power operation. Table B-2 also includes comparison of the CRACKFLO adjustment factor and the a factor by Eq (18). Similar to Table B-2, Table B-3 presents the comparison for a variety of pressure differentials under steam line break.

The Belgian α adjustment factor for Plant E decreases faster than the CRACKFLO and exponential adjustment factors for decreases in Δp from the reference point. Use of the exponential adjustment factor is then conservative in estimating the leak rate when the adjustment is toward a lower Δp. Adjustment to Westinghouse measurements in this report are to lower pressure differentials such that the use of the exponential form (Eq (18)) leads to higher adjusted leak rates than if Eq (15) were applied.

B.4 Temperature and Flashing Adjustment Factors

Temperature adjustment factor β is defined by Eq (16). Flashing adjustment factor γ is defined by Eq (17).

B.4.1 Temperature Factor β Only and Leak Rate Adjustment (i.e., without Flashing)

For water without flashing at T_o and T and $\Delta p = \Delta p_o = \Delta p_{mo}$, it follows that

$$L(\Delta p, T)_{T_o} = \beta \, L(\Delta p_{mo}, T_o)$$

This β factor can be compared with the CRACKFLO calculated adjustment factor under non-flashing conditions. Table B-4 presents the comparison for the case without water flashing. Similar results were obtained for crack lengths of 0.4 and 0.6 inch. These results indicate that the approximation of Eq (18) to Eq (13) yields good agreement with the more detailed crack area models in CRACKFLO for leak rate ratios between different temperatures.

B.4.2 Adjustment Factors β and γ from Room to Operating Temperature under SLB Conditions

For water flashing at T and non-flashing at T_o and $\Delta p_o = \Delta p_{mo}$, it follows that

$$L(\Delta p, T)_{T_o} = \beta \, \gamma \, L(\Delta p_{mo}, T_o)$$

where β is given in Eq (16) and γ by the second expression of Eq (17). Table B-5 presents the comparison of leak rate adjustment between the CRACKFLO code and the proposed expressions with a pressure coefficient $C_p = 1.0$.

For $C_p = 1.0$, the proposed expressions of β and γ factors yield an adjustment 18% to 25% lower than the CRACKFLO calculated factor. The deviation comes from the flashing point. A $C_p = 1.0$ implies that flashing takes place at the saturation pressure corresponding to upstream temperature T_1. For $T_1 = 616°F$, the saturation pressure $p_{1f} = 1735$ psia. However, because of heat transfer and friction along the leakage passage, the water flashing will occur at lower pressure, or a saturation pressure corresponding to a temperature lower than the upstream temperature T_1. In fact, the CRACKFLO code predicts a flow choking at a pressure less than p_{1f}.

To bring the proposed equation to yield a result equal to the CRACKFLO calculation, a C_p is obtained for each case. Table B-6 presents the results for C_p. The longer the crack length the

larger the pressure coefficient for a given pressure differential. A longer crack length means a larger crack opening, and thus less friction and smaller heat transfer effect. It approaches the ideal case: an isentropic (i.e., frictionless and adiabatic) process -- a situation with less leak rate. We can use C_p = 0.85 for p_1 = 2350 psia, and C_p = 0.77 for p_1 = 2665 psia.

B.4.3 Adjustment Factors α and γ for Primary Δp Changes at Temperatures with Flashing

Westinghouse model boiler leak rate tests of pulled tubes are conducted at a primary pressure higher than the typical pressure during steam line break. The tests were conducted at a temperature of 616°F. The leak rate must be adjusted to the typical primary pressure. The relevant adjustment factors are the mechanical adjustment factor a and the flow flashing adjustment factor γ. It follows that

$$L\big(\Delta p,T\big)_{T_o} = \alpha\gamma L\big(\Delta p_{mo},T_o\big)$$

where the α factor is defined by Eqs (18), and the g factor by the first expression of Eq (17). Note that $T_o = T$ = 616°F. To convert the leak rate to the equivalent volumetric rate at the room temperature (70°F), the following expression is used:

$$L\big(\Delta p,T\big)_{70} = \frac{\rho_{T_o}}{\rho_{70}} L\big(\Delta p,T\big)_{T_o}$$

Eq (18) involves a constant parameter b = 725 psi. Use of b = 725 was fitted from the Belgian data. For Westinghouse data, a specific parameter will be later fitted b for each tube tested.

As an illustration, Table B-7 presents some results of the adjustment factors for scaling from one flashing conditions to another flashing ones. Table B-7 also lists the comparison between the CRACKFLO code prediction and the proposed expressions with appropriate choice of the pressure coefficient C_p. There are good agreements. These lead to confidence in using the proposed expressions of the adjustment factors α and γ.

B.5 Leak Rate Adjustment to Belgian Plant E-4 Data

Table B-8 presents leak rates measured for Plant J-1 cracked tubes for both normal operating and steam line break conditions. Both conditions simulate the typical pressure differentials across the tube, but tests were conducted at room temperature. It is desired to scale these room temperature data to hot temperature of 616°F. First, normal operating data are scaled.

B.5.1 Adjustment for Normal Operating Data

All of normal operating conditions involve no flashing of water. So the adjustment factors are as follows.

$$L\big(\Delta p,T\big)_{T_o} = \alpha\beta L\big(\Delta p_{mo},T_o\big)$$

where the factor a is defined by Eq (15) and the factor β by Eq (16). The Δp_{mo} is 1450 psi and T_o = 70°F. We will scale to Δp_o = 1450 psi and T = 616°F. When there is no water flashing $\Delta p = \Delta p_o$ so γ = 1. The properties of flow stress, Young's modulus and water density can be found in Table B-4. Table B-9 presents leak rate results at the desired conditions.

B- 7

The above table uses $\beta = 1.15 \times 0.81 = 0.93$, and $\gamma = 1$ for scaling from 70°F to 616°F with $\Delta p = 1450$ psi.

B.5.2 Adjustment for Steam Line Break Data

The steam line break (SLB) data may be now adjusted. Table B-8 lists the measured leak rate and pressure differentials Δp_{mo}. To scale them to $T = 616$°F and $\Delta p_o = 2650$ psi and 2335 psi, respectively, the following is used:

$$L(\Delta p, T)_{T_o} = \alpha \beta \gamma L(\Delta p_{mo}, T_o)$$

where the α and β factors are defined by Eqs (15) and (16), respectively, and the γ factor by the second expression of Eq (17) with $C_p = 1.0$. Eq (15) is appropriate for the Plant J-1 data, which had significant ligament tearing. For the same reason of the significant ligament tearing, the pressure coefficient C_p is taken to be unity. Tables 11 and 12 list the adjusted leak rate at a pressure differential of 2650 psi and 2335 psi, respectively.

B.6 Adjustment to Leak Rate Data Base for Alternate Δp

Table B-12 lists the model boiler tests and plant data. Leak rate adjustment for these data was made using both mechanical and hydraulic factors as described in Sect. 4.3. Table B-13 presents the adjusted leak rate for the normal operating (NOP) and SLB conditions. Four sample tubes results in adjusted leak rates for SLB being less than the adjusted leak rate under NOP. For conservatism, the measured SLB leak rate are retained as the final value for those four tubes.

Table B-1
Results of Leak Rate Tests under Room Temperature
and Typical Pressure Differentials during Steam Line Break

<u>Normal Operation Conditions</u>   <u>Steam Line Break Conditions</u>

⌐   ┐ g

└   ┘

Table B-2
Comparison of the Pressure Adjustment Factor α between
the CRACKFLO Prediction and Proposed Correlation at Tempereture
--Power Operating Pressure Differentials--

Crack Length (in)	Upstream Pressure (psia)	Downstream Pressure (psia)	Upstream Temperature (°F)	Leak Rate (gpm)	Adjustment Factor α		
					CRACKFLO	Exponent	Plant E

⌐   ┐ g

└   ┘

Table B-3
Comparison of the Pressure Adjustment Factor α between the CRACKFLO Prediction and Proposed Correlation at Temperature
--Steam Line Break Pressure Differentials--

Crack Length (in)	Upstream Pressure (psia)	Downstream Pressure (psia)	Upstream Temperature (°F)	Leak Rate (gpm)	Adjustment Factor α		
					CRACKFLO	Exponent	Plant E

a, g

Table B-4
Comparison of the Temperature Adjustment Factor β between the CRACKFLO Prediction and Proposed Expression for the Case without Water Flashing

a, g

Table B-5
Comparison of the Temperature and Flashing Adjustment Factors between the CRACKFLO prediction and Proposed Expression for the Case with Water Flashing

a, g

Table B-6
Pressure Coefficient C_p

a, g

Table B-7
Comparison of the Mechanical and Flashing Adjustment Factors α and γ between the CRACKFLO Prediction and Proposed Correlations at Operating Temperature

Crack Length	Pressure, psia p_1	p_2	Temp $T_1(°F)$	Leak Rate @ 616°F (gpm)	Adjustment Factors α and γ CRACKFLO	Q_2	α	γ	$\alpha\gamma$	a, g

Table B-8
Results of Leak Rate Tests for Plant J-1 Tubes under Room Temperature
and Typical NOP and SLB Pressure Differentials

g

Table B-9
Adjusted Leak Rate from Measured Value at 70°F to a Normal Operating
Pressure Differential of 1450 psi and a Temperature of 616°F

a, g

Table B-10
Adjusted Leak Rate from Measured Value at 70°F to
a SLB Pressure Differential of 2650 psi and a Temperature of 616°F

a, g

Table B-11
Adjusted Leak Rate from Measured Value at 70°F to
a SLB Pressure Differential of 2335 psi and a Temperature of 616°F

a, g

Table B-12
**Results of Leak Rate Tests at 616°F and Normal Operating and
Steam Line Break Pressure Differentials**

Sample Model Boiler	Temperature °F	Normal Operating Pressure Diff. psi	Leak Rate liter/hr	Steam Line Break Pressure or Pressure Differential Primary p_p, psia	Secondary p_s, psia	Differential Δp, psia	Leak Rate liter/hr	g

Table B-13
Results of Leak Rate Tests and Their Adjustments at 616°F and Normal Operating and Steam Line Break Pressure Differentials

Sample Model Boiler	Measured Leak Rate, liter/hr		Adjusted NOP Δp =1300 psi Leak Rate liter/hr	Adjusted SLB Δp=2650 psi Leak Rate liter/hr	Adjusted SLB Δp =2335 psi Leak Rate liter/hr	
	NOP	SLB				a, g.

* Adjustments not included. SLB leak rates are close to normal operating results such that further adjustment is not considered to be appropriate.

† Not reliable data. Measured leak rate at limit of facility prior to modifications for later tests.

Appendix C: Regression Analysis

C.1 Introduction

The analysis of the relationship between two variables is generally termed either *regression* analysis or *correlation* analysis. In addition, one may also find the term *confluence* analysis. For each, the objective is to establish a mathematical model describing a predictive relationship between the variables. The use of the term regression is frequently interpreted to imply that some sort of causal relationship exists while correlation has been reserved for non-causal relationships. Other differentiations between the two terms involve the nature of the variables, i.e., whether or not one or both is stochastic. In additon, the term regression is also frequently used to mean the process by which the parameters of a relationship are determined.

For the purposes of the evaluations reported herein the name *regression analysis* is used in the broad sense of covering the aspects of the fitting of a curve, i.e, equation, to observed data points, where concern is with the slope and position of the curve that best fits the data, and to the analysis of how well the data points can be represented by the curve, i.e., the correlation analysis. The correlation analysis has two aspects, one is a measure of the degree of covariablility between two variables, and the second is as a measure of the closeness of fit of a regression line to the distribution of the observations. The statistical analysis is performed for the purpose of establishing a stochastic dependence, and does not, nor does it have to, demonstrate the existence of a causal dependence.

For the analyses dealing with the APC it is desired that models be developed relating the burst strength and leak rate of degraded tubes to the morphology of the degradation. Unfortunately, the degradation morphology is only known exactly for tubes which have been destructively examined. However, a third variable, based on the non-destructive examination of the tubes, is available which is also directly related to the morphology of the degradation. Each degradation state is taken to correspond to a set of quantifiable characteristics or variables, such as the burst strength (measured by a burst pressure test), the leak rate (measured as a function of differential pressure), and a non-destructive examination (NDE) response, e.g., eddy current bobbin coil signal amplitude in either an absolute or differential mode. Since the field examination of the tubes is based on the NDE response it is appropriate to examine the relationships between the first two variables and the third.

The degradation process determines the magnitude of the evolution of each variable; however, the degradation process is complex and the morphology and time history will vary even under conditions which would normally be termed identical. Thus, it is expected that the correlation between any pair of the three variables may have significant scatter. This is expected even if each of the variables is measured with perfect accuracy and contains no measurement error.

It is to be noted that the causative factor relative to the magnitude of each variable is the crack morphology, and that none of the three characteristic variables can be considered to be the cause of the other. This means that for any pair, either may be treated as the predictor and the remaining variable treated as the response. Once a correlating relationship has been established, either variable may be used to predict an expected value for the other. For example, a correlating relationship may be mathematically determined using burst pressure as the response and bobbin amplitude as the predictor. Onca the relationship is known the bobbin amplitude associated with a given burst pressure can be calculated.

The general, linear, first order analysis model relating two variables is given by

$$y_i = a_0 + a_1 x_i + \varepsilon \tag{C.1}$$

where y_i is taken here as the response or predicted variable, and x_i as the predictor. The ε, or error term, accounts for deviations from a perfect prediction. In order to establish confidence and prediction limits on y_i the error is assumed to be normally distributed with a mean value of zero and a variance that is uniform over the range of interest. An analysis is then performed to determine the best values of a_0 and a_1 to use in equation C.1. Three methods are commonly used for the analysis, maximum likelihood estimation, least squares (LS), and weighted least squares (WLS). For maximum likelihood analysis the values of a_0 and a_1 are found that maximize the probability of obtaining the observed responses. The use of maximum likelihood analysis is formally correct, however, if the errors are normally distributed, the maximum likelihood estimators (MLE) will be identical to the estimators obtained using least squares. If both variables are stochastic and the errors are normally distributed then the application of least squares still leads to the maximum likelihood estimators of a_0 and a_1.

The LS method is based on minimizing the sum of the squares of the errors, also referred to as residuals, between the observed and predicted values, thus, the best values of a_0 and a_1 are those that make

$$\sum_{i=1}^{n} (Y_i - \hat{Y}_i)^2 \tag{C.2}$$

a minimum, where the caret indicates the predicted value,

$$\hat{Y}_i = a_0 + a_1 x_i . \tag{C.3}$$

Expression C.2 is differentiated with respect to a_0 and a_1 and the resulting expressions set equal to zero and solved for the coefficients. For WLS the same expres-

sion for the errors is established by considering the error term, ε_i to be weighted non-uniformly, i.e., the error distribution is

$$\varepsilon_i \sim N(0, \Sigma_i \sigma^2) \qquad \cdot (C.4)$$

and the expression to be minimized becomes

$$\sum_{i=1}^{n} w_i (Y_i - \hat{Y}_i)^2, \qquad (C.5)$$

where the Σ_i and hence the w_i are known. In situations where the variance of the response is not uniform it is possible to find appropriate weights such that the resulting estimators are MLE's.

For the unweighted LS analysis the slope of the regression or correlation line is found to be

$$a_1 = \frac{\sum (x_i - \bar{x})(y_i - \bar{y})}{\sum (x_i - \bar{x})^2}, \qquad (C.6)$$

where the summation limits are understood. The intercept is then found as

$$a_0 = \bar{y} - a_1 \bar{x} \qquad (C.7)$$

if y has been regressed on x. If x is regressed on y the slope will be

$$\frac{\sum (x_i - \bar{x})(y_i - \bar{y})}{\sum (y_i - \bar{y})^2} \qquad (C.8)$$

relative to the ordinate axis. If this is reckoned to a coordinate system in which x is the abscissa then the slope relative to the abscissa is

$$a_1 = \frac{\sum (y_i - \bar{y})^2}{\sum (x_i - \bar{x})(y_i - \bar{y})}. \qquad (C.9)$$

If the data used for the analysis contains significant scatter the values found by (C.6) and (C.9) can be quite different. A rough visualization of this can be obtained by picturing the smallest ellipse that can be drawn that envelopes all of the data points. A line connecting the largest and smallest abscissa values of the ellipse will approximate the regression of the y variable on the x variable, while the line connecting the maximum and minimum ordinate values will approximate the regression of the x varaible on the y variable.

For the APC analyses the objective is to relate burst pressure and leak rate to bobbin voltage. This means that bobbin amplitude is depicted as the abscissa variable while burst pressure and leak rate are depicted as ordinate variables respectively. Such depiction does not imply the direction of the regression analysis performed.

C.2 Consideration of Variable Error

If there is measurement error present in the predictor variable the slope obtained from the regression analysis will be biased. For the predictor, say X, the total variance will be

$$\sigma_X^2 = \sigma_x^2 + \sigma_m^2 \tag{C.10}$$

where the subscript m indicates measurement error. It can be shown that in this case the expected value of the calculated slope, a_1, will be

$$a_1 = \frac{\alpha_1}{1 + \frac{\sigma_m^2}{\sigma_x^2}}, \tag{C.11}$$

where α_1, is the true value or the value that would result if no measurement error was present, and

$$\sigma_x^2 = \frac{\sum (x_i - \bar{x})^2}{n-1}. \tag{C.12}$$

It is noted that a_0 would be found from equation (C.7) as before. A key point to note is that the calculated slope underpredicts the true slope (without measurement error). If the measurement error is known, and is uniform, its effect on the analysis slope can be calculated directly and the appropriate slope to be used for prediction would be

$$\alpha_1 = a_1 \left(1 + \frac{\sigma_m^2}{\sigma_x^2} \right). \tag{C.13}$$

When the error varianca is known and can be expressed as a fraction of the variable variance the slope will be affected by a like amount.

When the error varianca is not known an estimate of the true slope can be made using the partitioning technique developed by Wald and subsequently improved upon by Bartlett. The technique consists of partitioning the data into three groups based upon the ordered predictor variable. The line joining the centroids of the upper and lower groups is an unbiased and consistent estimator of the true slope. If the slope thus found is close to the slope determined without considering measurement errors then the measurement errors are not significant.

It is noted that the consideration of measurement errors does not lead to any criteria for selection of a regression direction.

C.3 Detection of Outliers

If the errors are normally distributed the application of LS to determine the coeffi-cients of the regression equation minimizes the varianca of these estimators. The coefficients are also the MLE's. A drawback of the LS technique is that it is not very robust. This means that the fitted line may not be the best estimator of the correct relationship because it can be significantly influencad by potentially outlying data. In addition, the resulting fit may be such that potential outliers become hidden if exam-ined after the analysis is performed. There are established methods for identifying influential data that may result in a distortion of the regression line. Such methods fall into the categories of regression diagnostics and robust regression. Robust regression methods are designed to be insensitive to potential outliers, and can be used to identify outliers based on the residual errors from the robust regression line. A rather simple example of improving the robustness of the fit would be simply minimize the sum of the absolute values of the residuals instead of the sum of the squares. This provides significant improvement if the outlier is in the y-direction for a y on x regression, but is not resistant to outliers in the x-direction.

One very robust technique is termed the "least median of squares," or LMS. The best regression line (or polynomial) is the one for which the median of the squared residuals is a minimum. The drawbacks to this technique are that there is no closed form solution, and techniques for the determination of inferenca regions would be difficult to apply. However, the determination of a reasonable solution is quite easy using a computer. The algorithm proceeds by drawing sub-samples of a given size from the data set. For each sub-sample regression line coefficients and the median of the squared residuals are calculated. The coefficients of the minimum median solution are designated as the LMS solution. A median based scale estimate (analogous to the standard deviation) is determined for the identification of outliers at a two-sided 98% confidence level, or a one-sided 99% confidence level.

The data for the APC were examined using the LMS robust regression program PROGRESS by Rousseeuw and Leroy. It is noted that the application of robust regression is not for the automatic deletion of improbable data points, only for the identification of potential outliers. The rejection of any data is then based on an evaluation of the circumstances surrounding the data collection to search for possible errors.

C.4 Selection of a Regression Coordinate System

For the analysis of continuous variable data, four alternatives were examined for each correlation. These choicas are listed in Table C.1. For each case, the *correla-tion coefficient, r*, measuring the "goodness-of-fit" of the regression line was calculated. The correlation coefficient is a measure of the variation of the data explained by the regression line, thus the largest value is indicative of the best fit. The expression for the square of the correlation coefficient, known as the *index of*

Table C.1: Fitting Options Considered for LS Regression

Abscissa	Ordinate	Relation
Linear	Linear	$y_i = a_1 + a_1 x_i$
Logarithmic	Linear	$y_i = a_1 + a_1 \log(x_i)$
Linear	Logarithmic	$\log(y_i) = a_1 + a_1 x_i$
Logarithmic	Logarithmic	$\log(y_i) = a_1 + a_1 \log(x_i)$

determination (also termed coefficient of determination), is

$$r^2 = \frac{\sum (\hat{y}_i - \bar{y})^2}{\sum (y_i - \bar{y})^2} . \tag{C.14}$$

The index of determination is the proportion of the total variation about the mean of the predicted variable that is explained by the regression line. The scale combination yielding the largest index of determination, and henca, the largest correlation coefficient, was selected for the analysis. In the event that the predicted variable for the regression is the logarithmic tranformation of a physicel variable, the above calculation is performed on the untransformed variable. It is readily apparent, however, that for data with a range of several orders of magnitude, e.g., bobbin amplitude ranging from O(0.1 volt) to O(100 volts), the use of a logarithmic scale is appropriate. It is also to be expected that the variation of observed voltages would be normally distributed about the log of the voltage. The same is true for the leak rate which ranged from O(0.02 l/hr) to O(500 l/hr) for specimens for which leakage was observed.

C.5 Selection of a Regrsssion Direction

As noted in the introduction to this appendix, the bobbin amplitude does not cause the observed burst pressure and vice versa. The same is true for the relation between bobbin voltage and leak rate. Thus, the regression direction is not specified by the choice of variates.

The objective of performing the regression analysis is prediction. For purposes of this analysis the bobbin voltage will be used as a predictor of burst pressure and leak rate. However, the intended use does not dictate the designation of predictor and response for the regression analysis. The LS fit simply finds the line such that the variance of the responses is minimized relative to the regression line. As previously noted, onca the LS fit has been performed either variable can be predicted from the other. In addition, inference regions or bands established for prediction in one

direction may be similarly used in the reverse direction (although the terminology is changed to *discrimination*).

For a regression of y on x, a future value of y_0 for a given x_0 is bounded with a $(1-\alpha)\cdot 100\%$ level of confidence by

$$\left[y_0 - a_0 - a_1 x_0\right]^2 \geq t^2_{1-\alpha/2, n-2} \, s^2 \left[1 + \frac{1}{n} + \frac{(x_0 - \bar{x})^2}{\sum (x_i - \bar{x})^2}\right], \qquad (C.15)$$

where s^2 is the "standard error of regression," i.e.,

$$s^2 = \frac{\sum (y_i - \hat{y}_i)^2}{n-2} \qquad (C.16)$$

and $t_{1-\alpha/2, n-2}$ is found from the student's t-distribution. However, for a given y_0 the bounds on x_0 are found by solving equation C.15 for the values of x_0 that satisfy the equality.

If the scatter of the data is small, the regressions of x on y and y on x will yield slopes that are similar. However, for APC analyses the data exhibit significant scatter and the two regression lines have significantly different slopes. In this case it is appropriate to select the regression line based on non-statistical considerations. Such considerations may be known end points of the regression line, e.g., burst pressure for non-degraded tubes, or comparison of the slope with theory based results. For either regression direction, inferenca regions can be determined.

REFERENCES:

1. Fuller, W.A., <u>Measurement Error Models</u>, John Wiley & Sons, New York (1987).

2.. Draper, N.R., and Smith, H., <u>Applied Regression Analysis, Second Edition, Second Edition</u>, John Wiley & Sons, New York (1981).

3. Hald, A., <u>Statistical Theory with Engineering Applicetions</u> John Wiley & Sons, New York (1952).

4.. Bartlett, M.S., *Fitting a Straight Line When Both Variables are Subject to Error*, Annals of Mathematical Statistics, Vol. 5, pp. 207-212 (1949).

5. Wald, A. *Fitting a Straight Line When Both Variables are Subject to Error*, Annals of Mathematical Statistics, Vol. 11, pp. 284-300 (1940).

6. Rousseeuw, P.J., and Leroy, A.M., <u>Robust Regression and Outlier Detection</u>, John Wiley and Sons, New York (1987).

7. Yamane, T., <u>Statistics: An Introductory Analysis</u>, 2nd Edition, Harper & Row, New York (1967).

8. Hosmer, D.W., and Lemeshow, S., <u>Applied Logistic Regression</u>, John Wiley & Sons, New York (1989).

9. Weisberg, S., <u>Applied Linear Regression</u>, John Wiley & sons, New York (1985).

10. Lipson, C., and Sheth, N. J., <u>Statistical Design and Analysis of Engineering Experiments</u>, McGraw-Hill, New York (1973).

11. <u>CSS: Statistica Users Manual</u>, Statsoft (1991).

12. <u>SAS/STAT User's Guide</u>, Revision 6, Fourth Edition, Volume 2, Chapter 27, The Logistic Procadure, SAS Institute, Inc., Cary, North Carolina (1990?).